PETROLOGY OF VOLCANIC ROCKS FROM SAO MIGUEL AND FAIAL, AZORES ISLANDS

Thesis submitted for the degree of Doctor of Philosophy

by

MICHAEL STOREY

Department of Geology
Bedford College
Regent's Park
London NW1 4NS

April 1985

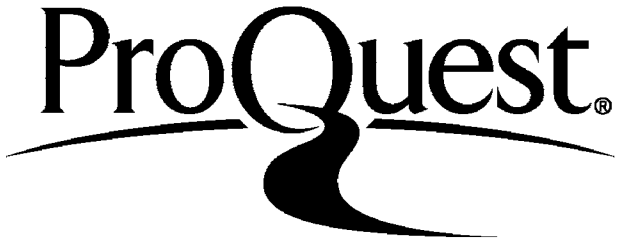

To

Michael O'Neil

ABSTRACT

Volcanic rocks from Sao Miguel form two distinct alkaline (potassic) magma series. Recent eruptives comprise Ne-normative basalts and derivatives (Main Series). Older basalts associated with the extinct stratovolcano Povoacao are either Ne or Hy-normative (Povoacao Series) and have lower P/Zr, Ba/Zr and Sr/Zr ratios. Faial volcanic rocks form a single series, basaltic compositions being Ne-normative. Differentiates on both islands range through intermediate compositions to metaluminous and peralkaline trachytes. The latter are strongly enriched in the incompatible elements (eg Th, Rb, Ta, Nb, Zr and the rare-earths) and are depleted in Mg, Ni, Cr, V, Ti, P, Sr, Eu and Ba. Fractional crystallization of the observed phenocryst assemblages can account for most chemical variations, incompatible element abundances indicating that the trachytes result from some 60-85% solidification of a parental basalt.

Mixed-magma lavas occur on both Faial and Sao Miguel. They form two distinct groups. (1) M-type lavas. These have high Ni, Cr and MgO and low CaO, Sr, P_2O_5, TiO_2 and V. Modelling suggests they are a mix of trachyte (70%) and MgO-rich basalt (30%). (2). AM-type lavas. They show similar geochemical features but also have high Ba and Eu and large K/Rb ratios. They are best modelled by mixing hawaiite, trachyte and alkali feldspar. AM-type lavas and geochemically heterogeneous pumice deposits suggest compositionally zoned (basalt-intermediate-trachyte) magma chambers beneath both islands.

Compositional variations in recent pumice deposits from Agua de Pau volcano show temporal control. Trends up the succession include the depletion of Sr, Ba and Eu coupled with stepwise enrichment in the incompatible elements. These suggest the deposits represent successive samples of an evolving body of trachytic magma. The lack of similar variations in the Furnas pumice succession is attributed to a high magma viscosity, inhibiting crystal/liquid fractionation.

Pre-eruptive temperatures for trachytic pumice deposits, from coexisting magnetite and ilmenite, ranged between 960°C - 880°C. fO_2 varied between $10^{-10.9}$ - $10^{-13.4}$. Thermodynamic-based estimates of magmatic water contents were between 6.5 - 7.2 wt.%. These values are compatible with field data. Estimates of S_2, H_2S, SO_2, SO_3, H_2, CO_2, HCl and HF suggest they are several orders of magnitude less abundant than H_2O.

Lastly, Azores basalts exhibit inter and intra-island compositional heterogeneity. Relative to N-type m.o.r.b., they are characterized by high La/Yb, Ba/La, $^{87}Sr/^{86}Sr$ ratios and low $^{143}Nd/^{144}Nd$, Zr/Nb, Zr/Ta and K/Rb ratios. Sao Miguel shows a systematic increase in $^{87}Sr/^{86}Sr$ ratios from west to east (up to 0.70522). Most of these features represent source characteristics and suggest a complexly heterogeneous mantle.

ACKNOWLEDGEMENTS

Much of this work was carried out while I held a Research Assistantship at South London College, London SE27 OTX. This was funded by the Inner London Education Authority to whom I am grateful. I thank Dr. R. Croasdale, who initially suggested the project and supplied research material, and Prof. G.P.L. Walker for providing samples and unpublished data and for his tutition in the methods of study of pyroclastic rocks during a visit to Tenerife in January 1978. Prof. A.J. Smith was most generous in his support and provision of facilities while I was at Bedford College. I am especially thankful to my supervisor Dr. A.D. Saunders for critically reading this thesis and also for his patience, encouragement and invaluable advice during its protracted preparation. Sue Smith and Pat Storey kindly typed the final draft.

Use of analytical facilities were provided by the University of London Reactor Centre and the Departments of Geology at Bedford College, University College London, Goldsmiths College and Cambridge University. Thanks go to my 'blood brother' Alan Fever for help in thin-section making, Susan Parry, Nick Rogers and Alan Mann for advice and assistance in INAA analysis and Dr. J. Long, Pete Treloar and Ian Young for instruction in the use of the electron-microprobe. I am especially grateful to Giz Marriner for passing on her "unrivalled" expertise in XRF techniques.

Some of the most interesting and useful discussion held during the course of this research were with Andy Saunders, Mike Norry, John Wright and John Wolff. Research collaboration with John Wolff at the Pied Bull, and elsewhere was particularly stimulating and productive.

Lastly, I thank my family and friends for their encouragement and toleration, especially Pat and George, Moira Ann, Sue, John Wolff, Mike Mullholland, John Digance and Rick Gosling.

TABLE OF CONTENTS

CHAPTER 2

CHAPTER 4

PLATES

CHAPTER 2

CHAPTER 3

TABLES

CHAPTER 1

CHAPTER 2

CHAPTER 3

CHAPTER 4

CHAPTER 5

APPENDIX 1

APPENDIX 2

APPENDIX 3

CHAPTER 1

INTRODUCTION AND GEOLOGICAL SETTING

1.1 INTRODUCTION

The Azores (Fig. 1.1) are nine oceanic volcanic islands situated in the North Atlantic on the important triple junction between the American, Eurasian and African Plates. Five of the islands are known to be volcanically active, compositions of erupted rocks ranging from basalt through to trachyte, comendite and pantellerite differentiates. Basaltic rocks occur as lavas, scoria cones and off-shore ash-rings whereas salic rocks occur as air-fall pumice deposits, ignimbrites, lavas and extrusive domes. The wet-temperate climate of the Azores is such that luxuriant vegetation and soil soon develop on and effectively anchor any newly erupted pyroclastic material. The result is that a remarkably complete record of the explosive eruptions is preserved, in which the successive deposits are clearly demarcated by the soil horizons that separate them. Several of the islands, therefore, are ideal for tephrochronological studies. These techniques were applied in the Azores by Prof. G.P.L. Walker and co-workers who in the late nineteen sixties and early seventies initiated studies to document the recent volcanology of Sao Miguel (Booth et al., 1978; Walker and Croasdale, 1971), Terceria (Self, 1976) and Faial (Walker and Croasdale, unpub. data). While this work was in progress, a comprehensive collection of volcanic rocks from Faial and Sao Miguel was made. Prof. Walker kindly made these samples available for this petrological study. (Sample details and locations being given in Appendix 1).

Chemical variations exhibited by volcanic rocks from oceanic islands are often complex and suggest compositional control by one or more factors/processes; for example, source heterogeneity, variable partial melting, fractional crystallization, magma-mixing. This thesis presents new whole-rock and mineral analyses for volcanic rocks from Faial (Chapter 2) and Sao Miguel (Chapter 3). The data are

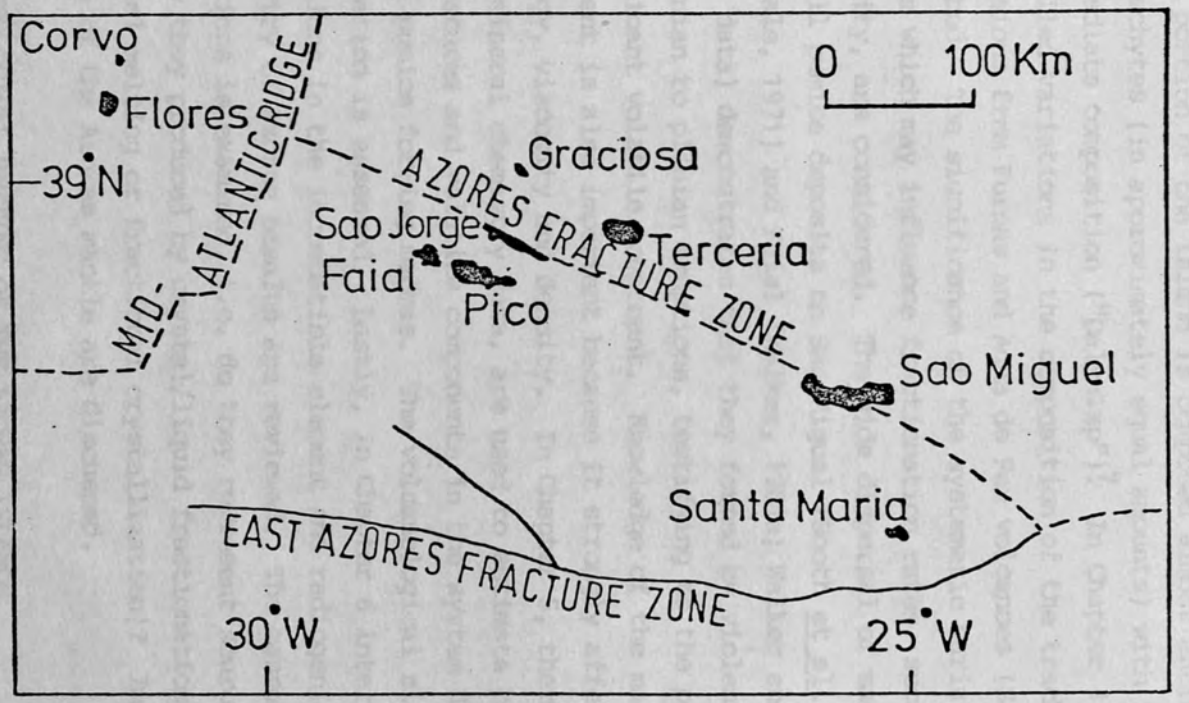

Fig 1.1 The Azores archipelago. Dashed line indicates active plate boundary (after Laughton and Whitmarsh, 1975). Azores fracture zone (after Flower et al., 1976).

examined in terms of theoretical models of element behaviour in igneous systems, the relative importance of different processes being assessed. Where relevant, consistency between theoretical models and field data is discussed. For example, is a fractional crystallization hypothesis for most of the major and trace element variations in Sao Miguel magmas reconcilable with the observation that the visible sub-aerial portion of the island is composed almost entirely of basalts and trachytes (in approximately equal amounts) with few rocks of intermediate composition ("Daly Gap")? In Chapter 4, temporal-controlled variations in the composition of the trachytic pyroclastic successions from Furnas and Agua de Pau volcanoes (Sao Miguel) are described. The significance of the systematic variations found and factors which may influence fractionation rates, such as magma viscosity, are considered. The wide dispersal of many of the trachytic air fall pumice deposits on Sao Miguel (Booth et al., 1978; Walker and Croasdale, 1971) and Faial (Walker, 1981a; Walker and Croasdale, unpub. data) demonstrates that they formed by violently explosive subplinian to plinian eruptions, testifying to the presence of a significant volatile component. Knowledge of the magmatic volatile component is also important because it strongly affects magma rheology, viscosity and density. In Chapter 5, thermodynamic methods, using mineral chemistry data, are used to estimate pre-eruptive temperatures and volatile components in the system H-O-S for some Azores pumice forming magmas. The volcanological significance of this information is assessed. Lastly, in Chapter 6 inter and intra-island variations in the incompatible element and radiogenic isotope chemistry of Azores basalts are reviewed. The cause of these variations is examined, i.e. do they represent source heterogeneities or are they produced by crystal/liquid fractionation processes (partial melting or fractional crystallization)? Implications for the nature of the Azores mantle are discussed.

1.2 GEOLOGICAL SETTING OF THE AZORES ISLANDS

The Azores archipelago, which comprises nine Tertiary-Quaternary volcanic islands and the tidally submerged Formigas islets, are

situated in the Atlantic approximately 1,400 km west of Portugal, lying between latitudes 36° 55' and 39° 43'N and longitudes 25° 00' and 31° 17'W (Fig 1.1). The islands trend west northwest for 600 km, straddling the Mid-Atlantic Ridge (MAR) on a tectonically complex, topographic high known as the Azores Platform, which has unusually thick oceanic crust (8 km), being some 60 percent greater than average (Searle, 1976). The seven islands to the east of the MAR (Fig 1.1) are associated with a seismically active complex transform fracture zone (Laughton and Whitmarsh, 1975); Krause and Watkins (1970) had previously interpreted this zone to be a secondary axis of crustal spreading. As stated earlier the Azores are the locus of the important 'triple junction' where the American, Eurasian and African plates come together at the meeting of the MAR and the western end of the Azores-Gibralter fracture zone (AFZ; Fig 1.1).

The oldest volcanic rocks known in the Azores are of Miocene age. For example, K-Ar dating of basalt from the upper part of the 'Old Basaltic Complex' on Santa Maria (Zbyszewski and Ferreira, 1962), the most southerly island in the archipelago, gave 8.12 ± .85 Ma (Abdel-Monem et al., 1975). Volcanism continues to the present with eruptions on Sao Jorge, Faial, Pico, Terceria and Sao Miguel, since the time of settlement. All but the deeply eroded island of Santa Maria, have one or more large Quaternary stratovolcanoes, the highest being the 2,351 m cone on Pico, the others all having calderas. The best known calderas are those on Sao Miguel (Sete Cidades, Fogo, Furnas and Povoacao). In addition to the stratovolcanoes, there are more than one thousand basaltic scoria cones in the Azores, many of them aligned along fissures. Also, several islands have off-shore ash-rings or tuff-rings due to surtseyan-type eruptions in shallow water. Comprehensive summaries of the geology of the Azores have been given by Mitchell-Thome (1976) and Ridley et al. (1974) where full bibliographies may be found. More detailed descriptions of the geological setting of Faial and Sao Miguel are given in Chapters 2, 3 and 4.

1.2.1 Classification of volcanic rocks from the Azores

Volcanic rocks from the Azores belong to the alkali-basalt/trachyte suite. Basaltic (*) compositions, including those with minor Hy in the norm, lack a Ca-poor pyroxene having a typical alkalic phenocryst assemblage of olivine, titaniferous augite and plagioclase with accessory Cr-spinel, Fe-Ti oxides and pyrrhotite. The groundmass consists of the same minerals along with some alkali feldspar. In a plot of total alkalis versus silica (Fig 1.2) the majority of analyses of Azores basaltic rocks plot in the alkali-basalt field of Macdonald and Katsura (1964).

Undersaturated volcanic rocks from oceanic islands have been broadly divided into two suites based on the compositions of the derivatives (Coombs and Wilkinson, 1969):

(i) a strongly undersaturated basanite-phonolite suite having more than 5% normative Ne (eg Tenerife, Ridley 1970)

(ii) the alkali-basalt/trachyte suite, having less than 5% normative Ne.

This arbitrary division between the two suites does not easily apply to the Azores alkali-basalt/trachyte series, where basaltic compositions may contain significantly more than 5% normative Ne. A saturated to oversaturated transitional suite with normative Hy also occurs on some oceanic islands including Terceria (Self and Gunn, 1976) and Sao Miguel (Fernandez, 1980, 1982; Chapter 3, this thesis) in the Azores. Petrological studies of the Atlantic islands have shown significant inter-island differences in alkalinity and Na/K ratios of

---

* The term "basaltic" is used here in a broad sense and is taken to include both basalts and hawaiites (ie Differentiation Index < 45).

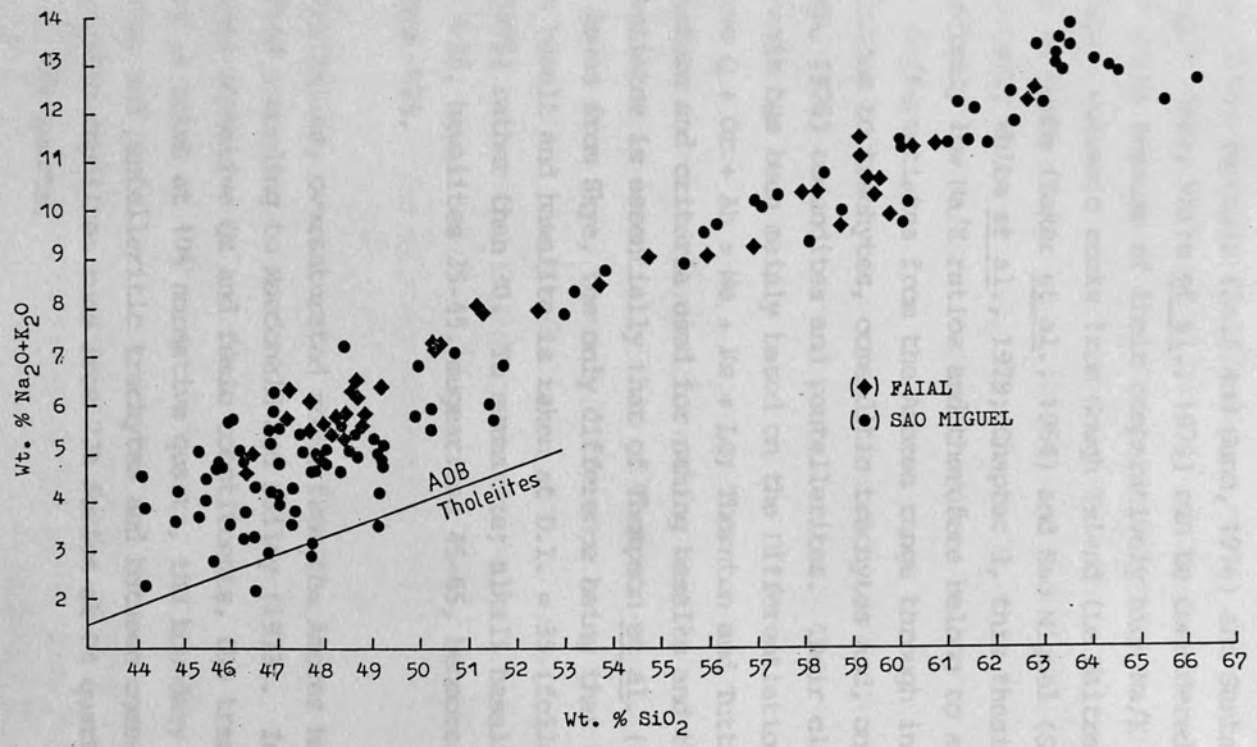

Fig 1.2. Total alkalis versus SiO_2 for volcanic rocks from Faial and Sao Miguel. Data is from Fernandez (1980), Metrich et al. (1981), White et al. (1979) and this thesis. The solid line discriminates between Hawaiian tholeiites and alkali basalts (Macdonald and Katsura, 1964).

basaltic rocks. Thus, some workers have advocated a dual nomenclature based on the Na/K ratio (Coombs and Wilkinson, 1969). For example, volcanic rocks from Maderia (Hughes and Brown, 1972; Schmincke and Weibel, 1972), Terceria (Self and Gunn, 1976) and Santa Maria (B.M. Gunn unpub. data; White et al., 1979) can be considered to belong to a 'sodic' suite because of their comparatively high Na/K ratios. Conversely, volcanic rocks from Gough Island (Le Maitre, 1962), Tristan da Cunha (Baker et al., 1964) and Sao Miguel (Schmincke and Weibel, 1972; White et al., 1979; Chapter 3, this thesis) have comparatively low Na/K ratios and therefore belong to a 'potassic' suite. Differentiates from the Azores range through intermediate compositions to trachytes, comenditic trachytes and, on Terceria (Self and Gunn, 1976) comendites and pantellerites. Their classification in this thesis has been mainly based on the Differentiation Index (D.I. = normative Q + Or + Ab + Ne + Ks + Lc; Thornton and Tuttle, 1960). The nomenclature and criteria used for naming basalts and their differentiates is essentially that of Thompson et al. (1972) for Eocene lavas from Skye, the only difference being that the division between basalt and hawaiite is taken at D.I. = 35 (following Self and Gunn, 1976) rather than 30. To summarize; alkali basalts have D.I. values < 35, hawaiites 35-45, mugearites 45-65, benmoreites 65-75 and trachytes >75.

Peralkaline, oversaturated rocks from the Azores have been classified according to Macdonald and Bailey (1973). In this scheme, which uses normative Qz and femic constituents, the trachyte-rhyolite boundary is taken at 10% normative quartz, the boundary between comenditic and pantelleritic trachytes and between comenditic and pantelleritic rhyolites runs from 22% femics at 0% quartz to 9.2% femics at 40% quartz.

1.3 THE USE OF TRACE ELEMENTS IN UNDERSTANDING MAGMATIC PROCESSES

A trace element in magmatic systems is defined as one which follows Henry's law in the phases considered. An element may be present in trace quantities and not follow Henry's law, being an

essential structural constituent of a mineral phase. An example would be a granitic melt containing only a few hundred parts per million (ppm) Zr but which was crystallizing zircon. The purpose of this section is to briefly review the uses of trace elements in understanding the origin and evolution of igneous rocks. For example, the composition of basalts is a complex function of fractional crystallization, partial melting and mantle heterogeneity. As will be shown in this and subsequent Chapters study of suitable trace elements allows discrimination between these different factors.

Particularly valuable in this regard is the rare-earth group of elements (REE). With the exception of Eu which normally occurs as the divalent ion in magmas, the REE (normally trivalent in natural melts), which show a small but progressive increase in field strength (ionic charge/ionic radius) with increasing atomic number, behave in a chemically coherent and systematic manner in fractionation processes. The common method of displaying REE data is in a 'chondrite normalised' plot. The chondrite normalizing values from Evensen et al. (1978) are used in this study (Table 1.1).

1.3.1 Classification of trace elements

The partioning of a trace element between solid and melt is described by its bulk distribution coefficient (D); equation 1.1

$$D = \Sigma_i^n X^i Kd^i \quad \text{(Eq. 1.1)}$$

where X^i is the weight fraction of mineral i and Kd^i is its mineral/melt partition coefficient for a given trace element.

Depending on their D values, trace elements may behave in one of two ways during fractionation processes. Elements with $D < 1$ are termed incompatible and are preferentially concentrated in the liquid phase during melting and crystallization. In contrast elements with $D > 1$ are termed compatible and are preferentially retained or extracted by the residual or crystallizing phases respectively. The D value of

La	0.2446
Ce	0.6379
Nd	0.4738
Sm	0.1540
Eu	0.05802
Gd	0.2043
Tb	0.03745
Dy	0.2541
Ho	0.05670
Er	0.1660
Yb	0.1651
Lu	0.02539

Table 1.1 Average chondrite REE abundances (data from Evensen et al., 1978).

a particular element may vary through the course of magma differentiation. For example, in Sao Miguel magmas D_{Ba} < 0.01 in basaltic and intermediate compositions but in the trachytes D_{Ba} > 1 due to alkali feldspar fractionation (Table 1.2). Wood et al. (1979) used the term "hygromagatophile" (HYG), for those elements with D's < 1. These are subdivided into "more-HYG" for those elements with D < 0.01 and "less-HYG" for those elements with D $\sim$0.1. In ocean basalt suites examples of more-HYG elements are Cs, Rb, K, U, Th, Ta, Nb, Ba, La, Ce (Zr, Hf). Less-HYG elements are Sr, P, Ti, Y, (Zr, Hf) and the heavy REE. The classification reflects the relative bulk distribution coefficients of the elements rather than their atomic structure, D values being strongly dependent upon the mineralogical components, PH_2O, PO_2, P and T of the system. For example, it is apparent from studies of trace elements in orogenic suites (eg Saunders et al., 1980) where PH_2O is probably higher than in most non-orogenic suites (eg Ringwood, 1974), that the small highly charged ions (eg Nb^{5+}) behave in a different manner to the larger, univalent ions (eg Rb^{+}). Thus, alternative groupings based on field strengths of trace elements have been proposed (eg Saunders et al., 1979). In this classification, incompatible elements are subdivided according to their radius/charge ratio. For example, high field strength (HFS) elements, defined as having a radius/charge ratio of less than 0.2, include Zr, Hf, Ti, P, Nb, and Ta. Examples of low field strength (LFS) elements (radius/charge ratio greater than 0.2) include Cs, Rb, K, Ba, Sr, Th, U, and Pb. Strictly speaking, the REE and Y belong to the LFS group because they have radius/charge ratios between 0.3 and 0.34. However, because many aspects of their behaviour resemble those of the HFS elements, Saunders et al. (1979) treat them as a separate (third) group.

The terms mobile and immobile, respectively refer to elements which are prone or resistant to post eruptive/emplacement alteration processes. For example, the rare-earth and HFS elements are considered to be immobile during the alteration of basalt (Pearce, 1975) whereas the mobility of LFS elements (especially the alkali and alkaline earths but excluding the REE) is well known (for example,

	Cs	Ba	Rb	K	Sr	La	Ce	Nd	Sm	Eu	Gd	Dy	Er	Yb
Basaltic/intermediate rocks														
Clinopyroxene*	.0011	.0011	.0011	.002	.067	.069	.098	.21	.26	.31	.30	.33	.30	.28
Orthopyroxene*		.001	.0006	.001	.007		.0030	.0068	.010	.013	.016	.022	.030	.049
Olivine*	.00043	.00011	.00018	.00018	.00019		.0005	.0010	.0013	.0016	.0015	.0017	.0015	.0015
Garnet *		.0015	.0007	.001	.0011		.021	.087	.217	.320	.498	1.06	2.00	4.03
Augite		.026	.031	.038	.12		.15	.31	.50	.51	.61	.68	.65	.62
Hornblende		.42	.29	.96	.46		.20	.33	.52	.59	.63	.64	.55	.49
Phlogopite		1.09	3.06	2.65	.081		.034	.032	.031	.030	.030	.030	.034	.042
Plagioclase		.23	.071	.17	1.83		.012	.081	.067	.34	.063	.055	.063	.067
Rhyolitic rocks														
Clinopyroxene		.131	.032	.037	.516		.50	1.11	1.67	1.56	1.85	1.93	1.66	1.58
Hornblende		.044	.014	.081	.022		1.52	4.26	7.47	5.14	10.0	13.0	12.0	8.4
Biotite		9.7	2.24				.32	.29	.26	.24	.28	.29	.35	.44
Apatite							34.7	57.1	62.8	30.4	56.3	50.7	37.2	23.9
Zircon							2.64	2.20	3.14	3.14	12.0	45.7	135	270
K-feldspar		6.12	.37		3.87		.044	.025	.18	1.13	0.011	0.006	0.006	0.012

Table 1.2 Partition coefficients for basaltic, intermediate and rhyolitic rocks. * From compilation of Hanson (1977) for basaltic melts. Rest of data from compilations of Arth and Hanson (1975)

during low to medium temperature alteration of basalt by seawater: Hart, 1971; Hart et al., 1974; Wood et al., 1976; Mitchell and Aumento, 1977).

In this thesis the terms compatible and incompatible will suffice. These may be distinguished as highly incompatible ($D \leq 0.01$) or moderately incompatible ($D > 0.01, < 1$), terms broadly equivalent with more-HYG and less-HYG respectively.

1.3.2 Models of trace element behaviour

(a) Crystal fractionation

The variation of a trace element during fractional crystallization, where D is constant, is given by the Rayleigh fractionation law (Neumann et al., 1954) which describes the trace element concentration of the differentiated melt, C_L, relative to the parent melt C_O; equation 1.2.

$$C_L/C_O = F^{(D-1)} \quad \text{(Eq. 1.2)}$$

In Eq. 1.2, which specifically relates to crystals that are only in surface equilibrium with a homogenous melt, conditions believed to prevail in a crystallizing magma body (Allegre and Minster, 1978), F is the weight fraction of melt left relative to the parent. D, the bulk partition coefficient for minerals crystallizing out of the melt, is given by Eq. 1.1. For highly incompatible elements, D approaches zero and the enrichment of the element relative to the parental melt varies inversely with F. Elements with D values significantly greater than 1 will show a large decrease in concentration for a small amount of crystallization (Fig 1.3).

(b) Partial melting

Magmas are formed by partial melting of a multi-phase solid assemblage. The simplest model of this process is batch melting in

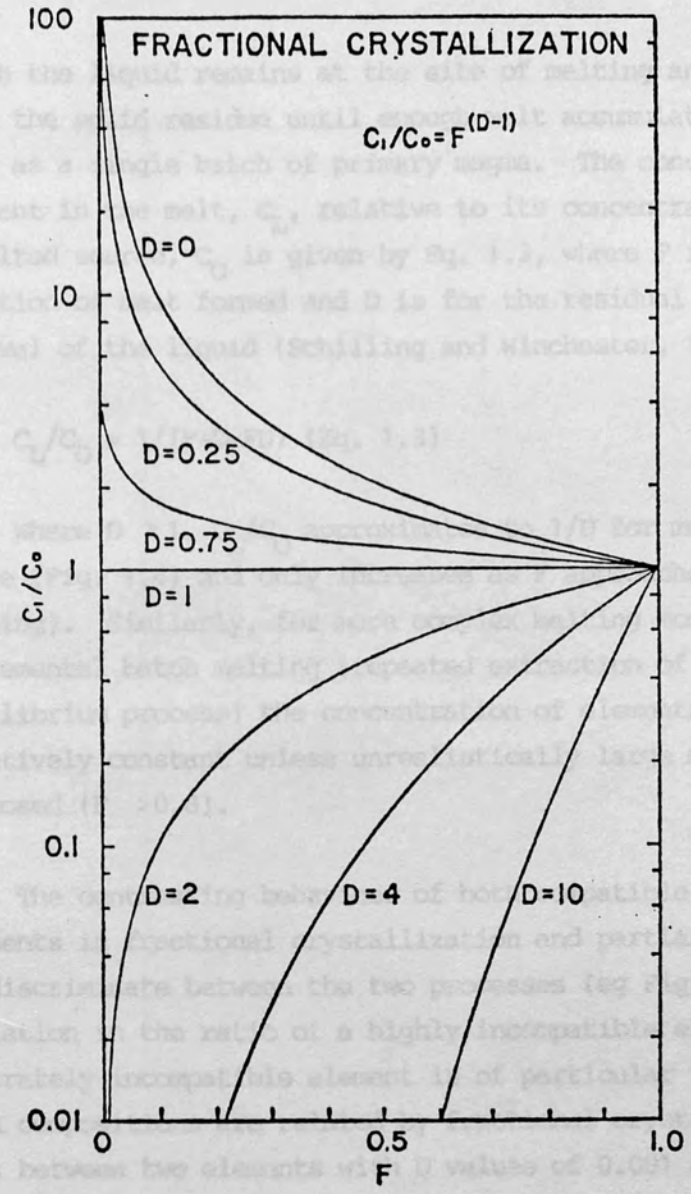

Fig 1.3 Plot of C_L/C_O versus F for fractional crystallization.

which the liquid remains at the site of melting and is in equilibrium with the solid residue until enough melt accumulates to allow it to rise as a single batch of primary magma. The concentration of a trace element in the melt, C_L, relative to its concentration in the original unmelted source, C_O is given by Eq. 1.3, where F is the weight fraction of melt formed and D is for the residual solid at the time of removal of the liquid (Schilling and Winchester, 1967).

$$C_L/C_O = 1/(F+D-FD) \quad \text{(Eq. 1.3)}$$

Where $D > 1$, C_L/C_O approximates to $1/D$ for much of the melting range (Fig. 1.4) and only increases as F approaches 1 (ie almost total melting). Similarly, for more complex melting models such as incremental batch melting (repeated extraction of melts formed by an equilibrium process) the concentration of elements with $D > 1$ remains relatively constant unless unrealistically large melt fractions are proposed ($F > 0.8$).

The contrasting behaviour of both compatible and incompatible elements in fractional crystallization and partial melting may be used to discriminate between the two processes (eg Fig. 2.25). The variation in the ratio of a highly incompatible element to a moderately incompatible element is of particular value. If a group of rock compositions are related by fractional crystallization, a biaxial plot between two elements with D values of 0.001 and 0.1 repectively, would approximate to a colinear trend. For example, based on mineral/liquid partition coefficents (Table 1.2) the light REE/heavy REE ratio (eg Ce/Yb) should remain relatively constant in a basaltic magma series related by low pressure fractionation (eg plagioclase, olivine, clinopyroxene). In contrast, such ratios would show considerable variation between melts produced by different values of F (Fig 1.4). Theoretically, small degrees of partial melting of garnet lherzolite could produce basalts with Ce/Yb ratios an order or so magnitude greater than the source.

Lastly, it follows that in a biaxial plot between two highly

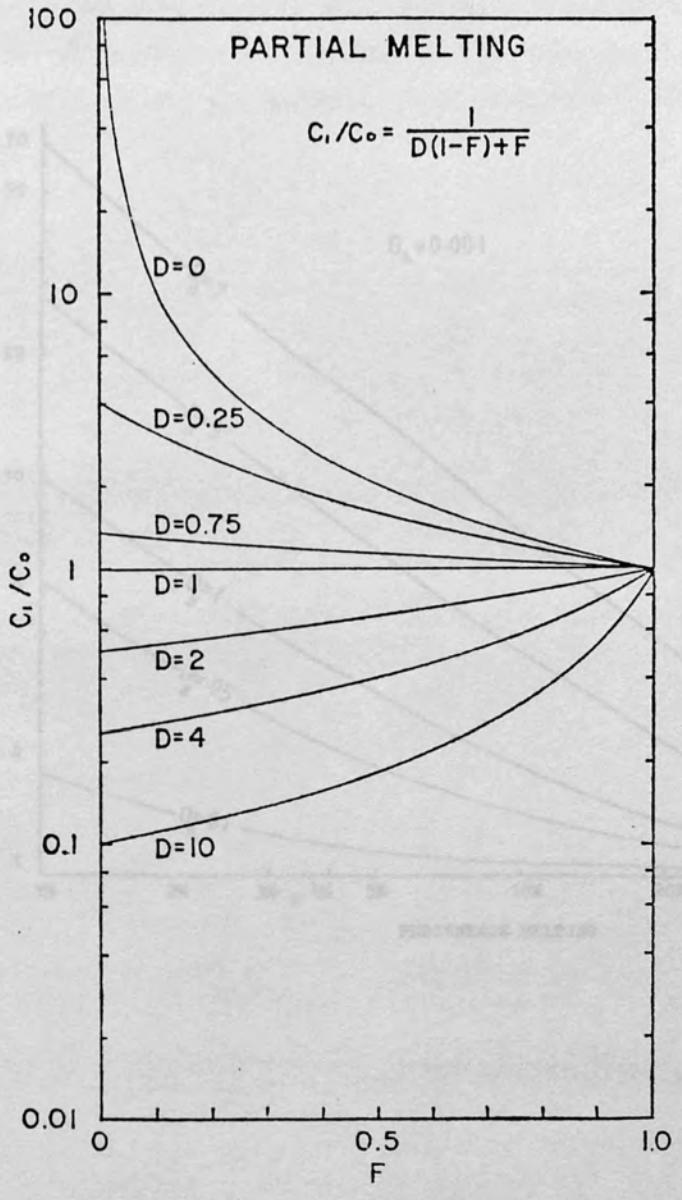

Fig 1.4 Plot of C_L/C_O, the concentration of a trace element in the liquid relative to its concentration in the original parent versus F, the fraction of melting.

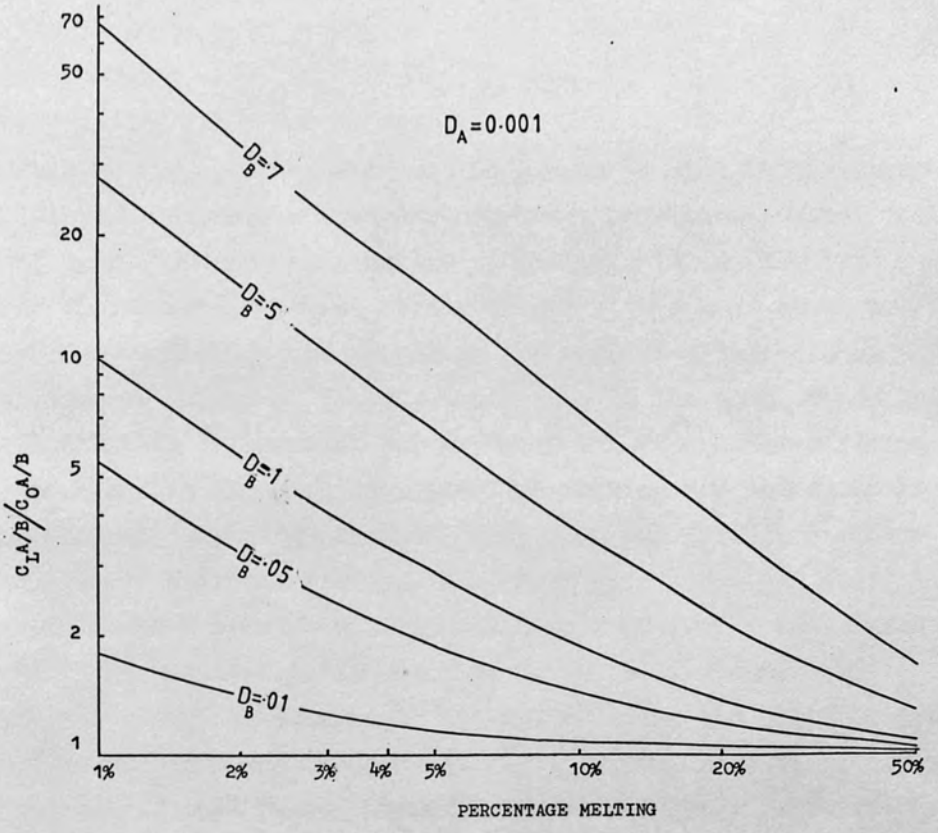

Fig 1.5 The variation in the ratio of a highly incompatible element (A) to a moderately incompatible element (B) in the liquid (C_L A/B), for various degrees of partial melting and D_B values (0.01 to 0.7), relative to their ratio in the parent (C_O A/B).

incompatible elements it is not possible to distinguish (unless F is very small) between partial melting and fractional crystallization processes. Thus, large variations in the K/Rb ratios of basaltic magmas, for example, are suggestive of source heterogeneties.

CHAPTER 2

THE PETROLOGY OF VOLCANIC ROCKS FROM FAIAL

2.1 INTRODUCTION

Faial is the most westerly of the Azores Islands on the European Plate, sitting on the youngest oceanic crust and being nearest to the MAR (Fig 1.1). Volcanically active in historic times, the island consists of a single, central stratovolcano with a well developed caldera (Cabeco Gordo), the slopes of the volcano being mantled with air fall pumice deposits. Fissural activity in the west of the island and rift activity in the east has produced a number of lava flows, mainly of basaltic composition. Previous work on the petrology and geochemistry of lavas from the island by Assunaco (1959), Assunaco and Canilho (1970), Berthois (1953), Metrich et al. (1981) and White et al. (1979) have shown that compositions range from alkali basalt to trachyte. The basaltic rocks occur as lavas, scoria cones and offshore ash-rings, an example of the latter being the historic 1957-58 eruption at Ponta dos Capelinhos. Silicic compositions occur as large volume air fall pumice deposits (Walker, 1981a), ignimbrites, lavas and domes (Metrich et al., 1981). Volcanic rocks from Faial are therefore diverse in terms of both their occurence and composition, the island providing a good setting to study physical and chemical aspects of volcanism in the oceanic environment. Although the major-element variation of lavas from Faial is fairly well documented by Metrich et al. (1981) comprehensive trace element data on the volcanic rocks are limited to a total of eight analyses published by Flower et al. (1976) and White et al. (1979). Furthermore, published analyses of the silicic pyroclastic rocks, either of major or trace elements are lacking. The aim of this chapter therefore, is:

(a) to present new major and trace element analyses of twenty-seven recently erupted Faial volcanic rocks consisting of lavas, pyroclastics and, two syenite xenoliths from trachytic pumice fall deposits S and T.

(b) to present data on the compositions of the main mineral phases found in Faial volcanic rocks.

(c) to examine both whole rock and mineral chemical variations in terms of processes such as partial melting, fractional crystallization and magma-mixing.

2.2 GEOLOGICAL SETTING

The nearest island to Faial is Pico which together form a WNW-ESE alignment parallel to the AFZ (Fig 1.1). This regional trend controls the orientation of the majority of volcanic structures on Faial as shown (Fig 2.1) by the geological maps made by Zbyszewski et al. (1959) and Metrich et al. (1981). The latter workers, to which most reference is made here, distinguish four volcanic units on Faial based on the location and age of the eruptive centres. These comprise:

(a) Eruptives from the 'eastern rift' and other volcanic rocks preceeding the formation of the caldera.

(b) Post-caldera activity of the stratovolcano, composed mainly of lavas and pyroclastics of trachytic composition.

(c) The recent basaltic activity of the Horta volcanic field in the SE of the island.

(d) Recent and historic basalts produced by fissural activity in the west of the island.

Apart from the stratovolcano, pre-caldera volcanic rocks are also associated in the low-lying tract of land to the east with a number of WNW-ESE trending structures which Metrich et al. (1981) interpret as normal faults, forming a graben which they refer to as the 'eastern rift' of Faial (Fig 2.1). This is based on their observation that the sequence of lavas in the axial zone of the 'eastern rift' differs from

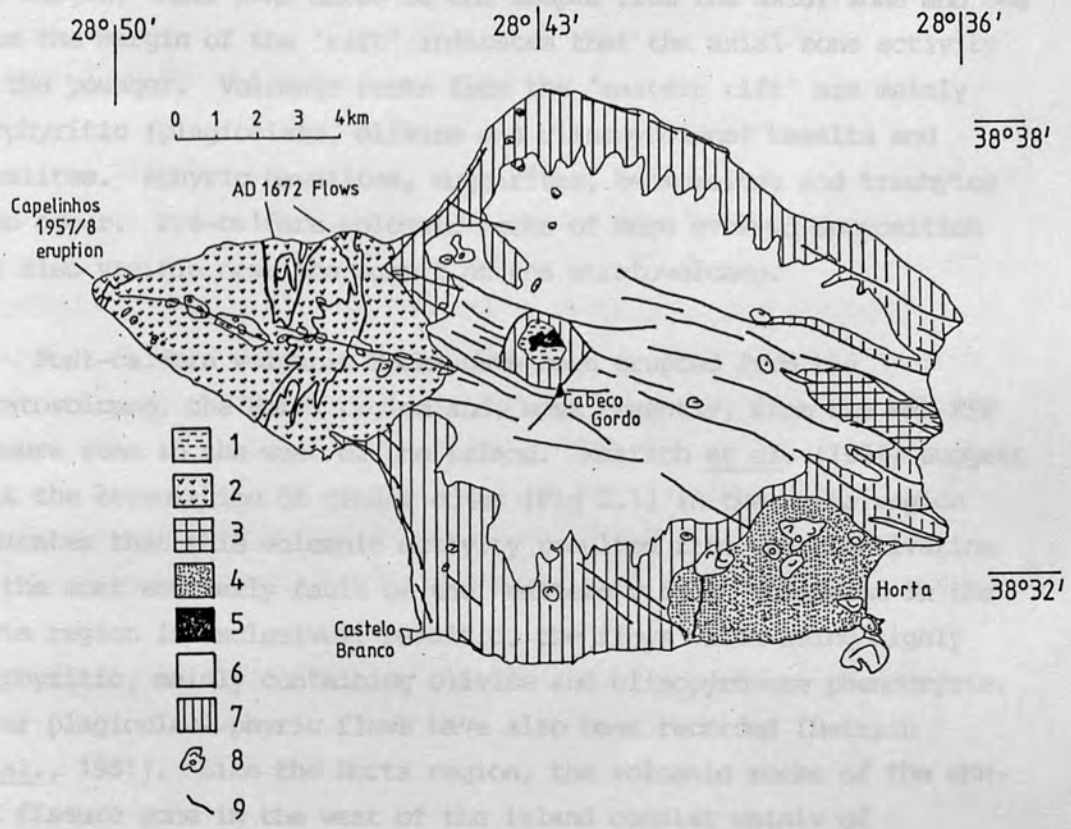

Fig 2.1 Geological map of Faial; simplified after Metrich et al. (1981).

1 - Alluvium, beach deposits, talus.
2 - Basaltic rocks produced by fissural activity in the west.
3 - Eruptives associated with the 'eastern rift'.
4 - Basaltic rocks associated with the Horta volcanic field.
5 - Post-caldera volcanic rocks of intermediate composition.
6 - Mostly trachytic pyroclastics.
7 - Pre-caldera eruptives.
8 - Scoria cones.
9 - Faults, fissures.

the margin; their K-Ar dates of one sample from the axial zone and one from the margin of the 'rift' indicates that the axial zone activity is the younger. Volcanic rocks from the 'eastern rift' are mainly porphyritic (plagioclase, olivine and clinopyroxene) basalts and hawaiites. Aphyric hawaiites, mugearites, benmoreites and trachytes also occur. Pre-caldera volcanic rocks of more evolved composition are also visible near the summit of the stratovolcano.

Post-caldera volcanic rocks have been erupted from the stratovolcano, the Horta region and, most recently, from the WNW-ESE fissure zone in the west of the island. Metrich et al. (1981) suggest that the orientation of cinder cones (Fig 2.1) in the Horta region indicates that this volcanic activity resulted from the reactivation of the most southerly fault of the 'eastern rift'. Volcanism in the Horta region is exclusively basaltic, the flows often being highly porphyritic, mainly containing olivine and clinopyroxene phenocrysts. Rarer plagioclase-phyric flows have also been recorded (Metrich et al., 1981). Like the Horta region, the volcanic rocks of the WNW-ESE fissure zone in the west of the island consist mainly of porphyritic basaltic rocks containing phenocrysts of olivine, clinopyroxene and rarer plagioclase. Volcanic rocks erupted from the caldera-region of the stratovolcano are predominantly trachytes. Many occur as air-fall pumice deposits, some with volumes in excess of $1km^3$, produced by plinian-type eruptions (Walker, 1981a). Other trachytes occur as lava flows, domes and ignimbrites. The recent volcanology of Faial has been the subject of a study by Walker and Croasdale (unpublished data). Part of this was a tephrochronological study on a number of the large trachytic air-fall pumice deposits erupted from the stratovolcano. The petrology of several of these deposits (field designation A, B, D, S, T, U) will be detailed in this and subsequent chapters.

2.2.1 Historic Volcanicity

There have been two volcanic eruptions from the western fissure zone during historic times. The first eruption documented on Faial

occured in A.D. 1672 (Machado, 1967) and was of strombolian type with several resulting lava flows (Fig 2.1). The second eruption occured between 1957-58 off Ponta dos Capelinhos (Fig 2.1) and was very well documented, for example see Machado (1967) and references cited therein. The initial volcanic activity of the 1957 eruption (preceded by some two hundred earth tremors) was surtsyean and quite violent, ejecta being hurled up to 2km in the air. The resultant cinder ring eventually became joined to the main island by a sand isthmus. Later activity in May 1958 was of strombolian type and was accompanied by a number of lava emissions and the growth of a spatter cone inside the cinder ring. Tazieff (1958) estimated that the volume of basalt erupted equalled $778m^3$. Although Faial has a number of large volume trachytic pyroclastic deposits (Walker, 1981a) no plinian-type eruptions have occured during historic times. However, the trachytic pumice fall deposit I has been dated as 1500 B.P. (Walker, 1981a) suggesting that future volcanic activity of this type is possible.

2.2.2 Mixed-magma Eruptions

For most volcanic settings it has been shown, both from lavas (eg Blake et al., 1965; Gibson and Walker, 1963) and pyroclastic deposits (eg Anderson, 1976; Eichelberger, 1975, 1978; Sakuyama, 1979, 1981; Luhr and Carmichael, 1980; Wolff et al., 1980; Wolff and Storey, 1984) that the products of individual eruptions are often made up of two or more compositionally distinct magmas. On Faial good examples are provided by pumice fall deposit A and a lava (samples AZ3410, AZ3411) from near Castelo Branco. Faial A consists of a buff-coloured trachytic pumice (57.3 wt% SiO_2) which grades upwards into a denser, darker less vesicular variety (benmoreite; 56.0 wt% SiO_2). A further example of a mixed-magma eruption, a lava from near Castelo Branco, consists of basic inclusions (54.8 wt% SiO_2) in a trachytic host (62.9 wt% SiO_2). Textural relationships (Walker pers. comm.) suggest both components were fluid at the time of eruption. Both these cases of 'mixed magma' eruptions are described in more detail in subsequent sections.

2.3 CLASSIFICATION OF FAIAL VOLCANIC ROCKS

In the plot of alkali elements versus silica (Fig 1.2) all the basaltic analyses given here for Faial plot in the alkali-basalt field for Hawaii of Macdonald and Katsura (1964). In terms of their Na/K ratio they have values intermediate between 'sodic' islands such as Terceria and 'potassic' islands such as Sao Miguel (Fig 2.14). Unlike some Azores Islands, for example Terceria (Self and Gunn, 1976) and Sao Miguel (Fernandez 1980, 1982; Chapter 3 this thesis), transitional, Hy-normative basaltic rocks appear to be absent on Faial, all being strongly silica undersaturated, normative Ne varying between 5 and 10% with the proportion of Ne increasing from basalt to hawaiite (Fig 2.2). Differentiates on Faial range through intermediate compositions to metaluminous and peralkaline trachytes. Fig 2.3 is a plot of D.I. against the normative An/An+Ab ratio for Faial volcanic rocks (the plot includes the date of Metrich et al., 1981). A feature is that by themselves neither the range of analyses of Metrich et al. (1981) or the new data given here can be considered fully representative of the Faial magma series. In particular, the paucity of intermediate rocks in the latter data set is notable, a feature which may be due to deliberate sampling bias in favour of post-caldera eruptives, samples being collected during a study of the recent volcanology of Faial (Walker and Croasdale, unpublished data).

Fig 2.4 is a plot of the silica saturation (normative Ne or Qz + Qz in Hy) against D.I. Compositions more evolved than hawaiite show a decrease in normative Ne with differentiation, the majority of trachytes being transitional in terms of silica saturation. Two trachyte samples (AZ3401, AZ3426) have minor Hy in the norm, however no particular significance is attached as a small change in the Fe_2O_3/FeO ratio can shift transitional compositions either side of the plane of silica undersaturation. Similarly, post-eruptive leaching of alkali elements would result in an apparently more silica saturated composition. Trachytes are also classified by their molecular alkali/aluminium ratio. All are metaluminous with the exception of Faial D (AZ3401) and the trachytic component (AZ3410) of the mixed

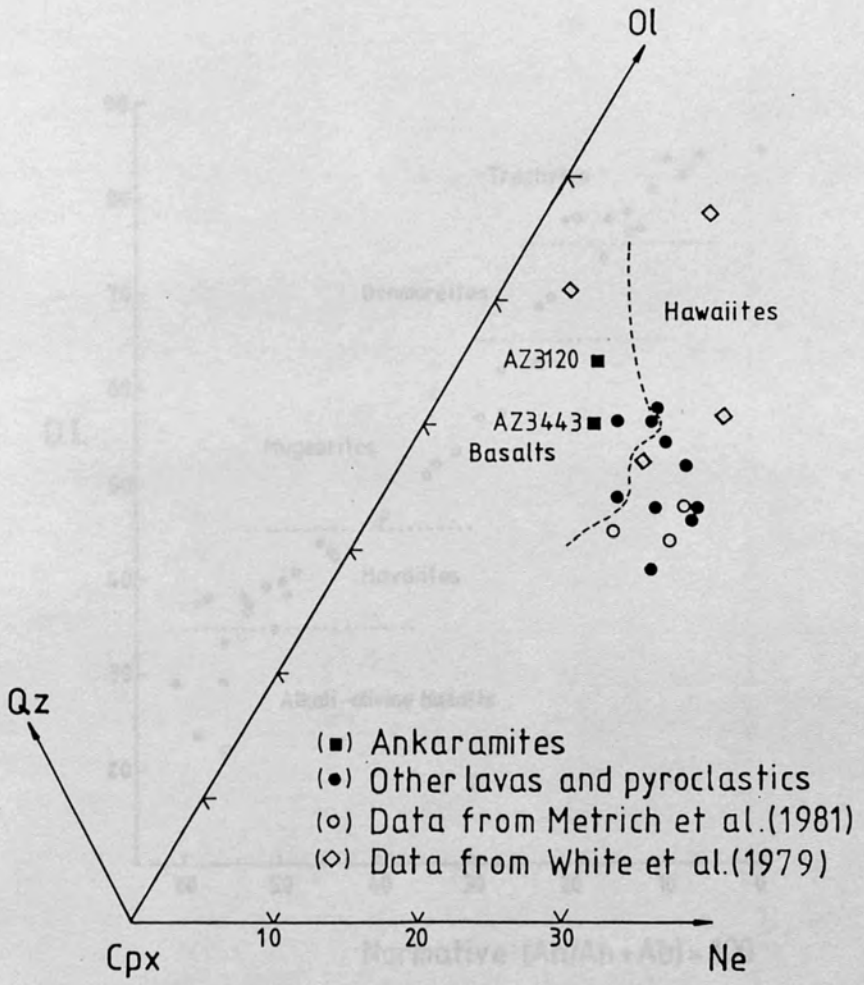

Fig 2.2 Projection of Faial basalts and hawaiites (DI < 45) in the normative tetrahedron of Yoder and Tilley (1962).

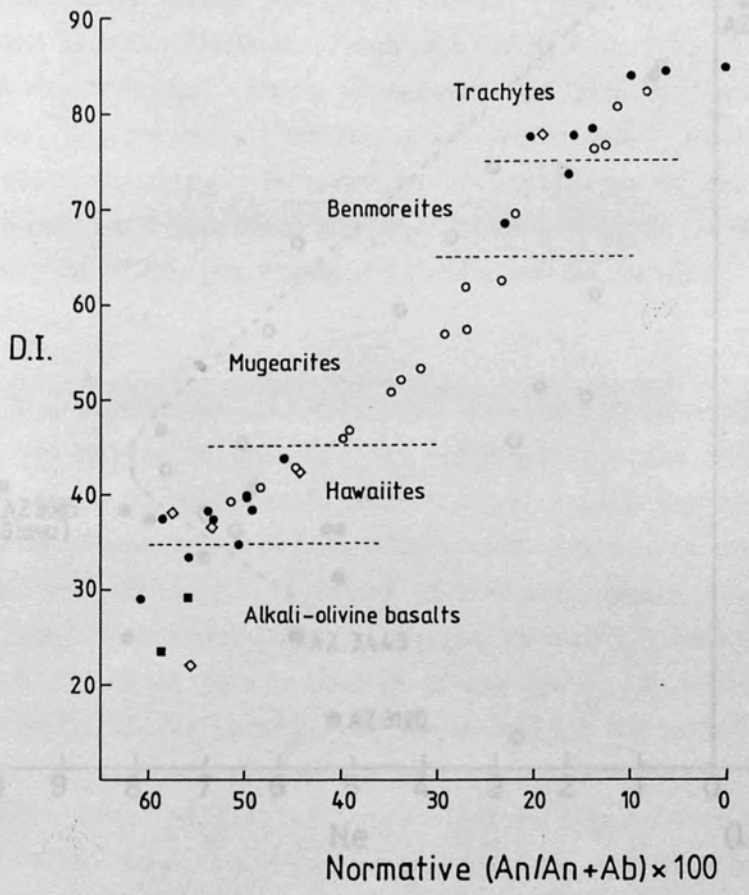

Fig 2.3 A plot of Faial volcanic rocks in terms of their normative anorthite content and DI. Symbols as Fig 2.2.

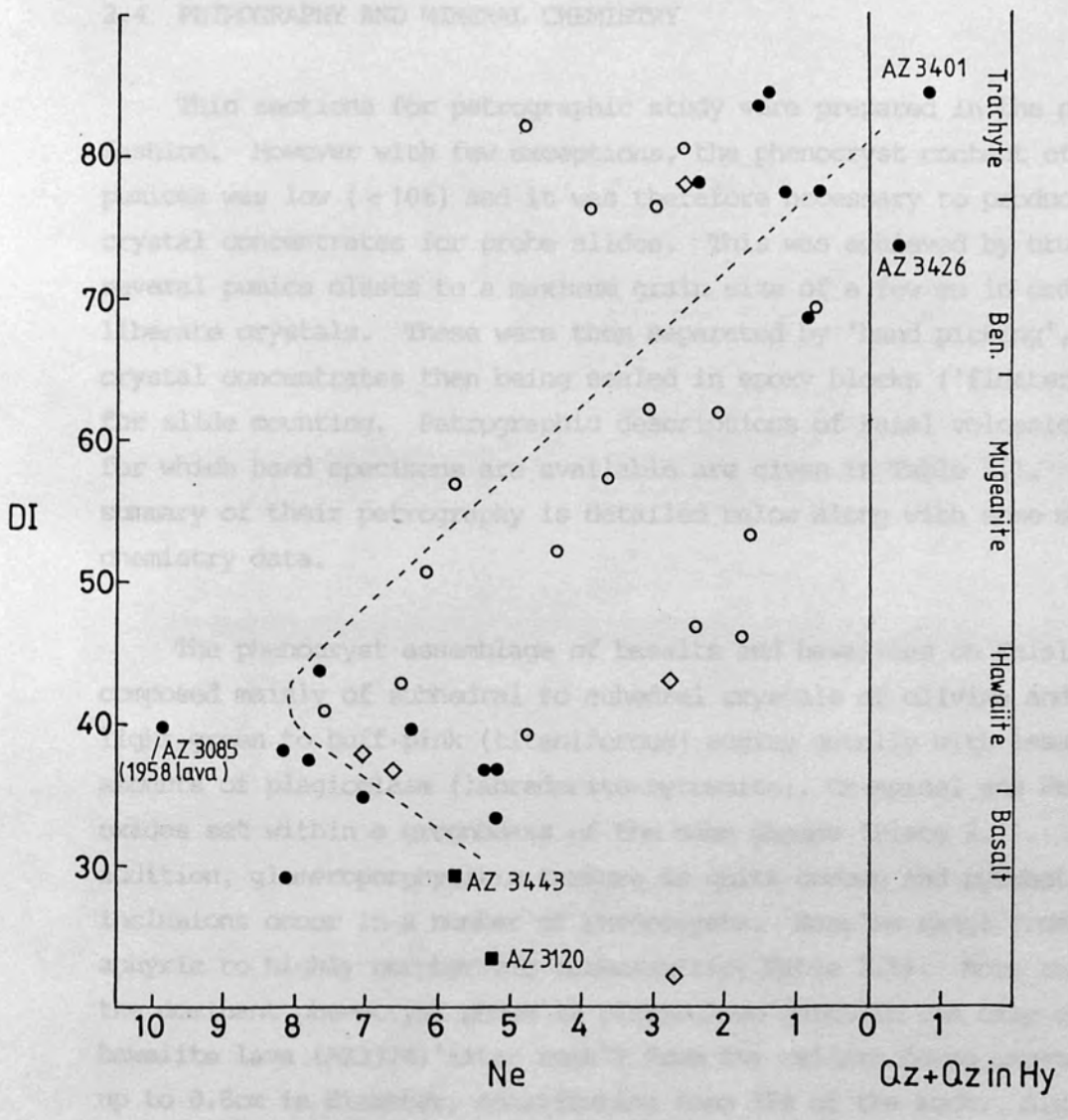

Fig 2.4 Silica saturation versus DI for Faial volcanic rocks. Dashed line is the inferred liquid-line of descent. Mixed lava and syenite samples not shown. Symbols as Fig 2.2.

lava from Castelo Branco, both of which are mildly peralkaline.

2.4 PETROGRAPHY AND MINERAL CHEMISTRY

Thin sections for petrographic study were prepared in the normal fashion. However with few exceptions, the phenocryst content of the pumices was low (< 10%) and it was therefore necessary to produce crystal concentrates for probe slides. This was achieved by crushing several pumice clasts to a maximum grain size of a few mm in order to liberate crystals. These were then separated by 'hand picking', the crystal concentrates then being sealed in epoxy blocks ('floaters') for slide mounting. Petrographic descriptions of Faial volcanic rocks for which hand specimens are available are given in Table 2.1. A summary of their petrography is detailed below along with some mineral chemistry data.

The phenocryst assemblage of basalts and hawaiites on Faial is composed mainly of subhedral to euhedral crystals of olivine and light-green to buff-pink (titaniferous) augite usually with lesser amounts of plagioclase (labradorite-bytownite), Cr-spinel and Fe-Ti oxides set within a groundmass of the same phases (Plate 2.1). In addition, glomeroporphyritic texture is quite common and pyrrhotite inclusions occur in a number of phenocrysts. Samples range from aphyric to highly porphyritic (ankaramitic; Table 2.1). More rarely, the dominant phenocryst phase is plagioclase which in the case of the hawaiite lava (AZ3374;'Altar rock') from the caldera forms crystals up to 0.8cm in diameter, constituting some 35% of the rock. Similar 'big plagioclase' hawaiites have been reported from Santa Barbara volcano on Terceria (Self and Gunn, 1976) and on Gran Canaria, Canary Islands by Schmincke (1969).

In volcanic rocks of more evolved composition (benmoreites and trachytes) the phenocryst assemblage consists of fayalite, augite, aegerine-augite, kaersutitic amphibole, biotite, Fe-Ti oxides, anorthoclase and alkali feldspar. Microphenocrysts of apatite and small oval blebs of pyrrhotite occur as accessory phases, most

Sample No.	Rock type	% pheno's	Phenocrysts	Groundmass
AZ3120	Alkali basalt lava.	29%	Olivine (76%),titaniferous augite (24%).Sparse microphenocrysts of Cr-spinel, Fe-Ti oxides,pyrrhotite and plagioclase.	Olivine,plagioclase, Fe-Ti oxides and interstitial glass.
AZ3115	Alkali basalt lava	5%	Olivine,augite and occasional plagioclase.	Vesicular with plagioclase, olivine,clinopyroxene, Fe-Ti oxides and glass.
AZ3443	Alkali basalt lava	21%	Olivine (75%) which is partly altered to iddingsite, titaniferous augite (25%). Sparse microphenocrysts of Cr-spinel,Fe-Ti oxides, pyrrhotite and plagioclase.	Plagioclase,olivine, clinopyroxene,Fe-Ti oxides.
AZ3099	Alkali basalt lava	10%	Olivine,titaniferous augite and plagioclase.	Plagioclase,olivine, clinopyroxene and Fe-Ti oxides.
AZ3374	Hawaiite lava	37%	Predominantly plagioclase (93%) showing strong optical zonation (labradorite-bytownite) with lesser amounts of olivine (6%), titaniferous augite (1%) and Fe-Ti oxides.	Plagioclase,olivine, clinopyroxene and devitrified glass.
AZ3504	Hawaiite lava	<5%	Olivine,titaniferous augite and plagioclase (labradorite).	Plagioclase,olivine, clinopyroxene,Fe-Ti oxides.
AZ3339	Hawaiite lava	10%	Predominantly plagioclase (labradorite-andesine) frequently showing glomeroporphyritic texture, with occasional crystals having resorption textures. Augite/titaniferous-augite (showing hour glass zoning), olivine, partly altered to iddingsite.	Plagioclase,Fe-Ti oxides, olivine and clinopyroxene.
AZ3328	Hawaiite lava	5%	Plagioclase and olivine.	Plagioclase,Fe-Ti oxides, olivine,clinopyroxene.
AZ3527	Hawaiite lava	20%	Predominantly plagioclase (labradorite) with olivine and augite/titaniferous-augite showing glomeroporphyritic texture.	Plagioclase,Fe-Ti oxides, olivine,clinopyroxene.
AZ3085	Hawaiite lava	10%	Olivine,augite,plagioclase.	Plagioclase,Fe-Ti oxides, olivine,clinopyroxene.
AZ3533	Hawaiite lava	<5%	Plagioclase (some crystals showing resorption textures), olivine,Fe-Ti oxides.	Plagioclase,Fe-Ti oxides, olivine,clinopyroxene.
AZ3411	Intermediate component of mixed lava	<5%	Occasional plagioclase (labradorite) phenocrysts showing resorption textures.	Relatively coarse grained (crystals ~0.3mm) containing approximately 20% biotite (v. elongated) the rest of the groundmass consisting of a granular aggregate of alkali feldspar,plagioclase, Fe-Ti oxides
AZ3410	Trachytic component of mixed lava	<5%	Rare phenocrysts of Fe-Ti oxides,microphenocrysts of clinopyroxene (with oxide rims),alkali feldspar and opaque pseudomorphs after unknown mineral.	Predominantly alkali feldspar showing trachytic texture.
AZ3360	Trachyte block in ash	30%	Large (~1cm),strongly zoned plagioclase phenocrysts ($An_{?}$-$_{5\%}$). Sparse phenocrysts of pleochroic (light-medium green) fayalitic olivine, light green augite,pleochroic (light-dark brown) kaersutite with oxidized rims,Fe-Ti oxides.	Predominantly alkali feldspar showing trachytic texture,with Fe-Ti oxides and aegerine-augite.
AZ3446 F500 AZ3435 Az3432 AZ3426 AZ3424	Mafic (benmoreite) pumice from Faial A Trachytic pumice from air-fall deposits A,T,S	<5%-10%	Anorthoclase,light green (low Al-Ti) augite,aegerine-augite, kaersutite,Fe-Ti oxides (low Al,Mg).Xenocrysts of forsteritic olivine,titaniferous augite, plagioclase(andesine-bytownite), magnetite(high Al,Mg),ilmenite (high Mg),Cr-spinel.	Colourless to light-dark brown glass,sometimes in streaky association, frequently microlitic.
AZ3417 AZ3436 AZ3401	Trachytic pumice from air-fall deposits D,U,D	<5%	Anorthoclase,alkali feldspar, augite/aegerine-augite,biotite, Fe-Ti oxides.	Colourless to brown glass,microlitic.
AZ3437 AZ3428	Syenite xenolith:		Alkali feldspar,light-medium green aegerine-augite,biotite,Fe-Ti oxides.	

Table 2.1 Petrography of Faial volcanic rocks.

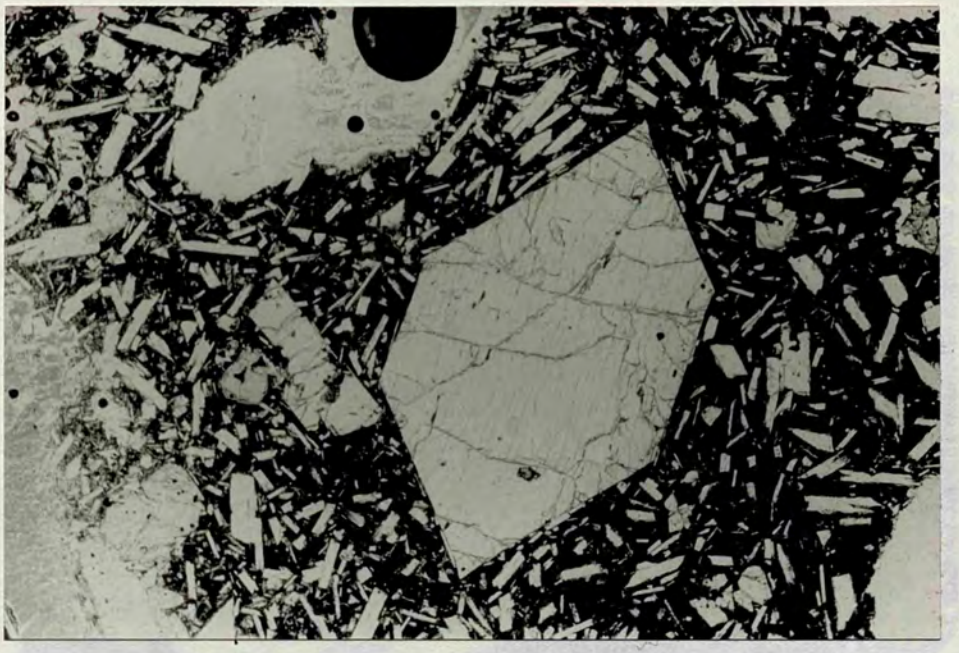

(a)

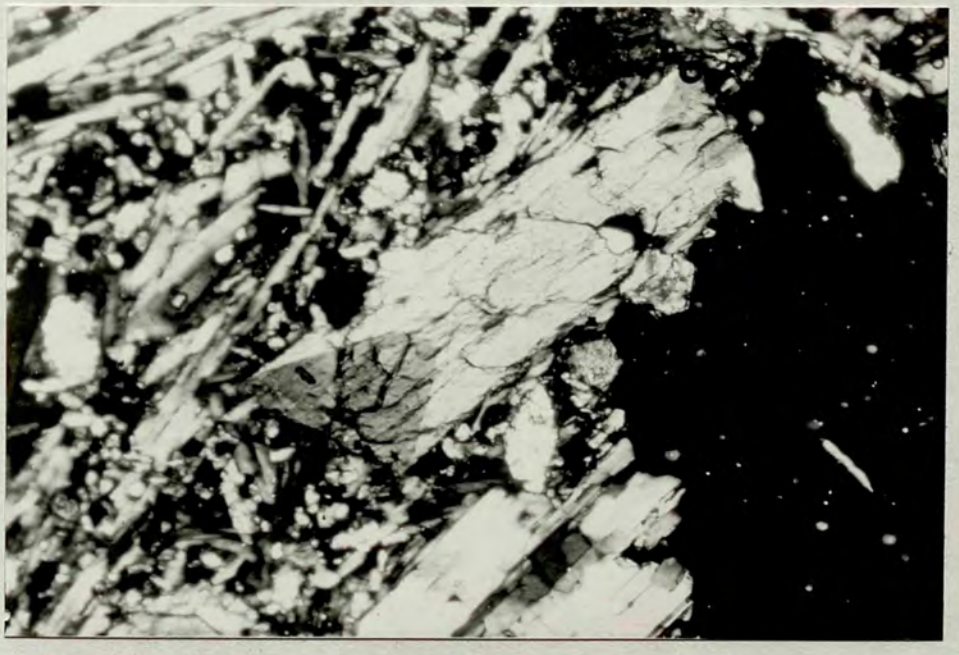

(b)

Plate 2.1 Photomicrographs of Faial basaltic rocks.
(a) Euhedral olivine phenocryst and plagioclase microphenocrysts in glassy matrix; AZ3115, plane-polarised light (ppl), Mag x45. (b) Euhedral titanaugite showing hourglass zoning; AZ3339, xpl, x150. (c) Zoned plagioclase microphenocrysts; AZ3533, xpl, x150.

(c)

Plate 2.1 (continued).

frequently as inclusions in other minerals. The groundmass of the lavas consists of plagioclase and alkali feldspar (showing trachytic texture) with minor agerine-augite, Fe-Ti oxides and occasional alkali amphibole. Pumice samples have a glassy to partly devitrified matrix, the glass varying from very light to dark brown (Plate 2.2). Phenocryst contents of the pumice clasts do not usually exceed 5-10%, however one trachyte lava (AZ3360) is highly porphyritic containing 30% phenocrysts (Table 2.1). Also of interest is the contrast in the occurrence of amphibole phenocrysts in this lava with the pumice deposits S, A and T. In the former the amphibole is heavily altered to a fine grained mass of Fe-Ti oxides (Plate 2.3) as opposed to their unaltered nature in the pumice deposits. Lastly, occuring in some pumice deposits (S, A and T) are a number of 'basaltic' xenocrysts which include one or more of the following, namely calcic plagioclase, forsteritic olivine, titaniferous augite, Cr-spinel and Fe-Ti oxides (having large contents of the minor elements Al and Mg). These features are discussed further in subsequent sections.

2.4.1 Feldspars

Feldspar phenocrysts have been analysed in seven volcanic rocks from Faial ranging in composition from hawaiite to trachyte; analyses (along with other mineral chemistry data for Faial) are given in Appendix 3, and are plotted in Fig 2.5. Also shown are analyses of some feldspar microphenocrysts and groundmass crystals from the lavas. Phenocryst compositions range from bytownite (An_{83}) in basaltic rocks to compositions transitional between anorthoclase and sanidine in trachytic pumice deposits B and S ($An_{0.5}Ab_{62.8}Or_{36.7}$). The most potassic of these, occuring in Faial B, are probably sanidine, monoclinic symmetry being suggested by the presence of carlsbad twinning and the lack of pericline twinning. Zoning in the feldspar phenocrysts analysed is generally small and may be either normal or reverse. In addition to phenocrysts of alkali feldspar, the trachytic pumice deposits S, A and T contain plagioclase xenocrysts, showing strong resorption textures, which range in composition between bytownite and andesine (Figs 2.5 and 2.6).

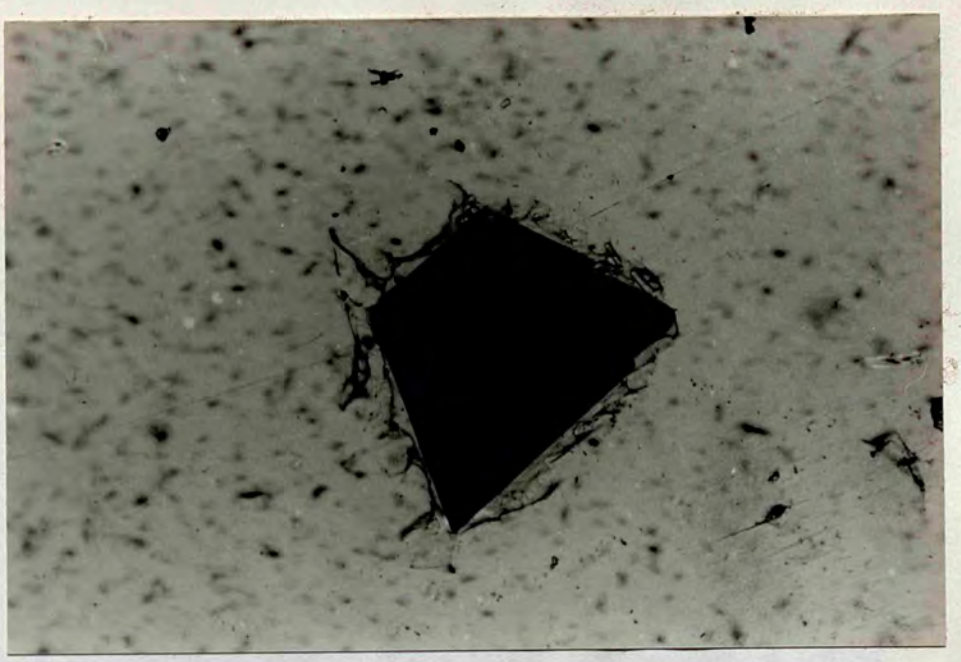

(a)

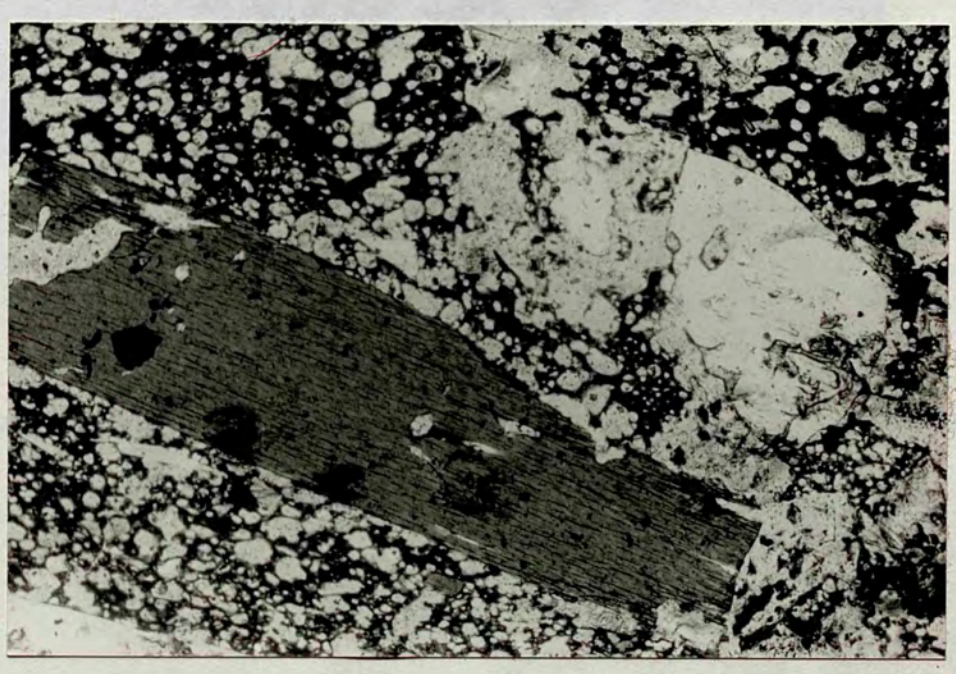

(b)

Plate 2.2 Titanomagnetite with sheath of colourless glass; mineral separate form trachyte AZ3417, ppl, X150. (b) Biotite phenocryst, resorbing plagioclase xenocryst and brown glass from Faial A(top); AZ3446, X45, ppl.

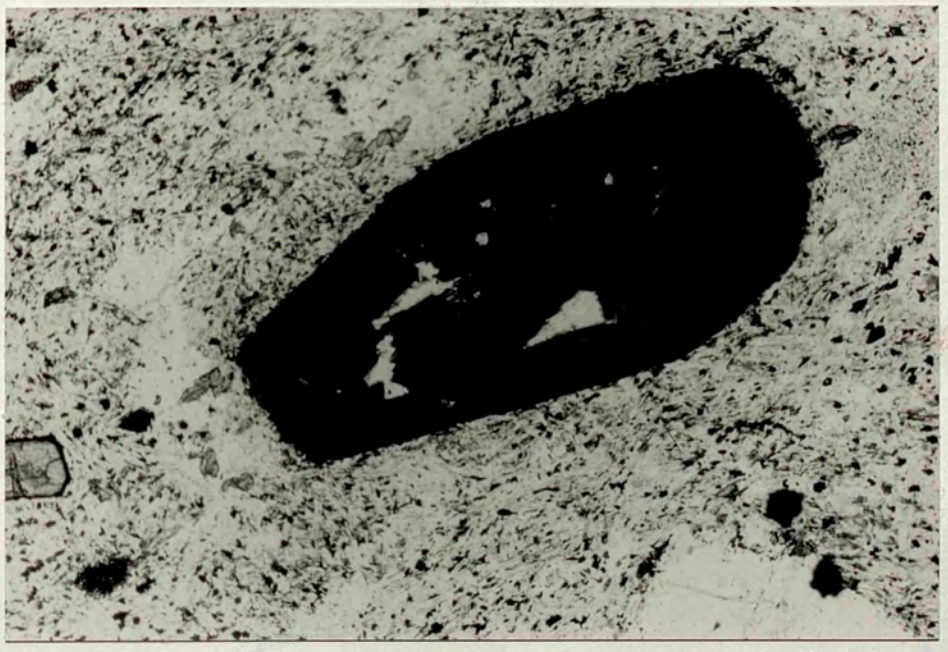

Plate 2.3 Kaersutite phenocryst with oxide rim in trachyte (AZ3360); ppl, X45.

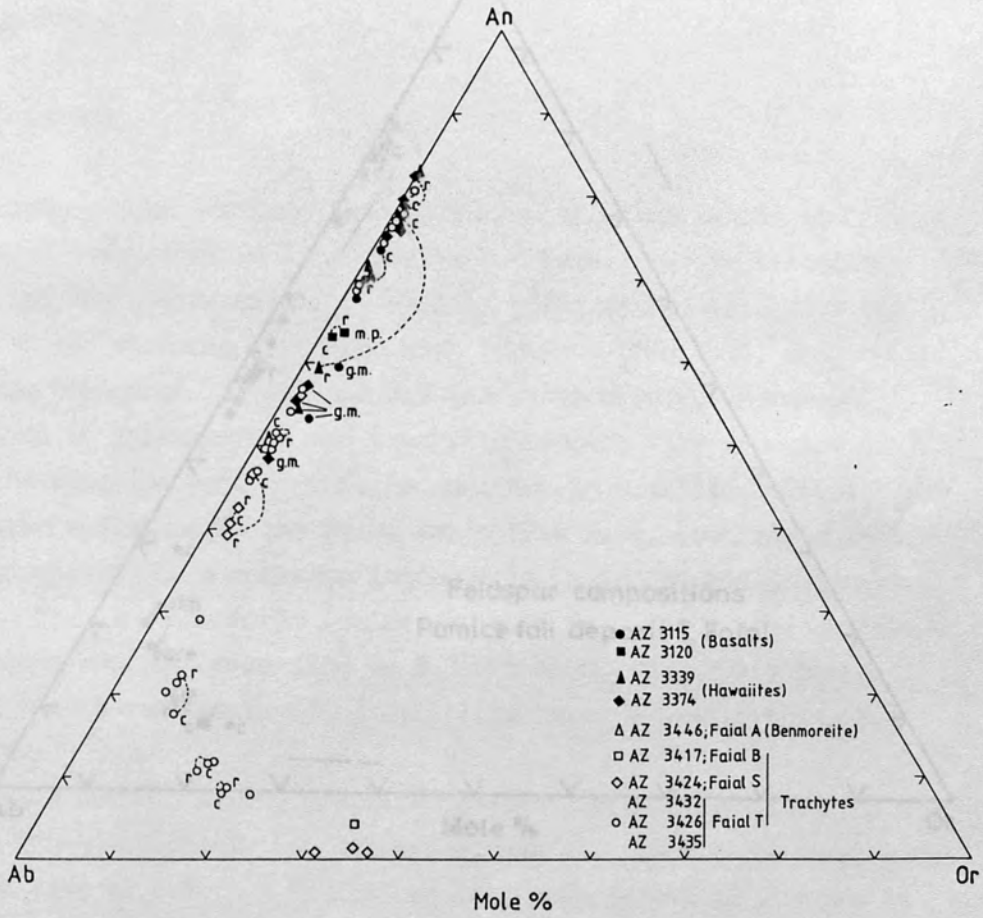

Fig 2.5 Feldspar phenocryst and groundmass (gm) compositions in Faial volcanic rocks, (c=core;r=rim); (m.p.) microphenocryst.

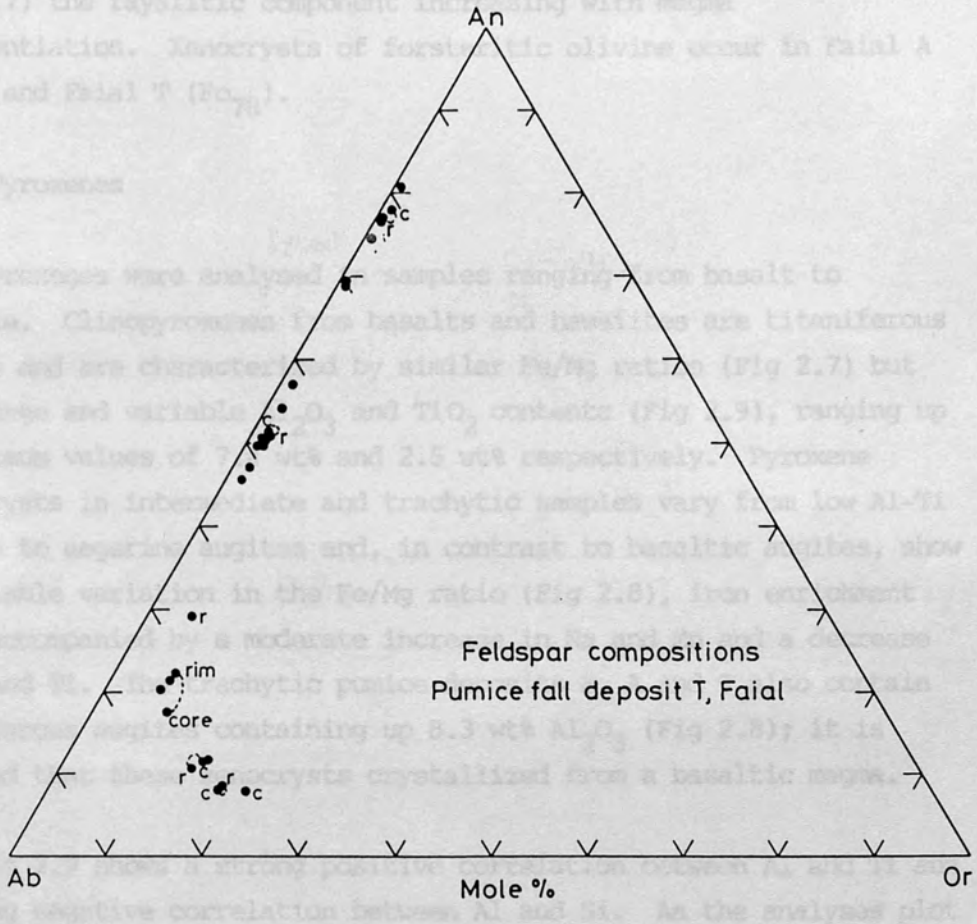

Fig 2.6 Feldspar compositions in trachytic air fall pumice deposit Faial T.

2.4.2 Olivines

Analyses of olivine phenocrysts from Faial range from Fo_{83}-Fo_{51} (Fig 2.7) the fayalitic component increasing with magma differentiation. Xenocrysts of forsteritic olivine occur in Faial A (Fo_{69}) and Faial T (Fo_{78}).

2.4.3 Pyroxenes

Pyroxenes were analysed in samples ranging from basalt to trachyte. Clinopyroxenes from basalts and hawaiites are titaniferous augites and are characterized by similar Fe/Mg ratios (Fig 2.7) but with large and variable Al_2O_3 and TiO_2 contents (Fig 2.9), ranging up to maximum values of 7.4 wt% and 2.5 wt% respectively. Pyroxene phenocrysts in intermediate and trachytic samples vary from low Al-Ti augites to aegerine augites and, in contrast to basaltic augites, show appreciable variation in the Fe/Mg ratio (Fig 2.8), iron enrichment being accompanied by a moderate increase in Na and Mn and a decrease in Al and Ti. The trachytic pumice deposits S, A and T also contain titaniferous augites containing up 8.3 wt% Al_2O_3 (Fig 2.8); it is inferred that these xenocrysts crystallized from a basaltic magma.

Fig 2.9 shows a strong positive correlation between Al and Ti and a strong negative correlation between Al and Si. As the analyses plot above the line Al + Si = 2 it follows that some of the Al must be in tetrahedral coordination. The Al^{iv}/Al^{vi} ratio is about 3 with Al^{vi} being approximately equal to Ti, with Ca remaining relatively constant this suggests the following substitution.

$$Ti^{vi} + Al^{vi} + 3Al^{iv} = 2(Mg, Fe^{2+}, Mn)^{vi} + 3Si^{iv}$$

Selected pyroxene analyses have been recalculated into theoretical end-members (Table 2.2), the procedure being similar to the method described by Cawthorn and Collerson (1974). The main differences are firstly, because of an excess of Al^{iv}, after all other

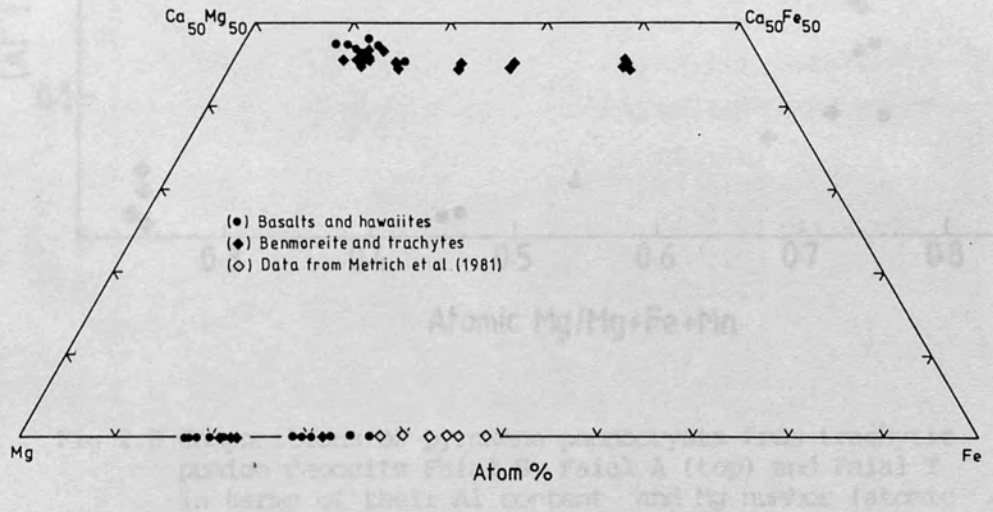

Fig 2.7 Pyroxene phenocryst compositions in terms of their Ca, Mg and Fe components. Also shown on the Mg-Fe join are coexisting olivine phenocrysts.

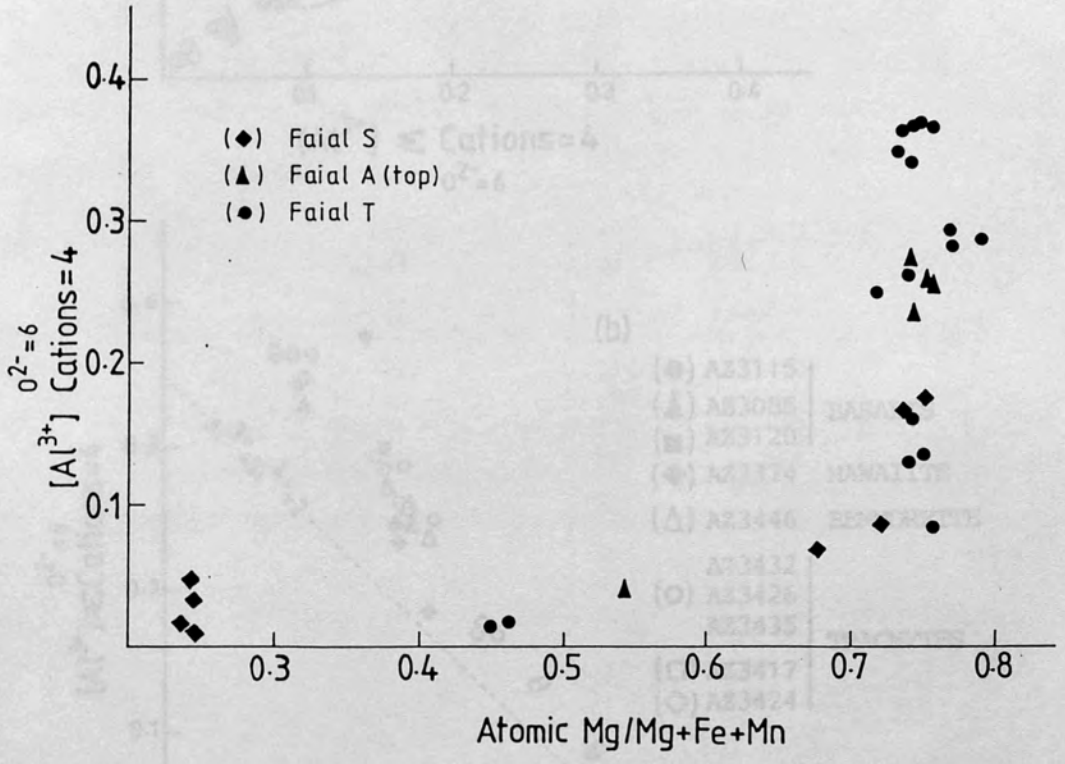

Fig 2.8 Compositions of pyroxene phenocrysts from trachytic pumice deposits Faial S, Faial A (top) and Faial T in terms of their Al content and Mg number (atomic Mg/Mg + Fe + Mn).

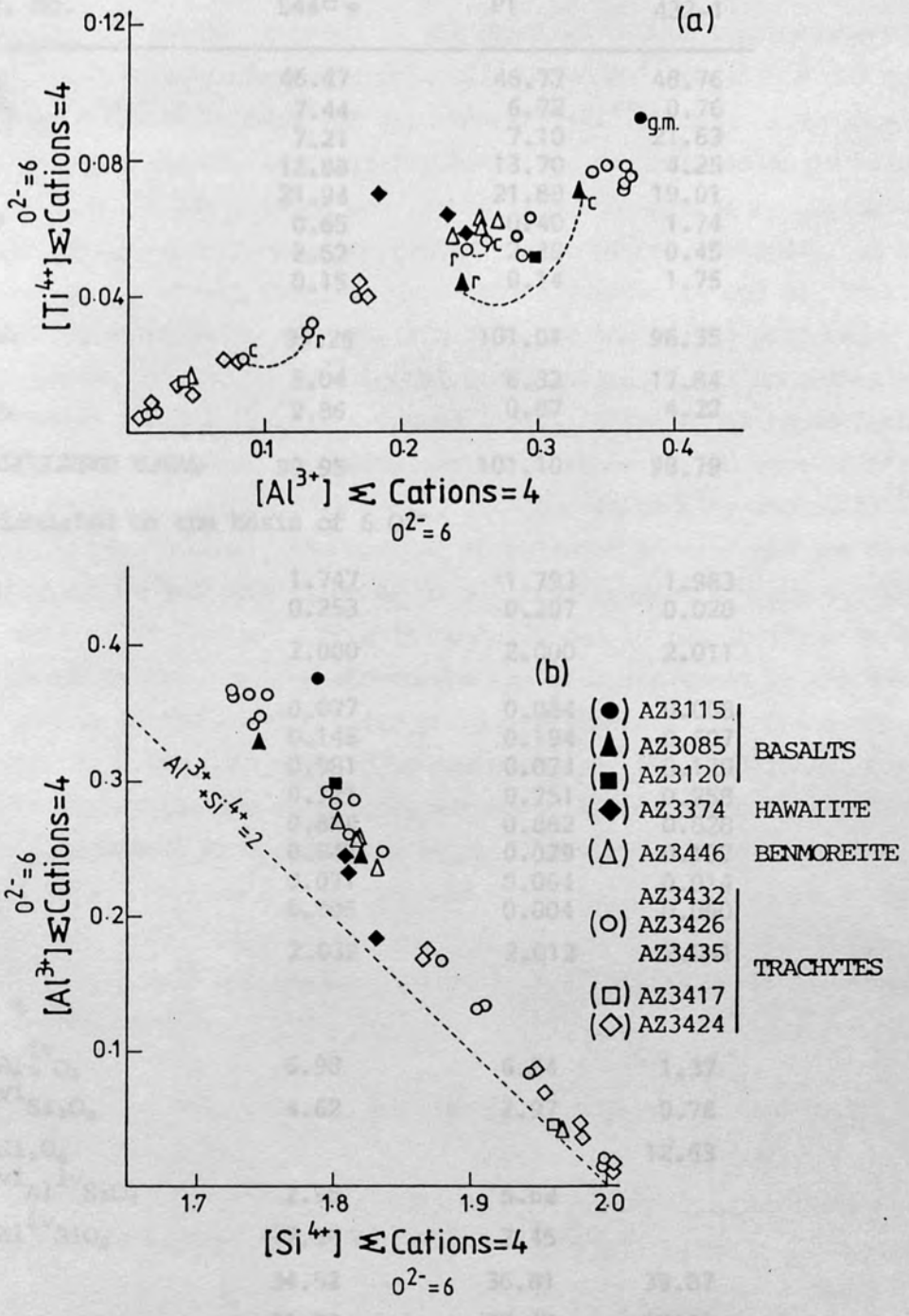

Fig 2.9 Pyroxene compositions from Faial in terms of (a) Al and Ti. (b) Si and Al. All analyses are of phenocrysts unless otherwise stated.

Anal. No.	AZ3085 (1958 lava) 544c ♀	Faial T P1	Faial S 432-1
SiO_2	46.47	48.77	48.76
Al_2O_3	7.44	6.72	0.76
* FeO	7.21	7.10	21.63
MgO	12.88	13.70	4.25
CaO	21.94	21.88	19.01
Na_2O	0.65	0.40	1.74
TiO_2	2.52	2.30	0.45
MnO	0.15	0.14	1.75
TOTAL	99.26	101.01	98.35
FeO	5.04	6.32	17.84
Fe_2O_3	2.86	0.87	4.22
RECALCULATED TOTAL	99.95	101.10	98.79
Recalculated on the basis of 6 O^{2-}			
Si	1.747	1.793	1.983
Al^{iv}	0.253	0.207	0.028
ΣZ	2.000	2.000	2.011
Al^{vi}	0.077	0.084	0.008
Fe^{2+}	0.146	0.194	0.607
Fe^{3+}	0.081	0.024	0.129
Mg	0.721	0.751	0.258
Ca	0.884	0.862	0.828
Na	0.047	0.029	0.137
Ti	0.071	0.064	0.014
Mn	0.005	0.004	0.060
ΣWXY	2.032	2.012	2.041
Mol. %			
$CaTiAl_2^{iv}O_6$	6.98	6.54	1.37
$NaAl^{vi}Si_2O_6$	4.62	2.97	0.78
$NaFeSi_2O_6$			12.63
$CaAl^{vi}Al^{iv}SiO_6$	2.95	5.62	
$CaFeAl^{iv}SiO_6$	7.96	2.45	
Wo	34.52	36.81	39.87
En	35.50	38.45	12.63
Fs	7.47	7.16	32.72

* All iron as FeO

Table 2.2 Recalculated pyroxene analyses.
For method see text.

components had been formed, it was considered more appropriate to calculate ferri-tschermak's molecule ($CaFe^{3+}Al^{iv}SiO_6$) in order to maintain charge balance and stoichometry ($Al^{iv}+Si=2$). Also knowledge of both the amounts of ferri-tschermak's and acmite molecule allows estimation of the ferrous and ferric iron contents of the pyroxene; this cannot be determined by electron microprobe. Secondly, on the basis of the strong positive correlation between Ti and Al, their negative correlation with Si (Fig 2.9) and the strong preference of Ti for octahedral rather tetrahedral coordination, Ca-Ti tschermak's component ($CaTiAl_2^{iv}O_6$) was formed first. For most of these pyroxene compositions it does not matter at which stage in the recalculation procedure this molecule is formed as there is usually enough Al^{iv} to satisfy Ti. However, the mineral formulae of some of the low Al-Ti ferrosalites indicate there is no Al^{iv} even though there are small amounts of Ti present. This is probably due to inaccuracies in Si analysis by the electron microprobe, as also suggested by the excess of silica in the recalculation procedure (Table 2.2). Therefore, enough Al^{iv} has been assumed so as to satisfy the requirement for Ti in Ca-Ti tschermak's component, although this occasionally results in the tetrahedral site occupancy being slightly > 2. To summarise, the recalculation procedure of pyroxene analyses, used here, is as follows:

1. Enough Al^{iv} was assigned to utilize all Ti in Ca-Ti tschermak's component.

2. Any remaining tetrahedral site deficiency was filled by Al ($Al^{iv}+Si = 2$).

3. Na was used to form jadeite ($NaAl^{iv}Si_2O_6$).

4. If $Na>Al^{iv}$ then enough Fe^{3+} was assumed to form acmite ($NaFe^{3+}Si_2O_6$).

5. If $Na<Al^{iv}$ then enough Al^{iv} was assigned to form Ca-tschermak's component ($CaAl^{vi}Al^{iv}SiO_6$).

6. If there was an excess of Al^{iv} at this stage then it was used to form Ca-Al-ferri-tschermak's component ($CaFe^{3+}Al^{iv}SiO_6$).

7. Remaining Ca, Mg and Fe^{2+}+Mn were calculated as wollastonite, enstatite and ferrosilite respectively.

Results (Table 2.2) show a high proportion of tschermak's component (~18 mol%) in the titanaugites. Aegerine-augite from the trachytes have a significant acmite component (up to 12.6 mol%).

2.4.4 Amphiboles

Pleochroic, pale yellow-dark brown amphibole phenocrysts occur in some intermediate and trachytic volcanic rocks from Faial. Crystals from pumice fall deposits S, A and T have been analysed by electron-microprobe. They are fairly homogenous, the ionic Mg/Mg+Fe ratio only varying between 0.64-0.69 and showing a positive correlation with Ti (Fig 2.10). Chemically the amphiboles are distinguished by their low Si and high Al and Ti contents (~6wt% TiO_2), with insufficient Si in the formula unit requiring most of the Al to be in the tetrahedral site. As these are titaniferous and contain more than two Mg atoms in the formula unit on the basis of 23 O^{2-} they classify as kaersutite rather than barkevikite (Wilkinson, 1961).

2.4.5 Biotites

Euhedral pleochroic phenocrysts of biotite occur in several of the trachytes, analyses of biotites from pumice deposits B, A (top) and T being given in Appendix 3. Their Mg numbers vary between 0.43-0.60 and thus classify as biotites rather than phlogopites (Deer et al., 1966). The most Mg rich compositions occur in Faial A (top), the Mg/Mg + Fe ratio of the biotite mirroring the relatively high Mg/Mg + Fe ratio of this sample. The Faial biotites, like those from Sao Miguel (Chapters 3 and 4), are notable for their high Ti content (up to 8.8 wt% TiO_2). On the basis of 22 O^{2-} in the formula unit the sum of Al and Si is less than the eight required to fill the tetrahedral

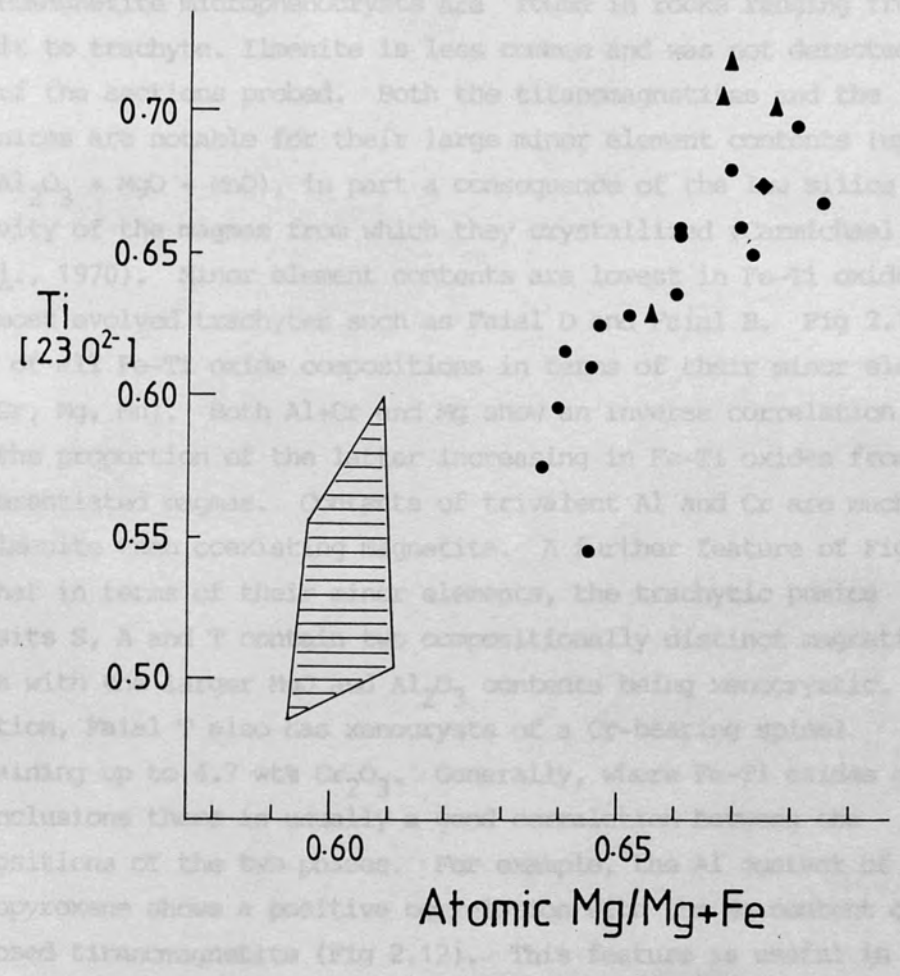

Fig 2.10 Compositions of kaersutite phenocrysts from Faial S, Faial A (top) and Faial T in terms of their Ti content and Mg number. Ruled area shows compositional range of kaersutite phenocrysts from a layered amphibole-plagioclase-magnetite-apatite nodule (AZ1035; Section 3.4.4) from Sao Miguel. Symbols as Fig 2.8.

site. This cation deficiency could presumably be filled by Ti or Fe^{3+}. As with kaersutite, the Mg/Mg+Fe ratio of the biotites show a positive correlation with their Ti content. Substitution mechanisms for biotites are discussed further in Section 5.3.2.

2.4.6 Fe-Ti oxides

Ubiquitous euhedral to subhedral, occasionally anhedral, titanomagnetite microphenocrysts are found in rocks ranging from basalt to trachyte. Ilmenite is less common and was not detected in all of the sections probed. Both the titanomagnetites and the ilmenites are notable for their large minor element contents (up to 10 wt% Al_2O_3 + MgO + MnO), in part a consequence of the low silica activity of the magmas from which they crystallized (Carmichael et al., 1970). Minor element contents are lowest in Fe-Ti oxides from the most evolved trachytes such as Faial D and Faial B. Fig 2.11 is a plot of all Fe-Ti oxide compositions in terms of their minor elements (Al+Cr, Mg, Mn). Both Al+Cr and Mg show an inverse correlation with Mn, the proportion of the latter increasing in Fe-Ti oxides from more differentiated magmas. Contents of trivalent Al and Cr are much lower in ilmenite than coexisting magnetite. A further feature of Fig 2.11 is that in terms of their minor elements, the trachytic pumice deposits S, A and T contain two compositionally distinct magnetites, those with the larger MgO and Al_2O_3 contents being xenocrystic. In addition, Faial T also has xenocrysts of a Cr-bearing spinel containing up to 4.7 wt% Cr_2O_3. Generally, where Fe-Ti oxides occur as inclusions there is usually a good correlation between the compositions of the two phases. For example, the Al content of a host clinopyroxene shows a positive correlation with the Mg content of the enclosed titanomagnetite (Fig 2.12). This feature is useful in assisting the establishment of equilibrium phenocryst assemblages. In Chapter 5 analyses of coexisting titanomagnetites and ilmenites (mainly from trachytes) were recalculated into their end-members ulvospinel and haematite respectively (using the procedure of Carmichael, 1967), allowing an estimate of the equilibration temperature and oxygen fugacity (Fig 5.2). Results showed that mol%

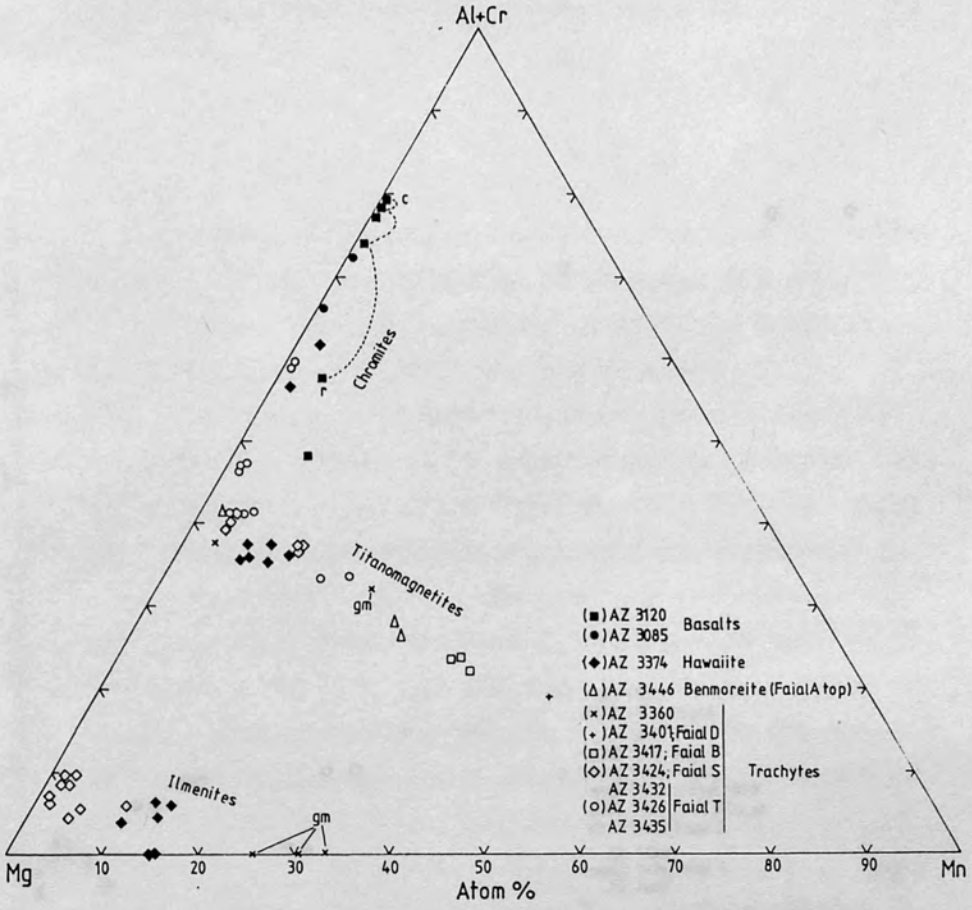

Fig 2.11 Fe-Ti oxides in terms of the minor elements Al+Cr, Mg and Mn. All analyses are of phenocrysts unless otherwise stated.

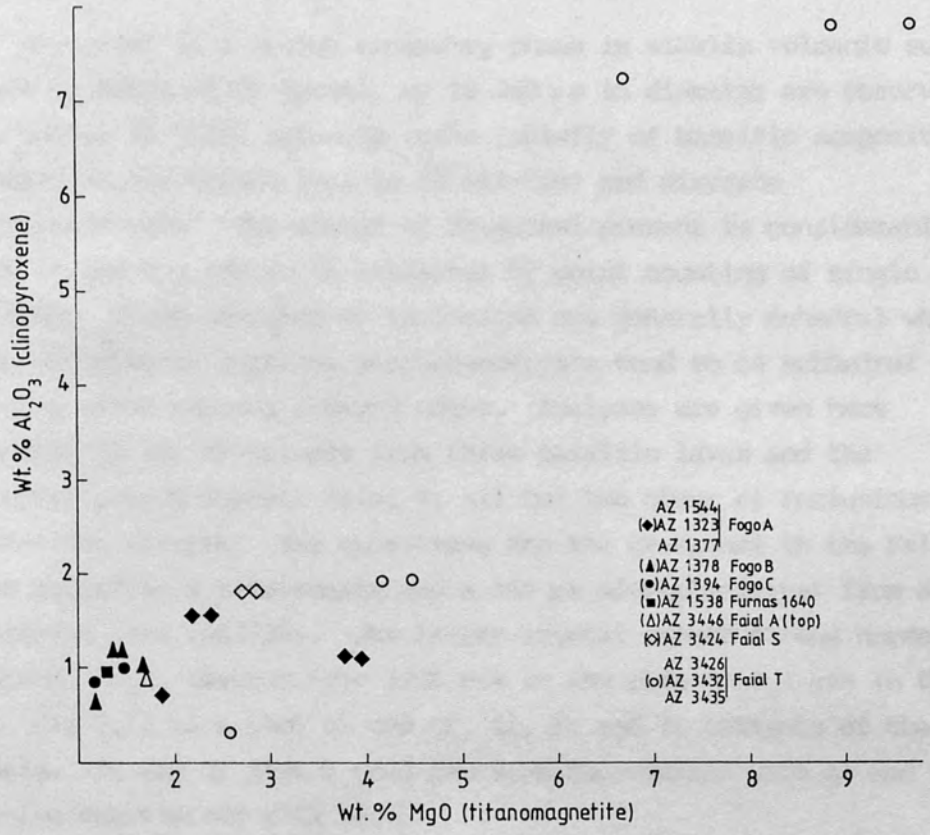

Fig 2.12 Poikilitic relationships. A plot of the MgO content of enclosed titanomagnetites against the Al_2O_3 content of host clinopyroxenes. Examples from Sao Miguel are also shown.

Usp. varied between 47-66% and mol% Haem. between 1.6-6.5%, the former showing a negative correlation with the minor element content of the magnetite.

2.4.7 Cr-spinels

Cr-spinel is a common accessory phase in alkalic volcanic suites. Opaque crystals of Cr-spinel, up to 250 µm in diameter are observed in a number of Faial volcanic rocks (chiefly of basaltic composition) occurring as inclusions (mainly in olivine) and discrete microphenocrysts. The amount of Cr-spinel present is considerably below 1% and too low to be estimated by point counting of single thin sections. Those occurring as inclusions are generally euhedral while those occurring as separate microphenocrysts tend to be subhedral to anhedral often showing embayed edges. Analyses are given here (Appendix 3) for Cr-spinels from three basaltic lavas and the trachytic pumice deposit Faial T, all but two occur as inclusions in forsteritic olivine. The exceptions are the Cr-spinel in the Faial T which occurs in a titanaugite and a 150 µm microphenocryst from an ankaramite lava (AZ3120). The latter crystal showed strong normal zonation, Cr_2O_3 varying from 31.5 wt% in the core to 4.4 wt% in the rim. Fig 2.13 is a plot of the Cr, Al, Fe and Ti contents of the Cr-spinels. Fe and Cr show a good positive correlation with Al and a negative correlation with Ti.

2.4.8 Sulphides

Pyrrhotite (Fe_7S_8-FeS) is a minor accessory phase occurring in Faial rocks of most compositions. It occurs as opaque, small, round to elongated grains up to 100 µm in diameter being found in most phenocrysts. Pyrrhotites from rocks of basaltic, intermediate and trachytic composition have been analysed. Those included in phenocrysts of forsteritic olivine (Fo_{79-82}) from the hawaiite lava of the 1958 Capelinhos eruption and from an ankaramite (AZ3120) are notable for their large contents of Ni (up to 40,000 ppm) and to a lesser extent Cu (up to 6,000 ppm). Pyrrhotites from rocks of more

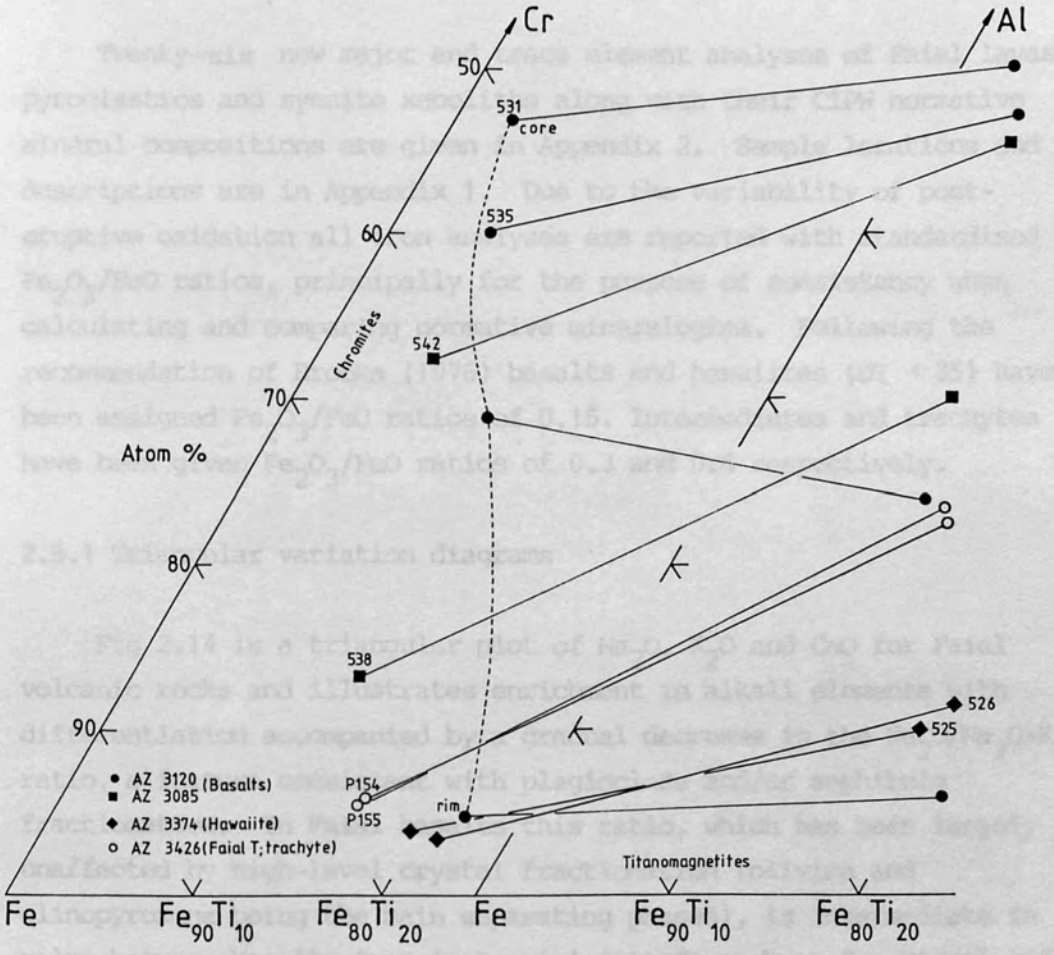

Fig 2.13 Compositions of Cr-bearing spinel microphenocrysts and xenocrysts in terms of Fe, Ti, Cr and Al. (Numbers refer to analyses in Appendix 3).

evolved composition have little or no Ni, mirroring its rapid depletion with magma differentiation. A solitary Cu-Fe (30% Cu) sulphide grain was observed in Faial T, having the formula $Fe_{0.57}Cu_{0.54}S_{1.0}$.

2.5 WHOLE-ROCK CHEMISTRY

Twenty-six new major and trace element analyses of Faial lavas, pyroclastics and syenite xenoliths along with their CIPW normative mineral compositions are given in Appendix 2. Sample locations and descriptions are in Appendix 1. Due to the variability of post-eruptive oxidation all iron analyses are reported with standardised Fe_2O_3/FeO ratios, principally for the purpose of consistency when calculating and comparing normative mineralogies. Following the recommendation of Brooks (1976) basalts and hawaiites (DI < 35) have been assigned Fe_2O_3/FeO ratios of 0.15. Intermediates and trachytes have been given Fe_2O_3/FeO ratios of 0.3 and 0.6 respectively.

2.5.1 Triangular variation diagrams

Fig 2.14 is a triangular plot of Na_2O, K_2O and CaO for Faial volcanic rocks and illustrates enrichment in alkali elements with differentiation accompanied by a gradual decrease in the Na_2O/Na_2O+K_2O ratio, a feature consistent with plagioclase and/or amphibole fractionation. In Faial basalts this ratio, which has been largely unaffected by high-level crystal fractionation (olivine and clinopyroxene being the main separating phases), is intermediate in value between basalts from 'potassic' islands such as Sao Miguel and 'sodic' islands such as Terceria (Fig 2.14).

With increasing differentiation, Faial volcanic rocks show the slight iron, strong alkali enrichment trend characteristic of oceanic island volcanism (Fig 2.15). By contrast, tholeiitic basalts from the Azores Plateau exhibit a trend towards strong iron enrichment (Schilling, 1975).

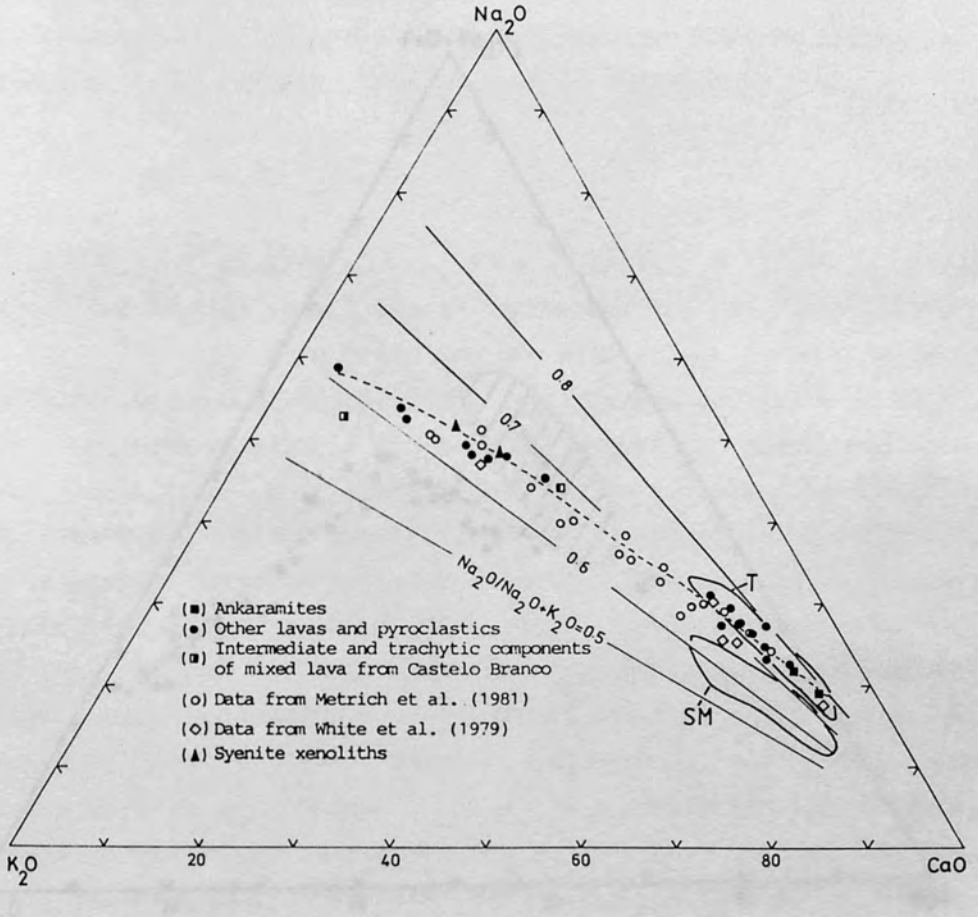

Fig 2.14 Plot of Faial volcanic rocks in the Na_2O-K_2O-CaO triangle. Dashed line equals the inferred liquid line of descent. Shown for comparison are data for basaltic rocks from Sao Miguel (SM;Chapter 3) and Terceria (T; data from Self and Gunn, 1976).

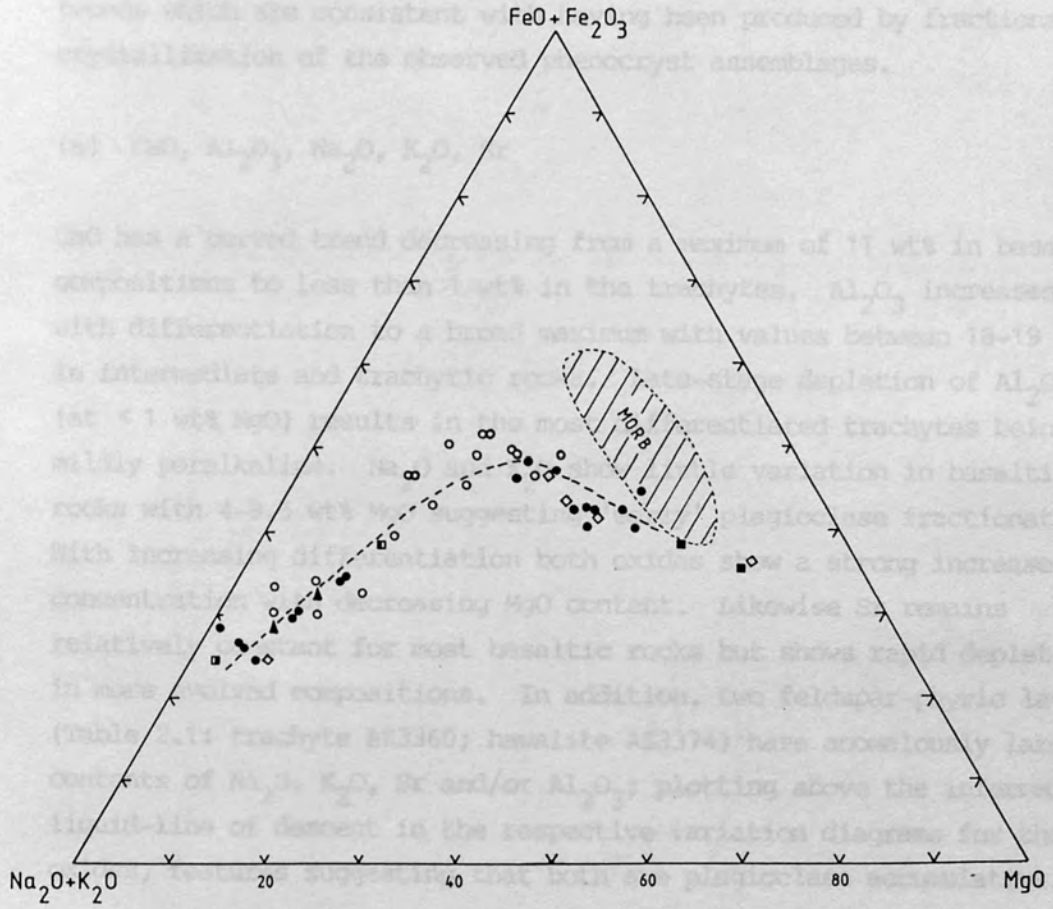

Fig 2.15 Plot of Faial volcanic rocks in the AFM triangle. Field of morb from the Azores Plateau (data from Schilling, 1975) is shown for comparison. Dashed line equals the inferred liquid-line of descent. Symbols as Fig 2.14.

2.5.2 MgO variation diagrams

Fig 2.16 shows most major element oxides and some trace elements plotted against MgO as abscissa. Also shown are data from Metrich et al., (1981). The largest MgO contents (11.0% and 14.9wt%) are observed in two ankaramitic lavas (AZ3443 and AZ3120) suggesting they may be accumulative in origin. The data define smooth continuous trends which are consistent with having been produced by fractional crystallization of the observed phenocryst assemblages.

(a) CaO, Al_2O_3, Na_2O, K_2O, Sr

CaO has a curved trend decreasing from a maximum of 11 wt% in basaltic compositions to less than 1 wt% in the trachytes. Al_2O_3 increases with differentiation to a broad maximum with values between 18-19 wt% in intermediate and trachytic rocks. Late-stage depletion of Al_2O_3 (at < 1 wt% MgO) results in the most differentiated trachytes being mildly peralkaline. Na_2O and K_2O show little variation in basaltic rocks with 4-9.5 wt% MgO suggesting 'early' plagioclase fractionation. With increasing differentiation both oxides show a strong increase in concentration with decreasing MgO content. Likewise Sr remains relatively constant for most basaltic rocks but shows rapid depletion in more evolved compositions. In addition, two feldspar-phyric lavas (Table 2.1: trachyte AZ3360; hawaiite AZ3374) have anomalously large contents of Na_2O, K_2O, Sr and/or Al_2O_3; plotting above the inferred liquid-line of descent in the respective variation diagrams for these oxides, features suggesting that both are plagioclase accumulative.

(b) SiO_2, P_2O_5, TiO_2, V

SiO_2 ranges from 46 wt% in basalts and hawaiites to maximum values of about 63 wt% in the trachytes. SiO_2 remains relatively constant in basaltic compositions; however, at approximately 4 wt% MgO there is a marked inflection with silica showing strong enrichment with decreasing MgO. The variation of TiO_2 and V mirrors that of silica, both showing little change until 4 wt% MgO whereupon they decrease

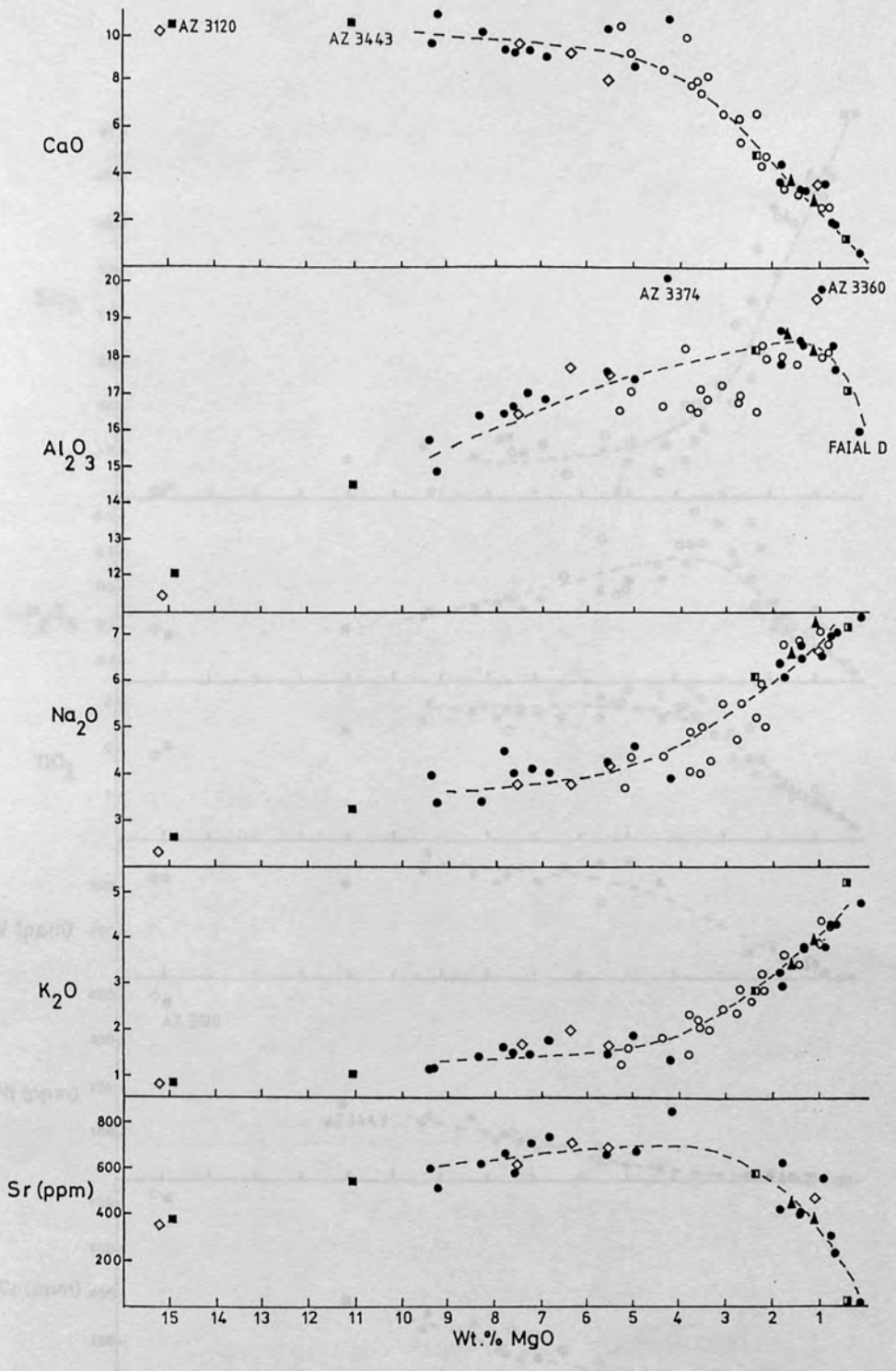

Fig 2.16 Plot of most major element oxides and selected trace elements against MgO for Faial volcanic rocks. Dashed line equals inferred liquid-line of descent. All values as wt.% unless otherwise stated.

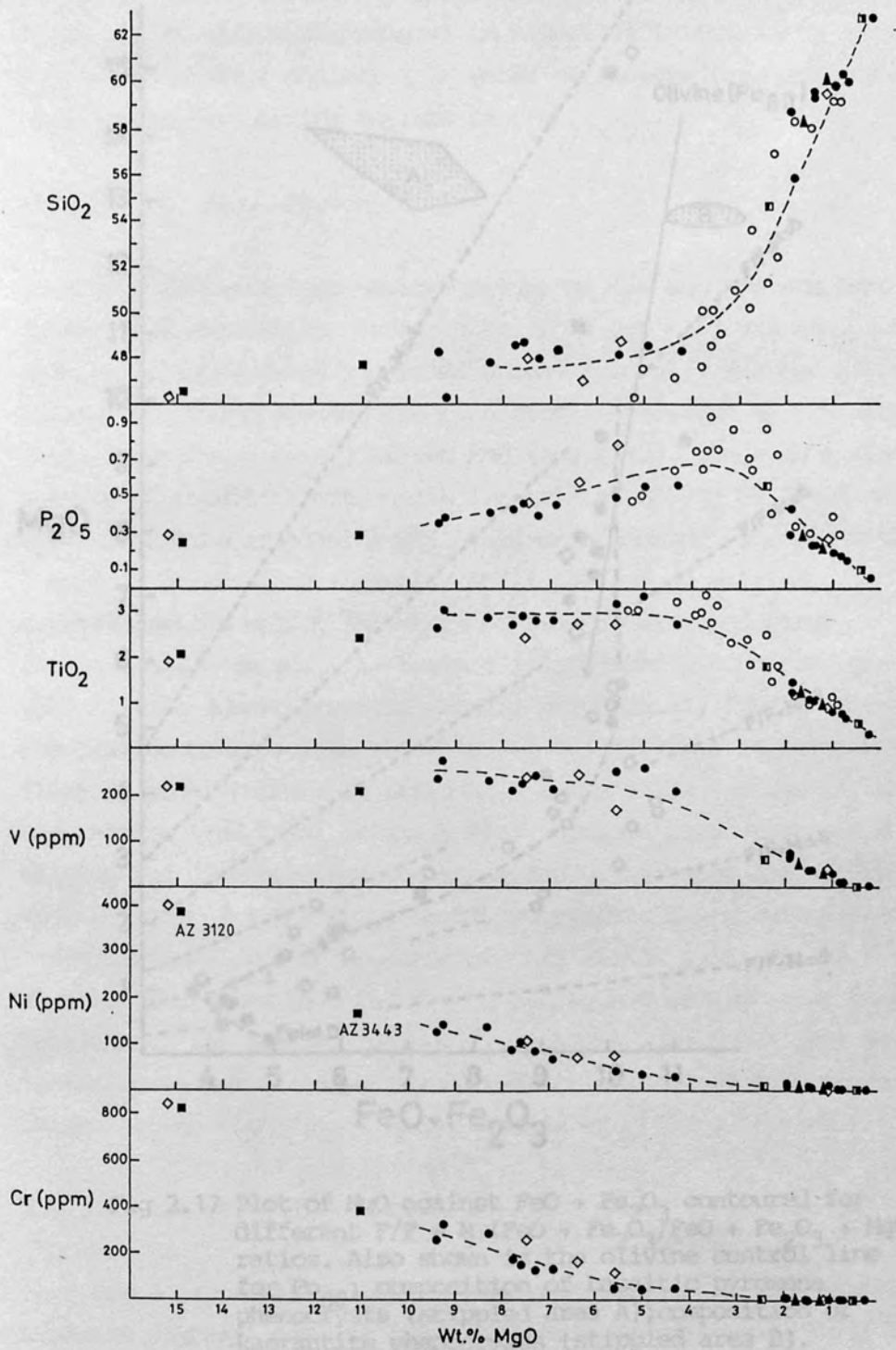

Fig 2.16 continued.

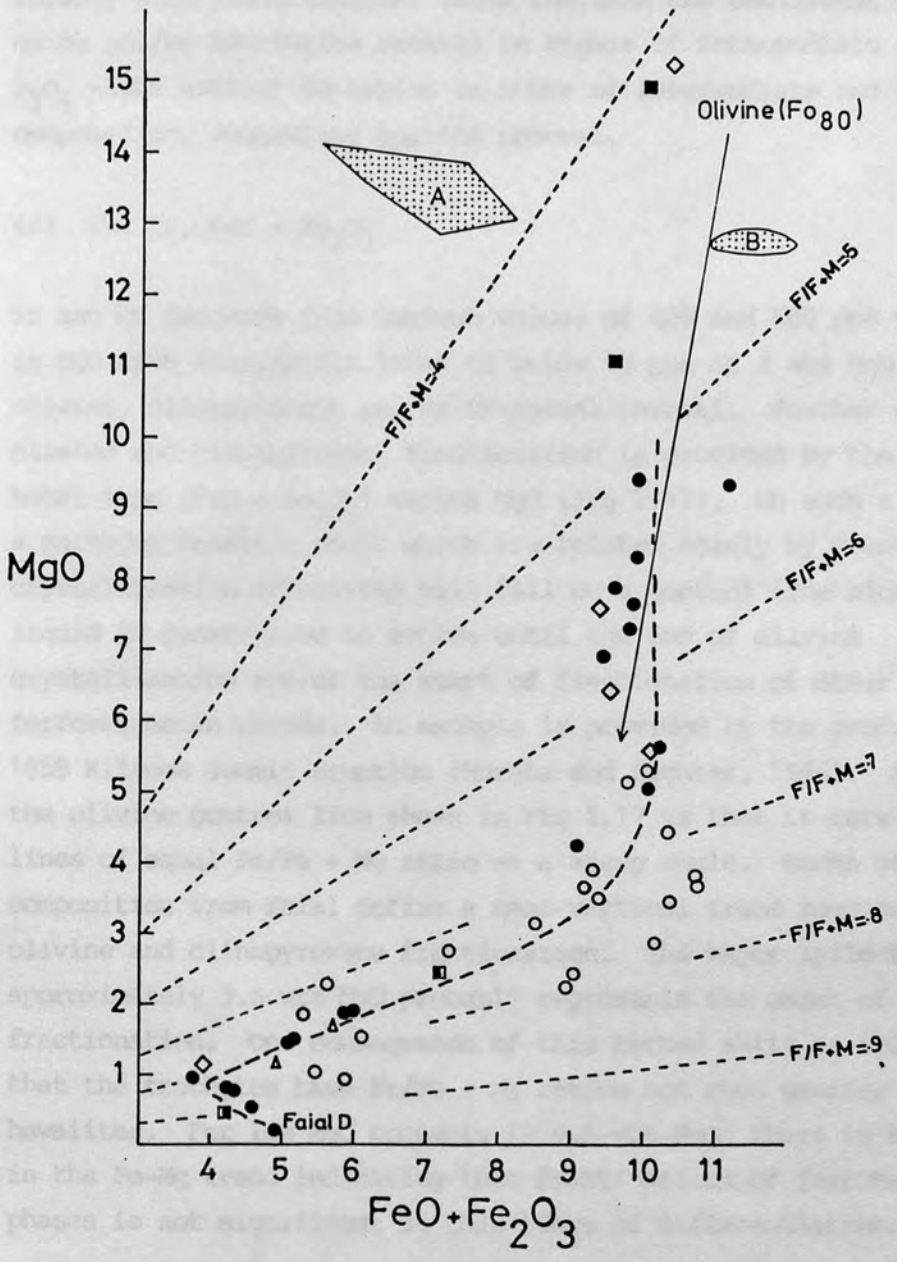

Fig 2.17 Plot of MgO against FeO + Fe_2O_3 contoured for different F/F + M (FeO + Fe_2O_3/FeO + Fe_2O_3 + MgO) ratios. Also shown is the olivine control line for Fo_{80}; composition of basaltic pyroxene phenocrysts (stippled area A);composition of kaersutite phenocrysts (stippled area B). Heavy dashed line equals inferred liquid-line of descent. MgO and iron values in wt.%; symbols as Fig. 2.14.

rapidly with fractionation. These features are consistent with Fe-Ti oxide and/or kaersutite removal in magmas of intermediate composition. P_2O_5 shows similar depletion in rocks of intermediate and trachytic composition, suggesting apatite removal.

(c) Ni, Cr, FeO + Fe_2O_3

Ni and Cr decrease from maximum values of 400 and 800 ppm respectively in MgO-rich ankaramitic lavas to below 10 ppm at 4 wt% MgO, suggesting olivine, clinopyroxene and/or Cr-spinel removal. Further evidence for olivine and clinopyroxene fractionation is provided by the plot of total iron (FeO + Fe_2O_3) versus MgO (Fig 2.17). On such a diagram, a suite of basaltic rocks which are related solely by fractional crystallization of olivine will fall on a control line along which the liquid is constrained to evolve until the end of olivine crystallization and/or the start of fractionation of other ferromagnesian phases. An example is provided by the products of the 1959 Kilauea summit eruption (Murata and Richter, 1966). A feature of the olivine control line shown in Fig 2.17 is that it cuts across lines of equal Fe/Fe + Mg ratio at a steep angle. Rocks of basaltic composition from Faial define a near-vertical trend suggesting both olivine and clinopyroxene fractionation. The major inflection at approximately 3.5 wt% MgO probably represents the onset of Fe-Ti oxide fractionation. One consequence of this marked shift in the trend is that the trachytes have Fe/Fe + Mg ratios not much greater than the hawaiites. For low MgO contents (< 0.5 wt% MgO) there is a reversal in the Fe-Mg trend indicating that fractionation of ferromagnesian phases is not significant at this stage of differentiation.

2.5.3 Zr variation diagrams

Fig 2.18 shows the covariation of Zr with other incompatible elements in Faial basalts and hawaiites. Zr was chosen as a 'reference' element because, firstly, the intercepts of the best-fit lines (Fig 2.18) indicate that it is has a very small D value, secondly it is relatively insensitive to alteration and, lastly, it

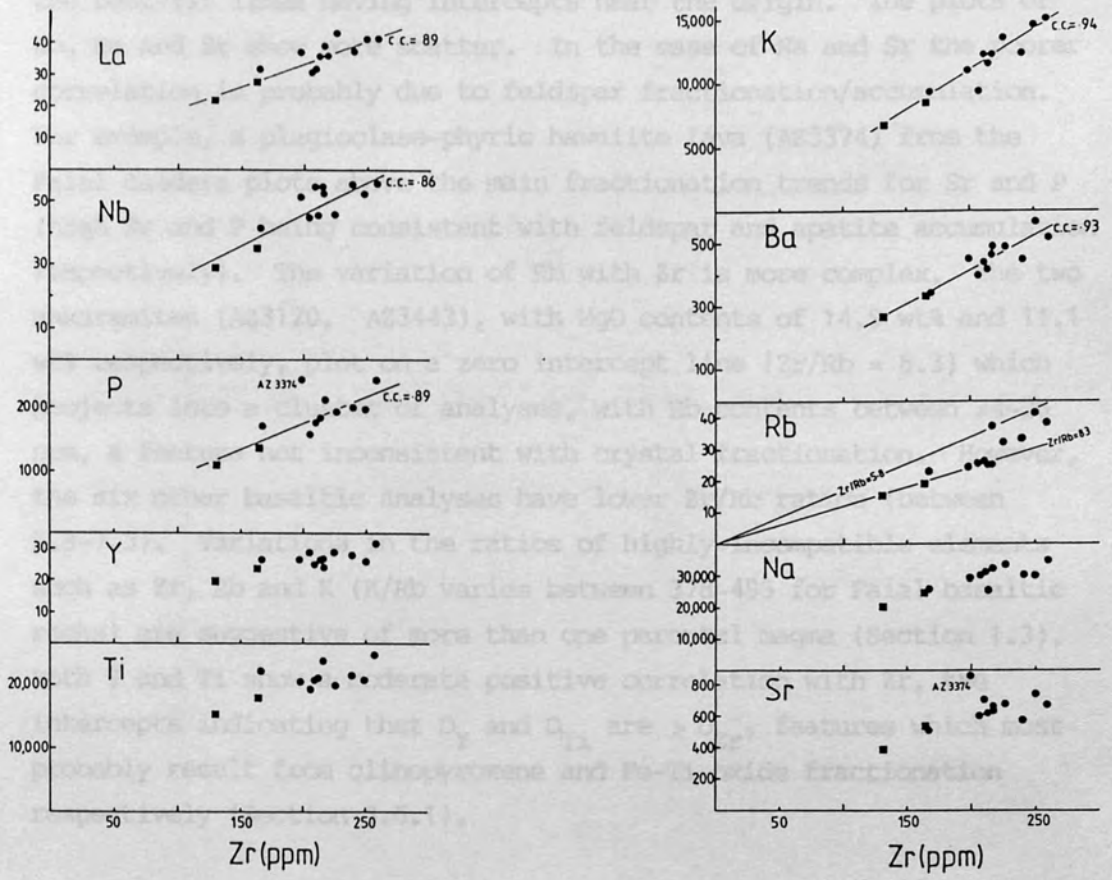

Fig 2.18 Biaxial plots of selected incompatible elements against Zr for Faial basalts and hawaiites. Best fit lines and correlation coefficients (c.c.) shown for K, Ba, La, Nb, and P. All values in parts per million (ppm).

can be determined with high precision by XRF techniques (Tarney et al.,1977).

K, Ba, La, Nb and P show a strong positive correlation with Zr, the best-fit lines having intercepts near the origin. The plots of Rb, Na and Sr show more scatter. In the case of Na and Sr the poorer correlation is probably due to feldspar fractionation/accumulation. For example, a plagioclase-phyric hawaiite lava (AZ3374) from the Faial caldera plots above the main fractionation trends for Sr and P (high Sr and P being consistent with feldspar and apatite accumulation respectively). The variation of Rb with Zr is more complex. The two ankaramites (AZ3120, AZ3443), with MgO contents of 14.9 wt% and 11.1 wt% respectively, plot on a zero intercept line (Zr/Rb = 8.3) which projects into a cluster of analyses, with Rb contents between 24-26 ppm, a feature not inconsistent with crystal fractionation. However, the six other basaltic analyses have lower Zr/Rb ratios (between 5.9-7.3). Variations in the ratios of highly incompatible elements such as Zr, Rb and K (K/Rb varies between 378-495 for Faial basaltic rocks) are suggestive of more than one parental magma (Section 1.3). Both Y and Ti show a moderate positive correlation with Zr, the intercepts indicating that D_Y and D_{Ti} are $> D_{Zr}$, features which most probably result from clinopyroxene and Fe-Ti oxide fractionation respectively (Section 3.6.1).

Fig 2.19 is a plot of Nb, Y, Rb and Ba against Zr for all Faial compositions ranging from basalt to trachyte. Nb shows a linear fractionation trend, the mildly peralkaline trachytic pumice deposit Faial D having the most evolved chemistry in terms of its incompatible element abundances (eg Zr = 1316 ppm). In Fig 2.18, Y exhibits a moderate positive correlation with Zr for basaltic compositions but, in intermediate and some trachytic samples (Fig 2.19) this element shows little variation (suggesting $D_Y \sim 1$), resulting in an increase in the Zr/Y ratio with differentiation (eg Zr/Y $\sim$ 21 in the trachytic pumice deposit, Faial U). A similar trend is shown by the variation of Y with Zr for Sao Miguel rocks (Fig 3.20) and is indicative of significant apatite and/or amphibole fractionation in intermediate and

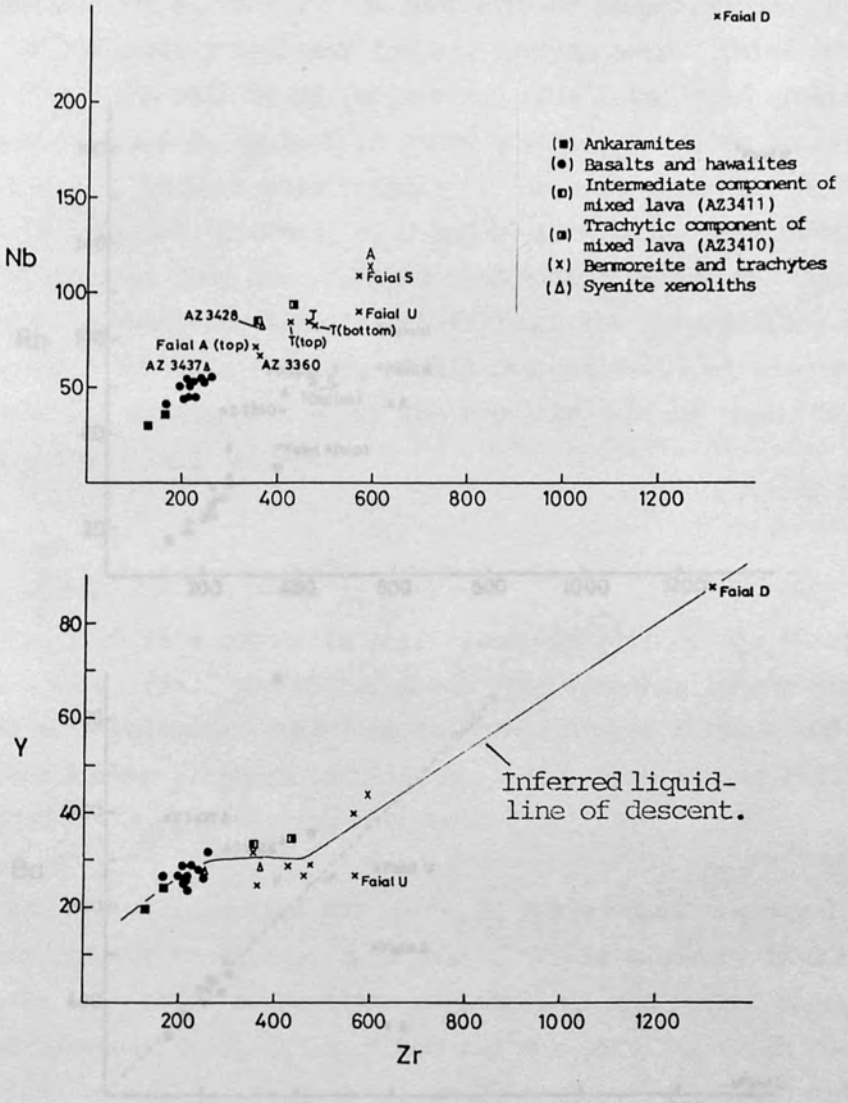

Fig 2.19 Biaxial plots of Nb, Y, Rb and Ba against Zr for all Faial compositions. Note the anomalously high Ba contents of the syenite xenoliths, Faial A (top) and the intermediate and trachytic components of the mixed lava from Castelo Branco. All values in ppm.

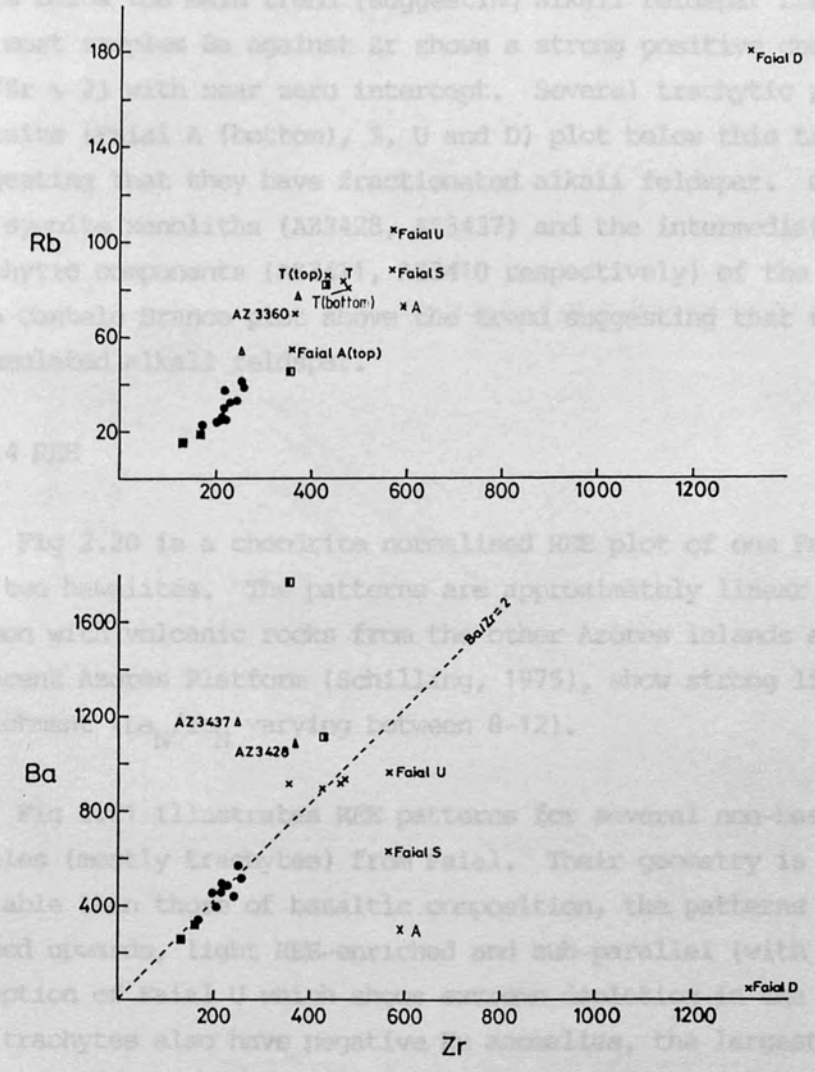

Fig 2.19 continued.

the less evolved trachytic compositions. In the same plot, Faial D, A and S fall on a line colinear with the origin and other trachytes suggesting that $D_Y << 1$ in the most evolved compositions. Rb against Zr is approximately colinear for all samples except Faial D which plots below the main trend (suggesting alkali feldspar fractionation). For most samples Ba against Zr shows a strong positive correlation ($Ba/Zr \sim 2$) with near zero intercept. Several trachytic pumice deposits (Faial A (bottom), S, U and D) plot below this trend suggesting that they have fractionated alkali feldspar. Conversely, two syenite xenoliths (AZ3428, AZ3437) and the intermediate and trachytic components (AZ3411, AZ3410 respectively) of the mixed lava from Castelo Branco plot above the trend suggesting that they have accumulated alkali feldspar.

2.5.4 REE

Fig 2.20 is a chondrite normalised REE plot of one Faial basalt and two hawaiites. The patterns are approximately linear and, in common with volcanic rocks from the other Azores islands and the adjacent Azores Platform (Schilling, 1975), show strong light REE enrichment (La_N/Yb_N varying between 8-12).

Fig 2.21 illustrates REE patterns for several non-basaltic samples (mostly trachytes) from Faial. Their geometry is more variable than those of basaltic composition, the patterns are dish-shaped upwards, light REE-enriched and sub-parallel (with the exception of Faial U which shows extreme depletion in the middle REE). The trachytes also have negative Eu anomalies, the largest occurring in Faial D ($Eu/Eu^* = 0.16$), a deposit that is mildly peralkaline in composition and which is also characterized by a large Rb/Sr ratio (15) and small K/Rb ratio (219).

2.5.5 Mixed-magma samples

The compositional variations in two mixed-magma eruptions from Faial are detailed here, their occurrence being briefly described in

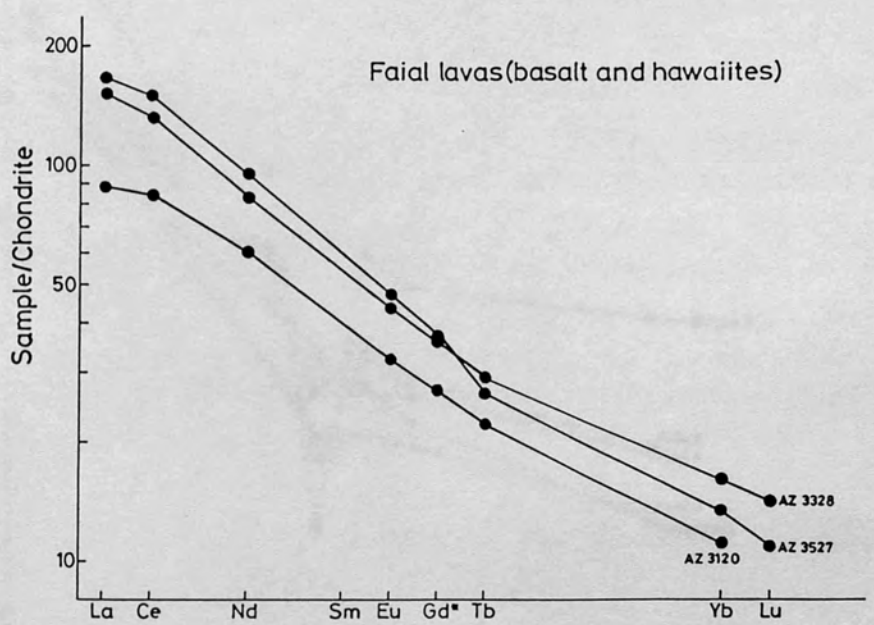

Fig 2.20 Chondrite normalised REE concentrations of basaltic lavas from Faial. Gd values interpolated (Gd*).

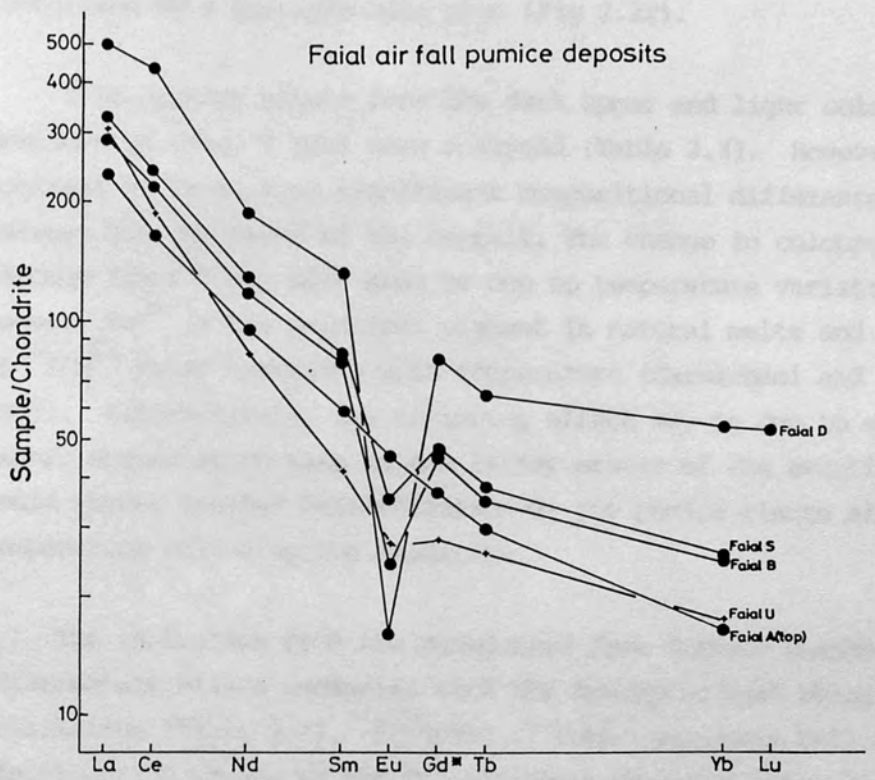

Fig 2.21 Chondrite normalised REE patterns of a benmoreite (Faial A, top) and four trachytes. Gd values interpolated.

Section 2.2.2.

Faial A zones upward from a buff-coloured pumice (0.5wt% MgO) to a darker, more mafic variety (1.9 wt%MgO), analyses being given in Table 2.3. The lower part of the deposit is relatively enriched in the incompatible elements and is depleted in Ba, Sr, Eu, P, Ti, V. The element enrichment/depletion pattern between mafic and salic pumice from Faial A is summarised by a sample/sample plot (Fig 2.22).

Also, pumice clasts from the dark upper and light coloured lower portions of Faial T have been analysed (Table 2.3). However, in contrast to Faial A no significant compositional difference was found between the two parts of the deposit. The change in colouration through Faial T may have been be due to temperature variations in the magma. Fe^{3+} is the principal pigment in natural melts and the Fe^{3+}/Fe^{2+} ratio increases with temperature (Carmichael and Nicholls, 1967). Alternatively, the colouring effect may be due to a higher tephra accumulation rate in the latter stages of the eruption. This would favour greater heat retention by the pumice clasts allowing high-temperature post-eruptive oxidation.

The inclusions from the mixed lava from Castelo Branco have intermediate silica contents, with the trachytic host being mildly peralkaline (Table 2.3). Analyses of both components fall on crystal fractionation trends in the MgO variation diagrams (Figs 2.16, 2.17). However, consideration of trace element abundances suggests that neither is a simple derivative. For example, in the plot of Ba against Zr (Fig 2.19) both the intermediate and trachytic components plot above the linear fractionation trend (defined by basaltic analyses where $D_{Zr} \sim D_{Ba}$) indicating that they are accumulative in alkali feldspar. This is supported by their large K/Rb ratios (Table 2.3) and the small, positive Eu anomaly of the intermediate component (Fig 2.23). In the chondrite normalised REE plot (Fig 2.23) the affinities of the two components are illustrated by their quite different patterns. Typically, the trachyte shows relative depletion in the middle REE which, in this instance, results in a cross over with

Sa. No.	Faial A(top) AZ3446	Faial A(base) F500	Faial T(top) AZ3435	Faial T(base) AZ3432	Mixed lava, Castelo Branco AZ3411	AZ3410
SiO_2	56.03	57.29	59.61	59.41	54.80	62.90
TiO_2	1.44	1.18	1.05	1.04	1.82	0.57
Al_2O_3	18.77	20.74	18.55	18.40	18.25	17.21
Fe_2O_3	2.20	1.85	1.92	1.90	1.66	1.59
FeO	3.66	3.08	3.20	3.16	5.53	2.65
MnO	0.16	0.21	0.16	0.15	0.19	0.18
MgO	1.88	0.54	1.45	1.42	2.43	0.45
CaO	4.42	1.18	3.24	3.16	4.87	1.20
Na_2O	6.12	5.87	6.55	6.79	6.14	7.20
K_2O	2.98	4.20	3.82	3.85	2.88	5.23
P_2O_5	0.44	0.17	0.24	0.24	0.55	0.10
H_2O^+	1.1	2.6				
Total	99.20	98.91	99.79	99.52	99.28	99.64
			Trace elements			
Ni	3	1	4	8	4	
Cr			2			
V	62	14	34	35	75	2
Rb	54	72	85	83	45	82
Sr	611	100	410	401	574	24
Y	32	44	29	27	34	35
Hf	9.4	13.8			10.4	11.9
Zr	354	595	427	462	358	433
Nb	72	119	84	84	85	93
Ta	5.0	7.2			7.0	7.7
Th	5.9	10.0	9.4	9.7	5.7	8.9
Ba	908	294	890	909	1759	1109
La	51	75	62.0	59.0	63.1	65.5
Ce	105	150	120	124	148	139
Nd	461	62	41.0	41.3	63.7	54.0
Sm	8.9	10.9	10.5	10.7	11.2	8.8
Eu	3.3	1.9	2.26	2.26	4.30	2.56
Tb	0.9	1.3	0.9	0.8	1.4	1.1
Ho	1.1	1.7			1.4	1.3
Yb	2.7	4.8	2.8	2.8	3.3	3.6
Lu	0.3	0.6	0.7	0.4	0.48	0.47
Eu/Eu*	1	0.6	1	1	1.1	1
K/Rb	458	484	373	385	531	529
Rb/Sr	0.09	0.72	0.21	0.21	0.08	3.42
La_N/Yb_N	12.7	10.5	14.9	14.2	13.0	12.3
La_N/Sm_N	3.6	4.3	3.7	3.5	3.5	4.7
			CIPW normative minerals			
Or	17.6	25.8	22.6	22.8	17.0	30.9
Ab	50.0	51.6	54.1	53.1	44.8	56.2
An	14.9	5.0	9.9	8.4	13.7	
Ne	1.0		0.7	2.4	3.9	1.7
Ac						1.3
Di	3.4		3.8	4.7	5.7	4.5
Hy		4.1				
Ol	4.3		3.4	2.9	6.9	1.6
Mt	3.2	2.8	2.8	2.6	2.4	1.6
Ilm	2.7	2.3	2.0	2.0	3.5	1.1
Ap	1.0	0.4	0.6	0.6	1.3	0.2

Table 2.3 Major and trace element (ppm) analyses of Faial A, Faial T and separates of the mixed lava from Castelo Branco.

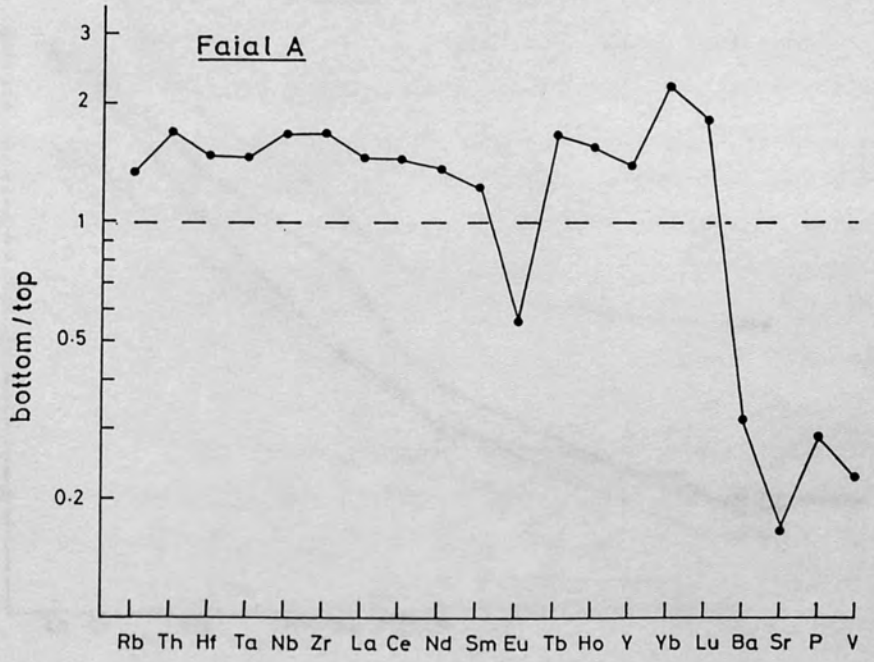

Fig 2.22 Trace element variation in trachytic pumice deposit Faial A. Each plotted point is the concentration of an element in the basal salic pumice (F500), divided by its concentration in the topmost mafic pumice (AZ3446). The compositional stratigraphy of the deposit is assumed to qualitatively represent an inversion of the magma body prior to eruption.

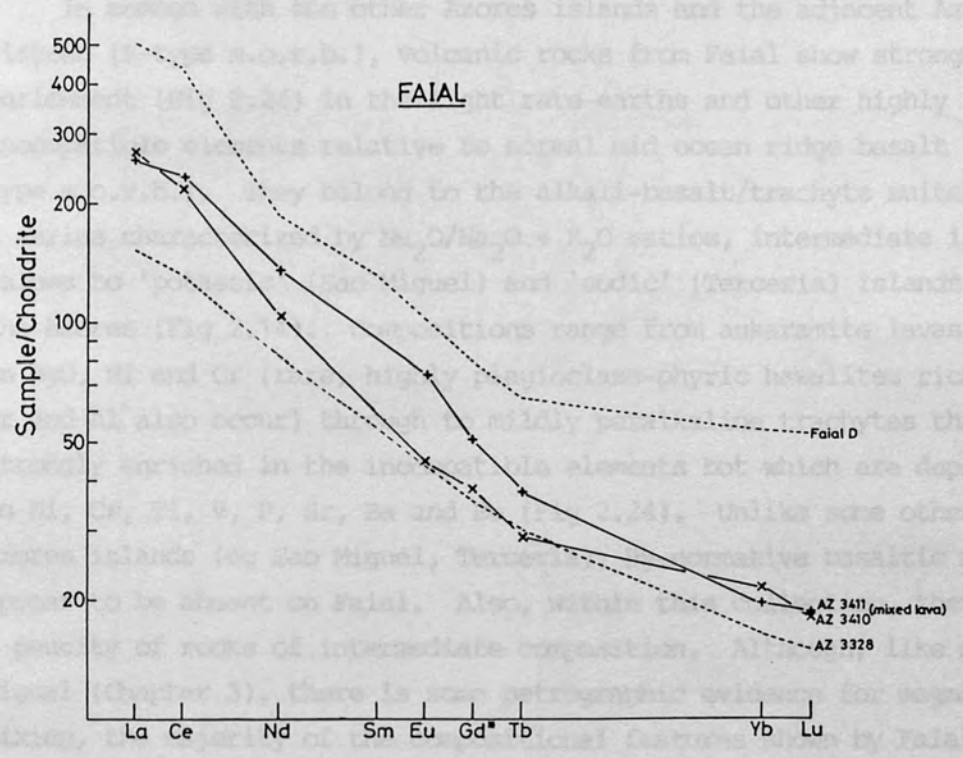

Fig 2.23 Chondrite normalised REE patterns of trachytic (AZ3410) and intermediate (AZ3411) components of mixed lava from Castelo Branco. A hawaiite (AZ3328) and trachyte (AZ3401) are shown for comparison. Gd values interpolated.

the more linear pattern of the 'basic' component. The higher concentration of elements such as Ba and the middle rare-earths in the latter suggests that the two components cannot be easily related by fractional crystallization or magma-mixing. This is discussed in Section 2.6.2.

2.6 DISCUSSION

In common with the other Azores islands and the adjacent Azores Plateau (E-type m.o.r.b.), volcanic rocks from Faial show strong enrichment (Fig 2.24) in the light rare-earths and other highly incompatible elements relative to normal mid ocean ridge basalt (N-type m.o.r.b.). They belong to the alkali-basalt/trachyte suite, forming a series characterized by $Na_2O/Na_2O + K_2O$ ratios, intermediate in values to 'potassic' (Sao Miguel) and 'sodic' (Terceria) islands from the Azores (Fig 2.14). Compositions range from ankaramite lavas rich in MgO, Ni and Cr (rare, highly plagioclase-phyric hawaiites rich in Sr and Al also occur) through to mildly peralkaline trachytes that are strongly enriched in the incompatible elements but which are depleted in Ni, Cr, Ti, V, P, Sr, Ba and Eu (Fig 2.24). Unlike some other Azores islands (eg Sao Miguel, Terceria), Hy-normative basaltic rocks appear to be absent on Faial. Also, within this collection, there is a paucity of rocks of intermediate composition. Although, like Sao Miguel (Chapter 3), there is some petrographic evidence for magma-mixing, the majority of the compositional features shown by Faial volcanic rocks are qualitatively consistent with being produced from fractional crystallization of a basaltic parent by the observed phenocryst assemblage.

Whether a series of comagmatic rocks are related by fractional crystallization or variable partial melting can often be determined by application of equations governing trace element distribution in crystal-liquid fractionation processes. For example, trace element studies on suites of alkaline rocks from Reunion island in the Indian Ocean by Zelinski (1975) and Grenada in the Iesser Antilles by Shimizu and Arculus (1975) demonstrated the variations to be best explained by fractional crystallization and partial melting respectively. As was

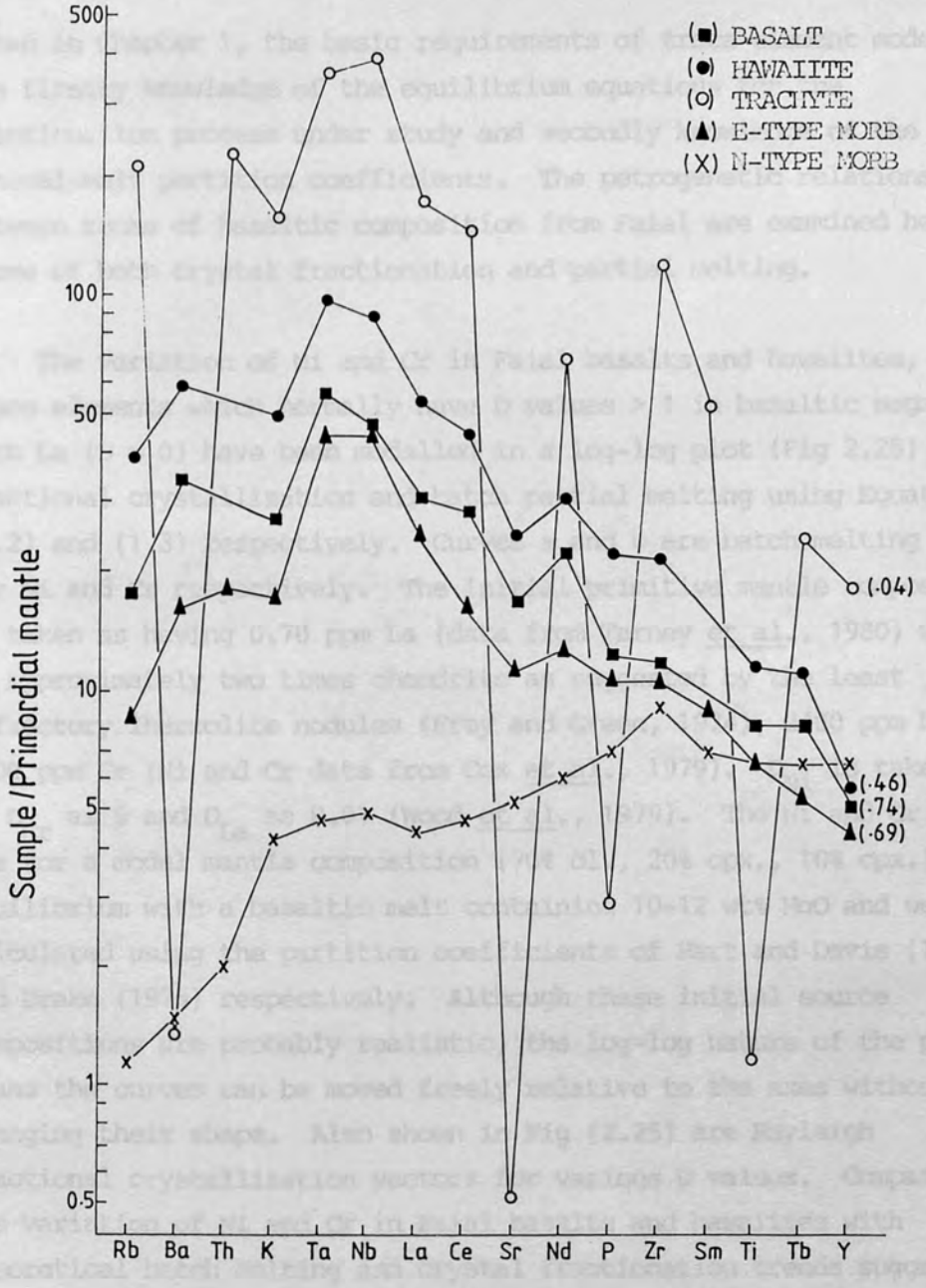

Fig 2.24 Incompatible element abundances in a basalt (AZ3120), hawaiite (AZ3328) and mildly peralkaline trachyte (AZ3401) from Faial, normalised to a primordial mantle composition. Shown for comparison are E-type m.o.r.b. from 36°N mid-Atlantic ridge (DSDP site 413) and average N-type m.o.r.b. Primordial mantle values and m.o.r.b. data from Tarney et al. (1980). Mg numbers in brackets. Order of incompatibilty decreases from left to right.

shown in Chapter 1, the basic requirements of trace-element modelling are firstly knowledge of the equilibrium equations for the fractionation process under study and secondly knowledge of the mineral-melt partition coefficients. The petrogenetic relationships between rocks of basaltic composition from Faial are examined here in terms of both crystal fractionation and partial melting.

The variation of Ni and Cr in Faial basalts and hawaiites, (two trace elements which normally have D values > 1 in basaltic magmas) with La ($D \sim 0$) have been modelled in a log-log plot (Fig 2.25) for fractional crystallization and batch partial melting using Equations (1.2) and (1.3) respectively. Curves a and b are batch melting models for Ni and Cr respectively. The initial primitive mantle composition is taken as having 0.78 ppm La (data from Tarney et al., 1980) which is approximately two times chondrite as suggested by the least refractory lherzolite nodules (Frey and Green, 1974), 2400 ppm Ni and 2700 ppm Cr (Ni and Cr data from Cox et al., 1979). D_{Ni} is taken as 9, D_{Cr} as 6 and D_{La} as 0.01 (Wood et al., 1979). The Ni and Cr values are for a model mantle composition (70% ol., 20% opx., 10% cpx.) in equilibrium with a basaltic melt containing 10-12 wt% MgO and were calculated using the partition coefficients of Hart and Davis (1978) and Drake (1976) respectively. Although these initial source compositions are probably realistic, the log-log nature of the plot means the curves can be moved freely relative to the axes without changing their shape. Also shown in Fig (2.25) are Rayleigh fractional crystallization vectors for various D values. Comparing the variation of Ni and Cr in Faial basalts and hawaiites with theoretical batch melting and crystal fractionation trends suggest that:

(1) The depletion of Ni and Cr with increasing La cannot easily be explained by variable partial melting. Based on measured partition coefficients, however, their variation is consistent with fractional crystallization of olivine and clinopyroxene (and/or chromite) respectively.

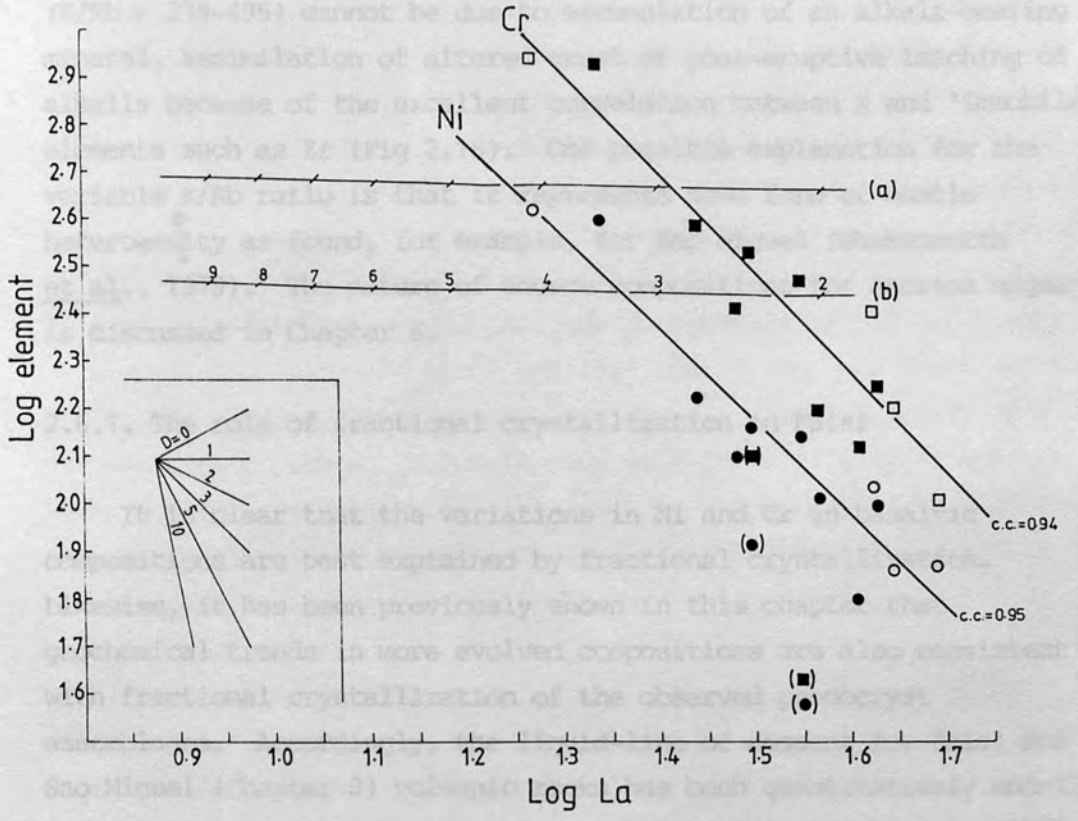

Fig 2.25 A log-log plot of Cr (squares) and Ni (circles) against La for Faial basaltic rocks. Unfilled circles and squares; data from White et al. (1979). Best fit lines shown, with data in brackets not being included in linear regressions. Curves a and b are batch melting models of mantle composition with 70% olivine, 20% orthopyroxene and 10%clinopyroxene for Cr and Ni respectively (numbers are melt proportions in percent). Rayleigh fractional crystallization vectors for various D values shown in bottom left hand corner of diagram.

(2) The correlation between La and Ni and La and Cr suggests one lineage only. This indicates that parental melts had similar La concentrations and were therefore the products of comparable degrees of partial melting.

Finally, the variable K/Rb ratios of Faial basalts and hawaiites (K/Rb = 378-495) cannot be due to accumulation of an alkali-bearing mineral, assimilation of altered crust or post-eruptive leaching of alkalis because of the excellent correlation between K and 'immobile' elements such as Zr (Fig 2.18). One possible explanation for the variable K/Rb ratio is that it represents some form of mantle heterogeneity as found, for example, for Sao Miguel (Hawkesworth et al., 1979). The nature of source compositions for Azorean magmas is discussed in Chapter 6.

2.6.1. The role of fractional crystallization on Faial

It is clear that the variations in Ni and Cr in basaltic compositions are best explained by fractional crystallization. Likewise, it has been previously shown in this chapter that geochemical trends in more evolved compositions are also consistent with fractional crystallization of the observed phenocryst assemblages. Accordingly, the liquid-line of descent for Faial and Sao Miguel (Chapter 3) volcanic rocks has been quantitatively modelled using the least-squares mass balance method of Bryan et al., (1968) and Wright and Docherty (1970). In least-squares mass balance modelling calculations the measure of how accurately a proposed phenocryst assemblage can relate two liquids is given by the sum of the squares of the residuals (Σr^2). Although it is not possible to apply rigorous statistical criteria to the acceptability of least-squares solutions (Banks, 1979), previous workers have assumed arbitrary upper limits of $\Sigma r^2 = 1.5$ (eg Luhr and Carmichael, 1980). Large residuals suggest, either that the liquids are not related by crystal fractionation or that the model mineral assemblage is incorrect. Model fractional crystallization solutions for the Faial magma series, with acceptably low residuals and which are in general agreement with

the trace element variations are shown in Table 2.4. These are discussed below along with other evidence in support of a fractional crystallization model.

2.6.1. (a) Basalt-hawaiite

Differentiation trends consist of enrichment of the incompatible elements, an increase in normative Ne and the F/F + M ratio coupled with depletion of Ni and Cr. Silica remains relatively constant throughout this compositional range. Least-squares mixing calculations (Table 2.4) suggest a fractionating assemblage consisting of 41% olivine and 59% clinopyroxene best accounts for the derivation of hawaiite from basalt. In the hawaiite compositional range, results also suggest that further differentiation involves plagioclase in the fractionating assemblage (as indicated by Sr contents, Fig 2.18), one model solution having 30% olivine, 27% clinopyroxene and 43% plagioclase (Table 2.4). The moderately incompatible behaviour of Y in Faial basalts and hawaiites is consistent with clinopyroxene fractionation, Kd_Y cpx/melt having been estimated to equal approximately 0.3 in compositionaly similar magmas from Sao Miguel (Section 3.6.1).

2.6.1 (b) Intermediate rocks

Modelling of the liquid-line of descent through the intermediates is more problematical because of the relatively large compositional gap. However, the variation diagrams provide useful constraints on the nature of the fractionating assemblage. For example, the inflections in the variation trends of SiO_2, TiO_2, V (Fig 2.16) and FeO + Fe_2O_3 (Fig 2.17) at 3-4 wt% MgO are consistent with significant Fe-Ti oxide fractionation, whereas the maximum in P_2O_5 at 3 wt% MgO and the depletion of Sr are consistent with apatite and plagioclase fractionation respectively. The 'plateau' in Y contents for intermediate compositions (Fig 2.19) suggests that $D_Y \sim 1$. As detailed in Section 3.6.1 for Sao Miguel, the strong inflection in the variation trend of Y with Zr suggests that the increase in D_Y is due to a change in the fractionating assemblage rather than an increase in

Sa. No.	Hawaiite AZ3328	Ol.	Cpx.	Basalt AZ3099 observ.	Basalt AZ3099 estim.	Resid. (r)
SiO_2	48.80	38.74	47.14	48.40	48.48	0.0848
TiO_2	2.88		2.02	2.62	2.73	0.1125
Al_2O_3	16.71		6.43	15.75	15.56	- 0.1872
FeO	9.68	18.44	6.32	9.73	9.86	0.1296
MnO	0.16	0.28	0.15	0.15	0.16	0.0145
MgO	7.61	41.76	13.44	9.39	9.25	- 0.1354
CaO	9.21	0.29	21.83	9.68	9.60	- 0.0843
Na_2O	4.08		0.64	4.03	3.75	- 0.2813
K_2O	1.50			1.14	1.37	0.2252
P_2O_5	0.46			0.36	0.42	0.0587
%	90.7	3.8	5.5			$\Sigma r^2 = 0.2307$

Sa. No.	Hawaiite AZ3533	Ol.	Cpx.	Plag.	Hawaiite AZ3328 observ.	Hawaiite AZ3328 estim.	Resid. (r)
SiO_2	48.66	37.79	46.00	52.63	48.80	48.64	- 0.1579
TiO_2	3.34		2.50		2.88	2.68	- 0.1963
Al_2O_3	17.44		7.37	29.45	16.71	16.90	0.1856
FeO	9.90	27.01	7.14	0.41	9.68	10.11	0.4278
MnO	0.17	0.32	0.15		0.16	0.16	0.0034
MgO	5.02	35.17	12.75		7.61	7.45	- 0.1616
CaO	8.72	0.38	21.72	11.93	9.21	9.46	0.2502
Na_2O	4.65		0.64	4.30	4.08	4.01	- 0.0672
K_2O	1.83			0.31	1.50	1.41	- 0.0933
P_2O_5	0.56				0.46	0.42	- 0.0401
%	74.1	7.8	7.1	11.0			$\Sigma r^2 = 0.3845$

Sa. No.	Benmoreite AZ3446	Cpx.	Plag.	Amp.	Mag.	Ap.	Hawaiite AZ3533 observ.	Hawaiite AZ3533 estim.	Resid.(r)
SiO_2	56.03	50.19	55.46	40.49	0.36		48.66	48.67	0.0133
TiO_2	1.44	1.00		5.40	16.98		3.34	3.05	- 0.2647
Al_2O_3	18.77	2.16	27.25	11.67	5.68		17.44	17.45	0.0127
FeO	5.64	10.87	0.94	12.95	68.39		9.90	9.95	0.0540
MnO	0.16	0.39		0.28	0.45		0.17	0.18	0.0133
MgO	1.88	12.61		12.04	6.12		5.02	5.14	0.1232
CaO	4.42	22.07	9.65	10.91	0.28	55.84	8.72	8.60	- 0.1172
Na_2O	6.12	0.62	5.78	2.97			4.65	4.67	0.0206
K_2O	2.98		0.44	0.82			1.83	1.56	- 0.2734
P_2O_5	0.44					42.05	0.56	0.72	0.1556
%	39.7	2.6	21.2	30.7	4.5	1.3			$\Sigma r^2 = 0.2017$

Sa. No.	Trachyte AZ3432	Plag.	Amp.	Mag.	Ap.	Benmoreite AZ3446 observ.	Benmoreite AZ3446 estim.	Resid. (r)
SiO_2	59.41	58.94	40.49			56.03	56.03	- 0.0025
TiO_2	1.04		5.40	25.30		1.44	1.55	0.1075
Al_2O_3	18.40	25.65	11.67	1.80		18.77	18.68	- 0.0865
FeO	4.87	0.37	12.95	67.40		5.64	5.60	- 0.0363
MnO	0.15		0.28	1.00		0.16	0.14	- 0.0164
MgO	1.42		12.04	2.30		1.88	1.84	- 0.0428
CaO	3.16	7.02	10.91		55.84	4.42	4.49	0.0698
Na_2O	6.79	7.22	2.97			6.12	6.39	0.2650
K_2O	3.85	0.72	0.82			2.98	2.95	- 0.0336
P_2O_5	0.24				42.05	0.44	0.35	- 0.0927
%	72.7	18.6	6.5	1.8	0.4			$\Sigma r^2 = 0.1073$

Table 2.4 Fractional crystallization least-squares model for volcanic rocks from Faial. Mineral analyses from Appendix 3; apatite analysis from Deer et al. (1966).

Kd_Y values for clinopyroxene. These features are consistent with apatite and/or amphibole (kaersutite) fractionation, both of which occur as phenocrysts or microphenocrysts in intermediate and trachytic rocks. Moreover, both these phases also preferentially incorporate the middle REE (Table 1.2), thus providing an explanation for the concave-upwards patterns of more evolved rock compositions (Fig 2.21). Fractionation of kaersutite and apatite is also indicated by results from the least-squares mixing calculations. The best model solution for the derivation of benmoreite from hawaiite (Table 2.4) suggests a fractionating assemblage consisting of 51% amphibole (kaersutite), 35% plagioclase, 8% magnetite with minor clinopyroxene (4%) and apatite (2%). More detailed evidence for the importance of this fractionating assemblage in Azorean magmas of intermediate composition is given in Section 3.6.1.

2.6.1 (c) Trachytes

The elemental abundance patterns of trachytes from Faial provides convincing evidence for a fractional crystallization origin (Figs 2.16, 2.19, 2.21 and 2.24). They are depleted in P, Ti, V, Mg, Ni, Cr, Sr and Eu and enriched in incompatible elements such as Zr, Nb, Th, Y and the REE. The air fall pumice deposits A (bottom), D, S and U are depleted in Ba (Fig 2.19) suggesting that alkali feldspar fractionation is important in trachytic magmas. This diagram also demonstrates that the mafic top of Faial A (AZ3446), the syenite xenoliths and both the intermediate and trachytic components of the mixed lava from Castelo Branco are probably accumulative in alkali feldspar plotting above the linear fractionation trend. With the possible exception of Faial U (which shows extreme depletion in the middle REE) the importance of amphibole and/or apatite fractionation diminishes in the more evolved trachytes, Faial A, D and S falling on a simple fractionation line which projects to the origin in the plot of Y against Zr (Fig 2.19). This is consistent with the experimental data of Merril and Wyllie (1975) which suggests that a high TiO_2 content in the melt increases the thermal stability of amphibole whereas its stability decreases with an increase in the SiO_2 content

and $Na_2O/Na_2O + K_2O$ ratio. The mildly peralkaline nature of Faial D and the trachytic component of the mixed lava from Castelo Branco is consistent with a fractionation assemblage consisting of biotite, Al-bearing clinopyroxene and alkali feldspar (Chapter 4). Table 2.4 shows results from least-squares modelling for the derivation of trachyte from intermediate melt. A fractionating assemblage consisting of 68% plagioclase, 24% amphibole, 7% magnetite and 1% apatite provides a possible solution. Abundances of incompatible elements in the most evolved trachyte (Faial D) suggest that it was produced by about 85% soldification of a basalt parent.

2.6.2 Mixed-magma eruptions

Evidence for compositionally zoned (intermediate-trachyte) magma bodies on Faial is provided by pumice air-fall deposit A. The mixed-lava from Castelo Branco shows, in most respects, similar compositional features to one from SE of Queimado on Sao Miguel. Both the intermediate and trachytic components of the Castelo Branco lava have probably accumulated alkali feldspar. However, it is evident that the two components cannot be related by simple magma mixing as the intermediate component has larger Eu (4.3 ppm) and Ba (1759 ppm) compared to the trachyte (2.6 ppm and 1109 ppm respectively).

In Section 3.6 results from least-squares mass balance calculations are given in which it is suggested that such (mixed) lavas come from a zoned magma chamber and represent samples adjacent to a compositional interface in which underlying intermediate magma has accumulated settling alkali feldspar (possibly in the form of glomeroporphyritic lumps with interstitial trachytic melt. Disruption of a stably zoned magma chamber provides a simple explanation for the presence of basaltic and intermediate xenocrysts in some trachytic pumice deposits (eg Faial S, A and T).

2.6.3 Summary and conclusions

(1) Compositional variations in the basalts and hawaiites are

produced by fractional crystallization of clinopyroxene, olivine and plagioclase. The presence of only one lineage in the plot of La against Ni and Cr suggests that parental magmas were produced by similar degrees of partial melting.

(2) Rocks of intermediate silica content were produced from basaltic magmas by fractional crystallization. Modelling of the liquid-line of descent suggests a separating assemblage consisting principally of kaersutite and plagioclase with lesser amounts of Fe-Ti oxides, clinopyroxene and apatite.

(3) The trachytes were produced from intermediate magma by fractional crystallization of plagioclase with lesser amounts of kaersutite, magnetite and apatite. To produce the total compositional (liquid) range of Faial magmas requires some 85% soldification of a basalt parent.

(4) Air-fall pumice deposit A and the mixed-lava from Castelo Branco provide evidence for compositional zonation of magma bodies beneath Faial.

CHAPTER 3

THE PETROLOGY OF VOLCANIC ROCKS FROM SAO MIGUEL

3.1 INTRODUCTION

Sao Miguel is the largest and most populated of the nine Azores Islands forming (with Santa Maria and the Formigas Bank) the most easterly component of the archipelago. The island, which overlies a WNW-ESE fracture zone (Fig 1.1) has three active stratovolcanoes, each having a long record of explosive trachytic eruptions (Fig 3.1 and Fig 3.2). There is also a volcanically active fissure zone (predominantly basaltic) in the low-lying tract of land ('waist') between Sete Cidades and Agua de Pau volcanoes (Fig 3.3). At the eastern end of the island there is a fourth, much older stratovolcano (Povoacao) which is believed to be long extinct.

Previous petrological studies of volcanic rocks from Sao Miguel (Schmincke and Weibel, 1972) have shown that they belong to a potassic series in the alkali-basalt/trachyte suite, akin to other Atlantic islands such as Gough (Le Maitre, 1962) and Tristan de Cunha (Baker et al., 1964). Early reconnaissance studies of the Azores were made by Esenwein (1929) and Berthois (1953). Assuncao (1961) and Assuncao and Canilho (1970) made a general petrological study of Sao Miguel while studies on individual volcanoes have been made by Jeremine (1957) on Furnas and by Marriner et al. (1982), Storey (1981) and Wolff and Storey (1983, 1984) on lavas and pyroclastics from Agua de Pau. Fernandez (1980, 1982) made a study of volcanics from the old, predominantly basaltic Nordeste Complex in northeastern Sao Miguel demonstrating that the oldest flows (4.0 m.y.; Abdel-Monem et al., 1975) are transitional in composition containing normative Hy. Other geochemical data on Sao Miguel is given by Schmincke (1973) and Schmincke and Weibel (1972) who analysed a number of non-basaltic lavas and pyroclastics, while Cann (1967) gives analyses of co-magmatic syenite xenoliths occuring in trachytic pumice fall deposits from Agua de Pau volcano. Some major element, trace element and

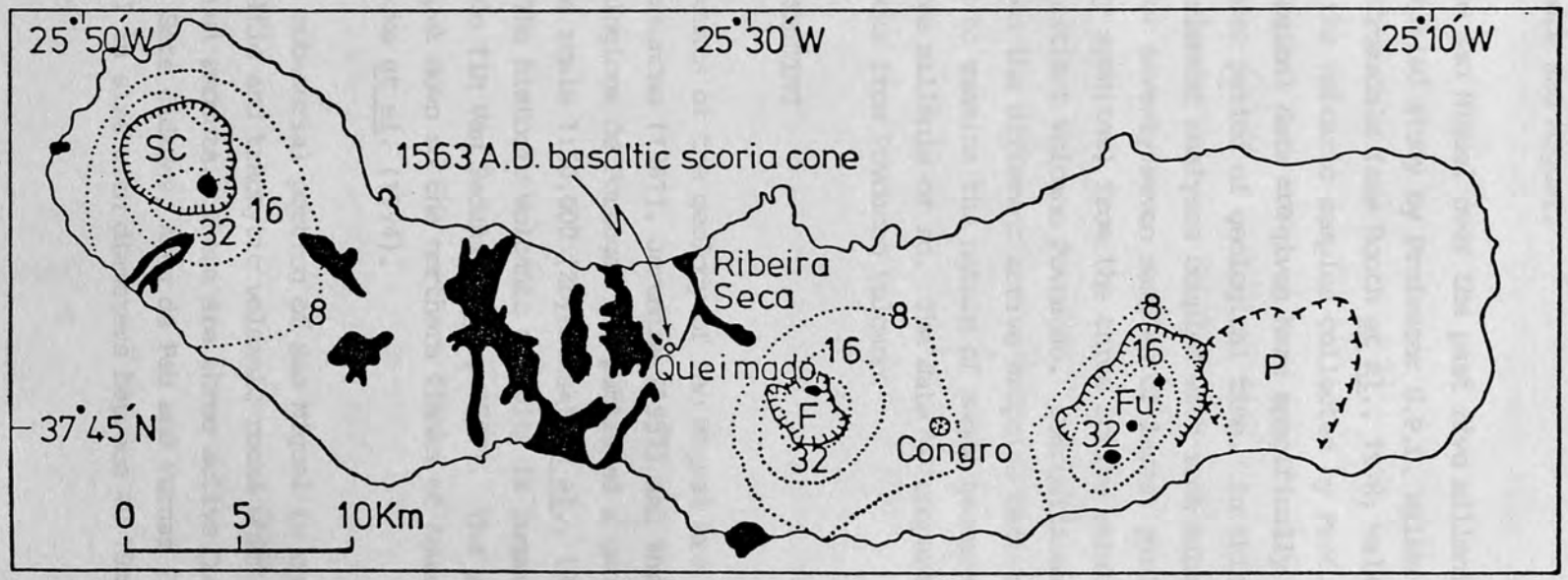

Fig. 3.1 Map of Sao Miguel showing isopachs (metres) for the total thickness of trachytic pumice deposits formed in the past 5,000 years; simplified after Booth et al. (1978). Also shown, in solid black, are trachyte and basalt lava extrusions formed during the same period; the former are found only in the calderas and the Congro crater. Caldera: SC, Seta Cidades; F, Fogo (Agua de Pau); Fu, Furnas; P, Povoacao.

isotope data for Sao Miguel are also given by Flower et al. (1976), Hawkesworth et al. (1979) and White et al. (1979). The $^{87}Sr/^{86}Sr$ isotope data of Hawkesworth et al. (1979) provide evidence for source heterogeneity beneath Sao Miguel.

Volcanism on Sao Miguel over the past five millenia has been the subject of a detailed study by Professor G.P.L. Walker, Dr. B. Booth and Dr. R Croasdale (see Booth et al., 1978; Walker and Croasdale 1971). Most of the volcanic samples collected by Prof. Walker and for which petrological data are given here specifically relate to this comparatively short period of geological time. In this chapter new major and trace element analyses coupled with some mineral chemistry data are given for seventy-seven samples of lavas, pyroclastics and xenoliths (mostly syenites) from the three active stratovolcanoes, the 'waist' and the extinct volcano Povoacao. Compositional variations within and between the different active eruptive centres are used here and in Chapter 4 to examine the nature of magma genesis on Sao Miguel over the past five millenia or so. The data are compared to analyses of much older rocks from Povoacao volcano.

3.2 GEOLOGICAL SETTING

General accounts of the geology of Sao Miguel are given by Branco et al. (1957), Assuncao (1961), Jeremine (1957) and Zbyszewski (1961). The Servicos Geologicos de Portugal has published a geological map of Sao Miguel on the scale 1:50,000 (Zbyszewski et al., 1958; Zbyszewski et al., 1959). The historic volcanic activity is summarised by Weston (1964) and Machado (in Van Padang et al., 1967). The geology of a 981m deep drill hole put down on the northern flanks of Agua de Pau is described by Muecke et al. (1974).

The visible sub-aerial portion of Sao Miguel is composed almost entirely of basaltic and trachytic volcanic rocks which occur in approximately equal amounts. There are three active Quaternary stratovolcanoes, Sete Cidades, Agua de Pau and Furnas (Fig 3.1). They are roughly equal in size with diameters between 10-15km at sea-level

rising to heights of between 800-950m. Each possesses a central caldera and a long record of explosive volcanic eruptions, the resulting trachytic pumice fall deposits thickly mantling the slopes of the volcanoes and accounting for more than half their visible bulk (Fig 3.1); the volume of each of the volcanoes above sea-level is in the order of $70km^3$. The Fogo caldera of Agua de Pau (Plate 3.1) is believed to be a collapse structure mainly attributable to a large plinian eruption some 4,550 years ago (Walker and Croasdale, 1971). The syn-caldera air fall pumice deposit Fogo A (Plate 3.2) forms the base for the study of 5,000 years of volcanism on Sao Miguel by Booth et al. (1978). As previously stated rocks as old as 4.0 m.y. (Abdel-Monem et al., 1975) occur at the eastern end of the island in an area known as the Nordeste Complex and in association with a fourth stratovolcano, Povoacao, which is believed to be long extinct.

The quantitative study of recent volcanism on Sao Miguel by Booth et al. (1978) showed that there have been some 57 eruptions during the past five millenia. Twenty-seven of these produced trachytic air fall pumice deposits (Fig 3.2), explosive eruptions having taken place during this period from vents in each of the calderas and from the maar-like crater of Lagoa do Congro on the eastern side of Agua de Pau volcano (Fig 3.1). Although the majority of trachytic rocks on Sao Miguel occur as air-fall pumice deposits there are examples of lavas, domes and ignimbrites. The final stages of several of the explosive pumice eruptions were accompanied by the extrusion of a trachyte dome (eg Congro ash). Also, as on Faial, magmatically heterogenous lavas and pumice deposits occur (G.P.L. Walker pers. comm.; Walker and Croasdale, 1971). Good examples are provided by the Fogo A deposit which consists of a buff coloured pumice (Plate 3.2) overlain by a streaky (Plate 3.3) and then a dark, more mafic pumice (Section 4.5.2). A second example is a mixed lava (sa. no. AZ1721) from the NW flanks of Agua de Pau which consists of numerous small basic inclusions in a trachytic host. Textural relationships (G.P.L. Walker pers. comm.) suggest that both components were fluid at the time of eruption. Syenite xenoliths, with chemical compositions similar to the trachytes, occur in the air fall pumice deposits Fogo A, Fogo 1563

Plate 3.1 The Fogo caldera (looking east).

(a)

(b)

Plate 3.2. (a) East side of cutting along track 2km NNE of Vila Franco do Campo. The buff-coloured ash is Fogo A (some 4.3m thick) which rests on red-brown soil. (b) Road cutting 2km east of Lagoa, Sao Miguel. Fogo A ash here is $\frac{3}{4}$ way up the section and is 1.3m thick. This is not the true thickness as the top has been eroded away.

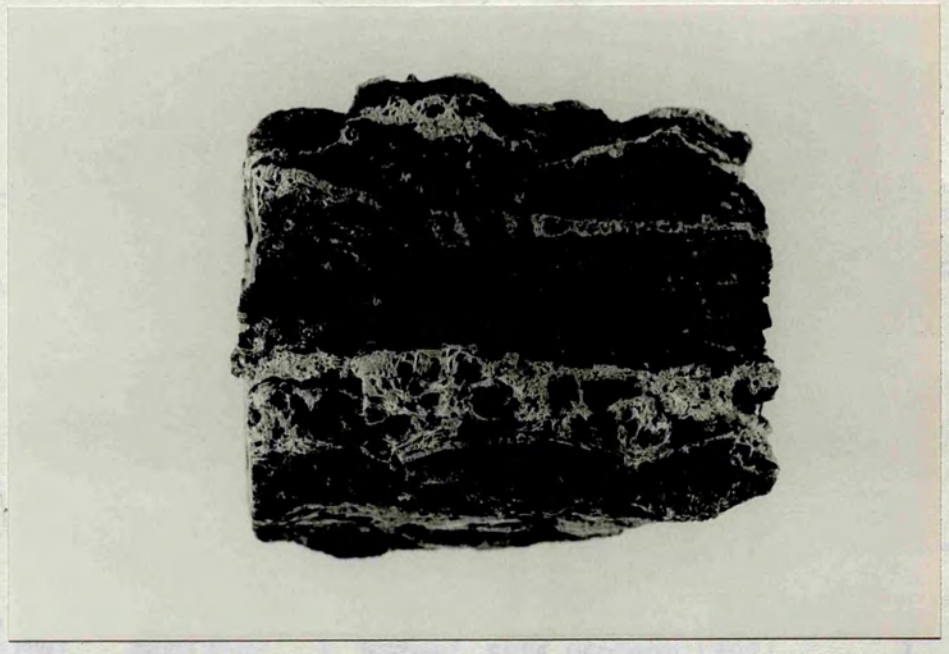

Plate 3.3 Streaky pumice clast (AZ1323) from Fogo A containing the light and dark coloured components from the lower and upper parts of the deposit respectively. Magnification (X 1.5).

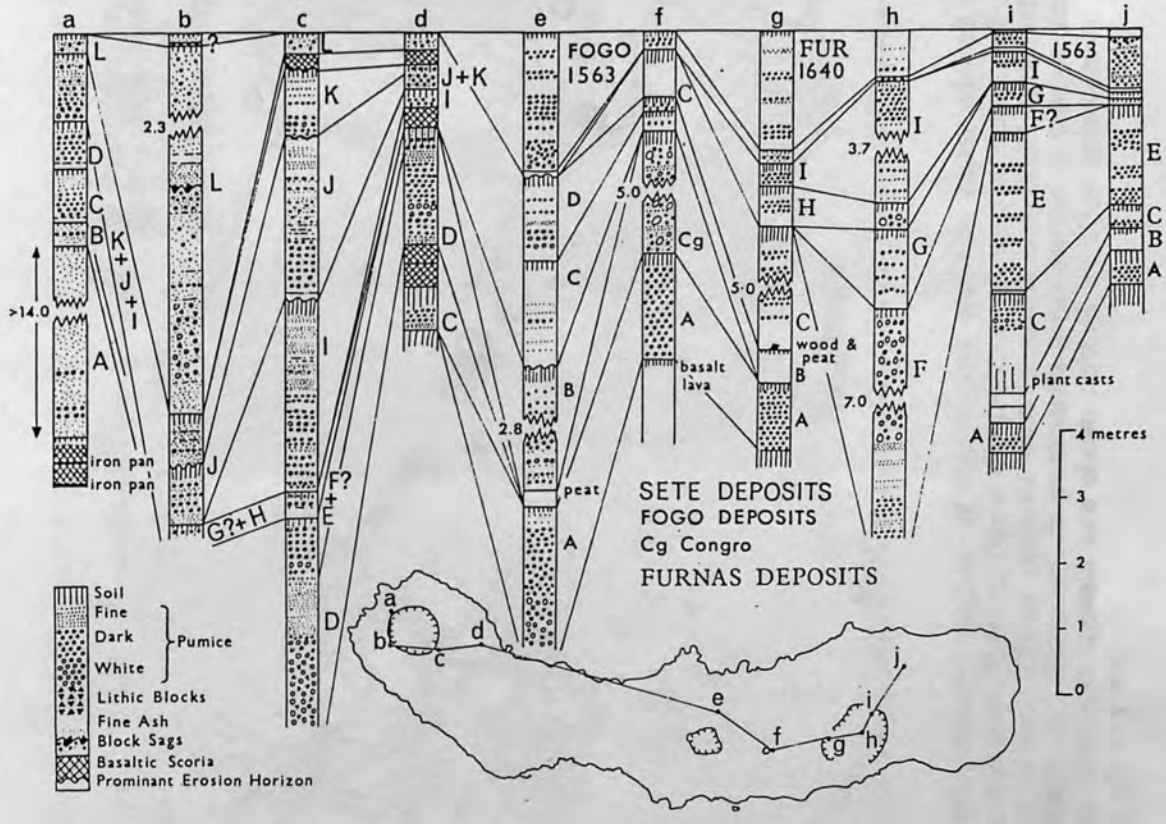

Fig. 3.2 Selected sections showing stratigraphic successions and summarizing depositional features of the pyroclastic fall deposits of the past 5,000 years. The three styles of lettering employed for the deposits identify the three source volcanoes. Locations of the sections are shown on the map at the bottom of the figure. From Booth et al. (1978)

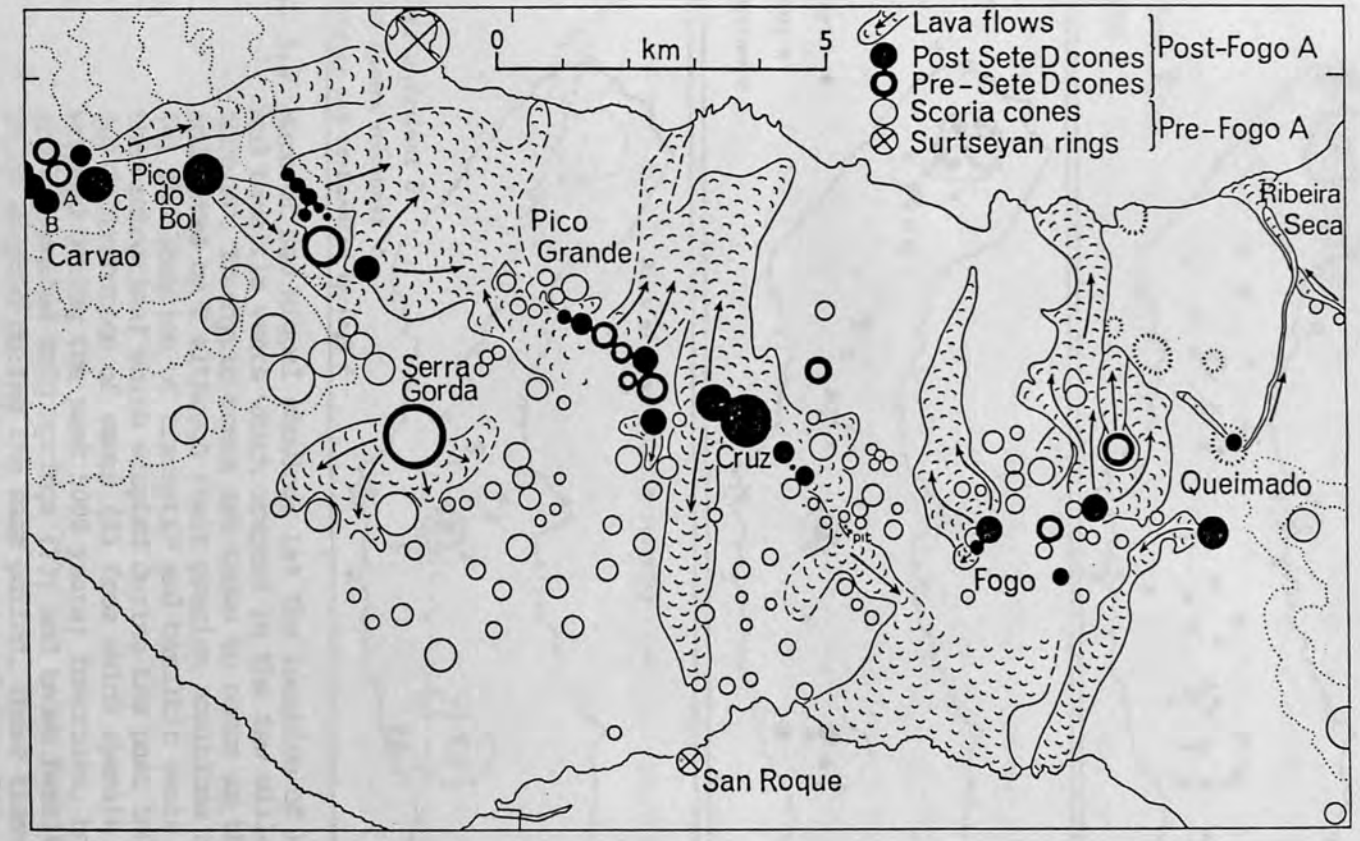

Fig. 3.3 Map of the 'waist' region of Sao Miguel and the lower slopes of Sete Cidades volcano showing the distribution of scoria cones and young basaltic lavas. Three ages of scoria cones are distinguished. The lavas shown are those which post-date Fogo member A pumice fall deposit. Contours 400m and upward are shown dotted at 100m intervals. From Booth et al. (1978).

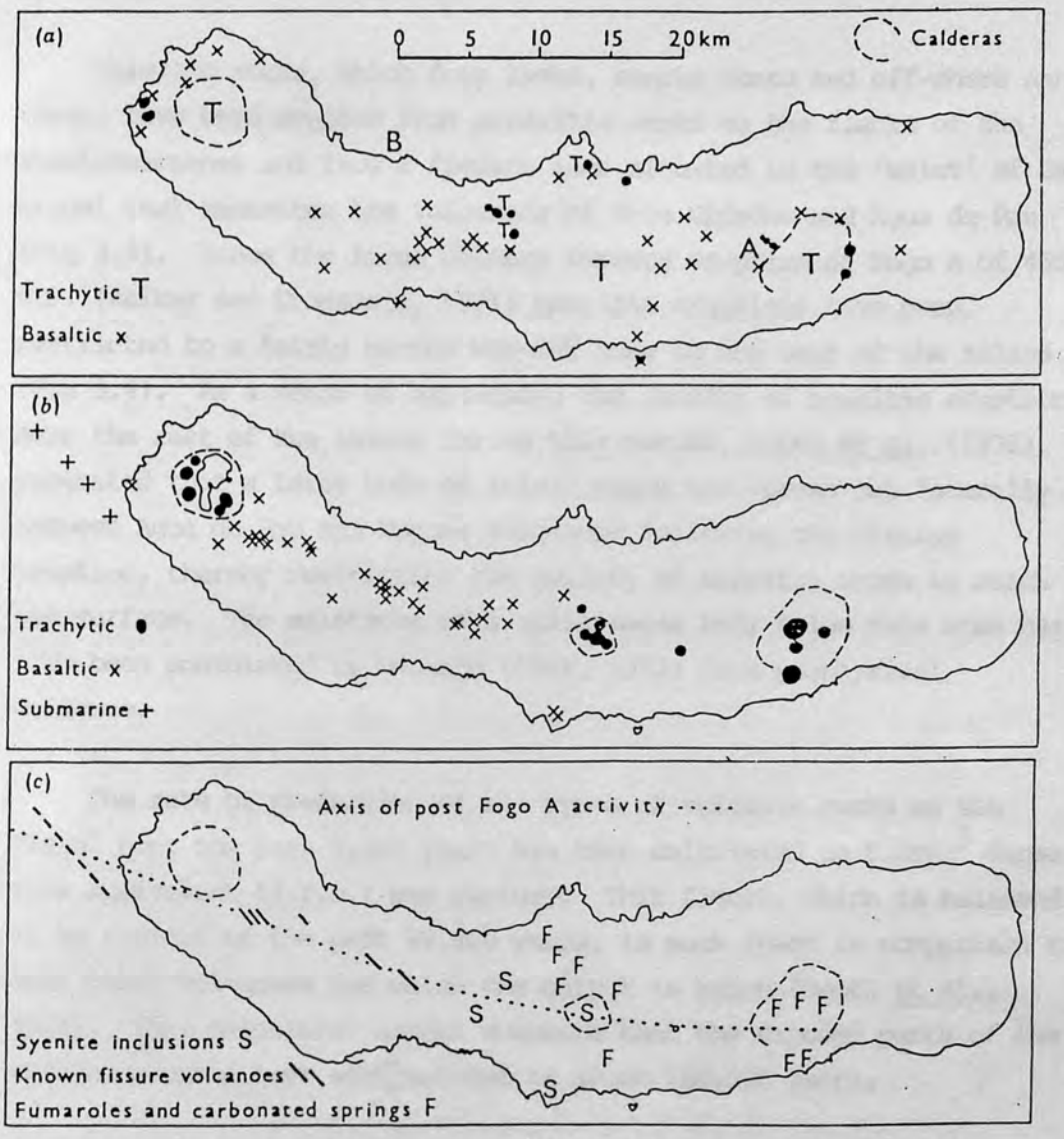

Fig. 3.4 Maps of Sao Miguel showing: (a) The location of known trachytic and basaltic vents which erupted in the few millennia before 5000 BP. Trachytic vents are known to occur in the areas indicated by T although their precise positions are uncertain. (b) The location of trachytic and basaltic vents (some of them submarine) which erupted during the past 5000 years. (c) Distribution of vents (S) from which syenite has been erupted during the past 5000 years; fumaroles, hot springs and carbonated cold springs (F); and known basaltic fissures which erupted during the same period. These fissures, and two of the calderas, delineate the axis of post Fogo A activity. The dashed lines indicate the present extent of the calderas. From Booth et al. (1978).

and some of the older pyroclastic rocks.

Basaltic rocks, which form lavas, scoria cones and off-shore ash rings, have been erupted from parasitic vents on the flanks of the stratovolcanoes and from a fissure zone situated in the 'waist' of Sao Miguel that separates the volcanoes of Sete Cidades and Agua de Pau (Fig 3.3). Since the large caldera forming eruption of Fogo A of 4550 B.P. (Walker and Croasdale, 1971) basaltic eruptions have been restricted to a fairly narrow WNW-ESE zone in the west of the island (Fig 3.4). As a means of explaining the paucity of basaltic eruptions over the rest of the island during this period, Booth et al. (1978) suggested that a large body of felsic magma had spread out laterally between Agua de Pau and Furnas volcanoes following the plinian eruption, thereby restricting the ability of basaltic magma to reach the surface. The existence of a salic magma body below this area has also been postulated by Machado (1966, 1973) from geophysical evidence.

The rate of production of all types of volcanic rocks on Sao Miguel over the past 5,000 years has been calculated as $0.09km^3$ dense rock equivalent (d.r.e.) per century. This figure, which is believed to be typical of the past 50,000 years, is much lower in comparison to most other volcanoes for which the output is known (Booth et al., 1978). This calculated output suggests that the exposed parts of the volcanoes could have accumulated in about 150,000 years.

3.3 CLASSIFICATION

Volcanic rocks from Sao Miguel belong to the alkali-basalt/trachyte suite being amongst the most alkalic and potassic in the Azores (Schminke and Weibel, 1972). Basalts and hawaiites, including those with minor Hy in the CIPW norm, lack a Ca-poor pyroxene, and have a typical alkalic phenocryst assemblage of olivine, titaniferous augite and plagioclase with accessory Fe-Ti oxides, Cr-spinel and pyrrhotite. The groundmass consists of the same minerals along with some alkali feldspar. In the plot of total alkalis versus

silica (Fig 1.2) all the basaltic analyses given here for Sao Miguel plot in the alkali-basalt field of Macdonald and Katsura (1964).

Basaltic rocks from Sao Miguel form two distinct groups in the projection of the normative Ne-Ol-Di-Qz tetrahedron (Fig 3.5). Recent basaltic eruptions (many are younger or contemporaneous with Fogo A) from Sete Cidades, Agua de Pau, Furnas and the 'waist' are moderately to strongly silica undersaturated containing between 1.6 - 8.1% normative Ne, the proportion of normative Ne increasing with differentiation from basalt to hawaiite. This group of lavas are here referred to as the Main Series. In contrast to the silica undersaturated trend shown by basalts and hawaiites of the Main Series, much older basaltic rocks associated with the extinct volcano of Povoacao have transitional compositions, forming a magma series (Povoacao Series) which trends towards more silica saturated compositions with differentiation. Fernandez (1980, 1982) has shown that basalts from the oldest part of the Nordeste Complex also have transitional compositions. The opposing trends towards more Ne and Hy normative compositions shown by derivatives from the Main Series and Povoacao Series respectively (Fig 3.5 and Fig 3.7) indicate the operation of the low pressure thermal divide in the system Ol-Di-Ne-Qz (Yoder and Tilley, 1962).

Differentiates on Sao Miguel range through intermediate compositions to trachytes and have been mostly classified here according to the Thornton-Tuttle differentiation index using the nomenclature outlined in Chapter 1 (Fig 3.6). As was shown quantitatively by Booth et al. (1978) there is a paucity of rocks of intermediate composition in the products of recent volcanism on Sao Miguel (Fig 3.6). This feature (Daly Gap) is important because of its implications for crystal fractionation models and will be referred to again in subsequent sections. With the exception of two samples containing normative corundum (AZ1544, AZ1204) the trachytes and syenites are either metaluminous or mildly peralkaline. In terms of silica saturation they are transitional in character having either minor Ne or Qz and/or Hy (Fig 3.7). The silica saturated peralkaline

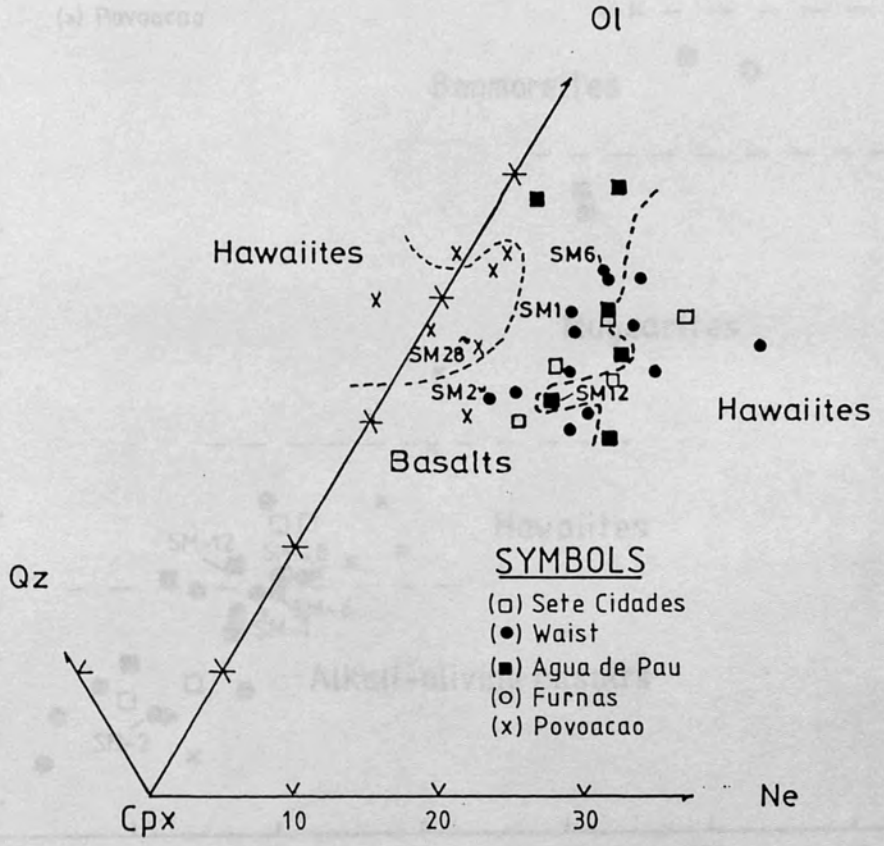

Fig. 3.5 Plot of Sao Miguel basalts and hawaiites (DI<45) in projection of normative tetrahedron of Yoder and Tilley (1962) Samples with prefix SM from White et al. (1979)

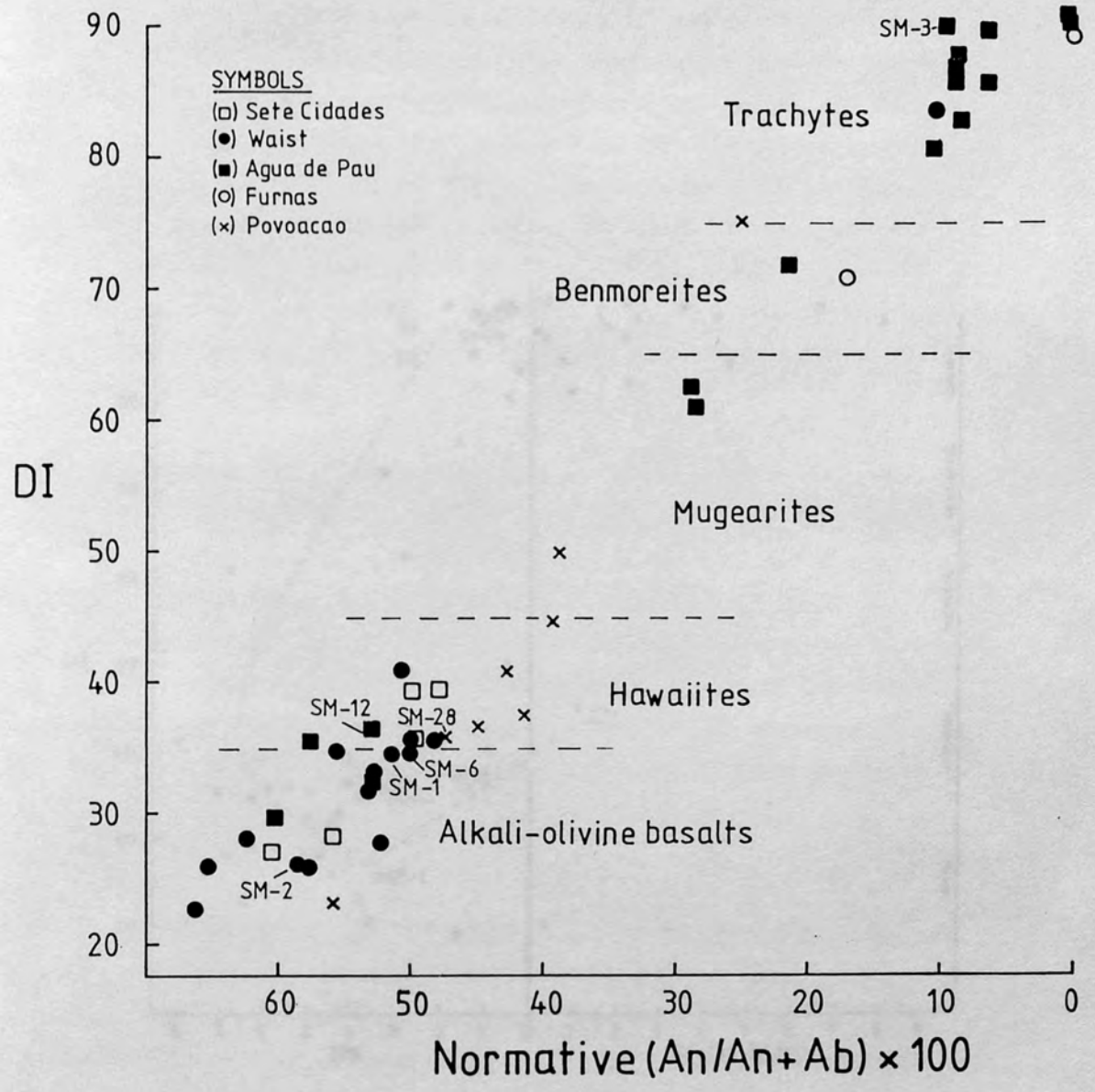

Fig. 3.6 Plot of Sao Miguel volcanic rocks in terms of their normative anorthite content and Differentiation Index (Thornton and Tuttle, 1960). Strongly accumulative and magma mixed samples not shown. Samples with prefix SM from White et al. (1979).

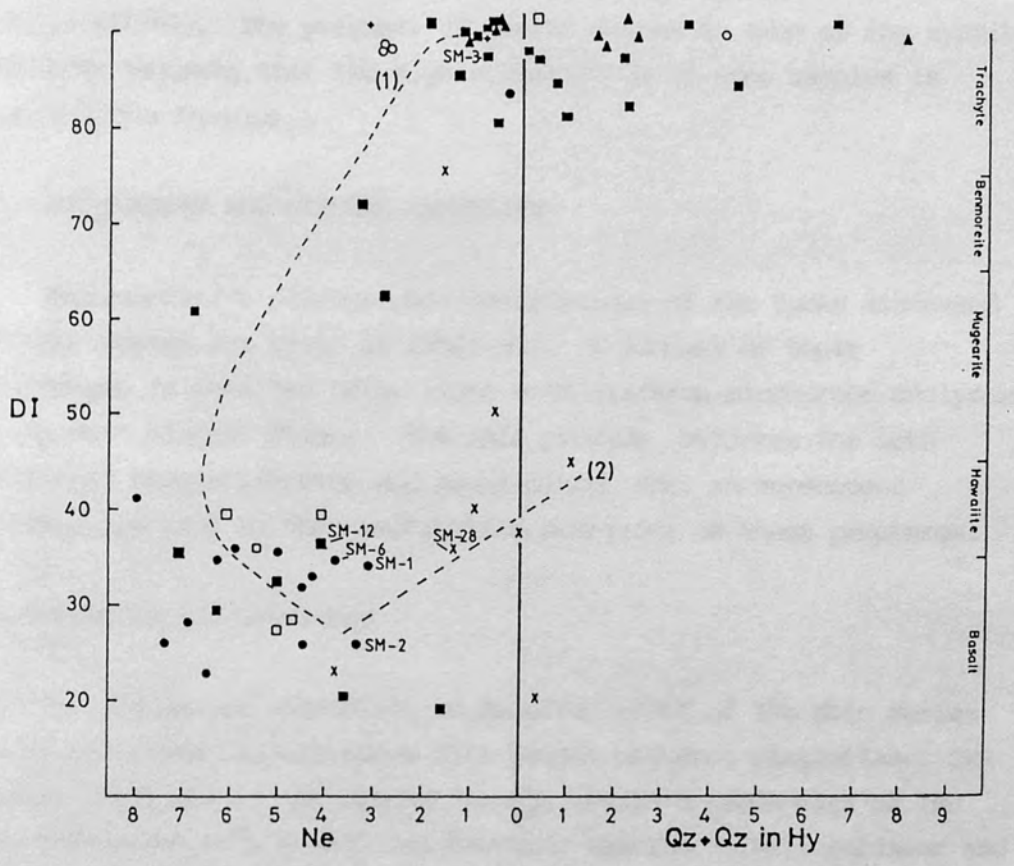

Fig. 3.7 Silica saturation versus the Differentiation Index (DI) for Sao Miguel rocks. Dashed lines are the inferred liquid-line of descent for the Main series (1) and the Povoacao series (2). Mixed magma samples not shown.
Symbols: triangles = syenite xenoliths; crosses = obsidian fiamme; other symbols as Fig. 3.6

types classify as comenditic trachytes under the scheme of Macdonald and Bailey (1973); however it is possible that the Hy-normative character of some of the samples of trachytic pumice deposits (eg AZ1544, AZ1678) is due to post-eruptive leaching of Na. In terms of their proportions of the normative components Qz, Ab, Or and Ne (Appendix 2) the trachytes have values near the thermal minimum on the Ab-Or join (Bowen and Tuttle, 1950). The syenites have similar normative compositions to the trachytes although the majority are silica saturated containing up to 7% normative quartz (sample AZ1204). The presence of quartz druses in some of the syenite xenoliths suggests that the high normative Qz of some samples is a sub-solidus feature.

3.4 PETROGRAPHY AND MINERAL CHEMISTRY

Representative petrographic descriptions of the rocks discussed in this chapter are given in Table 3.1. A summary of their petrography is detailed below along with electron-microprobe analyses of the main mineral phases. The data provide evidence for both fractional crystallization and magma-mixing and, in subsequent sections,are used in the quantitative modelling of these processes.

3.4.1 Basalts and hawaiites

The phenocryst assemblage of basaltic rocks of the Main Series mainly comprises clinopyroxene with lesser olivine, plagioclase, Cr-spinel, Fe-Ti oxides and pyrrhotite set within a groundmass of the same phases but with occasional biotite, apatite, alkali feldspar and interstitial glass. Basaltic rocks from Povoacao have a similar phenocryst assemblage although the proportion of ore and plagioclase is usually greater, notably in the hawaiites. Samples from both magma-series range from being near aphyric to highly porphyritic containing up to 40% phenocrysts in some ankaramitic lavas from Agua de Pau and Povoacao volcanoes (Table 3.2). Within the porphyritic lavas glomeroporphyritic texture is common. Olivine and clinopyroxene crystals range up to 5mm, particularly in the ankaramitic lavas, the

SETE CIDADES

Sample No.	Rock type	% pheno's	Phenocrysts	Groundmass
6SM	Alkali basalt lava	<5%	Olivine frequently showing glomeroporphyritic texture	Olivine,clinopyroxene, Fe-Ti oxides with some interstitial glass
AZ1704	Alkali basalt lava	<5%	Olivine and augite	Olivine,clinopyroxene, plagioclase and Fe-Ti oxides
AZ1883	Hawaiite lava	27%	Olivine,titaniferous augite plagioclase (An_{45}) and Fe-Ti oxides.	Olivine,clinopyroxene, plagioclase,Fe-Ti oxides and glass
AZ1034	Hawaiite lava	10%	Titaniferous augite,olivine, labradorite and Fe-Ti oxides Xenocrysts of andesine and kaersutite (with oxide rim)	Olivine,clinopyroxene, plagioclase and Fe-Ti oxides
AZ1168	Hawaiite ejected block	28%	Titaniferous augite, plagioclase (An_{64}),rare olivine,Fe-Ti oxide microphenocrysts	Olivine,clinopyroxene, plagioclase,Fe-Ti oxides,glass,sparse biotite and apatite
AZ1172	Trachyte dome	<5%	Alkali feldspar with microphenocrysts of Fe-Ti oxides	Trachytic texture consisting of alkali feldspar with minor sodic plagioclase,Fe-Ti oxides and apatite
			'WAIST'	
AZ1872	Alkali basalt lava	32%	Augite with titanifeous rims,olivine	Olivine,clinopyroxene, plagioclase,Fe-Ti oxides, glass
AZ1880	Alkali basalt lava	10%	Olivine,augite	Olivine,clinopyroxene, plagioclase and Fe-Ti oxides
AZ1322	Alkali basalt lava	13%	Olivine,titaniferous augite	Olivine,clinopyroxene plagioclase,Fe-Ti oxides, glass
2SM	Hy-normative pahoehoe lava	<5%	Olivine with rare resorbing plagioclase	Olivine,titaniferous augite,plagioclase, Fe-Ti oxides,glass
AZ1039	Alkali basalt lava	25%	Zoned titaniferous augite, sparse olivine and labradorite	Olivine,plagioclase, Fe-Ti oxides,glass
AZ1308	Alkali basalt lava	<5%	Olivine	Olivine,clinopyroxene, Fe-Ti oxides
AZ1874	Alkali basalt 'bomb'	10%	Olivine,titaniferous augite, occasional Fe-Ti oxides some showing resorption features	Olivine,clinopyroxene, plagioclase,Fe-Ti oxides
AZ1691	Alkali basalt lava	<5%	Titaniferous augite	Olivine,clinopyroxene plagioclase,Fe-Ti oxides
AZ1689	Hawaiite lava	<5%	Predominantly olivine (sometimes with oxidised rims), augite,rare microphenocrysts of plagioclase and Fe-Ti oxides	Olivine,clinopyroxene, plagioclase,Fe-Ti oxides, glass
AZ1315	Hawaiite lava	<5%	Olivine	Olivine,plagioclase, Fe-Ti oxides,glass
AZ1324	Hawaiite lava	<5%	Plagioclase,kaersutite (with oxidised rims),microphenocrysts of olivine and Fe-Ti oxides	Olivine,clinopyroxene, plagioclase,Fe-Ti oxides
AZ1879	Trachyte lava (1652 eruption)	<5%	Rare plagioclase	Alkali feldspar,plagioclase biotite (oxidised),glass

Table 3.1 Petrography of Sao Miguel volcanic rocks

AGUA DE PAU

Sample No.	Rock type	% pheno's	Phenocrysts	Groundmass
MA23/3	Alkali basalt lava	35%	Olivine,augite, sparse Fe-Ti oxides	Clinopyroxene,plagioclase, Fe-Ti oxides
AZ1017	Alkali basalt lava	*	Olivine,augite,sparse Fe-Ti oxides. Some of the phenocrysts are probably xenocrystic;olivines having deformation lamellae and the augite orienated exsolved rods	Clinopyroxene,plagioclase, Fe-Ti oxides
10SM	Alkali basalt lava	18%	Titaniferous augite,olivine, plagioclase (An_{60}),Fe-Ti oxides	Clinopyroxene,plagioclase, Fe-Ti oxides
AZ1027	Alkali basalt lava	10%	Titaniferous augite,partly oxidised olivine,sparse plagioclase	Olivine,clinopyroxene, plagioclase,Fe-Ti oxides, glass
36AP	Hawaiite lava	<5%	Olivine with microphenocrysts of augite (some with green cores),plagioclase,Fe-Ti oxides	Olivine,clinopyroxene, plagioclase,Fe-Ti oxides
AZ1705	Mixed intermediate lava	6%	Predominantly xenocrysts of strongly resorbing alkali feldspar and occasional rectangular pseudomorphs composed of Fe-Ti oxides (probably after biotite) Phenocrysts of titaniferous augite and Fe-Ti oxides	Titaniferous augite, plagioclase,Fe-Ti oxides, apatite
AZ1018	Mugearite lava	<5%	Rare phenocrysts of plagioclase (An_{33}) and Fe-Ti oxides	Plagioclase,augite,Fe-Ti oxides,sparse olivine and biotite
AZ1396	Benmoreite lava	<5%	Plagioclase (An_{38}),Fe-Ti oxides kaersutite (mostly altered to granular mass of Fe-Ti oxides)	Plagioclase,clinopyroxene, biotite,alkali feldspar
MA239	Mixed intermediate lava	11%	Augite with titaniferous rims, olivine,strongly resorbing anorthoclase and K-feldspar, Fe-Ti oxides,biotite (with oxide rims),green low Al-Ti clinopyroxene,apatite microphenocrysts	Trachytic texture consisting of plagioclase, alkali feldspar,clinopyroxene,Fe-Ti oxides, apatite
AZ1721(B)	Intermediate component of mixed lava	5%	Strongly resorbing anorthoclase and K-feldspar,titaniferous augite,olivine(with oxide rims), Fe-Ti oxides	Plagioclase,alkali feldspar, Fe-Ti oxides,partly devitrified glass
AZ1721(T)	Trachyte component of mixed lava	5%	Alkali feldspar,aegerine-augite Fe-Ti oxides,occasional titan-augite xenocrysts	Mostly devitrified brown glass with alkali feldspar and Fe-Ti oxides
AZ1672	Trachyte lava	24%	Mostly alkali feldspar showing glomeroporphyritic texture with aegerine-augite, biotite and Fe-Ti oxides	Alkali feldspar,glass
AZ1604	Trachyte lava	*	Alkali feldspar,clinopyroxene, Fe-Ti oxides,rectangular pseudomorphs of Fe-Ti oxides probably after biotite	Alkali feldspar,aegerine, alkali amphibole
AZ1202	Trachyte 'bomb'	*	Alkali feldspar,clinopyroxene, biotite(strongly oxidised), Fe-Ti oxides	Trachytic groundmass of alkali feldspar,clinopyroxene, alkali amphibole,Fe-Ti oxides, isotropic feldspathoid or analcite,secondary calcite
AZ1213	Trachyte lava	*	Alkali feldspar,clinopyroxene, biotite(strongly oxidised), Fe-Ti oxides,sparse olivine	Trachytic groundmass of alkali feldspar,blue-green alkali amphibole,Fe-Ti oxides

Table 3.1 continued

AGUA DE PAU (cont.)

Sample No.	Rock type	% pheno's	Phenocrysts	Groundmass
AZ1019 AZ1394 AZ1188 AZ1024	Trachyte air-fall pumice deposits	<5%	Alkali feldspar,biotite, light-green clinopyroxene, Fe-Ti oxides	Colourless to light brown glass,rich in microlites in places
AZ1544 AZ1323 AZ1377 AZ1378 AZ1149	Trachyte air-fall pumice deposits	<5%-10%	Alkali feldspar,biotite, light-medium green (aegerine-augite) clinopyroxene,Fe-Ti oxides.Xenocrysts of olivine, augite,titanaugite,anorthoclase, labradorite,Fe-Ti oxides	Colourless to dark brown glass, rich in microlites in places
			FURNAS	
AZ1014	Mixed intermediate lava	7%	Predominatly xenocrysts of strongly resorbing alkali feldspar,biotite (with oxide rims). Phenocrysts of titaniferous augite,forsteritic olivine, plagioclase and Fe-Ti oxides	Plagioclase,alkali feldspar clinopyroxene,Fe-Ti oxides
29SM	Mixed intermediate lava	6%	as above	as above
AZ1538 AZ1629 AZ1678 AZ1686	Trachytic air-fall pumice deposits	<5%	Alkali feldspar,biotite, aegerine-augite,Fe-Ti oxides	Colourless to light brown glass, rich in microlites in places
			POVOACAO	
AZ1126	Alkali basalt lava	37%	Olivine,augite,plagioclase, Fe-Ti oxides	Olivine,clinopyroxene, plagioclase,Fe-Ti oxides
AZ1129	Alkali basalt lava	39%	Olivine,augite with titaniferous rims,Fe-Ti oxides	Olivine,clinopyroxene, plagioclase,Fe-Ti oxides
AZ1138	Hawaiite lava	26%	Olivine (partly altered to iddingsite),titaniferous augite with microphenocrysts of labradorite and Fe-Ti oxides	Olivine,clinopyroxene, plagioclase,Fe-Ti oxides, sparse biotite
AZ1139	Hawaiite block from agglomerate	<5%	Andesine,augite,olivine, microphenocrysts of Fe-Ti oxides	Clinopyroxene,plagioclase Fe-Ti oxides,sparse biotite
AZ1131	Hawaiite lava	17%	Olivine,titaniferous augite, labradorite,Fe-Ti oxides	Clinopyroxene,plagioclase, Fe-Ti oxides
AZ1135	Hawaiite-Mugearite dyke	*	Olivine,titaniferous augite, plagioclase,Fe-Ti oxides	Olivine,clinopyroxene, plagioclase,Fe-Ti oxides
AZ1134	Mugearite dyke	11%	Labradorite,olivine showing partial alteration to iddingsite, Fe-Ti oxides	Plagioclase,olivine,titaniferous augite,Fe-Ti oxides, biotite,apatite
AZ1344	Trachyte lava	*	Alkali feldspar,plagioclase, Fe-Ti oxides,strongly resorbed and oxide rimmed amphibole and biotite	Trachytic groundmass of alkali feldspar with clinopyroxene,biotite and Fe-Ti oxides

* Petrographic description of GPL Walker; no hand specimen available

Table 3.1 continued

Volcano	SETE CIDADES			'WAIST'		AGUA DE PAU				FURNAS		POVOACAO				
Sa. No.	AZ1883 Basalt	AZ1168 Hawaiite	AZ1035 Kaersutitic nodule	AZ1872 Basalt	AZ1322 Basalt	HA23/3 Basalt	10SM Basalt	AZ1705 Intermediate (Mixed)	HA239 Intermediate (Mixed)	AZ1672 Trachyte	AZ1014 Intermediate (Mixed)	29SM Intermediate (Mixed)	AZ1126 Basalt	AZ1129 Basalt	AZ1138 Hawaiite	AZ1131 Hawaiite	AZ1134 Mugearite
Phenocrysts																	
Olivine	1.8			9.6	6.5	19.2	2.6		3.6		0.2	0.3	15.6	9.4	7.2	4.8	0.4
Clinopyoxene	15.3	13.3		20.9	6.0	16.1	7.7	0.6	3.0	0.4	0.9	1.2	21.3	20.2	13.0	4.3	
Amphibole			62.3														
Biotite								tr	tr	tr	tr	tr					
Plagioclase	8.8	11.9	26.2	1.0		tr	4.9	tr	tr		tr	tr	tr		4.8	7.6	10.0
Alkali feldspar								5.5	3.9	24.4	6.2	4.0					
Fe-Ti oxides	0.8	2.6	7.8			tr	2.6	0.2	0.3	tr	0.2	0.2	tr	0.8	1.2	0.4	0.9
Apatite		tr	3.7						tr								
TOTAL (Phenocrysts)	26.7	27.8	100	31.5	12.5	35.3	17.8	6.3	10.8	24.4	7.5	5.7	36.9	39.4	26.2	17.1	11.3
GROUNDMASS	73.3	72.2		68.5	87.5	64.7	82.2	93.7	89.2	75.6	92.5	94.3	63.1	60.6	73.8	82.9	88.7

Table 3.2 Percent modal analyses (on 1000 points over standard petrographic slide) of some porphyritic Sao Miguel rocks.

olivine occurring as colourless subhedra or euhedra although it occasionally shows evidence for being xenocrystic in the form of rounded crystals, oxidized rims or deformation lamellae. Other alteration is limited to the secondary development of iddingsite along rims and fractures of olivine crystals. Analysed compositions from two basalts range from Fo_{75-78} (Appendix 3); a study of the mineral chemistry of basaltic lavas from Agua de Pau volcano by Marriner et al, (1982) records olivine compositions between Fo_{76-90}.

In the basalts and hawaiites clinopyroxene occurs as subhedra or euhedra typically ranging from a light green to colourless diopsidic augite in the basalts to a buff-pink titaniferous augite in the hawaiites. Normal, reverse, oscillatory and hour-glass zoning are observed. Occasionally augites zone outwards to buff-pink titaniferous rims. Analyses of pyroxenes from the Main Series show that an increase of Ti and Al is accompanied by an increase in the Fe/Mg ratio (Fig 3.12a) indicating that the normal trend for basaltic pyroxenes, with magma evolution, is towards more titaniferous and aluminous compositions. This can be accounted for by the slightly more Ne-normative character of the hawaiites of the Main Series compared to the basalts (Fig 3.5); a decrease in $aSiO_2$ favouring Al and Ti enrichment in the pyroxenes (Verhoogen, 1962). Also noteworthy of the titaniferous augites is the trend towards the Ca apex in the Ca-Mg-Fe diagram (Fig 3.13b) indicating an increase in Ca-tschermak's component with increasing Al and Ti.

Subhedral to euhedral plagioclase phenocrysts occur in some Main Series and Povoacao Series hawaiites and occasional basalts. Crystals may show normal, reverse or oscillatory zoning with carlsbad and/or albite twinning being typical. Maximum extinction angles of sections perpendicular to the albite-twin lamellae suggest plagioclase compositions typically range from bytownite in basalts to andesine in the hawaiites. Plagioclase phenocrysts from one basalt and two hawaiites, analysed by electron-microprobe span from $An_{81}Ab_{18}Or_1$, to $An_{51}Ab_{40}Or_4$ (Fig 3.8). Some lavas contain plagioclase crystals showing evidence for resorption in the form of rounded corners and embayments (Plate 3.4). In one example from a hawaiite lava (AZ1034),

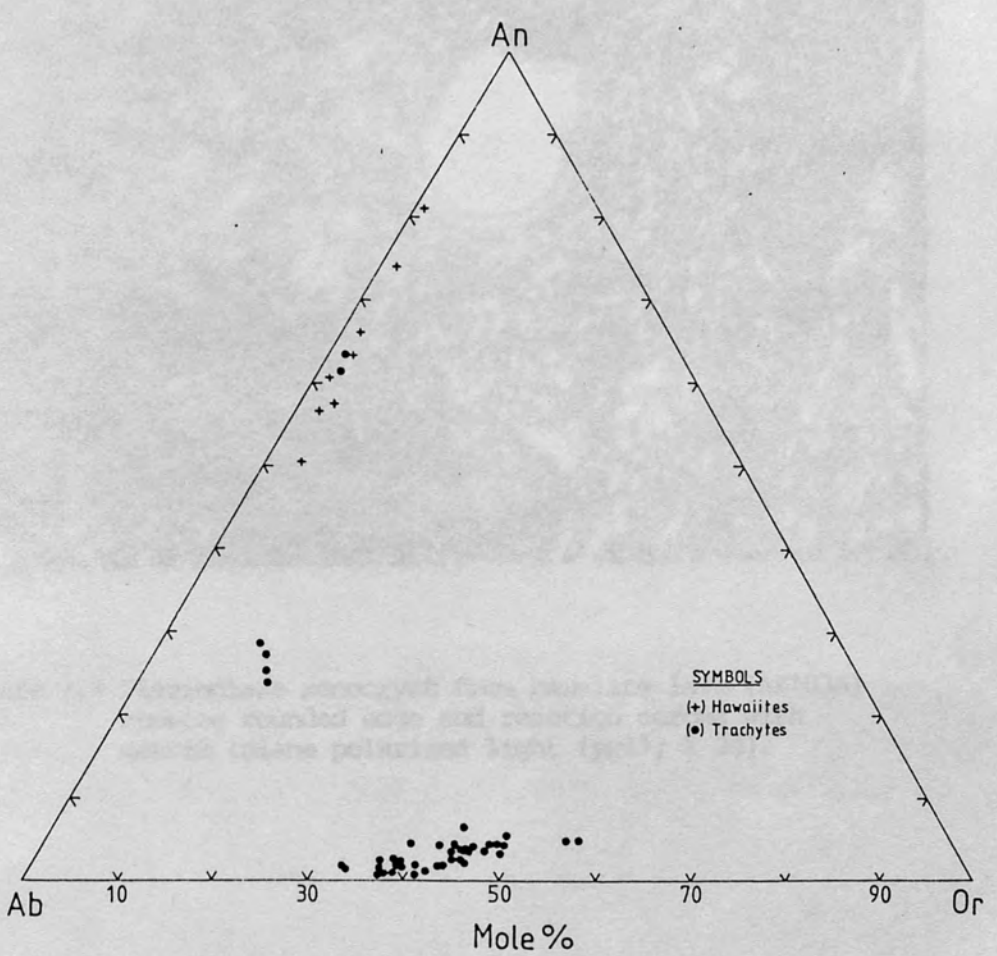

Fig. 3.8 Feldspar phenocryst compositions in Sao Miguel volcanic rocks.

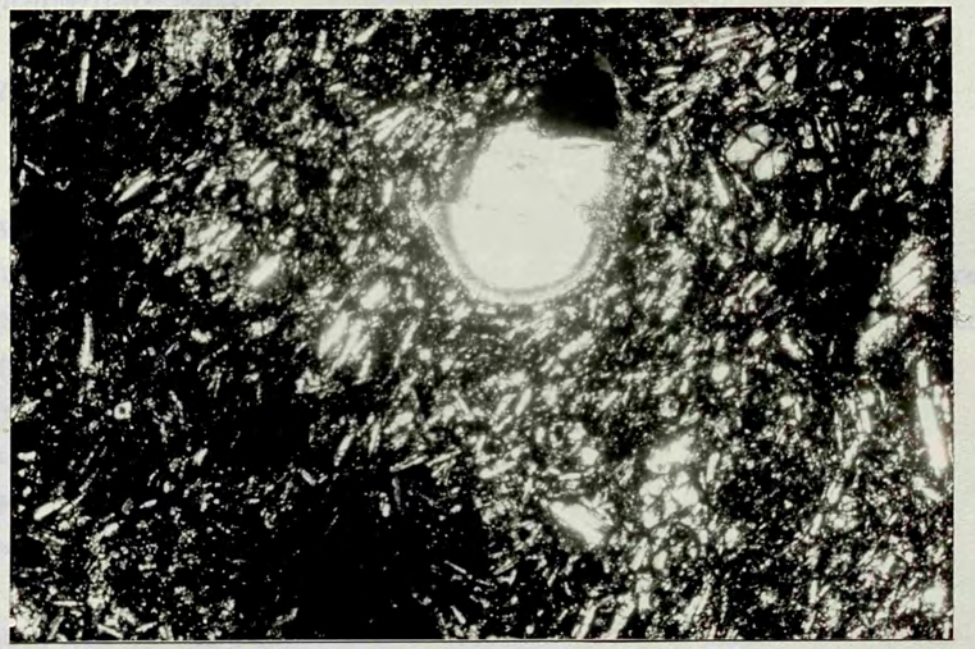

Plate 3.4 Plagioclase xenocryst from hawaiite lava (AZ1034) showing rounded edge and reaction corona with matrix (plane polarized light (ppl); X 30).

a plagioclase phenocryst has a partially resorbed core which has been preserved by an overgrowth of a more calcic composition. Analysis (Fig 3.9) shows the core to be andesine ($An_{43}Ab_{54}Or_3$) and the rim labradorite ($An_{61}Ab_{38}Or_1$), inferring that the former crystallized from an intermediate magma.

3.4.2 Intermediate compositions

Rocks of intermediate silica content (51-58 wt% SiO_2) are comparatively rare on Sao Miguel relative to those of basaltic or trachytic compositions (Fig 3.6). Mineralogically, however, they are extremely complex and are here divided into three groups according to their phenocryst content and occurrence. These consist of two dykes belonging to the Povoacao Series, three lavas belonging to the Main Series and lastly, six lavas from Agua de Pau and Furnas volcanoes which show both mineralogical and whole-rock compositional evidence for magma-mixing. Each group is described in turn below:

(a) Povoacao Series

The two mugearites belonging to the Povoacao series are only marginally more evolved than hawaiite, having a similar phenocryst assemblage of olivine, titaniferous augite, plagioclase (labradorite - andesine) and Fe-Ti oxides. Full descriptions are given in Table 3.1.

(b) Main Series

Only three lavas of intermediate composition show geochemical evidence for being simple differentiates from basaltic (Main Series) magma. Hand specimens were available for two of these lavas, a mugearite (AZ1018) and a benmoreite (AZ1396). Both are near-aphyric containing rare phenocrysts of andesine-feldspar and Fe-Ti oxides set in a groundmass of sodic plagioclase, augite, Fe-Ti oxides, alkali feldspar, olivine and biotite. The benmoreite contains phenocrysts of strongly pleochroic (pale brown-dark brown) kaersutitic amphibole, which are heavily altered to, and sometimes completely pseudomorphed

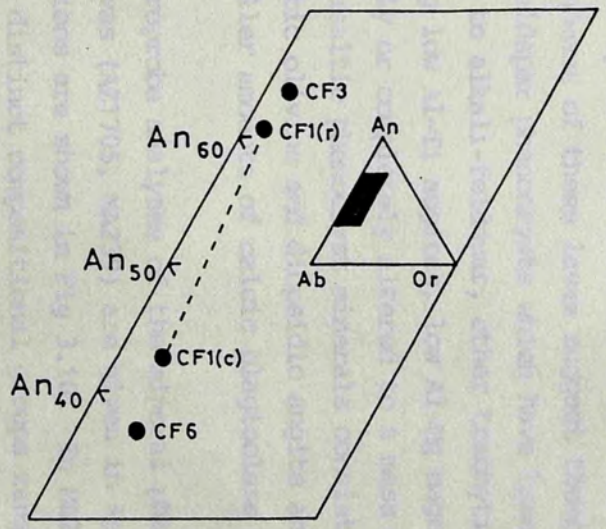

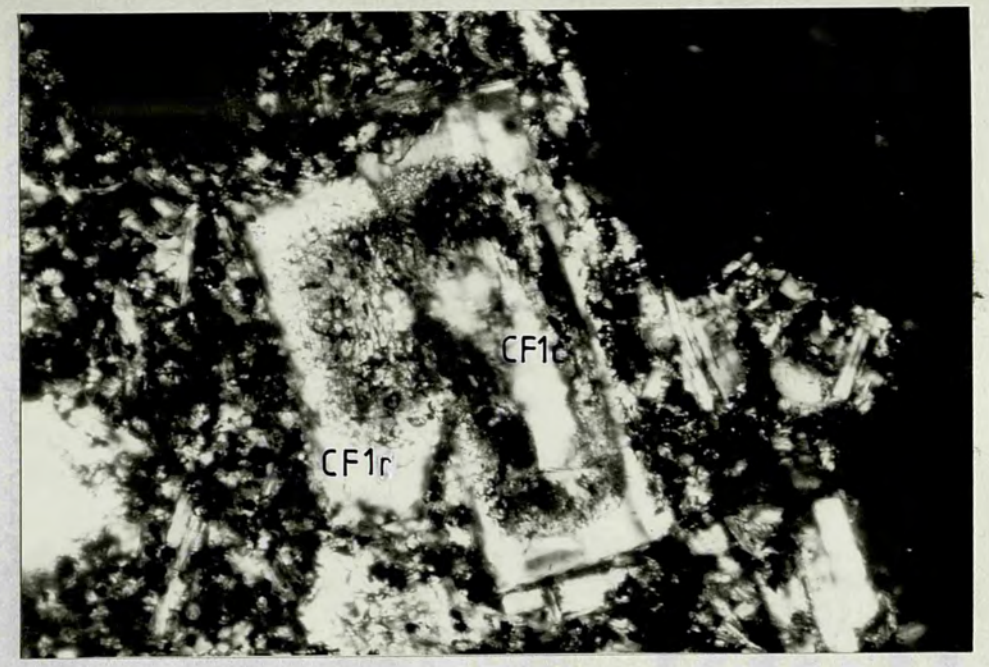

Fig. 3.9 Analyses of phenocryst (CF3), xenocryst (CF6) and labradorite overgrowth over partially resorbed andesine phenocryst in hawaiite lava (Sa. no. AZ1034). Note in the accompanying plate the reaction surface between the two components.

by, a fine grained mass of Fe-Ti oxides (Plate 3.5). The heavily altered nature of amphibole phenocrysts in the lavas contrasts strongly with their pristine condition in some pumice samples from Faial (eg Faial A, B and T; Chapter 2). As kaersutite is unstable below about 1.4 kbars H_2O (Le Maitre, 1969) this feature indicates that reasonable preservation is only likely to occur where PH_2O and T drop very rapidly from magmatic to atmospheric values (as is the case in explosive pumice-forming eruptions).

(c) Mixed intermediate lavas

Several intermediate lavas (sa no's MA239, AZ1197, AZ1705, AZ1721, AZ1014, 29SM) have been termed mixed because they show both mineralogical and whole-rock geochemical evidence for magma-mixing. In hand specimen they appear homogeneous with the exception of the lava from SE of Queimado on the NW flanks of the Agua de Pau volcano (sa no AZ1721) which consists of numerous small basic inclusions in a trachytic host (G.P.L. Walker pers comm.). The most prominent feature of these intermediate lavas/components is the presence of strongly resorbing crystals of cross-hatched and carlsbad twinned alkali feldspar often showing glomeroporphyritic texture (Plate 3.6) and which form up to 6% of the rock (Table 3.2). Feldspathic patches in the groundmass of these lavas suggest themselves as remnants of alkali-feldspar phenocrysts which have been completely resorbed. In addition to alkali-feldspar, other trachytic minerals are found including low Al-Ti augites, low Al-Mg magnetites and biotites which are partly or completely altered to a mass of Fe-Ti oxides (Plate 3.7). Basaltic phenocryst minerals consist predominantly of forsteritic olivine and diopsidic augite and/or titaniferous augite with smaller amounts of calcic plagioclase and high Al-Mg magnetites.

Microprobe analyses of the mineral phases found in two of these mixed lavas (AZ1705, MA239) are given in Appendix 3. Feldspar compositions are shown in Fig 3.10. In MA239 feldspar xenocrysts fall into two distinct compositional groups ranging between $An_8Ab_{55}Or_3$-$An_4Ab_{45}Or_{51}$ and $An_{33}Ab_{55}Or_{12}$-$An_{19}Ab_{59}Or_{22}$. In AZ1705 alkali feldspar

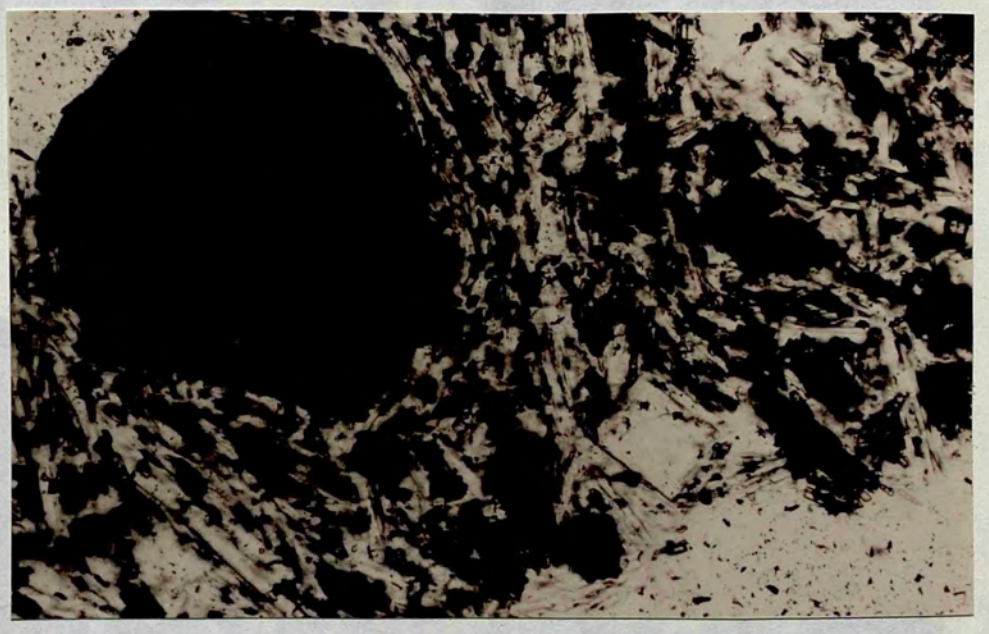

Plate 3.5 Intermediate lava (AZ1396) showing kaersutite phenocryst heavily altered to a fine-grained mass of Fe-Ti oxides (ppl; X 180).

(a)

(b)

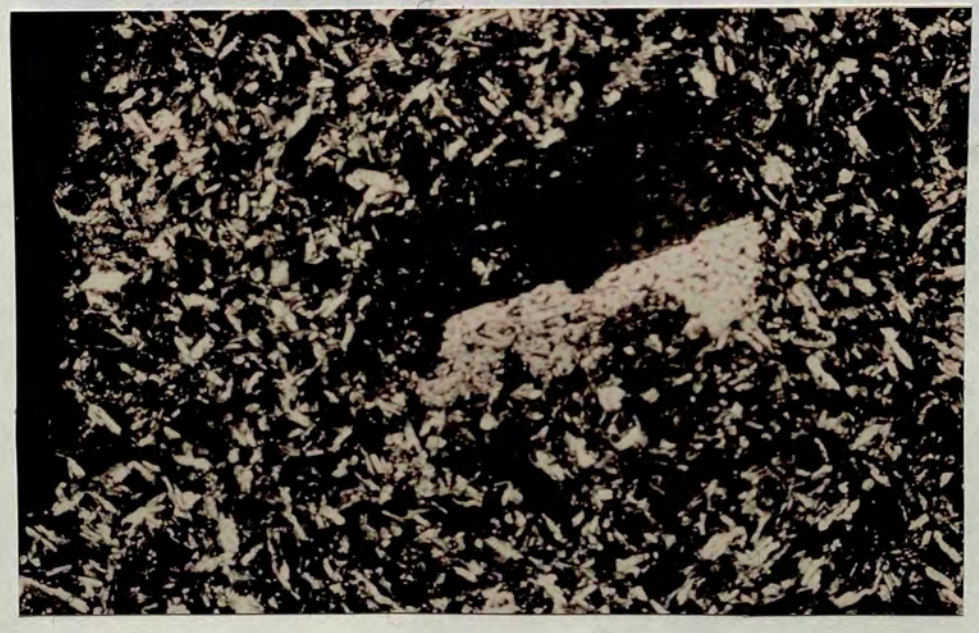

Plate 3.6 Anorthoclase and K-feldspar xenocrysts in mixed lavas of intermediate composition showing resorption textures and (a) cross-hatched twinning (anorthoclase in AZ1014), (b) carlsbad twinning (K-feldspar in AZ1705). (xpl; X 45). (c) Resorbing 'clump' of feldspars in AZ1705 (xpl; X45).

(c)

Plate 3.6 continued.

Plate 3.7 Intermediate lava (MA239) containing both trachytic and basaltic phenocryst assemblages. Note xenocrysts of biotite (partly altered to Fe-Ti oxides), titanaugite (lower middle) and forsteritic olivine (upper left hand corner). (xpl; X 45).

xenocrysts ($An_{13}Ab_{47}Or_{38}$-$An_5Ab_{31}Or_{64}$) coexist with labradorite feldspar ($An_{57}Ab_{39}Or_4$-$An_{51}Ab_{46}Or_4$). It is particularly noteworthy that the K-feldspars in these mixed lavas have an anomalously large anorthite content (Fig 3.10), which is presumably a consequence of their incorporation into hotter more basic magma. Pyroxene compositions from AZ1705 and MA239 are shown in Fig 3.12. The diopsidic augites from MA239, which are the least evolved of all analysed pyroxenes from Sao Miguel (including those from basaltic samples), are associated with olivines having compositions between Fo_{83-89}. Likewise in AZ1705 there are basaltic, titaniferous augites containing up to 3.5 wt% TiO_2. The light green, low Al-Ti augites which occur in both MA239 and AZ1705 have compositions similar to the pyroxene phenocrysts found in the trachytes. The basaltic and trachytic affinities of the different pyroxenes along with their fractionation trends are indicated on Fig 3.12.

3.4.3 Trachytes

The phenocryst assemblage of the trachytes mainly consists of alkali feldspar with ubiquitous but minor clinopyroxene, biotite and Fe-Ti oxides. Microphenocrysts of apatite and small oval blobs of pyrrhotite occur as accessory phases, most frequently as inclusions in other minerals. The groundmass of the lavas is alkali feldspar showing typical trachytic texture (Plate 3.8) with minor aegerine-augite, Fe-Ti oxides and occasional alkali amphibole and feldspathoid or analcite. Secondary calcite was observed in one trachyte lava thin-section (AZ1202). Trachytic pumice samples have a glassy to partly devitrified matrix, the glass varying from colourless to dark brown (Plate 3.9). Phenocryst contents of the pumice clasts do not usually exceed 5-10%, the lavas, however are generally more porphyritic containing up to 25% phenocrysts.

Alkali feldspar phenocrysts in seven pumice deposits, analysed by electron-microprobe, ranged between $An_1Ab_{66}Or_{33}$-$An_5Ab_{39}Or_{56}$ (Fig 3.8), compositions becoming more sodic with magma evolution and trending towards the low pressure minimum liquidus temperature on the Ab-Or join (Bowen and Tuttle, 1950). Also occurring in the trachytic pumice

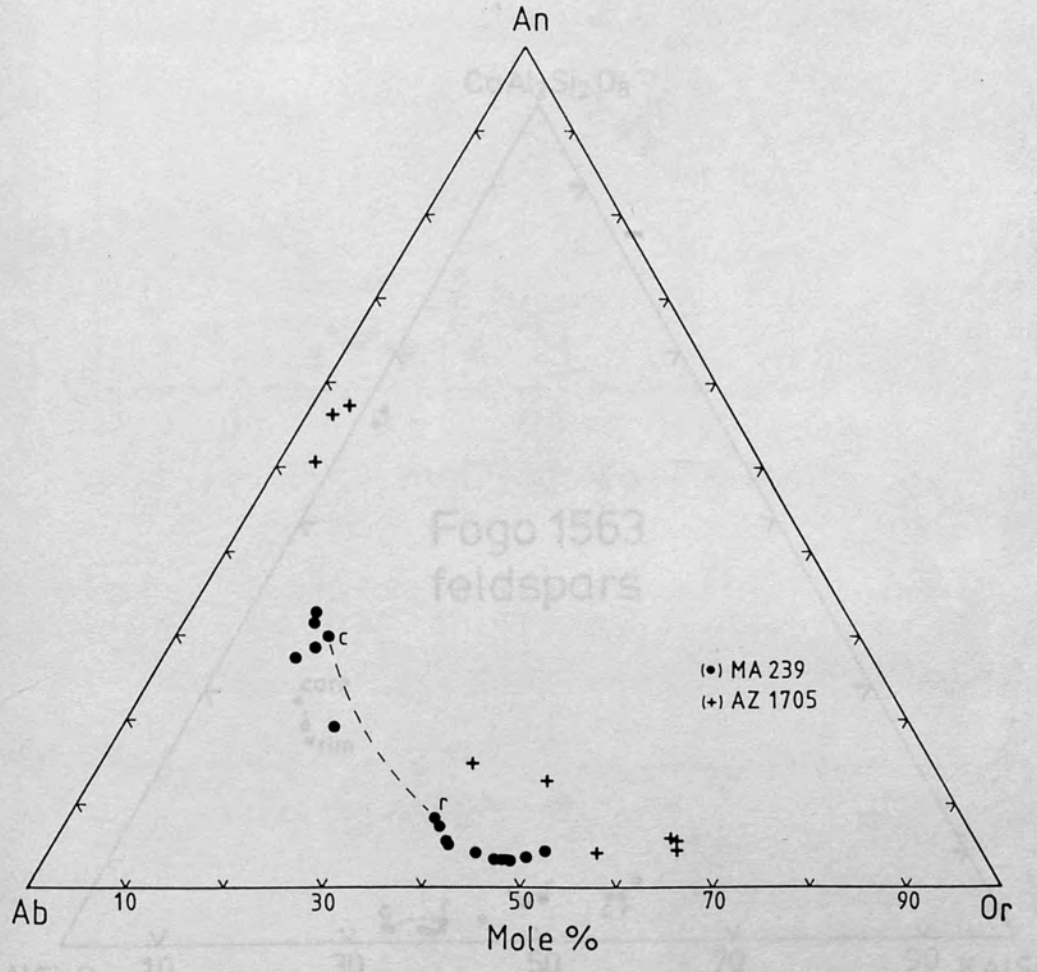

Fig. 3.10 Feldspar compositions in two mixed-intermediate lavas from Agua de Pau.

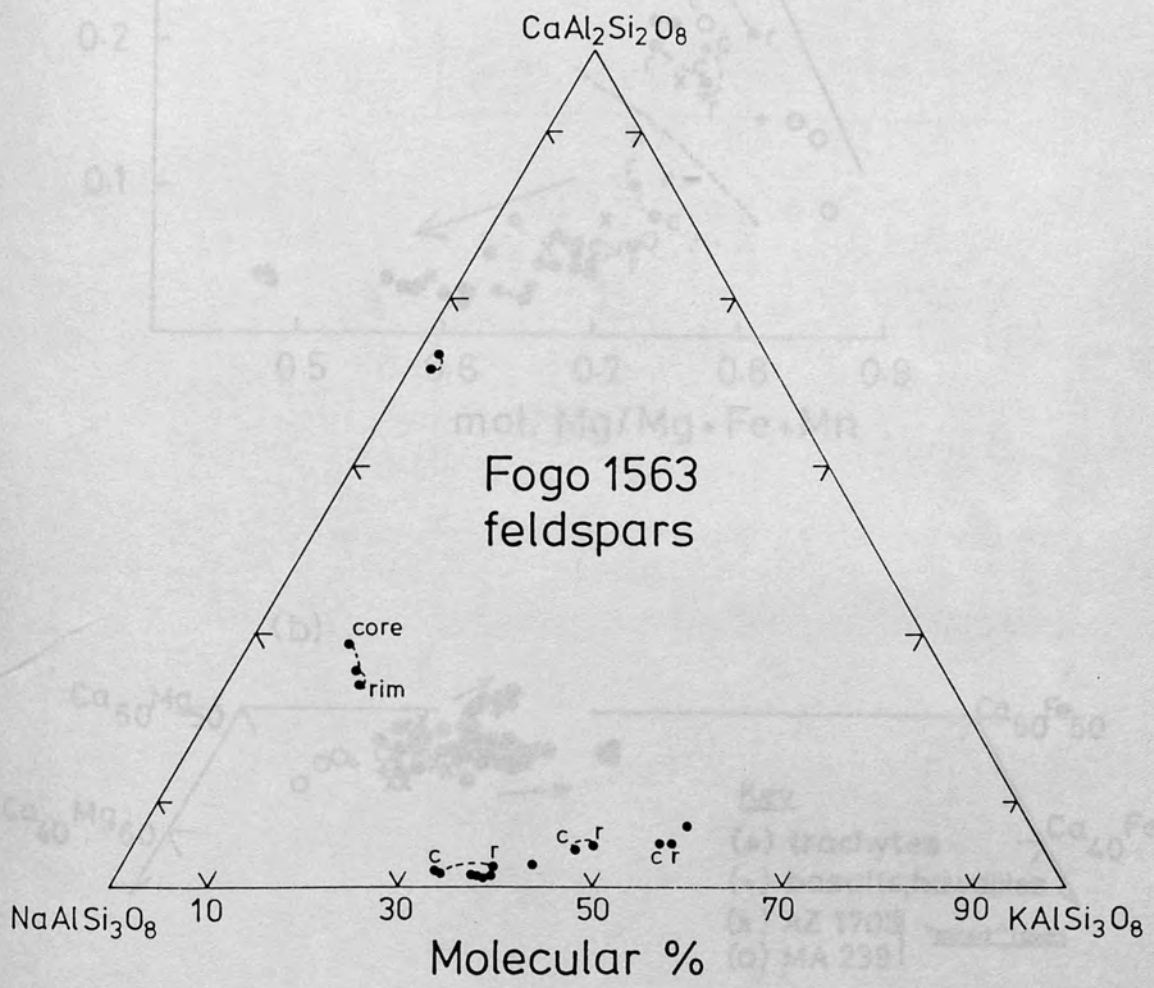

Fig. 3.11 Feldspar compositions in trachytic air fall pumice deposit Fogo 1563.

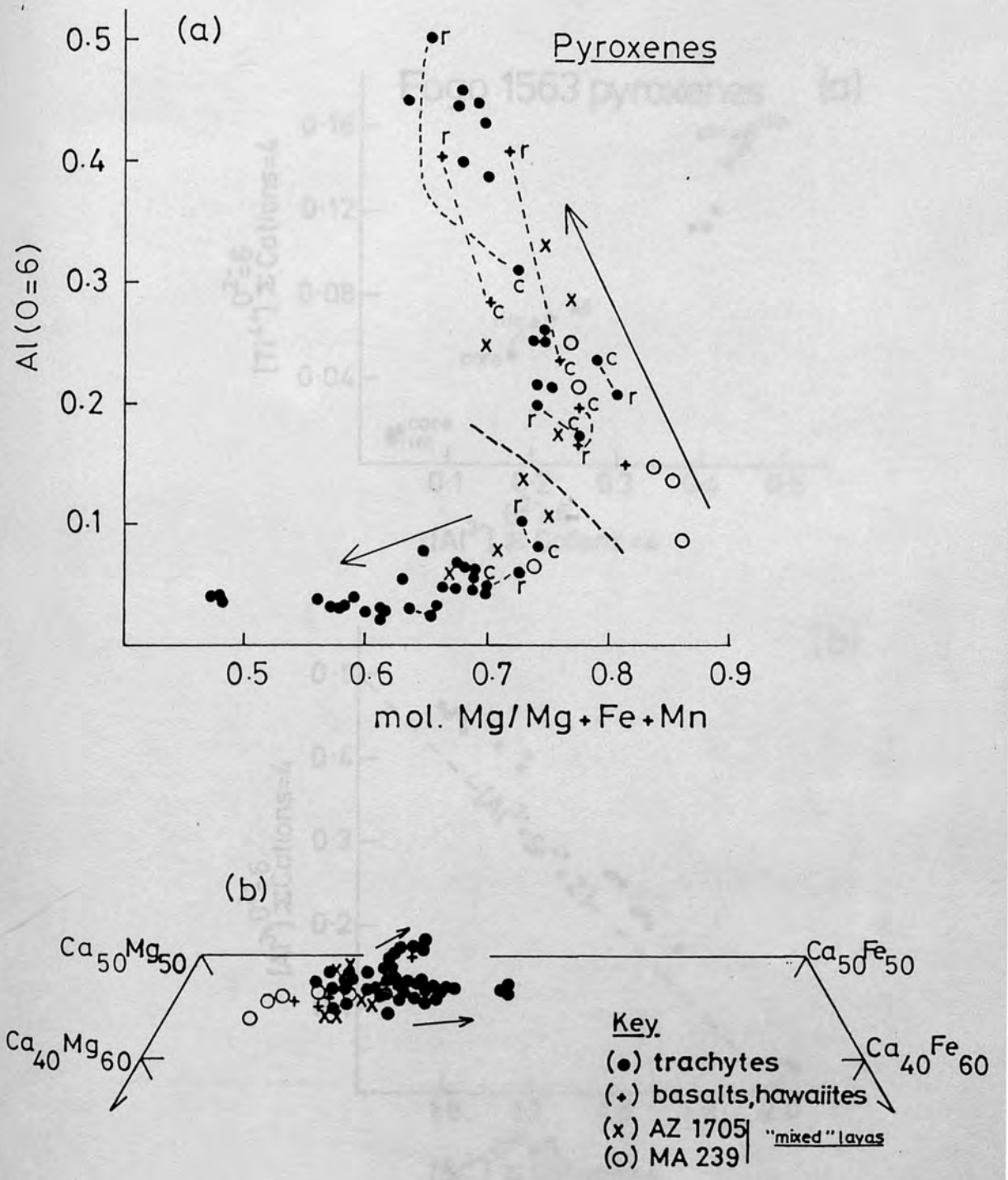

Fig. 3.12 Pyroxene compositions in terms of (a) Al and mol.Mg/Mg+Fe+Mn ratio (b) Ca, Fe and Mg. Arrows show deduced fractionation trends. The heavy dashed line in (a) separates the opposing trends of equilibrium basaltic and trachytic pyroxenes. The zoning relationships and whole rock compositions indicate that basaltic pyroxenes show a decrease in the Mg/Mg+Fe+Mn ratio and an increase in Al with differentiation. Note the presence of 'basaltic' pyroxene compositions in some trachytic pyroclastic deposits.

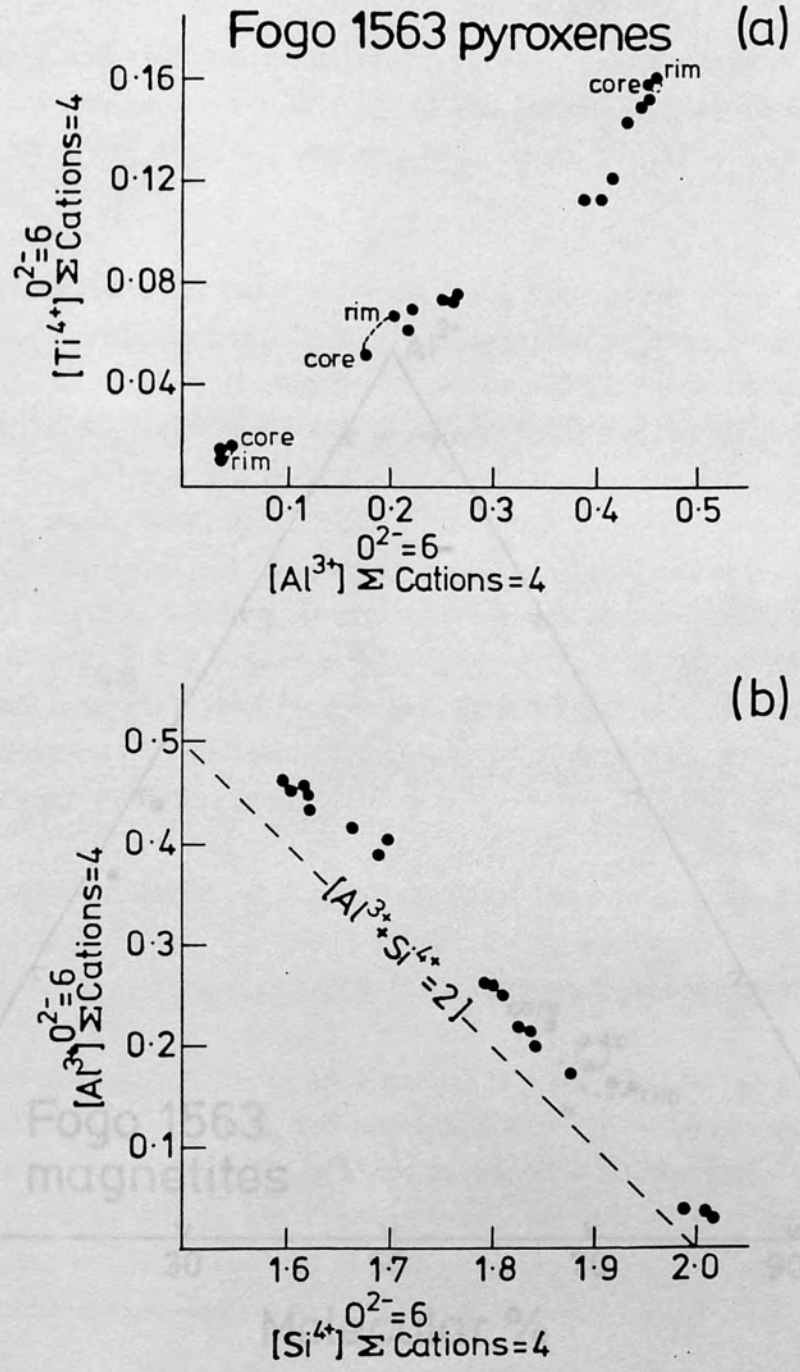

Fig. 3.13 Pyroxene compositions from Fogo 1563 in terms of (a) Al and Ti. (b) Si and Al.

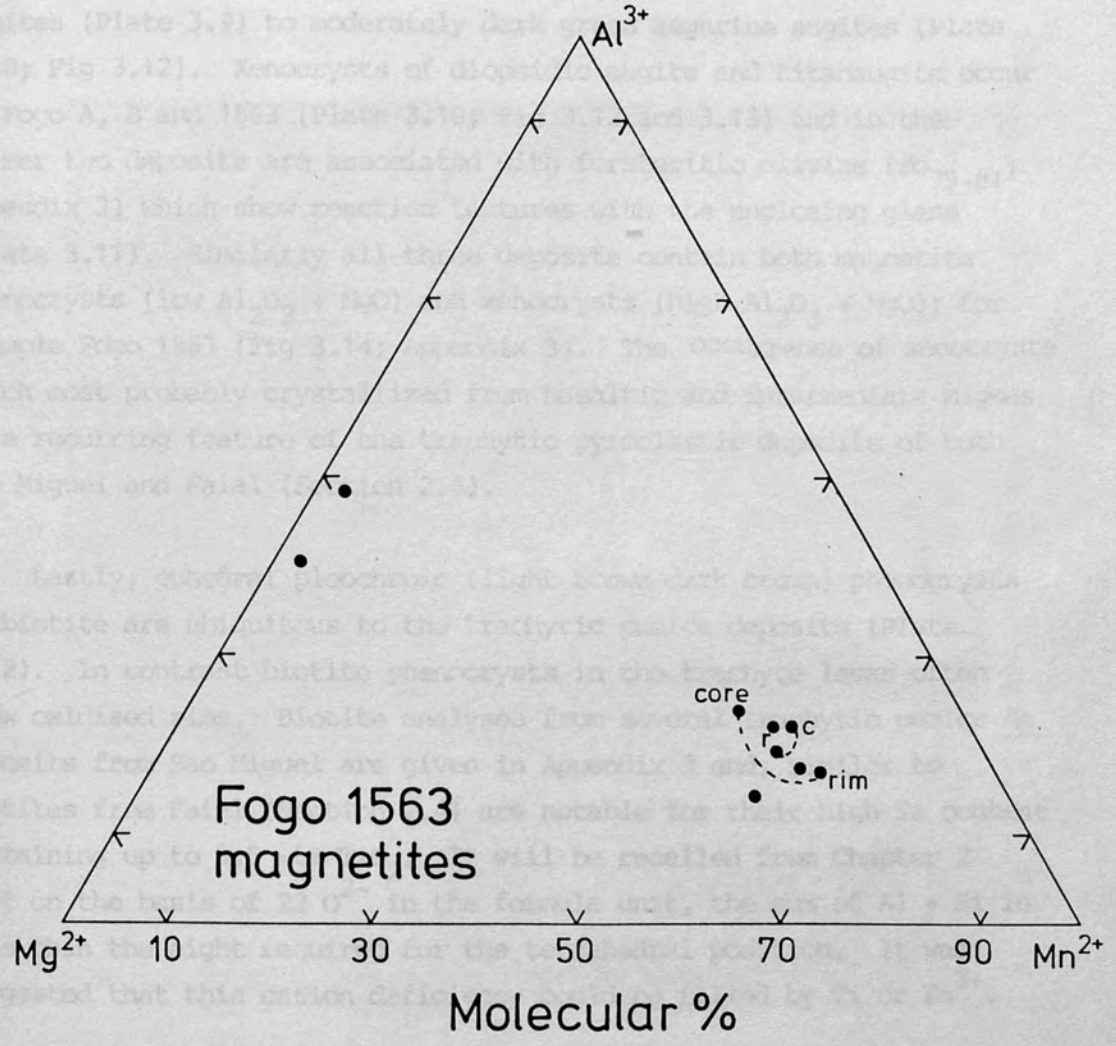

Fig. 3.14 Titanomagnetites from Fogo 1563 shown in terms of their minor elements Al, Mg and Mn.

deposits Fogo A, B and 1563 are resorbing crystals of anorthoclase and calcic plagioclase analysed compositions in the latter deposit ranging between $An_{29}Ab_{61}Or_{10}$-$An_{24}Ab_{62}Or_{14}$ and $An_{63}Ab_{35}Or_{2}$-$An_{62}Ab_{36}Or_{2}$ respectively (Fig 3.11).

Pyroxene phenocrysts in the trachytes range from green low Al-Ti augites (Plate 3.9) to moderately dark green aegerine augites (Plate 3.10; Fig 3.12). Xenocrysts of diopsidic augite and titanaugite occur in Fogo A, B and 1563 (Plate 3.10; Fig 3.12 and 3.13) and in the former two deposits are associated with forsteritic olivine (Fo_{79-81}; Appendix 3) which show reaction textures with the enclosing glass (Plate 3.11). Similarly all three deposits contain both magnetite phenocrysts (low Al_2O_3 + MgO) and xenocrysts (high Al_2O_3 + MgO); for example Fogo 1563 (Fig 3.14; Appendix 3). The occurrence of xenocrysts which most probably crystallized from basaltic and intermediate magmas is a recurring feature of the trachytic pyroclastic deposits of both Sao Miguel and Faial (Section 2.4).

Lastly, euhedral pleochroic (light brown-dark brown) phenocrysts of biotite are ubiquitous to the trachytic pumice deposits (Plate 3.12). In contrast biotite phenocrysts in the trachyte lavas often show oxidised rims. Biotite analyses from several trachytic pumice deposits from Sao Miguel are given in Appendix 3 and, similar to biotites from Faial (Section 2.4) are notable for their high Ti content containing up to 9.5 wt% TiO_2. It will be recalled from Chapter 2 that on the basis of 22 O^{2-} in the formula unit, the sum of Al + Si is less than the eight required for the tetrahedral position. It was suggested that this cation deficiency could be filled by Ti or Fe^{3+}.

3.4.4 Xenoliths

(a) Syenites

Syenite xenoliths up to several tens of centimetres in diameter are common in the Fogo A and Fogo 1563 pumice deposits erupted from Agua de Pau volcano (Booth et al., 1978). Similar nodules also occur in

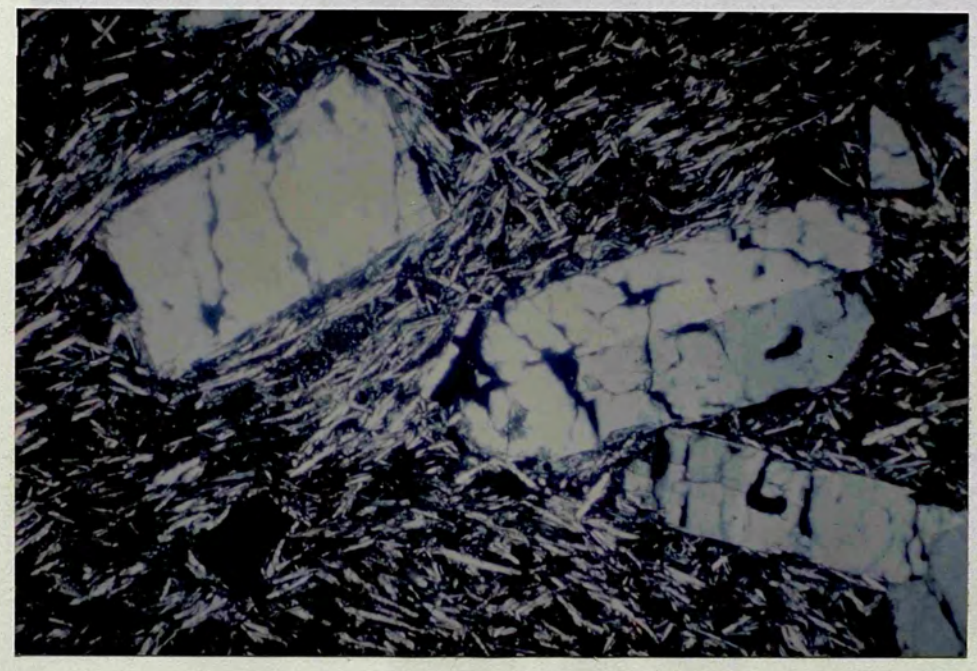

Plate 3.8 Highly porphyritic trachyte lava (AZ1672) showing Carlsbad-twinned alkali feldspar and typical trachytic texture. (xpl; X 30).

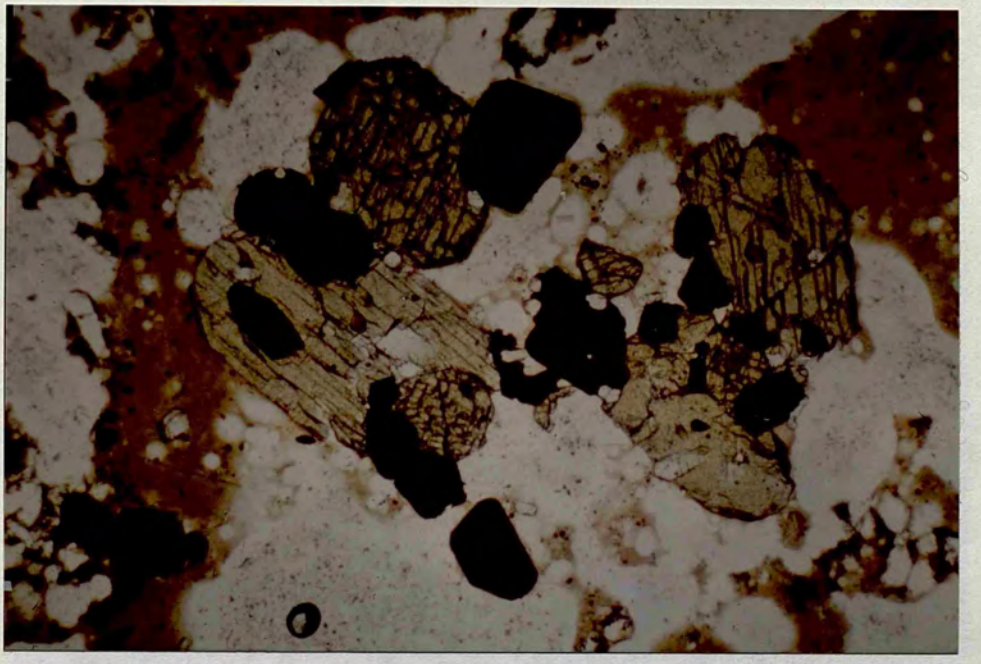

Plate 3.9 Trachytic pumice deposit (Fogo A) with brown glass and phenocrysts of Fe-Ti oxides, light-green augite and apatite in glomeroporphyritic association. (ppl; X 30).

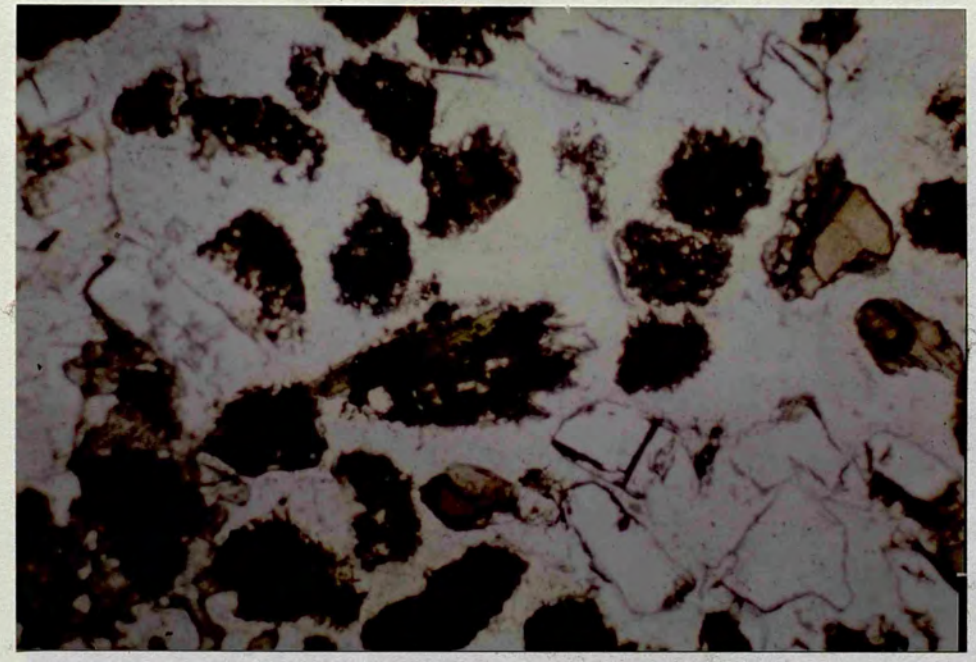

Plate 3.10 Mineral concentrate ('floater') from trachytic pumice deposit Fogo 1563 showing feldspar, dark-green aegerine augite, buff-coloured titanaugite and dark coloured (partly devitrified) glass. (ppl; X 30).

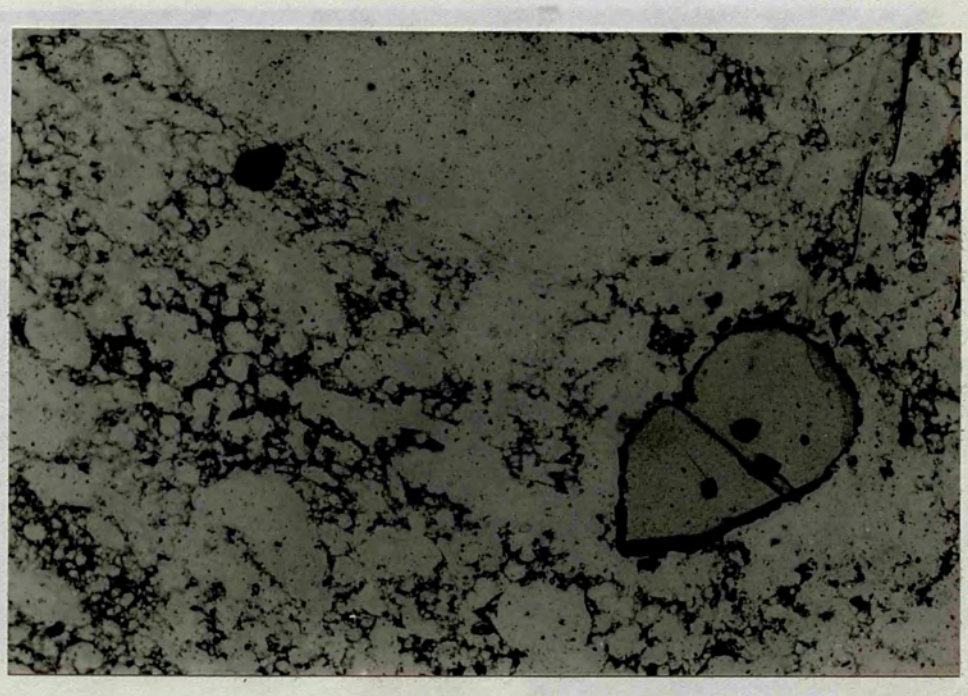

Plate 3.11 Resorbing xenocryst of forsteritic olivine in Fogo A (AZ1377). (xpl; X 30).

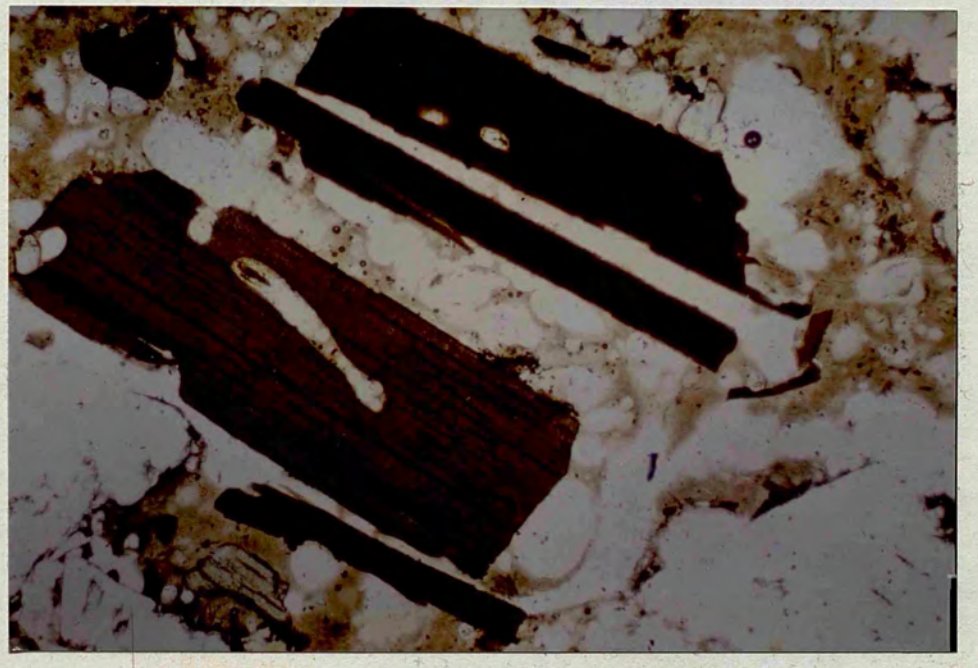

Plate 3.12 Euhedral phenocrysts of biotite in Fogo A (ppl; X 30).

several of the older pumice deposits on Sao Miguel. The petrology of syenite nodules from Agua de Pau has been studied by Cann, 1967 (and references cited therein). Nine syenite xenoliths have been analysed here to allow comparison with the volcanic rocks with which they are associated. A detailed petrological study was not intended and only a brief resume of their petrography is given below.

In hand specimen fresh blocks show white platy alkali feldspar crystals and brilliant black striated prisms of amphibole. Drusy cavities are abundant and contain well terminated crystals of feldspar, amphibole and quartz. In thin section the feldspar varies from an optically homogeneous sanidine, showing carlsbad twinning, to well-developed perthitic intergrowths. The amphibole, sometimes containing cores of aegerine-augite or fayalite, shows intense absorption and considerable pleochroism from yellow to a near opaque dark-brown. Microprobe analysis shows it to be arfvedsonite (Appendix 3).

Aegerine prisms also occur sometimes in association with the rims of arfvedsonite crystals. Other accessory phases include Fe-Ti oxides, quartz, apatite, biotite and zircon. Cann (1967) also found dalyite and astrophyllite (at the apparent expense of biotite and zircon) in the most chemically evolved of the syenites in his study, although neither of these were present in the samples examined here.

(b) Amphibole-plagioclase nodule

Coarse-grained inclusions of an amphibole and plagioclase bearing rock up to 30cm in size are extremely abundant in the Ponta da Ferraria hawaiite lava. Hand specimen samples (AZ1035) show a pronounced layering of feldspar and amphibole on the scale of several millimetres. The amphibole is strongly pleochroic (light-dark brown) occuring as subhedral to anhedral crystals up to 5mm in length forming some 62% of the rock; microprobe analysis showing it to be kaersutite (Appendix 3). The remainder of the mineral assemblage consists of plagioclase (26%), magnetite (8%), apatite (4%) and

numerous small inclusions of pyrrhotite (<400 μm). Plagioclase occurs as subhedra to euhedra up to 3mm in length, occasionally showing uneven extinction, compositions ranging from $An_{73}Ab_{26}Or_1$ - $An_{47}Ab_{50}Or_3$. Although zoning patterns are complex, core compositions tend to be more calcic (Appendix 3). Magnetite occurs as anhedral-subhedral crystals up to 1mm in diameter. Apatite occurs as colourless subhedral-euhedral prisms up to 0.75mm in length.

3.5 WHOLE-ROCK CHEMISTRY

Seventy-seven new major and trace element analyses, with CIPW norms, of lavas, pyroclastics and xenoliths (mostly syenites) from Sete Cidades, Agua de Pau, Furnas, Povoacao and the 'waist' are given in Appendix 2. Norms were calculated using standardised Fe_2O_3/FeO ratios as detailed in Chapter 2. Analyses of separates of the two components of the mixed lava (sample AZ1721) from the NW flanks of Agua de Pau are given in Table 3.3. All the data are discussed below with the aid of variation diagrams.

3.5.1 Triangular variation diagrams

Fig 3.15 is a triangular plot of Na_2O, K_2O and CaO and illustrates the comparatively potassic nature of basaltic rocks from Sao Miguel, the $Na_2O/Na_2O + K_2O$ ratio varying between 0.5 and 0.7, contrasting with more sodic islands such as Terceria and Faial (shown for comparison in Fig 3.15). On Sao Miguel the Na/K ratio decreases with fractionation reaching low values in rocks of intermediate and trachytic compositions but increasing to maxima in the most evolved (peralkaline) trachytes and syenites. The AFM plot (Fig 3.16) shows a small to moderate iron and strong alkali enrichment from basaltic to intermediate compositions, a feature characteristic of many alkalic oceanic islands. Such a trend is consistent with the early crystallization of Fe-Ti oxides in the differentiation sequence and is indicative of a high Fe^{3+}/Fe^{2+} ratio in the melt. Also of interest is that several of the mineralogically mixed intermediate lavas described in Section 3.4.2 plot below the inferred liquid line of descent.

Major elements		
Sa.No.	AZ1721(B)	AZ1721(T)
SiO_2	53.59	61.75
TiO_2	2.53	1.06
Al_2O_3	16.98	17.30
Fe_2O_3	1.06	1.10
FeO	7.06	3.65
MnO	0.17	0.20
MgO	3.38	0.99
CaO	5.21	1.58
Na_2O	4.65	6.30
K_2O	4.00	5.54
P_2O_5	0.42	0.18
TOTAL	99.05	99.65
Trace elements		
Ni	31	7
Cr	132	3
V	150	26
Rb	58	115
Sr	777	257
Y	39	37
Zr	328	812
Hf	9.2	20.9
Nb	72	158
Ta	4.3	10.2
Ba	3905	1258
La	101.5	133.3
Ce	152.5	223.9
Nd	85.8	93.9
Sm	15.8	15.5
Eu	5.80	3.26
Tb	1.1	1.5
Ho	1.2	1.4
Yb	2.5	3.1
Lu	0.30	0.39
Th	5.5	15.6
Eu/Eu*	1.6	0.8
K/Rb	572	400
Rb/Sr	0.07	0.45
La_N/Yb_N	27.2	29.0
La_N/Sm_N	4.0	5.4
CIPW normative minerals		
Or	23.9	32.9
Ab	34.3	52.5
An	13.8	2.6
Ne	2.9	0.5
Di	8.8	3.8
Ol	9.2	3.7
Mt	1.6	1.6
Ilm	4.9	2.0
Ap	1.0	0.4

Table 3.3 Analyses of separates of basic and trachytic components of a mixed lava from 0.75km S.E. of Queimado on the N.W. flanks of Agua de Pau volcano.

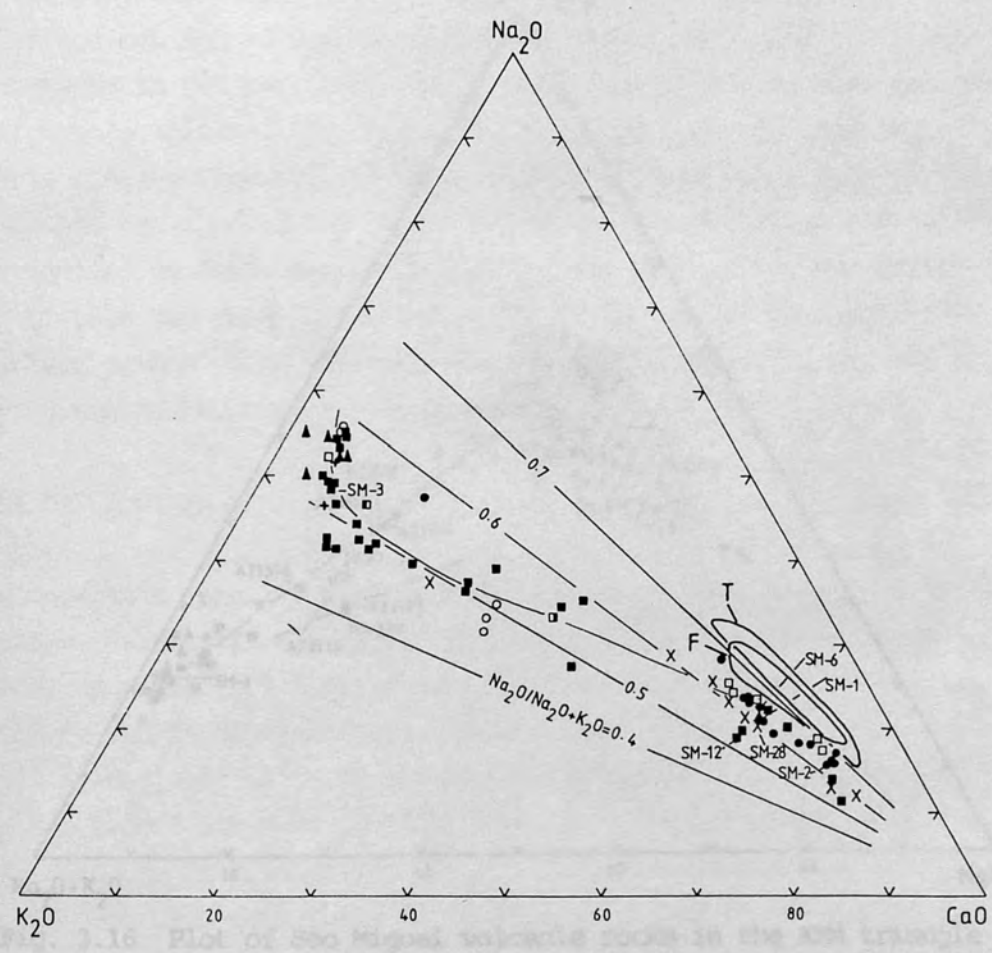

Fig. 3.15 Plot of Sao Miguel volcanic rocks in the Na_2O-K_2O-CaO triangle. Solid line equals inferred liquid line of descent. Note their potassic nature compared to basaltic rocks from other Azores Islands such as Faial (F) and Terceria (T; data from Self and Gunn, 1976). Symbols as Fig. 3.17 Samples with prefix SM from White et al. (1979).

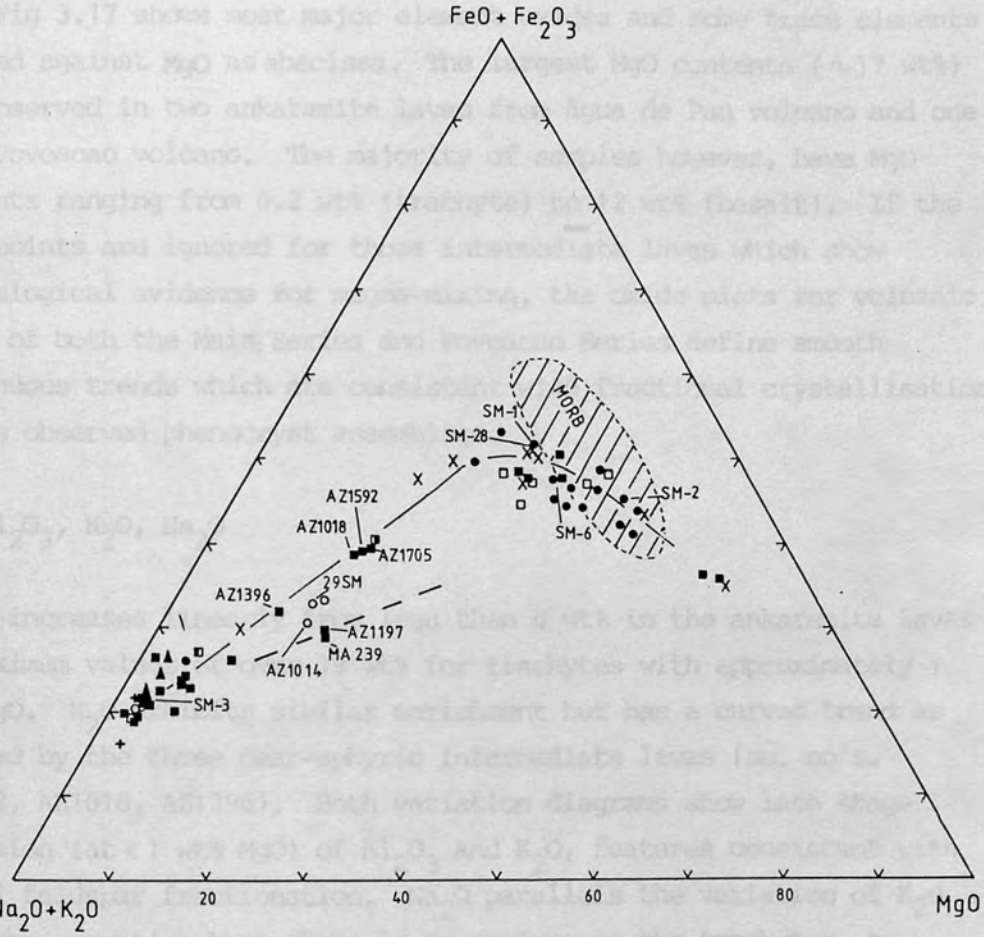

Fig. 3.16 Plot of Sao Miguel volcanic rocks in the AFM triangle . Solid line equals inferred liquid line of descent; heavy dashed line represents possible compositions resulting from magma-mixing between basalt and trachyte. Field of m.o.r.b. from the Azores Plateau (Schilling 1975) is shown for comparison. Symbols as Fig. 3.17. Samples with prefix SM from White et al.(1979).

(defined for intermediate compositions in the Main Series by the three near-aphyric lavas AZ1592, AZ1018, AZ1396) showing a possible mixing trend (heavy dashed line in Fig 3.16) between basaltic and trachytic compositions.

3.5.2 MgO variation diagrams

Fig 3.17 shows most major element oxides and some trace elements plotted against MgO as abscissa. The largest MgO contents ($\sim$17 wt%) are observed in two ankaramite lavas from Agua de Pau volcano and one from Povoacao volcano. The majority of samples however, have MgO contents ranging from 0.2 wt% (trachyte) to 12 wt% (basalt). If the data points are ignored for those intermediate lavas which show mineralogical evidence for magma-mixing, the oxide plots for volcanic rocks of both the Main Series and Povoacao Series define smooth continuous trends which are consistent with fractional crystallisation of the observed phenocryst assemblage.

(a) Al_2O_3, K_2O, Na_2O

Al_2O_3 increases linearly from less than 8 wt% in the ankaramite lavas to maximum values of over 19 wt% for trachytes with approximately 1 wt% MgO. K_2O exhibits similar enrichment but has a curved trend as defined by the three near-aphyric intermediate lavas (sa. no's. AZ1592, AZ1018, AZ1396). Both variation diagrams show late stage depletion (at < 1 wt% MgO) of Al_2O_3 and K_2O, features consistent with alkali feldspar fractionation. Na_2O parallels the variation of K_2O with the exception that there is no maximum in the trachytes, a consequence of the melt having a higher sodium content than the coexisting alkali feldspar (Tables 4.2 and 4.5). Lastly, one notable feature of the K_2O plot, prominent because of the curvature in the variation trend at intermediate MgO contents, is that the mineralogically mixed lavas (labelled in Fig 3.17) plot above the liquid line of descent on what is interpreted as a magma-mixing trend between basaltic and trachytic compositions.

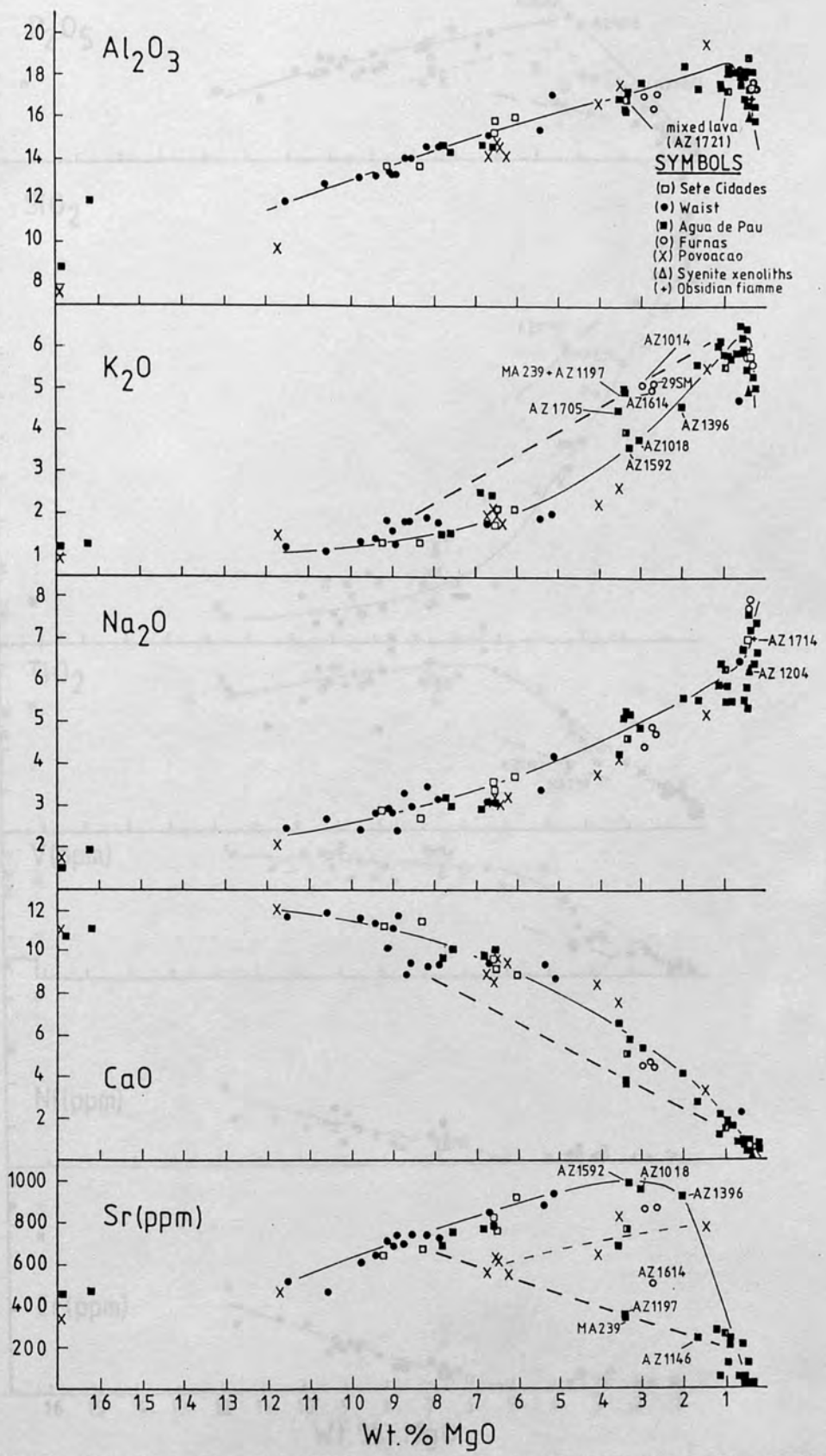

Fig. 3.17 Plots of major element oxides and selected trace elements against MgO for Sao Miguel rocks. Solid and light dashed lines represent the inferred liquid lines of descent for volcanic rocks of the Main series and Povoacao series respectively; heavy dashed line represents basalt-trachyte mixing trend. AZ1592, AZ1018 and AZ1396 are 3 aphyric intermediate lavas. All values as wt% unless otherwise stated. Samples with prefix SM from White et al. (1979).

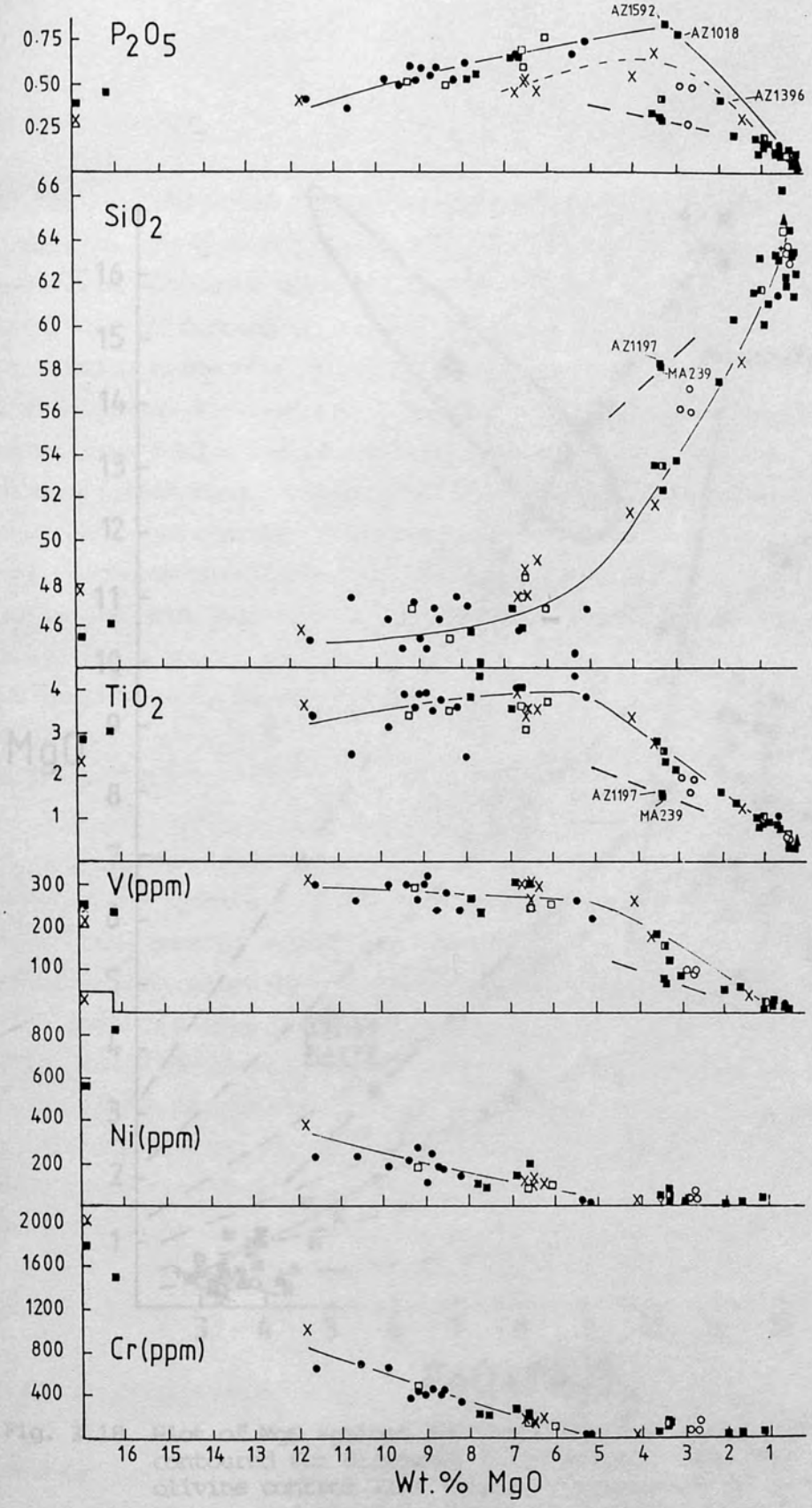

Fig. 3.17 (continued)

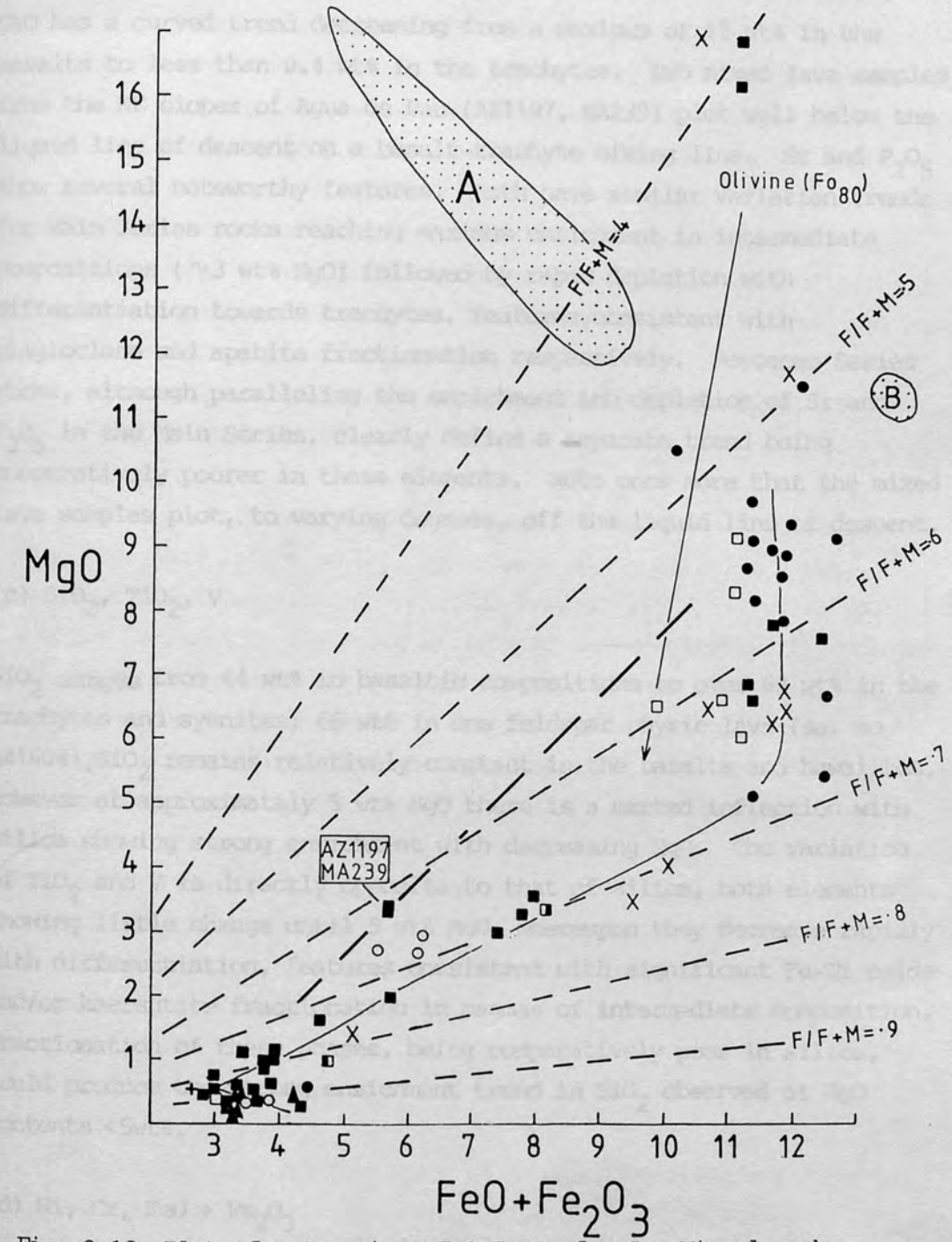

Fig. 3.18 Plot of MgO against $FeO+Fe_2O_3$ for Sao Miguel rocks contoured for different F/F+M values. Also shown is the olivine control line (Fo_{80}); compositions of basaltic pyroxenes (stippled area A); kaersutite compositions from nodule AZ1035 (stippled area B). Heavy dashed line represents basalt-trachyte mixing trend. All values in wt% and symbols as Fig. 3.17.

(b) CaO, Sr, P_2O_5

CaO has a curved trend decreasing from a maximum of 12 wt% in the basalts to less than 0.4 wt% in the trachytes. Two mixed lava samples from the NE slopes of Agua de Pau (AZ1197, MA239) plot well below the liquid line of descent on a basalt-trachyte mixing line. Sr and P_2O_5 show several noteworthy features. Both have similar variation trends for Main Series rocks reaching maximum enrichment in intermediate compositions ($\sim$3 wt% MgO) followed by rapid depletion with differentiation towards trachytes, features consistent with plagioclase and apatite fractionation respectively. Povoacao Series rocks, although paralleling the enrichment and depletion of Sr and P_2O_5 in the Main Series, clearly define a separate trend being comparatively poorer in these elements. Note once more that the mixed lava samples plot, to varying degrees, off the liquid line of descent.

(c) SiO_2, TiO_2, V

SiO_2 ranges from 44 wt% in basaltic compositions to over 64 wt% in the trachytes and syenites; 66 wt% in one feldspar phyric lava (sa. no AZ1604). SiO_2 remains relatively constant in the basalts and hawaiites, however at approximately 5 wt% MgO there is a marked inflection with silica showing strong enrichment with decreasing MgO. The variation of TiO_2 and V is directly opposite to that of silica, both elements showing little change until 5 wt% MgO, whereupon they decrease rapidly with differentiation, features consistent with significant Fe-Ti oxide and/or kaersutite fractionation in magmas of intermediate composition. Fractionation of these phases, being comparatively poor in silica, would produce the strong enrichment trend in SiO_2 observed at MgO contents <5wt%.

(d) Ni, Cr, FeO + Fe_2O_3

Ni and Cr decrease from values of around 200-300 ppm and 400-1000 ppm, respectively, in basalts, to less than 20 ppm in the most evolved hawaiites ($\sim$5 wt% MgO), trends generally consistent with olivine,

clinopyroxene and/or Cr-spinel fractionation. However, a number of basalts with MgO contents spread between about 9-12 wt%, have very similar Ni concentrations ($\sim$200 ppm). Also of interest are the large Ni and Cr contents of several of the mixed lavas, particularly those from the NE flanks of Agua de Pau (sa. no's AZ1197, MA239) which contain up to 60 ppm Ni and 165 ppm Cr. If, as the mineralogical and geochemical evidence indicates, these lavas were produced by magma-mixing the high Ni and Cr levels suggest the involvement of a fairly primitive basaltic component in the mixing process. Lastly, the very large Ni and Cr contents (up to 800 ppm and 2000 ppm respectively) of the three ankaramite lavas with between 16-17 wt% MgO indicates they are probably accumulative.

In a plot of FeO + Fe_2O_3 against MgO (Fig 3.18) basalts and hawaiites show little or no depletion of iron, defining a near vertical trend (similar to the Faial series; Fig 2.18) which produces a rapid increase in the Fe/Mg ratio with differentiation through to intermediate compositions; suggestive of combined olivine and clinopyroxene fractionation. The major inflection at approximately 5 wt% MgO, which results in iron depletion and a more gradual increase in the Fe/Mg ratio is consistent with Fe-Ti oxide fractionation in intermediate magmas as also suggested by the variation trends of SiO_2, TiO_2 and V (Fig 3.17). The Fe/Mg ratio continues to increase in the trachytes but the most evolved, peralkaline types actually show an iron enrichment trend indicating that fractionation of ferromagnesian minerals is no longer significant.

3.5.3 Zr variation diagrams

Fig 3.19 shows the variation of several incompatible elements, plotted against Zr, in rocks of basaltic composition (DI<45). La, Nb, K and Rb exhibit a strong positive trend with Zr, having intercepts near the origin. The variation of Y, with the best-fit line intersecting the Y axis suggests that it is considerably more compatible than Zr, possibly due to clinopyroxene fractionation. The general order of incompatibility of these elements in basaltic magmas from Sao Miguel, as inferred from the intercepts of the best-fit lines is Rb > K > Zr >

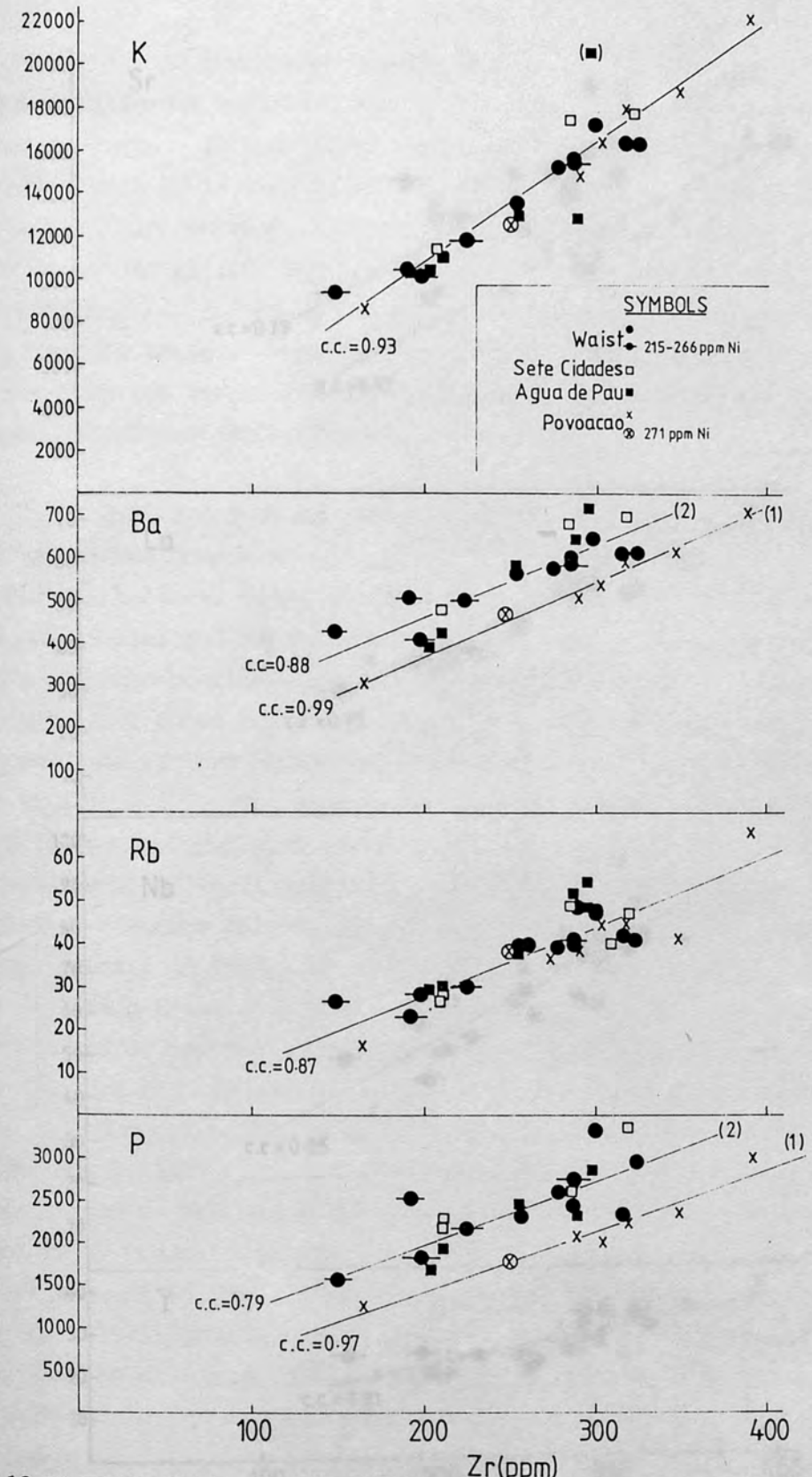

Fig. 3.19 Biaxial plots of selected incompatible elements against Zr for rocks of basaltic composition (DI<45). Best-fit lines and correlation coefficients (c.c.) shown. Note different intercepts between Main series and Povoacao series basaltic rocks for Ba, P and Sr. All values in ppm.

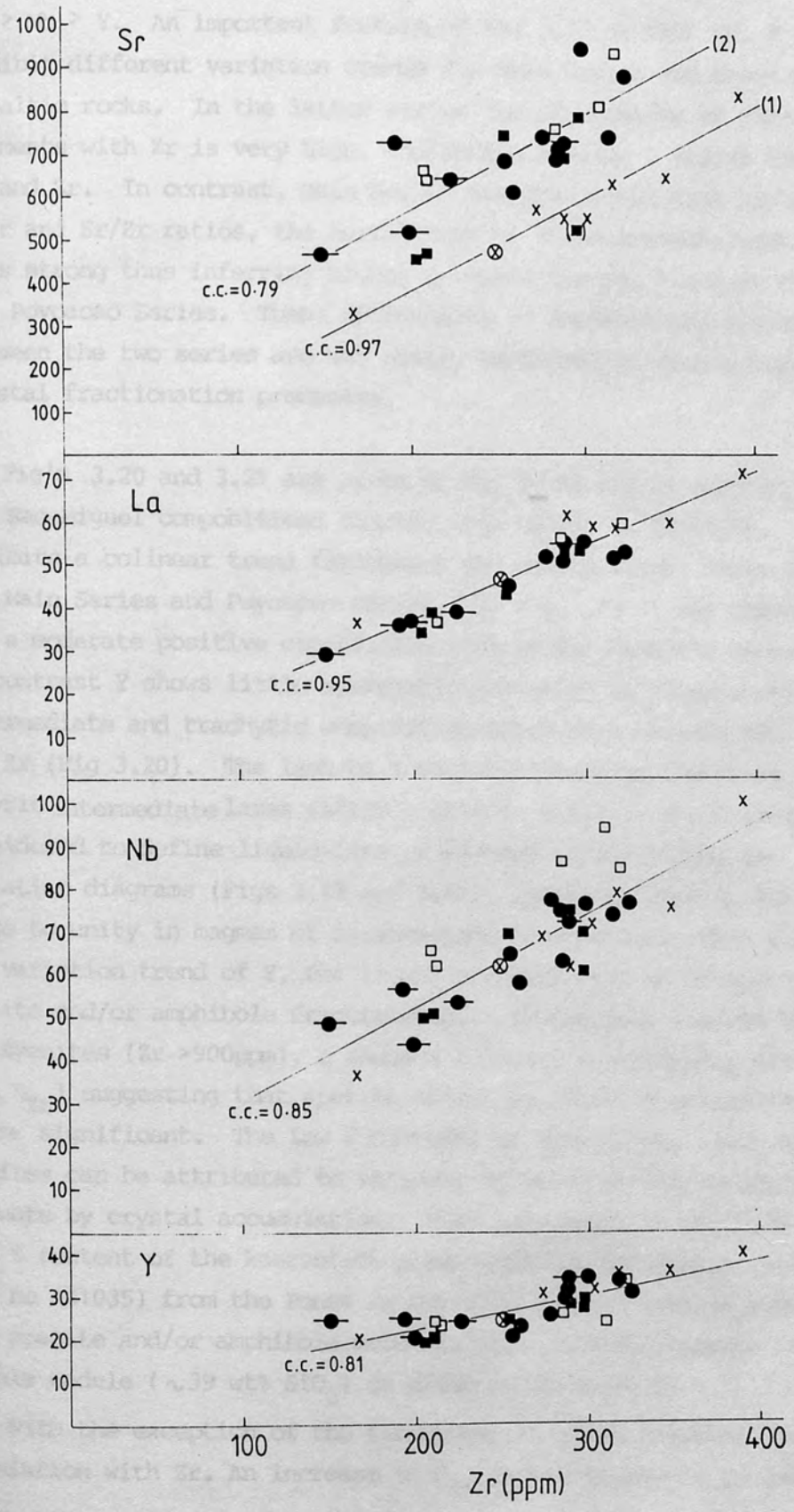

Fig. 3.19 (continued)

La > Nb > Y. An important feature of Fig 3.19 is that Ba, P and Sr exhibit different variation trends for Main Series and Povoacao Series basaltic rocks. In the latter series the correlation of these elements with Zr is very high, indicating similar D values for Ba, P, Sr and Zr. In contrast, Main Series basaltic rocks have higher Ba/Zr, P/Zr and Sr/Zr ratios, the correlation of these elements with Zr being less strong thus inferring higher D values for Ba, P and Sr than in the Povoacao Series. These differences in incompatible element ratios between the two series are not easily explained by simple high-level crystal fractionation processes.

Fig's 3.20 and 3.21 are plots of Nb, Y, Rb and Ba against Zr for all Sao Miguel compositions ranging from basalt to trachyte. Nb exhibits a colinear trend throughout the compositional range of both the Main Series and Povoacao Series. In Fig 3.19 it was shown that Y has a moderate positive correlation with Zr for basaltic compositions. In contrast Y shows little systematic variation in those rocks of intermediate and trachytic composition which have between 400 - 900 ppm Zr (Fig 3.20). The lack of Y variation between the three near-aphyric intermediate lavas (AZ1396, AZ1018, AZ1592), which are considered to define liquid-line of descent trends in the MgO variation diagrams (Figs 3.17 and 3.18), indicates that D_Y must be close to unity in magmas of intermediate composition. This plateau in the variation trend of Y, for liquid compositions, is consistent with apatite and/or amphibole fractionation. In the more evolved trachytes and syenites (Zr >900ppm), Y shows a colinear relationship with Zr (ie $D_Y \sim D_{Zr}$) suggesting that apatite and/or amphibole fractionation is no longer significant. The low Y contents of some of the trachytes and syenites can be attributed to variable dilution of the incompatible elements by crystal accumulation. Also noteworthy in Fig 3.20 is the high Y content of the kaersutite-plagioclase-magnetite-apatite nodule (sa. no AZ1035) from the Ponta da Ferraria lava, a feature consistent with apatite and/or amphibole accumulation. A full chemical analysis of this nodule ($\sim$39 wt% SiO_2) is given in Appendix 2.

With the exception of the trachytes, Rb shows a strong positive correlation with Zr. An increase in D_{Rb} in the trachytes is indicated by the

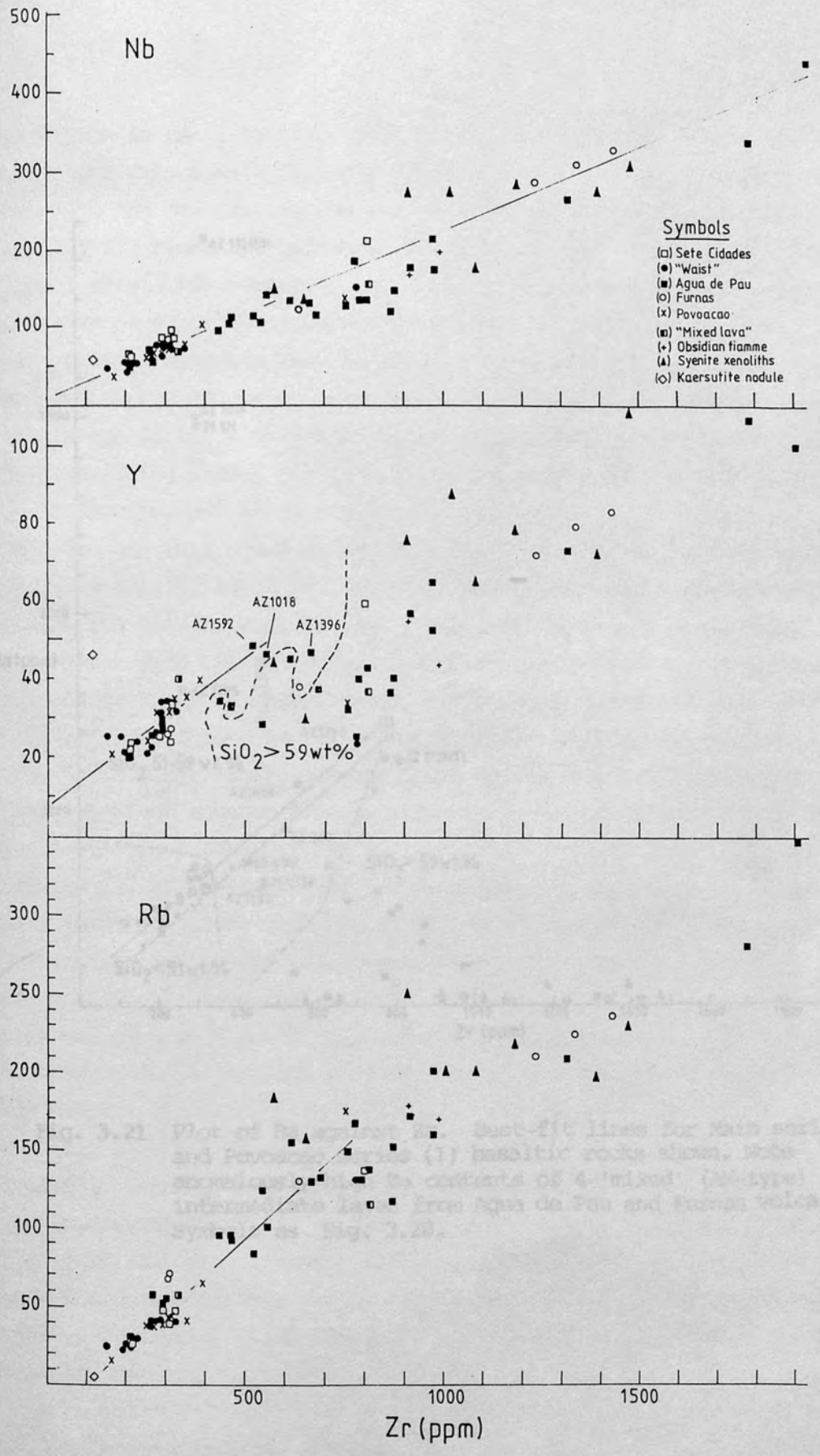

Fig. 3.20 Biaxial plots of Nb, Y and Rb against Zr for all Sao Miguel rock compositions. Best-fit lines are for basaltic rocks (Fig. 3.19). All values in ppm.

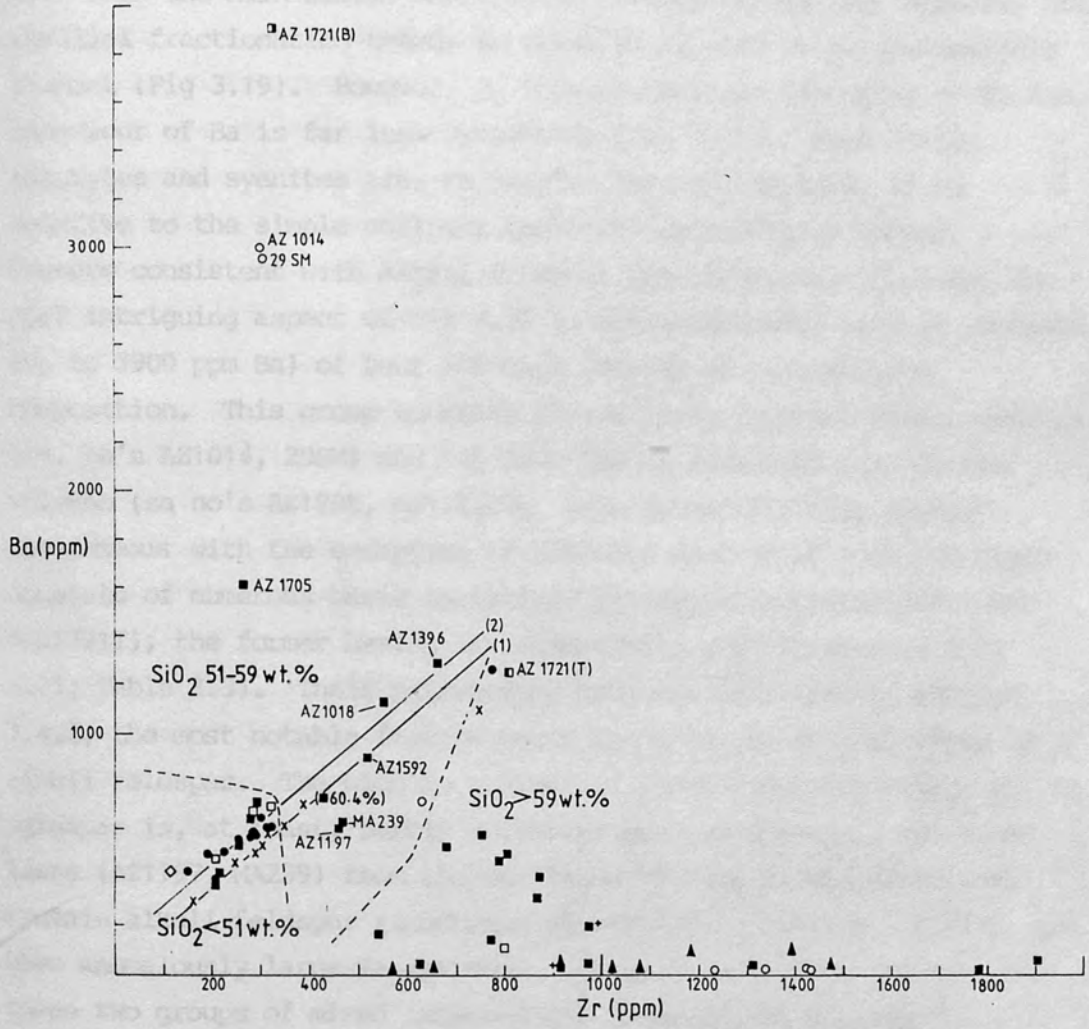

Fig. 3.21 Plot of Ba against Zr. Best-fit lines for Main series (2) and Povoacao series (1) basaltic rocks shown. Note anomalously high Ba contents of 4 'mixed' (AM-type) intermediate lavas from Agua de Pau and Furnas volcanoes Symbols as Fig. 3.20.

inflection in the variation trend at approximately 800 ppm Zr and is consistent with alkali feldspar fractionation. Lastly, basaltic rocks from both the Main Series and Povoacao Series define two separate, but parallel fractionation trends in which Ba behaves as an incompatible element (Fig 3.19). However, in intermediate and trachytic rocks the behaviour of Ba is far less systematic (Fig 3.21). Most of the trachytes and syenites are, to varying degrees, depleted in Ba relative to the simple colinear basaltic fractionation trends, a feature consistent with alkali feldspar fractionation. However, the most intriguing aspect of Fig 3.21 is the anomalously high Ba contents (up to 3900 ppm Ba) of four volcanic samples of intermediate composition. This group consists of two lavas from the Furnas caldera (sa. no's AZ1014, 29SM) and two from the NW flanks of Agua de Pau volcano (sa no's AZ1705, AZ1721B). Macroscopically they appear homogeneous with the exception of the lava from SE of Queimado which consists of numerous basic inclusions (AZ1721B) in a trachytic host (AZ1721T); the former having an anomalously high Ba content (Fig 3.21; Table 3.3). Their petrography has been described in Section 3.4.2, the most notable feature being the presence of xenocrysts of alkali feldspar. The high Ba content of these lavas suggests that the feldspar is, at least, partly accumulative. In contrast, two mixed lavas (AZ1197, MA239) from the NE flanks of Agua de Pau which also contain alkali-feldspar xenocrysts (described in Section 3.4.2) do not have anomalously large Ba contents. It is important to distinguish these two groups of mixed intermediate lavas in the subsequent discussion, since although they have similar petrographic features, they exhibit significant compositional differences. Therefore, according to their Ba contents the mixed intermediate lavas are divided into two groups, those with large Ba contents being termed AM-type (accumulative-mixed), the remaining two lavas from the NE flanks of Agua de Pau being referred to as M-type (mixed). Also included in the latter group is lava sample AZ1614 from Furnas volcano (no hand specimen available) which plots off a number of liquid-line of descent variation trends.

3.5.4 K/Rb and Zr versus SiO_2.

Fig 3.22 is a plot of the K/Rb ratio versus SiO_2. In basaltic compositions the K/Rb ratio varies between 320 - 430. The four AM-type lavas have anomalously large K/Rb ratios of between 572 - 653, a feature consistent with alkali feldspar accumulation. M-type lavas have K/Rb ratios similar to the basaltic rocks. With increasing SiO_2 the K/Rb ratio decreases to values below 200 in some of the trachytes and syenites, a feature consistent of alkali feldspar fractionation. The plot of Zr against SiO_2 (Fig 3.23) illustrates several important features of differentiates from Sao Miguel, many of which have been detailed for Agua de Pau by Marriner et al. (1982). Firstly, the AM-type lavas show no enrichment in Zr over the levels present in basaltic rocks, which is in strong contrast to the two-three fold enrichment shown by the three near-aphyric intermediate lavas (AZ1592, AZ1018, AZ1396). The low Zr contents of the AM-type lavas is consistent with the hypothesis that they are partly feldspar accumulative. In the trachytes Zr shows a rapid increase with little variation in SiO_2 reaching maximum values in the peralkaline pumice deposits (Fogo D, Fogo 1563). However, several of the syenite xenoliths and feldspar-phyric trachytes have comparatively low Zr contents (430 - 650 ppm) indicating that they are probably partly accumulative in nature.

3.5.5 REE

Representative, chondrite normalised REE abundance patterns of volcanic rocks from Sao Miguel ranging in composition from basalt to peralkaline trachyte are shown in Fig 3.24. The REE patterns of the basalts and hawaiites are sub-parallel, approximately linear and show similar degrees of light REE enrichment (La_N/Yb_N = 11.5-15.5). Within this compositional range there is no systematic variation in the degree of light REE enrichment with increasing Fe/Mg ratio. Also, as suggested by the biaxial plots of La and Y against Zr (Fig 3.19) there is no significant difference between the REE patterns of basaltic rocks from the Main Series and Povoacao Series. The REE patterns of the intermediate and trachytic rocks are similarly enriched in the

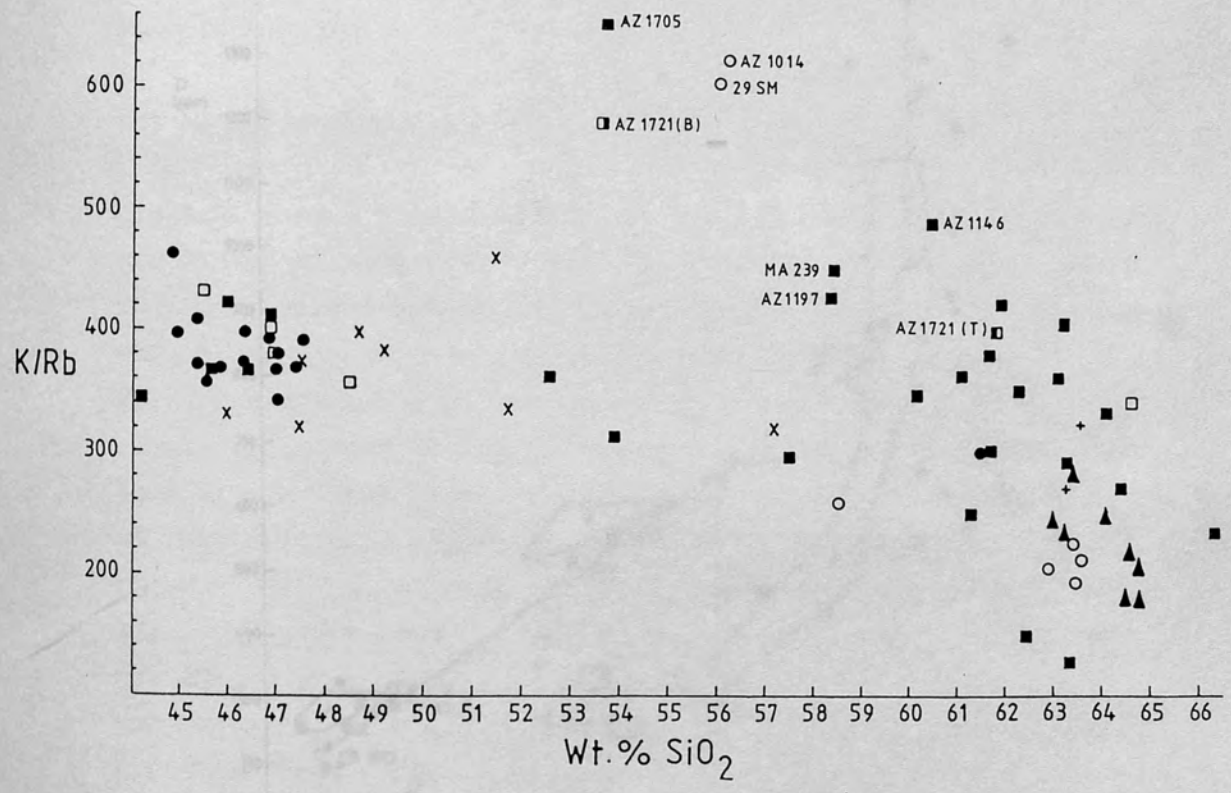

Fig. 3.22 Plot of the K/Rb ratio against SiO_2. Note the anomalously high values of the four 'mixed' (AM-type) intermediate lavas. Symbols as Fig. 3.20.

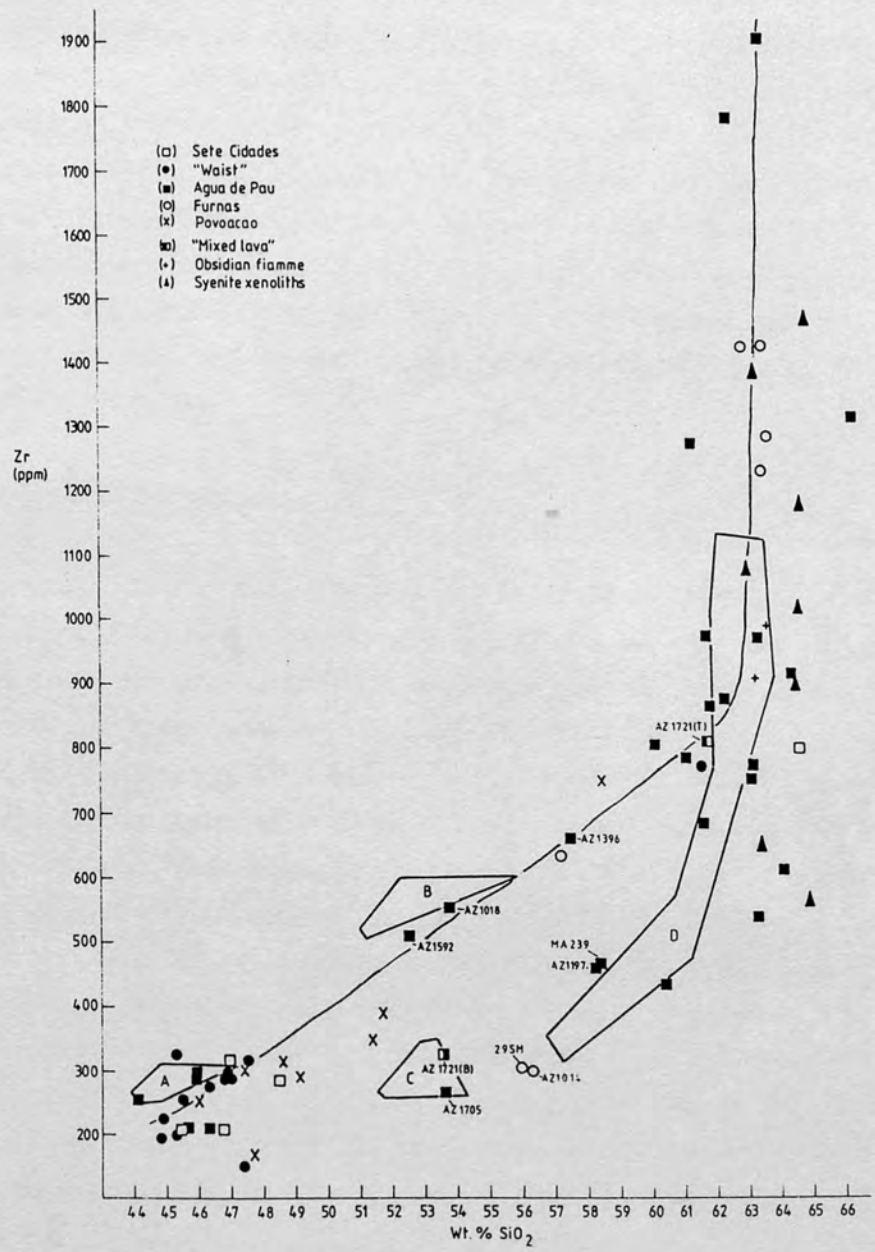

Fig. 3.23 Plot of Zr against SiO_2 for Sao Miguel volcanic rocks. Solid line shows the inferred liquid line of descent for the Main series. Note that the 4 AM-type lavas have similar Zr contents to basaltic compositions suggesting the former are partly accumulative. Boxes define the compositional range of the data of Marriner et al. (1982) for lavas from Agua de Pau, corresponding to basalts and hawaiites (A); aphyric intermediate lavas (B); intermediate lavas with similar mineralogical and chemical features to AM-types described here (C); trachyte lavas (D).

light REE although they differ from the basalts and hawaiites in that their patterns are concave upwards; La_N/Sm_N varies between 3.5-4.5 for intermediate and trachytic rocks compared to 2.5-3.0 for basalts and hawaiites. This feature results in a crossover in patterns, at the middle REE for some samples. The trachytes are distinguished by the parallelism of their REE patterns and also by the presence of negative Eu anomalies, the size of which varies in inverse proportion to the abundances of the other REE and incompatible elements, the largest anomalies occuring in the mildly peralkaline trachytes (eg Eu/Eu* = 0.05 in Fogo D).

(a) AM and M-type lavas

Fig 3.25 shows a chondrite normalised plot of two AM-type lavas from the Furnas caldera (AZ1014) and the NW flanks of Agua de Pau (AZ1705). They have concave-upwards REE patterns and are distinguished for their strong positive Eu anomalies (Eu/Eu*: AZ1705 $\sim$ 1.3; AZ1014 $\sim$ 1.7), a feature consistent with feldspar accumulation. Also shown in Fig 3.25 is the REE pattern of an M-type lava (MA239) from the NE flanks of Agua de Pau. This lava, which contains xenocrysts of forsteritic olivine, diopsidic augite and alkali feldspar is strongly light REE enriched (La_N/Yb_N = 20) with a concave pattern (La_N/Sm_N = 48) and a small negative Eu anomaly suggesting feldspar removal. Fig 3.26 shows the REE patterns of the intermediate (AM-type) and trachytic components of the mixed lava sample (AZ1721) from SE of Queimado. Both have concave-upward REE patterns, the intermediate component having a positive Eu anomaly (Eu/Eu* $\sim$ 1.6) similar to the AM-type lavas in Fig 3.25.

(b) Syenites and amphibole plagioclase bearing nodule

Fig 3.27 shows the chondrite normalised REE patterns of three syenite xenoliths from trachytic pumice deposits and, secondly a nodule, with the mineral assemblage kaersutite + plagioclase + magnetite + apatite + pyrrhotite, collected from the Ponta de Ferraria

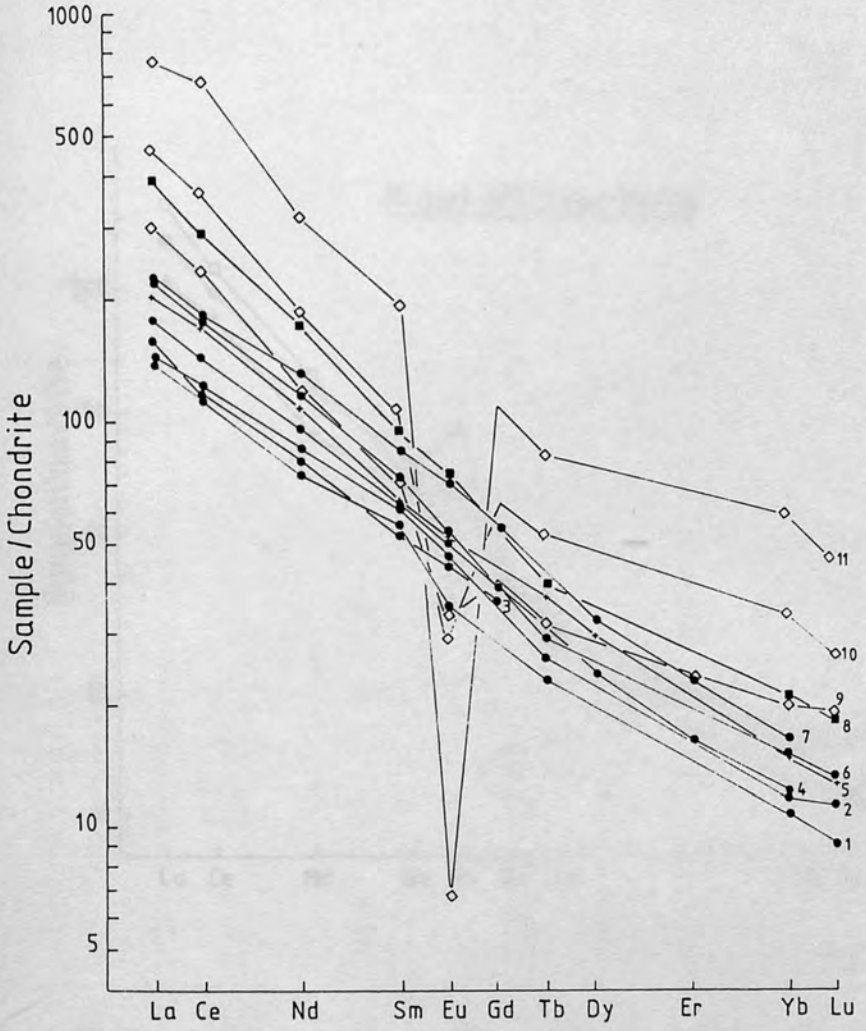

Fig. 3.24 Chondrite normalised REE contents of volcanic rocks from Sao Miguel. Key: 1, ankaramite (MA 23/3); 2, basalt (2SM); 3, basalt (AZ1322); 4, basalt (AZ1039); 5, hawaiite (SM-28, data from White et al., 1979); 6, hawaiite (36AP); 7, hawaiite (AZ1324); 8, mugearite (SM61, Marriner pers. comm.); 9, trachyte (AZ1377); 10, trachyte (AZ1378); 11, peralkaline trachyte (AZ1188). Sample numbers in brackets. All samples are from the Main series with the exception of (5) which is from the extinct stratovolcano Povoacao.

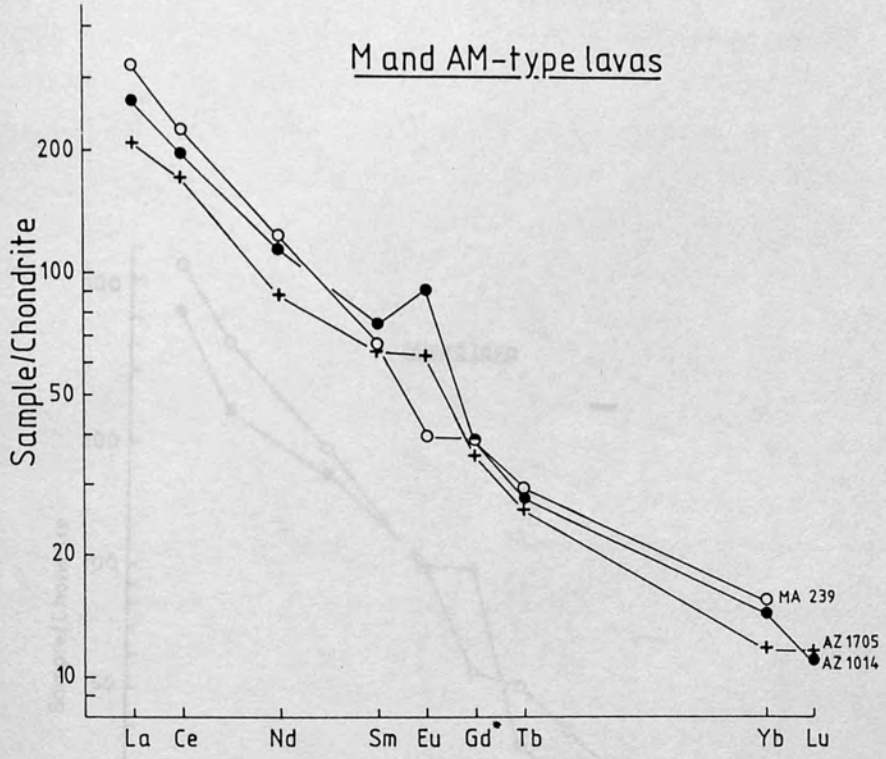

Fig. 3.25 Chondrite normalised REE contents of three mixed intermediate lavas from Agua de Pau and Furnas volcanoes. Note the strong positive Eu anomalies of AM-type lavas (sample numbers AZ1705, AZ1014). Gd values interpolated.

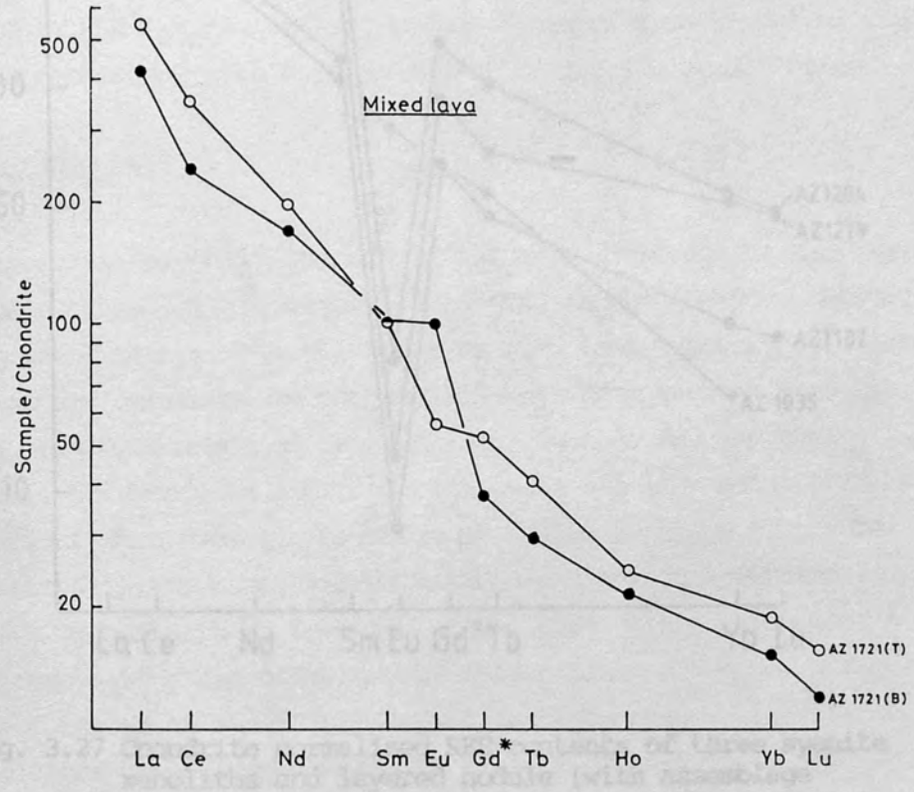

Fig. 3.26 Chondrite normalised REE contents on intermediate and trachytic components of a mixed lava from the NW flanks of Agua de Pau volcano. Note positive Eu anomaly of intermediate component (AM-type). Gd values interpolated.

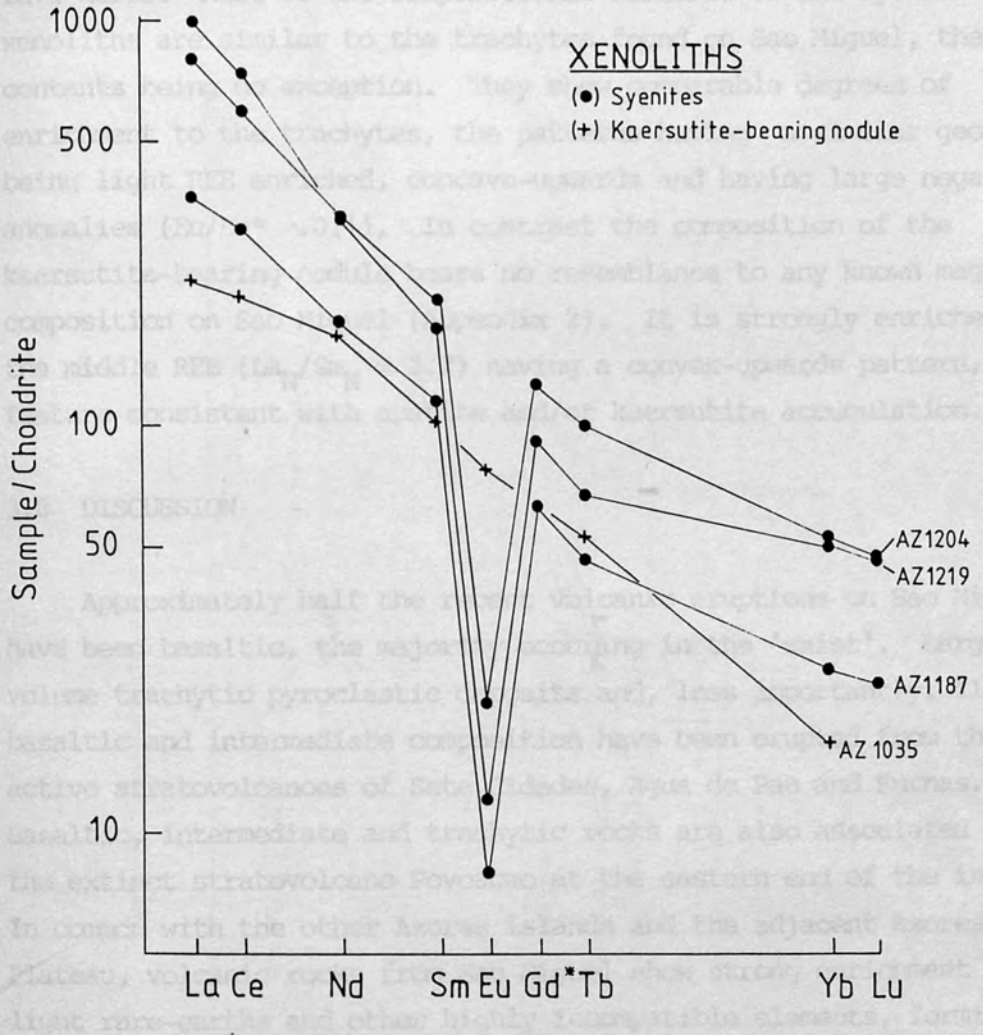

Fig. 3.27 Chondrite normalised REE contents of three syenite xenoliths and layered nodule (with assemblage kaersutite + plagioclase + magnetite + apatite). Gd values interpolated.

lava delta. Most of the compositional features of the syenite xenoliths are similar to the trachytes found on Sao Miguel, their REE contents being no exception. They show comparable degrees of enrichment to the trachytes, the patterns having a similar geometry being light REE enriched, concave-upwards and having large negative Eu anomalies ($Eu/Eu^* \sim 0.1$). In contrast the composition of the kaersutite-bearing nodule bears no resemblance to any known magma composition on Sao Miguel (Appendix 2). It is strongly enriched in the middle REE ($La_N/Sm_N = 2.2$) having a convex-upwards pattern, a feature consistent with apatite and/or kaersutite accumulation.

3.6 DISCUSSION

Approximately half the recent volcanic eruptions on Sao Miguel have been basaltic, the majority occurring in the 'waist'. Large volume trachytic pyroclastic deposits and, less importantly, flows of basaltic and intermediate composition have been erupted from the three active stratovolcanoes of Sete Cidades, Agua de Pau and Furnas. Basaltic, intermediate and trachytic rocks are also associated with the extinct stratovolcano Povoacao at the eastern end of the island. In common with the other Azores islands and the adjacent Azores Plateau, volcanic rocks from Sao Miguel show strong enrichment in the light rare-earths and other highly incompatible elements, forming a potassic series in the alkali-basalt/trachyte suite. Like Faial, compositions range from ankaramite lavas rich in MgO, Ni and Cr through to mildly peralkaline trachytes that are strongly enriched in the incompatible elements but which are highly depleted in Ni, Cr, Ti, V, P, Sr, Ba and Eu. Although some samples show evidence for magma-mixing and/or crystal accumulation, the majority of the compositional features of volcanic rocks from Sao Miguel (summarised in Fig 3.28) are qualitatively consistent with being derived from a basaltic parent by fractional crystallization of the observed phenocryst assemblages (discussed in section 3.6.1).

Important compositional differences exist between the old volcanics from the extinct stratovolcano Povoacao (Povoacao Series) and the Ne-

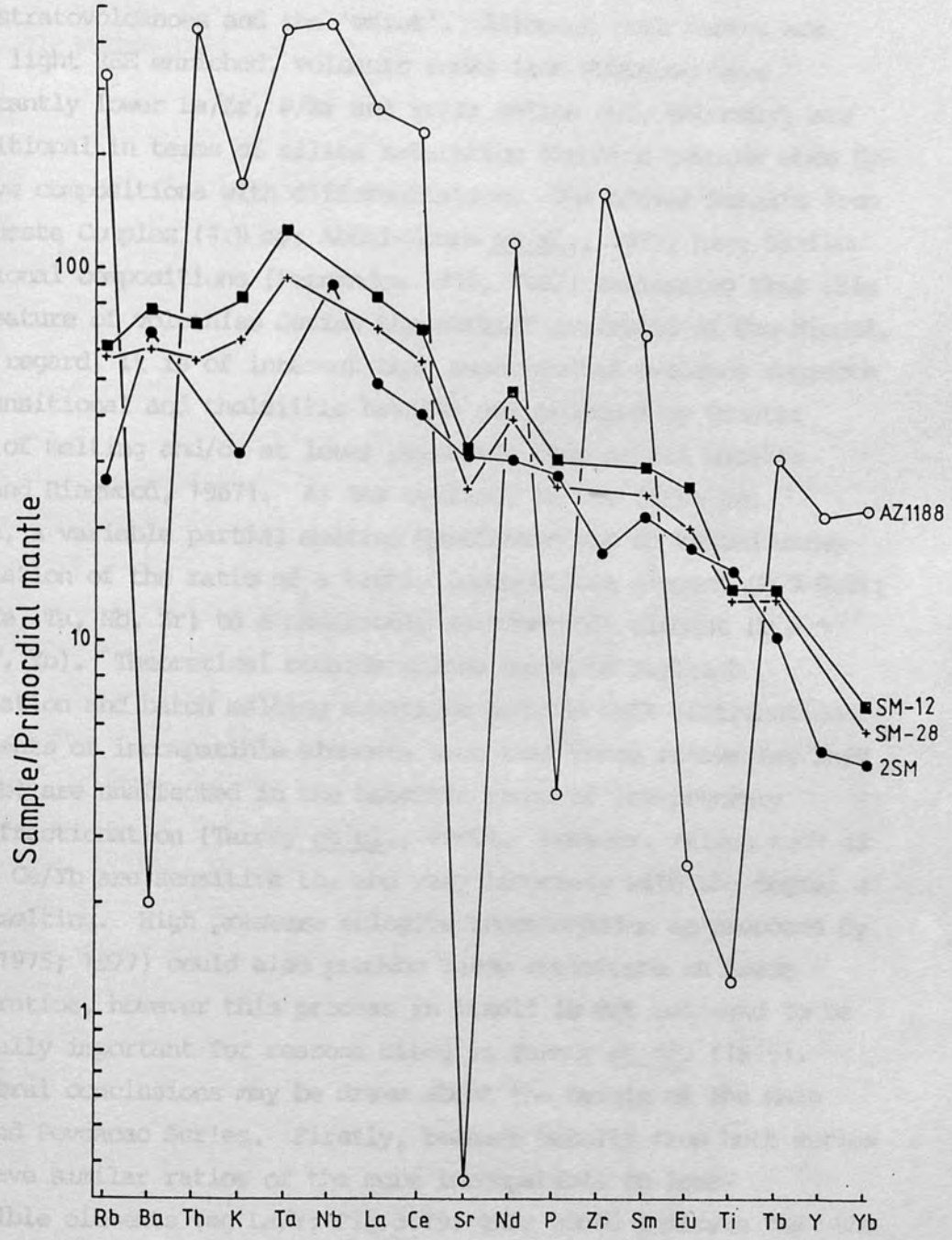

Fig. 3.28 Normalised plot of elemental abundances of basalt (2SM), hawaiite (SM-12) and peralkaline trachyte (AZ1188) from the Main series and hawaiite (SM-28) from the Povoacao series. SM-12 and SM-28 data from White et al. (1979). Primordial mantle values from Tarney et al. (1980).

normative basalts and their derivatives (Main Series) from the three active stratovolcanoes and the 'waist'. Although both series are equally light REE enriched, volcanic rocks from Povoacao have significantly lower Ba/Zr, P/Zr and Sr/Zr ratios and, secondly, are transititional in terms of silica saturation trending towards more Hy-normative compositions with differentiation. The oldest basalts from the Nordeste Complex (4.0 my; Abdel-Monem et al., 1975) have similar transitional compositions (Fernandez 1980, 1982) indicating that this was a feature of volcanism during the earlier evolution of Sao Miguel. In this regard, it is of interest that experimental evidence suggests that transitional and tholeiitic basalts are produced by greater degrees of melting and/or at lower pressures than alkali basalts (Green and Ringwood, 1967). As was outlined in the first two chapters, a variable partial melting hypothesis can be tested using the variation of the ratio of a highly incompatible element ($D \leq 0.01$; eg La, Ce, Ta, Nb, Zr) to a moderately incompatible element ($D = \sim 0.1$ eg Y, Yb). Theoretical considerations based on Rayleigh fractionation and batch melting equations and the bulk distribution coefficients of incompatible elements show that these ratios (eg La/Y and Ce/Yb) are unaffected in the basaltic range of low-pressure crystal fractionation (Tarney et al., 1980). However, ratios such as La/Y and Ce/Yb are sensitive to, and vary inversely with the degree of partial melting. High pressure eclogite fractionation as proposed by O'Hara (1975; 1977) could also produce large variations in these element ratios, however this process in itself is not believed to be geologically important for reasons cited in Tarney et al. (1979). Thus several conclusions may be drawn about the origin of the Main Series and Povoacao Series. Firstly, because basalts from both series series have similar ratios of the more incompatible to less-incompatible elements (eg La/Y; Fig 3.19) this would indicate that the respective primary magmas were produced by similar degrees of melting; partial melting at lower pressures could explain the transitional nature of the Povoacao basalts. Secondly, variations in the ratios Ba/Zr, P/Zr and Sr/Zr between the Main Series and Povoacao Series are not easily accounted for by either low or high pressure crystal

fractionation but rather, suggest compositionally distinct parental magmas and possible different source compositions. Strong evidence for mantle heterogeneity beneath Sao Miguel is also provided by the Sr and Nd data of Hawkesworth et al. (1979) who demonstrated that the $^{87}Sr/^{86}Sr$ ratio shows a systematic increase in value from the west to the east of the island. These matters are considered more fully in Chapter 6.

3.6.1 The role of fractional crystallization on Sao Miguel

A quantitative study by Booth et al. (1978) of volcanism on Sao Miguel has shown that rocks erupted over the past five millenia have consisted predominantly of basalt and trachyte, both types forming in closely comparable amounts. The paucity of volcanic rocks of intermediate composition led these authors to question the importance of fractional crystallization as a means of producing the large volume of trachytes which occur on the island. Bimodal volume relationships in the basalt-trachyte magma series of oceanic islands was first noted for St Helena by Daly (1925), subsequent studies having shown the 'Daly gap' to be a feature of many oceanic volcanic islands including, for example, Terceria in the Azores (Self and Gunn, 1976) and Iceland (Sigurdsson, 1977). To account for the Daly gap alternative processes to fractional crystallization have been suggested for the origin of salic rocks on oceanic islands. These include partial melting of a suitable source rock; for example, the mantle (Yoder, 1973), a plagiogranite layer within the oceanic crust (Sigurdsson, 1977) or hydrous partial melting of basalts (Onions and Gronvold, 1973). However, despite the reservations expressed by other workers about the ability of fractional crystallization to account for the volume relationships commonly observed on oceanic islands, it has previously been shown in this chapter that the majority of rock compositions from Sao Miguel fall on geochemical trends which are entirely consistent with fractional crystallization processes involving the observed phenocryst assemblages. Inflection points in the geochemical variation trends correspond to changes in the relative modal abundances of the separating phases or to a change in the

phenocryst mineralogy. Moreover, chemical features such as the degree of light REE enrichment and K/Na ratio, which distinguishes basaltic rocks from the different Azores islands (White et al., 1979) also distinguishes the more evolved rocks, implying that in the latter the salient chemical characteristics of the basalts have been retained through the fractional crystalization process. Accordingly, the liquid-line of descent has been modelled, using the least-squares mass balance method of Bryan et al. (1968) and Wright and Docherty (1970), for volcanic rocks belonging to both the Main Series and Povoacao Series. An aphyric (<5% phenocrysts) basalt lava from the 'waist' (AZ1308) with MgO, Ni and Cr contents of 9.2 wt%, 266ppm and 452 ppm respectively was taken as the parental composition for liquid-line of descent calculations in the Main Series. A number of basalts have higher contents of MgO (up to 17 wt%), Ni (up to 954 ppm) and Cr (up to 2029 ppm) coupled with higher normative olivine and diopside, however these lavas are considered to be moderately to strongly accumulative in olivine and/or clinopyroxene because:

(i) They are porphyritic containing up to 40% phenocrysts (mainly olivine and clinopyroxene; Table 3.1 and 3.2) in three ankaramite lavas from Agua de Pau and Povoacao volcanoes with approximately 17 wt% MgO. Using AZ1308 as a parental melt composition this figure is similar to the estimate (44.5%) obtained in least squares calculations for the proportion of accumulated phenocrysts in these lavas (Table 3.4).

(ii) Using the criteria of Hart and Davis (1978) it is apparent that the Ni contents of several of the ankaramite lavas are too high (even for a primary magma) for them to be in equilibrium with mantle olivine.

It is noteworthy that the most strongly accumulative compositions (MgO $\sim$17wt%) are associated with the three stratovolcanoes, basalts from the 'waist' having MgO contents <12 wt%.

Model fractional crystallization solutions for least-squares mass

Sa. No.	Basalt AZ1308	Ol	Cpx.	Ankaramite MA23/3 obser.	Ankaramite MA23/3 estim.	Resid.(r)
SiO_2	47.00	39.14	48.43	45.60	45.47	- 0.1338
TiO_2	3.68		2.26	2.91	2.57	- 0.3379
Al_2O_3	13.70		5.29	8.90	8.82	- 0.0594
FeO	11.17	17.79	7.64	10.87	11.60	0.7254
MnO	0.18	0.28	0.16	0.17	0.19	0.0243
MgO	9.17	41.95	13.24	16.91	16.73	- 0.1843
CaO	10.24	0.29	21.75	10.72	10.92	0.2048
Na_2O	2.94			1.51	1.62	0.1117
K_2O	1.87			1.28	1.03	- 0.2485
P_2O_5	0.62			0.39	0.34	- 0.0480
%	55.5	20.4	24.1			Σr^2= 0.8146

Table 3.4 Least-squares crystal accumulation model for ankaramite sample MA23/3 from Agua de Pau volcano. Basalt sample AZ1308 taken as melt composition (< 5% phenocrysts; 9.2 wt% MgO; 266 ppm Ni)

balance calculations which give acceptably low residuals and which are in general agreement with the trace element variations are shown in Table 3.5. These are discussed below along with other major and trace element evidence in support of a fractional crystallization model.

3.6.1 (a) Main Series

(i) Basalts- hawaiites

Differentiation trends in the Main Series consist of variable degrees of enrichment of the incompatible elements, an increase in normative Ne and the F/F+M ratio coupled with a rapid depletion of Ni and Cr. Silica remains relatively constant throughout. Least-squares mixing calculations (Table 3.5) suggest that a fractionation assemblage consisting of 70% clinopyroxene, 26% olivine and minor amounts of Fe-Ti oxides (<4%) best accounts for the derivation of hawaiite from basalt. The lack of negative Eu anomalies and the moderately incompatible behaviour of Sr in basaltic magmas (Fig 3.19) suggests that plagioclase fractionation is not important as Kd_{Sr}plag/liq = 1.8-2.0 (Irving, 1978). The degree of enrichment shown by incompatible elements indicates the following order of D values in the basaltic range of crystallization $D_Y > D_{Nb} > D_{La} > D_{Zr} > D_K > D_{Rb}$. If it is assumed that $D_{Rb} \sim 0$, then D_Y must equal 1-m where m is the slope of the best-fit line in a log-log plot between Rb and Y. For Main Series basaltic rocks this suggests that $D_Y \sim 0.2$. Also, as Kd_Y olivine/melt ~ 0.01 (Pearce and Norry, 1979), Kd_Y cpx/melt must be ~ 0.3 assuming clinopyroxene constitutes 70% of the fractionating assemblage. Fractionation of Fe-Ti oxides early in the differentiation sequence is supported by the near constant Ti and V levels and the limited iron enrichment of Sao Miguel basalts and hawaiites compared to basalts erupted from the adjacent ocean ridge (Fig 3.16).

(ii) Intermediates

As stated earlier, a comparatively small proportion of Sao Miguel volcanic rocks have intermediate silica contents (Fig 3.17). Fewer still, show

Sa.No.	Hawaiite AZ1883	Ol	Cpx.	Mag.	Basalt AZ1308 obser.	Basalt AZ1308 estim.	Resid. (r)
SiO_2	46.90	39.14	45.12	0.26	47.00	46.84	- 0.1590
TiO_2	3.78		3.56	20.46	3.68	3.59	- 0.0908
Al_2O_3	16.00		7.42	3.78	13.70	14.01	0.3138
FeO	11.04	17.79	7.57	66.78	11.17	11.17	- 0.0023
MnO	0.17	0.28		0.60	0.18	0.16	- 0.0249
MgO	6.08	41.95	12.67	5.82	9.17	9.32	0.1485
CaO	8.90	0.29	21.89	0.12	10.24	10.38	0.1397
Na_2O	3.77		0.98		2.94	3.19	0.2501
K_2O	2.15				1.87	1.74	- 0.1315
P_2O_5	0.77				0.62	0.62	0.0026
%	79.6	6.0	14.3	0.1			Σr^2= 0.2540

Sa.No.	Mugearite 1018	Amp.	Mag.	Plag.	Ap.	Hawaiite AZ1883 obser.	Hawaiite AZ1883 estim.	Resid.(r)
SiO_2	53.80	40.64	0.38	57.25		46.90	46.95	0.0540
TiO_2	2.19	4.54	13.67			3.78	3.29	- 0.4909
Al_2O_3	17.60	12.93	3.46	25.96		16.00	15.91	- 0.0859
FeO	7.25	13.18	76.04	0.87		11.04	11.13	0.0882
MnO	0.18	0.21	0.85			0.17	0.20	0.0263
MgO	3.02	11.59	2.23			6.08	6.20	0.1155
CaO	5.51	11.53		8.70	55.84	8.90	8.77	- 0.1297
Na_2O	4.89	2.42		6.08		3.77	3.82	0.0549
K_2O	3.85			0.56		2.15	1.89	- 0.2604
P_2O_5	0.79				42.05	0.77	0.94	0.1723
%	47.5	40.0	3.0	8.2	1.3			Σr^2= 0.3904

Sa.No.	Benmoreite AZ1396	Amp.	Mag.	Plag.	Ap.	Mugearite AZ1018 obser.	Mugearite AZ1018 estim.	Resid. (r)
SiO_2	57.50	40.64	0.38	59.15		53.80	53.82	0.0162
TiO_2	1.16	4.54	13.67			2.19	1.70	- 0.4888
Al_2O_3	18.40	12.93	3.46	25.50		17.60	17.48	- 0.1158
FeO	5.63	13.18	76.04	0.45		7.25	7.34	0.0916
MnO	0.17	0.21	0.85			0.18	0.18	- 0.0032
MgO	2.00	11.59	2.23			3.02	3.07	0.0512
CaO	4.20	11.53		7.79	55.84	5.51	5.57	0.0622
Na_2O	5.63	2.42		6.82		4.89	5.11	0.2242
K_2O	4.60			0.78		3.85	3.78	- 0.0736
P_2O_5	0.42				42.05	0.79	0.71	- 0.0826
%	82.0	12.2	1.5	3.4	0.9			Σr^2= 0.3300

Sa.No.	Trachyte AZ1544	Cpx.	Amp.	Mag.	K-fl.	Ap.	Benmoreite AZ1396 obser.	Benmoreite AZ1306 estim.	Resid. (r)
SiO_2	61.80	51.27	40.64	0.38	60.70		57.50	57.56	0.0620
TiO_2	0.63	1.00	4.54	13.67			1.16	1.31	0.1534
Al_2O_3	18.90	1.83	12.93	3.46	24.34		18.40	18.43	0.0339
FeO	2.74	8.36	13.18	76.04	0.32		5.63	5.60	- 0.0261
MnO	0.13	0.39	0.21	0.85			0.17	0.14	- 0.0277
MgO	0.46	13.99	11.59	2.23			2.00	1.90	- 0.1015
CaO	1.28	21.55	11.53		5.85	55.84	4.20	4.13	- 0.0712
Na_2O	5.40	0.39	2.42		6.89		5.63	5.09	- 0.5404
K_2O	5.96				1.82		4.60	4.36	- 0.2427
P_2O_5	0.08					42.05	0.42	0.51	0.0946
%	67.1	2.0	10.6	2.7	16.5	1.1			Σr^2= 0.4052

Table 3.5 Fractional crystallization least-squares models for volcanic rocks of the Main Series. Mineral analyses from Appendix 3. Apatite analysis from Deer et al (1966).

evidence for being simple derivatives from basaltic magma, the majority of intermediate lavas having both petrographic and geochemical features which suggest magma-mixing. The liquid-line of descent is traced through intermediate compositions by reference to three, near aphyric lavas (sa no's AZ1592, AZ1396, AZ1018) from the SE flanks of Agua de Pau (Figs 3.17, 3.18, 3.20, 3.21 and 3.22). Intermediate lavas (AM and M-type), which are characterised by having some or all of the following features, namely the presence of a strongly disequilibrium phenocryst assemblage made up of trachytic and basaltic components including alkali feldspar and forsteritic olivine, anomalously high K/Rb ratios and Ba contents, positive Eu anomalies and low concentrations of the incompatible elements, do not plot on liquid-line of descent trends in many of the variation diagrams. These 'mixed' lavas are referred to in a subsequent section and can be eliminated from the present discussion.

A number of the whole-rock variation trends suggests a change in the nature of the fractionating assemblage from basaltic magmas. For example, the maximum of Sr and P_2O_5 at 3wt% MgO (Fig 3.17) is consistent with the onset of plagioclase and apatite fractionation respectively whilst the inflection in the variation trends of SiO_2, TiO_2, V and FeO + Fe_2O_3 (Figs 3.17 and 3.18) at 5wt% MgO suggests increased fractionation of the Fe-Ti oxides. The similar Y contents (46-48 ppm) of the three aphyric intermediate lavas ('liquids') is also noteworthy as the enrichment factor of the most incompatible elements (eg Zr) indicates solidification values of about 35% between the least and most evolved of them. This suggests that $D_Y \sim 1$ in intermediate magmas, moreover, the similar charge/radius ratio of Ho and Y indicates that light/middle REE ratios should be higher than for basaltic compositions. This is shown by the concave-upwards REE pattern of one aphyric intermediate lava (Fig 3.24). The strong inflection in the variation trend in the plot of Y against Zr (Fig 3.20) suggests that the increase in D_Y is due to a change in the fractionating assemblage rather than increase in Kd_Y cpx/melt due to P, T, X variations. Fractionation of amphibole (kaersutite) and apatite (Kd_Y amp/melt ~ 2.5, Kd_Y apatite/melt ~ 20; Pearce and Norry,

1979), both of which occur as phenocrysts or microphenocrysts in lavas of intermediate composition, provides a simple explanation for this variation trend. Evidence for kaersutite and apatite fractionation is also given by results from least-squares mixing calculations (Table 3.5). In models for the derivation of the intermediates from a hawaiite only phenocryst assemblages which contain kaersutite give low residuals. Other model assemblages involving clinopyroxene, olivine, plagioclase and magnetite were found to give unacceptably large residuals ($\Sigma r^2 > 5$). The best solution (Table 3.5) suggests a fractionating assemblage consisting of 76% kaersutite, 16% plagioclase, 5.5% Fe-Ti oxides and 2.5% apatite. These results and the opposing fractionation trends shown by basaltic and trachytic clinopyroxenes (Fig 3.12) possibly suggests that titaniferous augite reacts to kaersutite in intermediate magmas. With increasing differentiation (53-58wt% SiO_2) mixing calculations indicate that kaersutite (68%) still forms the bulk of the fractionating assemblage, however, the proportion of plagioclase (19%), Fe-Ti oxides (8%) and apatite (5%) all increase (Table 3.5). These calculated proportions are remarkably similar to the modal abundances of phenocrysts of kaersutite (62%), plagioclase (26%), Fe-Ti oxides (8%) and apatite (4%) in the layered nodules (sa no AZ1035) which occur in the Ponta da Ferraria lava delta. Also, compared to volcanic rocks from Sao Miguel, AZ1035 shows relative enrichment in Sr, Nb, Y, P and the middle REE, evidence consistent with these phases being accumulative. Both the mineralogy and chemistry of these nodules provide very strong evidence for the proposed fractionating assemblage in intermediate magmas of the Main Series.

(iii) Trachytes

The elemental abundance patterns of the trachytes provide convincing evidence for a fractional crystallization origin (Fig 3.28). Most show extreme depletion of Sr, Eu, Ba, P, Ti, V, Mg, Ni and Cr coupled with enrichment of incompatible elements such as Zr, Nb Th, Y and the REE. Least-squares modelling of the derivation of trachyte from intermediates illustrates the importance of anorthoclase in

controlling the liquid-line of descent at this stage of differentiation. A fractionating assemblage consisting of 51% anorthoclase, 32% kaersutite, 6% clinopyroxene, 8% titanomagnetite and 3% apatite provides one possible solution (Table 3.5). The very strong maxima in K_2O and Al_2O_3 at approximately 0.6wt% MgO (Fig 3.18) demonstrates the importance of alkali feldspar fractionation in the trachytes. Further evidence is provided by the increasing $Na_2O/Na_2O + K_2O$ and Eu/Eu* ratios and decreasing K/Rb ratio with differentiation and also by the inflection in the variation trend of Rb with Zr (Fig 3.20). Estimates of D_{Rb}, assuming $D_{Zr} \sim 0$, give values of about 0.25 for trachytic melts. As alkali feldspar constitutes 80% or more of the total phenocryst content of the trachytes this indicates that Kd_{Rb} a.fl/melt ~ 0.2. The low P_2O_5 contents of the trachytes, their parallel REE patterns and the colinear variation trend of Y with Zr (Fig 3.20) indicates a decrease in D_Y from intermediate compositions to trachytes and suggests that kaersutite and/or apatite fractionation are no longer important. The mildly peralkaline nature of the most evolved trachytes is consistent with an origin involving biotite, Al-bearing clinopyroxene and alkali feldspar. A number of the syenite xenoliths are also mildly peralkaline having compositions ('liquid') very similar to the trachytes, plotting on crystal fractionation trends in the whole-rock variation diagrams. The origin of these peralkaline rocks is discussed in more detail in Chapter 4.

3.6.1 (b) Povoacao Series

Samples from the extinct volcano Povoacao range in composition from basalt to trachyte, major and trace element variation trends are consistent with fractional crystallization and suggest fractionating assemblages similar to those proposed for the Main Series. However, the Povoacao Series is distinguished from the Main Series by lower values of the incompatible element ratios Ba/Zr, P/Zr and Sr/Zr and also by their transitional nature in terms of silica saturation. It was suggested earlier that many of these compositional differences cannot be easily explained by fractional crystallization or variable partial melting but, rather, indicate source heterogeneity. With

Sq.No.	Mugearite AZ1134	Ol.	Cpx.	Mag.	Hawaiite AZ1138 obser.	Hawaiite AZ1138 estim.	Resid. (r)
SiO_2	51.70	38.11	48.43	0.26	47.50	47.53	0.0275
TiO_2	2.75		2.26	20.46	3.90	3.26	- 0.6395
Al_2O_3	17.60		5.29	3.78	14.10	14.00	- 0.0991
FeO	9.37	22.41	7.64	66.78	11.72	11.93	0.2144
MnO	0.17	0.48	0.16	0.60	0.16	0.20	0.0371
MgO	3.51	38.34	13.24	5.82	6.74	6.59	- 0.1536
CaO	7.54	0.35	21.75	0.12	9.00	9.05	0.0471
Na_2O	4.14				3.00	3.06	0.0577
K_2O	2.67				1.98	1.97	- 0.0080
P_2O_5	0.68				0.46	0.50	0.0422
%	75.1	4.4	16.2	4.3			$\Sigma r^2 = 0.4979$

Table 3.6 Fractional crystallization least-squares model for basaltic/intermediate compositions of the Povoacao Series.

differentiation, the trend in the Povoacao Series is towards more Hy-normative compositions. In basaltic and intermediate compositions the variation trends suggest a fractionating assemblage of clinopyroxene, olivine and Fe-Ti oxides. Contrary to the model proposed for volcanic rocks from the Nordeste Complex by Fernandez (1980), the incompatible behaviour of Sr in basaltic and intermediate compositions shows that plagioclase fractionation is not important until MgO $\leq$ 3wt%. The liquid-line of descent has been modelled for this compositional range by least-squares mixing calculations. One possible solution (Table 3.6) suggests a separating assemblage composed of 6.5% clinopyroxene, 18% olivine and 17% Fe-Ti oxides.

3.6.1 (c) Summary and conclusions

Fig 3.29 is a plot of F against SiO_2 and summarises the results of the least-squares mixing calculations for the liquid-line of descent for both the Main Series and Povoacao Series. F values were taken to equal Co_{Zr}/Cl_{Zr} assuming Co_{Zr} = 280 ppm (based on Zr contents of aphyric, MgO rich basalts; eg AZ1308) and $D_{Zr} \sim 0$. Zr was chosen as an index of solidification because it behaves as an incompatible element throughout the compositional range of both magma series. Excluded from this plot are lavas which show evidence for magma-mixing or crystal accumulation; these are dealt with in a subsequent section. It should be noted that the F values based on Zr for each of the modelling stages are somewhat greater than those deduced from major-element modelling. This discrepency may be due to the choice of phenocryst compositions, or alternatively the assumption that $D_{Zr} \sim 0$. However this does not change the main conclusions to be drawn from Fig 3.29, which are:

(i) Evolution of basaltic melts is mainly controlled by the fractionation of clinopyroxene, olivine and Fe-Ti oxides. Clinopyroxene is the dominant phase in both magma series. Fe-Ti oxide fractionation is more important in rocks from the Povoacao Series than the Main Series.

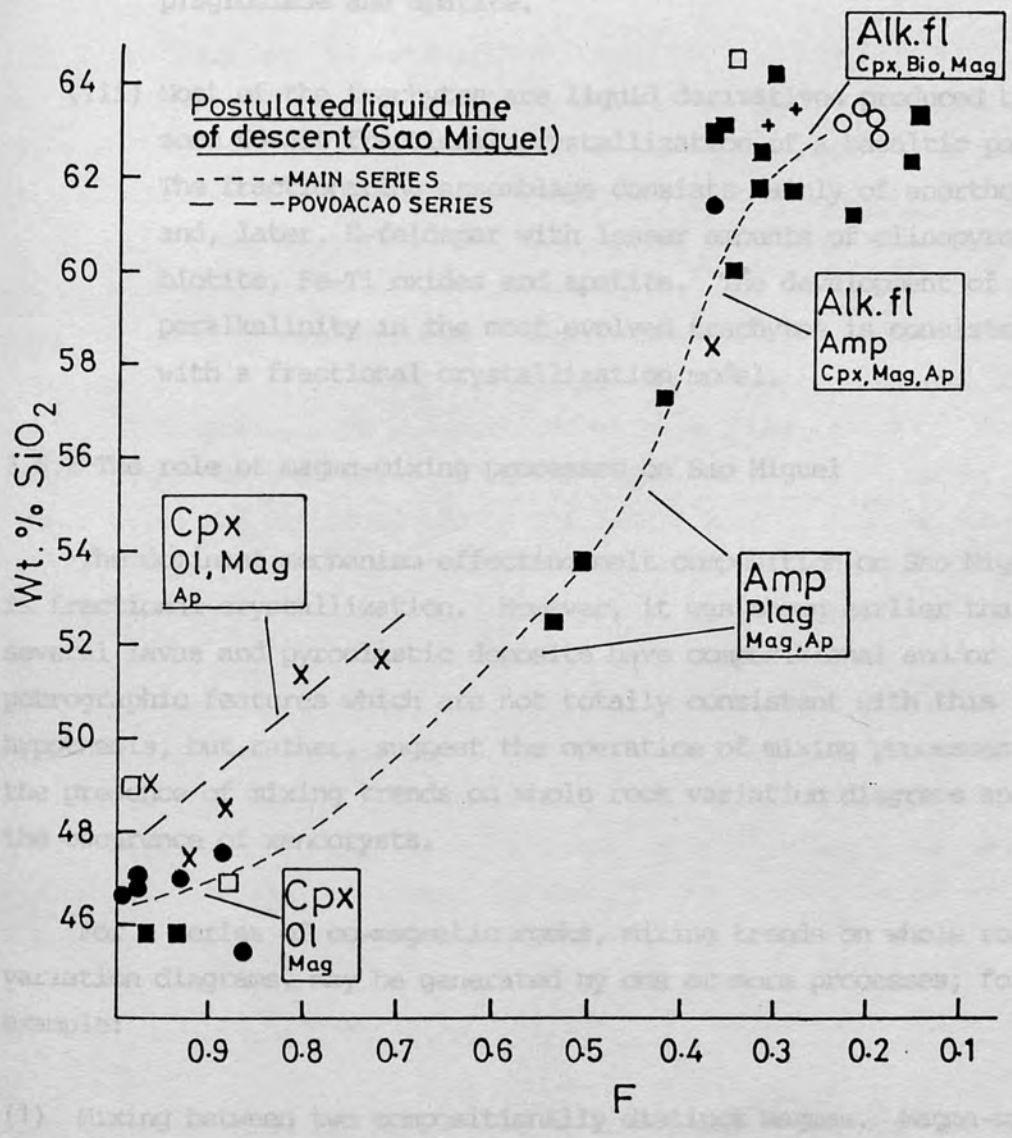

Fig. 3.29 Results from the least-squares modelling calculations for the liquid line of descent for the Main series and Povoacao series are summarised on this plot of F, the weight fraction of melt relative to the parent versus wt% SiO_2 . F values were taken to equal CoZr/ClZr assuming CoZr = 280 ppm and DZr = 0; see text for detailed explanation.

(ii) Rocks of intermediate silica content represent liquids generated by 30-60% fractional crystallization of a basaltic parent containing approximately 9wt% MgO. The observed liquid-line of descent from hawaiite to mugearite and benmoreite suggests a fractionating assemblage principally made up of kaersutite with lesser amounts of Fe-Ti oxides, plagioclase and apatite.

(iii) Most of the trachytes are liquid derivatives produced by some 60-85% fractional crystallization of a basaltic parent. The fractionating assemblage consists mainly of anorthoclase and, later, K-feldspar with lesser amounts of clinopyroxene, biotite, Fe-Ti oxides and apatite. The development of peralkalinity in the most evolved trachytes is consistent with a fractional crystallization model.

3.6.2 The role of magma-mixing processes on Sao Miguel

The dominant mechanism effecting melt composition on Sao Miguel is fractional crystallization. However, it was shown earlier that several lavas and pyroclastic deposits have compositional and/or petrographic features which are not totally consistent with this hypothesis, but rather, suggest the operation of mixing processes; ie the presence of mixing trends on whole rock variation diagrams and/or the occurence of xenocrysts.

For a series of co-magmatic rocks, mixing trends on whole rock variation diagrams, may be generated by one or more processes; for example:

(1) Mixing between two compositionally distinct magmas. Magma-mixing has been assigned an increasingly important role in igneous petrology, with particular emphasis being paid to island-arc magmas; for example, see the work of Anderson, 1976; Eichelberger, 1975, 1978; Luhr and Carmichael, 1980; Sakuyama 1979, 1981. Less attention has been paid to the role of this

process in alkaline magmas.

(2) Mixing between magma and phenocrysts. This could occur, for example, by crystal accumulation in the lower part of a magma body. Examples are provided by the accumulative basalts described earlier.

It is important to establish criteria for distinguishing between mixing, fractional crystallization and other processes. Of particular value in this respect are elements whose variation trends show a well defined maximum or inflection as a response to a change in the mineral components of the fractionating assemblage. For example, both P_2O_5 and Sr have maximum concentrations at about 3 wt% MgO (Fig 3.17) where upon they show a rapid decrease with differentiation due to fractionation of apatite and plagioclase respectively. In both these variation diagrams, rock compositions which are the result of simple binary mixing between basic and salic magma would plot on linear trends below the path followed by the liquid line of descent. A similar trend would result from mixing of silica rich phenocrysts, such as anorthoclase and K-feldspar, with a basic magma. The presence of xenocrysts provides further evidence for mixing, although of course such features do not necessarily imply magma-mixing. Several lavas of intermediate composition from Sao Miguel plot below the liquid-line of descent in the variation diagrams of P_2O_5 and Sr against MgO (Fig 3.27), although only one (AZ1721) shows textural evidence for magma-mixing. These lavas have been divided into two groups (M and AM-types) according to their composition.

(a) M-type intermediate lavas

This group consists of two lavas from the NE slopes of Agua de Pau volcano (MA239, AZ1197) and one from the southern flanks of Furnas volcano (AZ1614). The two from Agua de Pau fall off the main fractionation trends in the AFM plot and the variation diagrams of K_2O, CaO, Sr, P_2O_5, SiO_2, TiO_2, V and FeO + Fe_2O_3 versus MgO, falling between the clusters of basalt and trachyte analyses. They have unusually high

contents of Ni (47-60 ppm) and Cr (104-165 ppm) compared to intermediate lavas which are derivatives produced by crystal fractionation (ie < 10 ppm Ni and Cr). Also, forsteritic olivine (Fo_{71-88}) and diopsidic pyroxene occur with strongly resorbing crystals of anorthoclase and K-feldspar. These features are qualitatively consistent with mixing between basalt and trachyte magmas.

An estimate of the compositions of the mixing components can be obtained from the whole rock variation diagrams. For example, the two lavas from the NE flanks of Agua de Pau plot on a mixing trend in the AFM diagram which suggests an F/F+M ratio of about 0.53 for the basaltic component (Fig 3.16). For the liquid-line of descent of the Main Series, this ratio corresponds to a basaltic magma with between 9-11 wt% MgO (Fig 3.18). Similarly, the variation trend of K_2O against MgO, (Fig 3.17) suggests about 1 wt% MgO for the trachytic component. These compositional constraints coupled with the phenocryst assemblage have been used to select for least-squares mixing calculations whole rock analyses which are believed to approximate to the compositions of the mixing components. Results (Table 3.7) suggest that mixing of trachyte and alkali basalt in the ratio of about 5:2 by weight could produce the observed major element composition of the mixed lava sample MA239. Taking these proportions it is possible to calculate the concentration of individual trace elements in this hypothetical mix. This is represented in terms of a normalised plot (Fig 3.30). Agreement between calculated and trace element abundances is very good and thus provides further evidence for the mixing model. A magma-mixing origin is also suggested here for the intermediate lava (AZ1614) from the southern flanks of Furnas volcano. This lava falls off the fractionation trends in the plots of K_2O, Sr, P_2O_5, TiO_2 and V, but not in the plots of CaO, SiO_2 and FeO + Fe_2O_3. These mixing trends suggest that the basic and salic components had MgO contents of between 3-5wt% and 0.5-1wt% respectively.

Sa.No.	Trachyte AZ1377	Basalt AZ1704	M-type lava MA239 obser.	MA239 estim.	Residue(r)
SiO_2	61.60	46.80	58.40	58.30	- 0.1002
TiO_2	1.02	3.47	1.60	1.72	0.1214
Al_2O_3	17.60	13.60	16.50	16.72	0.2212
FeO	3.76	10.92	5.51	5.82	0.3107
MnO	0.14	0.17	0.15	0.15	0.0004
MgO	1.14	6.08	3.41	2.54	- 0.8683
CaO	2.18	8.90	3.86	4.10	0.2354
Na_2O	5.96	3.77	5.13	5.43	0.2980
K_2O	6.06	2.15	5.10	5.05	- 0.0531
P_2O_5	0.19	0.77	0.30	0.36	0.0553
%	72	28			$\Sigma r^2 = 1.0744$

Table 3.7 Magma-mixing model for M-type intermediate lavas (MA239).

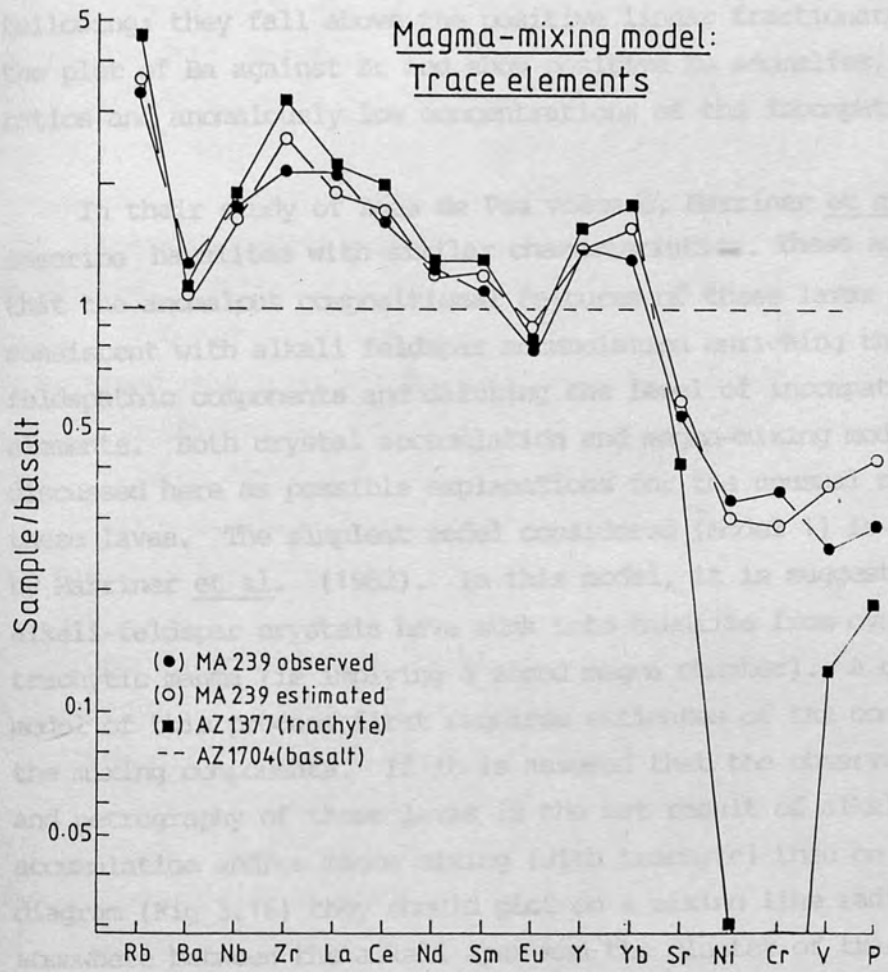

Fig. 3.30 Observed and estimated trace element abundances (normalised to basalt) in an M-type intermediate lava from the NE flanks of Agua de Pau volcano. Calculated trace element abundances are those for a binary mixing model between basalt (71%) and trachyte (29%). Mixing proportions are those obtained from least-squares modelling on major element compositions (Table 3.7); see text for full explanation of modelling details.

(b) AM-type lavas

This second group consists of two lavas from the north west flanks of Agua de Pau volcano (AZ1721B and AZ1705) and two lavas from the Furnas caldera (AZ1014 and 29SM). Their most distinguishing feature is the presence of strongly resorbing crystals of alkali feldspar. Compositionally, they are distinguished from M-type lavas by the following; they fall above the positive linear fractionation trend in the plot of Ba against Zr and show positive Eu anomalies, large K/Rb ratios and anomalously low concentrations of the incompatible elements.

In their study of Agua de Pau volcano, Marriner et al. (1982) describe hawaiites with similar characteristics. These authors suggest that the anomalous compositional features of these lavas are consistent with alkali feldspar accumulation enriching the melt in feldspathic components and diluting the level of incompatible elements. Both crystal accumulation and magma-mixing models are discussed here as possible explanations for the unusual chemistry of these lavas. The simplest model considered (Model 1) is that proposed by Marriner et al. (1982). In this model, it is suggested that alkali-feldspar crystals have sunk into hawaiite from overlying trachytic magma (ie implying a zoned magma chamber). A quantitive model of this process first requires estimates of the compositions of the mixing components. If it is assumed that the observed composition and petrography of these lavas is the net result of alkali feldspar accumulation and/or magma mixing (with trachyte) then on the AFM diagram (Fig 3.16) they should plot on a mixing line radiating from somewhere between the alkali apex and the cluster of trachyte analyses. Extrapolation of this mixing trend to the liquid-line of descent gives an estimate of the F/F+M ratio of the basic magmatic component prior to contamination. For example, in the case of AZ1705 this analysis would indicate an F/F+M ratio of ~ 0.7 for the basic mixing component implying an MgO content of between 5-6wt% (Fig 3.18). For modelling purposes, AZ1324 was assumed to approximate the composition of the basic component having 5.2wt% MgO and plotting on the liquid-line of descent trends on the variation diagrams. Major

element least-squares mixing calculations for Model 1 and which give low residuals are given in Table 3.7. Results indicate that the AM-type lava AZ1705 could be up to 50% accumulative, mostly in alkali feldspar. To test whether Model 1 is consistent with the trace element data, these mixing proportions were used to estimate theoretical abundances of incompatible elements in AZ1705. These calculations show a large discrepancy between observed and deduced values, the dilution of the incompatible elements being much less than expected. This cannot be due to the choice of mixing components as the relatively high Ni (40 ppm) and Cr (32 ppm) levels of AZ1705 suggest that if anything the assumed MgO content of the basic component is an underestimate. A larger MgO content would produce an even greater disparity between model and actual incompatible element abundances. Similar arguments also apply to the three other AM-type lavas. It would seem, therefore, that a model for the origin of these lavas based solely on accumulation of alkali feldspar is inconsistent with their chemistry. However, it is also apparent that simple binary mixing between basic and trachytic magma cannot account for the large Ba contents, positive Eu anomalies and low concentrations of the incompatible elements in AM-type lavas.

A more complex model (Model 2) for the origin of AZ1705 involving a combination of crystal accumulation and magma-mixing with trachyte also provides acceptably low residuals, least-squares calculations for major elements (Table 3.8) giving mixing proportions of 55% hawaiite, 18% trachyte and 27% crystals (mostly alkali feldspar). Moreover, using these mixing proportions there is very good agreement between observed and calculated incompatible element abundances (Fig 3.31). This three-component mixing model (Model 2) is considered to provide the best explanation for the origin of the anomalous chemical and petrographic features of the AM-type lavas.

An important question posed by this latter model is the nature of the mixing event/s; ie are the AM-type lavas the result of magma-mixing of hawaiite with alkali-feldspar accumulative trachyte or, alternatively do they represent samples, from below an

MODEL 1

Sa. No.	Hawaiite AZ1324	K-fl.	Anorthoclase	Cpx.	Mag.	AM-type lava AZ1705 observ.	AZ1705 estim.	Resid. (r)
SiO_2	46.90	64.72	62.00	52.01	0.38	53.70	53.62	- 0.0767
TiO_2	3.88			0.72	13.67	2.86	2.30	- 0.5567
Al_2O_3	17.10	19.60	19.99	1.84	3.46	16.90	17.13	0.2334
FeO	11.20	0.27	0.62	9.33	76.04	7.86	7.95	0.0887
MnO	0.19			0.64	0.85	0.13	0.16	0.0252
MgO	5.17			13.69	2.23	3.58	3.61	0.0285
CaO	8.66	1.02	3.14	22.16		6.62	6.75	0.1310
Na_2O	4.26	3.52	5.45	1.11		4.25	4.09	- 0.1602
K_2O	2.07	10.59	6.60			4.56	4.64	0.0750
P_2O_5	0.76					0.38	0.39	0.0143
%	51.3	21.5	19.0	6.4	1.8			$\Sigma r^2 = 0.4282$

MODEL 2

Sa. No.	Hawaiite AZ1324	K-fl.	Cpx.	Mag.	Trachyte AZ1377	AM-type lava AZ1705 observ.	AZ1705 estim.	Resid. (r)
SiO_2	46.90	64.72	52.01	0.38	61.60	53.70	53.68	- 0.0225
TiO_2	3.88		0.72	13.67	1.02	2.86	2.46	- 0.3964
Al_2O_3	17.10	19.60	1.84	3.46	17.60	16.90	17.00	0.0986
FeO	11.20	0.27	9.33	76.04	3.76	7.86	7.92	0.0607
MnO	0.19		0.64	0.85	0.14	0.13	0.17	0.0384
MgO	5.17		13.69	2.23	1.14	3.58	3.78	0.1958
CaO	8.66	1.02	22.16		2.18	6.62	6.53	- 0.0903
Na_2O	4.26	3.52	1.11		5.96	4.25	4.25	0.0023
K_2O	2.07	10.59			6.06	4.56	4.52	- 0.0388
P_2O_5	0.76				0.19	0.38	0.46	0.0761
%	55.1	21.4	5.0	0.7	17.9			$\Sigma r^2 = 0.2263$

Table 3.8 Two models for the origin of AM-type intermediate lavas (AZ1705); (1) is crystal accumulation model; (2) is crystal accumulation and magma mixing model. Mineral analyses from Appendix 3. See text for full explanation.

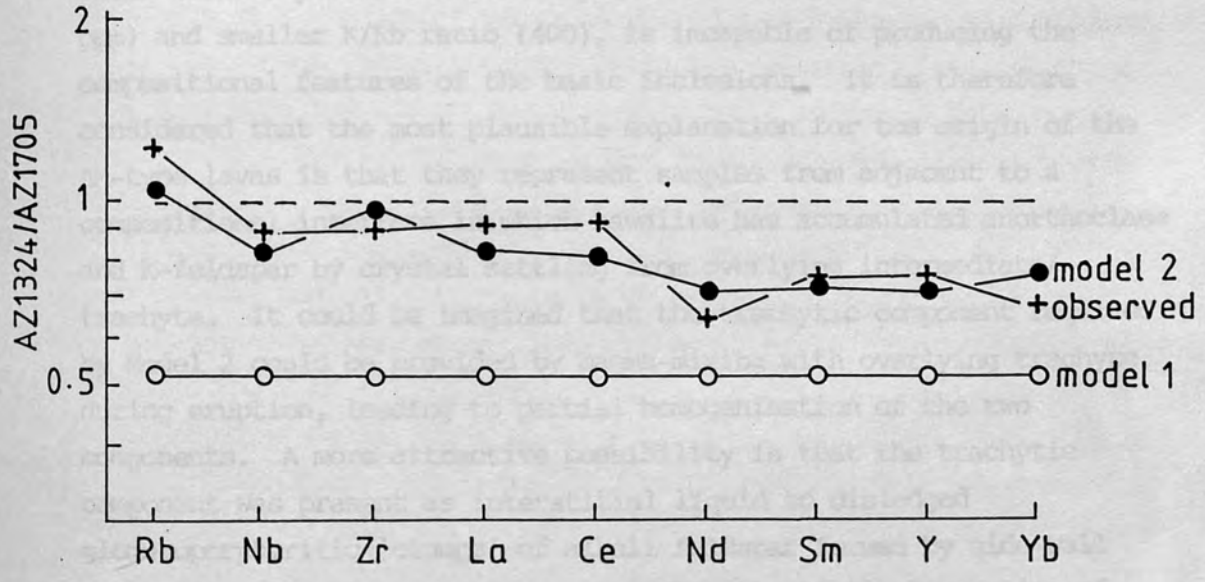

Fig. 3.31 Two models for the origin of the AM-type intermediate lavas from Furnas caldera and the NW flanks of Agua de Pau volcano. Shown are observed and calculated incompatible trace element abundances of lava sample AZ1705 (normalised to hawaiite; AZ1324). Model (1) is for a 48% accumulative hawaiite (mostly alkali feldspar). Model (2) is a three component mix between hawaiite (55%), trachyte (18%) and phenocrysts (27%; mostly alkali feldspar). Mixing proportions for each model are those obtained from least-squares solutions based on major elements (Table 3.8); see text for full explanation of modelling details.

intermediate/trachytic compositional interface, which has accumulated alkali feldspar by crystal settling. Evidence for the latter model is provided by the mixed lava from SE of Queimado (sa no AZ1721). It will be recalled that this flow is characterized by a blocky top which consists of numerous small inclusions of a more basic magma in a trachytic host. The former have petrographic and compositional features similar to the other AM-type lavas, namely alkali feldspar xenocrysts, a positive Eu anomaly, large Ba content (3905 ppm), high K/Rb ratio (572) and low incompatible element contents. Clearly, mixing between hawaiite and the trachytic host of the mixed lava, which lacks a positive Eu anomaly and has a lower content of Ba (1258 ppm) and smaller K/Rb ratio (400), is incapable of producing the compositional features of the basic inclusions. It is therefore considered that the most plausible explanation for the origin of the AM-type lavas is that they represent samples from adjacent to a compositional interface in which hawaiite has accumulated anorthoclase and K-feldspar by crystal settling from overlying intermediate/ trachyte. It could be imagined that the trachytic component required by Model 2 could be provided by magma-mixing with overlying trachyte during eruption, leading to partial homogenisation of the two components. A more attractive possibility is that the trachytic component was present as interstitial liquid to dislodged glomeroporphyritic 'clumps' of alkali feldspar formed by side-wall crystallization of trachytic magma. The potentially large size of such 'clumps' could overcome dynamic objections to a crystal settling model. Similar arguments apply to the mixed lava from Castelo Branco, Faial (Section 2.6.2).

(c) Trachytes

Occurring in the trachytic fall pumice deposits Fogo A, B and 1563 are a number of crystals showing disequilibrium textures with the enclosing glass. Forsteritic olivine (Fo_{78-80}), for example, occurs in Fogo A and B and shows a clear reaction relationship with the matrix. Similar textures are shown by crystal of titaniferous augite, Mg-Al rich titanomagnetite, calcic plagioclase (An_{63}) and

anorthoclase. The compositions of these minerals suggests that they are derived from basaltic to intermediate magmas. Their occurrence as xenocrysts in trachytic rocks could be due to magma-mixing. However, as few of the trachytes fall significantly off the liquid-line of descent trends on the whole rock variation diagrams, it suggests that if magma-mixing has occurred it has not been sufficient to significantly alter their bulk chemistry.

3.6.3 Sub-volcanic Sao Miguel

There is both geological and geophysical evidence for the existence of sub-volcanic magma chambers beneath Sao Miguel (Section 3.2). In recent years, numerous field and laboratory investigations have been made towards understanding magmatic processes in this environment. Studies of large volume pyroclastic deposits from both continental and oceanic settings (eg Eichelberger, 1980; Hildreth, 1979; Sigurdsson and Sparks, 1981) have been particularly fruitful and have pointed towards the existence of stratified magma bodies in which salic magma overlies, denser less evolved liquid. Theoretical studies (Huppert and Sparks 1980, Huppert et al., 1982a) and analogue experiments of magmas using aqueous solutions (McBirney, 1980; Sparks et al., 1984; Turner and Gustafson, 1981) predict that such systems develop compositional variation and density stratification as a result of crystal fractionation. This is envisaged to occur by wall-rock crystallization, yielding a low-density boundary layer of evolved magma which buoyantly rises until it is in gravitational equilibrium.

Hildreth (1979) on the basis of results obtained from his study of the Bishop Tuff, a large volume rhyolitic-andesitic sheet, proposed that the observed chemical zonation of the tuff resulted not from crystal fractionation but through a combination of convection and thermogravitational (Soret) diffusion. However, more recently Soret diffusion effects have been experimentally shown to be incapable of producing the geochemical variations displayed by the Bishop Tuff (Lesher et al., 1982; Walker and Delong, 1982). Furthermore, Michael (1983a, b), using the same data as Hildreth (1979) has successfully

modelled these chemical variations by crystal fractionation.

The applicability of such concepts to Sao Miguel depends on their ability to account for the following observations, some of which have been discused by Wolff and Storey (1984).

(1) The majority of trachytic pumice deposits have source vents located within the calderas (Booth et al., 1978; Walker and Croasdale, 1971).

(2) The trachytic air-fall deposit Fogo A is compositionally zoned with more mafic pumice overlying salic (Chapter 4).

(3) Pumice deposits show a greater degree of differentiation than trachyte lavas.

(4) The final stages of several of the explosive pumice eruptions were accompanied by the extrusion of a trachyte dome (eg the Congro deposit; Booth et al., 1978).

(5) The occurrence of 'basaltic' and 'intermediate' phenocrysts in the trachytic pumice deposits Fogo A, B and 1563.

(6) The occurrence of alkali-feldspar accumulative/magma-mixed intermediate lavas (AM-type) from the NW flanks of Agua de Pau volcano and the Furnas caldera.

(7) The association of intermediate and trachytic derivitives and strongly accumulative ankaramites ($\sim$17wt% MgO) with the stratovolcanoes and the virtual absence of such rocks in the 'waist'.

(8) The Daly gap.

(9) The occurrence of intermediate rocks (M-type) from the NE flanks of Agua de Pau which geochemical evidence suggests

were produced by magma-mixing between trachyte and a fairly primitive basalt (approximately 9wt% MgO, 140 ppm Ni, 370 ppm Cr).

Observation (1) provides evidence for the existence of trachyte magma bodies beneath the central calderas possessing chemical (2, 3) and possibly volatile gradients (4). Observations (5) and (6) suggest that basaltic, intermediate and trachytic magmas coexisted in the same chamber before eruption (shown by the cartoon for the Agua de Pau magma chamber in Fig 3.32). It was suggested earlier that the AM-type lavas (6) represent samples of or adjacent to a compositional interface in which hawaiite has accumulated anorthoclase and K-feldspar (possibly in the form of glomeroporphyritic clumps with interstitial trachytic liquid) by crystal settling from overlying, more salic magma. The association of the accumulative, MgO rich ankaramites with the stratovolcanoes (7) is attributed to extensive crystal settling after basalt has intruded into and ponded below more evolved, less dense magma. The ability of extensive high-level trachytic magma bodies to prevent eruption of more dense, basalts has been demonstrated for Sao Miguel by Booth et al., (1978). Similarly, if as suggested, intermediate magma is capped by a trachyte layer, then unless all the trachyte is first removed, there will be few eruptions of intermediate rocks (8).

Hybrid lavas (9) from the NE flanks of Agua de Pau suggest discrete trachyte magma bodies, rather than a zoned basalt-intermediate-trachyte chamber, beneath this region of the volcano. Modelling indicates that they are the result of mixing of alkali-basalt (28%) and trachyte (72%); there is no evidence for an intermediate component in the mixing process. Booth et al., (1978) have shown that laterally extensive bodies of trachytic magma can form, possibly as a response to caldera collapse, after large plinian-type eruptions (eg Fogo A). The large Ni and Cr contents estimated for the basaltic component (similar to the most primitive basalts from the 'waist') suggests that it had not undergone significant high-level crystal fractionation before mixing with trachyte. This observation

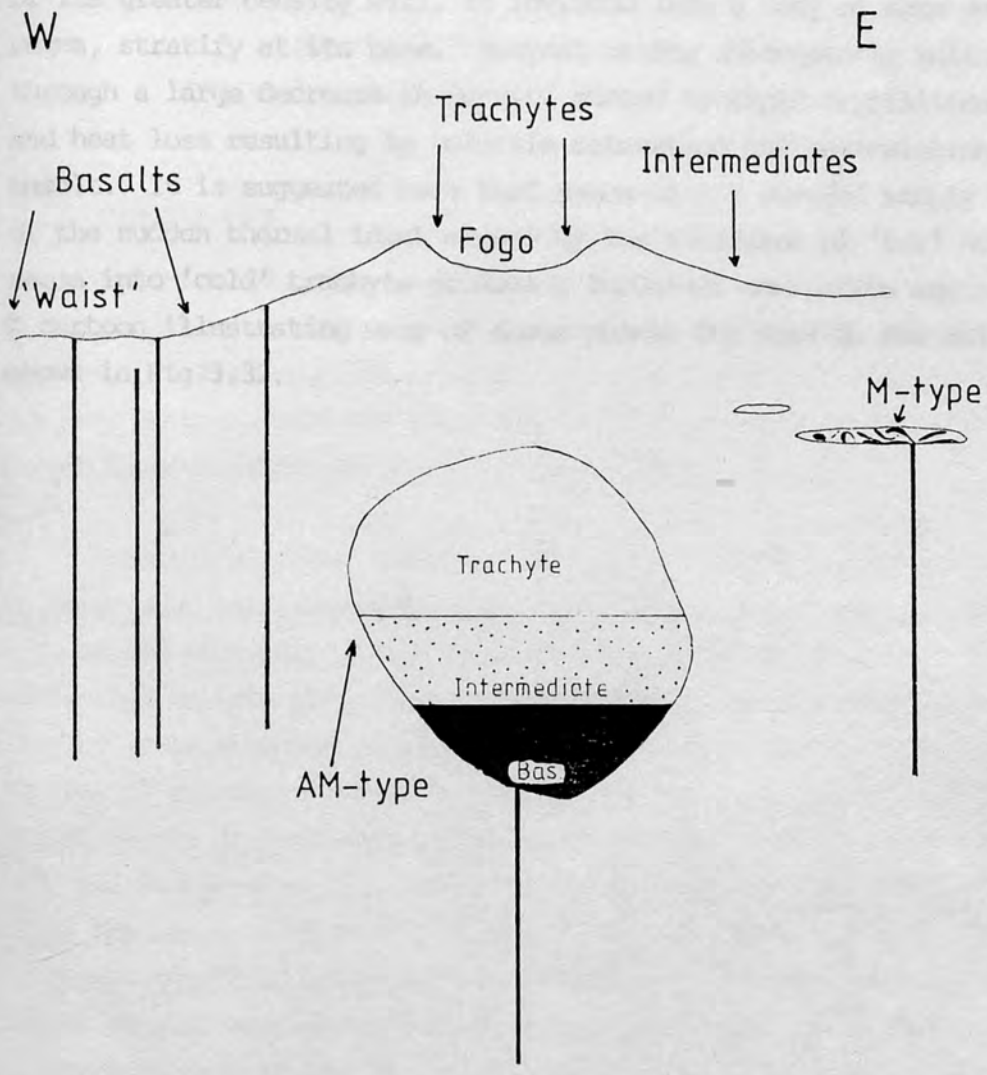

Fig. 3.32 Cartoon of proposed sub-volcanic magma chamber of Agua de Pau volcano. The roof (volatile rich) is postulated to lie under the Fogo caldera in view of the dominance of explosive trachytic eruptions from this region. The association of mixed lavas (AM-type) which may be samples of/or adjacent to an interface between intermediate and trachytic magma, with the NW flanks, and intermediate lavas which fall on crystal-liquid fractionation trends with the SE flanks of the volcano could be a function of chamber morphology. Stratification of basalt beneath intermediate magma would favour the development of highly accumulative ankaramites at the base of the chamber by crystal settling. Basalt-trachyte mixed lavas (M-type) from the NE flanks may suggest discrete cupolas of trachytic magma beneath this part of the volcano.

is at variance with the magma-mixing mechanism proposed by Eichilberger (1980) and Huppert et al . (1982b) who argue that basalt because of its greater density will, if intruded into a body of more evolved magma, stratify at its base. Buoyant mixing subsequently taking place through a large decrease in density caused by rapid crystallization and heat loss resulting in volatile saturation and vesiculation of the basalt. It is suggested here that magma-mixing occured simply because of the sudden thermal input caused by the intrusion of 'hot' basic magma into 'cold' trachyte producing turbulent convection and mixing. A cartoon illustrating many of these points for Agua de Pau volcano is shown in Fig 3.32.

CHAPTER 4

COMPOSITIONAL VARIATIONS IN THE TRACHYTIC PYROCLASTIC SUCCESSION OF SAO MIGUEL

4.1 INTRODUCTION

As previously stated in Chapter 3, the Recent stratigraphy of Sao Miguel records large numbers of trachytic pyroclastic deposits produced by sub-plinian to plinian eruptions. Most of these deposits have been erupted from the three active Quaternary stratovolcanoes of Sete Cidades, Agua de Pau and Furnas (Fig. 3.1).

Previous studies, mainly on composite basaltic/andesite volcanoes associated with destructive plate margins, have shown that knowledge of the volcanic history of a particular centre facilitates discrimination between processes capable of producing the more evolved volcanic rocks observed at any one volcano. For example, detailed sampling of stratigraphic sections exposed at the composite volcanoes of Santa Maria in Guatemala and Boqueron in El Salvador has respectively allowed Rose et al. (1977) and Fairbrothers et al. (1978) to define the temporal magmatic evolution of each centre. In each case fractional crystallization of a basaltic melt, rather than a partial melting origin, was identified as the process most likely responsible for the formation of the associated andesites.

Detailed field studies on Sao Miguel by Walker and Croasdale (1971) and Booth et al. (1978) have established, by superposition, the relative ages of the most recent trachytic air fall pumice deposits. It was shown that in the last 5,000 years there have been some 38 explosive trachytic eruptions from Sete Cidades, Agua de Pau and Furnas volcanoes. This Chapter examines the temporal variations in chemistry and mineralogy of part of this pyroclastic succession. Some of this work has recently been published as a separate paper (Storey 1981).

4.2 TEPHROCHRONOLOGY

The large central crater of Agua de Pau, the Fogo caldera, is believed to be a collapse structure attributed to a large plinian eruption (Walker and Croasdale 1971). The air fall pumice deposit produced, Fogo A, was named after the caldera. It has been dated at 4550 BP by ^{14}C measurements on carbonised wood fragments associated with the deposit (Shotton et al. 1968, 1969) and forms the base for the study of 5,000 years of volcanism on Sao Miguel by Booth et al. (1978). It was shown by these authors that since Fogo A, a further four trachytic air fall pumice deposits were erupted from the Fogo caldera, the last being the historic explosive eruption of 1563 AD. These subsequent deposits were designated as Fogo B, C, D, and 1563, indicating the order in which they occurred.

Fogo A bears special mention as the pumice clasts show marked changes in colour and physical characteristics through the deposit. The deposit grades upwards from the typical buff coloured pumice into first a streaky and then a more dense mafic variety of pumice, the latter two types being volumetrically subordinate to the first. The explosive 1563 AD eruption from the Fogo caldera is also of interest as it was shortly followed by the extrusion of two small basaltic flows from a scoria cone on the north-west flanks of Agua de Pau volcano near Queimado (Fig. 3.1 and 3.3).

Since the caldera-forming, plinian eruption of Fogo A (Walker & Croasdale, 1971), basaltic eruptions on Sao Miguel have been restricted to a fairly narrow WNW-ESE zone in the west of the island (Fig. 3.4). As a means of explaining the paucity of basaltic eruptions over the rest of the island during this period, Booth et al. (1978) suggested that perhaps a large body of trachytic magma had spread out laterally between Agua de Pau and Furnas volcanoes following the plinian eruption, thereby restricting the ability of basaltic magma to reach the surface. The existence of a salic magma body below this area has also been postulated by Machado (1966, 1973) from geophysical evidence.

During the same 5,000 year period, there were twenty two explosive trachytic eruptions from Furnas and Sete Cidades volcanoes. The

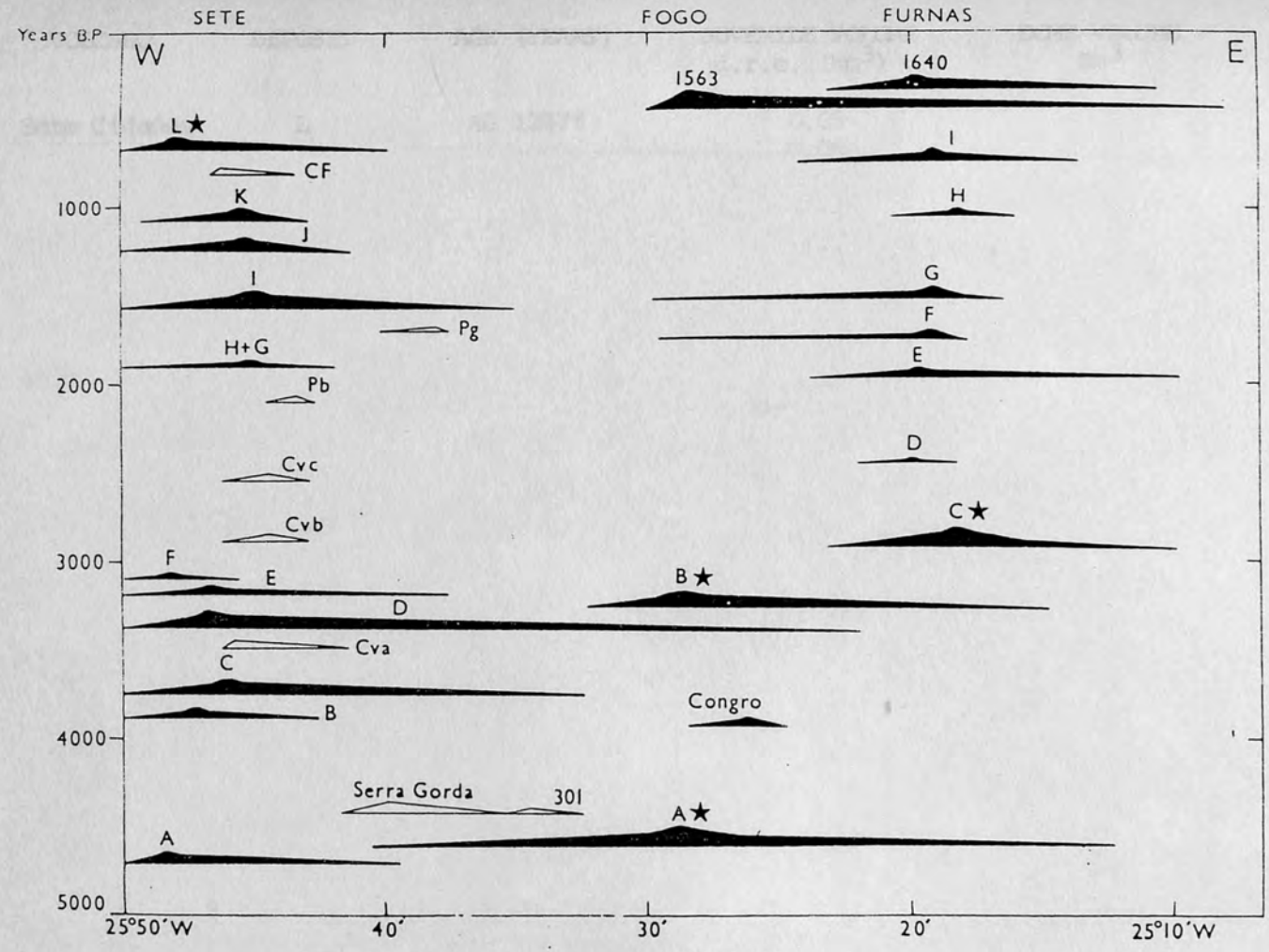

Fig. 4.1 Diagram summarising the chronological sequence of explosive eruptions on Sao Miguel during the past 5000 years. The width of the black bands show the approximate west to east extent of trachytic pyroclastic fall deposits and the thickness of each bar is crudely proportional to the thickness of the deposit. Stars indicate deposits for which radiocarbon ages are available. The open bars show some of the main basaltic pyroclastic fall deposits. From Booth et al. (1978).

VOLCANO	DEPOSIT	AGE (YEARS)	JUVENILE VOLUME d.r.e. (km^3)	DOME VOLUME Km^3
Sete Cidades	L	AD 1287*	0.05	
	K		0.06	
	J		0.08	
	I		0.11	
	G,H		0.07	
	E,F		0.05	
	D		0.13	0.25
	C		0.11	
	B		0.06	
	A		0.11	
Fogo	1563	AD 1563	0.17+	
	C,D			
	B	3242 BP*	0.23+	
	A	4550 BP*	0.94+	
Congro	Congro		0.01	< 0.01
Furnas	1640	AD 1640	0.08	0.04
	I		0.02	
	H		< 0.01	
	G		0.04	
	F		0.07	0.03
	E		0.06	
	D		< 0.01	
	C	2900 BP*	0.30	
	A,B		0.02	

*Radiocarbon dates from Shotton, Blundell and Williams (1968, 1969, 1970) and Shotton and Williams (1971)

+Calculated from revised total volumes given by Walker (1981a) see text for method

Table 4.1 The succession, ages and volumes of recent trachytic pumice deposits and associated domes from Sao Miguel (after Booth et al., 1978)

youngest deposit from Furnas is the product of the historic eruption of 1640 AD. In addition one other fall deposit originated from the small maar-like crater of Lagoa do Congro which is regarded by Booth et al. (1978) as a flank vent of Agua de Pau volcano. The chronological sequence of explosive volcanic eruptions on Sao Miguel during the last 5,000 years is summarised in Fig. 4.1. The pumice fall deposit successions with ages and juvenile volumes, where known are given in Table 4.1. With the exception of the three largest deposits, juvenile volumes, expressed as dense rock equivalent (d.r.e.), are taken from Booth et al. (1978). Walker (1981a)gives revised total volume estimates of Fogo A, B and 1563, based on the results of his independent crystal concentration method used to determine the volumes of three large air fall deposits in New Zealand (Walker 1980, 1981b). The method allows, on an area versus thickness plot of a pumice deposit, an accurate straight line extrapolation to a limiting thickness of 1 μm. The importance of the technique is that it allows the considerable proportion of fine ash released during a plinian eruption to be accurately quantified. Walker's revised volumes of Fogo A, B and 1563, minus their lithic volumes (Booth et al. 1978) are given in Table 4.1.

The geochemistry of the five Fogo deposits, the Congro ash and Furnas A, C, F and 1640 form the main basis of this Chapter.

4.3 MINERALOGY

A brief summary of the mineralogy of the pyroclastic deposits is given below. The reader is referred to Chapter 3 for a detailed discussion on their petrography.

Pumice clasts from the Fogo and Furnas trachytic air fall deposits, are generally glassy to cryptocrystalline, with crystal contents not usually exceeding 10% by volume. The phenocryst assemblage consists predominantly of alkali feldspar with ubiquitous but minor clinopyroxene, biotite and Fe - Ti oxides. Accessory phases include microphenocrysts of apatite and pyrrhotite grains both occurring as inclusions in other minerals. Also present are rare crystals of zircon which have only been found in Fogo 1563.

Occurring in several of the air fall pumice deposits, are a number of crystals showing disequilibrium textures with the enclosing glass. Forsteritic olivine (Fo_{78} - Fo_{80}), for example, occurs in Fogo A and B and shows a clear reaction relationship with the matrix. Similar textures are shown by crystals of aluminous titanaugite and plagioclase in Fogo A, B and 1563.

4.4 MINERAL CHEMISTRY

(1) Feldspars

Euhedral phenocrysts of alkali feldspar are volumetrically the most important mineral in the Fogo and Furnas pumice deposits. Microprobe analyses show they are calcium-bearing sanidines, with individual crystals showing limited compositional variation. Representative analyses are given in Table 4.2. Zoning, when present, can be one of two types; crystals become either more sodic from core to rim, or conversely they become more potassic from core to rim. An example of the latter type of zoning is shown by crystals from Fogo B. This may be seen in Fig. 4.2 where sanidines from the Fogo deposits are plotted in part of the An-Ab-Or triangle. Although there is compositional overlap between sanidine crystals from the different air fall pumice deposits, a general trend emerges consisting of a decrease in the anorthite and orthoclase components of crystals from successively younger deposits. Also shown, on the Ab-Or join, is the mol. $Na_2O/Na_2O + K_2O$ ratio for the whole pumice clast for each of the Fogo air fall deposits. It is evident that the increasing albite component of sanidine crystals up through the Fogo pyroclastic succession, is mirrored by an increase in the mol. $Na_2O/Na_2O + K_2O$ ratio of the whole pumice clast. In the system $NaAlSi_3O_8$-$KAlSi_3O_8$-H_2O both feldspars and the whole pumice clast fall on the potassium feldspar side of the thermal minimum on the Ab-Or join (Bowen and Tuttle 1950). As the Na/K ratio is lower for feldspar than the host pumice clast, then crystal fractionation would result in both the feldspar and liquid becoming more sodic with differentiation.

In strong contrast, the Furnas air fall deposits show no significant temporal variation in the mol. $Na_2O/Na_2O + K_2O$ ratio. Their values (0.67-0.69) are similar to those of Fogo D and 1563, the most compositionally evolved of the Agua de Pau pyroclastic deposits.

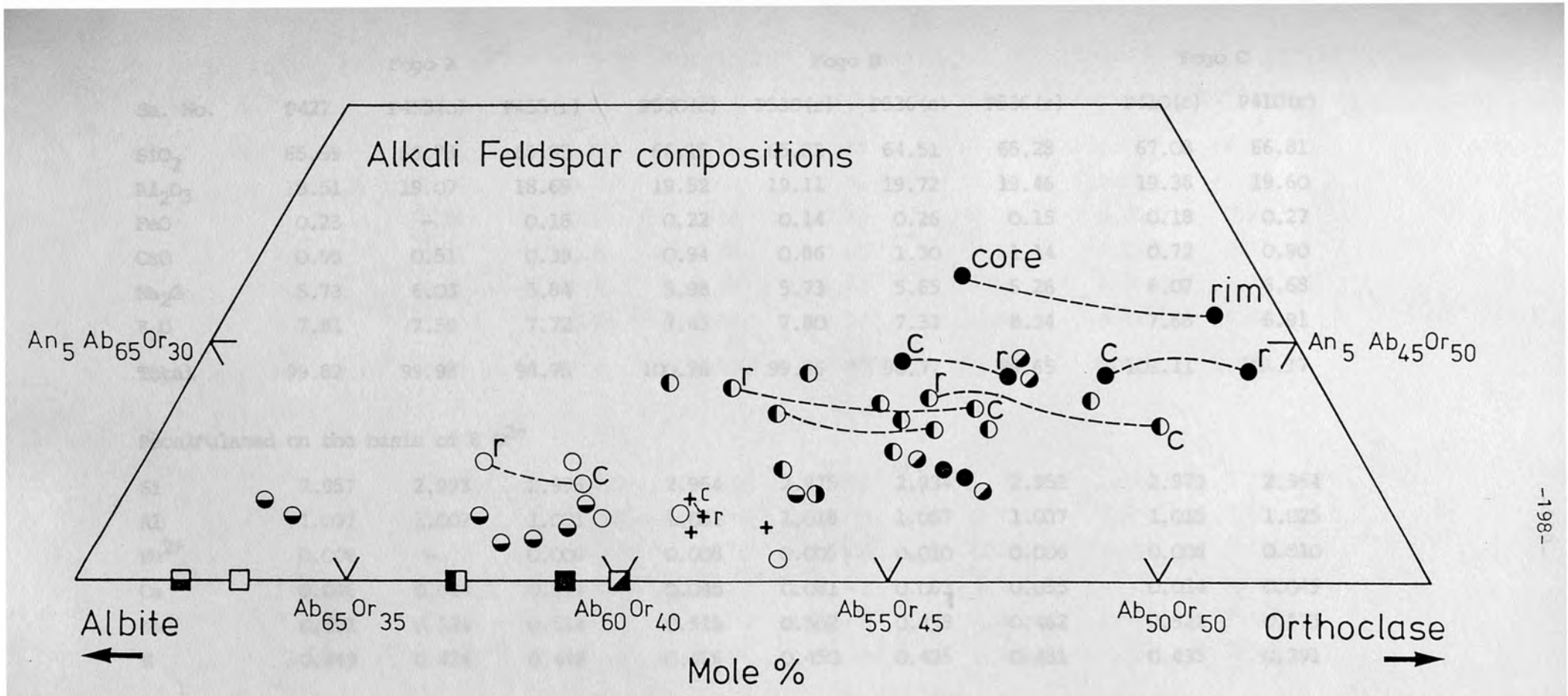

Fig. 4.2 Alkali feldspar compositions from the different Fogo pumice deposits and Furnas F, plotted in part of the An-Ab-Or triangle. Symbols: ◕ Fogo A, ● Fogo B, ◐ Fogo C, ○ Fogo D, ◒ Fogo 1563, + Furnas F. Also shown, on the Ab-Or join, is the mol. $Na_2O/Na_2O + K_2O$ ratio for the host Fogo pumice clasts (square symbols).

	Fogo A			Fogo B				Fogo C	
Sa. No.	P427	P455(c)	P455(r)	P530(c)	P530(r)	P536(c)	P536(r)	P410(c)	P410(r)
SiO_2	65.59	66.78	65.95	66.15	65.82	64.51	65.28	67.08	66.81
Al_2O_3	19.51	19.07	18.69	19.52	19.11	19.72	19.46	19.38	19.60
FeO	0.23	-	0.16	0.22	0.14	0.26	0.15	0.18	0.27
CaO	0.95	0.51	0.39	0.94	0.86	1.30	1.14	0.72	0.90
Na_2O	5.73	6.03	5.84	5.98	5.73	5.65	5.28	6.07	6.68
K_2O	7.81	7.59	7.72	7.45	7.80	7.33	8.34	7.68	6.91
Total	99.82	99.98	98.75	100.26	99.46	98.77	99.65	101.11	101.17
Recalculated on the basis of 8 O^{2-}									
Si	2.957	2.993	2.996	2.964	2.975	2.934	2.952	2.979	2.964
Al	1.037	1.007	1.001	1.031	1.018	1.057	1.037	1.015	1.025
Fe^{2+}	0.009	-	0.006	0.008	0.005	0.010	0.006	0.006	0.010
Ca	0.046	0.024	0.019	0.045	0.041	0.063	0.055	0.034	0.043
Na	0.501	0.524	0.514	0.519	0.502	0.498	0.462	0.522	0.575
K	0.449	0.434	0.448	0.426	0.450	0.425	0.481	0.435	0.391

(c) = crystal core (r) = crystal rim

Table 4.2 Selected feldspar analyses

	Fogo D			Fogo 1563		Furnas F		
Sa. No.	P450(c)	P450(r)	P502	P525(c)	P525(r)	P220	P222(c)	P2222(r)
SiO_2	66.82	66.03	66.92	67.15	67.78	67.26	66.67	66.99
Al_2O_3	19.07	19.16	19.18	19.04	18.96	18.96	19.31	19.20
FeO	0.19	0.18	0.25	0.18	0.19	0.19	0.26	0.26
CaO	0.42	0.53	0.35	0.34	0.21	0.24	0.32	0.27
Na_2O	6.87	7.20	7.45	6.78	7.20	6.29	6.36	6.44
K_2O	6.72	6.50	5.65	6.61	6.96	7.03	6.72	6.80
Total	100.09	99.60	99.80	100.10	101.30	99.97	99.64	99.98
Recalculated on the basis of 8 O^{-2}								
Si	2.988	2.971	2.988	2.997	2.997	3.005	2.988	2.994
Al	1.005	1.016	1.009	1.002	0.989	0.999	1.020	1.011
Fe^{2+}	0.007	0.007	0.009	0.007	0.007	0.007	0.010	0.010
Ca	0.020	0.025	0.017	0.016	0.010	0.011	0.016	0.013
Na	0.596	0.628	0.645	0.586	0.617	0.545	0.552	0.557
K	0.383	0.373	0.322	0.376	0.393	0.401	0.384	0.388

(c) = crystal core (r) = crystal rim

Table 4.2 contd

Finally, it should be mentioned that rarer crystals of plagioclase occur in some of the air fall deposits. These crystals generally have resorbing margins while their compositions also suggest that they were unlikely to have been in equilibrium with a trachytic melt. For example, in Fogo 1563 are calcium rich plagioclase crystals ranging in composition up to An_{63}.

(2) Biotites

Euhedral pleochroic phenocrysts of biotite are ubiquitous in the Fogo and Furnas air fall pumice deposits. Apart from a near opaque crystal in Fogo 1563 the biotites show no sign of oxidation. Listed in Table 4.3 are representative analyses showing the compositional range for the different Fogo air fall deposits. It can be seen that individual crystals show limited variation from core to rim. The biotites from the Fogo pumice deposits are notable for their high Ti content, containing 5.8-9.5 wt% TiO_2. The one biotite analysed from a Furnas pumice deposit had lower Ti containing 4.9% TiO_2.

The temporal variation of the Fogo biotite compositions is shown in Fig. 4.3 by a triangular plot of Ti, Mg and Fe. As with co-existing alkali feldspars, there is some compositional overlap in biotites from the different Fogo deposits, however there is a clear association of the more Fe-rich/Ti-poor crystals with the younger air fall pumice deposits. This trend mirrors a general increase in the Fe/Mg ratio of the whole pumice clast up through the Fogo pyroclastic succession.

(3) Clinopyroxenes

Commonly, the clinopyroxene present in the Fogo and Furnas pumice deposits, is a green low Al-Ti variety. Selected analyses (Table 4.4) show that clinopyroxenes associated with the youngest Fogo air fall pumice deposits have the highest Fe/Mg ratios. There is little compositional difference between clinopyroxene phenocrysts analysed from Furnas F and Furnas 1640. Also present, notably in Fogo 1563 where there are three types of clinopyroxene compositionally distinct in terms of Si, Al and Ti contents, are purple aluminous titanaugites containing up to 10 wt% Al_2O_3 (Table 4.4). Pyroxenes with the least evolved compositions

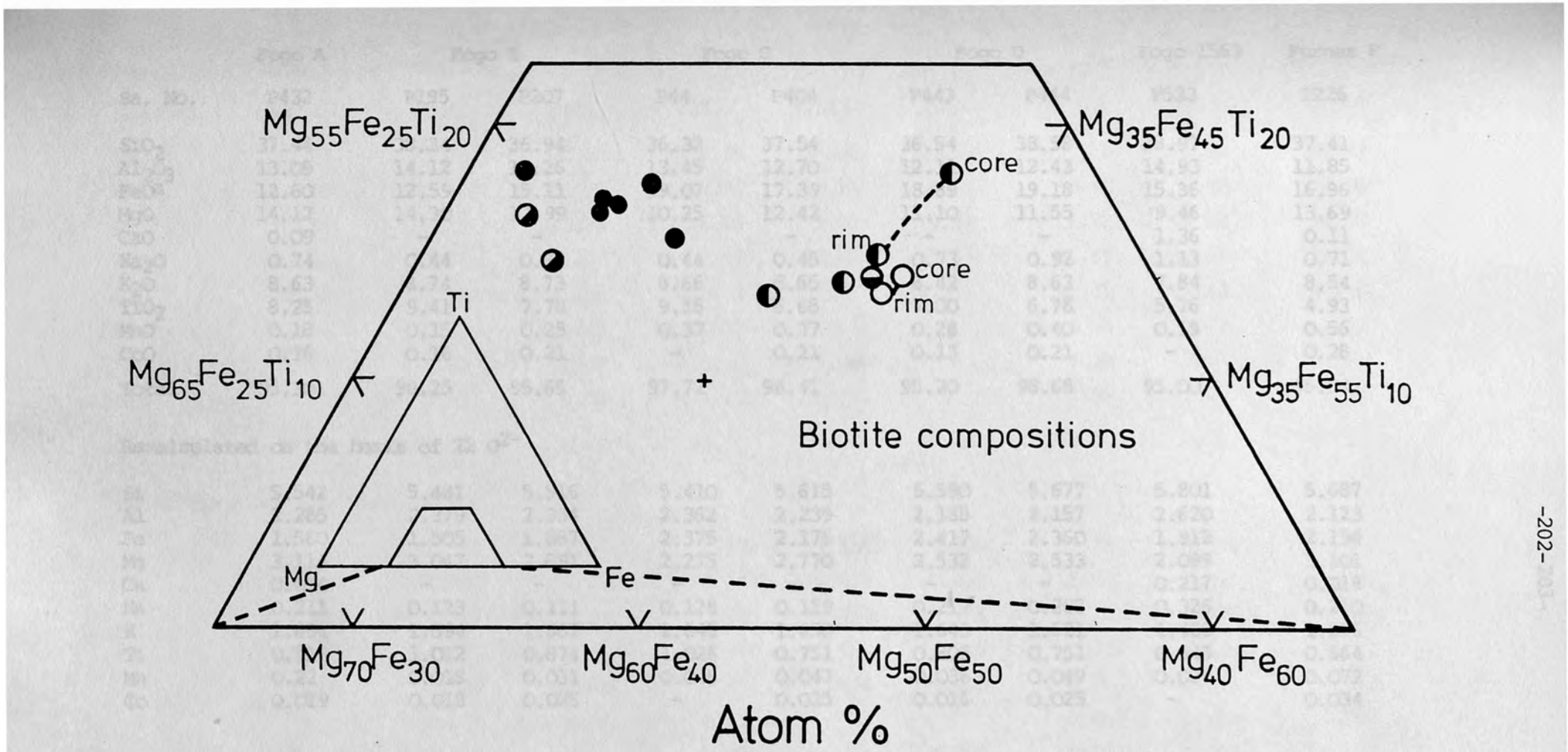

Fig. 4.3 Biotite compositions from the different Fogo pumice deposits plotted in terms of their Ti, Mg and and Fe contents. One biotite analysis from Furnas F is also shown. Symbols as Fig. 4.2.

	Fogo A	Fogo B		Fogo C		Fogo D		Fogo 1563	Furnas F
Sa. No.	P432	P195	P207	P44	P404	P443	P444	P523	P226
SiO_2	37.44	38.34	36.94	36.32	37.54	36.54	38.58	38.97	37.41
Al_2O_3	13.09	14.12	13.26	13.45	12.70	12.11	12.43	14.93	11.85
FeO[a]	12.60	12.59	15.11	19.07	17.39	18.89	19.18	15.36	16.96
MgO	14.12	14.30	12.99	10.25	12.42	11.10	11.55	9.46	13.69
CaO	0.09	-	-	-	-	-	-	1.36	0.11
Na_2O	0.74	0.44	0.38	0.44	0.45	0.73	0.92	1.13	0.71
K_2O	8.63	8.74	8.73	8.66	8.65	8.42	8.63	7.84	8,54
TiO_2	8.25	9.41	7.78	9.16	6.68	7.00	6.78	5.76	4.93
MnO	0.18	0.15	0.25	0.37	0.37	0.28	0.40	0.19	0.56
CoO	0.16	0.16	0.21	-	0.21	0.13	0.21	-	0.28
Total	95.30	98.25	95.65	97.72	96.41	95.20	98.68	95.00	95.04
Recalculated on the basis of 22 O^{2-}									
Si	5.542	5.481	5.516	5.410	5.615	5.590	5.677	5.801	5.687
Al	2.285	2.379	2.334	2.362	2.239	2.185	2.157	2.620	2.123
Fe	1.560	1.505	1.887	2.375	2.176	2.417	2.360	1.912	2.156
Mg	3.114	3.047	2.891	2.275	2.770	2.532	2.533	2.099	3.101
Ca	0.014	-	-	-	-	-	-	0.217	0.018
Na	0.211	0.123	0.111	0.128	0.129	0.217	0.262	0.326	0.210
K	1.631	1.594	1.662	1.645	1.650	1.643	1.621	1.488	1.656
Ti	0.919	1.012	0.874	1.026	0.751	0.805	0.751	0.645	0.564
Mn	0.22	0.018	0.031	0.046	0.047	0.036	0.049	0.024	0.072
Co	0.019	0.018	0.025	-	0.025	0.016	0.025	-	0.034

[a] All Fe as FeO

Table 4.3 Selected biotite analyses

	Fogo A	Fogo B	Fogo C	Fogo 1563			Furnas F		Furnas 1640
Sa. No.	P434	P534	P415	P231	P517	P522	P216 (c)	P216 (r)	UC558
SiO_2	52.97	52.30	52.64	51.45	42.03	49.36	52.54	52.59	51.42
Al_2O_3	0.96	0.70	0.76	0.90	10.25	4.89	0.45	0.82	0.94
FeO[a]	9.26	10.24	12.34	15.05	9.08	8.51	11.72	12.22	11.57
MgO	13.01	11.94	11.00	8.47	10.62	13.74	11.65	10.86	11.36
CaO	21.72	21.95	21.96	20.34	21.97	21.16	21.25	21.43	20.96
Na_2O	-	0.53	0.45	1.39	-	-	0.58	0.47	0.84
TiO_2	0.57	0.49	0.49	0.40	5.64	2.22	0.39	0.42	0.43
MnO	0.76	0.85	0.98	1.70	-	-	1.36	1.32	1.50
Total	99.25	99.00	100.62	99.70	99.59	99.88	99.94	100.13	99.02
Recalculated on the basis of 6 O^{2-}									
Si	1.992	1.988	1.986	1.992	1.596	1.840	1.992	1.995	1.972
Al	0.043	0.031	0.034	0.041	0.459	0.215	0.020	0.037	0.042
Fe^{2+}	0.291	0.325	0.389	0.486	0.288	0.265	0.372	0.388	0.371
Mg	0.729	0.677	0.619	0.487	0.601	0.763	0.658	0.614	0.650
Ca	0.875	0.894	0.888	0.844	0.894	0.845	0.863	0.871	0.862
Na	-	0.039	0.033	0.104	-	-	0.043	0.034	0.062
Ti	0.016	0.014	0.014	0.012	0.161	0.062	0.011	0.012	0.013
Mn	0.024	0.027	0.031	0.056	-	-	0.044	0.042	0.049

[a] All Fe as FeO

Table 4.4 Selected pyroxene analyses

commonly show a reaction relationship with the pumice glass. These disequilibrium features are discussed further in Chapter 3.

(4) Fe-Ti oxides

All of the Fogo and Furnas pumice deposits examined contained titanomagnetite. In addition Fogo A, B and C contained ilmenite. In the geothermometry section of Chapter 5, where the mineral chemistry of the Fe-Ti oxides is discussed in detail, pre-eruptive temperatures have been estimated from equilibrium titanomagnetite-ilmenite mineral pairs using the geothermometer and oxygen barometer of Buddington and Lindsley (1964). Temperature estimates, which have uncertainties of $\pm$ 30°C are 960°C, 910°C and 880°C for Fogo A, B and C respectively.

4.5 MAJOR ELEMENTS

Major element analyses and the normative mineralogies of the Fogo and Furnas air fall pumice deposits are given in Tables 4.5 and 4.6. To overcome the variable post-eruptive hydration and oxidation of the pumice glasses, and thereby facilitate comparison between the deposits, the analyses have been recalculated to 100% totals on a volatile free basis. Also, the normative mineralogies have been calculated using a constant FeO/Fe_2O_3 ratio of 1.36, which was the highest value measured in any of the deposits (Appendix 2). Only whole pumice clasts were analysed so as to avoid recording geochemical features resulting from crystal fractionation processes which occur during the actual pyroclastic producing eruption (Walker 1972). Care was also taken to select only fresh samples for analysis in order to minimise any deviation from the actual magma composition due to post eruptive leaching of alkali elements, a process to which volcanic glasses are particularly prone. The only suspected case of significant leaching of the alkali elements in the samples studied, is AZ1544 which contains normative corundum.

4.5.1 Classification

The analysed air fall pumice deposits are all trachytic with Thornton-Tuttle differentiation indices > 75 (Thornton and Tuttle 1960). Their compositions are transitional in two respects. Firstly, they straddle the silica saturation/undersaturation boundary being either

	Major elements								
	Fogo A	Fogo A (middle)	Fogo A (top)	Fogo B	Fogo C	Fogo D	Fogo 1563	Congro deposits (ash)	(lava)
Sa. No.	AZ1544	AZ1323	AZ1377	AZ1378	AZ1394	AZ1188	AZ1149	AZ1619	AZ1672
SiO_2	63.06	61.44	61.74	62.23	63.22	65.13	64.83	63.17	63.42
TiO_2	0.64	0.97	1.02	0.92	0.58	0.33	0.45	0.70	0.69
Al_2O_3	19.26	19.79	17.60	18.17	18.78	16.49	16.96	18.50	18.04
Fe_2O_3	1.47	1.70	1.67	1.62	1.40	1.92	1.39	1.29	1.44
FeO	1.99	2.39	2.28	2.23	1.91	2.62	1.89	1.75	1.96
MnO	0.13	0.13	0.14	0.15	0.15	0.29	0.22	0.12	0.10
MgO	0.47	0.94	1.14	0.96	0.33	0.22	0.27	0.49	0.59
CaO	1.31	1.99	2.18	1.70	0.98	0.64	0.85	1.34	1.44
Na_2O	5.51	5.64	5.97	6.00	6.68	7.00	7.61	6.01	5.65
K_2O	6.08	5.94	6.07	5.88	5.89	5.28	5.46	6.53	6.56
P_2O_5	0.08	0.15	0.19	0.14	0.08	0.08	0.07	0.10	0.11

Table 4.5 Analyses of pumice fall deposits from Agua de Pau volcano

CIPW normative minerals

	Fogo A	Fogo A (middle)	Fogo A (top)	Fogo B	Fogo C	Fogo D	Fogo 1563	Congro deposits (ash)	Congro deposits (lava)
Sa. No.	AZ1544	AZ1323	AZ1377	AZ1378	AZ1394	AZ1188	AZ1149	AZ1019	AZ1672
Q	3.7	-	-	-	-	2.3	-	-	1.6
Or	35.9	35.2	35.9	34.8	34.8	31.2	32.3	38.6	38.8
Ab	46.6	47.8	48.7	50.8	55.2	55.4	56.8	50.8	47.8
An	6.0	8.4	3.3	5.3	3.9	-	-	4.2	4.5
C	1.4	-	-	-	-	-	-	-	-
Ne	-	-	1.0	-	0.7	-	-	-	-
Ac	-	-	-	-	-	3.4	4.0	-	-
Mt	2.1	2.2	2.4	2.4	2.0	1.1	-	1.9	2.1
Il	1.2	1.8	1.9	1.8	1.1	0.6	0.9	1.3	1.3
Ap	0.2	0.4	0.4	0.3	0.2	0.2	0.2	0.2	0.3
Na_2OSiO_2	-	-	-	-	-	-	0.7	-	-
Di	-	0.6	5.1	1.8	0.4	2.3	3.3	1.5	1.6
Hy	2.8	2.9	-	2.8	-	3.5	1.2	0.7	2.1
Ol	-	0.8	1.3	0.2	1.7	-	0.7	0.7	-
D.I.	86.3	82.9	85.5	85.5	90.7	88.9	89.1	89.5	87.9
mol. $Na_2O/Na_2O + K_2O$	0.58	0.59	0.60	0.61	0.63	0.67	0.68	0.58	0.57
A.I.	0.81	0.84	0.93	0.89	0.92	1.04	1.09	0.92	0.91

D.I. Thornton-Tuttle differentiation index A.I. Agpaitic index

Table 4.5 contd

Trace elements

	Fogo A	Fogo A (middle)	Fogo A (top)	Fogo B	Fogo C	Fogo D	Fogo 1563	Congro (ash)	deposit (lava)
Sa. No.	AZ1544	AZ1323	AZ1377	AZ1378	AZ1394	AZ1188	AZ1149	AZ1019	AZ1672
La	74.4	78.8	80.7	112.7	136.2	189.7	197.1	95.3	72.9
Ce	150.6	195.0	172.8	230.8	290.6	439.9	362.3	187.6	164.6
Nd	55.3	75.2	58.8	87.1	99.8	151.0	129.7	59.3	54.0
Sm	11.8	14.1	12.0	16.7	17.5	30.1	27.3	13.6	11.0
Eu	1.90	2.12	2.43	1.69	1.16	0.39	0.62	2.30	2.64
Tb	1.2	1.6	1.3	1.9	2.1	3.1	2.7	1.3	1.0
Yb	3.3	3.9	3.6	5.4	6.1	9.8	8.1	3.9	2.9
Lu	0.49	0.66	0.49	0.65	0.87	1.19	1.13	0.58	-
Y	36.0	43.0	37.0	53.0	67.0	107.0	100.0	40.00	33
Zr	867.0	806.0	681.0	974.0	1274.0	1779.0	1906.0	875	753
Nb	121.0	136.0	118.0	176.0	222.0	339.0	442.0	149	127
Th	15.9	-	15.2	23.5	34.3	41.3	48.0	22.7	-
Rb	117.0	139.0	132.0	160.0	189.0	281.0	348.0	152	150
Sr	115.0	240.0	278.0	115.0	14.0	6.0	14.0	136	202
Ba	312.0	501.0	531.0	200.0	74.0	15.0	63.0	406	582
Eu/Eu*	0.60	0.52	0.72	0.35	0.19	0.05	0.08	0.61	0.84
K/Rb	432.0	354.0	382.0	305.0	259.0	156.0	130.0	357	363
Rb/Sr	1.0	0.58	0.5	1.4	13.5	46.8	24.9	1.1	0.74
Zr/Nb	7.2	5.9	5.8	5.5	5.7	5.3	4.3	5.9	5.9
Nb/Y	3.4	3.2	3.2	3.3	3.3	3.2	4.4	-	-
La_N/Yb_N	15.2	13.6	15.1	14.1	15.1	13.1	16.4	16.5	17.0
La_N/Sm_N	4.1	3.5	4.2	4.3	3.8	4.0	4.5	4.4	4.2

Table 4.5 contd

Major elements

	Furnas A	Furnas C	Furnas F	Furnas 1640
Sa. No.	AZ1686	AZ1678	AZ1629	AZ1538
SiO_2	63.43	63.38	63.67	63.47
TiO_2	17.19	17.15	17.27	17.27
Al_2O_3	17.19	17.15	17.27	17.27
Fe_2O_3	1.63	1.57	1.51	1.54
FeO	2.22	2.13	2.05	2.10
MnO	0.28	0.27	0.31	0.26
MgO	0.43	0.40	0.37	0.46
CaO	0.75	0.75	0.75	0.78
Na_2O	7.96	8.04	7.69	7.79
K_2O	5.57	5.72	5.81	5.72
P_2O_5	0.09	0.09	0.08	0.08

CIPW normative minerals

Q	-	-	-	-
Or	32.9	33.8	34.3	33.8
Ab	51.9	50.9	51.7	51.4
An	-	-	-	-
C	-	-	-	-
Ne	3.0	3.0	2.6	3.0
Ac	4.7	4.5	4.4	4.5
Mt	-	-	-	-
Il	0.9	0.9	0.9	1.0
Ap	0.2	0.2	0.2	0.2
Na_2SiO_2	1.1	1.5	0.8	0.9
Di	2.7	2.7	2.8	2.9
Hy	-	-	-	-
Ol	2.7	2.4	2.3	2.4
D.I.	87.8	87.7	88.6	88.2
mol. $Na_2O/Na_2O + K_2O$	0.68	0.69	0.67	0.67
A.I.	1.11	1.13	1.10	1.10

D.I. Thornton-Tuttle differentiation index A.I. Agpaitic index

Table 4.6 Analyses of pumice fall deposits from Furnas volcano

Trace elements

	Furnas A	Furnas C	Furnas F	Furnas 1640
Sa. No.	AZ1686	AZ1678	AZ1629	AZ1538
La	190.9	161.7	179.0	159.7
Ce	421.0	315.8	353.1	316.6
Nd	136.0	117.6	126.6	120.5
Sm	32.7	22.4	26.3	23.8
Eu	0.80	0.89	0.94	1.05
Tb	2.7	2.4	2.7	2.4
Yb	7.8	6.4	8.1	6.5
Lu	1.09	0.89	1.08	0.96
Y	83	79	86	72
Zr	1430	1337	1428	1232
Nb	329	309	334	284
Th	31.2	26.4	-	26.8
Rb	237	224	233	210
Sr	3	3	< 2	7
Ba	15	20	27	25
Eu/Eu*	0.10	0.12	0.14	0.14
K/Rb	195	212	207	226
Rb/Sr	79	75	-	30
Zr/Nb	4.3	4.3	4.3	4.3
Nb/Y	4.0	3.9	3.9	3.9
$La_N Yb_N$	16.5	17.1	14.9	16.6
La_N/Sm_N	3.7	4.5	4.3	4.2

Table 4.6 contd

nepheline or quartz and/or hypersthene normative. Secondly, they range between being metaluminous to mildly peralkaline. Of the latter those which are quartz normative fall into the comenditic trachyte field in the classification scheme devised for peralkaline rocks by Macdonald and Bailey (1973).

4.5.2 Compositional heterogeneity of individual deposits

To assess the significance of compositional variations between the different air fall pumice deposits it was first necessary to study the compositional range in a single deposit. This was achieved by analysing samples from the upper and lower portions of Fogo A for major and trace elements. Fogo A was chosen because firstly it has been recognised as a mixed pumice deposit (Walker and Croasdale 1971) and secondly because it is by far the most voluminous of the air fall deposits studied here. Major element analyses (Table 4.5) showed that the dark coloured pumice of the uppermost layer, was marginally less evolved, containing higher CaO and MgO than the underlying buff coloured pumice, which forms the bulk of the deposit. Curiously, the streaky pumice from the middle portion of the deposit was found to have the highest concentrations of incompatible trace elements. For compatible elements the dark top of Fogo A contained about twice the Sr and Ba content of the underlying part of the deposit (Fig. 4.4). The small volume Congro ash (< 0.01 km^3 d.r.e.) is only marginally more evolved than the accompanying lava dome (Fig. 4.5) which is thought by Booth et al. (1978) to represent the final stages of the Congro eruption. Similarly, Schmincke and Weibel (1972) give whole rock analyses of samples taken along vertical profiles across two welded trachytic ignimbrites from Sao Miguel, however no significant chemical zonation was observed. Schmincke and Weibel concluded that the probable reason for the lack of compositional variation was the small volume of the deposits (probably < 0.1 km^3). In comparison Fogo A has a juvenile volume of 0.94 km^3 d.r.e.

4.5.3 Temporal variation of major elements

Variations in major element concentrations up through the Fogo air fall pumice deposit succession, are systematic for most elements. CaO, MgO, Al_2O_3, TiO_2 and P_2O_5 decrease whilst SiO_2 and MnO increase.

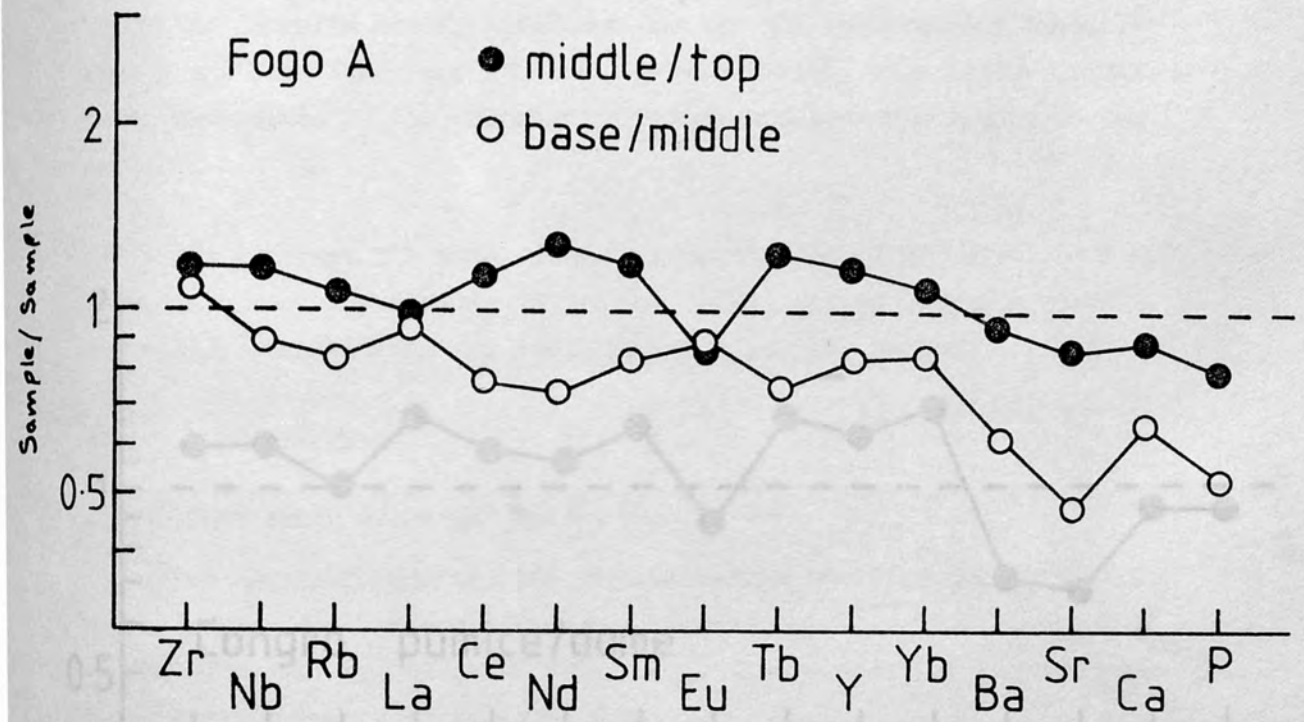

Fig. 4.4 Trace element variation in Fogo A. Filled circles: concentration of an element in the middle portion of the deposit divided by its concentration in the topmost part. Open circles: concentration of an element in basal pumice divided by its concentration in the middle portion.

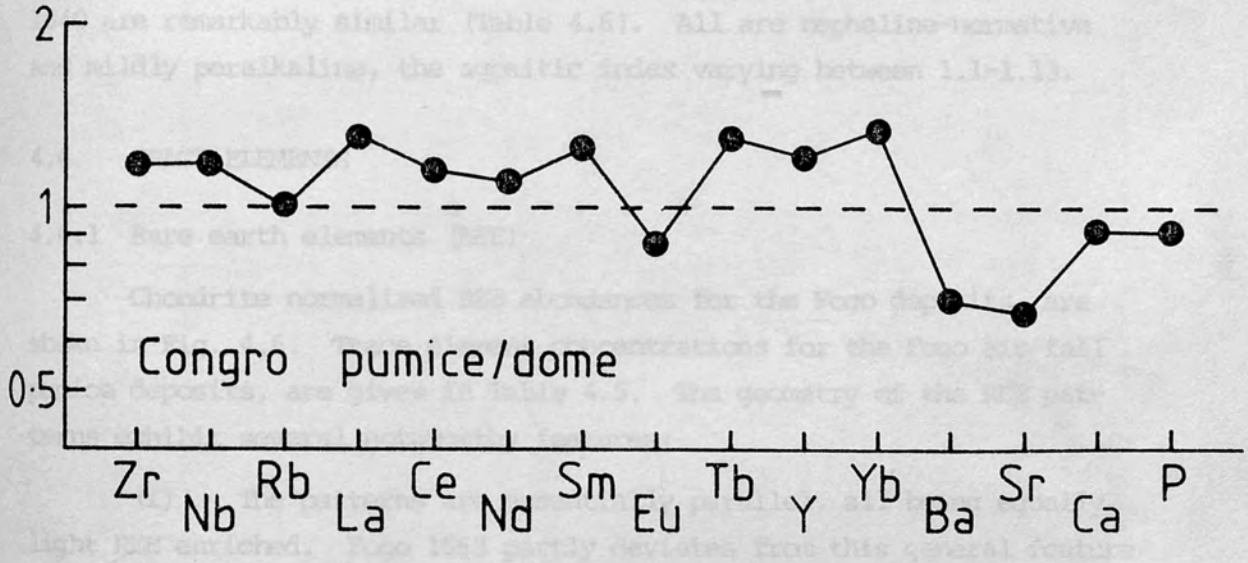

Fig. 4.5 Trace element variation among products of the Congro flank eruption from Agua de Pau, Sao Miguel. Each point is the concentration of an element in the pumice fall deposit divided by its concentration in the trachyte dome extruded at the close of the eruption.

The $FeO + Fe_2O_3/MgO$ and $Na_2O/ Na_2O + K_2O$ ratios increase to maximum values in the youngest deposits mirroring similar variations in the normative mineralogy (Table 4.5) and in the mineral chemistry of co-existing biotites, clinopyroxenes and alkali feldspars. Lastly, the agpaitic index (mol. $Na_2O + K_2O/Al_2O_3$) varies between 0.81 and 1.09. The older deposits are metaluminous whereas the two youngest deposits, Fogo D and Fogo 1563, are both mildly peralkaline, this latter condition being manifested by the presence of acmite and sodium silicate in the norm.

In contrast the major element compositions of Furnas A, C, F and 1640 are remarkably similar (Table 4.6). All are nepheline-normative and mildly peralkaline, the agpaitic index varying between 1.1-1.13.

4.6 TRACE ELEMENTS

4.6.1 Rare earth elements (REE)

Chondrite normalised REE abundances for the Fogo deposits, are shown in Fig. 4.6. Trace element concentrations for the Fogo air fall pumice deposits, are given in Table 4.5. The geometry of the REE patterns exhibit several noteworthy features;

(i) The patterns are essentially parallel, all being equally light REE enriched. Fogo 1563 partly deviates from this general feature because of its higher La_N/Sm_N ratio which results in a crossover of its REE pattern with that of Fogo D.

(ii) All the deposits have negative Eu anomalies, Eu/Eu* ranging between 0.72 for Fogo A and 0.05 for Fogo D; Eu/Eu* varies inversely to the abundance of the other REE.

(iii) The REE patterns are concave upwards. Although these patterns are similar to those of basalts from Agua de Pau, in that the latter are likewise light REE enriched, they differ in that the patterns of the basalts are linear.

In comparison, there is only a small degree of variation in REE abundances between the different Furnas air-fall pumice deposits (Table 4.6). Two chondrite normalised patterns are shown in Fig. 4.7. Their geometry is similar to the more compositionally evolved Fogo deposits (C, D and 1563), (C, D and 1563), having similar REE abundances with large negative

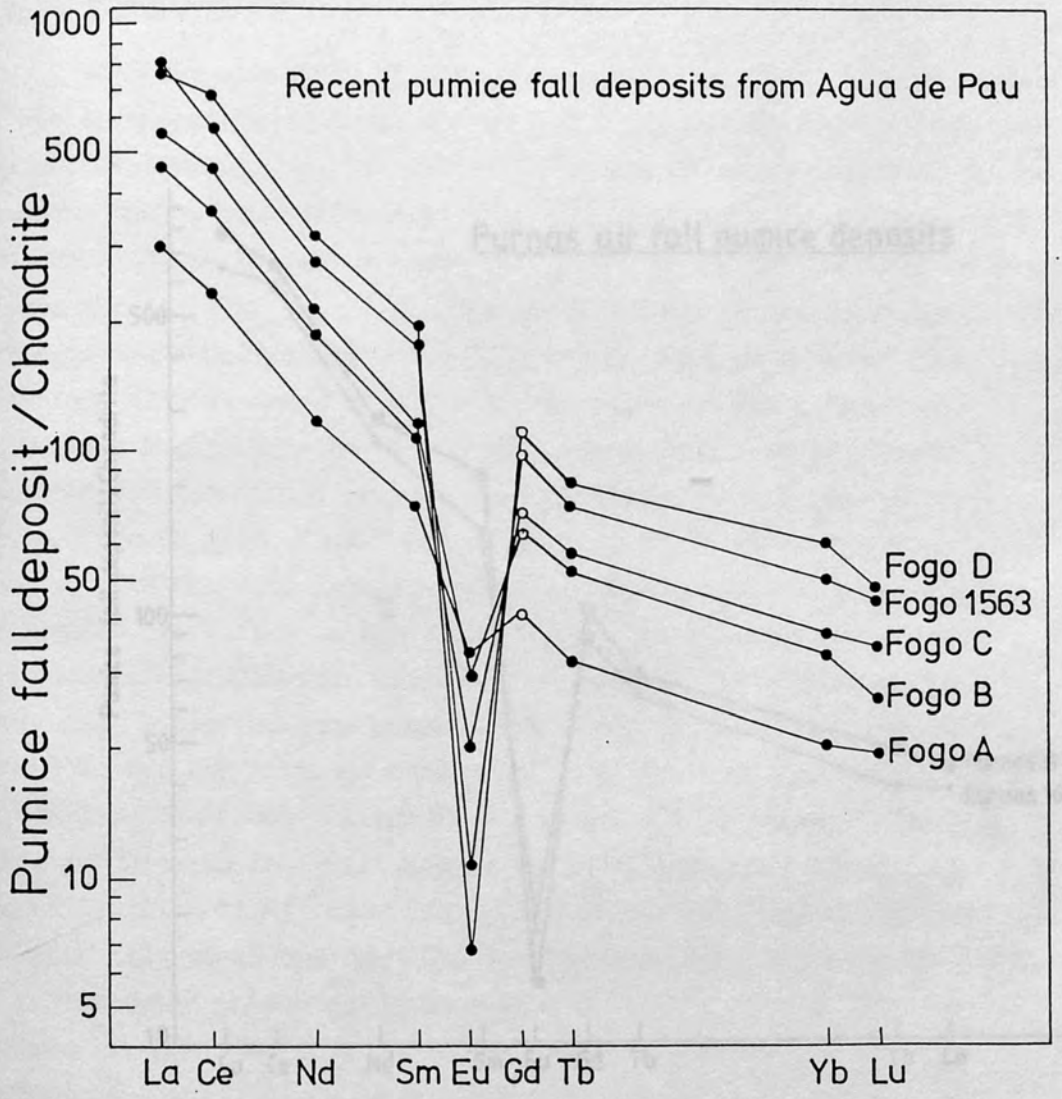

Fig 4.6 Chondrite normalised REE abundances for the Fogo air fall pumice deposits. Gd values interpolated.

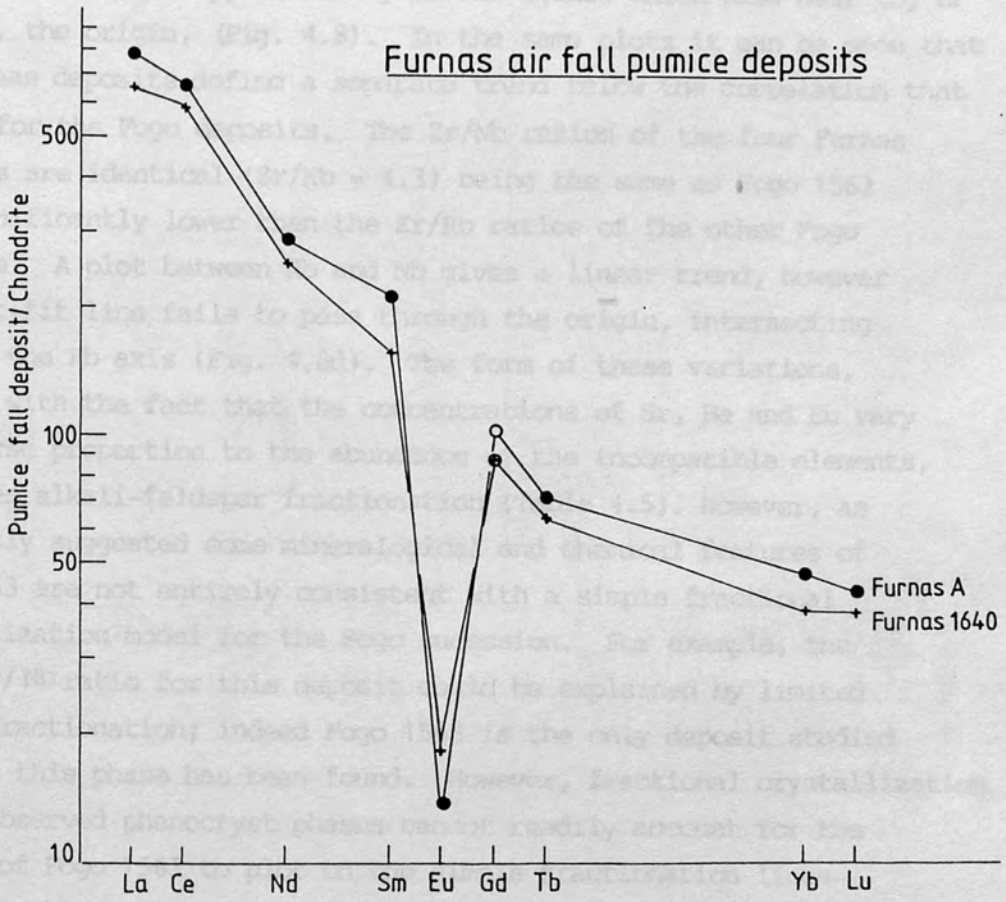

Fig 4.7 Chondrite normalised REE abundances for Furnas A and Furnas 1640. Gd values interpolated.

Eu anomalies (Eu/Eu* = 0.10-0.14)

4.6.2 Th, Zr, Nb, Y, Rb

With the exception of data points for Fogo 1563, biaxial plots of the incompatible elements Th, Zr and Y against Nb for the Fogo pumice deposits define approximately linear trends which pass near to, or through, the origin, (Fig. 4.8). In the same plots it can be seen that the Furnas deposits define a separate trend below the correlation that exists for the Fogo deposits. The Zr/Nb ratios of the four Furnas deposits are identical (Zr/Nb = 4.3) being the same as Fogo 1563 but significantly lower than the Zr/Rb ratios of the other Fogo deposits. A plot between Rb and Nb gives a linear trend, however the best-fit line fails to pass through the origin, intersecting instead the Rb axis (Fig. 4.8d). The form of these variations, coupled with the fact that the concentrations of Sr, Ba and Eu vary in inverse proportion to the abundance of the incompatible elements, indicates alkali-feldspar fractionation (Table 4.5). However, as previously suggested some mineralogical and chemical features of Fogo 1563 are not entirely consistent with a simple fractional crystallization model for the Fogo sucession. For example, the lower Zr/Nb ratio for this deposit could be explained by limited zircon fractionation; indeed Fogo 1563 is the only deposit studied in which this phase has been found. However, fractional crystallization of the observed phenocryst phases cannot readily account for the failure of Fogo 1563 to plot on the simple fractionation lines defined by biaxial plots of the other incompatible elements. This discrepancy suggests, in addition to fractional crystallization, the operation of magma mixing and/or other factors.

4.6.3 Temporal variation of trace elements

The variations of Zr and the K/Rb ratio up through the Fogo air fall pumice deposit succession are shown in Fig. 4.9. The concentration of Zr, which may be taken as an index of fractionation due to its incompatible nature, increases in a stepwise manner while the K/Rb ratio decreases in a likewise style. Similarly, La, Th, Nb and Rb increase in concentration in successively younger deposits attaining maxima in

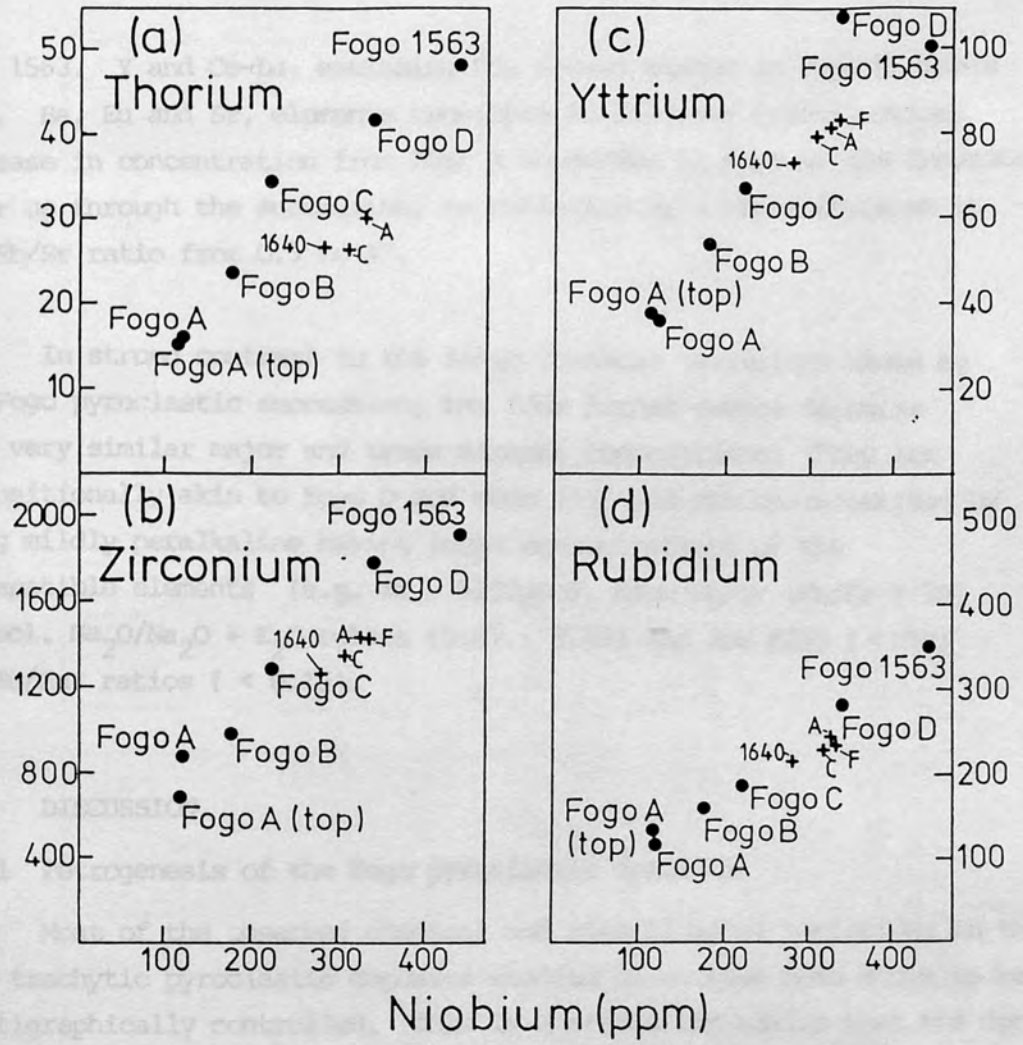

Fig 4.8 Biaxial plots of selected pairs of incompatible elements for the Fogo and Furnas pumice deposits. All values in ppm.

Fogo 1563. Y and Ce-Lu, excluding Eu, attain maxima in Fogo D (Table 4.6). Ba, Eu and Sr, elements sensitive to feldspar fractionation, decrease in concentration from Fogo A to minima in Fogo D; the decrease in Sr up through the succession, is reflected by a rapid increase in the Rb/Sr ratio from 0.5 to 47.

In strong contrast to the large chemical variations shown by the Fogo pyroclastic succession, the four Furnas pumice deposits have very similar major and trace element compositions. They are compositionally akin to Fogo D and Fogo 1563 and are characterized by being mildly peralkaline having large concentrations of the incompatible elements (e.g. Zr > 1200ppm), high Rb/Sr (Rb/Sr > 30) and mol. $Na_2O/Na_2O + K_2O$ ratios (0.67 - 0.69) and low K/Rb (< 230) and Eu/Eu* ratios (< 0.15).

4.7 DISCUSSION

4.7.1 Petrogenesis of the Fogo pyroclastic deposits

Most of the observed chemical and mineralogical variations in the Fogo trachytic pyroclastic deposits studied here, have been shown to be stratigraphically controlled. This is a strong indication that the deposits are cogenetic, as might be expected from their close spatial and temporal association.

Noteworthy trends up through the Fogo succession are;

(i) The rapid depletion of Ba, Sr and Eu, whereas incompatible elements such as Zr, Nb, Th, Y and the rare earths show stepwise enrichment.

(ii) A decrease in the K/Rb ratio.

(iii) An increase in the agpaitic index, the two youngest deposits being mildly peralkaline.

(iv) The Na/K ratio of pumice clast increases along with the albite content of the co-existing alkali feldspar. The pumice clast always has a higher Na/K ratio than the associated alkali feldspar.

(v) An increase in the Fe/Mg ratio of pumice clast and co-existing biotite and clinopyroxene.

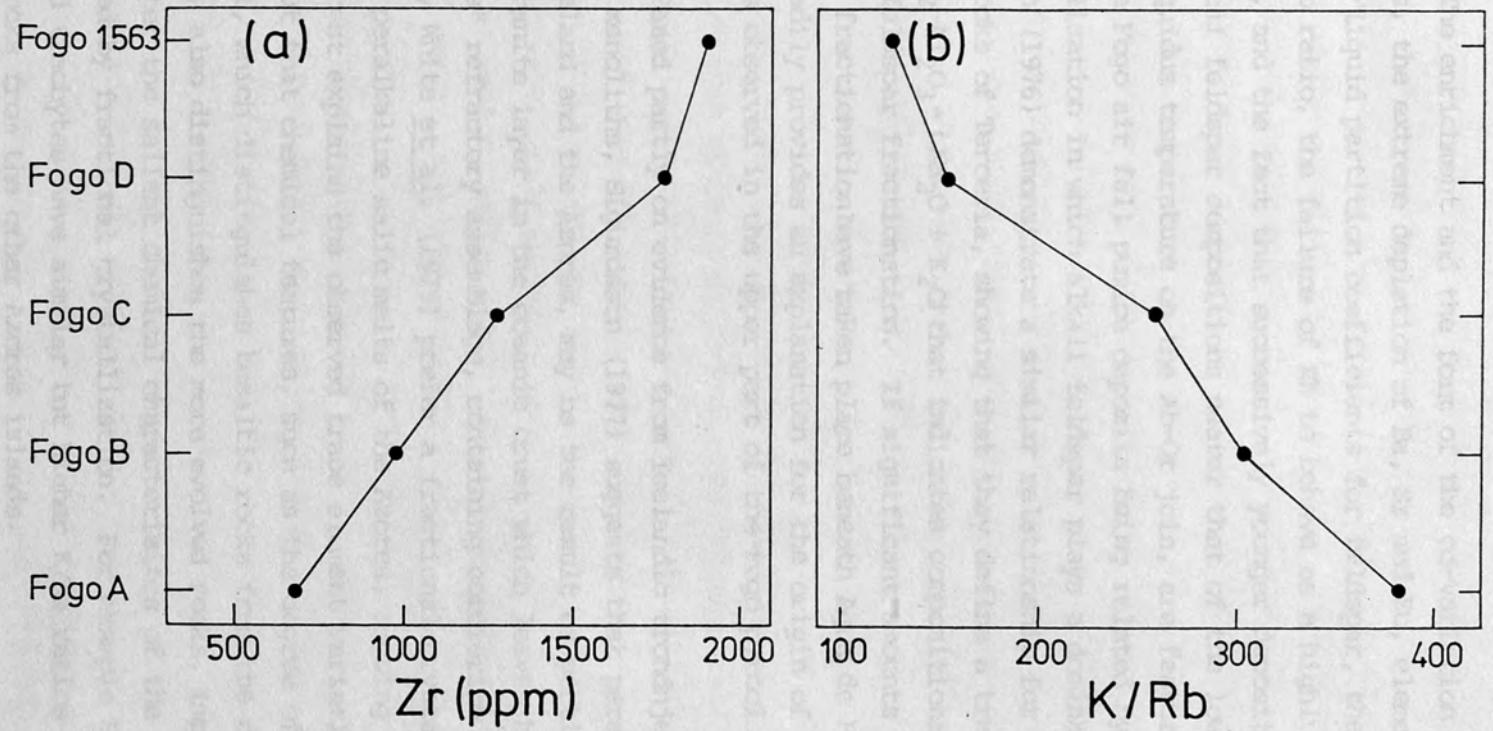

Fig. 4.9 (a) Variation of Zr and
(b) the K/Rb ratio up through the Fogo pyroclastic succession.

The enrichment and the form of the co-variation of incompatible elements, the extreme depletion of Ba, Sr and Eu, elements with high crystal/liquid partition coefficients for feldspar, the decrease in the K/Rb ratio, the failure of Rb to behave as a highly incompatible element, and the fact that successively younger deposits have liquid and alkali feldspar compositions nearer that of the low pressure minimum liquidus temperature on the Ab-Or join, are features consistent with the Fogo air fall pumice deposits being related by fractional crystallization in which alkali feldspar plays a dominant role. Self and Gunn (1976) demonstrate a similar relationship for the peralkaline salic rocks of Terceria, showing that they define a trend in the system SiO_2-Al_2O_3-(Na_2O + K_2O) that indicates compositional control by alkali feldspar fractionation. If significant amounts of high level crystal fractionation have taken place beneath Agua de Pau volcano, then this readily provides an explanation for the origin of the peralkaline deposits observed in the upper part of the Fogo pyroclastic succession.

Based partly on evidence from Icelandic trondhjemite and quartz diorite xenoliths, Sigurdsson (1977) suggests that peralkaline melts from Iceland and the Azores, may be the result of partial fusion of a plagiogranite layer in the oceanic crust which leaves behind a "peraluminous" refractory assemblage, containing cordierite and mullite. However, White et al. (1979) prefer a fractional crystallization origin for the peralkaline salic melts of the Azores, arguing that this hypothesis best explains the observed trace element variations. They also point out that chemical features, such as the degree of light REE enrichment, which distinguishes basaltic rocks from the different Azores islands, also distinguishes the more evolved rocks, implying that in the latter the salient chemical characterisitcs of the basalts have been inherited by fractional crystallization. For example Sao Miguel basalts and trachytes have similar but higher K/Na ratios than do basic and salic rocks from the other Azores islands.

For the peralkaline rocks of Agua de Pau it can be shown that the development of peralkalinity is consistent with fractional crystallization of the observed mineral assemblage of the trachytes. If the agpaitic indices for the older metaluminous deposits Fogo A, B and C

represent true melt values, then fractionation of alkali feldspar alone would not have led to an increase in this index due to similar mol. $Na_2O + K_2O/Al_2O_3$ ratios for pumice clast and coexisting alkali feldspar. In melts of these compositions however, the agpaitic index may have been increased by fractionation of "peraluminous" biotite and/or aluminous clinopyroxene. Such fractionation would have eventually evolved the trachytic melt to the critical point where its mol. $Na_2O + K_2O/Al_2O_3$ ratio exceeded that of its co-existing alkali feldspar; this ratio is < 1 due to the presence of a minor anorthite component. Once the melt exceeded this value, fractionation of alkali feldspar, the principal phenocryst phase, would have acted in unison with biotite and clinopyroxene in rapidly driving the melt towards the peralkaline condition witnessed in Fogo D and 1563.

The concave upwards REE patterns of the Fogo and Furnas trachytic pumice deposits may be explained by fractionation of amphibole and/or apatite at some stage in differentiation. Kaersutitic amphibole occurs as phenocrysts possessing opaque reaction rims in some of the intermediate lavas from Sao Miguel, while apatite microphenocrysts are observed in both intermediate lavas and trachytic lavas and pyroclastics. Measured crystal/melt partition coefficients for granitic melts, summarised in Hanson (1978), shows that both amphibole and apatite preferentially incorporate the middle REE.

The parallelism of the REE patterns suggests firstly the co-fractionation of feldspar and clinopyroxene from the trachytic melt, and secondly that significant fractionation of amphibole and/or apatite ceased at a previous stage in differentiation. This is supported by the low phosphorus content of the trachytic air fall deposits, and also by their apparent lack of amphibole and the presence of only minor amounts of apatite. It would appear likely that the concave REE patterns of the trachytic pumices are a legacy from some intermediate parental magma.

Allegre and Minster (1978) conclude that the physical properties of a crystallizing magma chamber are those for which the Rayleigh fractionation law is obeyed. Accordingly, a fractional crystallization model as a means of relating the Fogo air fall pumice deposits, can be more

rigorously tested by comparing observed trace element variations with those predicted by the Rayleigh fractionation law (Eq 1.1). In the case of Ba, Sr and Eu for the Fogo deposits, their bulk partition coefficients approximate to their respective Kd values for alkali feldspar. This is because the modal proportion of alkali feldspar is approximately 80% or more of the total phenocryst content and also because these elements have high crystal/melt partition coefficients for alkali feldspar (Hanson 1978). Recalling from Eq 1.2, that $C_L/C_O = F^{(D-1)}$, then for highly incompatible elements enrichment relative to the parental melt varies inversely with the amount of the melt remaining, F.

In Fig. 4.10 observed values of C_L/C_O for Eu, Sr and Ba are plotted against F. Also shown is the model variation of Eu, Sr and Ba assuming D values of 2, 4 and 6 respectively. Nb, because its incompatible behaviour approximates to a 1/F relationship, is used to estimate the amount of melt remaining. The top, more mafic, part of the Fogo A deposit has been assumed to be parental to the subsequent Fogo air fall pumice deposits. If fractional crystallization in a closed system is assumed to operate, then $C_{Nb_{Fogo\ A}}{}^{C_{Nb_{Fogo\ 1563}}}$ indicates that approximately 30% of the original melt volume was remaining prior to the eruption of Fogo 1563. It can also be seen that Ba, Sr and Eu show reasonable agreement with expected rates of removal by alkali feldspar fractionation, although they show slight increases in concentration in Fogo 1563*.

As detailed in Chapter 3, the presence in the Fogo pyroclastic succession of xenocrysts of forsteritic olivine, aluminous titanaugite and anorthite rich plagioclase suggests that some magma mixing may have occurred. Measured Fe^{2+}/Mg ratios for Fogo A average near 1.5, a value almost two times as high as that predicted for a melt in equilibrium

---

* It was stated by Storey (1981) that the behaviour of Ba, was anomalous, its variation through the succession being small and non-systematic. However, the same samples have been re-analysed for Ba, the new data showing parallel variation of this element with Sr and Eu. The initial analytical error is believed to have been caused by a failure to correct for the large interference from the Ceα1 peak.

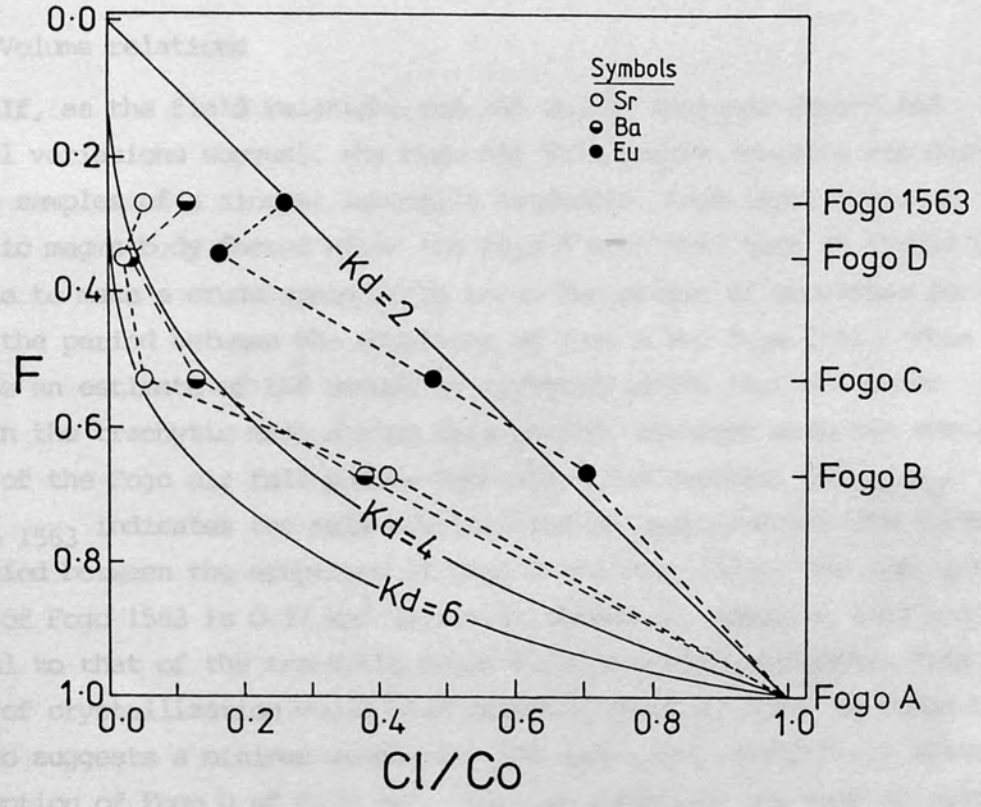

Fig. 4.10 Comparison of actual and calculated variation of Sr, Eu and Ba up through the Fogo pyroclastic succession. Fogo A taken as parental melt; see text for detailed explanation. F equals fraction of melt remaining relative to parent and C_L/C_O equals the concentration of the trace element of the differentiation melt, C_L, relative to the parent melt, C_O.

with the olivines of composition Fo_{80} that are found in this deposit (Roeder and Emslie 1970). The contemporaneous eruption in 1563 AD from Agua de Pau volcano of a trachytic air fall pumice deposit and a basaltic lava flow, coupled with the anomalous incompatible element ratios of Fogo 1563, provides additional support for magma mixing. Theoretically this would also act as a suitable mechanism for triggering explosive volcanic eruptions (Sparks et al. 1977).

4.7.2 Volume relations

If, as the field relations and the smooth temporal controlled chemical variations suggest, the Fogo air fall pumice deposits are successive samples of a single, laterally extensive, high level evolving trachytic magma body formed after the Fogo A eruption, then it should be possible to make a crude speculation as to the volume of cumulates formed in the period between the eruptions of Fogo A and Fogo 1563. This requires an estimate of the amount of crystallization that has taken place in the trachytic melt during this period, combined with the actual volume of the Fogo air fall pumice deposits. For example, $CNb_{Fogo\ D}/CNb_{Fogo\ 1563}$ indicates the melt crystallized by approximately 20% during the period between the eruptions of Fogo D and Fogo 1563. The juvenile volume of Fogo 1563 is 0.17 km^3 (d.r.e.); therefore, assuming this volume is equal to that of the trachytic magma body, a minimum estimate, this amount of crystallization would have produced about 0.05 km^3 of cumulates and also suggests a minimum volume for the magma body immediately after the eruption of Fogo D of 0.22 km^3. Similar reasoning was used to estimate the amount of crystallization that had taken place in the magma body between the other Fogo eruptions and the volume of cumulates that formed in the same period. Extrapolating backwards through the Fogo succession by adding the estimated cumulate volumes to the volumes of the Fogo deposits suggests that after the eruption of Fogo A the magma body had a minimum volume of about 1 km^3. The estimated volume of cumulates to have formed since this eruption is about 0.6 km^3. This, if anything, is an underestimate because, apart from using a minimum value for the size of the magma body, the effect of dilution of the incompatible elements by magma mixing has been ignored.

Finally, the estimated volume of cumulates is roughly comparable

with the combined volume of post Fogo A air fall pumice deposits of 0.45 km^3 (d.r.e.). The implication is that a crystalline, deep seated contribution to the salic crust of Agua de Pau, may be as significant as that due to the volcanic portion.

4.7.3 Furnas pumice deposits

In strong contrast to the Fogo trachytic pyroclastic deposits erupted over the past 5,000 years, where the chemical and mineralogical variations are stratigraphically controlled, the four Furnas pumice deposits show no significant variation in major or trace element composition. Chemically, the mildly peralkaline Furnas pumice deposits with large incompatible element contents and low Eu, Sr and Ba concentrations resemble Fogo D and 1563, suggesting that they are also differentiates produced from a metaluminous melt by alkali feldspar fractionation. The time span separating the eruptions of Furnas A and Furnas 1640 is some 3,000 years. If the four Furnas deposits are from the same body of magma then it appears that during this period of time the melt has not undergone any significant differentiation. The similarity in composition of the Furnas pumice deposits with Fogo D and 1563 and several of the syenite xenoliths (Chapter 3) coupled with the absence on Sao Miguel of more differentiated, highly peralkaline rocks suggests a limit to the degree of melt evolution possible. Physico-chemical controls on differentiation in trachytic magmas are examined in the subsequent sections of this discussion.

4.7.4 Melt rheology, density and viscosity; implications for convection and crystal settling

The rheological behaviour of magma as a fluid may be described as either newtonian or non-newtonian. A newtonian fluid is defined as one in which the shear rate (S_r) is directly proportional to the shear stress (σ) where the constant of proportionality is the newtonian viscosity (η_N)

$$Sr = \eta_N \sigma$$

Non-newtonian fluids may be described by one of several rheological models (Fig. 4.11). These are characterised by the possession of a yield

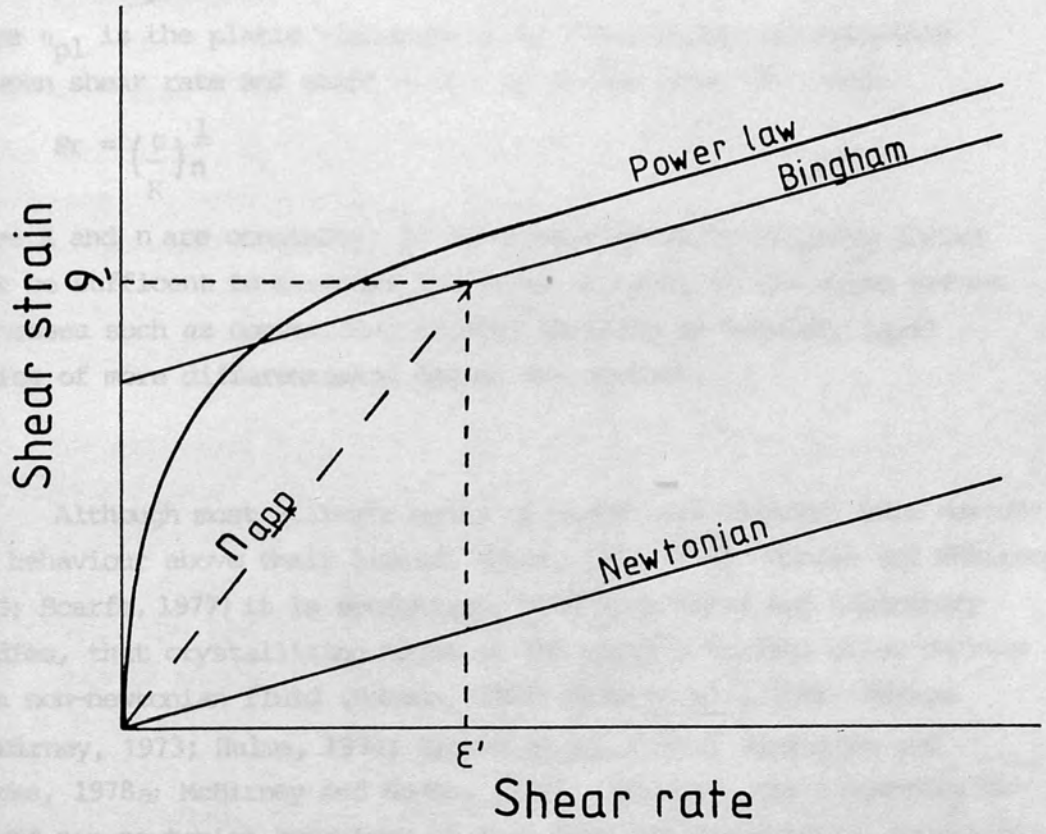

Fig. 4.11 Various rheological models for magma. The slope of the dashed line equals the apparent viscosity of a Bingham fluid at the given values of shear strain and shear rate.

strength (ψ) as in the Bingham model for non-newtonian fluids

$$Sr = \eta_{pl}\sigma + \psi$$

where η_{pl} is the platic viscosity or by a non-linear relationship between shear rate and shear strain as in the power law model

$$Sr = \left(\frac{\sigma}{K}\right)^{\frac{1}{n}}$$

where K and n are constants. In non-newtonian melts buoyancy forces must be sufficent to overcome the yield strength of the magma before processes such as convection, crystal settling or boundary layer uprise of more differentiated magma, can operate.

Although most silicate melts of geological interest show newtonian behaviour above their liquidi (Shaw, 1963, 1969; Murase and McBirney, 1973; Scarfe, 1977) it is recognised, both from field and laboratory studies, that crystallizing magma at the earth's surface often behaves as a non-newtonian fluid (Robson, 1967; Shaw et al., 1968; Murase & McBirney, 1973; Hulme, 1974; Sparks et al., 1976; Pinkerton and Sparks, 1978a; McBirney and Noyes, 1979). However, the frequently observed non-newtonian behaviour of lava does not necessarily imply similar rheological behaviour before eruption, rather it may simply reflect loss of volatiles from the magma on extrusion (Pinkerton and Sparks, 1978b). It is well known that H_2O and F act as network modifiers, consequently degassing of magma would lead to an increase in viscosity and yield strength by polymerization of the melt. A second consequence of volatile loss would be an increase in crystallization as solution of gases supresses the liquidus (Yoder and Tilley, 1962). A larger proportion of crystals and/or gas bubbles would lead to an increase in viscosity (Shaw, 1965).

To examine processes such as crystal settling requires some estimate of melt density and viscosity. Here, pre-eruptive trachytic densities have been calculated using the method of Bottinga and Weill (1970) from the following equation

$$p = \Sigma_i X_i M_i / X_i \bar{V}_i$$

where X_i = mole fraction of component i

$\bar{V}_i$ = partial molar volume of component i

M_i = gram formula weight of component i

Values for $\bar{V}Fe_2O_3$ and $\bar{V}H_2O$ have been estimated from the expressions given by Bottinga and Weill (1970) and Burnham and Davis (1969) respectively. P_{total} was assumed to equal P_{H_2O} in calculating $\bar{V}_{H_2O}$. Partial molar volumes for the other liquid components are those given by Nelson and Carmichael (1979).

The estimated density for trachytic magmas containing 6.5 wt% H_2O is around 2.2 g/cm^3. Calculated magmatic water contents were obtained using the compositions of co-existing biotite, sanidine and magnetite (Chapter 5). Anhydrous trachytic magma has a calculated density of 2.45 g/cm^3. The low density of trachytic magma implied by their high water contents indicates that K-feldspar phenocrysts would be denser by about 0.35 g/cm^3.

Melt viscosities are strongly dependent on both magmatic water content and temperature (Fig. 4.12). The large water contents of the pumice-forming trachytic magmas implies viscosities in the range 10^4 - 10^5 poise. On the basis of the equilibration temperatures obtained from the Fe - Ti oxides (Chapter 5) it would seem reasonable to suggest that the pre-eruptive temperature of Fogo D was some 100°C lower than for Fogo A. Over this temperature interval a trachytic melt with 6 wt% H_2O might be expected to show around a 5-fold increase in viscosity (Fig. 4.12). A large increase in viscosity would lead to a corresponding decrease in the efficiency of fractionation processes, such as crystal settling or boundary layer uprise of buoyant, more differentiated magma produced by wall-rock crystallization. A high viscosity provides a possible explanation for the lack of compositional variation in the Furnas pyroclastic succession.

For example, the existence of crystal accumulative lavas on Sao Miguel ranging from basalt to trachyte (Chapter 3) provides evidence for crystal settling. The settling velocity of a sphere in a newtonian

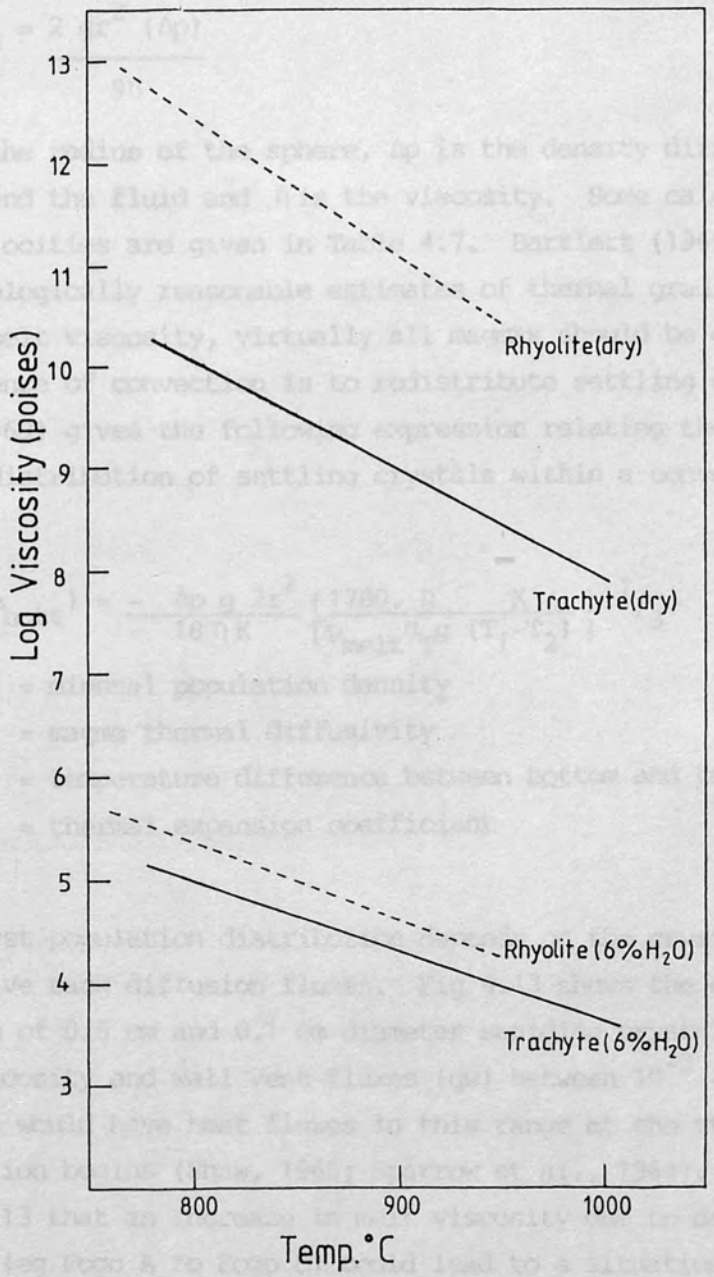

Fig. 4.12 Variation of the viscosity of trachytic magma with temperature, calculated using the empirical method of Shaw (1972). Rhyolite viscosities are shown for comparison. Rhyolite data are from Ewart and Stipp (1968) (averaged composition of Taupo rhyolitic pumice deposit)

fluid is described by Stokes law.

$$V_{sph} = \frac{2\ gr^2\ (\Delta p)}{9\eta}$$

where r is the radius of the sphere, Δp is the density difference between the sphere and the fluid and η is the viscosity. Some calculated terminal settling velocities are given in Table 4.7. Bartlett (1969) argues that for geologically reasonable estimates of thermal gradient, chamber height and melt viscosity, virtually all magmas should be convecting. One consequence of convection is to redistribute settling crystals. Bartlett (1969) gives the following expression relating the vertical population distribution of settling crystals within a convecting magma body.

$$\ln\ (Np_{top}/Np_{bott}) = \frac{-\ \Delta p\ g\ 2r^2}{18\ \eta\ K} \left\{ \frac{1700.\ \eta\ \ K}{\{p_{melt} \alpha_T g\ (T_1 - T_2)\}} \right\}^{1/3}$$

where Np = mineral population density

K = magma thermal diffusivity

$T_1 - T_2$ = temperature difference between bottom and top

α_T = thermal expansion coefficient

The phenocryst population distribution depends on the crystal settling and convective back diffusion fluxes. Fig 4.13 shows the calculated distribution of 0.5 cm and 0.1 cm diameter sanidine crystals as a function of magma viscosity and wall vent fluxes (qw) between 10^{-3} - 10^{5} cal $cm^{-2}s^{-1}$. Most plutons would have heat fluxes in this range at the stage when crystallization begins (Shaw, 1965; Sparrow et al., 1964). It is evident from Fig. 4.13 that an increase in melt viscosity due to decreasing temperature (eg Fogo A to Fogo D) could lead to a situation where the crystals are randomly distributed in the magma, with no significant fractionation by crystal settling. A high magma viscosity may explain the lack of compositional variation in the Furnas pyroclastic deposits, the absence of more extreme peralkaline differentiates on Sao Miguel and the "liquid compositions" of a number of syenite xenoliths from Agua de Pau volcano (Chapter 3).

Mineral	Crystal diameter			Viscosity (poise)
	0.1	0.2	0.5	
Alkali feldspar	6.9	27	170	
Clinopyroxene	22.3	89.2	567	10^4
Magnetite	51.4	206	1230	
Alkali feldspar	0.7	2.7	17	
Clinopyroxene	2.2	8.9	56.7	10^5
Magnetite	5.1	20.6	123	

Table 4.7 Terminal settling velocities (m/yr)

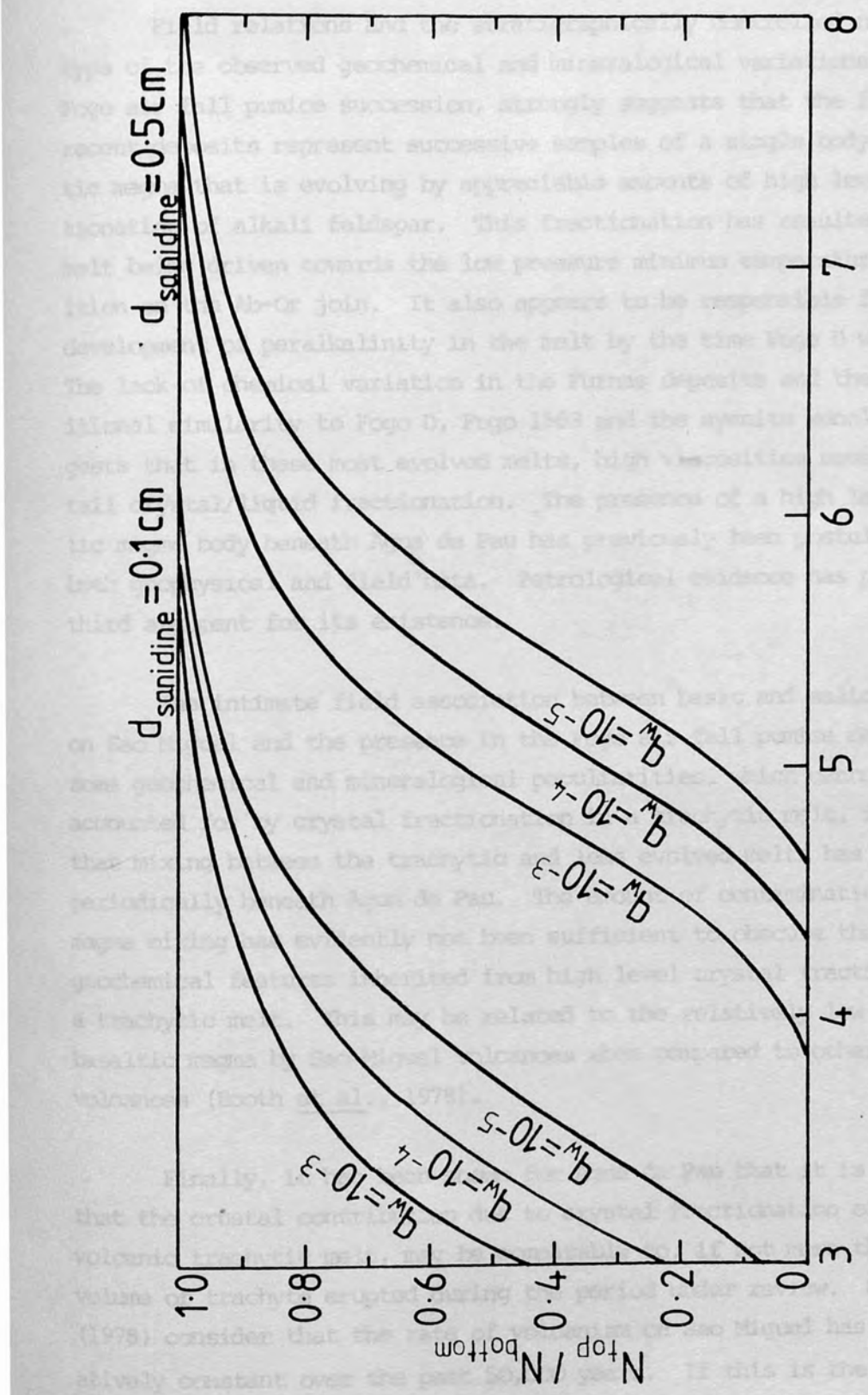

Fig. 4.13 Population distribution of 0.5 and 0.1 cm diameter sanidine crystals in a convective magma at selected cooling rates and melt viscosities.

4.8 CONCLUSIONS

Field relations and the stratigraphically controlled nature and type of the observed geochemical and mineralogical variations of the Fogo air fall pumice succession, strongly suggests that the five most recent deposits represent successive samples of a single body of trachytic magma that is evolving by appreciable amounts of high level fractionation of alkali feldspar. This fractionation has resulted in the melt being driven towards the low pressure minimum temperature composition on the Ab-Or join. It also appears to be responsible for the development of peralkalinity in the melt by the time Fogo D was erupted. The lack of chemical variation in the Furnas deposits and their compositional similarity to Fogo D, Fogo 1563 and the syenite xenoliths suggests that in these most evolved melts, high viscosities severely curtail crystal/liquid fractionation. The presence of a high level trachytic magma body beneath Agua de Pau has previously been postulated on both geophysical and field data. Petrological evidence has provided a third argument for its existence.

The intimate field association between basic and salic volcanism on Sao Miguel and the presence in the Fogo air fall pumice deposits of some geochemical and mineralogical peculiarities, which cannot be easily accounted for by crystal fractionation in a trachytic melt, indicates that mixing between the trachytic and less evolved melts has occurred periodically beneath Agua de Pau. The amount of contamination due to magma mixing has evidently not been sufficient to obscure the salient geochemical features inherited from high level crystal fractionation in a trachytic melt. This may be related to the relatively low output of basaltic magma by Sao Miguel volcanoes when compared to other composite volcanoes (Booth et al., 1978).

Finally, it has been shown for Agua de Pau that it is possible that the crustal contribution due to crystal fractionation of a subvolcanic trachytic melt, may be comparable to, if not more than, the volume of trachyte erupted during the period under review. Booth et al. (1978) consider that the rate of volcanism on Sao Miguel has been relatively constant over the past 50,000 years. If this is the case, the

total salic crustal contribution due to crystal fractionation of trachytic melts beneath the stratovolcanoes of Sao Miguel during this period, may be in the order of ten or so cubic kilometres.

CHAPTER 5

GEOTHERMOMETRY AND VOLATILE COMPONENTS OF THE PUMICE-FORMING MAGMAS

5.1 INTRODUCTION

Volcanic studies on the island of Sao Miguel (Booth et al., 1978; Walker and Croasdale, 1971) have shown that volumetrically the majority of rocks of trachytic composition occur as pumiceous, pyroclastic deposits. The wide dispersal of many of these pumice deposits shows that they formed by violently explosive sub-plinian to plinian eruptions (Booth et al., 1978; Walker and Croasdale, 1971), therefore demonstrating the presence of a significant magmatic volatile component (Wilson, 1976). The formation of ignimbrites and the welding of pyroclastic deposits are intimately associated with the concentration and composition of the volatile phase. The magmatic volatile component also strongly affects magma rheology, density and viscosity (Section 4.7.4). However, despite its obvious importance, the inherent difficulties in estimating the magmatic volatile phase have largely led to its omission from petrological studies. One approach, which has been developed, is that used by Sommer (1977) who analysed volatiles in pre-eruptive magma preserved as inclusions in tephra phenocrysts. A more routine method, as demonstrated by Heming and Carmichael (1973) and Rutherford and Heming (1978) on dacitic and rhyolitic magmas is to employ thermodynamic techniques on mineral chemistry data to determine the fugacities of volatile species in equilibrium with the phenocryst assemblage before eruption. The phenocryst assemblage of several of the trachytic pumice deposits from Sao Miguel and Faial are suitable for thermodynamic estimates of magmatic temperatures and volatile components in the system H-O-S. The purpose of this Chapter, therefore, is to present pre-eruptive temperature and volatile data for these samples, to compare the results with data for pumice-forming, salic magmas of other compositions and finally to assess the significance of this information in a volcanological context.

5.2 GEOTHERMOMETRY

Estimating the chemical activities of magmatic volatile components

from mineral chemistry by application of thermodynamic methods first requires knowledge of the pre-eruptive temperature. As most of the samples studied contained equilibrium pairs of titanomagnetite and ilmenite, temperatures have been estimated using the geothermometer and oxygen barometer of Buddington and Lindsley (1964).

5.2.1 Titanomagnetite-ilmenite geothermometer

The equilibrium reaction which forms the basis of this geothermometer is given by:

$$X\ Fe_2TiO_4 + (1-X)\ Fe_3O_4 + {}^1/_4O_2 = X\ FeTiO_3 + ({}^3/_2 - X)\ Fe_2O_3$$

ulvospinel magnetite ilmenite haematite

in which the reactants are oxygen and the ulvospinel-magnetite solid solution series (spinel phase) and the products the ilmenite-haematite solid solution series (rhombohedral phase). The equilibrium constant (K) for this reaction is given by:

$$K_{PT} = \frac{(a_{FeTiO_3}^{ilmenite})^X \; (a_{Fe_2O_3}^{ilmenite})^{(3/2-X)}}{(a_{Fe_2TiO_4}^{magnetite})^X \; (a_{Fe_3O_4}^{magnetite})^{(1-X)} \; (fO_2)^{1/4}}$$

hence at constant temperature and pressure, oxygen fugacity (fO_2) is defined by the mineral compositions. Thus, if analyses of magnetite-ilmenite pairs are recalculated, assuming stoichiometry, into the mole fractions of ulvospinel solid solution (X_{Usp}) in magnetite and haematite solid solution (X_{Hm}) in ilmenite, values for the equilibration temperature and oxygen fugacity can be obtained from the calibration curves of Buddington and Lindsley (1964). Recalculation of Fe-Ti oxides analyses to mole fractions of their end members also permits a summation test of the analytical accuracy as the electron-microprobe cannot distinguish between ferrous and ferric iron (Table 5.1).

Some of the Fe-Ti oxides studied contained substantial amounts of minor constituents such as Mg, Mn, Cr and Al, in part a consequence of the low silica activity of alkaline magmas (Carmichael et al., 1970). This introduces the added complexity of assigning the minor elements between the possible end members. Different recalculation procedures have been

	Fogo A	Fogo B	Fogo C	Faial T	Faial S	Faial B		
Sa. No.	AZ1544	AZ1378	AZ1394	AZ3432	AZ3424	AZ3417	AZ1034	10SM
Spinel phase								
SiO_2	0.42	0.44	0.39	0.30	0.21	0.26	0.28	0.35
TiO_2	18.12	17.15	17.66	16.88	17.52	23.74	21.48	18.56
Al_2O_3	1.68	1.11	1.22	3.84	4.74	0.89	4.02	6.43
Cr_2O_3	-	-	-	-	-	-	-	0.45
CaO	-	0.19	0.22	-	-	-	-	0.23
FeO	73.02	75.18	74.27	70.73	69.04	71.02	67.76	64.55
MnO	1.56	2.02	2.03	-	0.57	1.89	0.59	0.43
MgO	2.07	1.39	1.52	4.30	5.32	1.20	4.17	7.09
Total	96.87	97.48	97.31	96.05	97.40	99.00	98.30	98.09
Recalculated analyses (ulvo-spinel basis)								
Fe_2O_3	32.24	35.21	33.99	33.04	32.37	23.09	24.86	28.83
FeO	44.00	43.47	43.66	41.03	39.91	50.22	45.42	38.57
Total	100.09	100.98	100.69	99.39	100.64	101.29	100.82	100.94
mole% ulvospinel	51.7	48.7	50.3	47.0	47.2	66.2	58.4	49.1
Rhombohedral phase								
SiO_2	0.61	0.27	0.50	0.31	0.18	0.49	0.33	0.33
TiO_2	47.40	48.82	49.46	47.37	48.55	49.56	51.68	48.79
Al_2O_3	0.29	-	0.24	0.30	0.37	-	0.35	0.67
CaO	-	0.41	0.25	-	-	-	0.21	0.35
FeO	44.71	44.33	44.64	44.74	43.68	43.53	42.76	41.35
MnO	2.38	2.14	2.60	-	0.59	2.08	0.62	0.37
MgO	3.02	2.59	1.85	5.43	6.47	1.61	5.02	7.44
Total	98.41	98.56	99.54	98.15	99.84	97.27	100.97	99.30
Recalculated analyses								
Fe_2O_3	10.16	9.20	6.49	12.74	13.26	3.81	6.34	12.43
FeO	35.56	36.05	38.80	33.27	31.75	40.15	37.06	30.16
Total	99.42	99.48	100.19	99.42	101.17	97.70	101.61	100.54
mole% R_2O_3	10.0	8.6	6.5	12.2	12.5	3.8	6.2	12.1
Temp (°C)	960	910	880	960	965	900	940	970
fO_2	$10^{-11.3}$	$10^{-12.2}$	$10^{-13.2}$	$10^{-11.0}$	$10^{-10.9}$	$10^{-13.4}$	$10^{-12.1}$	$10^{-10.9}$

Table 5.1 Recalculated analyses of some titanomagnetite - ilmenite pairs with deduced equilibrium temperatures and oxygen fugacities

proposed for Fe-Ti oxide analyses by Anderson (1968), Buddington and Lindsley (1964), Carmichael (1967) and Lipman (1971). Where the minor element content is large there are significant differences between temperature and fO_2 estimates obtained by the different methods. For example, equilibrium magnetite-ilmenite pairs from pumice fall deposit Faial S have minor element contents ($MgO + MnO + Al_2O_3$) of approximately 10.5 wt% and 7 wt% respectively (Table 5.1). Temperatures yielded by the recalculation methods of Buddington and Lindsley (1964) and Carmichael (1967) are 1090°C and 965°C respectively. The recalculation methods of Anderson (1968) and Lipman (1971) give similar T-fO_2 estimates to those of Carmichael (1967). This discrepancy arises from the different procedures for assigning the divalent minor elements (RO) between magnetite ($FeO.Fe_2O_3$) and ulvospinel ($FeO.TiO_2$). Carmichael (1967) places all RO in the ulvospinel molecule, X_{Usp} being calculated as:

$$X_{Usp} = \frac{2(RO, FeO)\ TiO_2}{FeO(Fe_2O_3, R_2O_3) + 2(RO, FeO)\ TiO_2}$$

However, Buddington and Lindsley (1964) discard an amount of RO equal to R_2O_3 (principally Al_2O_3) and then equally assign excess RO (always the case in the Fe-Ti oxides studied here) between ulvospinel and magnetite, X_{Usp} being calculated as:

$$X_{Usp} = \frac{2(FeO)\ TiO_2}{FeO.Fe_2O_3 + 2(FeO)\ TiO_2}$$

with $2(RO)_2TiO_2$ and $FeO.R_2O_3$ being discarded. For magnetites with large proportions of minor constituents the estimate of X_{Usp} will be significantly larger than by the other methods. For ilmenite analyses, Carmichael (1967) calculates the mole fraction of haematite as:

$$X_{Hm} = \frac{R_2O_3, Fe_2O_3}{RO, FeO.TiO_2 + R_2O_3, Fe_2O_3}$$

Recalculation procedures using the other schemes gives little difference in the estimate of X_{Hm}. The necessity of using the recalculation procedure which best approximates the substitution behaviour of minor elements in magnetites is clear.

In this study the method of Carmichael (1967) was chosen, in preference to others, because:

(i) Experimental studies on the substitution of Mg in spinels (Speidel, 1970) suggests that Mg should be assigned to the ulvospinel molecule.

(ii) Hildreth (1979) has shown that temperatures and fO_2 values estimated from Fe-Ti oxides in the Bishop Tuff using the recalculation procedure of Carmichael (1967) differed by no more than $\pm$ 5°C and $\pm$ 0.15 log units fO_2 when compared to recalculation procedures recommended by Lindsley (pers. comm. Hildreth, 1979) for Fe-Ti oxides containing minor elements. Lindsley's procedures were based on studies by Mazzulo et al., (1975) and Pickney and Lindsley (1976) of the effects of Mg and Mn substitution in magnetite and ilmentite pairs on temperature and fO_2 values yielded by the original calibration curves for the pure Fe-Ti-O system given by Buddington and Lindsley (1964).

(iii) The estimated temperatures show good agreement with those obtained from another geothermometer (Table 5.2) based on Fe^{2+} - Mg exchange between clinopyroxene and ilmenite (Bishop, 1980).

Of the ten pumice deposits probed seven contained equilibrium magnetite-ilmenite pairs. Averaged analyses along with estimated temperatures and fO_2 values are given in Table 5.1. These temperatures are believed to closely approximate pre-eruptive magmatic values because rapidly quenched non-welded pumice fall deposits are unlikely to have undergone sub-solidus equilibration. Equilibrium is also suggested by the lack of zoning and the limited compositional variation between grains, except for those crystals which are obviously foreign. Strong supporting evidence that the deduced magnetite-ilmenite equilibrium temperatures represent pre-eruptive values is shown by their systematic correlation with whole rock composition. For example, compositions of equilibrium magnetite-ilmenite pairs from Fogo A, B and C imply pre-eruptive temperatures of 960°C, 910°C and 880°C respectively, correlating with Zr contents of 867 ppm (Fogo A), 974 ppm (Fogo B) and 1274 ppm (Fogo C).

It will be recalled from Chapters 2 and 3 that some of the pumice deposits studied here showed mineralogical evidence for contamination, by

the presence of two or more compositionally distinct magnetites, ilmenites, clinopyroxenes and feldspars. In such cases, the simplest means to establish equilibrium Fe-Ti oxide pairs was to use the observed enclosing relationships. Magnetites and ilmenites enclosed in compositionally similar phases were assumed to be in equilibrium. These and other Fe-Ti oxide pairs for which equilibrium has been assumed are shown linked by tie lines in a triangular plot of their minor elements Mn, Mg and Al (Fig. 5.1); the semi-parallelism of the tie lines provides strong support for the equilibrium criteria used. The plot also demonstrates the relationships found by Carmichael (1967), with ilmenite being marginally enriched in Mg and Mn whereas the magnetite is strongly enriched in Al. Also plotted in Fig. 5.1 are magnetites from Fogo D, Furnas A and Furnas 1640. No ilmenite was found in probe sections of these deposits. In a study of Fe-Ti oxide minerals from salic volcanics, Carmichael (1967) established that two of his samples, a phonolitic obsidian and a kenyte contained only magnetite. The minor element ratio R^{2+}/R^{3+} was found to be larger than for magnetites which coexisted with ilmenite. Carmichael's (1967) analyses of the magnetites from the phonolite and kenyte are plotted in Fig. 5.1. The observed relationships suggest that ilmenite is scarce rather than absent in Fogo D and the Furnas samples.

5.2.2 Accuracy of T-fO_2 data

Errors in probe analyses do not cause errors worse than $\pm$ 10°C and $\pm$ 0.25 log units fO_2. Buddington and Lindsley (1964) give accuracies of $\pm$ 30°C and $\pm$ 1 log unit fO_2 for their calibration curves in the pure Fe-Ti-O system. The results of Helz (1973), Ulmer et al. (1976) and Wright and Weilblen (1968), however, indicate the accuracy is even better than claimed. Hildreth (1979) considers an accuracy of $\pm$ 10°C and $\pm$ 0.25 log units fO_2 to be appropriate for his samples with their low minor element contents. An independent check of the accuracy of temperatures obtained from the Fe-Ti oxide geothermometer is provided by results obtained using the clinopyroxene-ilmenite geothermometer (Bishop, 1980). This geothermometer is based on Fe^{2+} - Mg partioning between ilmenite ($FeTiO_3$) - geikieite ($MgTiO_3$) solid solution and hedenbergite ($CaFeSi_2O_6$) - diopside ($CaMgSi_2O_6$) solid solution:

$$MgTiO_3 + CaFeSiO_2O_6 = FeTiO_3 + CaMgSi_2O_6$$

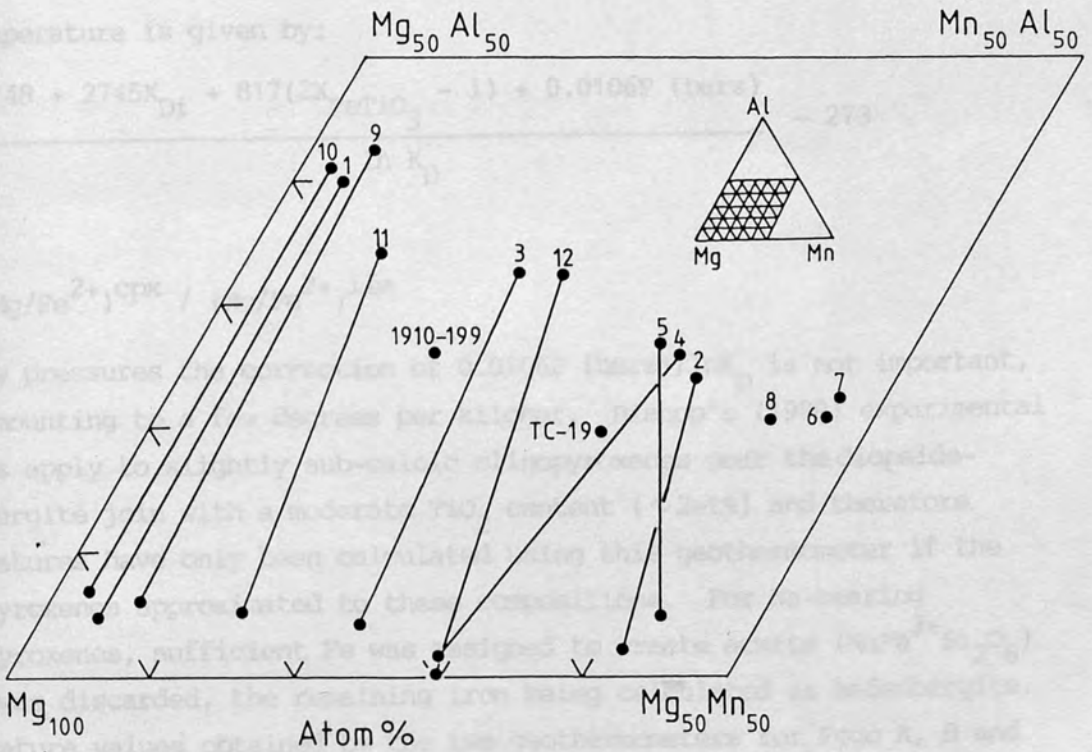

Fig. 5.1 Variation in minor elements of coexisting magnetite and ilmenite. Also shown are magnetite analyses from samples in which no ilmenite was found. 1910-199 (kenyte) and TC-19 (phonolite) are taken from Carmichael (1967).

Key - Pumice deposits: 1, Faial S; 2, Faial B; 3, Fogo A; 4, Fogo B; 5, Fogo C; 6, Fogo D; 7, Furnas F; 8, Furnas 1640.

Lavas: 9, AZ1034; 10, 10SM; 11, AZ3374; 12, AZ3360

The temperature is given by:

$$T°C = \frac{748 + 2745X_{Di} + 817(2X_{FeTiO_3} - 1) + 0.0106P \text{ (bars)}}{\ln K_D} - 273$$

where:

$$K_D = (Mg/Fe^{2+})^{cpx} / (Mg/Fe^{2+})^{ilm}$$

For low pressures the correction of $0.0106P \text{ (bars)}/\ln K_D$ is not important, only amounting to a few degrees per kilobar. Bishop's (1980) experimental results apply to slightly sub-calcic clinopyroxenes near the diopside-hedenbergite join with a moderate TiO_2 content ($\sim$2wt%) and therefore temperatures have only been calculated using this geothermometer if the clinopyroxenes approximated to these compositions. For Na-bearing clinopyroxenes, sufficient Fe was assigned to create acmite ($NaFe^{3+}Si_2O_6$) which was discarded, the remaining iron being calculated as hedenbergite. Temperature values obtained by the two geothermometers for Fogo A, B and C and from some phonolitic pyroclastic deposits from Tenerife (Wolff and Storey, 1983) are compared in Table 5.2. With one exception, the agreement is very good, the differences in temperatures being generally less than the errors initially suggested by Buddington and Lindsley (1964) for the Fe-Ti oxide geothermometer. It is therefore, suggested that errors of ± 30°C and ± 1 log unit fO_2 for the Fe-Ti oxide geothermometer are probably reasonable for most of the Azores samples.

5.3 VOLATILE COMPONENTS IN SOME PUMICE-FORMING MAGMAS FROM SAO MIGUEL AND FAIAL

This section is mainly concerned with the application of thermodynamic methods to mineral chemistry data as a means of estimating volatile components in the system H-O-S. The method is applied to those Azores pumice deposits with suitable phenocryst assemblages. The deduced volatile contents are compared with experimental data for the system Ab-Or-H_2) (Bowen and Tuttle, 1950) and with "rough" estimates for magnetic water obtained from field data.

5.3.1 Estimation of fO_2

The compositions of coexisting magnetite-ilmenite pairs defines

Eruptive unit	Temperature (^{o}C) from Fe-Ti oxides	Temperature (^{o}C) from cpx-ilm
[a]Ignimbrite O(i), Tenerife	940	980
[a]Ignimbrite O(ii), Tenerife	915	923
Boca de Tauce welded air fall tuff, Tenerife	835	810
Tajao ignimbrite, Tenerife	915	907
Adeje red ignimbrite, Tenerife	865	833
Fogo A pumice fall deposit, Sao Miguel	960	950
Fogo B pumice fall deposit, Sao Miguel	910	940
Fogo C pumice fall deposit, Sao Miguel	880	800

[a]Mixed-magma eruption: temperatures are given for two of the magmas represented in the pumice deposit

Table 5.2 Comparison of temperatures obtained by applying the Fe-Ti oxides geothermometer (Buddington & Lindsley, 1964) to analyses recast by the method of Carmichael (1967), with those given by the clinopyroxene-ilmenite geothermometer (Bishop, 1980), for those deposits where titanomagnetite, ilmenite and augite coexist. Tenerife data from Wolff and Storey (1983).

the fugacity of oxygen (fO_2) as well as the equilibration temperature (Buddington and Lindsley, 1964). Deduced fO_2 values for seven trachytic pumice deposits and two basic lavas are shown in Table 5.1 and Fig. 5.2. The data show a well-defined trend with fO_2 values approximately 0.5 log units above QFM at 1000°C, but trending towards this oxygen buffer (Wones and Gilbert, 1969) with decreasing temperature. This trend suggests that fayalite should be stable below approximately 900°C. Fayalite is an occasional phenocryst phase in trachytes from Faial and has also been reported from some co-magmatic syenite xenoliths erupted from Agua de Pau volcano on Sao Miguel (Cann, 1967). Previous workers (Carmichael, 1967; Ewart et al., 1971; Heming and Carmichael, 1973; Lipman, 1971; Rutherford and Heming, 1978) have shown that natural dacitic and rhyolitic liquids tend to plot on one of four curves in T-fO_2 space, each curve corresponding to the buffering of O_2 by the ferromagnesian minerals found in association with the Fe-Ti oxides (Fig. 5.2). Clearly the orthopyroxene and orthopyroxene-amphibole buffers do not apply to silica undersaturated magmas. All the trachytic pumice deposits plotted contain biotite and/or amphibole and yet fall up to two log fO_2 units below the biotite-amphibole curve for dacitic and rhyolitic liquids. Highly silica undersaturated phonolitic pumice deposits from Tenerife, with a similar ferromagnesian phenocryst assemblage to trachytes from the Azores, have higher fO_2 values than the Azores samples at a given magmatic temperature, although the Tenerife phonolites also plot some way below the biotite-amphibole buffer (Wolff and Storey, 1983). Therefore, the data suggest that either some phase/s other than biotite and/or amphibole are buffering O_2 or that the position of the biotite-amphibole curve varies with melt composition. For example, a similar study of dacitic and rhyolitic volcanics from California and the Rabaul caldera, Papau New Guinea (Heming & Carmichael, 1973) showed that the orthopyroxene buffer defined a different position in T-fO_2 space for the two provinces. This discrepancy was explained as resulting from the different silica activities of the two suites.

5.3.2 Estimation of fH_2O, PH_2O, XH_2O

Water fugacity (fH_2O) was estimated using the compositions of coexisting biotite, sanidine and magnetite from the equilibrium reaction:

$$\underset{\text{annite}}{KFe_3AlSi_3O_{10}(OH)_2} + \tfrac{1}{2}O_2 = \underset{\text{sanidine}}{KAlSi_3O_8} + \underset{\text{magnetite}}{Fe_3O_4} + H_2O$$

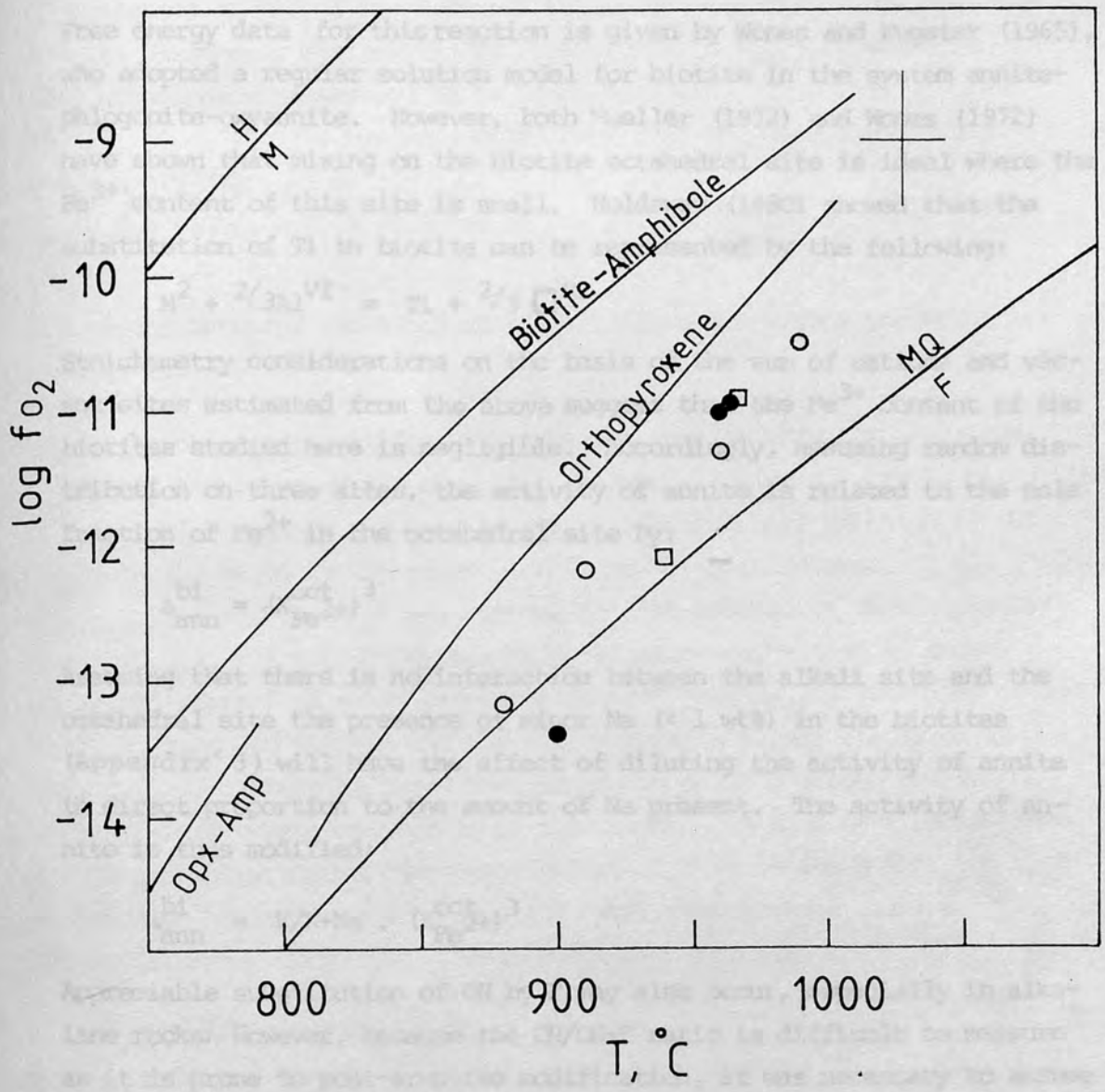

Fig. 5.2 Equilibration temperatures and fO_2 values derived from co-existing magnetite-ilmenite microphenocrysts. Open circles: Fogo trachytic pumice deposits, Sao Miguel; filled circles: Faial pumice deposits. Also shown are two basic lavas from Sao Miguel (open squares). MQF = magnetite-quartz-fayalite buffer; H-M = haematite-magnetite buffer. The biotite-amphibole, orthopyroxene-amphibole and orthopyroxene curves are mineral buffers found for dacitic and rhyolitic compositions (Carmichael, 1967; Ewart et al., 1971; Heming and Carmichael, 1973; Lipman, 1971; Rutherford and Heming, 1978).

Free energy data for this reaction is given by Wones and Eugster (1965), who adopted a regular solution model for biotite in the system annite-phlogopite-oxyannite. However, both Mueller (1972) and Wones (1972) have shown that mixing on the biotite octahedral site is ideal where the Fe^{3+} content of this site is small. Holdaway (1980) showed that the substitution of Ti in biotite can be represented by the following:

$$M^{2} + {}^{2}/_{3}Al^{VI} = Ti + {}^{2}/_{3}\square^{VI}$$

Stoichometry considerations on the basis of the sum of cations and vacant sites estimated from the above suggest that the Fe^{3+} content of the biotites studied here is negligible. Accordingly, assuming random distribution on three sites, the activity of annite is related to the mole fraction of Fe^{2+} in the octahedral site by:

$$a_{ann}^{bi} = (X_{Fe^{2+}}^{oct})^{3}$$

Assuming that there is no interaction between the alkali site and the octahedral site the presence of minor Na (< 1 wt%) in the biotites (Appendix 3) will have the effect of diluting the activity of annite in direct proportion to the amount of Na present. The activity of annite is thus modified:

$$a_{ann}^{bi} = K/K+Na \cdot (X_{Fe^{2+}}^{oct})^{3}$$

Appreciable substitution of OH by F may also occur, especially in alkaline rocks. However, because the OH/OH+F ratio is difficult to measure as it is prone to post-eruptive modification, it was necessary to assume that OH/OH+F = 1, and calculated values of fH_2O are thus maximum estimates. The activity of $KAlSi_3O_8$ in sanidine was calculated from the asymmetric regular solution treatment of Thompson and Waldbaum (1969) who give the following expressions for the margules parameters (W_G):

$$W_G^{albite} = 6326.7 + 0.0925P - 4.6321T$$

$$W_G^{orthoclase} = 7671.8 + 0.1121P - 3.8565T$$

where the activity coefficients are given by:

$$RT\ln\gamma_{ab} = (2W_G^{or} - W_G^{ab})\, X^{2}_{or} + 2(W_G^{ab} - W_G^{or})\, X^{3}_{or}$$

$$RT\ln\gamma_{or} = (2W_G^{ab} - W_G^{or})\, X^{2}_{ab} + 2(W_G^{or} - W_G^{ab})\, X^{3}_{ab}$$

For pressures of only a few kilobars it can be seen that values for the margules parameters are relatively insensitive to P_{total}. Magnetite solid solutions were assumed to be ideal following Carmichael et al. (1977). Thus, fH_2O values were calculated from the expression given by Wones (1972):

$$\log fH_2O = 7409/_T + 4.25 + 0.5 \log fH_2O + 3 \log a^{bi}_{amm} - \log a^{san}_{or} - \log a^{sp}_{mag}$$

fH_2O values obtained for 4 pumice deposits from Sao Miguel and Faial are given in Table 5.3.

Burnham et al. (1969) give fugacity coefficients for water over a range of temperatures and pressures thereby allowing P_{H_2O} to be calculated. If P_{total} is known, P_{H_2O} may be converted into the mole fraction of water (X_{H_2O}) in the magma by the expression given by Spera in Ewart et al. (1975). As P_{total} was not known it was assumed for the purpose of this study that $P_{H_2O} = P_{total}$. If the whole-rock major element composition is known, the weight percent of water can be calculated from X_{H_2O}. Estimated values for P_{H_2O}, X_{H_2O} and wt% H_2O for the pumice forming magmas are given in Table 5.3. It should be noted that these are maximum values for the magmatic water component because of the assumptions made of fluorine-free biotite and water saturation, nevertheless it will be shown that the high values (6.5-7.2 wt% H_2O) are compatible with the observed dispersal of lithic fragments associated with these pumice deposits.

5.3.3 Estimation of fH_2

Hydrogen fugacity (fH_2) may also be estimated from the biotite composition:

$$KFe_3AlSi_3O_{10}(OH)_2 = KAlSi_3O_8 + Fe_3O_8 + H_2$$

This reaction was used by Rutherford and Heming (1978) to estimate fH_2 for rhyolitic ignimbrites from New Zealand. However, the expression which they used assumes a regular solution model for biotite, which is inconsistent with the assumption of biotite ideality used to find fH_2O for the same mineral data. For the Azores samples, fH_2 values obtained using the thermodynamic data of Wones and Eugster (1965) and assuming biotite ideality seem unreasonably large (up to 900 bars). fH_2 has therefore been estimated from the water decomposition reaction:

Pumice deposit	a^{bi}_{ann}	a^{san}_{or}	$\log fH_2O$	PH_2O (bars)	XH_2O^a	$wt\%H_2O^a$	Total water[b]
Fogo A pumice fall deposit, Sao Miguel	0.0222	0.498	3.47	3000	0.22	6.6	0.15
Fogo B pumice fall deposit, Sao Miguel	0.0200	0.500	3.36	2500	0.21	6.5	0.03
Fogo C pumice fall deposit, Sao Miguel	0.0429	0.508	3.30	2300	0.21	6.5	0.008
Pumice fall deposit B, Faial	0.106	0.433	3.72	5300	0.23	7.2	-

[a]Calculated assuming water saturation of magma

[b]Total volume of water (calculated as liquid in km^3) released from the magma during the eruption. Based on total erupted volume of magma (Table 4.1)

Table 5.3 Estimated magmatic water contents

$$H_2O = H_2 + \tfrac{1}{2}O_2 \qquad \text{(Eq. 5.19)}$$

The variation of the equilibrium constant (K) with temperature for this reaction was obtained by regression of logK against $^1/_T$ using values given in the JANAF thermochemical tables (Stull and Prophet, 1971). This gave:

$$\log K = \frac{12795}{T} - 2.79 \qquad \text{c.c.} = 1.00$$

where c.c. is the correlation coefficient and,

$$\log fH_2 = \log fH_2O - \tfrac{1}{2} \log fO_2 - \log K \text{ reaction}$$

Deduced values of fH_2 are given in Table 5.4.

5.3.4 Estimation of fS_2

Sulphur fugacity (fS_2) has been estimated using the experimental results of Toulmin and Barton (1964) for the system Fe-S. fS_2 is related to temperature and pyrrhotite composition (Fe_7S_8 - FeS) by:

$$\log fS_2 = (70.03 - 85.83\, X_{FeS}^{pyrr})(1000/T - 1) + 39.3(1 - 0.9981 X_{FeS}^{pyrr})^{\frac{1}{2}} - 11.91$$

where fS_2 is relative to the ideal diatomic gas at one atmosphere, X_{FeS}^{pyrr} is the mole fraction of FeS in pyrrhotite in the system FeS-S and T is the absolute temperature. Pyrrhotite was found in a number of samples occurring as small oval black grains up to 100 μm across enclosed by phenocrysts. Microprobe analysis showed that some pyrrhotites, notably from the basalts, contained minor amounts of Ni (< 4%) and occasionally Cu (Appendix 3). Naldrett (1969) demonstrated that small amounts of Ni and Cu affect the pyrrhotite liquidus to much the same extent as comparable amounts of Fe. Thus minor elements were included with Fe in calculating the mole fraction of FeS. As the pyrrhotite grains are always found as inclusions it is possible that their compositions reflect fS_2 values at higher temperatures than those indicated by the Fe-Ti oxides. However, in the absence of data on their enclosing temperatures the values obtained by the Fe-Ti oxide geothermometer are used. Estimates of fS_2 for some volcanic rocks from Sao Miguel and Faial are shown in Fig. 5.3. Values of fS_2 are compared with data for dacites and rhyolites from Papua New Guinea and New Zealand (Heming and Carmichael, 1973; Rutherford and Heming,

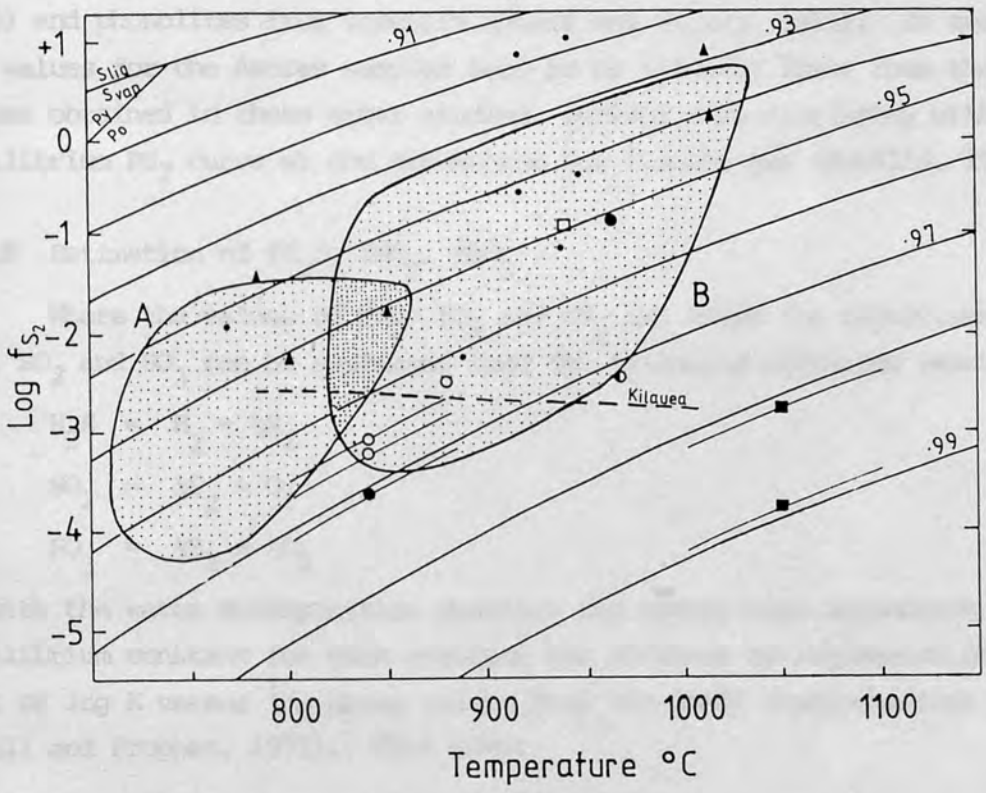

Fig. 5.3 fS_2 data for pyrrhotite bearing samples. Contours (calculated from the data of Toulmin and Barton, 1964) are the mole fraction of FeS in pyrrhotite solid solution (FeS-S_2). Also shown are the pyrite-pyrrhotite (P_y/P_o) and sulphur liquid-vapour equilibrium curve (S_{liq}/S_{vap}). Filled squares, Faial basalts; symbols for other Azores samples as Fig. 5.2. Bars represent possible equilibration temperature range for samples lacking ilmenite. Other symbols: small filled circles, Tenerife pumice deposits; triangles, sub volcanic cumulates from Tenerife; half filled circle, Green Tuff, Pantelleria (all from Wolff and Storey, 1983). Stippled field A is the range of fS_2 values found for New Zealand rhyolitic ignimbrites (Rutherford and Heming, 1978); B is the range of fS_2 values found for dacitic and rhyolitic pumice deposits from the Rabaul caldera, Papua New Guinea (Heming and Carmichael, 1973). Labelled Kilauea curve is best estimate for PS_2 (Nordlie, 1971)

1978) and phonolites from Tenerife (Wolff and Storey, 1983). On average, fS_2 values for the Azores samples tend to be slightly lower than the fS_2 values obtained in these other studies, showing more similarity with the equilibrium PS_2 curve at one atmosphere for Kilauea gas (Nordlie, 1971).

5.3.5 Estimation of fH_2S, fSO_2, fSO_3

Where the values of fS_2, fO_2 and fH_2 are known the fugacities of H_2S, SO_2 and SO_3 can be estimated from the following formation reactions:

$$H_2S = H_2 + \tfrac{1}{2}S_2$$

$$SO_2 = \tfrac{1}{2}S_2 + O_2$$

$$SO_3 = \tfrac{1}{2}S_2 + \tfrac{1}{2}O_2$$

As with the water decomposition reaction the temperature dependence of the equilibrium constant for each reaction was obtained by regression of a plot of log K versus $^1/_T$ using values from the JANAF thermochemical tables (Stull and Prophet, 1971). This gave:

$$\log fH_2S = \log K_{reaction} + \log fH_2 + \tfrac{1}{2} \log fS_2$$

where $\log K_{reaction} = \frac{1290}{T} - 0.65$ c.c. = 0.960

and,

$$\log fSO_2 = \log K_{reaction} + \tfrac{1}{2} \log fS_2 + \log fO_2$$

where $\log K_{reaction} = \frac{17520}{T} - 2.86$ c.c. = 0.999

and,

$$\log fSO_3 = \log K_{reaction} + \tfrac{1}{2} \log fS_2 + {}^3/_2 \log fO_2$$

where $\log K_{reaction} = \frac{22630}{T} - 7.60$ c.c. = 0.999

Only one of the pumice deposits studied (Fogo C.) contained the required phenocryst assemblage (magnetite + ilmenite + sanidine + biotite + pyrrhotite) for estimating all these sulphur bearing species. Calculated values of fH_2S, fSO_2 and fSO_3 (Table 5.4) can, at best, be only considered order of magnitude estimates due to uncertainties in the fO_2,

Sample	fH_2 [a]	fH_2 [b]	fH_2S	fSO_2	fSO_3
Fogo A	200	34	-	-	-
Fogo B	110	27	-	-	-
Fogo C	150	39	6.6	0.008	$10^{-9.0}$
Faial B	880	200	-	-	-
Faial T	-	-		0.83	$10^{-6.2}$
AZ1034	-	-	-	0.11	$10^{-7.5}$

[a] fH_2 estimated from biotite composition (see text for method)

[b] fH_2 estimated from the water decomposition reaction

Table 5.4 Volatile fugacities (H_2, H_2S, SO_2, SO_3)

fS_2 and fH_2 input data. For the limited data available from the Azores, results suggest that of the sulphur bearing species SO_3 is the least abundant and H_2S the most abundant. In this respect, this sample is similar to both rhyolites from New Zealand (Rutherford and Heming, 1978) and phonolites from Tenerife (Wolff and Storey, 1983).

5.4 LIMITATIONS AND ACCURACY

There are four main limitations to the accuracy of the data and the general applicability of this approach.

1) Errors in (a) mineral analyses and (b) thermodynamic data. (b) does not apply if results obtained by using the same calculation procedures are being compared, but errors from both sources are compounded when gas reactions are used (e.g. to find fSO_2, fSO_3) where the input data are fugacities already estimated from mineral data. Uncertainities in fugacity estimations, calculated by the error propogation method recommended by Powell (1978), are given in Table 5.5.

2) Errors due to assumptions made. These can usually be assessed with a degree of confidence, e.g. the assumption of fluorine-free biotite results in the calculation of maximum fH_2O values.

3) Pumice deposits often have very low phenocryst contents, and, if aggregate mineral grains are rare or absent, it may be difficult to establish equilibrium between phenocryst phases.

4) The required mineral phases may not be present. Just over half of the samples examined contained both magnetite and ilmenite, and fewer still contained biotite and/or pyrrhotite in addition. More seriously, the vast majority of erupted magmas do not bear a mineral assemblage which permits the determination of the important constituents CO_2, CO, HF and HCl.

Despite these problems, the approach is a powerful one, as it allows the rapid calculation of the composition of part of the volatile component of a range of salic magma types.

5.5 DISCUSSION

Fe-Ti oxide temperatures for the metaluminous trachytic pumice

T	30°C	log fS_2	0.5
log fO_2	0.5	log fSO_2	0.7
log fH_2O	0.3	log fSO_3	0.9
log fH_2	0.4	log fH_2S	0.5

Table 5.5 Uncertainties ($\pm$) in temperatures and fugacity values

deposits range between 860 - 960°C, similar to the range found for trachyandesitic and phonolitic pumice deposits from Tenerife (Wolff and Storey, 1983). These values may approximate to liquidus temperatures as the samples are near-aphyric. Due to the lack of ilmenite in the peralkaline trachytic pumice deposits (e.g. Fogo D, Furnas A, Furnas 1640) no temperature estimates using the Fe-Ti oxide geothermometer could be made. However, on the basis that these deposits are chemically more evolved than Fogo C, pre-eruptive temperatures < 850°C would seem reasonable.

Fugacities may be converted to molar abundances if it is assumed that volatile species mix ideally with each other and with magma, and if fugacity co-efficients are known for each volatile species. This has been done for Fogo C for the five principal species in H-O-S. Results (Table 5.6) show that volatile abundances are similar to the data for phonolites and rhyolites given by Wolff and Storey (1983). The general similarity in relative abundances is presumably a consequence of the relative stabilities of the various gas species under magmatic conditions; for example SO_2 will always predominate over SO_3 at the oxygen fugacities usually encountered in magmas. The data of Wolff and Storey (1983) suggest that the magmatic volatile component has a similar composition (at least in H-O-S) in a wide variety of pumice-forming salic melts, although it should be noted that a pantellerite sample for which they give data is much poorer in the sulphur species than the alkaline and calc-alkaline liquids (Fig. 5.3). Wolff and Storey (1983) give maximum estimated values for CO_2, HCl and HF in pumice-forming magmas from the Azores and Canary Islands. The levels they suggest for these components are comparable to the determined minor constituents in H-O-S but are several orders of magnitude less abundant than H_2O. Thus, water is the most important volatile constituent in the great majority of magmas, and a knowledge of magmatic water content is essential to the estimation of such parameters as the viscosity and density of magma before eruption (Chapter 4). Rutherford and Heming (1978) considered the water contents of New Zealand ignimbrite magmas to be unusually high, and ascribed this to an origin by anatexis of water-rich basement greywackes (for which there is a considerable body of evidence; see Carmichael et al., 1974, and references cited therein). The mean water content of the values tabulated by Rutherford

	Pumice fall deposit C, Sao Miguel	Pumice fall deposit E, Tenerife[b]	Average New Zealand ignimbrite[c]
H_2O	98.1%	99.4%	99%
H_2	1.6%	0.5%	0.5%
H_2S	0.3%	0.1%	0.5%
SO_2	(0.0003%)	(0.005%)	(0.0002%)
S_2	(0.0001%)	(0.0002%)	(0.0001%)

[a]Calculated using fugacity coefficients tabulated by Ryzhenko & Volkov (1971) and assuming ideal mixing

[b]From Wolff and Storey (1983)

[c]From data of Rutherford & Heming (1978)

Table 5.6 Molar abundances, as a percentage of total abundance of the five major species in the system H-O-S, for three cases[a]

and Heming corresponds to approximately 6.5% by weight, closely similar to the values obtained here. Sommer (1977) found volatile contents of up to 7% (average 5.4%) for the Bandelier Tuff, New Mexico, rhyolite magma; 92% of this consisted of H_2O, the remainder being mostly CO and and CO_2.

The estimated magmatic water contents of the Azores pumice deposits are compatible with both the experimentally determined relationships in the system Ab-Or-H_2O (Bowen and Tuttle, 1950) and field evidence for the violently explosive nature of the magmas. Fig. 5.4 shows that the liquidus for Ab-Or is lowered by increasing P_{H_2O} (Bowen and Tuttle, 1950). The composition of Fogo C, which contains 90% normative Ab + Or approximates to the simple Ab-Or system. Assuming the Fe-Ti oxide equilibration temperature of 880°C approximately equals the liquidus value, the experimental data of Bowen and Tuttle suggests a water content of about 1000 bars. This is a minimum estimate as the presence of accessory components in natural trachytic melts (such as anorthite) will have the effect of raising the liquidus.

The distribution of tephra in a plinian air-fall deposit can be used to estimate various physical parameters of the eruption (Wilson, 1976; Wilson et al., 1978). For pumice fall deposits it is possible to obtain a rough estimate of the magmatic volatile content from field data. Wilson (1980) and Wilson et al., (1980) have shown that the "muzzle" velocity of an explosive eruption depends on the mass eruption rate and magmatic volatile content (Fig. 5.5). However, dependence on eruption rate is very weak for the range of plinian eruption conditions (p on Fig. 5.5), and therefore volatile content, assumed to be entirely water, can be estimated from muzzle velocity. The error due to variations in the volatile composition is negligible if H_2O is > 80% of the total. The thermodynamic estimates given here and by Wolff and Storey (1983) suggest that other volatile species are greatly subordinate to water. Therefore, the muzzle velocity (μ) is given by Wilson (1976) where:

$$\mu^2 = (8\ gr_o\sigma_o)/3\ Cp \qquad \text{(Eq. 5.32)}$$

where r_o, σ_o are respectively the radius and density of the largest erupted clast, C is the drag coefficient and p is the effective gas density

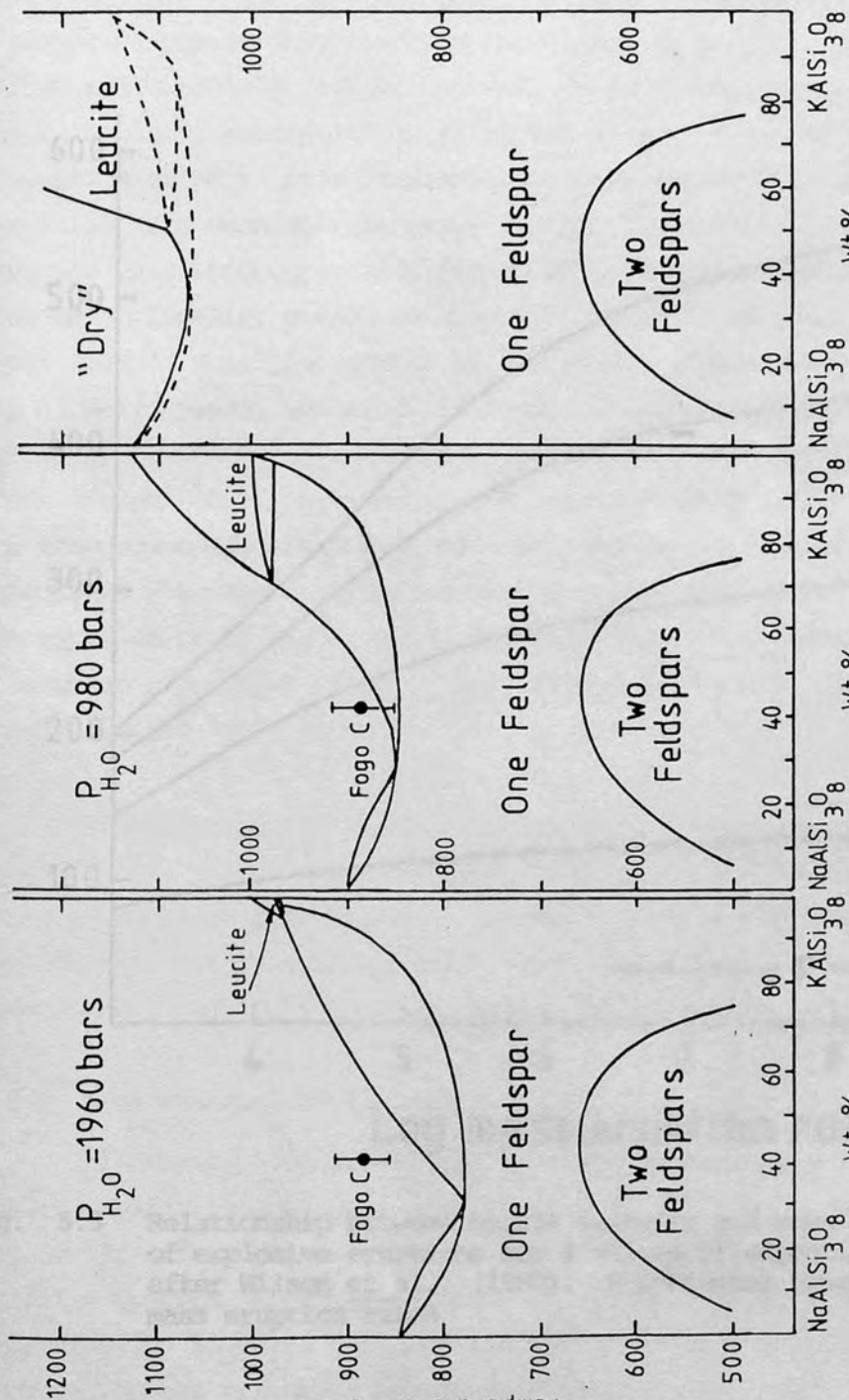

Fig. 5.4 Phase diagrams for the system $NaAlSi_3O_8$-$KAlSi_3O_8$-H_2O (after Bowen and Tuttle, 1950). Broken lines: phase boundaries not precisely determined. The normative $\left(\frac{Ab}{Ab + Or} \times 100\right)$ ratio and Fe-Ti oxide equilibrium temperature (880°C ± 30°C) for Fogo C also shown

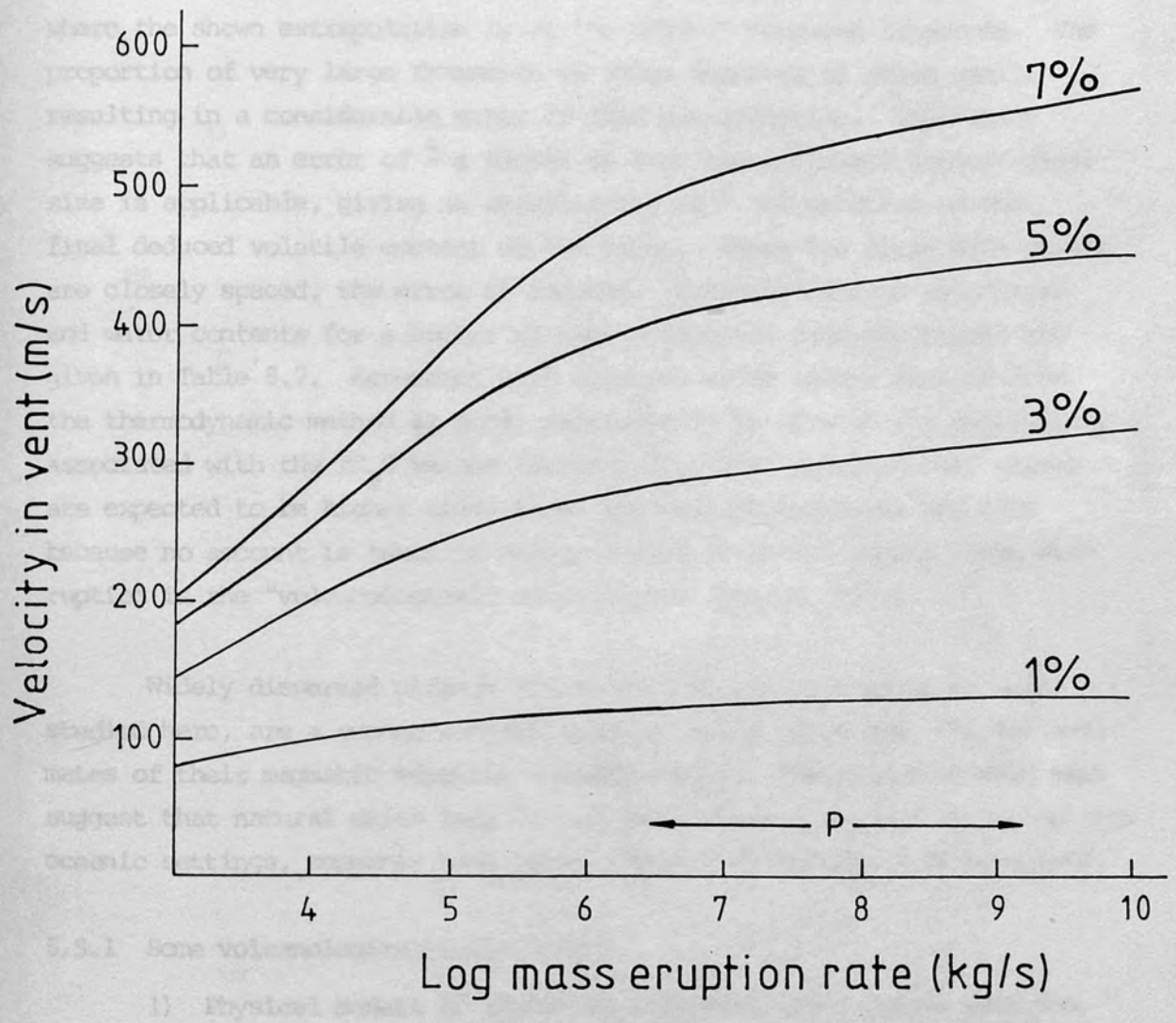

Fig. 5.5 Relationship between muzzle velocity and mass eruption rate of explosive eruptions for 4 values of magmatic water content, after Wilson et al., (1980). P indicates range of plinian mass eruption rates.

in the volcanic vent (values of p are tabulated by Wilson, 1976). The size of the largest erupted clast is found by extrapolation of the range dependence of clast size. Data on the three largest accessory lithic fragments (for which σ_o = 2.5 gcm^{-3}) at any one locality are given for a number of pumice deposits from Sao Miguel by Booth et al. (1978) and Walker and Croasdale (1971). An example is given by Fogo B (Fig. 5.6), where the shown extrapolation is of the largest measured fragments. The proportion of very large fragments in these deposits is often small, resulting in a considerable error in this extrapolation. Experience suggests that an error of $\pm$ a factor of 4 on the estimated largest clast size is applicable, giving an uncertainity of $\pm$ 30% relative on the final deduced volatile content of the magma. Where the field data points are closely spaced, the error is reduced. Estimated muzzle velocities and water contents for a number of pumice deposits from Sao Miguel are given in Table 5.7. Agreement with magmatic water values derived from the thermodynamic method is good, particularly in view of the uncertainty associated with the fH_2O values (Table 5.5). The "petrological" values are expected to be higher since these are maximum estimates and also because no account is taken of energy losses occurring during magma disruption in the "volcanological" calculations (Wilson, 1976).

Widely dispersed plinian pumice fall deposits, similar to those studied here, are a common manifestation of salic volcanism, yet few estimates of their magmatic volatile contents exist. The data discussed here suggest that natural salic liquids including those generated in intraplate, oceanic settings, commonly have water contents in excess of 5% by weight.

5.5.1 Some volcanological implications

1) Physical models of explosive processes often assume that the magmatic volatile component consists entirely of water, because of the negligible effect of the presence of small quanitites (< 10%) of other volatile species on eruption dynamics. These results indicate that this approximation is valid for alkaline salic magmas. An illustration is provided by the effect of gas density on a plinian eruption column. Dense columns tend to collapse to form ignimbrites (Sparks and Wilson 1976), whereas lighter columns more readily undergo convective uprise to form an

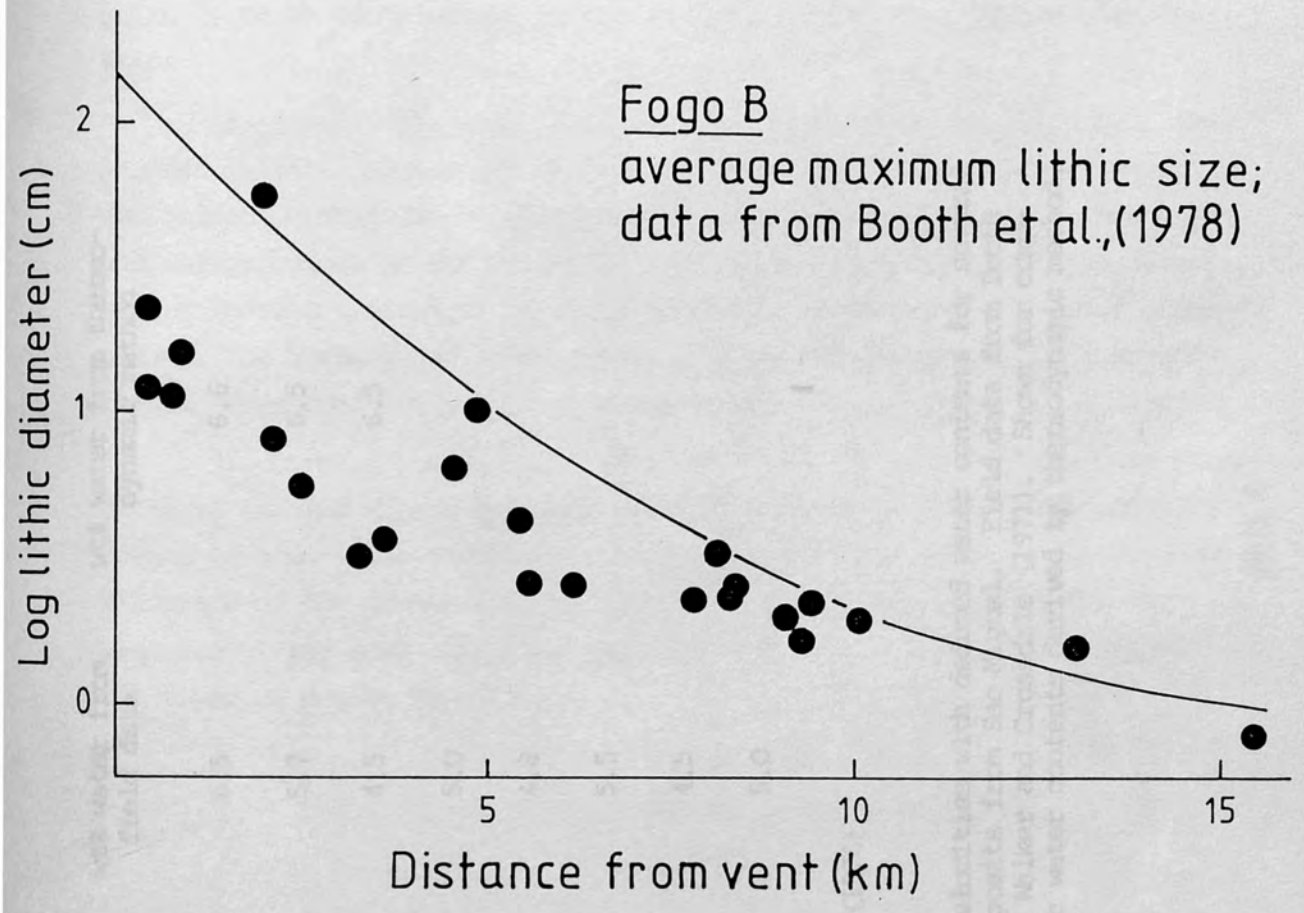

Fig. 5.6 Average of the three largest accessory lithic fragments found in Fogo B at a given locality plotted against distance from source; data from Booth et al., (1978). The largest measurements are extrapolated (solid line) to zero range to yield a value for the largest lithic clast which can just be supported by the eruption column at the vent

Deposit	Muzzle velocity ms^{-1}	wt% water from field data	wt% water from thermodynamic method
Fogo A	520[a]	6.5	6.6
Fogo B	470	5.7	6.5
Fogo C	400	4.5	6.5
Fogo D	420	5.0	
Fogo 1563	415[a]	4.8	
Congro ash	460	5.5	
Furnas C	400	4.5	
Furnas 1640	420	5.0	

[a]Muzzle velocities from Wilson (1976)

Table 5.7 Estimated muzzle velocities with deduced water contents for several air-fall pumice deposits from Sao Miguel. Field data from Booth et al., (1978) and Walker and Croasdale (1971). Shown for comparison are magmatic water contents derived by thermodynamic method.

eruption cloud some tens of kilometres high, fall-out from which produces a plinian pumice fall deposit (Wilson, 1976; Wilson et al., 1978). The data discussed here indicate that variations in the density of released gas, due to compositional variations in the system H-O-S, are unlikely to be great enough to significantly affect eruption column dynamics.

2) Appreciable quantities of combustible gases (H_2, S_2, H_2S) are present in salic magmas and will be released upon explosive eruption. The oxidation of these in the eruption cloud will contribute to the thermal energy budget of the eruption. Enthalpy calculations for the relevant combustion reactions indicate that this contribution is minor compared to the thermal and kinetic energy released, and is unlikely to exceed a few percent of the total eruption energy.

3) Large quantities of water are released during pumice eruptions. If it is assumed that a large proportion of released water falls as rain during or soon after eruption, then the formation of mudflows by remobilisation of the newly-deposited tephra is a virtually inevitable consequence of any such eruption. Mudflows are very common associates of all types of pumice deposit.

CHAPTER 6

GEOCHEMICAL CHARACTERISTICS OF AZORES BASALTS: IMPLICATIONS FOR SOURCE HETEROGENEITY

6.1 INTRODUCTION

Geochemical studies of ocean ridge basalts have revealed significant trace element and isotopic variations within the oceanic crust. Based mainly on the enrichment (or depletion), relative to a primitive reference composition (primordial mantle or chondrite), of the light rare-earths and other highly incompatible trace elements in basaltic magmas (eg Cs, Rb, Ba, Th, K, Ta, Nb) the results of these studies were used to classify mid-ocean ridge basalts (m.o.r.b.) into three types (Tarney et al.,1980); viz.

(1) Normal ridge segments (N-type m.o.r.b.). N-type m.o.r.b. are characterized by relatively low $^{87}Sr/^{86}Sr$ (<0.703) and $^{206}Pb/^{204}Pb$ ratios (17.5-18.5), high $^{143}Nd/^{144}Nd$ ratios (>0.5131) and are depleted in the highly incompatible elements.

(2) Enriched ridge segments (E-type m.o.r.b.) characteristic of ocean crust with positive, residual gravity and depth anomalies (eg the Azores Plateau; Searle, 1976). E-type m.o.r.b. have high $^{87}Sr/^{86}Sr$ (>0.703) and $^{206}Pb/^{204}Pb$ ratios (18-21), low $^{143}Nd/^{144}Nd$ ratios (<0.513) and are strongly enriched in the highly incompatible elements.

(3) Transitional ridge segments (T-type m.o.r.b.) As implied, these are transitional between the two previous types and are characterized by intermediate geochemical parameters.

Schilling (1975) observed all three types in a zone stretching SW from

the Azores Plateau to latitude 33°N, noting a progressive change southwards from light REE enriched (E-type) to light REE depleted (N-type) m.o.r.b. Thus, as noted by White et al. (1979), ridge basalts adjacent to the Azores have $^{87}Sr/^{86}Sr$ ratios and patterns of enrichment in the highly incompatible elements similar to alkali basalts from the islands (Fig 6.2).

In understanding the origin of ocean islands and ridges it is necessary to consider to what extent, if any, compositional differences between alkali basalts and the different m.o.r.b. types, represent variations in the mantle source composition. Tarney et al. (1980) attempted to model the observed variations in m.o.r.b. REE chemistry by a number of processes. It was demonstrated that it was highly unlikely that fractional crystallization in a closed system, zone refining or contamination by hydrothermally altered oceanic crust could produce the systematic regional differences observed in the REE ratios of m.o.r.b. However, it was the apparently evolved nature of most terrestial basalts which led O'Hara (1975) to propose that their light REE enriched nature may be due to substantial, open system, high pressure eclogite fractionation (Kd_{Yb} garnet/melt ~ 4; Hanson, 1977), low pressure equilibration and fractionation removing any evidence of this event. Using the equations of O'Hara (1977) for a continuously replenished magma chamber where Y is the fraction of liquid erupted from the magma chamber and X is the fraction of crystallization, Tarney et al. (1980) showed that for fractionation of an eclogite phase assemblage (86% clinopyroxene, 14% garnet), the REE variations in m.o.r.b. can only be produced if extreme X/Y and garnet/clinopyroxene ratios are invoked. These authors question whether such conditions are attainable in the upper mantle.

Their batch melting model (for $<15\%$ melting) of a garnet lherzolite source suggests that light REE/heavy REE ratios vary in direct relation to the proportion of melt produced (see also Fig 1.5, this thesis). For more than about 15% batch melting the light REE/heavy REE ratios of the melt are almost the same as the source. Experimental evidence and major element variations sugggest that m.o.r.b. is produced by 15-

30% partial melting of a peridotite source (Green and Ringwood, 1967) and thus REE ratios of the two should be similar. The batch melting model of Tarney et al. (1980) for a garnet lhezolite source might suggest that the same is not necessarily true of alkali basalts as these are probably produced by smaller degrees of partial melting than ocean ridge tholeiites (Green and Ringwood, 1967; Green, 1973). However, as previously stated there is a strong similarity in the incompatible element enrichment patterns between Azores island basalts and E-type m.o.r.b. from the adjacent Azores Plateau. This regional consistency provides good evidence that the mantle source for both basalt types is highly light REE enriched. Moreover, although it is conceivable that partial melting of a garnet lherzolite source or eclogite fractionation may be responsible for some (second order) variation in light REE/heavy REE ratios of alkali basalts, these factors cannot explain variations in the ratios of highly incompatible elements (eg their low Zr/Nb and K/Rb ratios relative to N-type m.o.r.b.) or radiogenic isotopes. The inescapable conclusion is that much of the compositional variation between alkali basalts, E-type m.o.r.b. and N-type m.o.r.b. is due to inhomogeneities in the sub-oceanic mantle.

On this premise, the purpose of this chapter is to review the incompatible element and radiogenic isotope chemistry for Azores basalts and to discuss what this implies about the nature of their mantle source.

6.2 MAJOR AND TRACE ELEMENT CHARACTERISTICS OF AZORES BASALTS

The Azores islands are composed predominantly of alkali basalt and its differentiation products which include trachytes, comendites and pantellerites (eg Self and Gunn, 1976; White et al.,1979; this thesis). This contrasts with the tholeiitic character of basalts from the adjacent Mid-Atlantic Ridge which transects the Azores Plateau (Schilling, 1975). It will be recalled from Section 1.2 that most Azores basalts are moderately to strongly silica undersaturated, those from Santa Maria having the highest normative Ne content (up to 18%;

White et al., 1979). Rarer, transitional mildly Hy-normative basalts are known to occur on Pico, Graciosa, Terceria and Sao Miguel. Similarly, in terms of their Na/K ratios Azores basalts show great variability (ie Santa Maria > Graciosa ∿ Terceria > Pico ∿ Faial ∿ Sao Jorge > Corvo ∿ Flores > Sao Miguel), both these features demonstrating that they represent a 'magma suite' in only the broad sense.

Although there is strong evidence that the compositions of some intermediate and trachytic lavas from the Azores are largely the result of magma-mixing processes (Chapters 2 and 3), for individual islands most major and trace element data define smooth trends on variation diagrams (eg data of Fernandez 1980, 1982; Metrich et al., 1981; Self and Gunn, 1976; White et al., 1979; this thesis) which are consistent with fractional crystallization of the observed phenocryst assemblages. However, variations in the incompatible element ratios Ba/Zr, P/Zr and Sr/Zr between the Main Series and Povoacao Series have been previously described (Section 3.5.3) providing evidence that there have been at least two compositionaly distinct magma sources on Sao Miguel. There are similarly significant inter-island variations in incompatible element ratios. For example, a plot of La against Yb (Fig 6.1), which is contoured for different La_N/Yb_N ratios, illustrates the variable degree of light REE enrichment shown by Azores basalts. Those from Sao Miguel and Flores consistently show the highest La_N/Yb_N ratios (12-15) while those from Terceria, Pico and Graciosa are the least light REE enriched (La_N/Yb_N varying between 7-11). The moderate positive correlation between the La_N/Yb_N ratio and La (coupled with a corresponding decrease in Cr) is probably due to clinopyroxene fractionation.

The incompatible element contents of basalts from all the Azores islands (except Corvo for which their are no data) are shown normalised to primordial mantle (bulk earth minus core) in Fig 6.2. The elements have been arranged approximately in order of increasing D values (left to right) for mantle mineralogies (after Tarney et al., 1980). Also shown in Fig 6.2 are data for 'average' N-type m.o.r.b. and

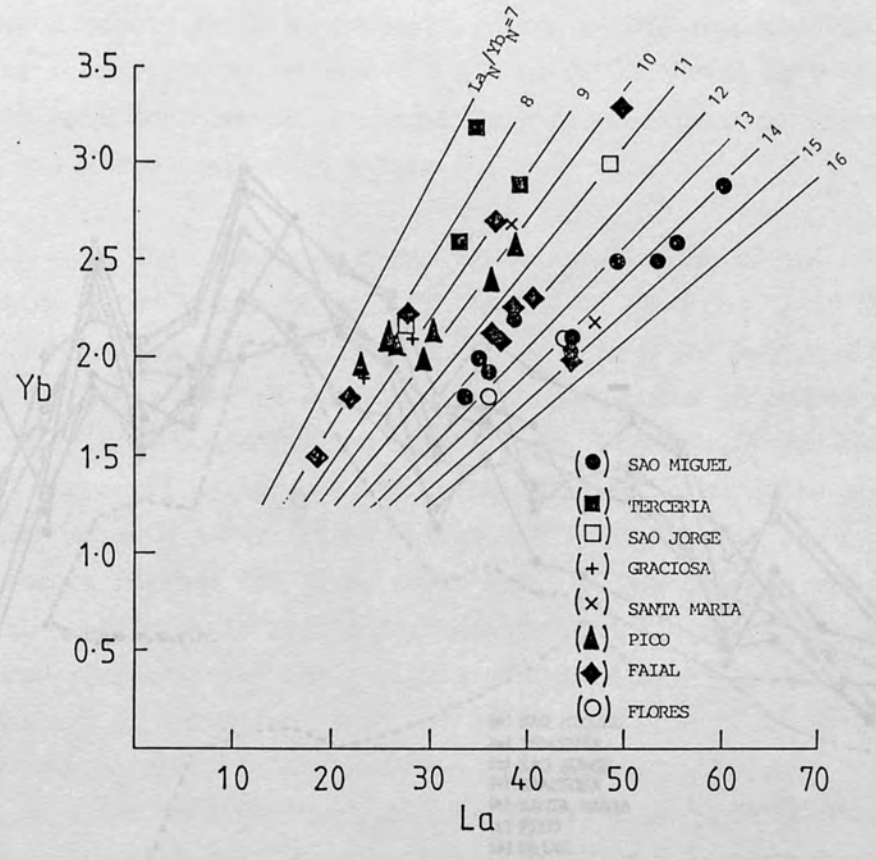

Fig 6.1. La versus Yb for basalts from the different Azores islands. The plot is contoured for different degrees of light REE enrichment in the form of chondrite normalised (La_N/Yb_N) ratios. Data from White et al. (1979) and this thesis.

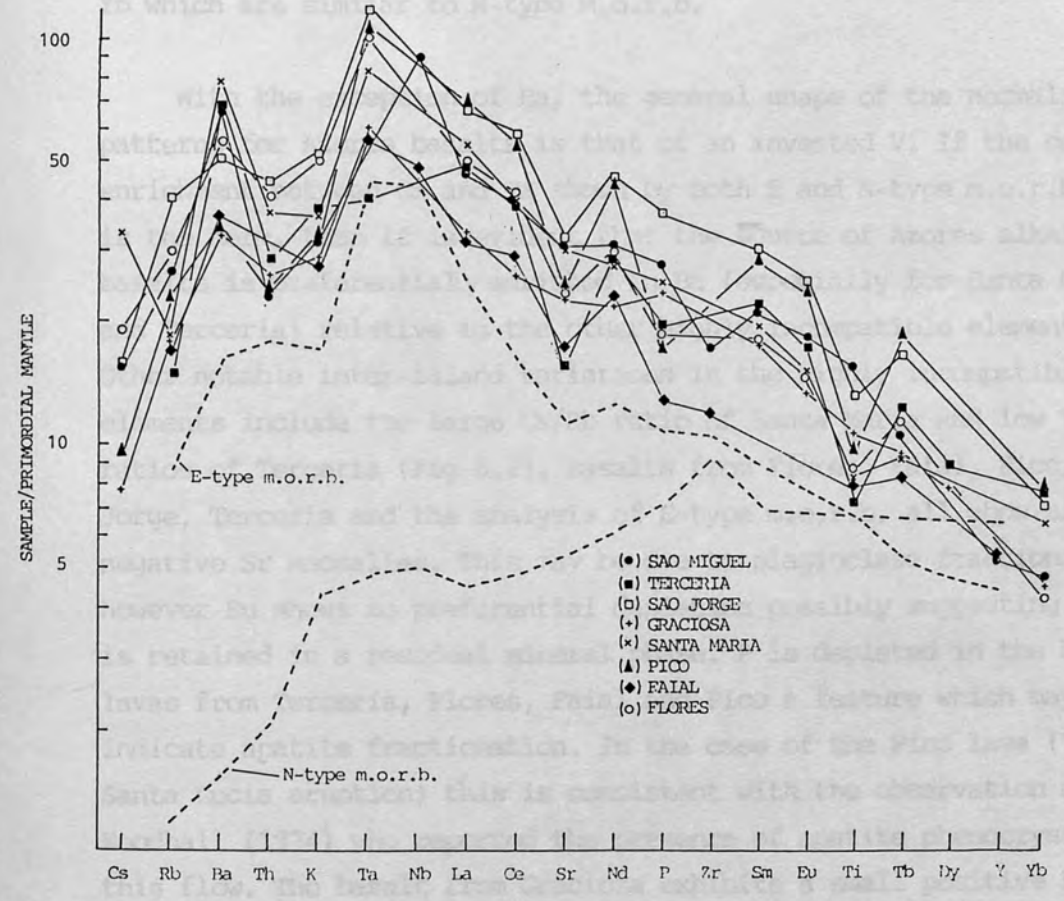

Fig 6.2. Incompatible element abundances in Azores basalts normalised to a primordial mantle composition. Shown for comparison are E-type m.o.r.b. from 36°N Mid-Atlantic Ridge (DSDP site 413) and average N-type m.o.r.b. Azores data from White et al. (1979) and this thesis. Primordial mantle values and m.o.r.b. data from Tarney et al. (1980). Order of incompatibilty decreases from left to right.

E-type m.o.r.b. Azores island basalts are strongly enriched in the highly incompatible elements showing similar normalised patterns to E-type m.o.r.b. from the Azores Plateau. The alkali basalts are approximately twice as enriched in the highly incompatible elements (for comparable Mg numbers and Ni and Cr contents) as E-type m.o.r.b. Both have contents of the moderately incompatible elements Dy, Y and Yb which are similar to N-type m.o.r.b.

With the exception of Ba, the general shape of the normalised patterns for Azores basalts is that of an inverted V. If the continuous enrichment between Cs and Ta shown by both E and N-type m.o.r.b. is the norm, then it is evident that the source of Azores alkali basalts is preferentially enriched in Ba (especially for Santa Maria and Terceria) relative to the other highly incompatible elements. Other notable inter-island variations in the highly incompatible elements include the large Cs/Rb ratio of Santa Maria and low Ta/La ratios of Terceria (Fig 6.2). Basalts from Flores, Faial, Pico, Sao Jorge, Terceria and the analysis of E-type m.o.r.b. all show sizeable negative Sr anomalies. This may be due to plagioclase fractionation, however Eu shows no preferential depletion possibly suggesting that Sr is retained in a residual mineral phase. P is depleted in the basalt lavas from Terceria, Flores, Faial and Pico a feature which may indicate apatite fractionation. In the case of the Pico lava (1718 Santa Lucia eruption) this is consistent with the observation of Woodhall (1974) who reported the presence of apatite phenocrysts in this flow. The basalt from Graciosa exhibits a small positive P anomaly. This suggests that either the source was enriched in P relative to adjacent incompatible elements (in Fig 6.2) or that this lava contains cumulus apatite.

In contrast to both E and N-type m.o.r.b. the majority of alkali basalts show negative Ti anomalies (Fig 6.2). This feature is in agreement with the limited iron enrichment trend shown by Azores basalts in AFM plots, as opposed to the strong iron enrichment (tholeiitic) trend of m.o.r.b. (Fig's 2.15 and 3.16) and indicates Fe-Ti oxide fractionation early in the differentiation sequence. Both

alkali basalts and m.o.r.b crystallize near the fayalite-magnetite-quartz buffer (White et al., 1979; Chapter 5, this thesis). However, Irvine (1967) showed that low silica activity favours the crystallization of magnetite, other factors being equal. Thus the absence of significant iron enrichment and the early appearence of Fe-Ti oxides in the island alkali basalts may simply reflect their lower silica activity relative to m.o.r.b.

6.3 $^{87}Sr/^{86}Sr$ and $^{143}Nd/^{144}Nd$ ISOTOPE GEOCHEMISTRY

$^{87}Sr/^{86}Sr$ and $^{143}Nd/^{144}Nd$ isotope data for the Azores islands and m.o.r.b. from the Azores Plateau is given by Hart and Brooks (1974), Hawkesworth et al. (1979), O'Nions and Pankhurst (1979), Richard et al. (1976), White and Schilling (1978), White et al. (1979) and White and Hoffman (1982). Except for samples from Faial, Pico and Sao Miguel and three felsic samples from Graciosa and Terceria, $^{87}Sr/^{86}Sr$ ratios in Azores island basalts range between 0.70332 to 0.70354 (White et al., 1979). These values are similar to those reported for adjacent E-type m.o.r.b. in the Azores Plateau (White and Schilling, 1978). Basalts from eastern Sao Miguel have $^{87}Sr/^{86}Sr$ ratios notably higher (up to 0.70522; Hawkesworth et al., 1979) than those from the west of the island where values more similar to the other Azores islands are found. In a plot of $^{143}Nd/^{144}Nd$ against $^{87}Sr/^{86}Sr$, Hawkesworth et al. (1979) observe that data for Sao Miguel define a distinct trend which is offset to the right of the 'normal' mantle array (defined by m.o.r.b. and islands such as Iceland, Bouvet and Tristan da Cunha) in the direction of values for continental crust, implying the presence of the latter as a component in the source (White and Hoffmann, 1982).

6.4 DISCUSSION

It is argued in Section 6.1 that the mantle source for alkali basalts from the Azores islands and ridge tholeiites from the Azores Plateau is strongly enriched in the light REE. Compared to the source of N-type m.o.r.b. it is also typically characterized by low Zr/Nb

(∿5) and K/Rb ratios (∿450). The incompatible geochemical characteristics of Azores basalts are summarised in Fig 6.3. Also shown is the estimated compositional field of melts generated by 5-10% batch partial melting of a garnet lherzolite (primordial) mantle (55% ol., 25% opx., 15% cpx., 5% gt.; with a melting mode of 10%:20%:40%:30% respectively and primordial incompatible element abundances of Tarney et al., 1980) using the mineral/liquid partition coefficents in Table 1.2. It is evident that while good agreement is obtained for the moderately incompatible trace elements, the highly incompatible elements are too enriched in Azores basalt magmas, even for low degrees of partial melting. This provides further evidence (relative to primordial mantle) for the light REE enriched nature of the Azores source.

Second order variations in geochemical parameters, such as highly incompatible element ratios (eg Ba/La, K/Rb), are also apparent when basalts from the different islands are compared. For example, those from Faial show variable K/Rb ratios (378-495) while those from Sao Miguel have the highest $^{87}Sr/^{86}Sr$ ratios (decreasing from east to west) recorded from the Azores, thus demonstrating both inter and intra island heterogenity.

As suggested by White et al. (1979) the similar concentrations of Dy, Y and Yb in Azores basalts and adjacent E-type m.o.r.b. indicates that garnet is probably a residual phase in the production of the alkali basalts. Neither apatite or phlogopite are thought to be important residual phases because both P and K show the same degree of enrichment in alkali basalt, relative to E-type m.o.r.b., as the other highly incompatible elements (approximately a factor of two for comparable Mg numbers, Ni and Cr contents). The similar incompatible element and $^{87}Sr/^{87}Sr$ ratios of Azores basalts and adjacent m.o.r.b. led White et al. (1979) to suggest that the most likely explanation for the higher abundances of the light REE in the former is that they are the product of smaller degrees of partial melting. On this basis, these authors constructed two batch melting models to account for the incompatible elemental abundances in the alkali basalts. They

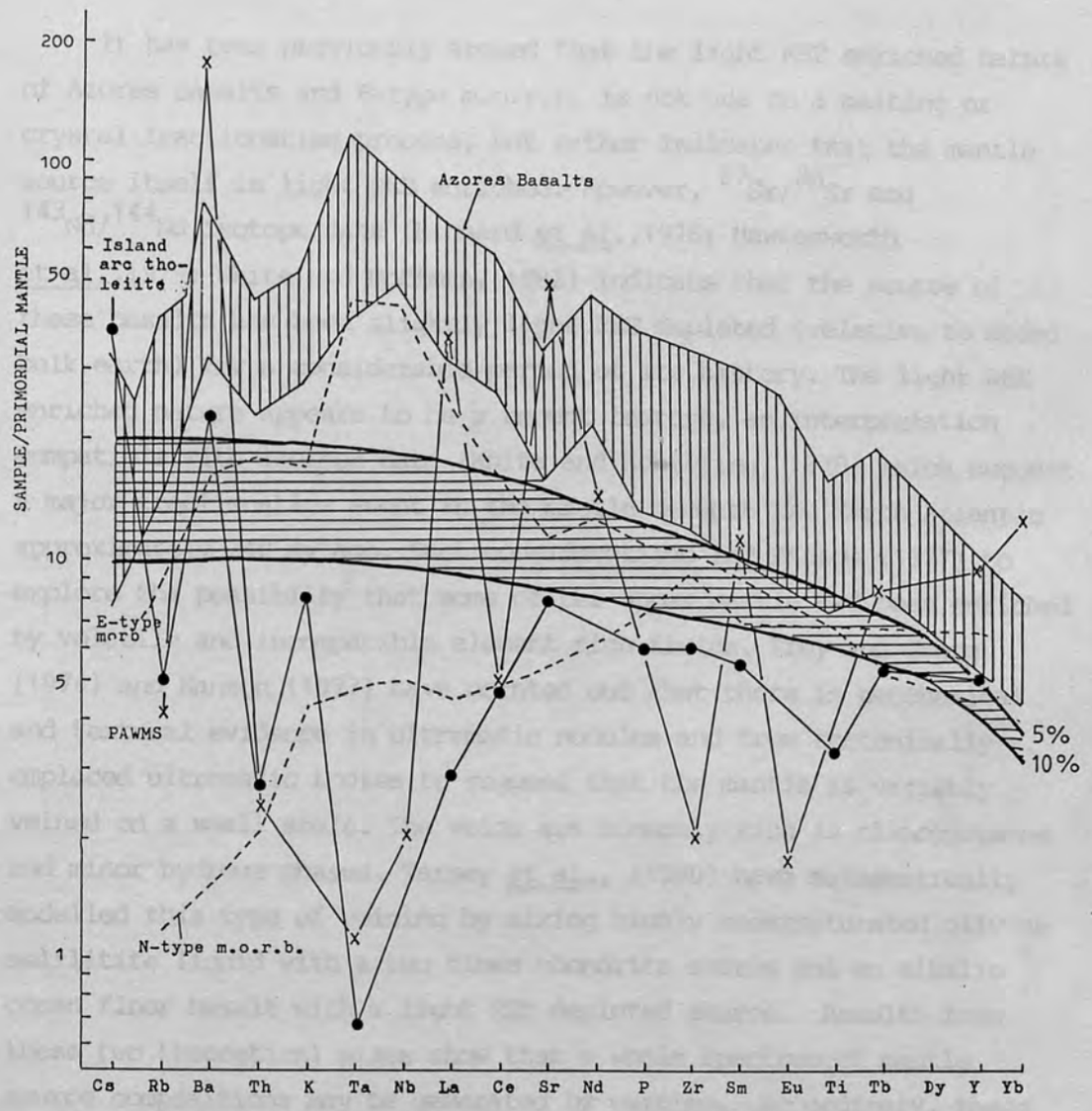

Fig. 6.3. Range of incompatible element abundances in Azores basalts normalised to a primordial mantle composition (vertical ruled lines). Horizontal ruled lines represent incompatible element abundances produced by 5-10% batch partial melting of primordial mantle having a phase assemblage of 55% ol., 25% opx., 15% cpx., 5% gt, with a melting mode of 10%:20%:40%: 30%; other modelling details are given in the text. Also shown are data for an island arc tholeiite (Joron and Treuil, 1977), PAWMS (Pacific authigenic weighted mean sediment; Hole et al., 1984) and E and N-type m.o.r.b.

considered the most plausible model to be 13% melting of a source consisting of 60% olivine, 25% orthopyroxene, 6% clinopyroxene and 9% garnet.

It has been previously argued that the light REE enriched nature of Azores basalts and E-type m.o.r.b. is not due to a melting or crystal fractionation process, but rather indicates that the mantle source itself is light REE enriched. However, $^{87}Sr/^{86}Sr$ and $^{143}Nd/^{144}Nd$ isotope data (Richard et al.,1976; Hawkesworth et al.,1979; White and Hoffman, 1982) indicate that the source of these basalts has been slightly light REE depleted (relative to model bulk earth) for a considerable period of its history. The light REE enriched nature appears to be a recent feature, an interpretation compatible with isotope data (White and Schilling, 1978) which suggest a major fractionation event in the mantle beneath the North Atlantic approximately 240 my ago. Such considerations led Hanson (1977) to explore the possibilty that some of the upper mantle had been enriched by volatile and incompatible element rich fluids. Frey and Green (1974) and Hanson (1977) have pointed out that there is geochemical and textural evidence in ultramafic nodules and from tectonically emplaced ultramafic bodies to suggest that the mantle is variably veined on a small scale. The veins are commonly rich in clinopyroxene and minor hydrous phases. Tarney et al., (1980) have mathematically modelled this type of veining by mixing highly undersaturated olivine melilitite liquid with a two times chondrite source and an alkalic ocean floor basalt with a light REE depleted source. Results from these two theoretical mixes show that a whole spectrum of mantle source compositions may be generated by veining. Accordingly, these authors suggest that incompatible element enrichment and the development of inhomogeneities in an evolving mantle are the result of veining by highly light REE enriched undersaturated melts (kimberlitic) produced by incipient melting of primitive mantle. This source may have variable geochemical characteristics depending on the geochemical nature of the mantle component from which the incipient melts have been produced. Subsequent melting of the variably veined mantle provides an explanation for the compositional variation in m.o.r.b.

The generally high and variable $^{208}Pb/^{204}Pb$ and $^{207}Pb/^{204}Pb$ ratios of oceanic islands coupled with $^{87}Sr/^{86}Sr$ ratios for Sao Miguel which are offset from the 'normal' mantle array towards values for continental material provides strong evidence for a crustal component in the source. Hole et al.(1984) have shown that to account for compositional features of basalts from the Marianas island arc much of the sediment approaching the trench is probably recycled into the upper mantle. This potential source component for alkali basalts is enriched in Ba, Sr, Th, and has high $^{87}Sr/^{86}Sr$, $^{208}Pb/^{204}Pb$ and $^{207}Pb/^{204}Pb$ ratios. In Fig 6.3, incompatible trace element abundances are shown for Nazca Plate pelagic sediments (Hole et al., 1984) and for an island arc tholeiite from Oshima, Japan (Joron and Treuil, 1977). It is evident that the geometry of the normalised incompatible element patterns between Cs and K generally shows a similar (zig-zag) enrichment/depletion patterns to alkali basalts from the Azores (particularly Santa Maria). Fig 6.4 is a plot the ratios La/Sm and Ba/La for Azores volcanic rocks. On such a diagram, two component mixes define straight lines. It is clear that the large variation in the Ba/La ratio (particularly for Santa Maria, Sao Miguel and Terceria) is not part of a mixing trend with E or N-type m.o.r.b. This implies a third, Ba-enriched component (ie pelagic sediment or arc/continental volcanics) in the Azores alkali-basalt source. Such contamination could also explain the large Cs contents of Santa Maria basalts. However, it is also clear from Fig 6.3 that this cannot account for the low Zr/Nb ratios of alkali basalts, subduction related volcanics (and derived sediments) being preferentialy depleted in Nb and Ta. Furthermore, there is a broad positive correlation between $^{87}Sr/^{86}Sr$ and the Nb/Zr ratio in the Atlantic (Wood et al., 1981) and Pacific (A. D. Saunders, unpub. data), implying that some of the ^{87}Sr-enriched component is also enriched in Nb (and Ta).

In summary, in order to satisfactorily account for the incompatible trace element and radiogenic isotopic characteristics of alkali basalts from the Azores it appears necessary to propose a mantle source composed of three components, namely:

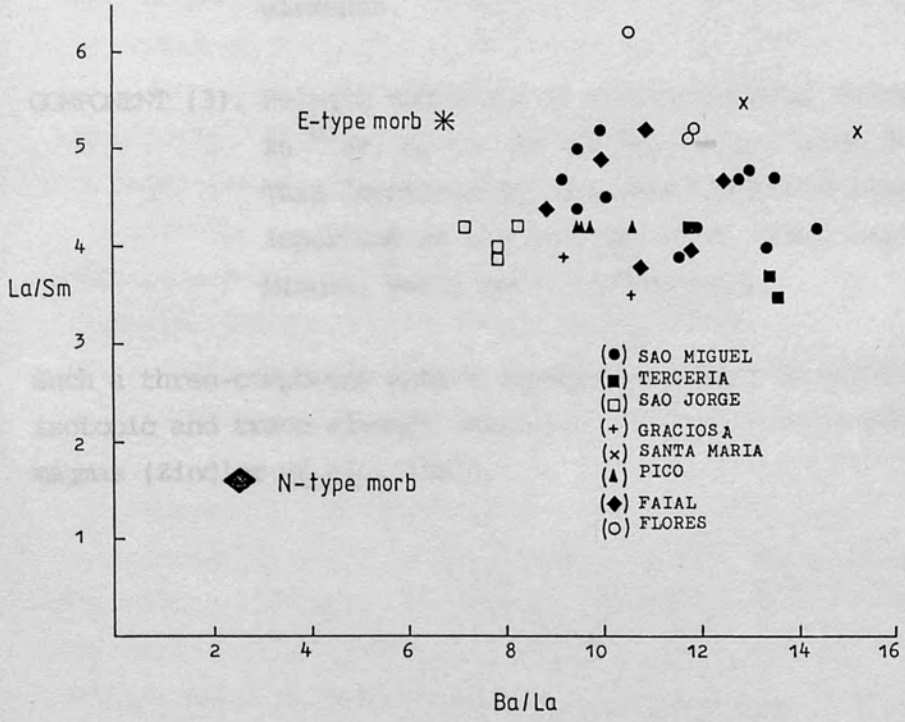

Fig 6.4. Plot of the La/Sm ratio against the Ba/La ratio for Azores basalts; data from White et al. (1979) and this thesis. E and N-type m.o.r.b. values from Tarney et al. (1980).

COMPONENT (1). Residual (ol. + opx. + cpx. +/- gt.), previously melted component slightly to highly depleted relative to primordial mantle in ^{87}Sr, the light REE and other highly incompatible elements, having high K/Rb and Zr/Nb ratios.

COMPONENT (2). Clinopyroxene rich veins produced by incipient melting of primitive mantle. This component is enriched in Nb, Ta, the light REE and other highly incompatible elements.

COMPONENT (3). Pelagic sediments or arc/continental volcanics enriched in ^{87}Sr, K, Rb, Cs and Ba, having large Ba/La ratios. This 'continental' component may have been particularly important in the production of alkali basalts from Sao Miguel, Santa Maria and Terceria.

Such a three-component mantle appears necessary to explain the isotopic and trace element characteristics of most mantle-derived magmas (Zindler et al., 1982).

CONCLUDING STATEMENT

This study has shown that volcanic rocks from Sao Miguel form two distinct alkaline magma series, being amongst the most potassic found on Atlantic Islands. Lower P/Zr, Ba/Zr and Sr/Zr ratios in the transitional, Povoacao Series suggests it is not related to the Main Series by either fractional crystallization or partial melting. Volcanic rocks from Faial form a single Ne-normative series. The process responsible for most compositional variations in each of the three magma series is fractional crystallization, incompatible element abundances suggesting that trachytes are produced by some 60-85% solidification of a parental basalt. The fractionating assemblages are olivine + clinopyroxene + plagioclase + Fe-Ti oxides in basalts and hawaiites; plagioclase + amphibole + Fe-Ti oxides + apatite + clinopyroxene in mugearites and benmoreites; alkali feldspar + anorthoclase + clinopyroxene + biotite + Fe-Ti oxides + apatite in trachytes. Separation of Fe-Ti oxides and kaersutite from intermediate magmas causes a rapid increase in SiO_2 for a relatively small amount of differentiation and partly accounts for the Daly Gap.

Beneath the stratovolcanoes of both islands fractional crystallization is envisaged to occur mainly in high-level, compositionally zoned (basalt-intermediate-trachyte) magma chambers. The roof-zone consists of trachytic (pumice-forming) magma having high incompatible element and water contents. This would act as a barrier to the eruption of underlying, more dense magma of less evolved composition and lower volatile content, this being a further factor in contributing to the Daly Gap. It is suggested that the high Ba and Eu contents and large K/Rb ratios of AM-type mixed lavas result from intermediate magma accumulating glomeroporphyritic clumps of alkali feldspar, with interstitial melt, by settling from overlying trachyte. Periodic replenishment at the base of the sub-volcanic magma chambers by intrusion and stratification of basalt would allow the development of accumulative, MgO-rich ankaramites. The thermal input resulting from basalt intrusion may cause magma-mixing and the triggering of the explosive pumice-forming, plinian-type eruptions.

Most (basaltic) eruptives from the fissure zones (eg in the 'waist') have not undergone much fractionation, presumably due to the absence of sub-volcanic magma bodies.

On Sao Miguel, trachyte also occurs as discrete, laterally extensive magma bodies, possibly forming in response to caldera-collapse (eg Fogo caldera). Field relations and the stratigraphically controlled nature and type of the observed geochemical and mineralogical variations of the Fogo air fall pumice succession, suggests that the five most recent deposits represent successive samples of a body of trachytic magma that is evolving principally by alkali feldspar fractionation. The lack of similar variation in the recent pumice succession from Furnas volcano, their compositional similarity to some syenite xenoliths and the absence of highly peralkaline differentiates on Sao Miguel is attributed to a high magma viscosity, inhibiting crystal-liquid fractionation processes. In the case of the five Fogo deposits, the sub-volcanic 'cumulate' crustal contribution due to crystal fractionation may be more than the volume of the trachyte erupted during the 4,000 year period under review.

Reliable temperature and fO_2 estimates can be obtained from titanomagnetite - ilmenite pairs containing appreciable quantities of minor elements. Pre-eruptive temperatures for trachytic pumice deposits from Faial and Sao Miguel ranged between 960 ^{o}C - 880 ^{o}C. Widely dispersed plinian pumice fall deposits are also common on other oceanic islands. The data discussed here indicates that natural salic liquids, including those generated in intraplate oceanic settings commonly have water contents in excess of 5 wt%. Estimates of the volatile species S_2, H_2S, SO_2, SO_3, CO_2, H_2, HCl and HF suggest they are several orders of magnitude less abundant than H_2O.

Theoretical models of trace element behaviour in magmatic processes indicate that Azores basalts are produced by about 13% partial melting of a garnet lherzolite mantle and that their high $^{87}Sr/^{86}Sr$, La/Yb, Ba/La ratios and low $^{143}Nd/^{144}Nd$, Zr/Nb, Zr/Ta and K/Rb ratios are close to source values. Inter and intra-island

variations in these parameters are suggestive of a complexly heterogeneous mantle consisisting of (1) a residual, previously melted, component depleted in ^{87}Sr and incompatible elements, (2) clinopyroxene-rich veins enriched in the highly incompatible elements, produced by incipient melting of primordial mantle and (3) a crustal component enriched in ^{87}Sr, Ba and Cs.

REFERENCES

Abbey, S 1973. Studies in "standard" samples of silicate rocks and minerals. Part 3: 1973 extension and revision of "usable" values. Geoloogical Survey of Canada paper. 73-36, 25pp.

Abdel-Monem, A.A., Fernandez, L.A. & Boone, G.M. 1975. K-Ar ages from the eastern Azores group (Santa Maria, Sao Miguel and the Formigas islands). Lithos. 8, 247-254.

Allegre, C.J. & Minster, J.F. 1978. Quantitative models of trace element behaviour in magmatic processes. Earth and Planetary Science Letters. 38, 1-25.

Anderson, A.T. 1968. The oxygen fugacity of alkaline basalt and related magmas, Tristan da Cunha. American Journal of Science. 266, 704-727.

Anderson, A.T. 1976. Magma mixing: petrological process and volcanological tool. Journal of Volcanology and Geothermal Research. 1, 3-33.

Arth, J.G. & Hanson, G.N. 1975. Geochemistry and origin of the early Precambrian crust of northeastern Minnesota. Geochimica et Cosmochimica Acta. 39, 325-362.

Assunaco, C.F.T. 1959. Contribucao para a petrografia dos produtos emitidos pelo vulcao dos Capelinhos (Faial). Mem. Servicos Geologicos de Portugal. 4, 57-64.

Assuncao, C.F.T. 1961. Estudo petrografico da ilha de S. Miguel (Azores). Comunicacoes dos Servicos Geologicos de Portugal. 45, 80-176

Assuncao, C.F.T & Canilho, M.H. 1970. Notas sobre petrografia comparada das ilhas Atlanticas. Boletin do Museu e Laboratorio Mineralogico da Faculdade de Ciencias, Lisboa University. 11, 305-342

Baker, P.E., Gass, I.G., Harris, P.G. & Le Maitre, R.W. 1964. The volcanological report of the Royal Society Expeditions to Tristan da Cunha. Philosophical Transactions of the Royal Society of London. A 256, 439-578.

Banks, R. 1979. The use of linear programming in the analysis of petrological mixing problems. Contributions to Mineralogy and Petrology. 70, 237-244.

Bartlett, P.W. 1969. Magma convection, temperature distribution and differentiation. American Journal of Science. 267, 1067-1082.

Berthois, L. 1953. Contribution a l'etude lithologique de l'Archipel des Azores. Comunicacoes dos Servicos Geologicos de Portugal. 34, 5-64.

Bishop, F.C. 1980. The distribution of Fe^{2+} and Mg between coexisting ilmenite and pyroxene with applications to geothermometry. American Journal of Science. 280, 46-77.

Blake, D.H., Elwell, R.W.D., Gibson, I.L., Skelhorn, R.R. & Walker, G.P.L. 1965. Some relationships resulting from the intimate association of acid and basic magmas. Quarterly Journal of the Geological Society of London. 121, 31-49.

Booth, B., Croasdale, R. & Walker, G.P.L. 1978. A quantitative study of five thousand years of volcanism on Sao Miguel, Azores. Philosophical Transactions of the Royal Society of London. A 288, 271-319.

Borley, G.D. & Rogers, N. 1979. Comparison of rare-earth element data obtained by neutron activation analysis using international rock and multi-element solution standards. Geostandards Newsletter. 3, 89-92.

Bottinga, Y. & Weill, D.F. 1970. Densities of liquid silicate systems calculated from partial molar volumes of oxide components. American Journal of Science. 269, 169-182.

Bowen, N.L. & Tuttle, O.F. 1950. The system $NaAlSi_3O_8$-$KAlSi_3O_8$-H_2O. Journal of Geology. 58, 489-511.

Branco, A.C., Zbyszewski, G., Medeiros, A.C. & Almeida, F.M. 1957. Etude geologique de la region de Furnas dans l'ile de S. Miguel (Acores). Comunicacoes dos Servicos Geologicos de Portugal. 38, 5-64.

Brooks, C.K. 1976. The Fe_2O_3/FeO ratio of basalt analyses: an a appeal for a standardised procedure. Bulletin of the Geological Society of Denmark. 25, 117-120.

Bryan, W.B., Finger, L.W. & Chayes, F. 1968. Estimating proportions in petrographic mixing equations by least-squares approximation. Science. 163, 926-927.

Buddington, A.F. & Lindsley, D.H. 1964. Iron-titanium oxide minerals and their synthetic equivalents. Journal of Petrology. 5, 310-357.

Burnham, C.W., and Davis, N.F. 1969. Partial molar volume of water in albite melts. Transactions of the American Geophysical Union 50, 338.

Burnham, C.W., Holloway, J.R. & Davis, N.F. 1969. Thermodynamic properties of water to 1,000° C and 10,000 bars. Geological Society of America Special Paper. 132, 1-96.

Cann, J.R. 1967. A second occurence of dalyite and the petrology of some ejected syenite blocks from Sao Miguel, Azores. Mineralogical Magazine. 36, 227-232.

Carmichael, I.S.E. 1967. The iron-titanium oxides of salic volcanic rocks and their associated ferromagnesian silicates. Contributions to Mineralogy and Petrology. 14, 36-64.

Carmichael, I.S.E. & Nicholls, J. 1967. Iron-titanium oxides and oxygen fugacities in volcanic rocks. Journal of Geophysical Research. 72, 4665-4687.

Carmichael, I.S.E., Nicholls, J. & Smith, A.L. 1970. Silica activity in igneous rocks. American Mineralogist. 55, 246-263.

Carmichael, I.S.E., Nicholls, J., Spera, F.J. Wood, B.J. & Nelson, S. 1977. High-temperature properties of silicate liquids: Applications to the equilibration and ascent of basic magma. Philosophical Transactions of the Royal Society of London. A 286, 373-431.

Carmichael, I.S.E., Turner, F.J. & Verhoogen, J. 1974. Igneous Petrology. McGraw-Hill, pp 739.

Cawthorn, R.G. & Collerson, K.E. 1974. The recalculation of pyroxene end-member parameters and the estimation of ferrous and ferric iron content from electron microprobe analyses. Ibid. 59, 1203-1208.

Coombs, D.S. & Wilkinson, J.F.G. 1969. Lineages and fractionation trends in undersaturated volcanic rocks from the East Otago Volcanic Province (New Zealand) and related rocks. Journal of Petrology. 10, 440-501.

Cox, K.J., Bell, J.D. & Pankhurst, R.J. 1979. The Interpretation of Igneous Rocks. George Allen & Unwin, 450pp.

Daly, R.A. 1925. The geology of Ascension Island. American Academy of Arts and Sciences. 5, 1-80.

Deer, W.A., Howie, R.A. & Zussman, J. 1966. An introduction to the rock forming minerals. Longman.

Drake, M.J. 1976. Evolution of major mineral compositions and trace element abundances during fractional crystallization of a model lunar composition. Geochimica et Cosmochimica Acta. 40, 401-411.

Eichelberger, J.C. 1975. Origin of andesite and dacite: evidence of mixing at Glass Mountain in California and the other circum-Pacific volcanoes. Ibid. 86, 1381-1391.

Eichelberger, J.C. 1978. Andesitic volcanism and crustal evolution. Nature. 275, 21-27.

Eichelberger, J.C. 1980. Vesiculation of mafic magma during replenishment of silicic magma reservoirs. Nature. 288, 446-450.

Essenwien, P. 1929. Sur petrographic der Azoren. Zeitschrift fur Volkanologie. 12, 108-227.

Evensen, N.M., Hamilton, P.J. & O'Nions R.K. 1978. Rare-earth abundances in chondritic meteorites. Geochimica et Cosmochimica Acta. 42, 1199-1212.

Ewart, A., Green, D.C., Carmichael, I.S.E. & Brown, F.H. 1971. Voluminous low temperature rhyolitic magmas in New Zealand. Contributions to Mineralogy and Petrology. 33, 128-144.

Ewart, A., Hildreth, W. & Carmichael, I.S.E. 1975. Quaternary acid magma in New Zealand. Contributions to Mineralogy and Petrology. 51, 1-27.

Ewart, A. & Stipp, J.J. 1968. Petrogenesis of the volcanic rocks of the Central North Island, New Zealand, as indicated by a study of $^{87}Sr/^{86}Sr$ ratios, and Sr, Rb, K, U and Th abundances. Geochimica et Cosmochimica Acta. 32, 699-735.

Fairbrothers, G.E., Carr, M.J. & Mayfield, D.G. 1978. Temporal magmatic variation at Boqueron volcano, El Salvador. Contributions to Mineralogy and Petrology. 67, 1-9.

Fernandez, L.A. 1980. Geology and petrolgy of the Nordeste volcanic complex, Sao Miguel, Azores. Bulletin of the Geological Society of America. 91, 2457-2557.

Fernandez, L.A. 1982. The petrology and geochemistry of the Nordeste volcanic complex, Sao Miguel, Azores. Proceedings of International Symposium on the Activity of Oceanic Volcanoes (IAVCEI), 1980. 145-158.

Flanagan, F.J. 1973. 1972 values for International Geochemical Reference Samples. Geochimica et Cosmochimica Acta. 37, 1189-1200.

Flower, M.F.J., Schmincke, H-U. & Bowman, H. 1976. Rare-earth and other trace elements in historic Azorean lavas. Journal of Volcanology and Geothermal Research. 1, 127-147.

Frey, F.A. & Green, D.H. 1974. The mineralogy, geochemistry and origin of lherzolite inclusions in Victorian basanites. Geochimica et Cosmochimica Acta. 38, 1023-1059.

Gibson, I.L. & Walker, G.P.L. 1963. Some composite rhyolite/basalt lavas and related composite dykes in eastern Iceland. Proceedings of the Geologists Association, London. 74, 301-318.

Green, D.H. 1973. Experimental melting studies on model upper mantle compositions at high pressure under both water-saturated and water-undersaturated conditions. Earth and Planetary Science Letters. 19, 37-53.

Green, D.H. & Ringwood, A.E. 1967. The genesis of basaltic magmas. Contributions to Mineralogy and Petrology. 31, 103-190.

Hanson, G.N. 1977. Evolution of the sub-oceanic mantle. Journal of the Geological Society of London. 134, 235-253.

Hanson, G.N. 1978. The application of trace elements to the petrogenesis of igneous rocks of granitic composition. Earth and Planetary Sciience Letters. 38, 26-43.

Hart, S.R. 1971. K, Rb, Cs, Sr, and Ba contents and Sr isotope ratios of ocean floor basalts. Philosophical Transactions of the Royal Society of London. A 268, 573-588.

Hart, S.R. & Brooks, C. 1974. Clinopyroxene-matrix partitioning of K, Rb, Cs, Sr and Ba. Geochimica et Cosmochimica Acta. 38, 1799-1803.

Hart, S.R. & Davis, K.E. 1978. Nickel partitioning between olivine and silicate melt. Earth and Planetary Science Letters. 40, 203-219.

Hart, S.R., Erlank, A.J. & Kable, E.J.D. 1974. Sea floor basalt alteration: some chemical and strontium isotope effects. Contributions to Mineralogy and Petrology. 44, 219-230.

Hawkesworth, C.J., Norry, M.J., Roddick, J.C. & Vollmer, R. 1979. $^{143}Nd/^{144}Nd$ and $^{87}Sr/^{86}Sr$ ratios from the Azores and their significance in LIL-element enriched mantle. Nature. 280, 28-31.

Helz, R.T. 1973. Phase relations of basalts in their melting range at PH_2O = 5 kbars as a function of oxygen fugacity. Journal of Petrology. 14, 249-302.

Heming, R.F. & Carmichael, I.S.E. 1973. High-temperature pumice flows from the Rabaul caldera, Papua New Guinea. Contributions to Mineralogy and Petrology. 38, 1-20.

Hildreth, W. 1979. The Bishop Tuff: evidence for the origin of compositional zonation in silicic magma chambers. Geological Society of America Special Paper. 180, 43-75.

Holdaway, M.J. 1980. Chemical formulae and activity models for biotite, muscovite and chlorite applicable to pelitic metamorphic rocks. American Mineralogist. 65, 711-719.

Hole, M.J., Saunders, A.D., Marriner, G.F. & Tarney J. 1984. Subduction of pelagic sediments: implications for the origin of Ce anomalous basalts from the Mariana Islands. Journal of the Geological Society of London. 141, 453-472.

Hughes, D.J. & Brown, G.C. 1972. Basalts from Madeira: a petrochemical contribution to the genesis of oceanic alkali rock series. Contributions to Mineralogy and Petrology. 37, 91-109.

Hulme, G. 1974. The interpretation of lava flow morphology Geophysical Journal of the Royal Astronomical Society. 39, 361-383.

Huppert, H.E. & Sparks, R.S.J. 1980. The fluid dynamics of a basaltic magma chamber replenished by influx of hot, dense ultrabasic magma. Contributions to Mineralogy and Petrology. 75, 279-289.

Huppert, H.E., Turner, J.S. & Sparks R.S.J. 1982a. Replenished magma chambers: effects of compositional zonation and input rates. Earth and Planetary Science Letters. 57, 345-357.

Huppert, H.E., Sparks, R.S.J. & Turner, J.S. 1982b. Effects of volatiles on mixing in calc-alkaline magma systems. Nature. 279, 554-557.

Irvine, T.N. 1967. Chromian spinel as petrogenetic indicator. Part 2. Petrologic applications. Canadian Journal of Earth Sciences. 4, 71-103.

Irving, A.J. 1978. A review of experimental studies of crystal/liquid trace element partitioning. Geochimica et Cosmochimica Acta. 42, 743-770.

Jeremine, E. 1957. Etude microscopique das roches de la region de Furnas (S. Miguel, Azores). Comunicacoes dos Servicos Geologicos de Portugal. 38, 65-90.

Joron, J.L. & Treuil, M. 1977. Utilisation des proprietes des elements fortement hygromagmatophiles pour l'etude de la composition chimique et de l'heterogeneite du manteau superieur. Bull. Soc. Geol. France. 19, 1197.

Krause, D.C. & Watkins, N.D. 1970. North Atlantic crustal genesis in the vicinity of the Azores. Geophysical Journal of the Royal Astronomical Society. 19, 261-283.

Laughton, A.S. & Whitmarsh, R.B. 1975. The Azores-Gibraltar plate boundary. In: L. Kristjansson (ed.) Geodynamics of Iceland and the North Atlantic. Reidel, Dordrecht. pp 63-81.

Le Maitre, R.W. 1962. Petrology of volcanic rocks, Gough Island, South Atlantic. Bulletin of the Geological Society of America. 73, 1309-1340.

Le Maitre, R.W. 1969 Kaersutite-bearing plutonic xenoliths from Tristan da Cunha, S. Atlantic. Mineralogical Magazine. 37, 185-197.

Lesher, L.E., Walker, D., Candela, P. & Jays, J.F. 1982. Soret fractionation of natural silicate melts of intermediate to silic composition. Geological Society of America. Abstracts 14, 545.

Lipman, P.W. 1971. Iron-titanium oxide phenocrysts in compositionally zoned ash-flow sheets from Southern Nevada. Journal of Geology. 79, 438-456.

Luhr, J.F. & Carmichael, I.S.E. 1980. The Colima volcanic complex, Mexico. Contributions to Mineralogy and Petrology. 71, 343-372.

Macdonald, G.A. & Katsura, T. 1964. Chemical composition of Hawaiian lavas. Journal of Petrology. 5, 82-133.

Macdonald, K. & Bailey, D.K. 1973. The chemistry of peralkaline oversaturated obsidians. US Geological Survey Professional Papers. 440-N, Pt. I.

Machado, F. 1967. Active volcanoes of the Azores. Catalogue of the Active Volcanoes of the World. IAVCEI. 21, 9-52.

Machado, F. 1966. Anomalias das intensidades do terramoto de S. Miguel (Acores) em 1522. Bull. Mus. Lab. Mineral. Geol., Fac. Cienc. Lisboa. 10, 109-117.

Machado, F. 1973. Acid volcanoes of Sao Miguel, Azores. Bulletin Volcanolgique. 36, 319-327

Marriner, G.F., Norry, M.J. & Gibson I.L. 1982. The petrology and geochemistry of Agua de Pau volcano, Sao Miguel, Azores. Proceedings of International Symposium on the Activity of Oceanic Volcanoes (IAVCEI), 1980. 159-173

Mazzulo, L.J., Dixon, S.A. & Lindsley, D.H. 1975. T-fO_2 relationships in Mn-bearing Fe-Ti oxides. Geological Society of America Abstract with programs. 7, 1192.

McBirney, A.R. 1980. Mixing and unmixing of magmas. Journal of Volcanology and Geothermal Research. 7, 357-371.

McBirney, A.R. & Noyes, R.M. 1979. Crystallization and layering of the Skaergaard Intrusion. Journal of Petrology. 20, 487-554.

Merril, R.B. & Wyllie, P.J. 1975. Kaersutite and kaersutite eclogite from Kakanni, New Zealand, water excess and water deficient melting to 30 kilobars. Bulletin of the Geological Society of America. 86, 555-570.

Metrich, N., Bizouard, H. & Varet, J. 1981. Petrologie de la Serie Volcanique de l'ile de Fayal (Acores). Bulletin Volcanologique. 44, 71-93.

Michael, P.J. 1983a. Chemical differentiation of the Bishop Tuff and other high-silica magmas through crystallization processes. Geology. 11, 31-34.

Michael, P.J. 1983b. Chemical differentiation of the Bishop Tuff and other high-silica magmas through crystallization processes: reply. Geology. 11, 623-624.

Mitchell, W.S. & Aumento, F. 1977. Uranium in oceanic rocks: Deep Sea Drilling Project Leg 37. Canadian Journal of Earth Sciences. 14, 794-808.

Mitchell-Thome, R.C. 1976. Geology of the Middle-Atlantic Islands. Gebruder Borntraeger. 382pp.

Muecke, G.K., Ade-Hall, J.M., Aumento, F., Macdonald, A. & Reynolds, P.H. 1974. Deep drilling in an active geothermal area in the Azores. Nature. 252, 281-285.

Mueller, R.F. 1972. Stability of biotite: a discussion. American Mineralogist. 57, 300-316.

Murase, T. & McBirney, A.R. 1973. Properties of some common igneous rocks and their melts at high temperatures. Bulletin of the Geological Society of America. 84, 3563-3592.

Murata, K.J. & Richter, D.H. 1966. Chemistry of the lavas, 1959-60 eruption of Kilauea volcano, Hawaii. U.S. Geological Survey Professional Papers. 537A, A1-A26.

Naldrett, A.J. 1969. A portion of the system Fe-S-O between 900°C to 1080° and its application to sulphide ore magmas. Journal of Petrology. 10, 171-201.

Nelson, S.A. & Carmichael, I.S.A. 1979. Partial molar volumes of oxide components in silicate liquids. Contributions to Mineralogy and Petrology. 71, 117-124.

Neumann, H., Mead, J & Vitaliano, C.J. 1954. Trace element variation during fractional crystallization as calculated from the distribution law. Geochimica et Cosmochimica Acta. 6, 90-99.

Nordlie, B.E. 1971. The composition of the magmatic gas of Kilauea and its behaviour in the near surface environment. American Journal of Science. 271, 417-463.

Norrish, K. & Hutton, J.T. 1969. An accurate x-ray spectrographic method for the analysis of a wide range of geological samples. Geochimica et Cosmochimica Acta. 33, 431-453.

O'Hara, M.J. 1975. Is there an Icelandic mantle plume. Nature. 253, 708-710

O'Hara, M.J. 1977. Geochemical evolution during fractional crystallization of a periodically refilled magma chamber. Nature. 226, 503-507.

O'Nions, R.K. & Pankhurst, R.J. 1974. Petrogenetic significance of isotope and trace element variations in volcanic rocks from the Mid-Atlantic. Journal of Petrology. 15, 603-634.

O'Nions, R.K. & Gronvold, K. 1973. Petrogenetic relationships of acid and basic rocks in Iceland: Sr-isotope and rare earth elements in late and post-glacial volcanics. Earth and Planetary Science Letters. 19, 397-409.

Padfield, T. & Gray, A. 1971. Major element rock analysis by X-ray fluorescence - a simple fusion method. Bulletin, Phillips Analytical Equipment.

Parker, R.J. & Willis, J.P. 1977. Programs SORT, REORD and MW for major element XRF data processing. Computers and Geosciences. 3, 115-172.

Pearce, J.A. 1975. Basalt geochemistry used to investigate past tectonic environments on Cyprus. Tectonophysics. 25, 41-67.

Pearce, J.A. & Norry, M.J. 1979. Petrogenetic implications of Ti, Zr, Y and Nb variations in volcanic rocks. Contributions to Mineralogy and Petrology. 69, 33-47.

Pickney, C.R. & Lindsley, D.H. 1976. Effects of magnesium on iron-titanium oxides. Geological Society of America Abstract with Programs. 8, 1051.

Pinkerton, H. & Sparks, R.S.J. 1978a. Field measurements of the rheology of lava. Nature. 276, 383-385.

Pinkerton, H. & Sparks, R.S.J. 1978b. Effect of degassing on rheology of basaltic lava. Nature. 276, 385-386.

Powell, R. 1978. Equilibrium thermodynamics in petrology. Harper and Row. pp 284.

Richard, P., Shimizu, N. & Allegre, C.J. 1976. $^{143}Nd/^{144}Nd$, a natural tracer: an application to oceanic basalts. Earth and Planetary Science Letters. 31, 269-278.

Ridley, W.I. 1970. The petrology of Las Canades volcanoes, Tenerife, Canary Islands. Contributions to Mineralogy and Petrology. 26, 124-160.

Ridley, W.I., Watkins, N.D. & McFarlane, D.J. 1974. The Azores: in The Ocean Basins and Margins. Volume 2 (AEM Nairn, F.G. Stehli, eds.), pp445-483. New York-London, Plenum Press.

Ringwood, A.E.M.1974. Petrological evolution of island arc systems. Journal of the Geological Society of London. 130, 183-204.

Robson, G.R. 1967. Thickness of Etnean lavas. Nature. 216, 251-252.

Roeder, P.L. & Emslie, R.F. 1970. Olivine-liquid equilibrium. Contributions to Mineralogy and Petrology. 29, 275-289.

Rose, W.I., Grant, N.K., Hahn, G.A., Lange, J.M., Powell, J.L., Easter, J. & Degraff, J.M. 1977. The evolution of Santa Maria volcano, Guatemala. Journal of Geology. 85, 63-87.

Rutherford, N.F. & Heming, R.F. 1978. The volatile component of Quaternary ignimbrite magmas from the North island, New Zealand. Contributions to Mineralogy and Petrology. 65, 401-411.

Ryzhenko, B.N. & Volkov, V.P. 1971. Fugacity coefficents of some gases in a broad range of temperatures and pressures. Geochemistry International. 468-481.

Sakuyama, M. 1979. Evidence of magma-mixing: petrological study of Shirouma-Oike calc-alkaline andesite volcano, Japan. Journal of Volcanology and Geothermal Research. 5, 197-208.

Sakuyama, M. 1981. Petrological study of the Myoko and Kurohime volcanoes, Japan: Crystallization sequence and evidence for magma mixing. Journal of Petrology. 22, 553-583.

Saunders, A.D., Tarney, J. & Marsh, N.G. 1979. Ophiolites as ocean crust or marginal basin crust: A geochemical study. Ophiolites (ed. A. Panayiotou). Proceedings of the International Ophiolite Symposium, Cyprus, 1979. pp193-204.

Saunders, A.D., Tarney, J. & Weaver, S.D. 1980. Transverse geochemical variations across the Antarctic Peninsula: Implications for the genesis of calc-alkaline magmas. Earth and Planetary Science Letters. 46, 344-360.

Scarfe, C.M. 1977. Viscosity of some basaltic glasses at one atmosphere. Canadian Mineralogist. 15, 190-194.

Schilling, J.-G. 1975. Azores mantle blob: rare-earth evidence. Earth and Planetary Science Letters. 25, 103-115.

Schilling, J.-G. & Winchester, J.W. 1967. Rare earth fractionation and magmatic processes, in: Mantles of the Earth and Terrestrial Planets. (S.K. Runcorn, ed.) Interscience, New York, N.Y. pp267.

Schmincke, H-U. 1969. Ignimbrite sequence on Gran Canaria. Bulletin Volcanologique. 33, 1199-1219.

Schmincke, H-U. 1973. Magmatic evolution and tectonic regime in the Canary, Madeira and Azores island groups. Bulletin of the Geological Society of America. 84, 633-648.

Schmincke, H-U. & Weibel,M. 1972. Chemical study of rocks from Maderia, Porto Santo and Sao Miguel, Terceria (Azores). Neues Jahrbuch Mineralogie Abhandlungen. 117, 253-281.

Searle, R.C. 1976. Lithospheric structure of the Azores Plateau from Rayleigh-Wave Dispersion. Geophysical Journal of the Royal Astronomical Society. 44, 537-546.

Self, S. 1976. The recent volcanology of Terceria, Azores. Journal of the Geological Society. 132, 645-666.

Self, S. & Gunn, B.M. 1976. Petrology, volume, and age relations of alkaline and saturated peralkaline volcanics from Terceria, Azores. Contributions to Mineralogy and Petrology. 54, 293-314.

Shaw, H.R. 1963. Obsidian-H_2O viscosities at 1000 and 2000 bars in temperature range 700° to 900° C. Journal of Geophysical Research. 68, 6337-6343.

Shaw, H.R. 1965. Comments on viscosity, crystal settling and convection in granite magmas. American Journal of Science. 263, 120-152.

Shaw, H.R. 1969. Rheology of basalt in the melting range. Journal of Petrology. 10, 510-535.

Shaw, H.R. 1972. Viscosities of magmatic silicate liquids: an empirical method of prediction. American Journal of Science. 272, 870-893.

Shaw, H.R., Wright, T.L., Peck, D.L. & Okamura, R. 1968. The viscosity of basaltic magma: an analysis of field measurements in the Makaopuhi lava lake, Hawaii. American Journal of Science. 266, 225-264.

Shimizu, N. & Arculus, R.J. 1975. Rare earth element concentration in a suite of basanitoids and alkali olivine basalts from Grenada, Lesser Antilles. Ibid. 50, 231-240.

Shotton, F.W., Blundell, D.J. & Williams, R.E.G. 1968. Birmingham University radiocarbon dates. II. Radiocarbon. 10, 200-206.

Shotton, F.W., Blundell, D.J. & Williams, R.E.G. 1969. Birmingham University radiocarbon dates. III. Radiocarbon. 11, 263-270.

Shotton, F.W., Blundell, D.J. & Williams, R.E.G, 1970. Birmingham University radiocarbon dates. IV. Radiocarbon. 12, 385-399.

Shotton, F.W. & Williams, R.E.G. 1971. Birmingham University radiocarbon dates. V. Radiocarbon. 13, 141-156.

Sigurdsson, H. 1977. Generation of Icelandic rhyolites by melting of plagiogranites in the oceanic layer. Nature. 269, 25-28.

Sigurdsson, H. & Sparks, R.S.J. 1981. Petrology of rhyolitic and mixed-magma ejecta from the 1875 eruption of Askja, Iceland. Journal of Petrology. 22, 41-84.

Sommer, M.A. 1977. Volatiles H_2O, CO_2 and CO in silicate melt inclusions in quartz phenocrysts from the rhyolitic Bandelier air-fall and ash-flow tuff, New Mexico. Journal of Geology. 85, 423-432.

Sparks, R.S.J., Pinkerton, H. & Hulme, G. 1976. Classification and formation of lava levees on Mount Etna, Sicily. Geology. 4, 269-271.

Sparks, R.S.J., Huppert, H.E. & Turner, J.S. 1984. The fluid dynamics of evolving magma chambers. Philosophical Transactions of the Royal Society of London. A 310, 511-34.

Sparks, R.S.J., Sigurdsson, H. & Wilson, L. 1977. Magma mixing: a mechanism for triggering acid explosive eruptions. Nature. 267, 315-318.

Sparks, R.S.J & Wilson, L. 1976. Model for ignimbrite formation by gravitational column collapse. Journal of the Geological Society of London. 132, 441-451.

Sparrow, E.M., Goldstein, R.J. & Jonsson, U.K. 1964. Thermal instabilty in a horizontal fluid layer. Fluid Mechanics. 18, 513-528.

Speidel, D.H. 1970. Effects of magnesium on the iron-titanium oxides. American Journal of Science. 268, 341-353.

Statham, P.J. 1976. A comparative study of techniques for quantitative analysis of the X-ray spectra obtained with a Si (Li) detector. X-Ray Spectrom. 5, 16-28.

Storey, M. 1981. Trachytic pyroclastics from Agua de Pau volcano, Sao Miguel, Azores: evolution of a magma body over 4,000 years. Contributions to Mineralogy and Petrology. 78, 423-432.

Stull, D.R. & Prophet, H. 1971. Joint Army Navy Air Force thermochemical tables. 2nd edition. Washington, D.C. : U.S. Government Printing Office.

Sweatman, T.R. & Long, J.V.P. 1969. Quantitative electron-probe microanalysis of rock forming minerals. Journal of Petrology. 10,332-379.

Tarney, J., Saunders, A.O. & Weaver, S.O. 1977. Geochemistry of volcanic rocks of the island arcs and marginal basis of the Scotia Sea region. In: Island arcs, deep sea trenches and back arc basins. (M. Talwani & U.C. Pitman, eds.) III Maurice Ewing Series, American Geophysical Union. pp 367-378.

Tarney, J., Wood, D.A., Saunders, A.D., Cann, J.R. & Varet, J. 1980. Nature of mantle heterogenity in the North Atlantic: evidence from deep sea drilling. Philosophical Transactions of the Royal Society of London. A 297, 179-202.

Taylor, S.R. & Gorton, M.P. 1977. Geochemical application of spark source mass spectrography - III: Element sensitivity, precision and accuracy. Geochimica et Cosmochimica Acta. 41, 1375-1380.

Tazieff, H 1958. L'eruption 1957-58 et la tectonique de Faial, (Acores). Bull. Soc. Belge. Geol. 67, 13-49.

Thompson, J.B. & Waldbaum, D.R. 1969. Mixing properties of sanidine crystalline solutions. III. Calculations based on two phase data. American Mineralogist. 54, 811-838.

Thompson, R.N., Esson, J. & Dunham, A.C. 1972. Major element chemical variation in the Eocene lavas of the Isle of Skye, Scotland. Journal of Petrology. 13, 219-253.

Thornton, C.P. & Tuttle, O.F. 1960. Chemistry of igneous rocks. I. Differentiation index. American Journal of Science. 258. 664-684.

Toulmin, P. & Barton, P.B. 1964. A thermodynamic study of pyrite and pyrrhotite. Geochimica et Cosmochimica Acta. 28, 641-671.

Turner, J.S. & Gustafson, L.B. 1981. Fluid motions and compositional gradients produced by crystallization or melting at vertical boundaries. Journal of Volcanology and Geothermal Research. 11, 93-125.

Ulmer, G.C., Rosenhauer, M., Woermann, E., Ginder, J., Drory-Wolff, A. & Wasilewski, P. 1976. Applicability of electrochemical oxygen fugacity measurements to geothermometry. American Mineralogist. 61, 653-660.

Van Pandang, Neumann, M., Richards, A.F., Machado, F., Bravo, T., Baker, P.E. & Le Maitre, R.W. 1967. Atlantic Ocean (Inter. Volcan. Assoc., Catalogue of active volcanoes-Pt. 21.).

Verhoogen, J. 1962. Distribution of titanium between silicates and oxides in igneous rocks. American Journal of Science. 260, 211-220.

Walker, D. & De Long, S.E. 1982. Soret separation of mid-ocean ridge basalt magma. Contributions to Mineralogy and Petrology. 79, 231-240.

Walker, G.P.L. 1972. Crystal concentration in ignimbrites. Contributions to Mineralogy and Petrology. 36, 135-146.

Walker, G.P.L. 1980. The Taupo Pumice: Product of the most powerful known (ultraplinian) eruption? Journal of Volcanology and Geothermal Research. 8, 69-94.

Walker, G.P.L. 1981a. Plinian eruptions and their products. Bulletin Volcanologique. 44, 223-240.

Walker, G.P.L. 1981b. The Waimiha and Hatepe plinian deposits from the rhyolitic Taupo Volcanic Centre. New Zealand Journal of Geology and Geophysics. 24, 305-324.

Walker, G.P.L. & Croasdale, R. 1971. Two plinian-type eruptions in the Azores. Journal of the Geological Society of London. 127, 17-55.

Weston, F.S. 1964. List of recorded volcanic eruptions in the Azores with brief reports. Bol. Mus. Lab. Miner. Geol. Fac. Ciencas. Lisboa. 10, 3-18.

White, W.M. & Schilling, J.-G. 1978. The nature and origin of geochemical variation in Mid-Atlantic basalts from the Central North Atlantic. Geochimica et Cosmochimica Acta. 42, 1501-1516.

White, W.M. & Hoffman, A.W. 1982. Sr and Nd isotope geochemistry of ocean basalts and mantle evolution. Nature. 296, 821-855.

White, W.M., Tapio, M.D.M. & Schilling, J-G. 1979. The petrology and geochemistry of the Azores islands. Contributions to Mineralogy and Petrology. 69, 201-213.

Wilkinson, J.F.G. 1961. Some aspects of the calciferous amphiboles oxyhornblende, kaersutite and barkevikite. American Mineralogist. 46, 340-354.

Wilson, A.D. 1955. A new method for the determination of ferrous iron in rocks and minerals. Bulletin of the Geological Survey of Great Britain. 9, 56-58.

Wilson, L. 1976. Explosive volcanic eruptions, III. Plinian eruption columns. Geophysical Journal of the Royal Astronomical Society. 45, 543-556.

Wilson, L. 1980. Relationships between pressure, volatile content and ejecta velocity in three types of volcanic explosion. Journal of Volcanology and Geothermal Research. 8, 297-313.

Wilson, L., Sparks, R.S.J., Huang, T.C. & Watkins, M.D. 1978. The control of volcanic column heights by eruption energetics and dynamics. Journal of Geophysical Research. 83, 1829-1836.

Wilson, L., Sparks, R.S.J. & Walker, G.P.L. 1980. Explosive volcanic eruptions, IV. The control of magma properties and conduit geometry on eruption column behaviour. Geophysical Journal of the Royal Astronomical Society. 63, 117-148.

Wolff, J.A. & Storey, M. 1983. The volatile component of some pumice-forming alkaline magmas from the Azores and Canary Islands. Contributions to Mineralogy and Petrology. 82, 66-74.

Wolff, J.A. & Storey, M. 1984. Zoning in highly alkaline magma bodies. Geological Magazine. 121, 563-575.

Wolff, J.A., Wright, J.V., Smith, A.L., Clough, B., Roobol, M.J. & Self, S. 1980. Mixed pumice deposits: field characteristics. Proceedings of IX Caribbean Conference. 1, 355-365.

Wones, D.R. 1972. Stability of biotite: a reply. American Mineralogist. 57, 316-317.

Wones, D.R. & Eugster, H.P. 1965. Stability of biotite: experiment, theory and application. American Mineralogist. 50, 1228-1272.

Wones, D.R. & Gilbert, M.E. 1969. The fayalite-magnetite-quartz assemblage between 600°C and 800°C. American Journal of Science. 267, 480-488.

Wood, D.A., Gibson, I.L. & Thompson, R.N. 1976. Element mobilty during zeolite facies metamorphism of the Tertiary basalts of eastern Iceland. Contibutions to Mineralogy and Petrology. 55, 241-254.

Wood, D.A., Tarney, J., Varet, J., Saunders, A.D., Bougault, H., Joron, J.L., Treuill, M. & Cann, J.R. 1979. Geochemistry of basalts drilled in the North Atlantic by IPOD Leg 49: implications for mantle heterogenity. Earth and Planetary Science Letters. 42, 77-97.

Wood, D.A., Tarney, J. & Weaver, B.L. 1981. Trace element variations in Atlantic Ocean basalts and Proterozoic dykes from northwest Scotland: their bearing upon the nature and geochemical evolution of the upper mantle. Tectonophysics. 75, 91-112.

Woodhall, D. 1974. Geology and volcanic history of Pico Island volcano, Azores. Nature. 248, 663-665.

Wright, T.L. & Doherty, P.C. 1970. A linear programming and least squares computer method for solving petrographic mixing problems. Bulletin of the Geological Society of America. 81, 1995-2008.

Wright, T.L. & Weilblen, P 1968. Mineral composition and paragenesis in tholeiitic basalt from Makuophi lava lake, Hawaii (abstract). Geological Society of America Special Paper. 115, 242-243.

Yoder, H.S. 1973. Contemporaneous basaltic and rhyolitic magmas. American Mineralogist. 58, 153-171.

Yoder, H.S. & Tilley, C.E. 1962. Origin of basalt magmas: an experimental study of natural and synthetic rock systems. Journal of Petrolgy. 3, 342-532.

Zbyszewski, G. 1961. Etude geologique de l'ile de S. Miguel (Acores). Comunicacoes dos Servicos Geologicos de Portugal. 46, 209-255.

Zbyszewski, G., Almeida, F.M., Ferrerira, O.V. & Assuncao, C.F.T. 1958. Carta Geologica de Portugal na escala de 1/50,000. Noticia explicativa da folha B, S. Miguel (Acores). Lisboa, Servicos Geologicos de Portugal. 37 pp.

Zbyszewski, G., Almeida, F.M., Ferrerira, O.V. & Assuncao, C.F.T. 1959. Carta Geologica de Portugal na escala de 1/25,000. Noticia explicativa da folha Faial (Acores). Lisboa, Servicos Geologicos de Portugal. 25pp.

Zbyszewski, G. & Ferreira, O.V. 1962. Etude geologique de l'ile de Santa Maria (Acores). Comunicacoes dos Servicos Geologicos de Portugal. 47, 209-246.

Zbyszewski, G., Ferreira, O.V. & Assuncao, C.F.T. 1959. Carta geologica de Portugal na escala de 1/50,000. Noticia explicativa da Folha A, S. Miguel (Acores). Lisboa, Servicos Geologicos de Portugal. 22 pp

Zelinski, R.A. 1975. Trace element evaluation of a suite of rocks from Reunion Island, Indian Ocean. Geochimica et Cosmochimica Acta. 39, 713-734.

Zindler, A., Jagoutz. E. & Goldstein S. 1982. Nd, Sr and Pb isotopic systematics in a three-component mantle: A new perspective. Nature. 298, 519-523.

APPENDIX 1

Sample Number	Occurrence	Grid Reference (N/E)
AZ 3099	Dyke in pre-Capelinhos vent, 0.6 km N of lighthouse	38.602/28.824
AZ 3085	Lava of 1958 eruption, NE Capelinhos	38.604/28.830
AZ 3339	Lava from old sea cliffs, Capelinhos	38.596/28.827
AZ 3533	Lava 0.9 km NNW of Cabeco do Canto	38.606/28.815
AZ 3527	Lava 1.7 km SW of Cabeco do Fogo	38.578/28.780
AZ 3504	Ejected block, scoria cone, Cabeco Verde	38.584/28.757
AZ 3120	Lava (matrix of ultramafic nodule), Faja	38.612/28.762
AZ 3443	Lava from cone 1.2 km WSW of Caldeira	38.580/28.738
AZ 3326	Sample from M. Quemada scoria cone, Horta	38.530/28.630
AZ 3408	Lava, Ponta Furada, 3.2 km SW of Horta	38.523/28.657
AZ 3328	Lava, Obras Rubheus, 0.6 km W of Horta harbour	38.527/28.732
AZ 3374	Lava, Altar rock, Caldeira	38.583/28.723
AZ 3115	Basalt (1958) lava, S. Capelinhos	38.594/28.830
AZ 3411	Basic component of mixed lava, Castelo Branco	38.524/28.750
AZ 3410	Trachytic component of mixed lava, Castelo Branco	38.524/28.750
AZ 3360	Block in ash, 2.2 km WSW Cedros	38.628/28.718
AZ 3446	Pumice (dark), top of ash A, 0.8 km SE of Caldeira	38.577/28.698
F 500	Pumice (buff), lower part of ash A	
AZ 3424	Pumice, ash S, 0.6 km W of Fontainhas	38.600/28.680
AZ 3426	Pumice, ash T, 2.6 km S of Cedros	38.615/28.702
AZ 3432	Pumice, base ash T, 0.9 km NNE of Caldeira	38.602/28.710
AZ 3435	Pumice (dark), top ash T, 0.9 km NNE of Caldeira	38.602/28.710
AZ 3436	Pumice, ash U, 0.9 km NNE of Caldeira	38.602/28.710
AZ 3417	Pumice, ash B, 1.4 km SE of Ribeira do Cabo	38.563/28.749
AZ 3401	Pumice, ash D, airfield Castelo Branco	38.520/28.723
AZ 3437	Syenite block in ash T, 0.8 km N of Ribeira Funda	38.623/28.728
AZ 3428	Syenite clast in ash S, 2.4 km NNE of Caldeira	38.615/28.702

Table A1.1 Faial Sample Descriptions and Grid References

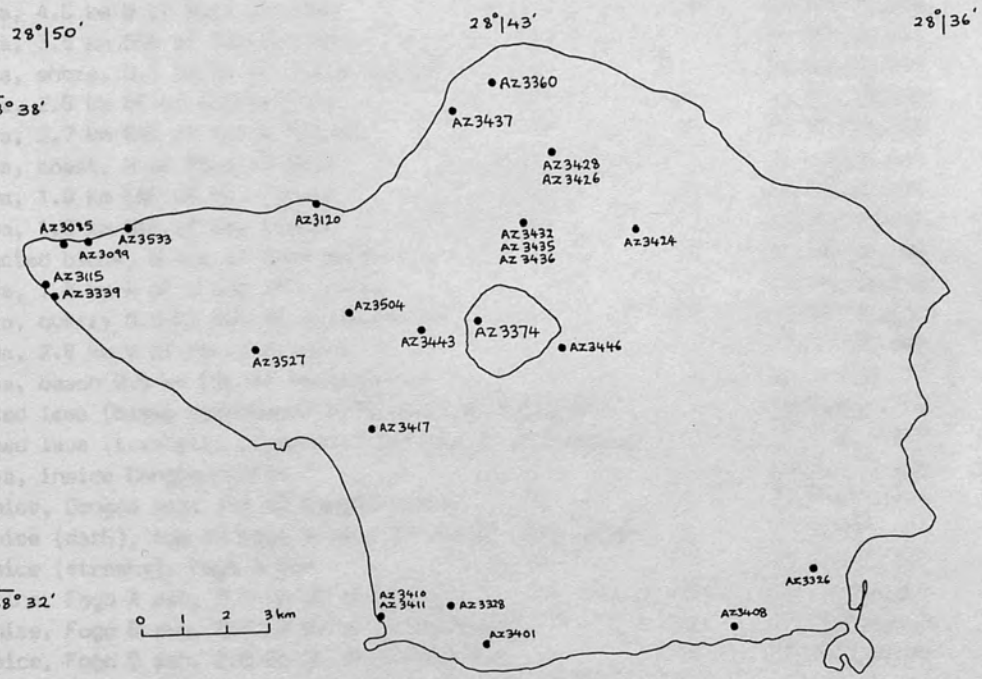

Fig A1.1 Faial sample locations.

Sample Number	Occurrence	Age (where known)	Grid Reference (N/E)
AZ 1139	Block from agglomerate, 0.4 km S of Lombo Gordo	P2	37.774/25.146
AZ 1138	Lava, 0.6 km S of Lombo Gordo	P2	37.771/25.146
AZ 1131	Lava, base of cliff E of Faial da Terra	P2	37.739/25.187
AZ 1134	Dyke, base of cliff E of Faial da Terra	P2	37.739/25.187
AZ 1135	Dyke, base of cliff E of Faial da Terra	P2	37.739/25.187
AZ 1129	Lava, base of cliff E of Faial da Terra	P2	37.739/25.187
AZ 1126	Lava, base of cliff E of Faial da Terra	P2	37.739/25.187
AZ 1127	Lava, base of cliff E of Faial da Terra	P2	37.739/25.187
AZ 1344	Lava, 0.4 km SE of Calhau Grande, Nordeste	P2	37.807/25.143
AZ 1014	Lava, caldera rim 1.0 km NW of Furnas	P1	37.777/25.321
29 SM	Lave, caldera rim 1.0 km NW of Furnas		37.777/25.321
AZ 1614	Lava, W end of beach, Ribeira Quente		37.724/25.314
AZ 1686	Pumice, Furnas A ash, 0.3 km NE of Lake Furnas	A	37.766/25.328
AZ 1678	Pumice, Furnas C ash, 0.2 km S of Furnas thermal springs	A	37.767/25.303
AZ 1629	Pumice, Furnas F ash, 0.5 km E of Gaspar	A	37.756/25.301
AZ 1538	Pumice, Furnas 1640 ash, 0.9 km SE of Azeitona	A	37.731/25.341
10 SM	Lava (Pico Enforcada)		37.720/25.410
AZ 1017	Lava, 0.7 km N of Agua d'Alto	P1	37.722/25.457
MA 23/3	Lava, 1.2 km W of Ribeira de Agua de Alto		37.725/25.445
36 AP	Lava, Agua de Pau		37.710/25.530
AZ 1027	Lava, 4.0 km W of Pico Barrosa	P1	37.761/25.539
AZ 1720	Lava, 3.5 km SSW of Ribeira Seoa		37.783/25.541
AZ 1592	Lava, shore, 0.7 km SW of Villa Franca		37.706/25.441
AZ 1396	Lava, 2.6 km NE of Ribeira Cha	P1	37.734/25.468
AZ 1018	Lava, 2.7 km ENE of Villa Franca	P1	37.721/25.408
AZ 1705	Lava, coast, N of Ribeira Seoa		37.820/25.541
AZ 1197	Lava, 1.9 km ENE of Mt. Escuro	P1	37.794/25.431
MA 239	Lava, 1.8 km NNE of Mt. Escuro		37.780/25.435
AZ 1202	Ejected block, W rim of Fogo caldera	P1	37.765/25.494
AZ 1213	Lava, 1.8 km N of W end of L. Fogo	P1	37.774/25.488
AZ 1604	Lava, quarry 0.5 km NNE of Villa Franca	P1	37.720/25.432
AZ 1634	Lava, 2.8 km W of Porto Formosa		37.817/25.445
AZ 1146	Lava, beach 0.9 km ESE of Ribeira Cha		37.713/25.477
AZ 1721B	Mixed lava (basic component) 0.75 km SE of Queimado		37.780/25.540
AZ 1721T	Mixed lava (trachytic component) 0.75 km SE of Queimado		37.780/25.540
AZ 1672	Lava, inside Congro crater	A	37.751/25.406
AZ 1019	Pumice, Congro ash, rim of Congro crater	A	37.750/25.411
AZ 1377	Pumice (dark), top of Fogo A ash, NW rim of Fogo caldera	A	37.768/25.493
AZ 1323	Pumice (streaky), Fogo A ash	A	37.768/25.493
AZ 1544	Pumice, Fogo A ash, 2.9 km SE of Furnas	A	37.754/25.287
AZ 1378	Pumice, Fogo B ash, 0.4 km NW of V. do Mulato	A	37.780/25.456
AZ 1394	Pumice, Fogo C ash, 2.6 km NE of Ribeira Cha	A	37.734/25.468
AZ 1024	Pumice, dark clast from Fogo D ash, 0.2 km SE of Ribeira Cha	A	37.714/25.485
AZ 1188	Pumice, Fogo D ash, 2.5 km NW of Villa Franca	A	37.727/25.456
AZ 1149	Pumice, Fogo 1563 ash, 1.0 km NE of Mt. Escuro	A	37.782/25.426
AZ 1015	Obsidian fiamme from ignimbrite Povoaco		
AZ 1714	Obsidian fiamme from ignimbrite, 1.6 km ESE of Ribeira Cha		37.711/25.466
AZ 1039	Lava, 1.2 km SE of Livramento	A	37.744/25.604
AZ 1308	Lava, Pico de Cava cone, ENE of Alagoa	A	37.783/25.563
AZ 1315	Lava, shore 1.5 km E of Rabo de Peixe	A	37.812/25.564
AZ 1880	Lava, Pico do Boi cone, 1.5 km SE of cone		37.818/25.705
AZ 1691	Lava, shore at Pocos, 2.2 km W of Fenaes da Luz		37.830/25.663
AZ 1324	Lava, 3.0 km SE of Fenaes da Luz	P1	37.803/25.621

Table A1.2 Sao Miguel Sample Descriptions and Grid References

Sample Number	Occurrence	Age (where known)	Grid Reference (N/E)
AZ 1322	Lava, 2.7 km N of Alagoa	P1	37.766/25.579
AZ 1874	Ejected block, Fogo cone		37.770/25.583
AZ 1872	Lava, 1.3 km NE of Fogo cone		37.777/25.570
AZ 1689	Lava, Morro de Rabo de Peixe		37.806/25.575
2 SM	Pahoehoe lava, Ponta Delgada		37.730/25.675
AZ 1326	Lava, 1.8 km SSE of Fenaes da Luz	P1	37.809/25.634
AZ 1164	Lava, 2.1 km NNE of Alagoa	A	37.583/25.567
AZ 1879	Lava of 1652 eruption, cone W of Fogo cone	A	37.768/25.587
AZ 1168	Ejected block, E side of Sete Cidades caldera	P2	37.864/25.770
6 SM	Carvao lava, 2 km ESE of Sete Cidades caldera		37.825/25.740
AZ 1883	Lava, N side of Cruz cone		37.856/25.750
AZ 1704	Lava, Ferrarias cone, 2.5 km NE of Feteiras		37.815/25.740
AZ 1172	Dome, Sete Cidades caldera		37.850/25.780
AZ 1034	Lava, Ponta da Ferraria lava delta		37.858/25.853
AZ 1035	Kaersutite-bearing nodule in AZ 1034 lava		37.858/25.853
AZ 1056	Ejected syenite block, 2.5 km NW of Villa Franca		37.727/25.456
AZ 1207	Ejected syenite block, W rim of Fogo caldera		37.765/25.494
AZ 1205	Ejected syenite block, W rim of Fogo caldera		37.765/25.494
AZ 1187	Syenite block in Fogo D		
AZ 1664	Syenite block in Fogo A		
AZ 1712	Syenite block in ancient pumice fall deposit, Ribeira Cha		
AZ 1204	Syenite block in Fogo A		
AZ 1219	Syenite block in Fogo A		
MA 18 E	Syenite block in Fogo A		

KEY TO AGES

A = contemporaneous with Fogo A or younger

P1 = immediately pre-Fogo A

P2 = pre-Fogo A (large time gap)

Table A1.2 Sao Miguel Sample Descriptions and Grid References (continued)

Fig A1.2 Sao Miguel sample locations.

APPENDIX 2

WHOLE-ROCK CHEMICAL ANALYSES

A2.1 ROCK POWDER PREPARATION

Each sample was cleaned and dried before passing through a jaw crusher to give a maximum grain size of 5mm. Samples were then ground to 400# in a tungsten carbide tema mill, taking on average 60 seconds. The powders were stored in glass bottles. Due to the fine grained nature of the majority of samples most were considered to be representative of that part of the lava flow or pumice deposit from which they were collected. For the latter, only whole pumice clasts were selected for analysis so as to avoid recording geochemical features resulting from crystal fractionation processes which occur during the actual pyroclastic producing eruption (Walker, 1972).

A2.2 METHODS OF ANALYSIS AND QUALITY OF RESULTS

A2.2.1 Major element analysis

For major element analysis, rock powder samples were first dried overnight at 105°C to remove H_2O^- and then cast into glass disks by the fusion method of Norrish and Hutton (1969). This technique has the advantage of eliminating the mineralogical, chemical and particle size effects inherent in the use of pressed powder pellets and secondly, of reducing inter-element absorption effects due to dilution of the rock in the flux. The procedure consisted of cooling the dried powder in a desiccator, weighing out into a 25cc platinum crucible (95% Pt, 5% Au) 0.4000 g of rock powder and 2.6000 g of lithium tetraborate flux (Johnson-Matthey spectroflux 104). The crucible was then placed into a furnace at 900-1000°C for 20 minutes after which it was removed and the mixture carefully swirled over three Meaker burners in order to eliminate gas bubbles and to ensure homogenity of the melt. At this point, the melt was quickly poured onto a 30mm diameter aluminium disc, resting on a hot plate at 240°C, and a

plunger was lowered on top. To ensure complete annealing, the resulting glass disc was wrapped in a clean paper towel and left to cool on an insulating plate to room temperature. The disc was then trimmed off around the rim, labelled on the reverse (curved) side and stored in a sealed polythene bag in a desiccator. Analysis was usually carried out within one to two weeks of manufacture due to the strongly hygroscopic nature of the discs. Duplicate samples were prepared in order to check for weighing errors. Analysis of Sao Miguel and Faial rocks for major and some trace elements (Tables A2.2 and A2.1) were carried out using Philips PW 1212 and PW 1400 X-ray spectrometers in the Department of Geology, Bedford College. The major elements Si, Ti, Al, Fe, Mn, Mg, Ca, K, Na and P were determined using a silver target X-ray tube (Padfield and Gray, 1971). Following the procedure of Parker and Willis (1977) calibration lines were erected by running four USGS and three Bedford College standard rocks having silica contents ranging between 40-70%. Raw data was processed by University of London computer programmes which, after correcting for machine drift, averaging the two sets of counts and applying mass absorption corrections, calculated oxide percentages. The quality of the major-element data was assessed by running USGS standard basalt (BCR-1) as an 'unknown' (Table A2.4).

For normative mineral calculations, Fe^{3+}/Fe^{2+} ratios were assigned using the criteria detailed in Section 2.5. A limited number of ferrous iron determinations, using the ammonium metavandate method of Wilson (1955) were carried out, data being given in Table A2.3.

A2.2.2 Trace element analysis (XRF)

The trace elements Nb, Zr, Y, Rb, Sr, Ba, La, Th, Ni, Cr and V were determined by XRF using pressed powder pellets. The pellets were prepared by weighing out 6.00 g of rock powder and 1.00 g of bakelite resin into a plastic phial. Four glass beads were added to facilitate homogenisation, the mixture being put on an automatic shaker for approximately 20 minutes. After removing the glass beads, the mixture

was pressed into a 30mm diameter pellet at a pressure of 15 tonnes by a standard piston-press assemblage. The pellet was then baked in an oven at 110°C for about 25 minutes to harden the resin. Calibrations were provided by running rocks standards with an artificial machine drift standard. Mass absorption corrections for Ba, La, Cr, Ni and V were calculated from the major element analyses. USGS standards were run as checks on the accuracy and precision of the data (Table A2.5).

A2.2.3 Trace element analysis (INAA)

The REE and, in a few cases, Ta, Hf, Th and Sc, were determined by Instrumental Neutron Activation Analysis (INAA) for selected samples (Tables A2.1 and A2.2). Approximately 0.1g of dried rock powder was accurately weighed into a polythene capsule and heat sealed. A high-purity multi-element nitrate solution was used as a standard (Borley and Rogers, 1979), 100 µl aliquots being pippeted on to 5mm diameter filter papers which were dried and sealed into polythene capsules. A total of eight unknown samples, one secondary rock standard (BCR-1) and three identical multi-element standard capsules were fitted into a polythene tube, which was then heat sealed. The multi-element standards were placed in the middle and at each end of the tube in order that neutron flux variations could be measured. The polythene tube was then placed in a lead pot and irradiated for approximately 30h in a thermal neutron flux of 1×10^{12} ncm^{-2} in the University of London Reactor at Silwood Park, Ascot. The samples were allowed to 'cool' for seven days after irradiation to allow short lived nucleides (principally ^{24}Na) to decay. This reduces the dead time and increases the peak to background ratio of the rare-earth activities. Samples were then analysed (at the University of London Reactor Centre) for La, Lu and Sc on a Li-drifted Ge solid-state detector. After further decay (usually one week) samples were counted on a Ge solid-state detector for determination of the remaining REE and Th, Ta and Hf. Both detectors were connected to a Link Systems Ltd. multi-channel analyser which output the data in

the form of counts, live counting times being around 10,000 s per sample. The counts were integrated to give peak areas which were then corrected for flux variations, background, radioactive decay and interfering nuclide peaks (using correction factors provided by N.W. Rogers). The USGS rock standard BCR-1 was run as an unknown, as a check on data quality, mean values being compared with published data in Table A2.6.

FAIAL

SAMPLE	AZ3099	AZ3085	AZ3339	AZ3533	AZ3527	AZ3120	AZ3443	AZ3326	AZ3408	AZ3328	AZ3374	AZ3504
SiO_2	48.40	48.72	48.30	48.66	48.46	46.77	47.91	47.91	46.43	48.80	48.43	48.02
TiO_2	2.62	2.69	3.18	3.34	2.81	2.06	2.41	2.85	3.04	2.88	2.75	2.80
Al_2O_3	15.75	16.53	17.67	17.44	16.88	12.10	14.62	16.46	14.95	16.71	20.26	17.10
Fe_2O_3	1.29	1.25	1.33	1.31	1.23	1.31	1.25	1.29	1.46	1.28	1.47	1.27
FeO	8.57	8.30	8.84	8.72	8.17	8.74	8.34	8.57	9.72	8.53	7.58	8.46
MnO	0.15	0.15	0.16	0.17	0.16	0.16	0.15	0.16	0.17	0.16	0.14	0.15
MgO	9.39	7.82	5.60	5.02	6.88	14.90	11.06	8.33	9.27	7.61	4.28	7.27
CaO	9.68	9.38	10.23	8.72	9.05	10.63	10.68	10.15	10.99	9.21	10.71	9.48
Na_2O	4.03	4.54	4.30	4.65	4.07	2.69	3.31	3.48	3.46	4.08	3.97	4.18
K_2O	1.14	1.64	1.49	1.83	1.79	0.83	1.05	1.41	1.14	1.50	1.35	1.49
P_2O_5	0.36	0.44	0.49	0.56	0.45	0.25	0.31	0.42	0.39	0.46	0.56	0.40
TOTAL	101.38	101.46	101.59	100.42	99.95	100.44	101.09	101.03	101.02	101.22	101.50	100.62
TRACE ELEMENTS												
Ni	127	86	38	30	63	391	167	138	143	105	26	81
Cr	258	172	43	31	131	834	382	290	333	155	41	125
Sc	8.1		21		19	30				22	16	
V	234	209	248	257	211	216	210	260	274	226	206	240
Rb	25	32	25	38	41	15	19	30	23	33	24	26
Sr	596	663	653	665	729	384	538	613	511	567	842	700
Y	29	29	27	32	26	20	24	26	27	28	27	25
Zr	206	226	216	259	250	131	164	213	167	240	198	210
Nb	44	45	54	55	52	29	35	45	41	55	51	54
Ta	7.0		4.2		4.0	2.3				4.2	4.3	
Ba	394	483	457	513	561	259	325	419	334	443	448	435
La	30	43	36	41	41	22	28	35	31	37	36	31
Ce	71		88	102	96	54	58			85	87	
Nd			41	38	45	29	30			40	41	
Sm				8.7			6.9					
Eu	2.3		2.7	2.6	2.5	1.9	2.1			2.5	2.7	
Tb	1.4		1.2	1.1	1.0	0.8	1.0			1.1	1.2	
Yb			2.8	2.5	2.3	1.8	2.2			2.7	2.5	
Lu	0.48		0.33	0.39	0.28	0.31	0.27			0.36	0.36	
CIPW NORMS												
Qz												
Or	6.7	9.7	8.8	10.8	10.6	4.9	6.2	8.3	6.7	8.9	8.0	8.8
Ab	21.1	20.2	21.2	25.2	22.6	13.1	17.3	19.8	14.3	23.7	23.6	20.9
An	21.5	19.9	24.5	21.3	22.5	18.5	21.9	25.1	21.9	22.9	33.5	23.5
Ne	7.0	9.9	8.2	7.7	6.4	5.2	5.8	5.2	8.1	5.9	5.4	7.9
Ac												
Di	19.5	19.3	18.9	15.0	15.8	26.1	23.3	18.2	24.4	16.1	13.1	17.0
Hy												
Mt	1.9	1.8	1.9	1.9	1.8	1.9	1.8	1.9	2.1	1.9	2.1	1.8
Ilm	5.0	5.1	6.0	6.3	5.3	3.9	4.6	5.4	5.8	5.5	5.2	5.3
Ap	0.8	1.0	1.1	1.3	1.0	0.6	0.7	1.0	0.9	1.1	1.3	0.9
Ol	17.8	14.6	10.9	10.9	13.9	26.2	19.4	16.1	16.8	15.5	9.3	14.5
D.I.	34.9	39.7	38.2	43.7	39.6	23.3	29.3	33.4	29.1	38.4	37.0	37.5

Major and trace element analyses of Faial samples AZ3446, F500, AZ3435, AZ3432, AZ3411 and AZ3410 are given in Table 2.3

D.I. = Thornton-Tuttle Differentiation Index.

Table A2.1 Whole rock analyses and CIPW norms of Faial volcanic rocks.

FAIAL

SAMPLE	AZ3360	AZ3424	AZ3426	AZ3436	AZ3417	AZ3401	AZ3437	AZ3428
SiO_2	59.94	60.89	58.84	60.44	58.94	62.82	58.47	60.24
TiO_2	0.80	0.61	1.20	0.75	0.69	0.30	1.22	0.97
Al_2O_3	19.91	17.73	17.90	18.43	19.56	16.09	18.68	18.33
Fe_2O_3	1.40	1.64	2.24	1.60	1.72	1.84	2.11	1.85
FeO	2.33	2.74	3.74	2.66	2.88	3.08	3.52	3.08
MnO	0.11	0.20	0.17	0.15	0.23	0.27	0.17	0.16
MgO	0.98	0.71	1.91	0.80	0.52	0.18	1.68	1.17
CaO	3.58	1.83	3.71	1.93	1.07	0.60	3.72	2.93
Na_2O	6.60	7.12	6.42	7.00	6.20	7.47	6.68	7.38
K_2O	3.80	4.29	3.25	4.32	4.24	4.74	3.46	3.96
P_2O_5	0.19	0.15	0.29	0.18	0.15	0.06	0.27	0.22
H_2O^+	n.d.	2.5	n.d.	2.1	3.2	1.9	n.d.	n.d.
TOTAL	99.64	100.41	99.67	100.36	99.40	99.35	99.98	100.29
TRACE ELEMENTS								
Ni	4	5	7	2	3	5	8	4
Cr			7				7	2
V	29	13	69	8			48	33
Rb	69	88	80	104	82	180	54	77
Sr	552	231	415	298	78	12	441	367
Y	27	40	29	27	52	88	27	29
Zr	361	564	475	567	617	1316	250	367
Nb	67	109	83	90	124	244	61	84
Ta					8.8	21.7		
Ba	1062	927	909	957	284	25	1175	1081
La	46	79	58	69	69	122	47	58
Ce	102	152		119	137	276		120
Nd	37	61		39	55	89		45
Sm	9.0	13		6.4	12	20		12
Eu	2.5	2.0		1.6	1.4	0.92		2.8
Tb	0.9	1.4		1.0	1.3	2.4		1.1
Yb	2.4	4.1		2.8	4.0	8.7		2.9
Lu	0.36	0.75		0.48	1.07	1.33		0.53
Th					8.8	22		
CIPW NORMS								
Qz					2.6			
Or	22.5	25.4	19.2	25.5	25.1	28.0	20.5	23.4
Ab	53.7	57.7	54.3	56.2	52.5	56.4	51.9	53.4
An	13.5	3.8	10.4	6.1	4.3		10.8	5.2
Ne	1.2	1.4		1.6			2.5	4.9
C					3.2			
Ac						5.3		
$Na_2O.SiO_2$						0.2		
Di	2.5	3.7	5.0	1.9		2.3	4.9	6.5
Hy		1.5			4.5	3.5		
Mt	2.1	2.4	3.3	2.3	2.5		3.1	2.7
Ilm	1.5	1.2	2.3	1.4	1.3	0.6	2.3	1.8
Ap	0.4	0.4	0.7	0.4	0.4	0.1	0.6	0.5
Ol	2.4	2.2	3.1	2.7		1.1	3.5	1.8
D.I.	77.3	84.4	73.5	83.4	80.1	84.4	74.8	81.7

n.d. not determined

Table A2.1 continued.

	Povoacao volcano								Furnas volcano		
SAMPLE	AZ1139	AZ1138	AZ1131	AZ1134	AZ1135	AZ1129	AZ1126	AZ1127	AZ1344	29SM	AZ1014	AZ1614
SiO_2	49.15	47.50	48.58	51.73	51.44	45.96	47.79		58.45	55.99	56.19	57.16
TiO_2	3.57	3.90	3.40	2.75	3.38	3.66	2.35		1.27	1.96	1.96	1.60
Al_2O_3	14.16	14.10	14.76	17.56	16.65	9.75	7.80		19.57	17.12	17.10	16.41
Fe_2O_3	1.52	1.55	1.39	1.24	1.31	1.54	1.36		1.20	1.42	1.43	1.28
FeO	10.14	10.33	9.26	8.26	8.74	10.29	9.02		3.99	4.72	4.78	4.26
MnO	0.16	0.16	0.16	0.17	0.14	0.17	0.17		0.14	0.14	0.14	0.18
MgO	6.27	6.74	6.52	3.51	4.05	11.78	16.95		1.45	2.69	2.93	2.74
CaO	9.52	9.00	8.59	7.54	8.42	12.09	11.12		3.31	4.47	4.52	4.58
Na_2O	3.21	3.00	3.27	4.14	3.74	2.03	1.67		6.58	4.77	5.18	5.05
K_2O	1.79	1.98	2.15	2.67	2.27	1.51	1.04		5.49	5.16	5.18	5.05
P_2O_5	0.47	0.46	0.52	0.68	0.54	0.41	0.29		0.31	0.48	0.49	0.26
TOTAL	99.96	98.72	98.70	100.24	100.68	99.10	99.56		100.43	98.92	99.18	98.44
TRACE ELEMENTS												
Ni	104	116	100	5	33	271	954		3	15	22	61
Cr	175	190	158		17	930	2029			48	57	166
V	292	301	260	177	260	307	212		37	92	57	166
Rb	39	44	45	66	41	38	16	37	176	71	69	131
Sr	548	549	632	826	643	468	330	573	778	860	855	498
Y		31	35	39	35	24	20	31	34	27	26	38
Zr	290	304	318	391	349	250	166	274	752	305	301	633
Nb	62	72	79	100	76	62	36	69	137	81	79	122
Ba	501	534	589	704	612	466	300		103	2959	3006	731
La	61	59	59	70	59	46	36		105	61	64	93
Ce						94					123	
Nd						42					54	
Sm						10.1					11.5	
Eu						2.3					5.2	
Tb						1.0					1.0	
Yb						2.3					2.4	
Lu						0.35					0.28	
CIPW NORMS												
Qz												
Or	10.6	11.9	12.9	15.7	13.3	9.0	6.2		31.4	30.8	30.9	30.1
Ab	26.8	23.9	26.3	33.7	31.4	10.4	14.2		40.8	36.2	36.8	38.6
An	18.9	19.4	19.6	21.4	21.8	13.1	10.8		13.5	10.2	11.4	7.9
Ne	0.2	1.0	0.9	0.7		3.8			1.8	2.5	0.7	2.0
Ac												
Di	20.9	18.8	16.7	9.9	13.6	36.1	34.2		1.1	8.1	7.2	11.2
Hy					3.4		0.9					
Mt	2.3	2.3	2.1	1.8	1.9	2.3	2.0		1.7	2.1	2.1	1.9
Ilm	6.8	7.5	6.5	5.2	6.4	7.0	4.5		2.4	3.8	3.8	3.1
Ap	1.1	1.1	1.2	1.6	1.3	1.0	0.7		0.7	1.1	1.2	0.6
Ol	12.5	14.2	13.8	10.1	6.9	17.4	26.5		5.6	5.4	6.2	4.3
D.I.	37.6	36.7	40.1	50.1	44.8	23.1	20.4		75.0	69.5	68.3	71.0

N.B. Analyses of AZ1686, AZ1678, AZ1629 and AZ1538 are given in Table 4.6.

Table A2.2 Whole rock analyses and CIPW norms of Sao Miguel volcanic rocks.

Agua de Pau volcano

SAMPLE	10SM	AZ1017	MA23/3	36AP	AZ1027	AZ1720	AZ1705	AZ1592	AZ1197	AZ1396	AZ1018	MA239
SiO_2	44.10	46.32	45.60	45.93	45.87		53.65	52.50	58.30	57.45	53.83	58.37
TiO_2	4.39	3.04	2.91	4.06	3.85		2.86	2.34	1.59	1.61	2.19	1.60
Al_2O_3	14.40	9.11	8.88	14.61	14.62		16.93	17.30	16.46	18.41	17.65	16.48
Fe_2O_3	1.62	1.44	1.44	1.48	1.52		1.04	1.02	1.32	1.33	0.96	1.30
FeO	10.79	9.61	9.58	9.87	10.11		6.92	6.75	4.40	4.43	6.39	4.34
MnO	0.18	0.18	0.17	0.16	0.17		0.13	0.18	0.15	0.17	0.18	0.15
MgO	7.62	16.22	16.91	6.61	7.83		3.58	3.30	3.40	2.00	3.02	3.41
CaO	10.17	11.11	10.72	10.02	9.68		6.62	5.95	3.83	4.20	5.51	3.86
Na_2O	3.00	1.93	1.51	3.15	3.25		4.25	5.28	5.31	5.63	4.89	5.13
K_2O	1.57	1.33	1.28	2.49	1.55		4.56	3.66	5.00	4.60	3.85	5.10
P_2O_5	0.56	0.45	0.39	0.66	0.53		0.38	0.89	0.31	0.42	0.79	0.30
TOTAL	98.40	100.74	99.39	99.04	98.98		100.92	99.17	100.07	100.25	99.26	100.04
TRACE ELEMENTS												
Ni	81	827	563	199	98		40	8	47	2	5	60
Cr	212	1506	1812	224	212		32	7	104			165
V	242	239	247	295	266		179	122	67	49	83	75
Rb	38	30	29	49	52	55	58	84	97	130	102	94
Sr	744	470	455	781	690	526	679	982	347	926	960	357
Y	25	21	20	27	28	29	26	48	33	47	46	33
Zr	254	210	204	297	289	297	265	520	462	661	554	464
Nb	70	51	50	70	75	61	55	113	109	131	140	111
Ba	566	418	392	717	640		1616	899	604	1286	1135	622
La	44	38	34	53	52		51	85	70	89	84	80
Ce			71	110		97	108					142
Nd			34	55		45	42					58
Sm			8.7	11.3		9.0	9.9					10.2
Eu			2.0	3.1		2.6	3.6					2.3
Gd						7.4						
Tb			0.9	1.1			1.0					1.1
Yb			1.8	2.5		2.3	2.0					2.6
Lu			0.23	0.34			0.29					
CIPW NORMS												
Qz												
Or	9.4	7.8	7.6	14.9	9.3		26.7	21.8	29.6	27.2	23.0	30.2
Ab	14.2	9.6	9.9	13.5	18.6		26.2	32.4	41.4	41.4	36.5	41.2
An	21.5	12.2	13.8	18.5	20.9		13.5	12.9	6.3	11.3	14.9	6.9
Ne	6.3	3.6	1.6	7.2	5.0		5.1	9.5	1.9	3.3	2.8	1.2
Ac												
Di	21.5	31.8	29.9	22.6	19.9		14.1	9.5	8.9	6.0	6.6	8.6
Hy												
Mt	2.4	2.1	2.2	2.2	2.3		1.5	1.5	1.9	1.9	1.4	1.9
Ilm	8.5	5.7	5.6	7.8	7.4		5.4	4.5	3.0	3.1	4.2	3.0
Ap	1.3	1.1	0.9	1.6	1.3		0.9	2.1	0.7	1.0	1.9	0.7
Ol	14.9	26.2	28.6	11.8	15.5		6.7	8.6	6.4	4.9	8.9	6.4
D.I.	29.9	21.0	19.1	35.6	32.8		58.0	61.0	72.8	71.9	62.3	72.6

N.B. Analyses of mixed lava samples AZ1721B and AZ1721T are given in Table 3.3.

Table A2.2 continued.

	Agua de Pau volcano						'Waist'						
SAMPLE	AZ1202	AZ1213	AZ1604	AZ1634	AZ1146	AZ1024	AZ1039	AZ1308	AZ1315	AZ1880	AZ1691	AZ1324	AZ1322
SiO_2	64.05	63.23	66.26	63.15	60.36	64.38	45.52	47.00	47.49	47.39	45.29	46.92	44.92
TiO_2	0.71	0.82	0.74	0.79	1.34	0.51	3.95	3.68	3.67	2.52	4.37	3.88	3.92
Al_2O_3	17.86	17.52	16.82	17.41	17.33	17.25	13.34	13.69	14.69	12.96	15.60	17.12	13.32
Fe_2O_3	1.36	1.44	1.13	1.28	1.73	1.38	1.51	1.48	1.48	1.31	1.64	1.48	1.55
FeO	2.27	2.41	1.88	2.14	2.89	2.30	10.08	9.84	9.94	8.77	10.92	9.86	10.35
MnO	0.15	0.17	0.21	0.14	0.14	0.19	0.17	0.18	0.17	0.17	0.20	0.19	0.17
MgO	0.53	0.63	0.52	1.11	1.66	0.38	9.01	9.17	8.20	10.61	5.41	5.17	9.41
CaO	1.05	0.91	0.77	1.22	2.88	0.80	11.34	10.24	9.35	11.95	9.52	8.66	11.48
Na_2O	6.82	6.69	6.70	6.47	5.59	7.29	2.88	2.94	3.51	2.71	3.05	4.26	2.85
K_2O	6.21	5.88	5.89	6.12	5.66	5.61	1.63	1.87	1.97	1.15	2.02	2.07	1.43
P_2O_5	0.11	0.10	0.08	0.11	0.21	0.08	0.53	0.62	0.53	0.36	0.69	0.76	0.50
TOTAL	101.12	99.80	101.00	99.94	99.79	100.17	99.96	100.71	100.90	99.90	98.71	100.37	99.90
TRACE ELEMENTS													
Ni	3	5	5	31	15		106	266	135	222	15	10	215
Cr		11		51	38		425	452	336	719	13	13	369
V		9		12	59		294	265	240	257	260	214	283
Rb	155	167	209	125	96	172	38	41	42	26	41	47	30
Sr	14	51	8	49	235	3	687	713	742	469	881	945	646
Y	45	25	73	28	34	57	21	34	34	25	31	34	24
Zr	614	774	1314	541	435	916	255	287	316	149	324	299	225
Nb	136	185	264	105	94	177	65	64	74	49	77	77	55
Ba	50	154	39	161	734	15	565	582	605	428	611	653	506
La	86	104	165	59	75	117	44	55	51	29	53	55	39
Ce			254			277	90					116	74
Nd			121			101	46					65	38
Sm			24			21	9.4					13	8.2
Eu			2.8			0.51	3.0					4.1	2.6
Gd							8.2					11.3	7.4
Tb			2.6			2.1							
Yb			6.6			5.6	2.0					3.0	
Lu			0.96			0.89							
CIPW NORMS													
Qz			2.7										
Or	36.3	34.9	34.5	36.2	33.5	33.1	9.6	11.0	11.5	6.8	12.1	12.2	8.5
Ab	53.1	55.5	53.1	52.6	46.6	55.5	11.4	16.3	18.3	14.5	18.6	21.0	10.3
An		0.4		0.4	5.5		18.7	18.5	18.3	19.8	23.3	21.4	19.3
Ne	1.9	0.6		1.2	0.5	1.0	7.0	4.6	6.0	4.6	4.1	8.1	7.5
Ac	0.4		2.6			3.7							
Di	3.7	2.9	2.8	4.1	6.2	3.0	27.9	22.9	19.9	30.1	16.8	13.9	28.1
Hy			2.3										
Mt	1.8	2.1	0.3	1.9	2.5	0.1	2.3	2.2	2.2	2.0	2.5	2.2	2.3
Ilm	1.3	1.6	1.4	1.5	2.6	1.0	7.5	6.9	6.9	4.8	8.4	7.3	7.5
Ap	0.3	0.2	0.2	0.3	0.5	0.2	1.3	1.5	1.2	0.9	1.7	1.8	1.2
Ol	1.2	1.7		1.9	2.2	2.3	14.4	16.4	15.6	16.6	12.7	12.3	15.5
D.I.	91.3	91.0	90.3	90.0	80.6	89.6	28.1	31.8	35.9	25.9	34.8	41.2	26.2

N.B. Analyses of samples AZ1544, AZ1323, AZ1377, AZ1378, AZ1394, AZ1188, AZ1149, AZ1019 and AZ1672 are given in Table 4.5.

Table A2.2 continued.

	'Waist'							Sete Cidades volcano				
SAMPLE	AZ1874	AZ1872	AZ1689	2SM	AZ1326	AZ1164	AZ1879	AZ1168	6SM	AZ1883	AZ1704	AZ1034
SiO_2	46.30	45.31	46.83	44.84			61.46	48.47	45.45	46.93	46.84	46.53
TiO_2	3.80	3.44	3.55	3.95			1.09	3.10	3.51	3.78	3.47	3.52
Al_2O_3	14.08	12.04	14.09	13.34			18.32	15.88	13.70	16.05	13.58	15.12
Fe_2O_3	1.53	1.57	1.46	1.55			1.67	1.28	1.44	1.46	1.44	1.41
FeO	10.23	10.47	9.73	10.30			2.78	8.54	9.57	9.73	9.62	9.38
MnO	0.18	0.17	0.18	0.19			0.13	0.17	0.17	0.17	0.17	0.18
MgO	8.59	11.57	8.71	8.92			0.61	6.57	8.35	6.08	9.23	6.64
CaO	9.50	11.79	8.98	11.79			2.37	9.15	11.61	8.90	11.32	9.61
Na_2O	3.03	2.50	3.37	2.37			6.58	3.61	2.71	3.77	2.92	3.56
K_2O	1.87	1.25	1.89	1.28			4.78	2.10	1.35	2.15	1.35	1.79
P_2O_5	0.59	0.42	0.55	0.58			0.15	0.61	0.50	0.77	0.52	0.67
TOTAL	99.70	100.53	99.34	99.11			99.94	99.48	98.36	99.79	100.46	98.41
TRACE ELEMENTS												
Ni	168	217	171	245				79		90	174	
Cr	469	648	402	445				171		85	459	
V	280	296	239	315			20	233		247	290	
Rb	39	28	40	23	49	40	132	49	26	47	28	40
Sr	742	520	694	739	722	609	696	766	666	931	649	803
Y	26	21	31	25	30	23	24	26	24	34	23	24
Zr	277	199	287	192	288	260	772	285	209	319	211	310
Nb	78	44	75	57	73	58	151	87	65	85	62	95
Hf							17					
Ba	574	404	593	504			1271	675		692	478	
La	51	37	51	35			55	55		59	36	
Ce				78			122				86	
Nd				40			42				45	
Sm				8.4			6.4				9.1	
Eu				2.7			2.5				2.9	
Gd											8.0	
Tb				1.0			0.83					
Ho							1.0					
Yb				2.0			2.3				1.9	
Lu				0.25			0.33					
CIPW NORMS												
Qz												
Or	11.1	7.3	11.2	7.6			28.3	12.5	8.1	12.7	7.9	10.7
Ab	17.5	9.0	19.2	13.1			54.7	23.0	14.1	20.5	15.8	20.5
An	19.4	17.8	17.9	22.0			6.3	21.0	21.6	20.6	19.9	20.3
Ne	4.4	6.5	5.2	3.8			0.5	4.2	5.0	6.2	4.8	5.5
Ac												
Di	19.8	30.5	19.2	26.6			4.1	17.1	27.5	15.6	26.6	19.3
Hy												
Mt	2.3	2.3	2.2	2.2			2.4	1.9	2.1	2.2	2.1	2.1
Ilm	7.2	6.5	6.8	7.5			2.1	5.9	6.8	7.2	6.6	6.8
Ap	1.4	1.0	1.3	1.3			0.4	1.5	1.2	1.8	1.2	1.6
Ol	17.0	19.0	17.2	15.1			1.2	13.1	13.7	13.3	15.2	13.2
D.I.	33.1	22.9	35.6	24.5			83.6	39.7	27.2	39.4	28.5	36.7

Table A2.2 continued.

SAMPLE	Sete Cidades AZ1172	Obsidians AZ1015	Obsidians AZ1714	Xenoliths AZ1035	Xenoliths AZ1056	Xenoliths AZ1207	Xenoliths AZ1205	Xenoliths AZ1187	Xenoliths AZ1664	Xenoliths AZ1712	Xenoliths AZ1204	Xenoliths AZ1219	Xenoliths MA18E
SiO_2	64.57	63.57	63.26	38.80	64.71	63.17	63.00	64.91	64.56	63.35	64.79	64.50	64.90
TiO_2	0.66	0.73	0.54	4.46	0.52	0.63	0.60	0.61	0.43	0.60	0.50	0.32	0.59
Al_2O_3	17.36	17.73	16.76	16.60	16.91	16.88	17.04	17.30	16.76	17.39	15.91	16.71	17.40
Fe_2O_3	1.15	1.00	1.38	15.58*	1.31	1.50	1.32	1.25	1.28	1.29	1.60	1.24	1.29
FeO	1.91	1.67	2.29		2.19	2.51	2.20	2.08	2.14	2.15	2.66	2.07	2.15
MnO	0.21	0.15	0.20	0.23	0.21	0.24	0.17	0.22	0.21	0.16	0.26	0.22	0.15
MgO	0.43	0.52	0.38	7.29	0.38	0.45	0.44	0.46	0.25	0.38	0.40	0.18	0.44
CaO	0.70	1.18	0.80	12.99	0.88	0.92	0.85	0.49	0.68	0.86	0.16	0.53	0.80
Na_2O	7.06	6.69	7.14	3.08	7.03	7.08	6.70	6.76	6.96	7.01	6.31	7.17	6.91
K_2O	5.71	6.60	5.80	0.82	5.47	5.51	5.98	5.76	5.32	5.53	4.96	5.42	6.25
H_2O^+	n.d.	n.d.	n.d.	n.d.	n.d.	1.0	0.9	n.d.	1.8	1.6	2.2	2.1	n.d.
TOTAL	99.84	99.94	98.63	102.50	99.65	100.06	99.30		100.44	100.40	99.83	100.50	100.98
TRACE ELEMENTS													
Ni	3	4	2	4	5	4					7	16	
Cr													
V		9		215									
Rb	138	170	178	3	219	197	200	184	202	159	231	250	
Sr	6	49	7	1212	40	52	8	3	3	6	6	7	
Y	59	44	56	46	78	72	65	44	88	30	111	76	
Zr	801	992	910	116	1180	1389	1080	568	1023	651	1473	907	
Nb	211	196	177	59	282	271	174	149	275	135	308	272	
Th								17			34	65	
Ba	115	205	26	430	91	105	31	25	21	28	47	38	
La	99	109	112	55	149	224	69	89	187	60	194	242	
Ce				30				194			382	469	
Nd				80				85			155	156	
Sm				16				18			31	27	
Eu				4.5				0.75			1.2	0.7	
Tb				2.0				1.8			3.8	2.6	
Yb				2.7				4.2			8.9	8.5	
Lu								0.6			1.2	1.2	
CIPW NORMS													
Qz					0.6			1.3	1.7		7.0	1.0	
Or	33.8	39.1	34.8		32.5	32.9	36.0	34.1	31.9	33.1	30.1	32.6	36.6
Ab	57.6	48.5	53.3		56.4	55.0	53.9	57.1	57.3	58.1	54.7	56.6	53.2
An											0.3		
Ne		3.2	0.7			1.0	0.7			0.6			0.5
C								0.3			0.1		
Ac	2.0	1.9	4.0				2.1		2.0	0.6		3.6	3.3
$Na_2O.SiO_2$			0.5									0.2	
Di	2.5	4.4	3.0		3.3	3.5	3.1	1.7	2.7	3.2		2.1	2.8
Hy	1.1				2.5			2.5	2.4		4.3	3.1	
Mt	0.7	0.5			0.5	0.6	0.9	1.7	0.8	1.6	2.4		0.2
Ilm	1.3	1.4	1.0		1.0	1.2	1.2	1.2	0.8	1.2	1.0	0.6	1.1
Ap	0.2	0.2	0.2		0.2	0.2	0.2	0.1	0.1	0.2	0.2	0.1	0.2
Ol	0.9	0.7	2.4			2.3	1.8			1.3			2.1
D.I.	91.4	90.8	88.8		89.5	89.0	90.6	92.5	91.0	91.9	91.7	90.2	90.3

* all iron reported as Fe_2O_3
n.d. not determined

Table A2.2 continued.

Sample	Wt.% FeO	Fe_2O_3/FeO
AZ1039	9.18	0.27
AZ1322	7.90	0.54
AZ1034	7.49	0.47
AZ1017	8.37	0.34
MA23/3	9.30	0.19
2SM	8.55	0.41
36AP	8.26	0.39
AZ1705	5.60	0.45
MA239	3.62	0.58
AZ1014	2.85	1.25
AZ1323	1.80	1.09
AZ1377	2.06	1.11
AZ1378	1.88	1.11
AZ1024	2.18	0.74
AZ1604	0.75	3.17
AZ1714	1.70	1.20
AZ1614	2.71	1.11
AZ1015	1.41	0.92
AZ1634	1.07	2.31

Table A2.3. Some ferrous iron determinations by method of Wilson (1955).

	$\bar{X}$	S	Abbey (1973)
SiO_2	54.67	0.68	54.85
TiO_2	2.31	0.03	2.22
Al_2O_3	13.70	0.13	13.68
Fe_2O_3*	13.52	0.13	13.54
MnO	0.19	0.01	0.19
MgO	3.52	0.05	3.49
CaO	6.93	0.10	6.98
Na_2O	3.44	0.10	3.29
K_2O	1.75	0.03	1.68
P_2O_5	0.34	0.02	0.33
Total	100.37		100.25

* all iron reported as Fe_2O_3

Table A2.4. Mean ($\bar{X}$) major element contents (wt.%) and their standard deviations (S) for six replicate analyses of USGS standard BCR-1. Shown for comparison are values recommended by Abbey (1973).

	$\bar{X}$	S.D.	(1)	(2)
Zr	196	15	190	185
Nb	15	1	13.5	14
Y	42	3	37	46
Rb	49	4	37	46
Sr	331	29	330	330

Table A2.5 Mean of four analyses (XRF) of BCR-1 for Zr, Nb, Y, Rb and Sr. Published values (1) are from Flanagan (1973) and (2) from Abbey (1973).

	$\bar{X}$	S	Ref. 1	Ref. 2
La (6)	25.1	1.1	24.2	26
Ce (5)	56.3	0.8	53.7	53.9
Nd (7)	30.4	1.4	28.5	29
Sm (4)	6.8	0.2	6.70	6.6
Eu (7)	1.97	0.06	1.95	1.94
Tb (4)	1.18	0.08	1.08	1.0
Yb (4)	3.7	0.15	3.48	3.36
Lu (7)	0.53	0.03	0.55	0.55

Ref. 1: Flanagan (1973).

Ref. 2: Taylor and Gorton (1977).

Table A2.6. Mean ($\bar{X}$) REE values (ppm) for USGS standard rock BCR-1, determined by INAA using multi-element solution. Figures in brackets are the number of determinations for each element, S is the standard deviation. Published data for BCR-1 is shown for comparison.

APPENDIX 3

MINERAL ANALYSES

A3.1 METHOD OF ANALYSIS AND QUALITY OF RESULTS

The mineral analyses presented in Tables A3.2 and A3.3 were carried out on polished, carbon coated thin sections using the electron microprobe designed and constructed in the Department of Earth Sciences, Cambridge and a Microscan V/EDS system at the Geology Department, University College, London. Cobalt metal was used as a standard, the intensities of the characteristic lines of all other elements being stored as ratios with respect to the intensity of the Co $K\alpha$ peak. Live count times were 80s and 100s at accelerating voltages of 20KV and specimen currents of 10nA and 25-35nA for the Cambridge and U.C. probes respectively. Energy spectra were automatically processed by mini-computer using an iterative peak stripping programme (Statham, 1976) and the compositions were estimated using ZAF correction procedures of Sweatman and Long (1969). Drift of the system was monitored by measuring the standard cobalt peak several times during the course of an analytical session. The quality of individual analyses was determined by the oxide weight percent totals and, where possible, mineral stoichiometry. This was particularly important for the alkali feldspars, some Na loss being found to occur under the higher specimen currents. Therefore, on the basis of 80^{2-}, alkali feldspar analyses were rejected if Ca+Na+K was less than about 0.95.

To check the reproducibility of the data, a standard olivine crystal was analysed several times during the course of probe work, the mean compositions and standard deviations for individual oxides being given in Table A3.1.

A3.2 THE DATA

Microporbe analyses of minerals from Faial and Sao Miguel

	$\bar{X}$	S
FeO	9.59	0.15
MgO	49.42	0.47
SiO_2	40.89	0.33
Total	99.90	

Table A3.1. Mean ($\bar{X}$) and standard deviation (S) for 14 replicate analyses (obtained during eight separate analytical sessions) for a single olivine crystal.

volcanic rocks are presented in Tables A3.2 and A3.3. All analyses are of phenocrysts unless otherwise stated (ie the suffix g.m. denotes groundmass crystal). The suffixes c and r denote core and rim respectively. For example, the numbers UC161(c), UC161 and UC161(r) refer to three analyses of the same crystal progressing from core to rim respectively. Crystals with the prefix U.C. were analysed on the Microscan V probe at University College, all other analyses being carried out on the Cambridge probe.

FAIAL MINERAL ANALYSES

	AZ3115					AZ3120				AZ3339		
	F13c	F13r	F11	F14gm	F16gm	F533c	F533r	F12gm	F17c	F17r	F18c	F18r
SiO_2	50.60	50.89	50.98	53.50	53.49	53.23	51.22	52.97	48.68	52.63	50.42	50.30
Al_2O_3	31.44	31.04	30.47	29.00	27.55	29.06	29.10	28.69	32.72	29.45	31.51	30.93
FeO	0.47	0.53	0.68	1.43	2.08	0.46	0.69	0.82	0.36	0.41	0.71	0.55
CaO	14.16	13.34	13.05	12.00	10.88	12.83	13.17	11.11	15.23	11.93	13.83	13.63
Na_2O	2.87	3.10	3.30	4.16	4.77	3.95	3.90	4.77	2.31	4.30	2.93	2.30
K_2O	0.15	0.18	0.21	0.58	0.65	0.31	0.35	0.24	0.11	0.31	0.15	0.20
TOTAL	99.69	99.08	98.69	100.67	99.43	99.84	98.43	98.60	99.61	99.03	99.55	98.73
Recalculated on the basis of 80^{2-}												
Si	2.313	2.330	2.344	2.408	2.437	2.416	2.367	2.430	2.238	2.405	2.304	2.318
Al	1.694	1.676	1.652	1.539	1.480	1.554	1.585	1.552	1.766	1.587	1.697	1.680
Fe	0.018	0.020	0.026	0.054	0.079	0.018	0.027	0.031	0.014	0.016	0.027	0.021
Ca	0.693	0.654	0.643	0.579	0.531	0.624	0.652	0.546	0.747	0.584	0.677	0.673
Na	0.256	0.280	0.294	0.361	0.422	0.348	0.349	0.425	0.205	0.380	0.259	0.268
K	0.009	0.011	0.012	0.033	0.038	0.018	0.021	0.014	0.006	0.018	0.009	0.012

	AZ3339	AZ3374								AZ3446	AZ3417
	F19	F110	F111	F112	F113	F114gm	F115gm	F116	UC224c	UC224r	F247	UC106
SiO_2	47.34	49.45	49.02	53.40	48.38	54.50	54.72	53.63	48.96	47.92	55.67	65.68
Al_2O_3	33.12	31.83	31.72	29.63	31.15	27.92	27.73	28.78	31.54	32.70	27.89	19.61
FeO	0.40	0.49	0.49	0.53	0.41	0.36	0.50	0.50	0.45	0.51	0.35	0.25
CaO	15.63	14.77	15.10	11.59	15.53	9.83	10.02	11.24	16.02	16.77	10.17	0.07
Na_2O	1.77	2.63	2.34	4.58	2.16	5.64	5.66	4.69	2.28	1.90	5.34	6.98
K_2O		0.12	0.19	0.32		0.39	0.40	0.25	0.13		0.24	5.66
TOTAL	98.26	99.29	98.86	100.05	98.63	98.64	99.05	99.29	99.38	99.86	99.86	99.05
Recalculated on the basis of 80^{2-}												
Si	2.202	2.273	2.265	2.414	2.241	2.493	2.496	2.440	2.251	2.194	2.517	2.953
Al	1.816	1.725	1.728	1.580	1.756	1.505	1.491	1.543	1.710	1.764	2.517	2.953
Fe	0.016	0.019	0.019	0.020	0.016	0.014	0.019	0.019	0.017	0.020	0.013	0.009
Ca	0.778	0.728	0.748	0.561	0.771	0.482	0.490	0.548	0.789	0.823	0.491	0.041
Na	0.160	0.235	0.210	0.402	0.194	0.500	0.502	0.431	0.203	0.174	0.466	0.608
K		0.007	0.011	0.018		0.023	0.023	0.015	0.008		0.014	0.325

	AZ3424								AZ3432			
	P70	P72	P74c	P74r	P86c	P86r	P90	UC430	P21c	P21r	P18	P18
SiO_2	67.88	66.01	58.26	57.84	56.58	58.73	67.97	54.61	50.95	60.92	56.38	57.00
Al_2O_3	19.36	18.93	26.66	27.23	27.49	26.65	19.38	28.53	31.34	24.72	28.74	26.72
FeO		0.23	0.24	0.22	0.30	0.24	0.19	0.54	0.31	0.40	0.35	0.29
CaO	0.11	0.21	8.29	8.76	9.44	8.07	0.14	11.03	14.03	5.81	10.57	9.11
Na_2O	6.95	7.06	6.51	6.30	5.79	6.59	7.64	4.63	3.37	7.33	5.33	5.84
K_2O	6.16	5.85	0.39	0.35	0.25	0.39	5.26	0.26	0.00	0.73	0.27	0.31
TOTAL	100.46	98.29	100.35	100.70	99.85	100.67	100.58	99.95	100.00	99.91	101.64	99.27
Recalculated on the basis of 80^{2-}												
Si	3.004	2.992	2.615	2.575	2.541	2.606	3.000	2.462	2.317	2.712	2.495	2.566
Al	1.010	1.012	1.387	1.429	1.455	1.394	1.006	1.516	1.680	1.298	1.499	1.430
Fe		0.009	0.001	0.008	0.011	0.009	0.007	0.020	0.012	0.015	0.013	0.011
Ca	0.005	0.010	0.392	0.418	0.454	0.384	0.007	0.550	0.684	0.277	0.501	0.443
Na	0.596	0.620	0.557	0.543	0.504	0.567	0.653	0.405	0.297	0.633	0.457	0.514
K	0.348	0.338	0.022	0.020	0.014	0.022	0.296	0.015	0.004	0.041	0.015	0.018

Table A3.2a Faial feldspar analyses.

	AZ3432							AZ3426				
	P29	PF58	P68	P69	UC161c	UC161	UC161r	P129	P141c	P142	P142r	P151
SiO_2	56.54	48.62	56.06	65.46	48.55	47.82	48.07	30.59	65.08	56.43	55.07	49.39
Al_2O_3	27.13	33.28	28.09	21.76	32.38	31.85	31.56	30.59	21.26	28.12	27.50	32.38
FeO	0.37	0.33	0.42	0.12	0.42	0.34	0.42	0.51	0.13	0.31	0.45	0.40
CaO	9.26	16.24	10.08	2.41	15.78	15.74	15.53	13.70	2.37	10.04	10.10	15.72
Na_2O	5.56	2.08	5.44	8.82	2.42	2.34	2.48	3.32	8.04	5.43	5.19	2.59
K_2O	0.30	0.11	0.30	2.35	0.11	0.18	0.12	0.17	2.49	0.28	0.32	0.08
TOTAL	99.18	100.62	100.39	100.92	99.58	98.35	98.27	98.81	99.37	100.61	98.63	100.56
Recalculated on the basis of $8O^{2-}$												
Si	2.554	2.212	2.514	2.872	2.237	2.241	2.229	2.872	2.891	2.521	2.515	2.248
Al	1.445	1.785	1.485	1.125	1.748	1.750	1.735	1.659	1.113	1.481	1.480	1.737
Fe	0.014	0.013	0.016	0.004	0.013	0.016	0.020	0.013	0.005	0.012	0.017	0.015
Ca	0.448	0.792	0.484	0.113	0.774	0.786	0.776	0.675	0.113	0.481	0.494	0.766
Na	0.489	0.183	0.473	0.750	0.214	0.212	0.224	0.296	0.692	0.470	0.460	0.226
K	0.017	0.006	0.017	0.131	0.006	0.011	0.007	0.010	0.141	0.016	0.019	0.005

						AZ3435						
	P104	P105c	P105r	P114	P120	P121c	P121r	P122c	P122r	P123c	P123r	P124c
SiO_2	53.23	53.86	55.26	49.12	66.22	61.89	62.16	64.07	64.64	65.98	65.66	56.03
Al_2O_3	29.39	28.69	28.13	32.34	20.83	22.95	23.15	21.04	21.16	20.90	21.15	27.99
FeO	0.30	0.36	0.46	0.38		0.21	0.23		0.11	0.12	0.13	0.43
CaO	11.45	11.22	10.06	15.35	1.57	4.30	4.70	2.32	2.32	1.71	1.73	10.45
Na_2O	4.66	5.06	5.40	2.62	7.90	8.61	8.40	8.32	8.90	8.69	8.42	5.62
K_2O	0.19	0.26	0.27	0.09	3.41	1.00	1.11	2.43	2.40	3.13	3.12	0.26
TOTAL	99.22	99.45	99.58	100.10	99.93	98.96	99.75	98.18	99.53	100.53	100.23	100.78
Recalculated on the basis of $8O^{2-}$												
Si	2.425	2.450	2.495	2.246	2.930	2.780	2.770	2.885	2.879	2.909	2.900	2.506
Al	1.579	1.539	1.497	1.743	1.087	1.215	1.216	1.117	1.111	1.086	1.101	1.477
Fe	0.012	0.013	0.017	0.015		0.008	0.009		0.004	0.004	0.005	0.016
Ca	0.559	0.547	0.487	0.752	0.074	0.207	0.225	0.112	0.110	0.081	0.082	0.501
Na	0.411	0.447	0.472	0.250	0.677	0.749	0.725	0.726	0.766	0.743	0.721	0.486
K	0.011	0.015	0.015	0.005	0.192	0.057	0.063	0.139	0.136	0.176	0.175	0.015

		AZ3435	
	P124r	P125c	P125r
SiO_2	55.29	63.66	62.60
Al_2O_3	28.55	22.68	23.22
FeO	0.27	0.14	0.19
CaO	10.84	3.67	4.59
Na_2O	5.65	8.61	8.40
K_2O	0.25	1.32	1.05
TOTAL	100.85	100.08	100.15
Recalculated on the basis of $8O^{2-}$			
Si	2.477	2.816	2.774
Al	1.508	1.183	1.218
Fe	0.010	0.005	0.007
Ca	0.520	0.174	0.218
Na	0.491	0.739	0.721
K	0.014	0.074	0.059

Table A3.2a continued.

	OL1c	OL1r	AZ3115 OL2	OL3	OL4gm	UC530	AZ3120 UC531	UC536	UC539	AZ3085 UC540	UC543	AZ3339 OL5
SiO_2	38.67	40.03	39.32	38.86	38.24	39.02	39.08	38.58	38.13	38.74	38.97	38.95
FeO	19.40	16.18	16.43	18.23	23.10	18.35	19.51	18.40	19.02	18.44	17.17	20.06
MnO	0.27	0.22	0.22	0.24	0.30		0.31	0.35	0.38	0.28	0.24	0.20
MgO	40.63	44.02	42.85	41.55	37.32	41.68	41.31	40.72	40.75	41.76	42.48	40.35
NiO		0.15	0.15	0.14								
CaO	0.32	0.22	0.23	0.16	0.44	0.19	0.24	0.23	0.22	0.29	0.24	0.32
TOTAL	99.29	100.82	99.20	99.18	99.40	99.44	100.45	98.28	98.50	99.51	99.10	99.88
Recalculated on the basis of 40^{2-}												
Si	0.999	1.002	1.003	1.000	1.004	0.992	0.991	1.000	0.992	0.988	0.994	1.003
Fe	0.419	0.339	0.351	0.393	0.507	0.390	0.414	0.399	0.414	0.393	0.366	0.432
Mn	0.006	0.005	0.005	0.005	0.007		0.007	0.008	0.008	0.006	0.005	0.004
Mg	1.564	1.643	1.629	1.594	1.460	1.580	1.562	1.573	1.580	1.586	1.616	1.549
Ni		0.003	0.003	0.003								
Ca	0.009	0.006	0.006	0.004	0.012	0.005	0.006	0.006	0.006	0.006	0.007	0.009

	OL6	OL7c	AZ3339 OL7r	OL8gm	OL9gm	UC527	AZ3374 UC528	OL10	OL11gm	OL12gm	AZ3435 P39	PF11
SiO_2	37.75	36.73	37.10	34.73	36.17	37.04	36.10	37.79	35.34	35.03	38.72	38.57
FeO	25.40	29.82	28.20	39.51	32.08	26.07	31.72	27.01	39.26	41.27	20.65	20.50
MnO	0.34	0.47	0.40	0.91	0.40	0.39	0.52	0.32	0.68	0.73	0.27	0.25
MgO	36.07	32.37	33.55	23.29	29.92	35.35	31.12	35.17	24.90	23.06	40.68	40.74
NiO												0.16
CaO	0.30	0.29	0.32	0.57	0.40	0.23	0.45	0.30	0.47	0.42	0.18	0.18
TOTAL	99.82	99.68	99.57	99.01	98.97	99.08	99.91	100.67	100.65	100.51	100.68	100.40
Recalculated on the basis of 40^{2-}												
Si	0.998	0.997	0.999	1.002	0.999	0.990	0.980	0.999	0.998	1.001	0.993	0.992
Fe	0.562	0.677	0.636	0.954	0.741	0.583	0.720	0.597	0.927	0.986	0.447	0.441
Mn	0.008	0.011	0.009	0.022	0.012	0.009	0.012	0.007	0.016	0.018	0.006	0.005
Mg	1.421	1.309	1.347	1.002	1.232	1.409	1.260	1.386	1.047	0.982	1.555	1.561
Ni												0.003
Ca	0.009	0.009	0.009	0.018	0.012	0.007	0.013	0.011	0.014	0.013	0.005	0.005

	AZ3446 P245	P246
SiO_2	37.05	37.46
FeO	27.50	27.70
MnO	1.02	0.91
MgO	33.56	33.57
NiO	0.40	0.43
CaO	0.20	0.18
TOTAL	99.73	100.25
Recalculated on the basis of 40^{2-}		
Si	0.998	1.003
Fe	0.619	0.620
Mn	0.023	0.021
Mg	1.340	1.339
Ni	0.009	0.009
Ca	0.006	0.005

Table A3.2b Faial olivine analyses.

	AZ3115	AZ3120	AZ3085			AZ3374				AZ3446		
	PX1gm	UC534	UC544c	UC544r	PX2	PX3	PX4	P241	P242	P250c	P250r	UC555
SiO_2	48.50	48.82	46.47	49.77	48.65	48.57	48.16	49.73	48.55	48.93	48.89	51.48
Al_2O_3	8.62	6.82	7.44	5.66	4.13	5.58	5.22	5.44	5.83	5.92	6.20	0.98
FeO	8.97	6.25	7.21	5.66	8.34	7.54	7.46	7.93	7.59	7.78	7.91	13.95
MnO			0.15				0.18	0.15	0.21		0.13	1.35
MgO	10.66	13.86	12.88	14.55	13.18	13.83	13.92	13.45	13.22	13.12	13.17	10.48
CaO	18.15	21.97	21.94	22.62	22.22	21.88	21.35	21.88	21.54	21.63	21.60	20.89
Na_2O	1.74		0.65		0.62	0.52	0.75	0.41	0.46	0.35	0.44	0.60
TiO_2	3.32	1.82	2.52	1.59	2.47	2.08	2.28	2.06	2.12	2.26	2.24	0.56
TOTAL	99.96	99.54	99.26	99.85	99.61	100.00	99.32	100.68	99.52	99.99	100.58	100.29
Recalculated on the basis of $6O^{2-}$												
Si	1.792	1.802	1.747	1.819	1.832	1.810	1.809	1.833	1.817	1.819	1.809	1.967
Al	0.375	0.297	0.330	0.244	0.183	0.245	0.231	0.236	0.257	0.259	0.271	0.044
Fe	0.277	0.193	0.227	0.173	0.263	0.235	0.234	0.244	0.238	0.242	0.245	0.446
Mn			0.005				0.006	0.005	0.007		0.004	0.044
Mg	0.587	0.763	0.721	0.793	0.740	0.766	0.780	0.739	0.737	0.730	0.726	0.597
Ca	0.718	0.869	0.884	0.885	0.897	0.874	0.860	0.864	0.864	0.862	0.856	0.856
Na	0.124		0.047		0.045	0.037	0.055	0.030	0.033	0.025	0.031	0.044
Ti	0.092	0.051	0.071	0.044	0.070	0.058	0.064	0.057	0.060	0.063	0.062	0.016

						AZ3432						AZ3426
	P1	P2c	P2r	P3	P4	P23	P53	UC156	UC157	UC156	UC159	P121c
SiO_2	48.77	52.74	51.05	51.07	50.68	46.81	48.49	45.91	46.19	45.71	49.55	45.90
Al_2O_3	6.72	1.91	3.04	3.82	2.96	6.25	6.47	8.10	8.32	8.14	6.63	7.60
FeO	7.10	8.14	8.17	8.46	8.32	7.08	7.05	7.65	7.65	7.55	6.50	7.72
MnO	0.14						0.16			0.20		
MgO	13.70	14.62	13.80	13.93	13.81	12.59	13.63	12.39	12.95	12.46	14.31	12.77
CaO	21.88	21.69	21.97	22.07	21.36	21.60	21.65	21.20	21.30	21.32	21.13	21.42
Na_2O	0.40	0.54		0.57	0.57	0.36	0.40	0.74	0.94	1.01	0.56	0.39
TiO_2	2.30	0.79	1.17	1.46	1.04	2.58	2.08	2.58	2.71	2.73	1.90	2.68
TOTAL	101.01	100.43	99.20	101.38	98.74	99.27	99.93	98.57	100.06	99.12	100.58	98.48
Recalculated on the basis of $6O^{2-}$												
Si	1.793	1.948	1.912	1.879	1.906	1.752	1.802	1.739	1.725	1.727	1.815	1.742
Al	0.291	0.083	0.134	0.166	0.131	0.364	0.283	0.362	0.366	0.362	0.286	0.340
Fe	0.218	0.251	0.256	0.260	0.262	0.222	0.219	0.242	0.239	0.239	0.199	0.245
Mn	0.004						0.005			0.006		
Mg	0.751	0.805	0.771	0.763	0.774	0.702	0.755	0.700	0.721	0.702	0.781	0.722
Ca	0.862	0.859	0.882	0.870	0.861	0.866	0.862	0.860	0.852	0.863	0.829	0.871
Na	0.029	0.039		0.040	0.042	0.027	0.029	0.054	0.068	0.074	0.040	0.029
Ti	0.064	0.022	0.033	0.040	0.029	0.072	0.058	0.073	0.076	0.078	0.052	0.077

Table A3.2c Faial Pyroxene analyses.

	AZ3426			AZ3435	
	P121r	P126	P136	P118c	P118r
SiO_2	48.95	52.48	51.26	48.59	49.02
Al_2O_3	7.91	0.44	0.30	5.91	5.59
FeO	7.92	16.99	16.81	7.98	8.58
MnO		1.29	1.48	0.16	0.25
MgO	12.52	8.90	8.46	13.10	12.80
CaO	21.57	20.67	20.59	21.94	21.52
Na_2O	0.49	0.61	0.39	0.37	
TiO_2	2.84	0.20	0.20	1.98	1.91
TOTAL	100.20	101.58	99.49	100.03	99.67
Recalculated on the basis of 60^{2-}					
Si	1.749	2.001	2.001	1.813	1.835
Al	0.348	0.020	0.014	0.260	0.246
Fe	0.247	0.542	0.549	0.249	0.268
Mn		0.042	0.049	0.005	0.008
Mg	0.695	0.506	0.492	0.729	0.714
Ca	0.861	0.844	0.861	0.877	0.863
Na	0.035	0.045	0.030	0.026	
Ti	0.079	0.006	0.006	0.056	0.054

Table A3.2c continued.

	AZ3424								AZ3417
	P76c	P76r	P79	P89	UC432/1	UC432/2	UC434	UC435	UC100
SiO_2	50.66	50.39	50.02	52.34	48.76	49.39	49.93	51.91	51.12
Al_2O_3	0.34	0.22	3.84	1.56	0.76	0.96	3.93	1.83	0.95
FeO	22.85	22.50	8.46	10.40	21.63	22.15	7.79	10.13	14.04
MnO	1.64	1.67	0.32	0.54	1.75	1.71	0.32	0.66	1.17
MgO	4.26	4.48	13.88	13.06	4.25	4.33	13.87	12.90	10.56
CaO	19.28	19.41	21.54	21.29	19.01	19.06	21.43	21.40	20.75
Na_2O	1.59	1.42	0.39	0.54	1.74	1.66	0.68	0.39	0.94
TiO_2	0.28	0.18	1.58	0.85	0.45	0.36	1.42	0.72	0.46
TOTAL	100.90	100.27	100.03	100.58	98.35	99.62	99.37	99.94	99.99
Recalculated on the basis of 6 O^{2-}									
Si	2.008	2.009	1.867	1.955	1.983	1.982	1.870	1.950	1.962
Al	0.016	0.010	0.169	0.068	0.036	0.046	0.174	0.081	0.043
Fe	0.757	0.751	0.264	0.325	0.736	0.744	0.244	0.318	0.451
Mn	0.055	0.056	0.010	0.017	0.060	0.058	0.010	0.021	0.038
Mg	0.251	0.266	0.772	0.727	0.258	0.259	0.775	0.723	0.604
Ca	0.819	0.829	0.862	0.852	0.828	0.820	0.860	0.861	0.853
Na	0.122	0.110	0.028	0.039	0.137	0.129	0.049	0.028	0.070
Ti	0.008	0.005	0.044	0.024	0.014	0.011	0.040	0.021	0.013

Table A3.2c continued.

		AZ3446			AZ3424				AZ3432			
	UC548	UC549	P243	P244	UC429	P24	P56	P57	P58c	P58r	P59	P60
SiO_2	39.64	39.57	39.92	41.39	39.82	40.12	41.18	41.24	42.72	42.24	41.92	40.72
Al_2O_3	12.72	12.82	12.95	11.92	12.08	12.75	11.97	12.19	11.93	11.54	11.76	12.91
FeO	11.11	11.20	10.84	12.01	10.84	11.40	12.39	12.62	10.92	11.34	12.22	11.64
MgO	12.46	12.59	12.71	12.79	12.58	12.96	12.35	12.39	13.42	13.09	12.48	12.67
CaO	11.85	11.91	11.68	11.23	11.46	11.68	11.45	11.20	11.04	11.54	11.78	11.73
Na_2O	2.98	2.36	2.28	2.30	2.52	2.63	2.45	2.74	3.00	2.57	2.47	2.40
K_2O	0.85	0.80	0.82	0.79	0.69	0.75	0.84	0.80	0.75	0.82	0.78	0.76
TiO_2	6.46	6.35	6.31	5.67	5.97	6.15	5.59	5.46	5.10	5.11	5.17	6.27
MnO				0.20	0.20		0.20	0.25	0.21	0.26	0.23	
TOTAL	98.07	97.60	97.51	98.30	96.18	98.44	98.57	98.97	99.09	98.51	98.83	95.10
Recalculated on the basis of 23 O^{2-}												
Si	5.855	5.865	5.898	6.085	5.976	5.898	6.070	6.052	6.183	6.191	6.157	5.940
Al	2.214	2.239	2.255	2.066	2.136	2.210	2.079	2.110	2.035	1.994	2.040	2.220
Fe	1.372	1.389	1.340	1.477	1.360	1.402	1.527	1.549	1.321	1.390	1.501	1.420
Mg	2.743	2.782	2.798	2.803	2.815	2.841	2.712	2.710	2.894	2.859	2.731	2.752
Ca	1.876	1.892	1.849	1.770	1.845	1.841	1.808	1.773	1.711	1.776	1.800	1.832
Na	0.854	0.678	0.654	0.655	0.733	0.749	0.700	0.779	0.841	0.732	0.703	0.677
K	0.159	0.151	0.156	0.148	0.131	0.141	0.158	0.150	0.139	0.154	0.145	0.141
Ti	0.718	0.708	0.701	0.627	0.674	0.680	0.620	0.602	0.555	0.564	0.571	0.690
Mn				0.025	0.026		0.025	0.031	0.026	0.031	0.029	

	AZ3432		AZ3426				AZ3435			
	P61	P52	P142	P143	P147	P149	P107	P108	P109	P113
SiO_2	40.17	41.10	40.37	40.35	40.86	41.42	41.09	41.03	40.23	40.22
Al_2O_3	12.90	12.64	12.99	12.86	12.77	11.95	11.73	11.90	13.02	11.91
FeO	11.44	11.90	10.93	11.22	11.17	12.30	12.13	12.11	10.78	11.64
MgO	12.42	12.83	12.96	12.82	12.96	12.27	12.45	12.55	13.10	12.22
CaO	11.94	11.37	11.63	11.60	11.81	11.38	11.25	11.10	11.77	10.99
Na_2O	2.68	2.54	2.54	2.82	2.63	2.60	2.91	2.81	2.82	2.58
K_2O	0.80	0.83	0.77	0.82	0.81	0.76	0.80	0.79	0.86	0.79
TiO_2	6.27	5.79	6.29	6.02	5.90	5.56	5.59	5.48	6.07	5.55
MnO	0.19				0.18	0.16	0.21	0.22	0.12	0.17
TOTAL	98.81	98.92	98.68	98.71	99.09	98.40	97.95	98.07	98.77	96.07
Recalculated on the basis of 23 O^{2-}										
Si	5.895	6.005	5.904	5.906	5.953	6.089	6.074	6.065	5.888	6.057
Al	2.232	2.177	2.240	2.219	2.193	2.071	2.044	2.074	2.247	2.115
Fe	1.404	1.444	1.336	1.373	1.362	1.512	1.499	1.498	1.320	1.466
Mg	2.717	2.794	2.824	2.797	2.814	2.689	2.743	2.766	2.857	2.742
Ca	1.878	1.780	1.855	1.851	1.844	1.793	1.781	1.771	1.845	1.774
Na	0.763	0.719	0.721	0.800	0.742	0.740	0.833	0.805	0.801	0.754
K	0.148	0.154	0.144	0.153	0.151	0.142	0.150	0.148	0.160	0.151
Ti	0.692	0.636	0.692	0.663	0.647	0.614	0.622	0.609	0.668	0.629
Mn	0.023				0.022	0.020	0.027	0.028	0.015	0.022

Table A3.2d Faial amphibole analyses.

	AZ3446	AZ3417	AZ3426	
	P249	UC107	P134c	P134r
SiO_2	37.36	36.08	36.62	37.07
Al_2O_3	14.87	11.88	13.31	13.41
FeO	15.26	22.13	21.13	21.07
MnO	0.22	0.42	0.30	0.34
MgO	13.67	9.39	9.81	9.92
Na_2O	0.87	0.67	0.77	0.47
K_2O	7.67	8.98	8.37	8.18
TiO_2	8.83	6.93	6.70	6.94
TOTAL	98.75	96.48	97.01	97.40
Recalculated on the basis of 22 O^{2-}				
Si	5.354	5.556	5.527	5.552
Al	2.513	2.156	2.367	2.367
Fe	1.912	2.850	2.667	2.639
Mn	0.027	0.055	0.039	0.043
Mg	2.918	2.154	2.207	2.214
Na	0.242	0.199	0.226	0.136
K	1.401	1.764	1.612	1.562
Ti	0.952	0.802	0.760	0.782

Table A3.2e Faial biotite analyses.

			AZ3374					AZ3446		AZ3360		AZ3401
	Mag1	Mag2	UC521	UC523	UC529/1	UC529/2	UC549	UC550/1	UC550/2	UC562	UC566gm	UC537
SiO_2	0.32	0.39	0.38	0.27	0.28	0.31	0.36	0.33	0.39	1.11	0.55	0.23
Al_2O_3	1.81	1.76	1.69	1.91	2.00	2.15	5.68	1.27	1.24	4.66	1.22	0.81
FeO	65.42	66.02	67.05	66.23	64.49	64.02	68.39	71.25	70.06	63.84	57.69	74.85
MnO	0.64	0.58	0.74	0.82	0.55	0.63	0.45	1.86	1.64	0.67	1.17	2.76
MgO	2.15	2.35	2.09	2.51	2.73	2.95	6.12	1.69	1.57	5.75	1.37	1.11
CaO							0.28		0.45			
TiO_2	25.06	27.18	27.03	27.68	28.47	28.34	16.98	22.44	22.06	19.95	33.21	16.76
TOTAL	95.57	98.28	98.98	99.42	98.52	98.40	98.26	98.84	97.80	95.98	95.21	96.54
Recalculated on the basis of 4 O^{2-}												
Si	0.013	0.015	0.014	0.010	0.010	0.012	0.014	0.013	0.016	0.043	0.021	0.010
Al	0.085	0.079	0.076	0.085	0.089	0.095	0.259	0.059	0.059	0.212	0.055	0.040
Fe	2.184	2.118	2.137	2.090	2.031	2.020	2.211	2.367	2.359	2.057	1.837	2.656
Mn	0.022	0.019	0.024	0.026	0.018	0.020	0.015	0.062	0.056	0.022	0.038	0.099
Mg	0.126	0.134	0.119	0.141	0.153	0.166	0.353	0.100	0.094	0.330	0.076	0.070
Ca							0.012		0.019			
Ti	0.752	0.784	0.775	0.785	0.806	0.804	0.493	0.670	0.668	0.578	0.951	0.535

		AZ3417				AZ3432				AZ3424		
	UC101	UC102/1	UC102/2	P6	P12	P13	Mag20	Mag21	P81	P91	P92	UC427
SiO_2	0.27	0.25		0.31	0.29	0.31	0.41	0.55	0.34	0.21	0.20	0.25
Al_2O_3	0.89	0.95	0.82	3.71	3.93	3.87	4.94	4.06	2.73	4.63	4.86	4.71
FeO	70.87	71.30	70.88	71.56	71.12	69.51	70.49	70.15	68.62	69.23	68.86	67.78
MnO	1.82	1.92	1.92				0.61	0.60	1.28	0.53	0.61	0.60
MgO	1.22	1.26	1.14	4.16	4.50	4.25	4.35	4.48	2.85	5.07	5.56	4.95
CaO						0.10	0.10	0.17				
TiO_2	23.67	23.83	23.73	16.63	17.00	17.00	15.87	16.91	21.39	17.34	17.69	17.64
TOTAL	98.74	99.49	98.48	96.37	96.81	95.04	96.77	96.92	97.41	97.01	97.78	96.13
Recalculated on the basis of 4 O^{2-}												
Si	0.011	0.010		0.013	0.012	0.013	0.016	0.022	0.014	0.008	0.008	0.010
Al	0.042	0.044	0.039	0.178	0.186	0.186	0.232	0.190	0.128	0.217	0.225	0.222
Fe	2.358	2.354	2.366	2.437	2.397	2.376	2.351	2.339	2.289	2.302	2.259	2.260
Mn	0.061	0.064	0.065				0.020	0.020	0.043	0.018	0.020	0.020
Mg	0.072	0.074	0.068	0.253	0.270	0.259	0.259	0.266	0.169	0.301	0.325	0.294
Ca						0.004	0.004	0.007				
Ti	0.708	0.707	0.712	0.509	0.515	0.523	0.476	0.507	0.640	0.519	0.522	0.535

Table A3.2f Faial magnetite analyses.

	AZ3424	
	UC436	UC437
SiO_2	0.35	0.20
Al_2O_3	2.74	2.58
FeO	68.65	68.15
MnO	1.32	1.17
MgO	2.92	2.78
CaO	0.27	0.12
TiO_2	21.46	21.83
TOTAL	97.71	96.83
Recalculated on the basis of 40^{2-}		
Si	0.014	0.008
Al	0.128	0.121
Fe	2.273	2.268
Mn	0.044	0.040
Mg	0.172	0.165
Ca	0.011	0.005
Ti	0.639	0.653

Table A3.2f continued.

	AZ3374						AZ3360			AZ3417	AZ3432	
	UC520c	UC520/2	UC520/3	UC520r	UC522	UC528	UC561	UC564	UC565	UC105	P8	P11
SiO_2	0.37	0.37	0.29	0.21	0.27	0.35	0.33	0.21	0.35	0.49	0.30	0.32
Al_2O_3	0.24		0.21		0.27	0.18					0.28	0.32
FeO	43.73	43.67	43.29	44.04	43.38	43.29	36.13	40.15	39.61	43.53	44.76	44.73
MnO	0.80	0.73	0.80	0.77	0.74	0.63	2.77	2.08	1.99	2.08		
MgO	2.49	2.42	2.70	2.42	2.74	2.93	4.55	2.31	2.53	1.61	5.65	5.21
CaO				0.12	0.09	0.11						0.12
TiO_2	52.30	52.35	52.22	51.78	51.54	51.82	55.85	54.64	54.84	49.56	47.13	47.60
TOTAL	99.93	99.54	99.51	99.34	99.03	99.31	99.80	99.39	98.97	97.27	98.12	98.30
Recalculated on the basis of 3 O^{2-}												
Si	0.009	0.009	0.007	0.005	0.007	0.009	0.008	0.005	0.009	0.013	0.007	0.008
Al	0.007		0.006		0.008	0.005					0.008	0.010
Fe	0.904	0.906	0.899	0.920	0.906	0.899	0.728	0.825	0.814	0.939	0.953	0.950
Mn	0.017	0.016	0.017	0.017	0.016	0.013	0.057	0.043	0.041	0.045		
Mg	0.092	0.089	0.100	0.090	0.102	0.109	0.164	0.085	0.093	0.062	0.215	0.197
Ca				0.003	0.002	0.003						0.003
Ti	0.973	0.977	0.975	0.971	0.968	0.968	1.012	1.010	1.013	0.961	0.902	0.909

	P83	P84	P85	P90	P94	AZ3424 UC428/1	UC428/2	UC431/1	UC431/2	UC433/1	UC433/2
SiO_2		0.33	0.18	0.18	0.26		0.18	0.22		0.34	0.18
Al_2O_3	0.69	0.96	0.78	0.37	0.71	0.93	1.02	1.00	0.94	0.55	0.42
FeO	41.17	41.23	40.85	43.68	41.55	40.76	41.30	40.01	40.64	42.56	43.22
MnO	0.27	0.31	0.26	0.59	0.24	0.28	0.43	0.27	0.41	0.90	1.00
MgO	8.05	8.29	8.01	6.47	8.40	7.62	7.41	7.57	7.46	5.20	4.86
CaO		0.01									
TiO_2	47.98	47.84	48.63	48.55	48.41	48.97	48.45	48.40	48.39	47.85	47.61
TOTAL	98.16	99.06	98.71	99.84	99.57	98.56	98.79	97.47	97.84	97.40	97.29
Recalculated on the basis of 3 O^{2-}											
Si		0.008	0.004	0.005	0.006		0.004	0.005		0.009	0.005
Al	0.020	0.028	0.023	0.011	0.021	0.027	0.030	0.029	0.027	0.017	0.013
Fe	0.860	0.850	0.846	0.908	0.854	0.841	0.850	0.832	0.845	0.904	0.922
Mn	0.006	0.006	0.005	0.012	0.005	0.006	0.009	0.006	0.009	0.019	0.022
Mg	0.300	0.304	0.295	0.240	0.308	0.260	0.272	0.281	0.277	0.197	0.185
Ca		0.003									
Ti	0.902	0.887	0.905	0.907	0.895	0.908	0.896	0.906	0.905	0.914	0.913

Table A3.2g Faial ilmenite analyses.

	AZ3085		AZ3120					AZ3374		AZ3426	
	UC538	UC542	UC531c	UC531c	UC531	UC531r	UC535	UC525	UC526	P154	P155
SiO_2	0.46	0.40	0.29	0.37	0.37	0.66	0.27	0.27	0.34	0.25	0.49
Al_2O_3	17.73	23.61	24.37	23.54	12.04	3.56	23.76	6.33	7.38	14.02	14.48
V_2O_3										0.44	0.55
Cr_2O_3	9.47	20.51	31.48	31.30	23.51	4.40	26.59	3.37	3.06	4.43	4.61
FeO*	50.67	36.56	31.70	31.93	46.45	63.59	34.46	64.40	62.96	57.07	55.60
MnO	0.31	0.27	0.32	0.42	0.51	0.64	0.49	0.38	0.43	0.30	0.29
MgO	9.61	11.25	9.14	9.35	7.37	3.39	9.48	4.95	4.40	8.84	9.45
NiO							0.27				
TiO_2	9.20	4.20	2.02	2.28	9.22	21.04	3.60	18.24	19.60	13.08	12.53
TOTAL	97.45	96.80	97.30	96.91	99.47	97.26	98.92	97.94	98.17	98.43	98.00
Recalculated on the basis of 4 O^{2-}											
Si	0.016	0.013	0.009	0.012	0.013	0.026	0.009	0.010	0.013	0.009	0.017
Al	0.730	0.922	0.922	0.895	0.496	0.162	0.910	0.285	0.325	0.567	0.603
V										0.125	0.129
Cr	0.262	0.537	0.799	0.798	0.650	0.134	0.683	0.102	0.090	0.125	0.129
Fe	1.480	1.013	0.851	0.861	1.359	2.053	0.937	2.057	1.969	1.694	1.644
Mn	0.009	0.008	0.009	0.011	0.015	0.021	0.013	0.012	0.014	0.009	0.009
Mg	0.500	0.555	0.437	0.449	0.384	0.195	0.459	0.262	0.245	0.468	0.490
Ni							0.007				
Ti	0.242	0.105	0.049	0.055	0.243	0.611	0.088	0.524	0.551	0.349	0.333

* All iron as FeO

Table A3.2h Faial Cr-spinel analyses.

	AZ3120		AZ3085	AZ3374		AZ3360	
	UC516	UC517	UC540	UC519/1	UC519/2	UC560/1	UC560/2
Fe	59.16	59.40	57.68	61.28	61.35	59.84	60.67
Ni	3.69	3.41	3.94	0.73	0.62		
Cu	0.51	0.56	0.31		0.31		
S	37.08	37.10	36.82	37.27	36.99	38.62	39.24
TOTAL	100.46	100.47	98.75	99.28	99.27	98.66	99.91

	AZ3446			AZ3401	AZ3432		
	UC547/1	UC547/2	UC548	UC541	UC227	UC228	UC229
Fe	62.24	62.45	62.49	61.99	57.57	58.20	57.85
Ni					2.95	2.99	3.01
Cu		0.29					
S	36.38	37.00	38.25	37.64	38.24	38.41	38.61
TOTAL	98.62	99.45	100.74	99.63	98.76	99.56	99.47

	AZ3432
	UCS230
Fe	34.49
Ni	0.53
Cu	29.79
S	34.42
TOTAL	99.23

Table A3.2i Faial sulphide analyses.

SAO MIGUEL MINERAL ANALYSES

	10SM			AZ1034				MA239						
	UC500	UC502c	UC502r	CF1c	CF1r	CF3	CF6	UC7c	UC7r	UC51	UC52	UC53	UC54	UC55
SiO_2	46.96	49.35	50.60	57.25	52.94	51.90	59.15	60.56	64.38	59.02	59.65	64.96	65.40	59.60
Al_2O_3	32.69	30.74	29.58	29.56	29.39	29.84	25.50	24.73	20.10	24.54	24.67	19.46	19.57	23.66
FeO	0.56	0.69	0.80	0.87	0.67	0.72	0.45	0.45	0.74	0.34	0.44	0.26	0.24	0.57
CaO	16.91	14.84	13.82	8.70	12.63	12.94	7.79	5.97	1.66	6.52	6.39	0.88	0.67	5.84
Na_2O	2.09	2.71	3.65	6.08	4.32	3.84	6.82	6.00	6.00	6.06	6.15	6.01	5.50	6.32
K_2O	0.13	0.25	0.28	0.56	0.27	0.30	0.78	2.58	6.25	2.12	2.26	7.52	7.97	2.46
TOTAL	99.35	98.58	98.73	99.42	100.22	99.54	100.49	100.29	99.13	98.60	99.56	99.10	99.55	98.45
Recalculated on the basis of 8 O^{2-}														
Si	2.171	2.283	2.332	2.592	2.402	2.369	2.640	2.697	2.909	2.673	2.682	2.948	2.955	2.714
Al	1.781	1.676	1.607	1.386	1.572	1.605	1.342	1.298	1.071	1.313	1.308	1.041	1.042	1.270
Fe	0.022	0.027	0.031	0.033	0.025	0.027	0.017	0.017	0.028	0.013	0.017	0.010	0.009	0.022
Ca	0.837	0.736	0.683	0.422	0.614	0.633	0.372	0.285	0.080	0.317	0.308	0.043	0.042	0.285
Na	0.187	0.243	0.327	0.534	0.380	0.340	0.590	0.519	0.526	0.533	0.536	0.529	0.482	0.558
K	0.008	0.015	0.017	0.032	0.016	0.018	0.045	0.147	0.361	0.123	0.130	0.436	0.459	0.143

	MA239									AZ170S				
	UC56	UC57	UC58	UC59	UC60	UC64	UC71	UC72	UC74	UC91	UC92	UC93	UC94	UC95
SiO_2	65.97	64.82	64.97	65.99	65.38	62.24	64.77	64.62	60.61	54.92	53.91	64.20	62.58	64.48
Al_2O_3	19.49	19.03	19.05	19.43	19.45	21.94	19.29	19.42	23.77	27.36	28.55	19.27	21.21	19.47
FeO	0.17	0.22	0.21	0.19	0.31	0.47	0.15	0.34	0.64	0.66	0.58	0.36	0.26	0.27
CaO	0.67	0.74	0.68	0.77	0.87	3.81	5.36	6.05	6.55	9.98	11.48	0.94	2.59	1.27
Na_2O	5.72	5.19	5.44	5.86	5.11	6.49	5.36	6.05	6.55	4.96	4.32	4.51	4.50	3.55
K_2O	7.81	8.11	7.92	8.15	8.64	3.59	7.73	6.65	2.26	0.63	0.62	9.57	7.68	10.59
TOTAL	99.83	98.11	98.27	100.39	99.76	98.54	98.04	98.18	99.32	98.51	99.46	98.85	98.82	99.63
Recalculated on the basis of 8 O^{2-}														
Si	2.968	2.969	2.972	2.960	2.956	2.819	2.964	2.951	2.726	2.510	2.452	2.939	2.851	2.940
Al	1.034	1.028	1.027	1.027	1.037	1.171	1.041	1.045	1.260	1.474	1.531	1.040	1.139	1.047
Fe	0.006	0.009	0.008	0.007	0.012	0.018	0.006	0.013	0.024	0.025	0.022	0.014	0.010	0.010
Ca	0.033	0.036	0.034	0.037	0.042	0.185	0.036	0.054	0.264	0.489	0.560	0.046	0.127	0.062
Na	0.499	0.461	0.482	0.510	0.448	0.570	0.475	0.536	0.571	0.440	0.381	0.401	0.397	0.314
K	0.448	0.474	0.462	0.467	0.498	0.207	0.451	0.388	0.130	0.037	0.036	0.559	0.447	0.616

	AZ170S				AZ1035									
	UC96	UC97	UC98	UC99	CF21	CF22c	CF22r	CF23c	CF23r	CF24c	CF24r	CF25c	CF25/2	CF25/3
SiO_2	64.72	64.61	53.57	62.00	53.11	55.36	54.22	52.83	56.54	53.18	52.93	53.40	50.99	49.89
Al_2O_3	19.60	19.86	28.21	19.99	30.19	29.25	29.53	30.18	27.76	30.28	30.17	19.96	32.16	32.12
FeO	0.27	0.30	0.62	0.62	0.29	0.41	0.37	0.31	0.65	0.34	0.34	0.42	0.41	0.36
CaO	1.02	1.23	11.22	3.14	12.09	10.82	11.53	12.36	9.60	12.15	12.13	11.70	14.02	14.68
Na_2O	3.52	3.61	4.48	5.45	4.49	5.16	4.57	4.08	5.55	4.31	4.60	4.76	3.48	2.94
K_2O	10.97	10.71	0.47	6.60	0.22	0.36	0.33	0.21	0.56	0.24	0.25	0.23	0.12	0.14
TOTAL	100.10	100.32	98.27	97.80	100.39	101.36	100.55	99.97	100.66	100.50	100.42	100.47	101.18	100.13
Recalculated on the basis of 8 O^{2-}														
Si	2.942	2.929	2.455	2.862	2.397	2.466	2.434	2.391	2.528	2.396	2.391	2.405	2.296	2.271
Al	1.051	1.061	1.524	1.089	1.606	1.536	1.563	1.610	1.463	1.608	1.606	1.591	1.707	1.726
Fe	0.010	0.012	0.024	0.024	0.011	0.015	0.014	0.012	0.024	0.013	0.013	0.016	0.015	0.014
Ca	0.050	0.060	0.551	0.156	0.584	0.516	0.554	0.599	0.460	0.587	0.587	0.565	0.676	0.717
Na	0.310	0.318	0.398	0.488	0.392	0.446	0.398	0.358	0.481	0.376	0.402	0.416	0.304	0.260
K	0.636	0.620	0.027	0.389	0.012	0.020	0.019	0.012	0.032	0.014	0.014	0.013	0.007	0.008

Table A3.3a Sao Miguel feldspar analyses.

	AZ1035				AZ1377	AZ1544		AZ1378				AZ1394		
	CF25r	CF26	CF27c	CF27r	P208	P427	P183c	P183r	P188	P189	P34c	P34r	P45c	P45r
SiO_2	55.66	52.72	54.41	54.71	60.70	65.51	66.06	66.62	66.94	67.08	66.09	65.83	67.10	66.35
Al_2O_3	28.28	30.20	28.70	28.49	24.34	19.27	19.53	19.58	19.50	19.25	19.52	19.46	19.67	19.54
FeO	0.33	0.32	0.36	0.60	0.32	0.20	0.23	0.19	0.20	0.21	0.18		0.17	0.13
CaO	9.98	12.32	10.49	10.66	5.85	0.66	0.85	0.85	0.43	0.45	0.62	0.77	0.71	0.73
Na_2O	5.30	4.23	5.27	4.73	6.89	5.65	5.35	5.00	5.91	5.91	5.26	5.78	5.68	5.43
K_2O	0.36	0.24	0.42	0.28	1.82	7.73	7.84	8.14	7.74	7.62	8.01	7.33	7.45	7.83
TOTAL	99.91	100.03	99.65	99.46	99.92	99.22	99.86	100.38	100.72	100.52	99.68	99.17	100.78	100.01
Recalculated on the basis of 8 O^{2-}														
Si	2.506	2.389	2.446	2.480	2.716	2.966	2.970	2.978	2.981	2.991	2.975	2.972	2.980	2.975
Al	1.501	1.613	1.534	1.523	1.284	1.028	1.035	1.032	1.024	1.012	1.036	1.036	1.030	1.033
Fe	0.012	0.012	0.014	0.023	0.012	0.008	0.009	0.007	0.007	0.008	0.007		0.006	0.005
Ca	0.482	0.598	0.509	0.518	0.281	0.042	0.041	0.041	0.020	0.021	0.030	0.037	0.034	0.035
Na	0.462	0.372	0.463	0.416	0.598	0.496	0.466	0.433	0.510	0.511	0.459	0.506	0.489	0.472
K	0.020	0.014	0.024	0.016	0.104	0.447	0.450	0.464	0.440	0.433	0.460	0.422	0.422	0.448

			AZ1394					AZ1024				AZ1149		
	P165	P400	P403	P408	P409	P410	P449	P453c	P453r	P239	P473	P476c	P476r	P476r/2
SiO_2	66.45	67.24	66.86	66.96	65.97	65.23	66.61	66.93	66.56	67.15	67.77	61.67	62.03	61.91
Al_2O_3	19.50	19.47	19.15	19.41	18.80	19.33	19.33	18.85	18.94	19.39	18.84	24.26	23.15	23.59
FeO	0.13	0.20	0.19	0.15	0.21	0.30	0.22	0.26	0.28	0.25	0.25	0.24	0.29	0.23
CaO	0.63	0.40	0.55	0.71	0.68	0.84	0.53	0.26	0.28	0.28	0.30	6.08	5.13	5.43
Na_2O	5.80	6.24	6.24	6.08	5.74	6.08	6.96	6.69	6.55	7.16	7.39	7.08	7.35	7.25
K_2O	7.41	7.56	7.74	7.54	7.60	7.05	6.71	6.65	6.93	5.54	6.62	1.85	2.48	2.27
TOTAL	99.92	101.11	100.73	100.85	99.00	98.83	100.36	99.55	99.39	99.79	101.17	101.18	100.43	100.68
Recalculated on the basis of 8 O^{2-}														
Si	2.978	2.982	2.983	2.979	2.980	2.958	2.974	3.002	2.995	2.991	2.999	2.723	2.766	2.748
Al	1.013	1.018	1.007	1.018	1.004	1.033	1.017	0.997	1.005	1.018	0.983	1.263	1.217	1.234
Fe	0.005	0.007	0.007	0.006	0.008	0.011	0.008	0.006	0.005	0.009	0.009	0.009	0.011	0.010
Ca	0.030	0.019	0.026	0.034	0.033	0.041	0.025	0.012	0.013	0.014	0.014	0.288	0.245	0.258
Na	0.504	0.536	0.539	0.524	0.504	0.535	0.602	0.582	0.571	0.620	0.634	0.606	0.635	0.624
K	0.424	0.428	0.441	0.428	0.440	0.408	0.382	0.381	0.398	0.315	0.374	0.104	0.141	0.128

			AZ1149							AZ1629
	P494c	P484r	P504c	P504r	P510c	P510r	P240	P520c	P520r	P221
SiO_2	67.53	67.60	66.11	65.75	65.16	65.96	67.02	52.38	52.61	66.64
Al_2O_3	18.82	18.78	19.58	19.01	19.32	19.65	19.51	29.93	29.75	19.13
FeO	0.31	0.29	0.27	0.21	0.28	0.18	0.20	0.46	0.56	0.28
CaO	0.16	0.16	0.90	0.91	0.98	0.98	0.38	12.80	12.58	0.17
Na_2O	7.20	7.02	5.74	5.40	4.58	4.45	6.12	3.86	4.10	6.46
K_2O	6.60	6.64	8.15	8.14	9.43	9.59	7.10	0.32	0.37	6.91
TOTAL	100.62	100.49	100.75	99.42	99.75	100.81	100.33	99.75	99.97	99.59
Recalculated on the basis of 8 O^{2-}										
Si	3.002	3.007	2.958	2.977	2.958	2.956	2.986	2.381	2.388	2.992
Al	0.986	0.985	1.033	1.015	1.034	1.038	1.025	1.604	1.592	1.013
Fe	0.011	0.011	0.010	0.008	0.011	0.007	0.007	0.017	0.021	0.010
Ca	0.008	0.009	0.043	0.044	0.048	0.047	0.018	0.624	0.612	0.008
Na	0.620	0.605	0.498	0.474	0.403	0.387	0.528	0.340	0.361	0.562
K	0.374	0.377	0.465	0.470	0.546	0.548	0.403	0.018	0.021	0.396

N.B. Additional feldspar analyses from samples AZ1377, AZ1544, AZ1378, AZ1394, AZ1024, AZ1149 and AZ1686 are given in Table 4.2.

Table A3.3a continued

	10SM		AZ1129	MA239				AZ1378		
	UC504c	UC504r	C100	UC80	UC81	UC82	UC83	P191	P201c	P201r
SiO_2	38.64	38.11	38.42	40.55	40.56	39.89	37.69	39.46	39.14	38.88
FeO	20.67	22.41	20.68	10.98	11.21	16.11	24.82	19.42	17.79	17.48
MnO	0.32	0.48	0.23	0.16	0.07	0.17	0.62	0.27	0.28	0.25
MgO	40.42	38.34	39.54	48.69	47.95	44.60	36.06	41.26	41.95	42.20
CaO	0.28	0.35	0.27	0.31	0.27	0.30	0.29	0.30	0.29	0.30
TOTAL	100.33	99.69	99.14	100.69	100.06	101.07	99.48	100.71	99.45	99.31
Recalculated on the basis of 4 O^{2-}										
Si	0.989	0.990	1.000	0.986	0.994	0.987	0.995	1.001	0.999	0.994
Fe	0.442	0.487	0.450	0.223	0.230	0.333	0.548	0.412	0.380	0.374
Mn	0.007	0.011	0.005	0.003	0.001	0.004	0.014	0.006	0.006	0.005
Mg	1.542	1.485	1.534	1.765	1.751	1.645	1.419	1.561	1.596	1.615
Ca	0.008	0.010	0.008	0.008	0.007	0.008	0.008	0.008	0.008	0.008
Mol.% Fo	77.7	75.3	77.3	88.8	88.4	83.2	72.1	79.1	80.8	81.2

Table A3.3b Sao Miguel olivine analyses.

	10SM			AZ1034			AZ1129				AZ1705			
	UC508c	UC508r	CP4c	CP4r	UC514c	UC514r	CP7	UC20	UC21	UC22	UC23	UC24	UC25	UC26
SiO_2	48.06	43.78	49.55	50.00	46.85	44.53	51.38	45.12	46.48	47.99	50.77	51.90	50.08	52.01
Al_2O_3	5.35	9.16	4.52	3.81	6.34	9.03	3.48	7.42	6.38	5.59	4.03	2.45	3.08	1.84
Cr_2O_3			0.16	0.17	0.17		0.29							
FeO	7.75	8.26	7.35	7.43	8.77	9.50	6.22	7.57	6.95	9.45	7.93	8.23	8.81	9.33
MnO			0.19			0.17	0.14			0.25	0.28	0.43	0.22	0.64
MgO	13.80	11.84	14.60	14.40	11.76	10.65	15.62	12.67	13.24	12.57	14.41	14.45	13.67	13.69
CaO	21.45	21.75	21.33	21.97	21.96	21.83	22.36	21.89	22.36	21.06	21.12	21.55	21.83	22.16
Na_2O		0.73	0.41		0.72	0.65		0.98	0.50	0.78	0.87	0.85	0.56	1.11
TiO_2	2.02	3.89	2.07	2.09	1.93	2.86	1.76	3.56	2.84	2.08	1.43	1.02	1.89	0.72
TOTAL	98.43	99.41	100.18	99.87	98.50	99.22	101.25	99.21	98.75	99.77	100.84	100.88	100.14	101.50
Recalculated on the basis of 6 O^{2-}														
Si	1.810	1.659	1.837	1.860	1.788	1.698	1.873	1.709	1.759	1.809	1.873	1.918	1.874	1.927
Al	0.238	0.409	0.197	0.167	0.285	0.406	0.150	0.331	0.285	0.249	0.175	0.107	0.136	0.080
Cr			0.005	0.005	0.005		0.008							
Fe	0.244	0.262	0.228	0.231	0.280	0.303	0.190	0.240	0.220	0.298	0.245	0.254	0.276	0.289
Mn			0.006			0.005	0.004			0.008	0.009	0.013	0.007	0.020
Mg	0.775	0.669	0.807	0.799	0.669	0.605	0.849	0.715	0.747	0.706	0.793	0.796	0.763	0.756
Ca	0.866	0.883	0.847	0.876	0.898	0.892	0.873	0.888	0.907	0.850	0.835	0.853	0.875	0.880
Na		0.054	0.029		0.054	0.048		0.072	0.037	0.057	0.062	0.061	0.040	0.080
Ti	0.057	0.111	0.058	0.058	0.055	0.082	0.048	0.102	0.081	0.059	0.040	0.028	0.053	0.020

	AZ1705				MA239				AZ1544			AZ1323		
	UC27	UC30	UC31	UC32	UC33	UC34c	UC34r	UC35	P459	P460	P216c	P216r	P312	UC214c
SiO_2	51.48	48.14	52.54	53.05	51.13	48.40	48.19	51.32	52.85	52.79	46.73	40.68	51.68	51.17
Al_2O_3	1.38	5.38	1.49	2.05	3.42	5.75	4.88	3.14	0.51	0.70	7.03	11.12	1.06	1.38
FeO	10.04	7.49	8.76	4.74	5.34	7.51	6.88	4.89	10.97	10.97	8.38	9.49	10.13	9.64
MnO	0.73	0.17	0.39	0.30	0.17	0.14	0.25		1.06	1.09	0.17	0.16	0.69	0.91
MgO	12.29	13.80	13.91	17.51	15.64	13.95	13.97	15.95	11.66	11.89	12.64	10.12	12.87	12.81
CaO	21.77	22.16	22.20	21.88	22.06	22.36	21.84	22.03	21.89	21.61	22.34	22.72	22.02	21.73
Na_2O	0.80	0.60	0.59	0.89	0.59	0.72	0.92	0.81		0.40			0.43	
TiO_2	0.63	2.22	0.42	0.79	1.49	2.58	2.24	1.19	0.37	0.40	3.01	5.33	0.45	0.60
TOTAL	99.12	99.96	100.30	101.21	99.84	101.41	99.17	99.33	99.31	99.85	100.44	99.62	99.33	98.24
Recalculated on the basis of 6 O^{2-}														
Si	1.957	1.800	1.957	1.923	1.885	1.785	1.813	1.897	2.003	1.995	1.747	1.557	1.960	1.952
Al	0.062	0.237	0.065	0.088	0.149	0.250	0.216	0.137	0.023	0.031	0.310	0.502	0.048	0.062
Fe	0.319	0.234	0.273	0.144	0.165	0.232	0.217	0.151	0.348	0.347	0.262	0.304	0.321	0.307
Mn	0.023	0.005	0.012	0.009	0.005	0.004	0.008		0.034	0.035	0.005	0.005	0.022	0.029
Mg	0.697	0.769	0.772	0.946	0.859	0.767	0.783	0.879	0.659	0.670	0.704	0.578	0.728	0.728
Ca	0.887	0.886	0.886	0.850	0.872	0.883	0.880	0.872	0.889	0.875	0.895	0.932	0.895	0.888
Na	0.059	0.043	0.042	0.062	0.042	0.051	0.067	0.058		0.030			0.032	
Ti	0.018	0.062	0.012	0.021	0.041	0.071	0.063	0.033	0.011	0.011	0.085	0.154	0.013	0.017

	AZ1323			AZ1377						AZ1378				
	UC214r	UC219	P434	P436	P437	P186	P196c	P196r	P200	P204c	P204r	P206	P212c	P212r
SiO_2	51.39	50.76	52.97	53.19	53.19	52.75	51.91	51.27	51.27	48.52	49.76	52.85	51.80	52.67
Al_2O_3	1.36	1.44	0.96	1.58	1.12	1.06	1.83	2.29	1.73	5.41	4.72	0.96	1.22	1.53
FeO	9.90	9.78	9.26	8.07	9.56	10.36	8.36	8.60	10.84	6.53	6.14	9.44	9.68	9.99
MnO	0.76	0.88	0.76	0.47	0.62	0.99	0.39	0.42	0.59			0.63	0.66	0.73
MgO	13.12	12.63	13.01	13.77	13.09	12.56	13.99	13.74	11.72	13.79	14.40	13.09	12.84	12.52
CaO	21.90	21.66	21.72	21.68	21.59	21.88	21.55	21.41	21,83	22.70	22.58	21.97	21.89	21.33
Na_2O	0.76	0.61				0.57	0.39	0.45	0.39			0.39	0.39	0.50
TiO_2	0.57	0.65	0.57	0.76	0.58	0.44	0.77	1.00	0.74	2.44	2.04	0.50	0.60	0.56
TOTAL	99.76	98.41	99.25	99.51	99.75	100.61	99.19	99.18	99.11	99.39	99.64	99.84	99.08	99.63
Recalculated on the basis of 6 O^{2-}														
Si	1.943	1.944	1.992	1.977	1.986	1.973	1.949	1.927	1.950	1.806	1.840	1.980	1.964	1.973
Al	0.061	0.065	0.043	0.069	0.049	0.047	0.081	0.101	0.077	0.238	0.206	0.042	0.055	0.068
Fe	0.313	0.314	0.291	0.251	0.298	0.324	0.262	0.270	0.345	0.203	0.190	0.296	0.307	0.313
Mn	0.024	0.029	0.024	0.015	0.019	0.031	0.012	0.017	0.019			0.020	0.021	0.023
Mg	0.739	0.722	0.729	0.763	0.728	0.700	0.782	0.770	0.665	0.765	0.794	0.730	0.726	0.699
Ca	0.887	0.889	0.875	0.864	0.863	0.877	0.867	0.862	0.890	0.905	0.895	0.882	0.889	0.856
Na	0.056	0.045				0.041	0.028	0.033	0.028			0.028	0.028	0.037
Ti	0.016	0.019	0.016	0.021	0.016	0.012	0.022	0.028	0.021	0.068	0.057	0.014	0.017	0.016

Table A3.3c Sao Miguel pyroxene analyses.

	AZ1378		AZ1394										AZ1149
	P544	UC226	P36c	P36r	P40	P161	P161r	P163	P170c	P170r	P175	P411	UC113r	P231c
SiO_2	41.40	51.21	51.80	51.85	52.58	52.11	51.39	51.79	52.66	52.88	52.23	52.46	50.92	51.02
Al_2O_3	9.85	1.15	1.14	0.64	0.60	0.62	0.84	0.67	1.04	1.08	0.60	1.01	1.40	0.86
Cr_2O_3						0.14	0.14	0.13						0.13
FeO	9.84	10.98	12.76	12.35	12.74	12.74	13.15	12.99	9.75	10.32	11.55	11.66	12.53	14.91
MnO	0.15	1.06				1.10	0.95	1.05	0.55	0.64	1.11	0.96	1.05	1.59
MgO	9.79	11.52	10.72	10.94	11.01	10.70	10.23	10.49	12.82	12.75	11.33	11.40	10.63	8.66
CaO	22.11	21.94	21.67	22.01	22.14	21.55	21.36	21.64	21.99	21.75	21.86	21.78	21.92	20.23
Na_2O		1.29	0.50	0.59	0.43	0.39	0.51	0.49		0.46	0.50	0.42	1.12	1.81
TiO_2	5.52	0.45	0.46	0.40	0.30	0.39	0.49	0.38	0.46	0.50	0.36	0.57	0.53	0.49
TOTAL	98.66	99.60	99.05	98.78	99.80	99.74	98.96	99.63	99.27	100.38	99.54	100.26	100.10	99.70
Recalculated on the basis of 6 O^{2-}														
Si	1.549	1.955	1.984	1.991	1.998	1.988	1.981	1.982	1.985	1.977	1.990	1.977	1.946	1.978
Al	0.449	0.052	0.051	0.029	0.027	0.028	0.038	0.030	0.046	0.047	0.027	0.045	0.063	0.039
Cr						0.004	0.004	0.004						0.004
Fe	0.318	0.350	0.409	0.397	0.405	0.406	0.424	0.416	0.307	0.323	0.368	0.367	0.400	0.484
Mn	0.005	0.034				0.036	0.031	0.034	0.018	0.020	0.036	0.031	0.034	0.052
Mg	0.563	0.656	0.612	0.626	0.623	0.608	0.582	0.598	0.720	0.710	0.644	0.640	0.605	0.500
Ca	0.915	0.898	0.889	0.906	0.902	0.881	0.882	0.887	0.888	0.871	0.893	0.879	0.898	0.841
Na		0.096	0.037	0.044	0.032	0.029	0.038	0.037		0.033	0.037	0.031	0.083	0.136
Ti	0.160	0.013	0.013	0.012	0.009	0.011	0.014	0.011	0.013	0.014	0.010	0.016	0.015	0.014

							AZ1149						AZ1629	
	P231r	P234	P235	P236	P237	P483	P507c	P507r	P496	P512c	P512r	P517c	P217	P218
SiO_2	51.39	47.84	42.78	45.03	48.86	47.54	44.86	48.29	42.44	50.07	49.12	42.05	52.60	52.48
Al_2O_3	0.87	5.71	9.98	8.77	4.86	5.57	9.00	5.99	9.63	3.95	4.53	10.02	0.40	0.46
Cr_2O_3	0.12	0.13												
FeO	14.98	8.23	9.14	9.08	7.93	7.65	9.08	7.82	8.64	7.25	8.44	8.79	12.57	12.47
MnO	1.68	0.14			0.18	0.15	0.15	0.18			0.17		1.51	1.56
MgO	8.58	13.13	10.66	11.86	13.75	13.03	10.89	13.21	11.05	14.11	13.79	10.94	10.89	11.42
CaO	20.29	22.02	22.19	21.61	21.90	21.53	20.86	21.98	21.81	21.83	21.18	21.92	21.03	21.32
Na_2O	1.42				0.35		0.47	0.42	0.41				0.76	0.70
TiO_2	0.46	2.67	5.25	4.01	2.05	2.59	3.96	2.69	4.98	1.80	2.38	5.50	0.42	0.36
TOTAL	99.79	99.87	100.00	100.36	99.88	98.06	99.27	100.58	98.96	99.01	99.61	99.22	100.31	100.77
Recalculated on the basis of 6 O^{2-}														
Si	1.987	1.791	1.620	1.687	1.825	1.807	1.698	1.794	1.620	1.874	1.839	1.603	1.995	1.983
Al	0.040	0.252	0.446	0.387	0.214	0.250	0.401	0.262	0.433	0.174	0.200	0.450	0.018	0.020
Cr	0.004	0.004												
Fe	0.484	0.258	0.290	0.285	0.248	0.243	0.287	0.243	0.276	0.227	0.264	0.280	0.399	0.394
Mn	0.055	0.004			0.006	0.005	0.005	0.006			0.005		0.048	0.050
Mg	0.495	0.733	0.601	0.662	0.765	0.738	0.614	0.731	0.629	0.787	0.770	0.622	0.616	0.643
Ca	0.841	0.883	0.900	0.867	0.876	0.877	0.846	0.875	0.892	0.875	0.850	0.895	0.855	0.863
Na	0.106				0.025		0.034	0.031	0.030				0.057	0.051
Ti	0.013	0.075	0.150	0.113	0.058	0.074	0.113	0.075	0.143	0.051	0.067	0.158	0.012	0.010

	AZ1629
	P223
SiO_2	52.31
Al_2O_3	0.69
FeO	11.73
MnO	1.42
MgO	11.06
CaO	21.10
Na_2O	0.63
TiO_2	0.28
TOTAL	99.22
Recalculated on the basis of 6 O^{2-}	
Si	1.999
Al	0.031
Fe	0.375
Mn	0.046
Mg	0.630
Ca	0.864
Na	0.047
Ti	0.008

N.B. Additional pyroxene analyses from samples AZ1377, AZ1378, AZ1394, AZ1149, AZ1629 and AZ1538 are given in Table 4.4.

Table A3.3c continued.

				AZ1035						AZ1712		AZ1219			
	CAM1	CAM2	CAM3c	CAM3/2	CAM3r	CAM4c	CAM4/2	CAM4/3	CAM4r	UC416c	UC416r	UC421/1	UC421/2	UC421/3	UC421r
SiO_2	40.64	40.34	40.46	40.45	40.62	39.62	40.14	39.61	42.51	45.25	44.93	43.58	43.62	47.07	46.67
Al_2O_3	12.93	13.03	12.93	12.65	12.50	12.96	12.96	12.84	13.77	4.23	3.45	5.20	4.25	1.84	2.40
FeO	13.18	13.41	13.49	13.28	13.41	13.33	13.52	13.38	12.04	24.03	29.63	22.21	25.28	31.81	29.66
MnO	0.21	0.21	0.22	0.28	0.28	0.21	0.27	0.15	0.30	1.51	1.76	1.54	1.87	2.57	2.33
MgO	11.59	11.73	11.60	11.31	11.50	11.30	11.20	11.16	9.61	6.52	2.39	7.42	5.36	1.64	2.82
CaO	11.53	11.81	11.71	11.61	11.82	11.54	11.61	11.86	10.81	8.15	5.60	10.21	8.32	4.20	5.72
Na_2O	2.42	2.79	2.71	2.49	2.62	2.54	2.43	2.75	2.87	5.26	6.08	4.32	4.31	6.32	5.69
K_2O	1.14	0.96	0.97	1.13	1.19	1.05	0.88	0.90	1.55	1.45	1.50	1.21	1.22	1.31	1.26
TiO_2	4.54	4.96	5.15	4.79	4.56	4.82	4.98	4.91	4.41	2.40	2.64	2.03	1.99	1.98	1.98
TOTAL	98.18	99.24	99.23	97.99	98.53	97.38	98.00	97.56	97.86	98.80	97.98	97.72	96.22	98.74	98.53
Recalculated on the basis of 23 O^{2-}															
Si	6.035	5.947	5.963	6.031	6.040	5.953	5.984	5.947	6.267	7.059	7.246	6.853	7.048	7.569	7.455
Al	2.264	2.265	2.246	2.224	2.184	2.296	2.278	2.272	2.393	0.778	0.657	0.964	0.810	0.348	0.452
Fe	1.637	1.653	1.662	1.656	1.668	1.675	1.686	1.679	1.484	3.135	3.997	2.921	3.416	4.278	3.962
Mn	0.026	0.026	0.027	0.035	0.035	0.027	0.034	0.019	0.037	0.200	0.240	0.205	0.256	0.349	0.316
Mg	2.565	2.576	2.547	2.514	2.548	2.530	2.489	2.498	2.112	1.515	0.574	1.740	1.292	0.393	0.671
Ca	1.835	1.866	1.850	1.854	1.883	1.858	1.854	1.907	1.708	1.363	0.967	1.720	1.441	0.723	0.978
Na	0.696	0.797	0.773	0.719	0.756	0.740	0.703	0.799	0.819	1.589	1.901	1.317	1.350	1.970	1.763
K	0.216	0.181	0.182	0.214	0.227	0.200	0.168	0.173	0.291	0.289	0.308	0.243	0.250	0.270	0.258
Ti	0.507	0.550	0.571	0.537	0.509	0.545	0.559	0.554	0.489	0.281	0.320	0.240	0.241	0.239	0.238

Table A3.3d Sao Miguel amphibole analyses.

	AZ1544			AZ1378			AZ1394			
	UC441	P185	P532	P533	UC220	UC223	P38	P46	P178	P405
SiO_2	36.24	37.93	36.12	37.66	34.31	35.84	36.64	36.72	36.43	36.91
Al_2O_3	13.02	13.89	12.92	13.80	13.58	13.23	13.21	13.24	13.23	12.82
FeO	13.32	14.11	13.59	13.77	13.26	14.21	18.35	18.84	18.58	17.32
MnO	0.24	0.16	0.12	0.23	0.17	0.28		0.36	0.39	0.33
CoO		0.24	0.19	0.24					0.26	0.16
MgO	14.17	13.76	13.25	13.15	12.74	12.89	11.75	11.52	10.40	12.09
CaO	0.16									
Na_2O	0.59	0.44		0.73	0.77	0.69	0.53	0.56	0.39	0.69
K_2O	8.69	8.93	8.38	8.42	8.34	9.02	8.70	8.76	8.46	8.66
TiO_2	7.54	8.56	8.46	8.42	10.56	8.84	6.94	7.58	9.05	6.65
TOTAL	93.97	98.02	93.03	96.42	93.75	95.00	96.12	97.58	97.19	95.63
Recalculated on the basis of 22 O^{2-}										
Si	5.724	5.488	5.498	5.525	5.212	5.395	5.522	5.472	5.444	5.577
Al	2.424	2.369	2.319	2.386	2.431	2.348	2.346	2.326	2.331	2.283
Fe	1.759	1.707	1.730	1.689	1.684	1.789	2.312	2.348	2.323	2.188
Mn	0.032	0.019	0.016	0.029	0.022	0.036		0.045	0.050	0.043
Co		0.028	0.023	0.029					0.032	0.019
Mg	3.335	2.967	3.005	2.874	2.886	2.893	2.639	2.558	2.316	2.723
Ca	0.027									
Na	0.180	0.124		0.207	0.225	0.201	0.154	0.163	0.112	0.203
K	1.751	1.649	1.627	1.576	1.617	1.732	1.672	1.667	1.613	1.670
Ti	0.895	0.932	0.968	0.929	1,206	1.001	0.786	0.850	1.017	0.756

N.B. Additional biotite analyses from samples AZ1377, AZ1378, AZ1394, AZ1024, AZ1538 and AZ1629 are given in Table 4.3.

Table A3.3e Sao Miguel biotite analyses.

	AZ1629		AZ1034				10SM					AZ1705		MA239
	P219	UC510	UC513c	UC513r	UC503c	UC503r	UC507/1	UC507/2	UC509/1	UC509/2	UC545	UC140	UC144	UC145c
SiO_2	0.57	0.23	0.28	0.34	0.26	0.44	0.40	0.44	0.18	0.38	0.28	0.36	0.35	0.35
Al_2O_3	0.91	3.98	4.01	4.09	3.78	4.01	7.28	7.17	5.79	5.48	3.70	2.80	2.73	2.18
Cr_2O_3					0.65	0.70	0.58	0.48	0.35	0.41	0.48			
FeO	75.76	67.04	67.99	67.98	66.79	66.14	63.92	63.79	65.19	65.32	66.71	67.50	67.16	68.18
MnO	2.68	0.58	0.62	0.57	0.60	0.50	0.30	0.41	0.49	0.54	0.69	0.64	0.60	0.99
MgO	1.03	4.31	4.26	3.93	5.82	5.54	7.29	7.37	6.88	6.82	6.10	3.04	3.32	3.08
CaO					0.12		0.26				0.12			
TiO_2	16.35	21.35	21.99	21.10	20.46	19.85	18.58	18.30	18.53	18.84	20.23	24.53	25.42	22.29
TOTAL	97.30	97.49	99.15	98.01	98.48	97.18	98.61	97.91	97.41	97.79	98.31	98.87	99.58	97.07
Recalculated on the basis of 4 O^{2-}														
Si	0.024	0.009	0.011	0.013	0.010	0.017	0.015	0.016	0.007	0.014	0.011	0.014	0.013	0.014
Al	0.045	0.182	0.180	0.187	0.171	0.184	0.319	0.315	0.262	0.246	0.168	0.127	0.122	0.102
Cr					0.020	0.022	0.017	0.014	0.011	0.012	0.015			
Fe	2.660	2.174	2.166	2.204	2.142	2.148	1.985	1.987	2.089	2.078	2.143	2.168	2.129	2.268
Mn	0.095	0.019	0.020	0.019	0.019	0.016	0.009	0.013	0.016	0.017	0.022	0.021	0.019	0.033
Mg	0.064	0.249	0.242	0.227	0.333	0.321	0.403	0.409	0.393	0.387	0.349	0.174	0.188	0.183
Ca					0.005		0.010				0.005			
Ti	0.516	0.623	0.630	0.615	0.590	0.580	0.519	0.513	0.534	0.539	0.584	0.708	0.725	0.667

	MA239		AZ1377				AZ1323					AZ1544		
	UC145r	P421	P422	P439	P440	P214	UC212	UC215c	UC215r	UC216	P454	P457	P458	P461
SiO_2	0.39	0.64	0.71	0.57	0.31	0.41	0.34	0.24	0.32	0.23	0.37	0.29	0.44	0.45
Al_2O_3	2.12	3.60	3.50	3.25	2.97	1.75	1.76	1.86	1.87	2.03	1.70	1.91	1.80	1.55
FeO	67.98	71.28	69.04	70.84	73.00	74.04	74.09	73.06	72.40	72.59	72.96	74.57	73.11	73.00
MnO	1.03	0.64	0.62	0.92	1.03	1.60	1.50	1.60	1.37	1.69	1.48	1.55	1.42	1.76
MgO	2.99	5.06	4.27	3.78	3.94	2.02	2.18	2.24	2.07	2.38	2.22	2.44	2.16	1.84
CaO				0.93						0.13				
TiO_2	22.08	17.50	17.19	17.65	17.50	17.72	18.44	18.31	17.73	18.24	18.13	18.27	17.86	18.36
TOTAL	96.59	98.72	95.33	97.94	98.75	97.54	98.31	97.31	95.76	97.29	96.86	99.03	96.78	96.96
Recalculated on the basis of 4 O^{2-}														
Si	0.016	0.025	0.029	0.022	0.012	0.017	0.014	0.010	0.014	0.010	0.015	0.011	0.018	0.018
Al	0.100	0.165	0.167	0.152	0.138	0.085	0.084	0.090	0.092	0.098	0.082	0.090	0.087	0.074
Fe	2.276	2.322	2.330	2.354	2.417	2.550	2.524	2.506	2.534	2.495	2.496	2.501	2.515	2.491
Mn	0.034	0.021	0.021	0.031	0.035	0.056	0.052	0.056	0.049	0.059	0.051	0.053	0.050	0.061
Mg	0.178	0.293	0.257	0.224	0.232	0.124	0.132	0.137	0.129	0.146	0.136	0.146	0.132	0.112
Ca				0.040						0.006				
Ti	0.665	0.513	0.522	0.528	0.521	0.549	0.565	0.565	0.558	0.564	0.558	0.551	0.553	0.563

	AZ1544			AZ1378			AZ1394							
	P462	P198	P546	P548	UC224	UC225	P41	P42	P43	P167	P168	P169	P174	P181
SiO_2	0.37	0.27	0.52	1.08	0.44		0.32	0.50	0.35	0.49	0.40	0.37	0.34	0.36
Al_2O_3	1.46	2.95	4.58	1.84	1.16	1.06	1.22	1.20	0.97	1.08	1.07	1.01	1.46	1.01
Cr_2O_3			0.96	0.14										
FeO	73.97	70.61	69.30	71.96	74.91	75.46	74.11	73.75	73.96	93.15	73.70	72.22	72.07	74.17
MnO	1.91	0.66	0.88	1.62	1.98	2.06		1.87	2.07	2.02	1.96	1.83	1.86	1.91
MgO	1.84	4.05	2.75	1.72	1.42	1.36	1.33	1.14	1.33	1.12	1.14	1.15	1.49	1.19
CaO		0.16	0.18	0.16	0.11	0.27	0.12	0.10	0.19				0.10	
TiO_2	18.66	16.77	15.90	17.54	17.24	17.06	19.11	19.07	18.07	17.49	17.74	18.42	18.38	16.36
TOTAL	98.21	95.47	95.07	96.06	97.26	97.27	96.21	97.63	96.94	95.35	96.01	95.00	95.70	95.00
Recalculated on the basis of 4 O^{2-}														
Si	0.015	0.011	0.021	0.045	0.018		0.013	0.021	0.015	0.021	0.017	0.015	0.014	0.015
Al	0.070	0.141	0.220	0.089	0.057	0.052	0.060	0.058	0.048	0.054	0.053	0.050	0.072	0.051
Cr			0.031	0.005										
Fe	2.515	2.401	2.360	2.483	2.624	2.644	2.592	2.542	2.589	2.589	2.576	2.540	2.506	2.654
Mn	0.066	0.023	0.030	0.057	0.070	0.073		0.065	0.073	0.072	0.069	0.065	0.065	0.069
Mg	0.111	0.246	0.167	0.106	0.088	0.085	0.083	0.070	0.083	0.070	0.071	0.072	0.092	0.076
Ca		0.007	0.008	0.007	0.005	0.012	0.005	0.004	0.009				0.004	
Ti	0.570	0.513	0.487	0.544	0.543	0.538	0.601	0.591	0.569	0.557	0.558	0.582	0.575	0.526

Table A3.3f Sao Miguel magnetite anlayses.

	AZ1394				AZ1024					AZ1149				
	UC110	UC111	UC115/1	UC115/2	P445	P446	P474	P479	P481	P482	P492	P494	P495	P500
SiO_2	0.28	0.63	0.21	0.44	1.27	0.35	0.55	0.76	0.38	0.44	0.39	0.56	0.46	0.66
Al_2O_3	1.29	1.03	1.35	1.21	0.83	0.65	0.72	1.03	4.72	4.90	0.48	0.68	0.45	0.62
FeO	75.53	72.78	74.71	74.05	68.71	69.11	79.14	72.90	68.56	67.80	77.95	79.06	79.32	78.24
MnO	2.07	2.16	2.02	1.86	2.11	2.05	2.22	1.91	0.36	0.47	2.49	2.33	2.37	1.97
MgO	1.53	1.40	1.73	1.43	1.12	0.99	0.39	1.11	5.55	5.62	0.66	0.54	0.38	0.41
CaO		0.34	0.11		0.26									
TiO_2	17.11	17.36	18.34	17.83	22.75	22.97	12.47	19.74	18.35	18.31	12.17	11.14	11.22	12.83
TOTAL	97.81	95.70	98.47	96.82	97.05	96.12	95.49	97.45	97.92	97.54	94.14	94.31	94.20	04.73
Recalculated on the basis of 4 O^{2-}														
Si	0.012	0.027	0.008	0.018	0.050	0.014	0.024	0.031	0.014	0.017	0.017	0.025	0.021	0.029
Al	0.063	0.051	0.065	0.060	0.039	0.031	0.037	0.050	0.215	0.223	0.026	0.036	0.024	0.032
Fe	2.620	2.579	2.554	2.583	2.278	2.351	2.923	2.491	2.213	2.185	2.925	2.978	3.009	2.885
Mn	0.073	0.078	0.070	0.066	0.071	0.071	0.083	0.066	0.012	0.015	0.095	0.089	0.091	0.073
Mg	0.094	0.088	0.105	0.089	0.066	0.060	0.025	0.067	0.319	0.323	0.044	0.037	0.025	0.027
Ca		0.015	0.005		0.011									
Ti	0.534	0.553	0.564	0.559	0.678	0.702	0.414	0.606	0.533	0.531	0.411	0.377	0.383	0.425

	AZ1149	AZ1538
	P524	UC559
SiO_2	0.55	0.27
Al_2O_3	6.14	0.91
FeO	67.51	73.61
MnO	0.55	2.65
MgO	5.07	1.31
TiO_2	18.59	17.78
TOTAL	98.41	96.53
Recalculated on the basis of 4 O^{2-}		
Si	0.021	0.012
Al	0.274	0.045
Fe	2.138	2.591
Mn	0.018	0.094
Mg	0.286	0.082
Ti	0.530	0.563

Table A3.3f continued.

	10SM				AZ1034		AZ1544		AZ1323			AZ1378		AZ1394
	UC501	UC505/1	UC505/2	UC506	UC511/1	UC511/2	UC438	UC440	UC213c	UC213/2	UC213r	UC221/1	UC221/2	P171
SiO_2	0.56	0.18	0.27		0.28	0.35	0.49	0.71	0.38	0.29		0.26	0.29	0.40
Al_2O_3	0.66	0.74	0.80	0.50	0.26	0.36		0.28						
FeO	40.28	42.03	41.80	41.30	42.73	42.11	44.28	43.26	44.43	44.90	45.22	44.15	44.51	44.45
MnO	0.31	0.34	0.30	0.54	0.56	0.67	2.73	1.92	1.86	1.72	1.88	2.16	2.13	2.47
MgO	7.82	7.47	7.32	7.16	4.99	5.15	2.96	2.95	3.35	3.46	3.57	3.05	2.98	2.13
CaO	0.56	0.27	0.42	0.12	0.17	0.28				0.20		0.37	0.46	
TiO_2	49.08	48.28	48.08	49.73	51.66	51.27	45.46	47.39	48.68	49.17	49.61	48.76	48.89	49.08
TOTAL	99.27	99.31	98.99	99.35	100.65	100.19	95.92	96.51	98.70	99.74	100.28	98.75	99.26	98.53
Recalculated on the basis of 3 O^{2-}														
Si	0.014	0.004	0.007		0.007	0.009	0.013	0.018	0.010	0.007		0.007	0.007	0.010
Al	0.019	0.021	0.023	0.014	0.008	0.010		0.009						
Fe	0.823	0.867	0.866	0.843	0.873	0.862	0.979	0.937	0.942	0.940	0.942	0.938	0.945	0.945
Mn	0.006	0.007	0.006	0.011	0.012	0.014	0.061	0.042	0.040	0.037	0.040	0.047	0.046	0.053
Mg	0.285	0.275	0.270	0.261	0.182	0.188	0.117	0.114	0.127	0.129	0.132	0.116	0.113	0.081
Ca	0.015	0.007	0.011	0.003	0.004	0.007				0.005		0.010	0.004	
Ti	0.902	0.896	0.896	0.913	0.949	0.943	0.904	0.923	0.928	0.926	0.929	0.932	0.933	0.938

	AZ1394	
	UC114c	UC114r
SiO_2	0.30	0.71
Al_2O_3		0.24
FeO	45.41	43.87
MnO	2.59	2.60
MgO	1.85	1.85
CaO	0.20	0.30
TiO_2	50.35	48.57
TOTAL	100.70	98.14
Recalculated on the basis of 3 O^{2-}		
Si	0.008	0.018
Al		0.007
Fe	0.953	0.942
Mn	0.055	0.057
Mg	0.069	0.071
Ca	0.005	0.008
Ti	0.950	0.938

Table A3.3g Sao Miguel ilmenite analyses.

	10SM	AZ1034			AZ1538		AZ1394
	UC546	UC515/1	UC515/2	UC512	UC556	UC557	UC565
Fe	37.81	60.22	60.74	60.82	61.99	61.15	61.24
Ni	0.35						
Cu	26.92	0.14		0.14			0.35
S	34.27	38.17	38.89	38.67	38.27	37.56	38.08
TOTAL	99.35	98.53	99.63	99.63	100.26	98.71	99.67

Table A3.3h Sao Miguel sulphide analyses.

Contrib Mineral Petrol (1981) 78:423–432

Contributions to Mineralogy and Petrology

Trachytic Pyroclastics from Agua de Pau Volcano, Sao Miguel, Azores: Evolution of a Magma Body over 4,000 Years

Michael Storey
Department of Geology, Bedford College, Regents Park, London NW1 4NS, England

Abstract. The Recent stratigraphy of Sao Miguel records large numbers of trachytic pyroclastic deposits produced by sub-plinian to plinian eruptions. Tephrochronological studies by Walker and Croasdale (1971) and Booth et al. (1978) have shown that in the last 5,000 years there have been five such eruptions from the caldera of Agua de Pau, one of the three active stratovolcanoes on Sao Miguel.

A geochemical and electron microprobe study made on the resultant pyroclastic succession, revealed significant variations in pumice clast chemistry and mineralogy between the individual deposits: most of these variations show temporal control. For example, Sr and Eu/Eu* decrease in value up through the succession, whereas incompatible elements such as La, Zr and Nb show stepwise enrichment, attaining highest concentrations in the most recent deposit. It is proposed that the five air fall pumice deposits represent successive samples of an evolving trachytic magma body in which fractionation of alkali feldspar has largely controlled the liquid line of descent. This crystal fractionation had resulted in the development of peralkalinity in the melt by the time Fogo D, the second youngest deposit, was erupted.

The presence of some mineralogical and chemical peculiarities suggest that the trachytic melt has been periodically contaminated by less evolved magmas.

Introduction

The Recent stratigraphy of Sao Miguel, the largest of the nine Azores volcanic islands, records large numbers of trachytic pyroclastic deposits produced by sub-plinian to plinian eruptions. Most of these deposits have been erupted from three active Quaternary stratovolcanoes on the island (Fig. 1b).

The origin of alkaline/peralkaline salic rocks on Sao Miguel and other oceanic islands has been mainly attributed to two distinct processes, namely fractional crystallization from a basaltic melt (White et al. 1979) or alternatively by partial melting of a suitable source rock: for example, the mantle. (Yoder 1973) or a plagiogranite layer within the oceanic crust (Sigurdsson 1977).

Previous studies, mainly on composite basaltic/andesitic volcanoes associated with destructive plate margins, have shown that knowledge of the volcanic history of a particular centre facilitates discrimination between processes capable of producing the more evolved volcanic rocks observed at any one volcano. For example, detailed sampling of stratigraphic sections exposed at the composite volcanoes of Santa Maria in Guatemala and Boqueron in El Salvador has respectively allowed Rose et al. (1977) and Fairbrothers et al. (1978) to define the temporal magmatic evolution of each centre. In each case fractional crystallization of a basaltic melt, rather than a partial melting origin, was identified as the process most likely responsible for the formation of the associated andesites.

Detailed field studies on Sao Miguel by Walker and Croasdale (1971) and Booth et al. (1978) have established, by superposition, the relative ages of the five most recent trachytic air fall pumice deposits erupted from the Fogo caldera of Agua de Pau volcano. This work examines the temporal variations in chemistry and mineralogy of this pyroclastic succession with the aim of further understanding the origin of alkaline/peralkaline salic rocks in the oceanic island environment.

Geological Setting

The Azores islands are situated in the Atlantic approximately 1,400 km west of Portugal (Fig. 1a). The islands straddle the Mid-Atlantic Ridge on a topographic high known as the Azores Platform, those islands to the east of the ridge being associated with a seismically active complex transform fracture zone (Laughton and Whitmarsh 1975). Krause and Watkins (1970) had previously interpreted this zone to be a secondary axis of crustal spreading.

Volcanic rocks from the Azores belong to the alkali basalt/trachyte series: compositional differences within and between islands show that the rocks represent a suite in only a broad sense. For example, volcanic rocks from Sao Miguel are more potassic than those from the other Azores islands (Schmincke and Weibel 1972 and White et al. 1979). Also, Hawkesworth et al. (1979) have shown that the $^{87}Sr/^{86}Sr$ ratios of Sao Miguel basalts, increase systematically from the west to the east of the island.

The visible sub-aerial portion of Sao Miguel is composed almost entirely of basaltic and trachytic rocks which occur in approximately equal amounts. There are few rocks of intermediate composition. Possible explanations for the compositional gap are summarised by White et al. (1979). Sao Miguel has three active Quaternary stratovolcanoes, Sete Cidades, Agua de Pau and Furnas (Fig. 1b). Each possesses a central caldera and a long record of explosive volcanic eruptions. The resulting trachytic pumice fall deposits thickly mantle the slopes of the volcanoes and account for more than half their visible bulk. The volume of each of the volcanoes above sea level is of the order of 70 km^3. Rocks as old as 4.0 m.y. (Abdel-Monem et al. 1975) occur at the eastern end of the island and are associated with a fourth volcano, Povoacao, which is believed to be long extinct. Although the majority of trachytic rocks occur as air fall pumice deposits, there are examples of lavas, extrusive domes and ignimbrites.

0010-7999/81/0078/0423 $02.00

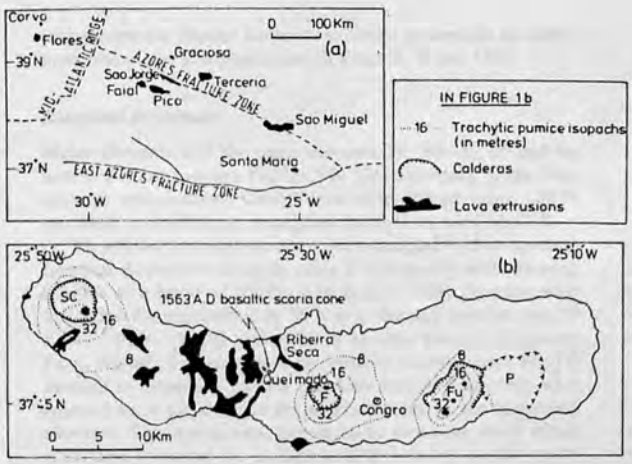

Fig. 1. *a* The Azores archipelago. *Dashed line* indicates active plate boundary (after Laughton and Whitmarsh 1975). Azores fracture zone (after Flower et al. 1976). *b* Map of Sao Miguel showing isopachs for the total thickness of trachytic pumice deposits formed in the past 5,000 years; simplified after Booth et al. (1978). Also shown, in *solid black*, are trachyte and basalt lava extrusions formed during the same period: the former are found only in the calderas and the Congro crater. Caldera: *SC*, Sete Cidades; *F*, Fogo; *Fu*, Furnas; *P*, Povoacao

Basaltic rocks, which form lavas, scoria cones and off-shore ash rings, have been erupted from parasitic vents on the flanks of the stratovolcanoes and from a fissure zone situated in the low lying tract of land that separates the volcanoes Sete Cidades and Agua de Pau. Since a large, caldera-producing, plinian eruption from Agua de Pau approximately 4550 B.P. (Walker and Croasdale 1971), basaltic eruptions have been restricted to a fairly narrow WNW-ESE zone in the west of the island. As a means of explaining the paucity of basaltic eruptions over the rest of the island during this period, Booth et al. (1978) suggested that a large body of trachytic magma had spread out laterally between Agua de Pau and Furnas volcanoes following the plinian eruption, thereby restricting the ability of basaltic magma to reach the surface. The existence of a salic magma body below this area has also been postulated by Machado (1966, 1973) from geophysical evidence.

The rate of production of all types of volcanic rock on Sao Miguel over the past 5,000 years, has been calculated as 0.09 km^3 dense rock equivalent (d.r.e.) per century. This figure, which is believed to be typical of the past 50,000 years, is much lower in comparison to most other volcanoes for which the output is known (Booth et al. 1978). This calculated output suggest that the exposed parts of the volcanoes could have accumulated in about 150,000 years.

Tephrochronology of Agua de Pau Volcano

Agua de Pau has a large central crater, the Fogo caldera, which is believed to be a collapse structure attributed to a large plinian eruption (Walker and Croasdale 1971). The air fall pumice deposit produced, Fogo A, was named after the caldera. It has been dated at 4550 B.P. by ^{14}C measurements on carbonised wood fragments associated with the deposit (Shotton et al. 1968, 1969) and forms the base for the study of 5,000 years of volcanism on Sao Miguel by Booth et al. (1978). It was shown by these authors that since Fogo A, a further four trachytic air fall pumice deposits were erupted from the caldera, the last being the historic explosive eruption of 1563 A.D. These subsequent deposits were designated as Fogo B, C, D, and 1563, indicating the order in which they occured. Samples collected from these five deposits form the main basis of the present study. Their succession, volume and age, where known, are given in Table 1.

Table 1. Volumes and ages of the Fogo pumice deposits

Deposit	Age (years)	Juvenile Volume d.r.e. (km^3)
Fogo 1563	A.D. 1563	0.14
Fogo D, C	–	0.05
Fogo B	3242 B.P.	0.14
Fogo A	4550 B.P.	0.55

Volume data from Booth et al. (1978)
Radiocarbon dates from Shotton, Blundell and Williams (1968, 1969, 1970)

Fogo A bears special mention as the pumice clasts show marked changes in colour and physical characteristics through the deposit. The deposit grades upwards from the typical buff coloured pumice into first a streaky and then a more dense mafic variety of pumice, the latter two types being volumetrically subordinate to the first. The explosive 1563 A.D. eruption from the Fogo caldera is also of interest as it was shortly followed by the extrusion of two small basaltic flows from a scoria cone on the north-west flanks of Agua de Pau volcano near Queimado (Fig. 1b).

Syenite nodules, with chemical compositions similar to the trachytes, occur in Fogo A and 1563. These have been described by Cann (1967) and Schmincke (1973).

Mineralogy

Pumice clasts from the Fogo trachytic air fall deposits, are generally glassy to cryptocrystalline, with crystal contents not usually exceeding 10% by volume. Some relative modal abundances are given by Schmincke and Weibel (1972). The phenocryst assemblage consists predominantly of alkali feldspar with ubtiquitous but minor clinopyroxene, biotite and Fe-Ti oxides. Accessory phases include microphenocrysts of apatite which most frequently occur as inclusions in other minerals. Also present are rare crystals of zircon which have only been found in Fogo 1563.

Occurring in several of the air fall pumice deposits, are a number of crystals showing disequilibrium textures with the enclosing glass. Forsteritic olivine (Fo_{78}–Fo_{80}), for example, occurs in Fogo A and B and shows a clear reaction relationship

with the matrix. Similar textures are shown by crystals of aluminous titanaugite and plagioclase in Fogo A, B and 1563.

Analytical Procedure

Major elements and the trace elements Zr, Nb, Y, Sr and Ba were determined using a Phillips PW 1212 automatic X-ray fluorescence spectrometer. Calibrations were erected using USGS standards and full mass absorption corrections were applied.

Th and the rare earth elements were analysed by Instrumental Neutron Activation Analysis using a high-purity multi-element solution as a standard (Borley and Rogers 1979). Samples were irradiated for approximately 30 h in a thermal neutron flux of 1×10^{12} n cm^{-2} in the University of London Reactor at Silwood Park, Ascot. The samples were initially counted on a Ge(Li) detector to determine La and Lu. After further decay they were counted on a Ge detector for determination of the remaining elements. The counts were integrated to give peak areas which were then corrected for background, interfering nuclide peaks and radioactive decay.

Mineral analyses were by a microprobe constructed by Dr. J. Long of the Department of Earth Sciences, University of Cambridge, UK. The acceleration voltage applied was 20 kv, the nominal beam current 50 nA and the counting period 80 seconds live time. Peaks were processed and measured by iterative peak stripping (Statham 1976) and the compositions were estimated using ZAF correction procedures by Sweatman and Long (1969).

Mineral Chemistry

Feldspars

Euhedral phenocrysts of alkali feldspar are volumetrically the most important mineral in the Fogo pumice deposits. Microprobe analyses show they are calcium bearing sanidines, with individual crystals showing limited compositional variation. Selected analyses are given in Table 2. Zoning, when present, can be one of two types: crystals become either more sodic from core to rim, or conversely they become more potassic from core to rim. An example of the latter type of zoning is shown by crystals from Fogo B. This may be seen in Fig. 2 where sanidines from the Fogo deposits are plotted in part of the An–Ab–Or triangle. Although there is compositional overlap between sanidine crystals from the different air fall pumice deposits, a general trend emerges consisting of a decrease in the anorthite and orthoclase components of crystals from successively younger deposits. Also shown, on the Ab–Or join, is the mol. Na_2O/Na_2O+K_2O ratio for the whole pumice clast for each of the Fogo air fall deposits. It is evident that the increasing albite component of sanidine crystals up through the pyroclastic succession, is mirrored by an increase in the mol. Na_2O/Na_2O+K_2O ratio of the whole pumice clast. In the system $NaAlSi_3O_8$–$KAlSi_3O_8$–H_2O both the feldspars and the whole pumice clast fall on the potassium feldspar side of the thermal minimum on the Ab–Or join (Bowen and Tuttle 1950). As the Na/K ratio is lower for feldspar than the host pumice clast, then crystal fractionation would result in both the feldspar and liquid becoming more sodic with differentiation.

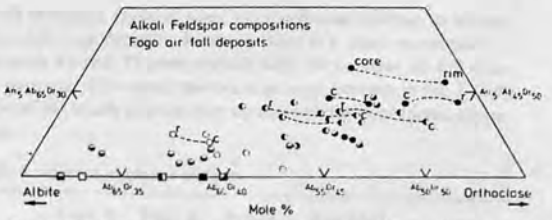

Fig. 2. Alkali feldspar compositions from the different Fogo pumice deposits plotted in part of the An–Ab–Or triangle. Symbols: ◕ Fogo A, ● Fogo B, ◑ Fogo C, ○ Fogo D, ◒ Fogo 1563. Also shown, on the Ab–Or join, is the mol. Na_2O/Na_2O+K_2O ratio for the host pumice clasts *(square symbols)*

Lastly it should be mentioned that rarer crystals of plagioclase occur in some of the air fall deposits. These crystals generally have resorbing margins while their compositions also suggest that they were unlikely to have been in equilibrium with a trachy-

Table 2. Selected feldspar analyses

	Fogo A			Fogo B				Fogo C		Fogo D		Fogo 1563		
Sa. No.	P427	P455(c)	P455(r)	P530(c)	P530(r)	P536(c)	P536(r)	P410(c)	P410(r)	P450(c)	P450(r)	P502	P525(c)	P525(r)
SiO_2	65.59	66.78	65.95	66.15	65.82	64.51	65.28	67.08	66.81	66.82	66.03	66.92	67.15	67.78
Al_2O_3	19.51	19.07	18.69	19.52	19.11	19.72	19.46	19.38	19.60	19.07	19.16	19.18	19.04	18.96
FeO	0.23	–	0.16	0.22	0.14	0.26	0.15	0.18	0.27	0.19	0.18	0.25	0.18	0.19
CaO	0.95	0.51	0.39	0.94	0.86	1.30	1.14	0.72	0.90	0.42	0.53	0.35	0.34	0.21
Na_2O	5.73	6.03	5.84	5.98	5.73	5.65	5.28	6.07	6.68	6.87	7.20	7.45	6.78	7.20
K_2O	7.81	7.59	7.72	7.45	7.80	7.33	8.34	7.68	6.91	6.72	6.50	5.65	6.61	6.96
Total	99.82	99.98	98.75	100.26	99.46	98.77	99.65	101.11	101.17	100.09	99.60	99.80	100.10	101.30
Recalculated on the basis of 8 O^{2-}														
Si	2.957	2.993	2.996	2.964	2.975	2.934	2.952	2.979	2.964	2.988	2.971	2.988	2.997	2.997
Al	1.037	1.007	1.001	1.031	1.018	1.057	1.037	1.015	1.025	1.005	1.016	1.009	1.002	0.989
Fe^{2+}	0.009	–	0.006	0.008	0.005	0.010	0.006	0.006	0.010	0.007	0.007	0.009	0.007	0.007
Ca	0.046	0.024	0.019	0.045	0.041	0.063	0.055	0.034	0.043	0.020	0.025	0.017	0.016	0.010
Na	0.501	0.524	0.514	0.519	0.502	0.498	0.462	0.522	0.575	0.596	0.628	0.645	0.586	0.617
K	0.449	0.434	0.448	0.426	0.450	0.425	0.481	0.435	0.391	0.383	0.373	0.322	0.376	0.393

(c) = crystal core
(r) = crystal rim

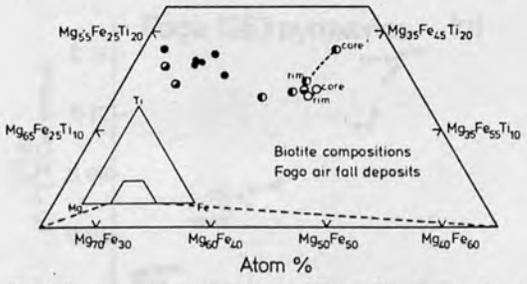

Fig. 3. Biotite compositions from the different Fogo pumice deposits plotted in terms of their Ti, Mg and Fe contents. Symbols as Fig. 2

tic melt. For example, in Fogo 1563 are calcium-rich plagioclase crystals ranging in composition up to An_{63} (authors data).

Biotites

Euhedral pleochroic phenocrysts of biotite occur in all five of the Fogo air fall pumice deposits. Apart from a near opaque crystal in Fogo 1563 the biotites show no sign of oxidation. Listed in Table 3 are selected analyses showing the compositional range for the different air fall deposits. The biotites are notable for their high Ti content, containing up to 9.5 wt.% TiO_2. On the basis of 22 oxygen atoms in the formula unit, the sum of Al and Si is less than the eight required for the tetrahedral position. This cation deficiency could presumably be filled by Ti or Fe^{3+}.

The temporal variation of biotite compositions is shown in Fig.3 by a triangular plot of Ti, Mg and Fe. As with coexisting alkali feldspars, there is some compositional overlap in biotites from different deposits, however there is a clear association of the more Fe-rich/Ti-poor crystals with the younger air fall pumice deposits. This trend mirrors a general increase in the Fe/Mg ratio of the whole pumice clast up through the pyroclastic succession.

Table 4. Selected pyroxene analyses

	Fogo A	Fogo B	Fogo C	Fogo1563		
Sa. No.	P434	P534	P415	P231	P517	P522
SiO_2	52.97	52.30	52.64	51.45	42.03	49.36
Al_2O_3	0.96	0.70	0.76	0.90	10.25	4.89
FeO [a]	9.26	10.24	12.34	15.05	9.08	8.51
MgO	13.01	11.94	11.00	8.47	10.62	13.74
CaO	21.72	21.95	21.96	20.34	21.97	21.16
Na_2O	–	0.53	0.45	1.39	–	–
TiO_2	0.57	0.49	0.49	0.40	5.64	2.22
MnO	0.76	0.85	0.98	1.70	–	–
Total	99.25	99.00	100.62	99.70	99.59	99.88
Recalculated on the basis of 6 O^{2-}						
Si	1.992	1.988	1.986	1.992	1.596	1.840
Al	0.043	0.031	0.034	0.041	0.459	0.215
Fe^{2+}	0.291	0.325	0.389	0.486	0.288	0.265
Mg	0.729	0.677	0.619	0.487	0.601	0.763
Ca	0.875	0.894	0.888	0.844	0.894	0.845
Na	–	0.039	0.033	0.104	–	–
Ti	0.016	0.014	0.014	0.012	0.161	0.062
Mn	0.024	0.027	0.031	0.056	–	–

[a] All Fe as FeO

Table 3. Selected biotite analyses

	Fogo A	Fogo B		Fogo C		Fogo D		Fogo 1563
Sa. No.	P432	P195	P207	P44	P404	P443	P444	P523
SiO_2	37.44	38.34	36.94	36.32	37.54	36.54	38.58	38.97
Al_2O_3	13.09	14.12	13.26	13.45	12.70	12.11	12.43	14.93
FeO[a]	12.60	12.59	15.11	19.07	17.39	18.89	19.18	15.36
MgO	14.12	14.30	12.99	10.25	12.42	11.10	11.55	9.46
CaO	0.09	–	–	–	–	–	–	1.36
Na_2O	0.74	0.44	0.38	0.44	0.45	0.73	0.92	1.13
K_2O	8.63	8.74	8.73	8.66	8.65	8.42	8.63	7.84
TiO_2	8.25	9.41	7.78	9.16	6.68	7.00	6.78	5.76
MnO	0.18	0.15	0.25	0.37	0.37	0.28	0.40	0.19
CoO	0.16	0.16	0.21	–	0.21	0.13	0.21	–
Total	95.30	98.25	95.65	97.72	96.41	95.20	98.68	95.00
Recalculated on the basis of 22 O^{2-}								
Si	5.542	5.481	5.516	5.410	5.615	5.590	5.677	5.801
Al	2.285	2.379	2.334	2.362	2.239	2.185	2.157	2.620
Fe	1.560	1.505	1.887	2.375	2.176	2.417	2.360	1.912
Mg	3.114	3.047	2.891	2.275	2.770	2.532	2.533	2.099
Ca	0.014	–	–	–	–	–	–	0.217
Na	0.211	0.123	0.111	0.128	0.129	0.217	0.262	0.326
K	1.631	1.594	1.662	1.645	1.650	1.643	1.621	1.488
Ti	0.919	1.012	0.874	1.026	0.751	0.805	0.751	0.645
Mn	0.022	0.018	0.031	0.046	0.047	0.036	0.049	0.024
Co	0.019	0.018	0.025	–	0.025	0.016	0.025	–

[a] All Fe as FeO

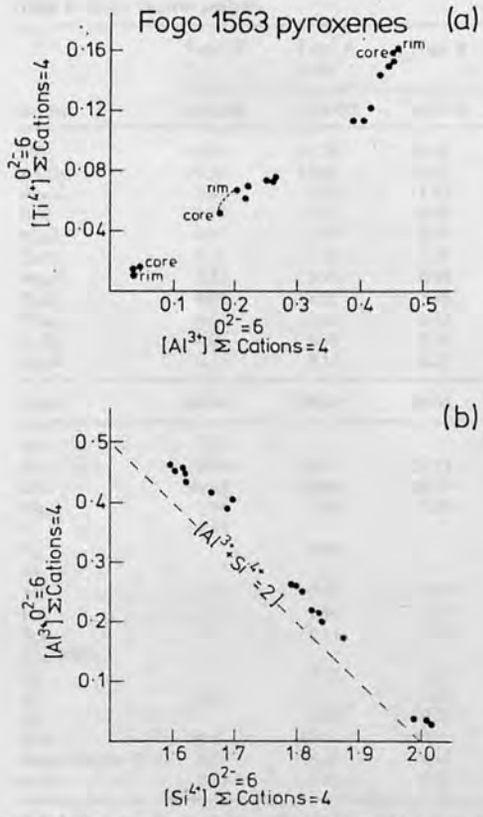

Fig. 4 a, b. Pyroxene compositions from Fogo 1563 in terms of (*a*) Al and Ti. (*b*) Si and Al

Clinopyroxenes

Commonly, the clinopyroxene present in the Fogo pumice deposits, is a green low Al-Ti variety. Selected analyses (Table 4) show that clinopyroxenes associated with the youngest air fall pumice deposits have the highest Fe/Mg ratios. Also present, notably in Fogo 1563, are purple aluminous titanaugites containing up to 10 wt.% Al_2O_3. In Fogo 1563 three types of clinopyroxenes are compositionally distinct in terms of Al, Si and Ti contents (Fig. 4). Pyroxenes with the least evolved compositions commonly show a reaction relationship with the pumice glass. In the plot of Al against Si, the pyroxenes plot above the line $Z=2$ indicating that some of the Al is in octahedral co-ordination.

Major Elements

Major element analyses and the normative mineralogies of the Fogo air fall pumice deposits are given in Table 5. To overcome the variable post-eruptive hydration and oxidation of the pumice glasses, and thereby facilitate comparison between the deposits, the analyses have been recalculated to 100% totals on a volatile free basis. Also, the normative mineralogies have been calculated using a constant FeO/Fe_2O_3 ratio of 1.36, which was the highest value measured in any of the deposits. Only whole pumice clasts were analysed so as to avoid recording geochemical features resulting from crystal fractionation processes which occur during the actual pyroclastic producing eruption (Walker 1972). Care was also taken to select only fresh samples for analysis in order to minimise any deviation from the actual magma composition due to post eruptive leaching of alkali elements, a process to which volcanic glasses are particularly prone. The only suspected case of significant leaching of the alkali elements in the samples studied, is AZ1544 which contains normative corundum.

Classification

The analysed Fogo air fall pumice deposits are all trachytic with Thornton-Tuttle differentiation indicies >75 (Thornton and Tuttle 1960). Their compositions are transitional in two respects. Firstly they straddle the silica saturation/undersaturation boundary being either nepheline or quartz and/or hypersthene normative. Secondly they range between being metaluminous to mildly peralkaline. The latter fall into the comenditic trachyte field in the classification scheme devised for peralkaline rocks by Macdonald and Bailey (1973).

Compositional Heterogeneity of Individual Deposits

To assess the significance of compositional variations between the different air fall pumice deposits it was first necessary to study the compositional range in a single deposit. This was achieved by analysing samples from the upper and lower parts of Fogo A for major and trace elements. Fogo A was chosen because firstly it has been recognised as a mixed pumice deposit (Walker and Croasdale 1971) and secondly because it is by far the most voluminous of the air fall deposits studied here. Major element analyses (Table 5) showed that the dark coloured pumice of the uppermost layer was marginally less evolved, containing higher CaO and MgO than the underlying buff coloured pumice, which forms the bulk of the deposit. With the exception of Zr, the difference in incompatible trace elements was small and not considered to be significant. The top of Fogo A however, contained about twice the Sr and Ba content of the underlying part of the deposit (Table 6).

Schmincke and Weibel (1972) give whole rock analyses of samples taken along vertical profiles across two welded trachytic ignimbrites from Sao Miguel: however no significant chemical zonation was observed. Schmincke and Weibel concluded that the probable reason for the lack of compositional variation was the small volume of the deposits (probably $<0.1\ km^3$). In comparison Fogo A has a juvenile volume of $0.55\ km^3$ d.r.e. The other analysed Fogo air fall deposits have relatively small volumes in comparison to Fogo A and present data suggest they show little variation in composition within individual deposits.

Temporal Variation of Major Elements

Variations in major element concentrations up through the Fogo air fall pumice deposit succession, are systematic for most elements. CaO, MgO, Al_2O_3, TiO_2 and P_2O_5 decrease whilst SiO_2 and MnO increase. The $FeO+Fe_2O_3/MgO$ and Na_2O/Na_2O+K_2O ratios increase to maximum values in the youngest deposits mirroring similar variations in the normative mineralogy (Table 5) and in the mineral chemistry of coexisting biotites, clinopyroxenes and alkali feldspars. Lastly, the agpaitic index (mol Na_2O+K_2O/Al_2O_3) varies between 0.81 and 1.09. The older deposits are metaluminous whereas the two youngest deposits, Fogo D and Fogo 1563, are both mildly peralkaline, this latter condition being manifested by the presence of acmite and sodium silicate in the norm.

Table 5. Major element analyses

	Fogo A	Fogo A (top)	Fogo B	Fogo C	Fogo D	Fogo 1563
Sa. No.	AZ1544	AZ1377	AZ1378	AZ1394	AZ1188	AZ1149
SiO_2	63.06	61.74	62.23	63.22	65.13	64.83
Al_2O_3	19.26	17.60	18.17	18.78	16.49	16.96
Fe_2O_3	1.47	1.67	1.62	1.40	1.92	1.39
FeO	1.99	2.28	2.23	1.91	2.62	1.89
MgO	0.47	1.14	0.96	0.33	0.22	0.27
CaO	1.31	2.18	1.70	0.98	0.64	0.85
Na_2O	5.51	5.97	6.00	6.68	7.00	7.61
K_2O	6.08	6.07	5.88	5.89	5.28	5.46
TiO_2	0.64	1.02	0.92	0.58	0.33	0.45
P_2O_5	0.08	0.19	0.14	0.08	0.08	0.07
MnO	0.13	0.14	0.15	0.15	0.29	0.22
Total	100.00	100.00	100.00	100.00	100.00	100.00
Q	3.72				2.28	
Or	35.93	35.87	34.75	34.81	31.20	32.26
Ab	46.62	48.69	50.77	55.16	55.42	56.84
An	5.98	3.30	5.28	3.86		
C	1.43					
Ne		0.99		0.74		
Ac					3.36	4.02
Mt	2.13	2.42	2.35	2.03	1.10	
Il	1.22	1.94	1.75	1.10	0.63	0.85
Ap	0.18	0.44	0.32	0.19	0.19	0.16
Na_2OSiO_2						0.70
Di		5.08	1.83	0.40	2.32	3.26
Hy	2.80		2.80		3.51	1.23
Ol		1.28	0.16	1.71		0.68
D.I. [a]	86.3	85.5	85.5	90.7	88.9	89.1
Na_2O/Na_2O+K_2O	0.58	0.60	0.61	0.63	0.67	0.68
A.I.[b]	0.81	0.93	0.89	0.92	1.04	1.09

[a] D.I. Thornton-Tuttle differentiation index [b] A.I. Agpaitic index

Table 6. Trace element analyses (ppm)

	Fogo A	Fogo A (top)	Fogo B	Fogo C	Fogo D	Fogo 1563
Sa. No.	AZ1544	AZ1377	AZ1378	AZ1394	AZ1188	AZ1149
La	74.4	80.7	112.7	136.2	189.7	197.1
Ce	150.6	172.8	230.8	290.6	439.9	362.3
Nd	55.3	58.8	87.1	99.8	151.0	129.7
Sm	11.8	12.0	16.7	17.5	30.1	27.3
Eu	1.90	2.43	1.69	1.16	0.39	0.62
Tb	1.2	1.3	1.9	2.1	3.1	2.7
Yb	3.3	3.6	5.4	6.1	9.8	8.1
Lu	0.49	0.49	0.65	0.87	1.19	1.13
Y	36	37	53	67	107	100
Zr	867	681	974	1.274	1.779	1.906
Nb	121	118	176	222	339	442
Th	15.9	15.2	23.5	34.3	41.3	48.0
Rb	117	132	160	189	281	348
Sr	115	278	115	14	6	14
Ba	396	616	343	267	365	410
Eu/Eu*	0.60	0.72	0.35	0.19	0.05	0.08
K/Rb	432	382	305	259	156	130
Rb/Sr	1.0	0.5	1.4	13.5	46.8	24.9
Zr/Nb	7.2	5.8	5.5	5.7	5.3	4.3
Nb/Y	3.4	3.2	3.3	3.3	3.2	4.4
La_N/Yb_N	15.2	15.1	14.1	15.1	13.1	16.4
La_N/Sm_N	4.1	4.2	4.3	3.8	4.0	4.5

Trace Elements

Rare Earth Elements (REE)

Chondrite normalised REE abundances for the Fogo deposits, are shown in Fig. 5. Trace element concentrations for the Fogo air fall pumice deposits, are given in Table 6. The geometry of the REE patterns exhibit several noteworthy features:

(1) The patterns are essentially parallel, all being equally light REE enriched. Fogo 1563 partly deviates from this general feature because of its higher La_N/Sm_N ratio which results in a crossover of its REE pattern with that of Fogo D.

(2) All the deposits have negative Eu anomalies, Eu/Eu* ranging between 0.72 for Fogo A and 0.05 for Fogo D; Eu/Eu* varies inversely to the abundance of the other REE.

(3) The REE patterns are concave upwards. Although these patterns are similar to those of basalts from Agua de Pau, in that the latter are likewise light REE enriched, they differ in that the patterns of the basalts are linear. This is illustrated in Fig. 6 where the chondrite normalised REE pattern of a basalt flow originating on the southern flanks of Agua de Pau is shown alongside the REE pattern of the trachytic air fall pumice deposit Fogo A – their respective differentiation indices are 19.2 and 86.3.

Th, Zr, Nb, Y, Rb

With the exception of data points for Fogo 1563, biaxial plots of the incompatible elements Th, Zr and Y against Nb define approximately linear trends which pass near to or through the origin (Fig. 7). A plot between Rb and Nb gives a linear trend, however the best fit line fails to pass through the origin, intersecting instead the Rb axis (Fig. 7d). The form of these variations, coupled with the fact that the concentrations of Sr and Eu vary in inverse proportion to the abundance of incompatible elements, indicates alkali feldspar fractionation (Table 6). However, as previously suggested some mineralogical and chemical features of Fogo 1563 are not consistent with this hypothesis. For example, the lower Zr/Nb ratio of this deposit could be explained by limited zircon fractionation: indeed Fogo 1563 is the only deposit studied in which this phase has been identified. However fractional crystallization of the observed phenocryst phases cannot readily account for the failure of this deposit to plot on the simple fractionation lines defined by biaxial plots of the other incompatible elements. This discrepency suggests, in addition to fractional crystallization, the operation of magma mixing and/or other processes in the trachytic melt that gave rise to Fogo 1563.

Temporal Variation of Trace Elements

The variation of Zr and the K/Rb ratio up through the Fogo air fall pumice deposit succession are shown in Fig. 8. The concentration of Zr, which may be taken as an index of fractionation due to its incompatible nature, increases in a stepwise manner while the K/Rb ratio decreases in a likewise style. Similarly La, Th, Nb and Rb increase in concentration in successively younger deposits attaining maxima in Fogo 1563. Y and Ce–Lu, excluding Eu, attain maxima in Fogo D (Table 6). Eu and Sr, elements sensitive to feldspar fractionation, decrease in concentration from Fogo A to minima in Fogo D; the decrease in Sr up through the succession, is reflected by a rapid increase in the Rb/Sr ratio from 0.5 to 47. Surprisingly, Ba, which is also sensitive to alkali feldspar fractionation, fails to show any systematic temporal variation in concentration.

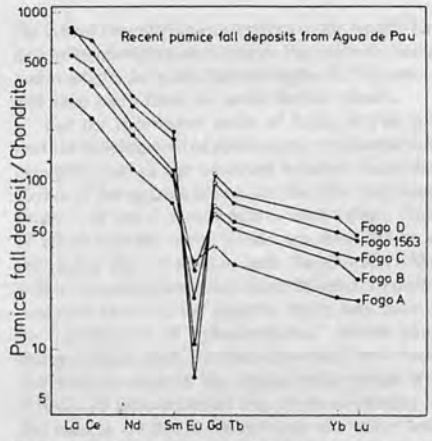

Fig. 5. Chondrite normalised REE abundances for the Fogo air fall pumice deposits. Chondrite data from Evensen et al. (1978)

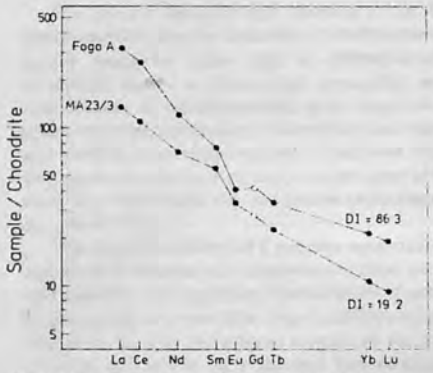

Fig. 6. Comparison of chondrite normalised REE patterns of a basalt (*MA/23*) and trachyte (*Fogo A*) from Agua de Pau volcano. *DI*, Thornton-Tuttle differentiation index

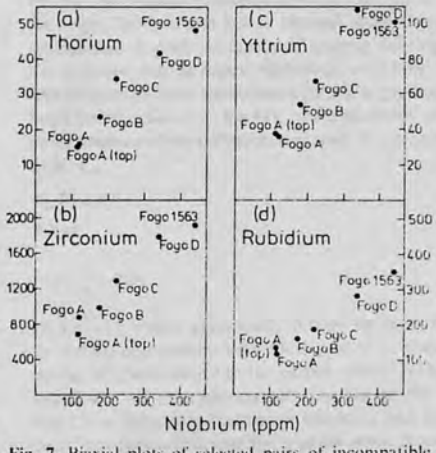

Fig. 7. Biaxial plots of selected pairs of incompatible elements. All values in ppm

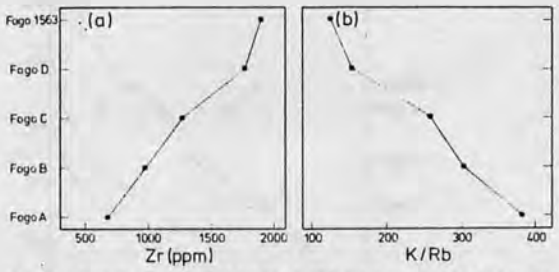

Fig. 8. *a* Variation of Zr and (*b*) the K/Rb ratio up through the Fogo pyroclastic succession

Discussion

Most of the observed chemical and mineralogical variations in the trachytic pyroclastic deposits studied here have been shown to be stratigraphically controlled. This is a strong indication that the deposits are cogenetic, as might be expected from their close spatial and temporal association.

Noteworthy trends up through the succession are:

(i) The rapid depletion of Sr and Eu, whereas incompatible elements such as Zr, Nb, Th, Y and the rare earths show stepwise enrichment.

(ii) A decrease in the K/Rb ratio.

(iii) An increase in the agpaitic index, the two youngest deposits being mildly peralkaline.

(iv) The Na/K ratio of pumice clast increases along with the albite content of the co-existing alkali feldspar. The pumice clast always has a higher Na/K ratio than the associated alkali feldspar.

(v) An increase in the Fe/Mg ratio of pumice clast and coexisting biotite and clinopyroxene.

The enrichment and the form of the covariation of incompatible elements, the extreme depletion of Sr and Eu, elements with high crystal/liquid partition coefficients for feldspar, the decrease in the K/Rb ratio, the failure of Rb to behave as a highly incompatible element, and the fact that successively younger deposits have liquid and alkali feldspar compositions nearer that of the low pressure minimum liquidus temperature on the Ab–Or join, are features consistent with the air fall pumice deposits being related by fractional crystallization in which alkali feldspar plays a dominant role. Self and Gunn (1976) demonstrate a similar relationship for the peralkaline salic rocks of Terceria, showing that they define a trend in the system $SiO_2-Al_2O_3-Na_2O+K_2O$ that indicates compositional control by alkali feldspar fractionation. If significant amounts of high level crystal fractionation has taken place beneath Agua de Pau volcano, then this readily provides an explanation for the origin of the peralkaline deposits observed in the upper part of the Fogo pyroclastic succession.

Based partly on evidence from Icelandic trondhjemite and quartz diorite xenoliths, Sigurdsson (1977) suggests that peralkaline melts from Iceland and the Azores, may be the result of partial fusion of a plagiogranite layer in the oceanic crust which leaves behind a "peraluminous" refractory assemblage, containing cordierite and mullite. However, White et al. (1979) prefer a fractional crystallization origin for the peralkaline salic melts of the Azores, arguing that this hypothesis best explains the observed trace element variations. They also point out that chemical features, such as the degree of light REE enrichment, which distinguishes basaltic rocks from the different Azores islands, also distinguishes the more evolved rocks, implying that in the latter the salient chemical characteristics of the basalts have been inherited by fractional crystallization. For example Sao Miguel basalts and trachytes have similiar but higher K/Na ratios than do basic and salic rocks from the other Azores islands.

For the peralkaline rocks of Agua de Pau it can be shown that the development of peralkalinity is consistent with fractional crystallization of the observed mineral assemblage of the trachytes. If the agpaitic indices for the older metaluminous deposits Fogo A, B and C represent true melt values, then fractionation of alkali feldspar alone would not have led to an increase in this index due to similar mol. Na_2O+K_2O/Al_2O_3 ratios for pumice clast and coexisting alkali feldspar. In melts of these compositions however, the agpaitic index may have been increased by fractionation of "peraluminous" biotite and/or aluminous clinopyroxene. Such fractionation would have eventually evolved the trachytic melt to the critical point where its mol. Na_2O+K_2O/Al_2O ratio exceeded that of its co-existing alkali feldspar; this ratio is <1 due to the presence of a minor anorthite component. Once the melt exceeded this value, fractionation of alkali feldspar, the principal phenocryst phase, would have acted in unison with biotite and clinopyroxene in rapidly driving the melt towards the peralkaline condition witnessed in Fogo D and 1563.

The concave upwards REE patterns of the Fogo trachytic pumice deposits may be explained by fractionation of amphibole and/or apatite at some stage in differentiation. Kaersutitic amphibole occurs as phenocrysts possessing opaque reaction rims in some of the intermediate lavas from Sao Miguel, while apatite microphenocrysts are observed in both intermediate lavas and trachytic lavas and pyroclastics. Measured crystal/melt partition coefficients for granitic melts, summarized in Hanson (1978), shows that both amphibole and apatite preferentially incorporate the middle REE.

The parallelism of the REE patterns suggests firstly the co-precipitation of feldspar and clinopyroxene from the trachytic melt, and secondly that significant fractionation of amphibole and/or apatite ceased at a previous stage in differentiation. This is supported by the low phosphorus content of the trachytic air fall deposits, and also by their apparent lack of amphibole and the presence of only minor amounts of apatite. It would appear likely that the concave REE patterns of the trachytic pumices are a legacy from some intermediate parental magma.

Allègre and Minster (1978) conclude that the physical properties of a crystallizing magma chamber are those for which the Rayleigh fractionation law is obeyed. Accordingly, a fractional crystallization model as means of relating the Fogo air fall pumice deposits, can be more rigorously tested by comparing observed trace element variations with those predicted by the Rayleigh fractionation law, Eq. (1), which describes the trace element concentration of the differentiated melt, C_L, relative to the parent melt, C_0:

$$C_L/C_0 = F^{(D-1)} \tag{1}$$

Where

$$D = \sum_{i}^{n} X^i K d^i \tag{2}$$

In Eq. (1), which specifically relates to crystals that are only in surface equilibrium with the liquid, F is the weight fraction of the melt left relative to the parent, and D is the bulk partition coefficient for minerals crystallizing out of the melt where X^i, Eq. (2), is the weight fraction of mineral i and Kd^i is its mineral melt partition coefficient for a given trace element. In the case of Ba, Sr and Eu for the Fogo deposits, their bulk partition coefficients approximate to their respective Kd values for alkali

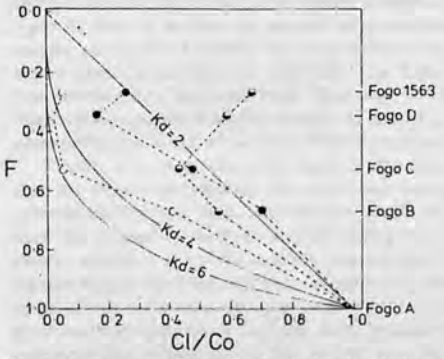

Fig. 9. Comparison of actual and calculated variation of Sr, Eu and Ba up through the Fogo pyroclastic succession. Fogo A taken as parental melt; see text for detailed explanation. Symbols: ○ Sr, ● Eu, ◒ Ba. F equals weight fraction of melt remaining relative to parent and C_L/C_0 equals the concentration of the trace element of the differentiated melt, C_L, relative to the parent melt, C_0

feldspar. This is because the modal proportion of alkali feldspar is approximately 80% or more of the total phenocryst content and also because these elements have high crystal/melt partition coefficients for alkali feldspar (Hanson 1978). For highly incompatible elements, the bulk partition coefficient approaches zero and the enrichment of the element relative to the parental melt varies inversely with the amount of the melt remaining, F.

In Fig. 9 both observed and calculated values of C_L/C_0 for Eu, Sr and Ba are plotted against F; alkali feldspar/melt partition coefficients for Eu, Sr and Ba are taken to be 2, 4 and 6 respectively. Nb, because its incompatible behaviour approximates to a $1/F$ relationship, is used to estimate the amount of melt remaining. The top, more mafic, part of the Fogo A deposit has been assumed to be parental to the subsequent Fogo air fall pumice deposits. If fractional crystallization in a closed system is assumed to operate, then $CNb_{Fogo\ A}/CNb_{Fogo\ 1563}$ indicates that approximately 30% of the original melt volume was remaining prior to the eruption of Fogo 1563. It can also be seen that both Sr and Eu show reasonable agreement with expected rates of removal by alkali feldspar fractionation, although both elements show slight increases in concentration in Fogo 1563. The behaviour of Ba is anomalous, its variation through the succession being small and non-systematic. This is unexpected because published partition coefficients (Hanson 1978) suggest that Ba is highly compatible with alkali feldspar.

The variation of Ba in the alkali-basalt/trachyte series, for example Reunion Island in the Indian Ocean (Zielinski 1975), the Azores (White et al. 1979) is such that it usually attains highest concentrations in the intermediate rocks, only becoming depleted when alkali feldspar or biotite are crystallizing phases. Conversely, removal of Eu^{2+} and Sr, mainly by plagioclase fractionation, tends to begin at an earlier stage in differentiation. It is therefore possible that the non-systematic variation of Ba might reflect contamination of the trachytic magma by material of intermediate composition. Magma mixing also provides a possible explanation for the presence of xenocrysts of forsteritic olivine, aluminous titanaugite and anorthite-rich plagioclase in some of the Fogo pumice deposits. Measured Fe^{2+}/Mg ratios for Fogo A average near 1.5, a value almost twice as high as that predicted for a melt in equilibrium with the olivines of composition Fo_{80} that are found in this deposit (Roeder and Emslie 1970). The contemporaneous eruption in 1563 AD from Agua de Pau volcano of a trachytic air fall pumice deposit and a basaltic lava flow, demonstrates the simultaneous availability of magmas of contrasting composition at Agua de Pau volcano. Theoretically magma mixing would also act as a suitable mechanism for triggering explosive volcanic eruptions (Sparks et al. 1977).

Volume Relations

If, as the field relations and the smooth temporal controlled chemical variations suggest, the Fogo air fall pumice deposits are successive samples of a single, high level evolving magma body, then it should be possible to make a crude speculation as to the volume of cumulates formed in the period between the eruptions of Fogo A and Fogo 1563. This requires an estimate of the amount of crystallization that has taken place in the trachytic melt during this period, combined with the actual volume of the Fogo air fall pumice deposits. For example, $CNb_{Fogo\ D}/CNb_{Fogo\ 1563}$ indicates that the melt crystallized by approximately 20% during the period between the eruptions of Fogo D and Fogo 1563. The juvenile volume of Fogo 1563 is 0.14 km^3 (d.r.e.): therefore, assuming this volume is equal to that of the trachytic magma body, a minimum estimate, this amout of crystallization would have produced about 0.04 km^3 of cumulates and also suggests a minimum volume for the magma body immediately after the eruption of Fogo D of 0.18 km^3. Similar reasoning was used to estimate the amount of crystallization that had taken place in the magma body between the other Fogo eruptions and the volume of cumulates that formed in the same period. Extrapolating backwards through the Fogo succession by adding the estimated cumulate volumes to the volumes of the Fogo deposits suggests that after the eruption of Fogo A the magma body had a minimum volume of about 1 km^3. The estimated volume of cumulates to have formed since this eruption is about 0.5 km^3. This, if anything, is an underestimate because, apart from using a minimum value for the size of the magma body, the effect of dilution of the incompatible elements by magma mixing has been ignored.

Finally, compared with the combined volume of post Fogo A air fall pumice deposits of 0.34 km^3 (d.r.e.), the estimated volume of cumulates is nearly one and a half times as great. The implication is that a crystalline deep seated contribution to the salic crust of Agu de Pau, may be as significant as that due to the volcanic portion.

Conclusions

Field relations and the stratigraphically controlled nature and type of the observed geochemical and mineralogical variations of the Fogo air fall pumice succession, strongly suggests that the five most recent deposits represent successive samples of a single body of trachytic magma that is evolving by appreciable amounts of high level fractionation of alkali feldspar. This fractionation has resulted in the melt being driven towards the low pressure minimum temperature composition on the Ab – Or join. It also appears to be responsible for the development of peralkalinity in the melt by the time Fogo D was erupted. The presence of a high level trachytic magma body beneath Agua de Pau has previously been postulated on both geophysical and field data. Petrological evidence has provided a third argument for its existence.

The intimate field association between basic and salic volcanism on Sao Miguel and the presence in the Fogo air fall pumice deposits of some geochemical and mineralogical peculariaties, which cannot be easily accounted for by crystal fractionation in a trachytic melt, indicate that mixing between the trachytic

and less evolved melts may have occurred periodically beneath Agua de Pau. If so then the amount of contamination due to magma mixing has evidently not been sufficient to obscure the salient geochemical features inherited from high level crystal fractionation in a trachytic melt. This may be related to the relatively low output of basaltic magma by Sao Miguel volcanoes when compared to other composite volcanoes (Booth et al. 1978).

Finally, it has been shown for Agua de Pau that it is possible that the crustal contribution due to crystal fractionation of a subvolcanic trachytic melt, may be comparable to, if not more than the volume of trachyte erupted during the period under review. Booth et al. (1978) consider that the rate of volcanism on Sao Miguel has been relatively constant over the past 50,000 years. If this is the case, the total salic crustal contribution due to crystal fractionation of trachytic melts beneath the stratovolcanoes of Sao Miguel during this period, may be in the order of several cubic kilometers.

Aeknowledgements. The author is especially indebted to G.P.L. Walker and R. Croasdale for providing samples; J.A. Wolff for discussion and critical review; A.D. Saunders and R. Croasdale for critical review; G.F. Marriner, S. Parry, N. Rogers and P. Treloar for providing analytical assistance; N. Sinclair-Jones for preparing diagrams and Pat Storey for drafting the final version of the manuscript. Much of this work was carried out while the author held a Research Assistantship at South London College, London SE27 0TX, funded by The Inner London Education Authorithy for which he is grateful.

References

Abdel-Monem AA, Fernandez LA, Boone GM (1975) K–Ar ages from the eastern Azores group (Santa Maria, Sao Miguel and the Formigas Islands). Lithos 8:247–254

Allègre CJ, Minster JF (1978) Quantitative models of trace element behaviour in magmatic processes. Earth Planet Sci Lett 38:1–25

Booth B, Croasdale R, Walker GPL (1978) A quantitative study of five thousand years of volcanism on Sao Miguel, Azores. Philos Trans R Soc London A288:271–319

Borley GD, Rogers N (1979) Comparison of rare-earth element data obtained by neutron activation analysis using international rock and multi-element solution standards. Geostandards Newsletter 3:89–92

Bowen NL, Tuttle OF (1950) The system $NaAlSi_3O_8$–$KAlSi_3O_8$–H_2O J Geol 58:489–511

Cann JR (1967) A second occurrence of dalyite and the petrology of some ejected syenite blocks from Sao Miguel, Azores. Mineral Mag 36:227–232

Evensen NM, Hamilton PJ, O'Nions RK (1978) Rare-earth abundances in chondritic meteorites. Geochim Cosmochim Acta 42:1199–1212

Fairbrothers GE, Carr MJ, Mayfield DG (1978) Temporal magmatic variation at Boqueron Volcano, El Salvador. Contrib Mineral Petrol 67:1–9

Flower MFJ, Schmincke H-U, Bowman H (1976) Rare earth and other trace elements in historic Azorean lavas. J Volcanol Geotherm Res 1:127–147

Hanson GN (1978) The application of trace elements to the petrogenesis of igneous rocks of granitic composition. Earth Planet Lett 38:26–43

Hawkesworth CJ, Norry MJ, Roddick JC, Vollmer R (1979) $^{143}Nd/^{144}Nd$ and $^{87}Sr/^{86}Sr$ ratios from the Azores and their significance in LIL-element enriched mantle. Nature 280:28–31

Krause DC, Watkins ND (1970) North Atlantic crustal genesis in the vicinity of the Azores. Geophys JR Astron Soc 19:261–283

Laughton AS, Whitmarsh RB (1975) The Azores-Gibraltar plate boundary. In: L Kristjansson (ed) Geodynamics of Iceland and the North Atlantic area. Reidel, Dordrecht 63–81

Macdonald K, Bailey DK (1973) The chemistry of peralkaline oversaturated obsidians. US Geol Surv Prof Pap 440-N Pt 1

Machado F (1966) Anomalias das intensidades do terramoto de S. Miguel (Acores) em 1522. Bull Mus Lab Mineral Geol. Fac Cienc Lisboa 10:109–117

Machado F (1973) Acid volcanoes of San Miguel, Azores. Bull Volcanol 36:319–327

Roeder PL, Emslie RF (1970) Olivine-liquid equilibrium. Contrib Mineral 29:275–289

Rose WI, Grant NK, Hahn GA, Lange JM, Powell JL, Easter J, Degraff JM (1977) The evolution of Santa Maria Volcano, Guatemala. J Geol 85:63–87

Schmincke H-U, Weibel M (1972) Chemical study of rocks from Madeira, Porto Santo and Sao Miguel, Terceria (Azores). Neues Jahrb Mineral Abh 117:253–281

Schmincke H-U (1973) Magmatic evolution and tectonic regime in the Canary, Madeira and Azores island groups. Bull Geol Soc Am 84:633–648

Self S, Gunn BM (1976) Petrology, volume and age relations of alkaline and saturated peralkaline volcanics from Terceria, Azores. Contrib Mineral Petrol 54:293–314

Shotton FW, Blundell DJ, Williams REG (1968) Birmingham University radiocarbon dates. II. Radiocarbon 10:200–206

Shotton FW, Blundell DJ, Williams REG (1969) Birmingham University radiocarbon dates. III. Radiocarbon 11:263–270

Shotton FW, Blundell DJ, Williams REG (1970) Birmingham University radiocarbon dates. IV. Radiocarbon 2:385–399

Sigurdsson H (1977) Generation of Icelandic rhyolites by melting of plagiogranites in the oceanic layer. Nature 269:25–28

Sparks RSJ, Sigurdsson H, Wilson L (1977) Magma mixing: a mechanism of triggering acid explosive eruptions. Nature 267:315–318

Statham PJ (1976) A comparative study of techniques for quantitative analysis of the X-ray spectra obtained with a Si(Li) detector. X-Ray Spectrom 5:16–28

Sweatman TR, Long JVP (1969) Quantitative electron-probe microanalysis of rock forming minerals. J. Petrol 10:332–379

Thornton CP, Tuttle OF (1960) Chemistry of igneous rocks. I. Differentiation index. Am J Sci 258:664–684

Walker GPL, Croasdale R (1971) Two plinian-type eruptions in the Azores. J Geol Soc Lond 127:17–55

Walker GPL (1972) Crystal concentration in ignimbrites. Contrib Mineral Petrol 36:135–146

White WM, Tapio MDM, Schilling J-G (1979) The petrology and geochemistry of the Azores Islands. Contrib Mineral Petrol 69:201–213

Yoder HS (1973) Contemporaneous basaltic and rhyolitic magmas. Am Mineral 58:153–171

Zielinski RA (1975) Trace element evaluation of a suite of rocks from Reunion Island, Indian Ocean. Geochim Cosmochim Acta 39:713–734

Received May 2, 1981; Accepted November 12, 1981

Contrib Mineral Petrol (1983) 82:66–74

Contributions to Mineralogy and Petrology

The Volatile Component of Some Pumice-Forming Alkaline Magmas from the Azores and Canary Islands

J.A. Wolff[1] and M. Storey[2]

[1] Department of Geology, Imperial College, London SW7 2BP, England
[2] Department of Geology, Bedford College, Regent's Park, London NW1 4NS, England

Abstract. The abundances of pre-eruptive magmatic volatile species in the system H-O-S may be determined by application of thermodynamic methods to phenocryst assemblages commonly found in volcanic rocks, as demonstrated by Rutherford and Heming (1978). These methods are applied to alkaline pumice deposits, of airfall and ignimbrite type, from Tenerife (Canary Islands), Sao Miguel and Faial (Azores). It is argued that reliable temperature and fO_2 estimates can be obtained from titanomagnetite-ilmenite pairs containing appreciable quantities of minor elements. fO_2 buffering mechanisms found in rhyolitic magmas appear not to operate in more alkaline liquids. fH_2O is estimated using biotite; the high values found are shown to be compatible with the violently explosive nature of the magmas concerned. fS_2 is estimated from pyrrhotite composition. fH_2, fH_2S, fSO_2, fSO_3 are calculated from gas equilibria. Water fugacity may be very roughly estimated for non-biotite bearing samples from data on the sulphur species. Abundances of these species are similar in alkaline and calc-alkaline salic magmas. Volcanological implications, relating to the release of volatiles during explosive eruptions, are considered.

Introduction

The magmatic volatile component may be defined as those species which are normally gaseous at magmatic temperatures and atmospheric pressure, and are thus largely released from the magma upon eruption. Of particular interest are the volatile contents of pumice-forming magmas, since their very formation is testimony to the presence of appreciable quantities of volatile constituents. The fugitive nature of volatiles necessitates that pre-eruptive abundances be determined from information preserved in the final pumice deposit. The most satisfactory method is to analyse samples of pre-eruptive magma preserved as glass inclusions in tephra phenocrysts (Sommer 1977; Druitt et al. 1982). Suitable inclusions are not ubiquitous and in some areas are uncommon. A more generally applicable approach is to use mineral chemistry data and to employ thermodynamic methods to deduce the fugacities of volatile species in equilibrium with the phenocryst assemblage before eruption. This approach has been demonstrated by Rutherford and Heming (1978), who determined species in the system H-O-S in dacitic and rhyolitic pyroclastics from New Zealand. However, very few similar studies appear to have been made. This paper, therefore, has three principal aims; firstly, to present temperature and volatile data for some phonolitic, trachytic and trachyandesitic pumice deposits from Atlantic islands; secondly, to reaffirm this approach as a rapid means of estimating the composition of the magmatic volatile component; thirdly, to attempt to assess the significance of this information in a volcanological context.

Offprint requests to: J.A. Wolff

Geological Settings

The Canary Islands lie in the Eastern Atlantic on a sea-floor fracture zone extending off the continental slope of North-West Africa (Fig. 1). Tenerife, the largest island, consists of a Tertiary alkali basalt shield capped by younger differentiated volcanics and later basalts (Fuster et al. 1968; Borley 1974). Petrologically the rocks show the evolutionary trend alkali basalt-trachybasalt-trachyandesite-phonolite (Borley 1974). An extensive late Quaternary pyroclastic series of dominantly phonolitic composition is prominent in the south and east of the island. The series has been mapped by Booth (1973) and Booth and Walker (to appear) who distinguish the products of some 40 individual eruptions from vents located in the central caldera of Las Cañadas. The series chiefly consists of non-welded plinian air-fall deposits and ignimbrites[1], although welded examples of both are found. All four types are represented in this study. Several of the deposits consist of mixed-magma pumice (Wolff et al. to appear), as evidenced by variability in glass chemistry and the presence of two or more distinct phenocryst assemblages.

The Azores islands straddle the Mid-Atlantic Ridge (Fig. 1) on a topographic high known as the Azores Platform, those to the east of the Ridge being associated with a seismically active transform fracture zone (Laughton and Whitmarsh 1975). Volcanic rocks from the Azores consist predominantly of alkali basalts and their differentiates which include trachytes and peralkaline types. On some islands, these evolved magmas have been explosively erupted to form extensive pumice deposits. These deposits have been quantitatively studied on Sao Miguel by Walker and Croasdale (1971), Booth et al. (1978) and Storey (1981), on Terceira by Self (1976) and on Faial by Walker and

[1] We adopt the terminology of Wright et al. (1980) when describing the physical characteristics of the rocks studied in this paper

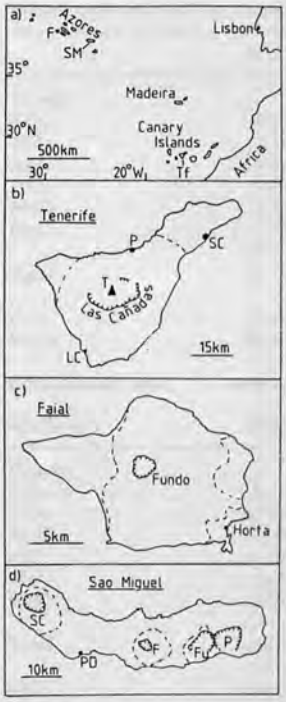

Fig. 1. Location maps. (a) Eastern Atlantic Ocean, showing location of Tenerife (Tf), Sao Miguel (SM) and Faial (F). (b) Tenerife, showing approximate extent of pumice series (dashed lines) erupted from vents in or near Las Cañadas caldera; greatest thicknesses are found south and east of Las Cañadas. T = volcanic peak of Teide. Principal towns: Santa Cruz (SC), Puerto de la Cruz (P), Los Cristianos (LC). (c) Faial, showing approximate extent of pumice series (dashed lines) erupted from the region of Fundo caldera. (d) Sao Miguel, showing the location of calderas associated with the three active volcanoes: Sete Cidades (SC); Fogo (F) caldera of Agua de Pau volcano, and Furnas (Fu). Dashed lines are the 8 m thickness contours for pumice successions erupted from each of the three centres (from Booth et al. 1978), although pumice occurs throughout the island. Also shown are the extinct centre of Povoacao (P) and the principal town, Ponta Delgada (PD)

Croasdale (unpub.). Sao Miguel, the largest island, has three active stratovolcanoes, Sete Cidades, Agua de Pau and Furnas. Faial island consists of a single stratovolcano rising to the peak of Carego Gordo. All four volcanoes possess a central caldera and a long record of explosive activity. Historic eruptions of trachytic pumice occurred from the Fogo caldera of Agua de Pau volcano in AD 1563 and from Furnas in AD 1640. In the last 5,000 years, there have been some 25 explosive trachytic eruptions on Sao Miguel, of which 6 were from the Agua de Pau volcano. As on Tenerife, magmatically heterogeneous pumice deposits are common (Walker and Croasdale 1971; Storey 1981).

Mineralogy and Petrology

The Tenerife deposits consist mainly of mildly peralkaline phonolite with a few modal percent of scattered phenocrysts. Most of the original pumice glass has devitrified to clay minerals, although unhydrated glass is preserved in some of the less vesicular clasts, and is common in welded tuffs. Samples showing evidence of alteration of phenocrysts were rejected. Many of the deposits studied contain a proportion of intermediate (trachyandesitic) tephra introduced by magma mixing shortly before eruption, and banded pumice clasts are common. In such cases detailed petrographic study is required to establish co-existing relationships within two (or more) crystal-magma populations (Wolff to appear). However aggregate phenocryst grains containing several minerals are common, and provide abundant evidence for equilibrium between phases at the time of quenching. Mineral assemblages in the pumice-forming magmas of Tenerife fall into three groups:

(i) Phonolitic:
Afsp + bi + mag ± ilm ± aeg-aug

(ii) Phonolitic:
Afsp + aeg-aug + bi + mag ± sph ± sod ± ne

(iii) Intermediate:
Plag + aug + amph + mag + ilm ± haüyne

Alkali feldspar in assemblages (i) and (ii) is usually sodic sanidine, occasionally anorthoclase. Xenocrysts derived from basaltic magma are common; these include olivine, titanaugite and calcic plagioclase.

The Azores samples are generally similar, except that the groundmass glass is trachytic. The usual phenocryst assemblage is Afsp + cpx + bi + mag ± ilm ± amph, with rare zircon. Basaltic xenocrysts are again common.

Apatite and pyrrhotite grains are found as inclusions in other phenocrysts in samples from both areas.

Analytical Procedure

Phenocryst phases in our samples have been analysed by electron microprobe. Tenerife samples were analysed on the Microscan V/EDS system at Imperial College using an accelerating voltage of 15 KV and a specimen current of 4 nA. Azores samples were analysed on a Microscan V/EDS at University College, London, using an accelerating voltage of 20 KV and a specimen current of 10 nA. The phases used in this study are homogenous within experimental error. Selected analyses for co-existing Fe-Ti oxides are given in Table 1.

Geothermometry

Knowledge of the equilibration temperature of the phenocryst-magma system is a necessary preliminary to determining the fugacities of magmatic volatile components. Nearly all the samples studied contain equilibrium mineral pairs of ilmenite and titanomagnetite, and temperatures have thus been estimated from the geothermometer and oxygen barometer of Buddington and Lindsley (1964), the mineral formulae first being recast in terms of end members by the method of Carmichael (1967). Both oxides contain substantial quantities of minor elements (4%–8% by weight $MgO + MnO + Al_2O_3$, Table 1), in part a consequence of the low silica activities of the magmas from which they precipitated (Carmichael et al. 1970). Powell and Powell (1977) recommend a different recalculation scheme which allows estimation of the maximum errors on the T-fO_2 determination due to the uncertainty involved in assigning minor elements to a particular end-member of the solid solutions. There is, however, evidence that Carmichael's (1967) procedure largely negates the effects of the minor elements. Hildreth (1979) has compared temperatures and oxygen fugacities obtained using Carmichael's method with those obtained by using recalculation procedures based on the actual effect of Mn and Mg components in the oxides (Mazzulo et al. 1975; Pinckney and Lindsley 1976), and finds a negligible discrepancy between results from the two methods. Furthermore, the estimated temperatures for our samples are corroborated by an independently derived geothermometer, the Fe^{2+}-Mg exchange between clinopyroxene and ilmenite (Bishop 1980). Agreement is generally very good (Table 2). We therefore believe that the Fe-Ti oxide

Table 1. Selected Fe-Ti oxide analyses recalculated following the method of Carmichael (1967), see text

	W.A.F.T., Tf[a]	Tajao ig., Tf[b]	Fogo B, S.M.[c]	Fogo C, S.M.[c]	Faial T
Ti mag.					
SiO_2	0.30	0.37	0.44	0.39	0.30
TiO_2	12.44	13.53	17.15	17.66	16.88
Al_2O_3	0.59	2.43	1.11	1.22	3.84
FeO	77.68	75.06	75.18	74.27	70.73
MnO	2.77	1.44	2.02	2.03	0.00
MgO	1.77	3.24	1.39	1.52	4.30
Total	95.55	96.07	97.29	97.09	96.05
FeO	37.57	38.07	43.47	43.66	41.03
Fe_2O_3	44.58	41.05	35.21	33.99	33.04
Recalculation total	100.02	100.13	100.79	100.47	99.39
Mol% usp	36.06	38.42	48.7	50.3	47.0
Ilmenite					
SiO_2	0.31	0.24	0.27	0.50	0.31
TiO_2	47.22	45.63	48.82	49.46	47.37
Al_2O_3	0.00	0.33	0.41	0.24	0.30
FeO	44.69	46.64	44.33	44.64	44.74
MnO	3.81	1.51	2.14	2.60	0.00
MgO	3.02	4.52	2.59	1.85	5.43
Total	99.05	98.87	98.56	99.29	98.15
FeO	33.60	31.97	36.05	38.80	33.27
Fe_2O_3	12.33	16.28	9.20	6.49	12.74
Recalculation total	100.29	100.48	99.48	99.94	99.42
Mol% ilm	88.54	84.52	91.4	93.5	87.8
Temperature (° C)	835	915	910	880	960
fO_2	$10^{-13.1}$	$10^{-11.4}$	$10^{-12.2}$	$10^{-13.2}$	$10^{-11.0}$

[a] W.A.F.T., Tf – Boca de Tauce welded air fall tuff, Tenerife
[b] Tajao ig., Tf – Tajao ignimbrite, Tenerife
[c] S.M. – Sao Miguel

temperatures closely approximate the actual temperatures prevailing at the moment when titanomagnetite-ilmenite-liquid equilibrium was quenched by eruption. Since the oxide phases are in equilibrium with the rest of the phenocryst assemblage in each sample, the temperature estimates apply to the whole assemblage and the associated magma. We have used the Fe-Ti oxide temperatures in the fugacity calculations, rather than temperatures derived from the Bishop (1980) geothermometer, since these phases were also used to find fO_2.

Estimation of fO_2

The composition of co-existing Fe-Ti oxides reflects the fugacity of oxygen as well as the equilibrium temperature (Buddington and Lindsley 1964). Results are shown in Table 1 and Fig. 2. The Tenerife samples show a higher oxygen fugacity for a given temperature than those from the Azores. Also, for individual volcanoes (Tenerife, Agua de Pau) the scatter of points is very small. This probably represents the effect of mineral and/or liquid component oxygen buffers. Several workers, using closely similar or identical Fe-Ti oxide recalculation schemes (Carmichael 1967; Ewart et al. 1971; Lipman 1971; Heming and Carmichael 1973; Rutherford and Heming 1978), have found that natural rhyolitic and dacitic liquids tend to plot on one of four curves in T-fO_2 space, each curve corresponding to the buffering of fO_2 by the ferromagnesian minerals found in association with the Fe-Ti oxides (Fig. 2). Clearly the *opx* and *opx-amph* buffers cannot apply to alkaline magmas. All of the studied samples contain biotite and/or amphibole, yet lie well below the *bi-amph* curve. None of the samples that plot near the QFM buffer curve contain quartz or olivine (with the exception of the Pantelleria sample, which is considerably more oversaturated). Thus it seems that either the mineral buffers found in acidic magmas do not operate in phonolitic and trachytic liquids, or else their effects are substantially modified by overall magma composition. Plausible reactions may be written for the mineral assemblages found in our rocks, but none are applicable over the entire range of assemblages observed.

As the assemblages do not permit an estimation of fH_2O which is independent of the fO_2 determination, we cannot test the possibility that the dissociation of water controls

Table 2. Comparison of temperatures obtained by applying the Fe-Ti oxides geothermometer (Buddington and Lindsley 1964) to analyses recast by the method of Carmichael (1967), with those given by the clinopyroxene-ilmenite geothermometer (Bishop 1980), for those deposits where titanomagnetite, ilmenite and augite coexist

Eruptive unit	Temperature (° C) from Fe-Ti oxides	Temperature (° C) from cpx-ilm
Ignimbrite O(i)[a], Tenerife	940	980
Ignimbrite O(ii)[a], Tenerife	915	923
Boca de Tauce welded air-fall tuff, Tenerife	835	810
Tajao ignimbrite, Tenerife	915	907
Adeje red ignimbrite, Tenerife	865	833
Fogo A pumice fall deposit, Sao Miguel	960	950
Fogo B pumice fall deposit, Sao Miguel	910	940
Fogo C pumice fall deposit, Sao Miguel	880	800

[a] Mixed-magma eruption: temperatures are given for two of the magmas represented in the pumice deposit

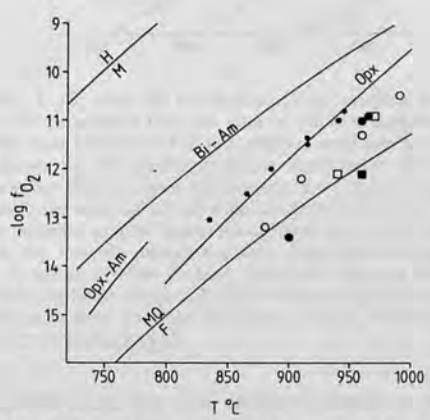

Fig. 2. Temperature, fO_2 data for pumice fall deposits and ignimbrites. Dots: Tenerife; open circles: Fogo deposits, Sao Miguel; filled circles: Faial. Also shown are two basic-intermediate lavas from Sao Miguel (open squares) and the pantelleritic Green Tuff (filled square), product of the largest documented eruption on Pantelleria, Italy (Wolff and Wright 1981). MQF = quartz-magnetite-fayalite buffer; HM = hematite-magnetite buffer. Curves labelled Bi-Am, Opx-Am, and Opx are explained in the text

fO_2. We can only conclude that magma type exerts a considerable effect on fO_2, but that the mechanism by which this effect operates remains open to question.

Estimation of fH_2O, P_{H_2O}, X_{H_2O}

The composition of co-existing biotite, sanidine and magnetite may be used to estimate the fugacity of water, by means of the reaction:

$$\underset{\text{biotite}}{KFe_3AlSi_3O_{10}(OH)_2} + \tfrac{1}{2}O_2 \rightleftharpoons \underset{\text{sanidine}}{KAlSi_3O_8} + \underset{\text{magnetite}}{Fe_3O_4} + H_2O$$

for which free-energy data is given by Wones and Eugster (1965), who adopted a regular solution model for biotite in the system annite-phlogopite-oxyannite. However Mueller (1972) and Wones (1972) have shown that mixing on the biotite octahedral site is approximately ideal, where the Fe^{3+} content of this site is small. Charge balance calculations show that the Fe^{3+} content of our biotites is negligible, and therefore the activity of annite in the biotites is equal to $(X_{Fe}^{oct})^3$, where X_{Fe}^{oct} is the octahedral site occupancy of Fe^{2+} in biotite. Appreciable substitution of Na for K and of F for OH may also occur, and the activity expression should therefore be modified by factors of $K/(K+Na)$ and $[OH/(OH+F)]^2$, assuming ideal mixing on both of these sites. Unfortunately the $OH/(OH+F)$ ratio is very readily changed by post-eruptive processes. We have therefore assumed $OH/(OH+F)=1$, and our calculated values of fH_2O (Table 3) are thus maximum estimates. The effect of fluorine in biotite on the calculated values may be readily assessed by inspection of the above reaction; for example, a fluorine site occupancy of 0.3 results in calculated log fH_2O being in excess by $\log(1-0{\cdot}3)^{-2}=0.3$. The activity of $KAlSi_3O_8$ in sanidine is calculated from the assymetric regular solution treatment of Thompson and Waldbaum (1969) and magnetite solid solutions are assumed to be ideal, following Carmichael et al. (1977).

Burnham et al. (1969) have determined the fugacity coefficient of water over a wide range of temperatures and pressures, and thus P_{H_2O} can be found for a given fH_2O and temperature. If P_{total} is known, the mole fraction of water in the magma (X_{H_2O}) can be calculated from the relationship given by Spera in Ewart et al. (1975). As we have no estimate of P_{total}, we have assumed that the magmas were water-saturated. X_{H_2O} may be readily converted into a primary wt% magmatic water content (Table 3). The water contents so found are maximum values, because of the assumptions of saturation and of fluorine-free biotite. Nonetheless they are compatible with the known explosive violence of the pumice eruptions, as evidenced by the wide dispersal of tephra from the source vents (Table 6 and below).

Estimation of fH_2

The fugacity of hydrogen may also be estimated from biotite composition:

$$\underset{\text{biotite}}{KFe_3AlSi_3O_{10}(OH)_2} \rightleftharpoons \underset{\text{sanidine}}{KAlSi_3O_8} + \underset{\text{magnetite}}{Fe_3O_4} + H_2$$

This reaction was used by Rutherford and Heming (1978) to estimate fH_2. However the expression for fH_2 which they used assumes a regular solution model for biotite, which is inconsistent with the assumption of biotite ideality in the expression used to find fH_2O from the same mineral data. We attempted to derive fH_2 values from the thermodynamic data of Wones and Eugster (1965) and assuming biotite ideality, but obtained unreasonably large results (up

Table 3. Estimated magmatic water contents

Pumice deposit	bi a_{ann}	san a_{or}	$\log fH_2O$	P_{H_2O}	X_{H_2O}[a]	wt% H_2O[a]	Total water[b]
Pumice fall E, Tenerife	0.0129	0.373	3.39	2,800	0.22	7.1	0.28
Adeje red ignimbrite, Tenerife	0.0117	0.391	3.20	1,900	0.18	5.6	0.006
Boca de Tauce welded air-fall tuff, Tenerife	0.0152	0.480	3.11	1,500	0.14	4.2	–
Fogo A pumice fall deposit, Sao Miguel	0.0222	0.498	3.47	3,000	0.22	6.6	0.09
Fogo B pumice fall deposit, Sao Miguel	0.0200	0.500	3.36	2,500	0.21	6.5	0.02
Fogo C pumice fall deposit, Sao Miguel	0.0429	0.508	3.30	2,300	0.21	6.5	0.008
Pumice fall deposit B, Faial	0.106	0.433	3.72	5,300	0.23	7.2	–

[a] Calculated assuming water saturation of magma

[b] Total volume of water (calculated as liquid in Km^3) released from the magma during the eruption. Based on total erupted volume of magma, taken from Booth et al. (1978) for Fogo A, B, C, Booth and Walker (in prep.) for Tenerife E, and Wolff (unpublished data) for Adeje, Tenerife. Tenerife volumes, based on present extent of deposits, are minima

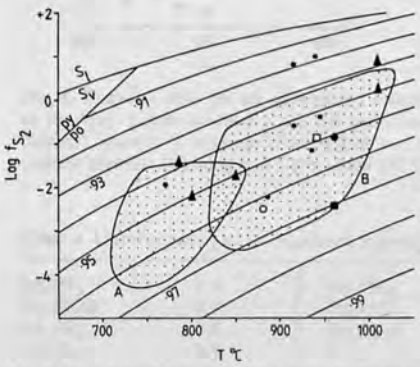

Fig. 3. fS_2 data for pyrrhotite-bearing samples. Numbered contours (calculated from the data of Toulmin and Barton 1964) are the mole fraction of FeS in pyrrhotite solid solution (FeS-S_2). Also shown are the pyrite-pyrrhotite equilibrium curve (py/po) and sulphur liquid-vapour equilibrium curve (S_l/S_v). Legend as Fig. 2, with the addition of sub-volcanic cumulates from Tenerife (filled triangles); sulphur fugacities of these fall within the range found in the Tenerife pumice deposits. Stippled field A is the range of fS_2 found in New Zealand ignimbrite magmas (Rutherford and Heming 1978); stippled field B is the range of fS_2 found for pumice deposits from the Rabaul caldera, Papua New Guinea (Heming and Carmichael 1973)

to 900 bars). We have therefore estimated fH_2 from the water decomposition reaction:

$$H_2O \rightleftharpoons H_2 + \tfrac{1}{2}O_2$$

using data given in the JANAF thermochemical tables (Stull and Prophet 1971). fH_2 data are given in Fig. 4.

Estimation of fS_2

Pyrrhotite occurs in a number of samples as inclusions in Fe-Ti oxides, pyroxene, amphibole, biotite, feldspar and (in the Tenerife pumices) haüyne. That enclosed in haüyne occurs as a fine dust, apparently formed after growth of the including crystal; in all other minerals it is found as blebs up to 100 μ across and is considered to have occurred as discrete grains before and/or during the growth of the principal phases. Pyrrhotite composition defines the fugacity of sulphur (fS_2) in the environment from which it crystallised (Toulmin and Barton 1964). The pyrrhotite grains ceased to be in equilibrium with the magma upon inclusion in other phases, which presumably occurred at slightly higher temperatures than those indicated by the present Fe-Ti oxide compositions. However the Fe-Ti oxide temperatures are used here in the absence of data on the enclosure temperatures of the pyrrhotite grains. Values of fS_2 show a degree of variation (Fig. 3) comparable to those found for dacitic and rhyolitic magmas (Heming and Carmichael 1973; Rutherford and Heming 1978).

Estimation of fH_2S, fSO_2, fSO_3

With a knowledge of fS_2, fH_2 and fO_2, the fugacities of three sulphur compounds may be estimated from the formation reactions:

$$H_2S \rightleftharpoons H_2 + \tfrac{1}{2}S_2$$
$$SO_2 \rightleftharpoons \tfrac{1}{2}S_2 + O_2$$
$$SO_3 \rightleftharpoons \tfrac{1}{2}S_2 + 1\tfrac{1}{2}O_2$$

using data from the JANAF thermochemical tables (Stull and Prophet 1971). Results are shown in Fig. 4.

Limitations

There are four main limitations to the accuracy of the data and the general applicability of this approach.

1. Errors arising from errors in (a) mineral analyses and (b) thermodynamic data. (b) does not apply if results obtained by using the same calculation procedures are being compared, but errors are compounded when gas reactions are used (e.g. to find fSO_2, fSO_3) where the input data are fugacities already estimated from mineral data. Uncertainties in fugacity estimations, calculated by the error propogation method recommended by Powell (1978), are given in Table 4.

2. Errors due to assumptions made. These can usually be assessed with a degree of confidence, e.g. the assumption of fluorine-free biotite results in the calculation of maximum fH_2O values.

3. Pumice deposits often have very low phenocryst contents, and, if aggregate mineral grains are rare or absent, it may be difficult to establish equilibrium between phenocryst phases.

4. The required mineral phases may not be present. We have examined some thirty erupted magmas, of which half bear iron-titanium oxides, and fewer still contain biotite

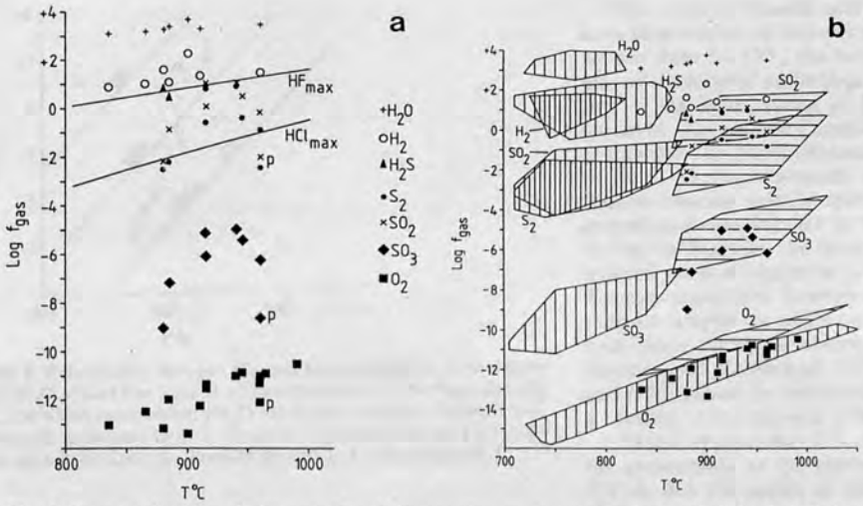

Fig. 4. Fugacity data for all determined volatile constituents in pyroclastics studied. (a) Labelled curves HF_{max}, HCl_{max} are explained in the text; points labelled p are the pantellerite sample. (b) Vertical rule: range of values for each species in H-O-S found in New Zealand ignimbrite magmas (Rutherford and Heming 1978). Horizontal rule: range of fS_2, fSO_2, fSO_3, fO_2 values in New Guinea pumice deposits (Heming and Carmichael 1973). Pantellerite omitted for sake of clarity

Table 4. Uncertainties (±) in calculated fugacity values

$\log fO_2$	0.5	$\log fSO_2$	0.7
$\log fH_2O$	0.3	$\log fSO_3$	0.9
$\log fH_2$	0.4	$\log fH_2S$	0.5
$\log fS_2$	0.5	T	30° C

and/or pyrrhotite in addition. More seriously, the vast majority of erupted magmas do not bear a mineral assemblage which permits the determination of the important constituents CO_2, CO, HF and HCl.

Despite these problems, the approach is a powerful one, as it allows the rapid calculation of the composition of part of the volatile component of a range of salic magma types.

Discussion

Our data are similar to those obtained by Heming and Carmichael (1973) and Rutherford and Heming (1978) for Quaternary pumice-forming magmas from Rabaul, New Guinea and North Island, New Zealand respectively (Fig. 4b). The New Zealand results are typically lower for each species than those for the Tenerife, Azores and Rabaul pumices; this is principally a reflection of their lower equilibration temperatures (729–810° C). fS_2 is on average slightly higher, at a given temperature, in the Atlantic magmas.

Fugacities may be converted to abundances if it is assumed that volatile species mix ideally with each other and with magma, and if fugacity co-efficients are known for each volatile species. When this is done for the five principal species in H-O-S, the similarity between the rhyolite, trachyte and phonolite data becomes even more apparent (Table 5). The general similarity in relative abundances is presumably a consequence of the relative stabilities of the various gas species under magmatic conditions; for example SO_2 will always predominate over SO_3 at the oxygen fugacities usually encountered in magmas. Thus we may conclude that the magmatic volatile component has a similar composition (at least in H-O-S) in a wide variety of pumice-forming salic melts, although it must be noted that the single pantellerite sample for which we have data is much poorer in the sulphur species than the alkaline and calcalkaline liquids (Fig. 4).

Table 5. Molar abundances, as a percentage of total abundance of the five major species in the system H-O-S, for three cases[a]

	Pumice fall deposit E, Tenerife	Pumice fall deposit C, Sao Miguel	Average New Zealand ignimbrite[b]
H_2O	99.4%	98.1%	99%
H_2	0.5%	1.6%	0.5%
H_2S	0.1%	0.3%	0.5%
SO_2	(0.005%)	(0.0003%)	(0.0002%)
S_2	(0.0002%)	(0.0001%)	(0.0001%)

[a] Calculated using fugacity coefficients tabulated by Ryzhenko and Volkov (1971) and assuming ideal mixing
[b] From data of Rutherford and Heming (1978)

Rough estimation of fH_2O for non-biotite bearing samples

The five principal species in the system H-O-S are related by the equilibrium:

$$S_2 + 2H_2O \rightleftharpoons H_2S + SO_2 + H_2$$

If the variation with temperature of three of these species can be characterised for a suit of samples, then a simple

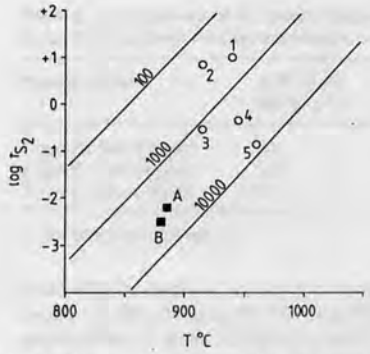

Fig. 5. Relationship between fS_2 and temperature for three values of fH_2O in bars (see text). A = Tenerife deposit E, B = Fogo deposit C, for which independent fH_2O values are available (Table 3). 1 = Tenerife ignimbrite O(i); 2 = Tenerife Tajao ignimbrite; 3 = Tenerife ignimbrite O(ii); 4 = Tenerife deposit J; 5 = Faial deposit T

relationship between the other two is found. We have applied this method to determine fH_2O for non-biotite bearing samples using the data in Fig. 4. Although this procedure is only qualitative owing to the substantial errors involved (particularly in the values of fH_2S, fSO_2 and fH_2 which form input data for this calculation), the results (Fig. 5) are compatible with other evidence; the high fH_2O value found for Faial deposit T is similar to the figure of 5,300 bars for an associated fall deposit (Faial B) which contains biotite; Tenerife ignimbrite O(ii) is very likely to be more water-rich than O(i), since it is derived from a cooler, more fractionated part of the same magma chamber (Wolff, to appear).

Constraints on the Fugacities of Undetermined Constituents

Under conditions of sufficiently high magmatic fCO_2, calcium-bearing minerals break down to form primary igneous calcite, as observed in carbonatites and some magmas of less extreme composition (Scott 1982). The absence of calcite from a given mineral assemblage thus defines an upper limit of fCO_2 for that assemblage. Several reactions between CO_2 and observed major components of solid phases may be written, for example:

$$3CaFeSi_2O_6 + 3CO_2 + \tfrac{1}{2}O_2$$
pyroxene
$$\rightleftharpoons 3CaCO_3 + Fe_3O_4 + 6SiO_2$$
calcite magnetite liquid

and for a sphene-bearing assemblage

$$2CaFeSi_2O_6 + CaTiSiO_5 + 3CO_2$$
pyroxene sphene
$$\rightleftharpoons 3CaCO_3 + Fe_2TiO_4 + 5SiO_2$$
calcite magnetite liquid

Using the thermodynamic data of Helgeson et al. (1978) and typical mineral compositions for our samples, maximum values of fCO_2 lie between 1 and 30 bars. This is in general agreement with the known low solubility of CO_2 in low-pressure, hydrous magmas (Mysen 1977).

The roles of fluoride and chloride species in magmas have been studied by Stormer and Carmichael (1970, 1971). As was done for CO_2, the lack of a fluoride-bearing phase among the mineral assemblage allows approximate calculation of maximum values of fF_2, using the reactions discussed by Stormer and Carmichael (1970) for the formation of fluorite (CaF_2) and villiaumite (NaF). With a knowledge of fH_2O or fH_2, maximum values of fHF, the principal fluorine-bearing volatile species, may be calculated. An overall maximum for fHF in the pumice magmas is plotted in Fig. 4a. Sodalite, the most widespread chloride-bearing igneous mineral occurs as a phenocryst in a few of the Tenerife phonolites; however it is unfortunately restricted to those samples for which no T-fO_2 estimate can be made, prohibiting direct calculation of fCl_2 by the method of Stormer and Carmichael (1971). Instead, maximum fCl_2 and $fHCl$ values for sodalite-free samples were found, and a "ceiling" $fHCl$ curve is given in Fig. 4a.

Thus it appears that CO_2, HCl and HF levels are possibly comparable to the determined minor constituents in H-O-S, but are orders of magnitude less abundant than H_2O.

Magmatic Water Contents

Water is the most abundant volatile constituent in the great majority of magmas, and a knowledge of magmatic water content is essential to the estimation of such parameters as the viscosity and density of magma before eruption. Rutherford and Heming (1978) considered the water contents of New Zealand ignimbrite magmas to be unusually high, and ascribed this to an origin by anatexis of water-rich basement greywackes (for which there is a considerable body of evidence; see Carmichael et al. 1974, and references cited therein). The mean water content of the values tabulated by Rutherford and Heming corresponds to approximately 6.5% by weight, closely similar to the values obtained here. Sommer (1977) found volatile contents of up to 7% (average 5.4%) for the Bandelier Tuff, New Mexico, rhyolite magma; 92% of this consisted of H_2O, the remainder being mostly CO and CO_2. Druitt et al. (1982) found a magmatic water content of 5% in the first erupted portion of the Bishop Tuff, California. Thus, when compared to other *pumice-forming* magmas, the New Zealand examples cannot be considered particularly water-rich.

The deduced water contents are compatible with field evidence for the violently explosive nature of the magmas. The distribution of tephra in a plinian air-fall deposit can be used to estimate various physical parameters of the eruption (Wilson 1976; Wilson et al. 1978). In particular, the dispersal of the largest dense (ballistic) fragments is unaffected by atmospheric transport. Extrapolation of the range dependence of ballistic clast size yields a value for the largest blocks which can be just supported by the eruption column at the vent, and thence maximum muzzle velocity (through a function given by Wilson 1976). Eruption velocity is directly related to the quantity of released gas and the primary magmatic volatile content (Wilson 1980; Wilson et al. 1980). The appropriate field data exist for the Fogo deposits (Booth et al. 1978; Walker and Croasdale 1971) and we have therefore calculated magmatic volatile contents for Fogo A, B and C. Our thermodynamic estimates indicate that other species are greatly subordinate to water, and thus actual water content will approximate

Table 6. Comparison of estimated values of water content with those deduced from field measurements on the dispersal of tephra[a]

Pumice deposit	wt% H_2O, this paper	wt% H_2O, from field data
Fogo A, Sao Miguel	6.6	6.7
Fogo B, Sao Miguel	6.5	5.7
Fogo C, Sao Miguel	6.5	4.5

[a] See text for method

total volatile content, permitting comparison with estimates based on the physical model. Agreement between the two approaches is good (Table 6), particularly in view of the uncertainty associated with the fH_2O values (Table 4). Although both methods give maximum estimates of water content, the "petrological" values are expected to be higher, since no account is taken of energy losses occurring during magma disruption in the "volcanological" calculations (Wilson 1980).

Widely dispersed plinian pumice fall deposits, similar to those studied here, are a common manifestation of salic volcanism, yet few estimates of their magmatic volatile contents exist. The data discussed here suggest that natural salic liquids commonly have water contents in excess of 5% by weight.

Some Volcanological Implications

1. Physical models of explosive eruptive processes often assume that the magmatic volatile component consists entirely of water, because of the negligible effect of the presence of small quantities (<10%) of other volatile species on eruption dynamics. Our results indicate that this approximation is valid for alkaline salic magmas. An illustration is provided by the effect of gas density on a plinian eruption column. Dense columns tend to collapse to form ignimbrites (Sparks and Wilson 1976), whereas lighter columns more readily undergo convective uprise to form an eruption cloud some tens of kilometres high, fall-out from which produces a plinian pumice fall deposit (Wilson 1976; Wilson et al. 1978). The data discussed here indicate that variations in the density of released gas, due to compositional variations in the system H-O-S, are unlikely to be great enough to significantly affect eruption column dynamics.

2. Appreciable quantities of combustible gases (H_2, S_2, H_2S) are present in salic magmas and will be released upon explosive eruption. The oxidation of these in the eruption cloud will contribute to the thermal energy budget of the eruption. Enthalpy calculations for the relevant combustion reactions indicate that this contribution is minor compared to the thermal and kinetic energy released, and is unlikely to exceed a few percent of the total eruption energy.

3. Large quantities of water are released during pumice eruptions (Table 3). If it is assumed that a large proportion of released water falls as rain during or soon after eruption, then the formation of mudflows by remobilisation of the newly-deposited tephra is a virtually inevitable consequence of any such eruption. Mudflows are very common associates of all types of pumice deposit.

Acknowledgements. J.A.W. wishes to thank the Natural Environment Research Council of Great Britain for a research studentship at Imperial College, and for funding fieldwork on Tenerife. Part of this work was carried out while M.S. held an Inner London Education Authority research assistantship at South London College, Knight's Hill, London SE27 OTX. M.S. thanks the Dept. of Geology, University College, London for the use of their electron microprobe facility and I.C. Young for analytical assistance. Pumice samples from the Azores were collected by Prof. G.P.L. Walker and Dr. R. Croasdale. Dr. J.V. Wright collected the Pantelleria sample. We are especially grateful to Prof. G.P.L. Walker, Dr. B. Booth and Dr. R. Croasdale for generous access to unpublished data. The original manuscript was substantially improved by the comments of Dr. A.D. Saunders and an anonymous reviewer. Pat Storey kindly typed the final draft.

References

Bishop FC (1980) The distribution of Fe^{2+} and Mg between coexisting ilmenite and pyroxene with applications to geothermometry. Am J Sci 280:46–77

Booth B (1973) The Granadilla pumice deposit of Southern Tenerife, Canary Islands. Proc Geol Assoc 84:353–370

Booth B, Croasdale R, Walker GPL (1978) A quantitative study of five thousand years of volcanism on Sao Miguel, Azores. Philos Trans R Soc London A288:271–319

Booth B, Walker GPL (to appear) Products of explosive volcanism on Tenerife, Canary Islands

Borley GD (1974) Aspects of the volcanic history and petrology of the island of Tenerife. Proc Geol Assoc 85:259–279

Buddington AF, Lindsley DH (1964) Iron-titanium oxide minerals and synthetic equivalents. J Petrol 5:310–357

Burnham CW, Holloway JR, Davis NF (1969) Thermodynamic properties of water to 1,000° C and 10,000 bars. Geol Soc Am Spec Paper 132:1–96

Carmichael ISE (1967) The iron-titanium oxides of salic volcanic rocks and their associated ferromagnesian silicates. Contrib Mineral Petrol 14:36–64

Carmichael ISE, Nicholls J, Smith AL (1970) Silica activity in igneous rocks. Am Mineral 55:246–263

Carmichael ISE, Nicholls J, Spera FJ, Wood BJ, Nelson S (1977) High-temperature properties of silicate liquids: Applications to the equilibration and ascent of basic magma. Philos Trans R Soc London A286:373–431

Carmichael ISE, Turner FJ, Verhoogen J (1974) Igneous Petrology. McGraw-Hill, pp 739

Druitt TH, Anderson AT, Nagle F (1982) Water in rhyolitic magma, Bishop, California. Eos 63:451

Ewart A, Green DC, Carmichael ISE, Brown FH (1971) Voluminous low temperature rhyolitic magmas in New Zealand. Contrib Mineral Petrol 33:128–144

Ewart A, Hildreth W, Carmichael ISE (1975) Quaternary acid magma in New Zealand. Contrib Mineral Petrol 51:1–27

Fuster JM, Arana V, Brandle JL, Navarro M, Alonso U, Aparicio A (1968) Geology and volcanology of the Canary Islands: Tenerife. Inst "Lucas Mallada", Madrid 218

Helgeson HC, Delaney JM, Nesbitt HW, Bird DK (1978) Summary and critique of the thermodynamic properties of rock-forming minerals. Am J Sci 278a:pp 229

Heming RF, Carmichael ISE (1973) High-temperature pumice flows from the Rabaul caldera, Papua New Guinea. Contrib Mineral Petrol 38:1–20

Hildreth W (1979) The Bishop Tuff: Evidence for the origin of compositional zonation in silicic magma chambers. Geol Soc Am Spec Paper 180:43–75

Laughton AS, Whitmarsh RB (1975) The Azores-Gibraltar plate boundary. In: Kristjansson L (ed) Geodynamics of Iceland and the North Atlantic area. Riedel, Dordrecht

Lipman PW (1971) Iron-titanium oxide phenocrysts in compositionally zoned ash-flow sheets from Southern Nevada. J Geol 79:438–456

Mazzulo LJ, Dixon SA, Lindsley DH (1975) T-fO_2 relationships

in Mn-bearing Fe-Ti oxides. Geol Soc Am Abstr with Prog 7:1192
Mueller RF (1972) Stability of biotite: a discussion. Am Mineral 57:300–316
Mysen BO (1977) The Solubility of H_2O and CO_2 under predicted magma genesis conditions and some petrological and geophysical implications. Rev Geophys Space Phys 15:351–361
Pinckney CR, Lindsley DH (1976) Effects of magnesium on iron-titanium oxides. Geol Soc Am Abstr with Prog 8:1051
Powell R (1978) Equilibrium thermodynamics in petrology. Harper & Row, London, pp 284
Powell R, Powell M (1977) Geothermometry and oxygen barometry using co-existing iron-titanium oxides: A reappraisal. Mineral Mag 41:257–263
Rutherford NF, Heming RF (1978) The volatile component of Quaternary ignimbrite magmas from the North Island, New Zealand. Contrib Mineral Petrol 65:401–411
Ryzhenko BN, Volkov VP (1971) Fugacity coefficients of some gases in a broad range of temperatures and pressures. Geochem Int 468–481
Scott S (1982) Evidence from Longonot volcano, Central Kenya, lending further support to the argument for a co-existing CO_2-rich vapour in peralkaline magma. Geol Mag 119:215–217
Self S (1976) The Recent volcanology of Terceira, Azores. J Geol Soc London 132:645–666
Sommer MA (1977) Volatiles H_2O, CO_2 and CO in silicate melt inclusions in quartz phenocrysts from the rhyolitic Bandelier air-fall and ash-flow tuff, New Mexico. J Geol 85:423–432
Sparks RSJ, Wilson L (1976) Model for ignimbrite formation by gravitational column collapse. J Geol Soc London 132:441–451
Storey M (1981) Trachytic pyroclastics from Agua de Pau volcano, Sao Miguel, Azores: evolution of a magma body over 4,000 years. Contrib Mineral Petrol 78:423–432
Stormer JC, Carmichael ISE (1970) Villiaumite and the occurrence of fluoride minerals in igneous rocks. Am Mineral 55:126–134
Stormer JC, Carmichael ISE (1971) The free-energy of sodalite and the behaviour of chloride, fluoride and sulphate in silicate magmas. Am Mineral 56:291–306
Stull DR, Prophet H (1971) Joint Army Navy Air Force thermochemical tables. 2nd edn. Washington, DC: US Govt Printing Office
Thompson JB, Waldbaum DR (1969) Mixing properties of sanidine crystalline solutions. III Calculations based on two phase data. Am Mineral 54:811–838
Toulmin P, Barton PB (1964) A thermodynamic study of pyrite and pyrrhotite. Geochim Cosmochim Acta 28:641–671
Walker GPL, Croasdale R (1971) Two plinian-type eruptions in the Azores. J Geol Soc London 127:17–55
Wilson L (1976) Explosive volcanic eruptions, III. Plinian eruption columns. Geoph JR Astron Soc 45:543–556
Wilson L (1980) Relationships between pressure, volatile content and ejecta velocity in three types of volcanic explosion. J Volcanol Geotherm Res 8:297–313
Wilson L, Sparks RSJ, Huang TC, Watkins ND (1978) The control of volcanic column heights by eruption energetics and dynamics. J Geoph Res 83:1829–1836
Wilson L, Sparks RSJ, Walker GPL (1980) Explosive volcanic eruptions, IV. The control of magma properties and conduit geometry on eruption column behaviour. Geoph JR Astron Soc 63:117–148
Wolff JA (to appear) Sampling of an alkaline magma series by individual eruptions of Tenerife, Canary Islands
Wolff JA, Wright JV (1981) Formation of the Green Tuff, Pantelleria. Bull Volcanol 44:681–690
Wolff JA, Wright JV, Smith AL, Clough BJ, Roobol MJ, Self S (to appear) Mixed pumice deposits: field characteristics. Proc IX Carib Conf Santo Domingo, 1980
Wones DR (1972) Stability of biotite: a reply. Am Mineral 57:316–317
Wones DR, Eugster HP (1965) Stability of biotite: experiment, theory and application. Am Mineral 50:1228–1272
Wright JV, Smith AL, Self S (1980) A working terminology of pyroclastic deposits. J Volcanol Geotherm Res 8:315–336

Received in revised from October 23, 1982;
Accepted November 18, 1982

Zoning in highly alkaline magma bodies

JOHN A. WOLFF* & MICHAEL STOREY†

* Geology Department, Imperial College, Prince Consort Road, London SW7 2BP, U.K.
† Geology Department, Bedford College, Regent's Park, London NW1 4NS, U.K.

(*Received* 11 January 1984; *accepted* 4 May 1984)

Abstract – We present chemical data on magmatically heterogeneous pyroclastic deposits of late Quaternary age erupted from zoned magma systems underlying Tenerife (Canary Islands), Sao Miguel and Faial (Azores), and Vesuvius. The most fractionated magmas present at each centre are respectively Na-rich phonolite, trachyte, and K-rich phonolite. Within any one deposit, chemical variation is either accompanied by changes in the phenocryst assemblage (petrographic zonation) or is largely manifested in trace element abundances, unaccompanied by any petrographic change (occult zonation). Zoning is analogous to that in calc-alkaline systems where the most fractionated products are high-silica rhyolites. When a range of magma types are considered, a correlation emerges between roofward depletion of trace elements (especially REE) in the zoned system and compatability of those same trace elements in the accessory phenocryst phases present. Thus, allanite- or chevkinite-bearing rhyolitic systems are light-REE depleted roofwards, the sphene-bearing Tenerife system is middle-REE depleted roofwards, the melanite-bearing Vesuvius system is heavy-REE depleted roofwards, while the Azores systems, which lack these phases, display roofward REE enrichment. Therefore, the behaviour of trace elements may in each case be explained by fractionation of observed phenocryst assemblages. The resemblance between features of zoned magma systems and published work on the dynamic consequences of cooling saturated aqueous solutions prompts us to suggest that sidewall crystallization and consequent boundary-layer uprise to form a capping layer at top of the system may be a plausible mechanism for the generation of both petrographic and occult zonation. Reverse zoning occurs among the first-erupted tephra of some deposits, demonstrating that the most highly differentiated magma available is not always the first to be tapped during an eruption from a zoned system.

1. Introduction

It is well established that large (10^2–10^4 km^3) silicic magma bodies, resident at high levels in continental crust, may develop vertical chemical gradients whilst in a largely liquid condition (Smith & Bailey, 1966; McBirney, 1968; Smith, 1979; Hildreth, 1979, 1981). In general, the topmost parts of these magma bodies are enriched in the most incompatible elements. Although such gradients have recently been documented from granites (Miller & Mittlefehldt, 1982; Mittlefehldt & Miller, 1983), evidence for zonation is most apparent in young, large-volume ignimbrite sheets, which may be zoned from andesitic to rhyolitic compositions (McBirney, 1968) or show more subtle internal variations largely manifested in trace-elements abundances (Hildreth, 1979). The glassy juvenile constituents of pyroclastic deposits are more faithful recorders of magmatic heterogeneities than equivalent crystalline igneous rocks (Anderson, 1976), and thus (if properly sampled) provide the most reliable guide to pre-eruptive magmatic processes.

The petrological study of such rocks received stimulus from the work of Hildreth (1979) on the Bishop Tuff. Hildreth rejected fractionation by crystal settling as a viable mechanism for inducing chemical zonation of magma and instead proposed a combination of convection and liquid-state thermogravitational (Soret) diffusion. Recently, several lines of evidence have led other workers to question Hildreth's preferred model. Soret diffusion effects so far observed in experiments are inconsistent with the geochemical patterns displayed by the Bishop Tuff (Lesher & Walker, 1983). Michael (1983*a*), using the same data set as Hildreth (1979), has successfully modelled the chemical profiles in the Bishop Tuff by crystal fractionation, and Mittlefehldt & Miller (1983) have likewise accounted for closely similar profiles in granites by crystallization processes. Finally, theoretical studies (Huppert & Sparks, 1980; Huppert, Sparks & Turner, 1982) and laboratory analogue experiments using aqueous solutions (McBirney, 1980; Turner & Gustafson, 1981; Sparks, Huppert & Turner, 1984) strongly suggest that crystallization-driven fluid dynamic processes are fully capable of producing chemical zoning in magma bodies; thus it may be unnecessary to invoke other than crystal-liquid processes to account for zoning.

We would raise two points here. Firstly, the debate on liquid state *vs.* crystal fractionation employing data from natural samples has been conducted principally with reference to one magmatic association, high-silica rhyolite–dacite–andesite. Secondly, there have been, to date, very few intensive studies on pyroclastic (or other volcanic) sequences which consider the new fluid dynamic concepts as possible models for magmatic

* Present address: Department of Geology, University of Texas at Arlington, UTA Box No. 19049, Arlington, Texas 76019, U.S.A.

evolution. In this paper, we petrologically examine chemical and mineralogical variation within individual eruptive units from four pyroclastic successions, of trachytic and phonolitic compositions, for which a rigorous stratigraphy has been compiled using tephrochronological techniques. We have three principle objectives: firstly, to establish that small-volume bodies of intermediate and felsic alkaline magma frequently display an analogous type of zonation to that found in much larger rhyolitic chambers; secondly, to assess the implications for a general behavioural model for highly differentiated magma bodies; thirdly, to consider the extent to which our observations justify the application of recent theoretical and laboratory fluid dynamic studies to real magmas.

2. Volcanology and petrology of studied units

There are very few alkaline volcanoes for which a detailed pyroclastic stratigraphy has been compiled; such a stratigraphy is a prerequisite for any meaningful geochemical sampling. The present study is based on the fieldwork of Booth (1973) and Booth & Walker (unpub. data) on the Canary Islands, and Booth, Croasdale & Walker (1978) and Walker & Croasdale (1971, and unpub. data) on the Azores Islands. We now describe the general features of these successions, and consider details displayed by individual units in succeeding sections. In volcanological terminology (Wright, Smith & Self, 1980), the units studied are subplinian to plinian pumice fall deposits and ignimbrites, some with associated lavas.

2.a. Tenerife, Canary Islands

The Canary Islands lie in the Eastern Atlantic on a sea-floor fracture zone extending off the continental slope of northwest Africa (Fig. 1). Tenerife, the largest island, consists of a Tertiary alkali basalt shield capped by younger differentiated volcanics and later basalts (Fuster *et al.* 1968). Petrologically the rocks show the evolutionary trend alkali basalt–trachybasalt–trachyandesite–phonolite (Borley, 1974).

The central caldera of Las Cañadas is the source of a late Quaternary pumice succession comprising some 40 airfall and ignimbrite deposits (Booth, 1973; Booth & Walker, unpub. data). The deposits, which are separated by soil/erosion horizons, are largely composed of near-aphyric white phonolitic pumice.

At least 15 deposits contain a proportion (1–50%) of black porphyritic trachyandesitic (i.e. intermediate in terms of normative mafic mineral content, Borley, 1974) pumice, the distribution of which within a deposit takes one of two forms. Some airfall units consist of phonolitic pumice overlain by a layer of dark and banded tephra (Fig. 2) with no evidence of any hiatus or change in the eruption between formation of the layers (an eruption break is usually recorded in the internal stratigraphy of a fall deposit as a fine ash bed or other discontinuity). More commonly, banded or streaky black-and-white pumice clasts are found

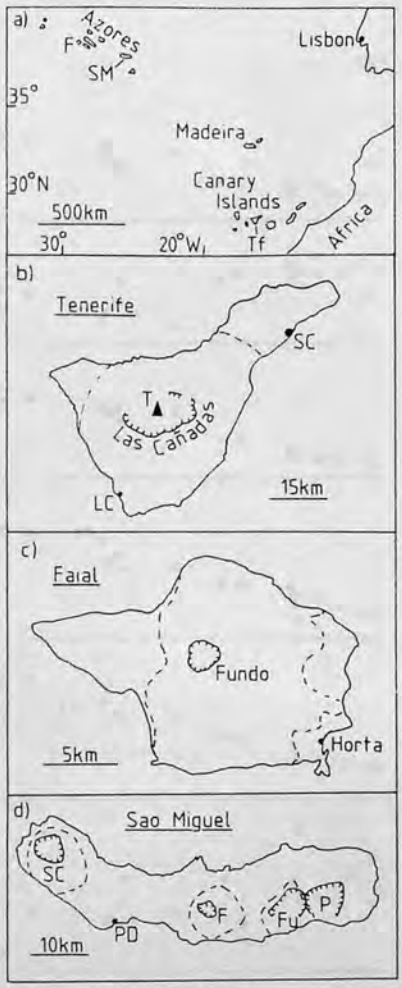

Figure 1. Location maps. (a) Eastern Atlantic Ocean, showing location of Tenerife (Tf), Sao Miguel (SM) and Faial (F). (b) Tenerife, showing approximate extent of pumice series (dashed lines) erupted from vents in or near Las Cañadas caldera; greatest thicknesses are found south and east of Las Cañadas. T = volcanic peak of Teide. Principal towns: Santa Cruz (SC), Los Cristianos (LC). (c) Faial, showing approximate extent of pumice series (dashed lines) erupted from the region of Fundo caldera. (d) Sao Miguel, showing the location of calderas associated with the three active volcanoes: Sete Cidades (Sc), Fogo (F) caldera of Agua de Pau volcano, and Furnas (Fu). Dashed lines are the 8 m thickness contours for pumice successions erupted from each of the three centres (from Booth, Croasdale & Walker, 1978), although pumice occurs throughout the island. Also shown are the extinct centre of Povoacao (P) and the principal town, Ponta Delgada (PD).

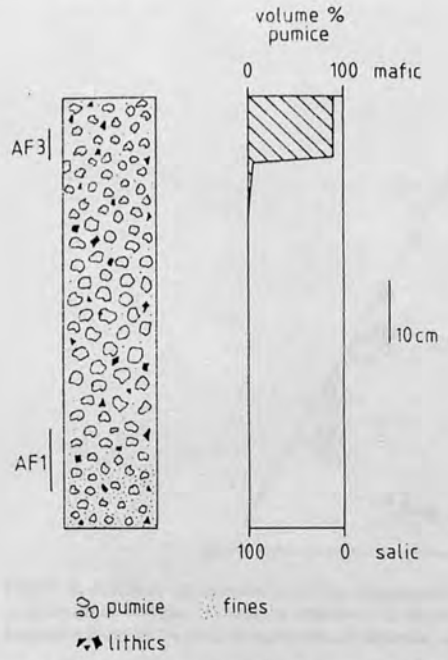

Figure 2. Section through Tenerife pumice fall A at the sampling locality, showing variation in mafic pumice content and positions from which samples were taken (vertical bars labelled with sample numbers).

dispersed through a deposit, often with a higher proportion of the mafic component among the last-erupted material.

The salic component is generally uniform in composition, or is characterized by subtle variations in trace-element content within any one deposit, while the mafic component, if present, is of variable composition (Fig. 3). The frequency and style of these associations strongly indicate that, prior to eruption, phonolitic magma was pooled in a discrete layer above denser, more mafic liquid.

The two types of heterogeneous pumice deposits (stratified and chaotically mixed) may simply reflect variation in the extraction pattern of magma from the chamber. If the capping layer is drawn from the chamber before the underlying material, a compositionally-stratified pumice deposit results. If both magma types are simultaneously drawn from the chamber, as in the model of Blake (1981), or due to 'stirring together' of mafic and felsic liquids immediately before eruption, banded pumice is erupted. The actual extraction pattern is determined by chamber morphology, and viscosity and density variation of the magma (Blake, 1981).

Over the whole succession, phonolitic components of magmatically heterogeneous pumice deposits are mineralogically uniform, whereas phenocryst assemblages of the mafic components are characteristically

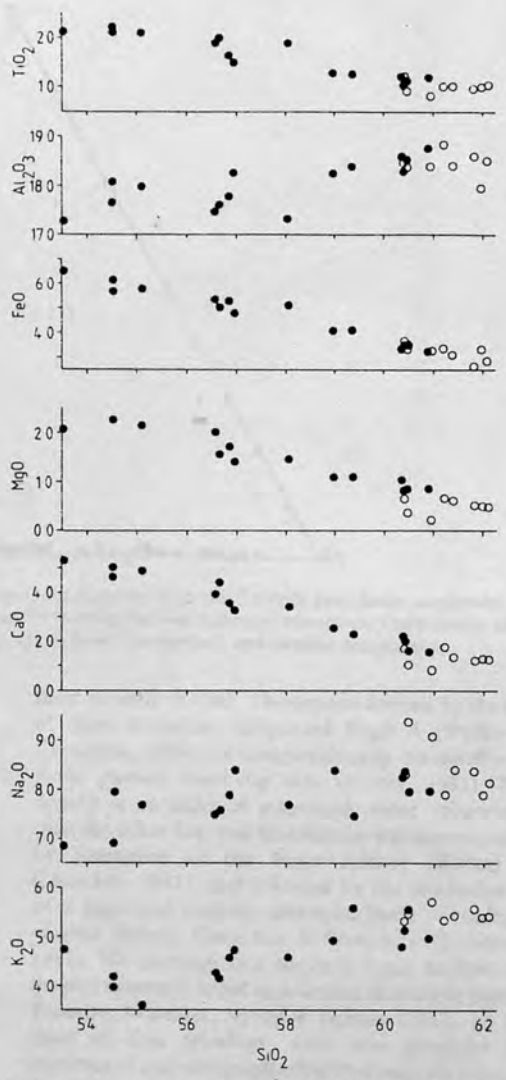

Figure 3. Variation diagrams vs. SiO_2 for streaky pumice glasses from Tenerife ignimbrite O. Filled circles: mafic glass; open circles: salic glass.

Table 1. Generalized phenocryst assemblages in salic and mafic components of heterogeneous pumice deposits, Tenerife, Canary Islands

Salic	Alkali-feldspar + biotite + sphene + Fe–Ti oxides + aegirine-augite ± amphibole ± nepheline ± sodalite
Mafic	Plagioclase (An_{20}–An_{40}) + augite + kaersutite + Fe–Ti oxides ± haüyne ± plagioclase (An_{55}–An_{90}) ± titanaugite ± olivine(Fo_{75}).

variable, implying a range of basic to mafic-intermediate magmas (Table 1). This contrast is clearly illustrated by feldspar compositions (Fig. 4); plagioclase from the mafic components varies from An_{22}

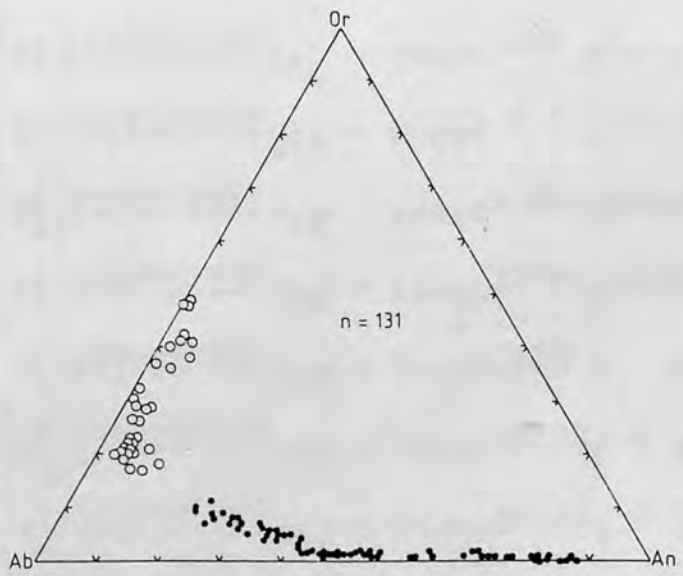

Figure 4. Feldspar compositions in five magmatically heterogeneous deposits from the Tenerife pyroclastic succession. All contain alkali feldspar, with sodic and/or calcic plagioclase typically showing varying degrees of resorption. Open circles: alkali feldspars from phonolitic components of deposits; dots: plagioclases from intermediate and basaltic components.

continuously to An_{88}. Other phenocryst species exhibit similar variation (Wolff, unpub. Ph.D. thesis, Univ. London, 1983). Mineralogical and compositional variations within the mafic components of the Tenerife magma system are mainly attributed to magma mixing (Wolff, unpub. Ph.D. thesis, Univ. London, 1983) and will be discussed elsewhere; we are here largely concerned with the origin and behaviour of the capping (phonolitic) layer of the magmatic system. The discrete nature of this layer is apparent from Figure 4; its volumetric dominance among the products of eruptions from the central caldera presumably reflects its position as the uppermost part of the magmatic system.

2.b. Sao Miguel and Faial, Azores Islands

The Azores Islands straddle the Mid-Atlantic Ridge (Fig. 1) on a topographic high known as the Azores Platform, those to the east of the ridge being associated with a seismically active transform fracture zone (Laughton & Whitmarsh, 1975). Volcanic rocks from the Azores consist predominantly of alkali basalts and their differentiates which include trachytes and peralkaline rhyolites. On Sao Miguel and Faial, extensive dominantly trachytic, pyroclastic fall deposits occur (Booth, Croasdale & Walker, 1978; Storey, 1981; Walker & Croasdale, 1971, and unpub. data). Sao Miguel, the largest island, has three active stratovolcanoes; we consider the products of one of these (Agua de Pau volcano) here. In the last 5000 years, Agua de Pau has explosively erupted six times, most recently in 1563. The deposit formed by the first of these eruptions, designated Fogo A (Walker & Croasdale, 1971), is compositionally stratified with mafic pumice overlying salic (Storey, 1981). This deposit is an order of magnitude more voluminous than the other five, and its eruption was accompanied by formation of the Fogo caldera (Walker & Croasdale, 1971), and followed by the establishment of a high-level laterally extensive body of trachytic magma (Booth, Croasdale & Walker, 1978; Storey, 1981). We envisage that beneath Agua de Pau, the magma system is zoned in a similar fashion to that on Tenerife. Marriner, Norry & Gibson (1982), on the basis of lava petrology, have also proposed the existence of a zoned magma chamber beneath Agua de Pau. The pyroclastic products of Carego Gordo caldera on Faial island also display evidence of derivation from the upper parts of a zoned magmatic system. Faial pumice fall A is a particularly good example of a compositionally zoned pumice fall; it closely resembles Fogo A and Tenerife A.

2.c. Vesuvius A.D. 79

The type plinian deposit, formed by the A.D. 79 eruption of Somma-Vesuvius, Italy, also displays marked vertical chemical and petrographic variation (Lirer *et al.* 1973; Barberi *et al.* 1981); again, mafic alkaline (phonolite–tephrite) pumice overlies more evolved phonolitic pumice within the products of the one eruption. We include this example here, firstly to demonstrate that zonation of highly evolved alkaline

Table 2. Major- and trace-element analyses of pumice fall deposits A, E and G from Tenerife, Faial A, Fogo A, and the Congro ash and lava dome from the Azores and the A.D. 79 deposit of Vesuvius

	Tenerife								Sao Miguel								
	Deposit A		Deposit E			Deposit G			Fogo A			Congro deposit		Faial A		Vesuvius A.D. 79	
Sample No.	base AF1	top AF3	base EF1	middle EF2	top EF4	base GF3	middle G678	top Gigl	base AZ1544	middle AZ1323	top AZ1377	ash AZ1019	lava AZ1672	base F500	top AZ3446	base 57/59	top 56/61
SiO_2	63.13	56.45	62.71	61.93	62.33	60.85	61.18	61.69	62.91	61.27	61.59	63.04	63.28	59.27	57.05	56.06	54.30
TiO_2	0.42	1.82	0.64	0.61	0.72	0.56	0.47	0.63	0.64	0.97	1.02	0.70	0.69	1.22	1.47	0.24	0.56
Al_2O_3	19.89	19.01	18.44	18.88	18.65	19.76	20.03	19.33	19.22	18.74	17.56	18.46	18.00	21.46	19.11	22.47	19.93
Fe_2O_3	2.84	6.53	3.14	3.16	3.26	3.40	3.47	3.29	3.67	4.26	4.19	3.24	3.61	5.45	6.38	2.56	4.72
MnO	0.24	0.22	0.19	0.21	0.20	0.25	0.26	0.24	0.13	0.13	0.14	0.12	0.10	0.22	0.16	0.13	0.14
MgO	0.26	1.77	0.56	0.46	0.54	0.43	0.38	0.53	0.47	0.94	1.14	0.49	0.59	0.56	1.91	0.18	1.66
CaO	0.78	4.87	0.65	0.64	0.79	0.75	0.59	0.73	1.31	1.99	2.17	1.34	1.44	1.22	4.50	2.55	5.52
Na_2O	5.09	5.27	7.13	7.51	7.18	8.13	7.49	6.67	5.50	5.63	5.95	6.00	5.64	6.07	6.23	5.94	4.27
K_2O	7.30	3.58	6.47	6.54	6.23	5.81	6.08	6.81	6.07	5.92	6.05	6.51	6.54	4.35	3.03	9.85	8.70
P_2O_5	0.05	0.48	0.07	0.06	0.10	0.06	0.05	0.08	0.08	0.15	0.19	0.10	0.11	0.18	0.16	0.02	0.20
Rb	200	85	98	135	112	177	191	141	117	139	132	152	150	72	54	411	350
Sr	69	935	5	6	13	40	13	16	115	240	278	136	202	100	611	414	981
Ba	142	1220	87	42	364	206	25	60	312	501	531	406	582	294	908	285	1312
Cu	11	16	17	28	21	16	8	23									
Ni	5	37	4	5	4	2	4	4	2	4	6	5	4	1	3	2	13
Zn	126	109	128	122	112	141	152	118									
V	23	105	38	38	43	37	30	42	6	25	32	15	16	14	62	28	113
Y	37	50	29	57	64	58	58	50	36	43	37	40	33	44	32	12	28
La	113	89	133	130	130		153	132	74	79	81	95	73	75	51	95	74
Ce	186	195	243	229	247	225	226	245	151	195	173	188	165	150	105	156	129
Nd	36	71	80	73	91	64	55	73	55	75	59	59	54	62	46	44	52
Sm	4.5	12.4	13.4	12.3	15.2	8.6	7.5	10.8	11.8	14.1	12.0	13.6	11	10.9	8.9		6.1
Eu	0.86	3.7	3.0	2.6	3.7	1.8	1.5	2.2	1.9	2.1	2.4	2.3	2.6	1.9	3.3	1.2	2.3
Tb	0.7	1.6	1.8	1.6	1.9	1.1	1.4	1.5	1.2	1.6	1.3	1.3	1.0	1.3	0.9		0.7
Yb	3.5	2.8	4.1	4.2	4.3	4.6	5.1	3.8	3.3	3.9	3.6	3.9	2.9	4.8	2.7	1.5	2.4
Lu									0.5	0.7	0.5	0.6		0.6	0.3		
Zr	1140	531	484	848	698	1130	1250	790	867	806	681	875	753	595	354	318	259
Hf			15.8	16.3	13.4	24	27							14	9.4	8.0	7.3
Th	30.5	12.1	17.8	20.4	17.6	30.7	34.0	23.8	15.9		15.2	22.7		11.5	5.8	52	35
U	7.3	3.0	4.4	4.4	3.0	7.3	9.0	6.9						2.5	2.1	10	6.8
Nb	286	199	161	290	265	368	377	293	121	136	118	149	127	119	72	75	57
Ta	13.9	15.8	20.9	19.5	20.9	21.1	21.0	22.0			8.2			7.2	5.0	3.5	3.0

Major-element abundances are expressed as oxide weight %, and trace elements as ppm. Total iron is reported as Fe_2O_3. To facilitate comparison the major-element analyses have been normalized to 100% on a water-free basis. The original totals, which include ater contents, are in the range 98.7–100.7 wt-%. Analytical methods: REE, Th, U, Hf, Ta by instrumental neutron activation; remainder by XRF. See Storey (1981) and Wolff (unpub. Ph.D. thesis, Univ. London, 1983) for details.

magmas is not restricted to the ocean-island setting but also occurs in K-rich magma bodies, and secondly to present new trace-element data on the deposit.

3. Geochemical features of zoned alkaline systems

Whole-pumice geochemical data are given in Table 2, and presented graphically in Figures 5–11.

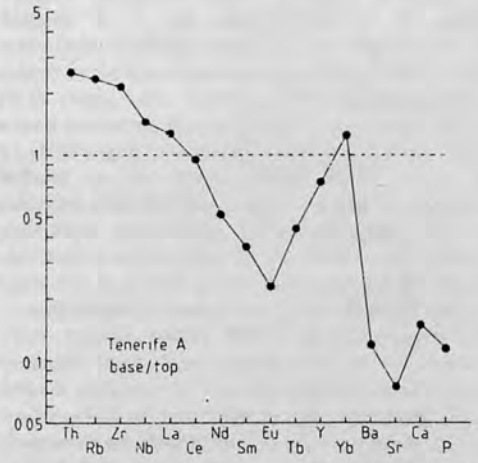

Figure 5. Trace element variation in Tenerife pumice fall A. Each plotted point is the concentration of an element in the basal salic pumice, divided by its concentration in the topmost mafic pumice. The compositional stratigraphy of the deposit is assumed to qualitatively represent an inversion of that of the magma body prior to eruption. Phenocryst assemblages are, mafic pumice: sodic plagioclase + haüyne + augite + kaersutite + Fe–Ti oxides; salic pumice: sanidine + sodic plagioclase + haüyne + augite + biotite + sphene + Fe–Ti oxides. Note that in this and all other deposits described here, apatite occurs in small amounts as inclusions in other phenocryst phases.

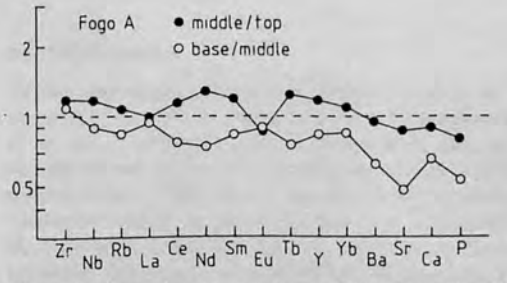

Figure 6. Trace element variation in Fogo A pumice fall deposit, Sao Miguel. Filled circles: concentration of an element in the middle portion of the deposit divided by its concentration in the topmost part. Open circles: concentration of an element in basal pumice divided by its concentration in the middle portion. Phenocryst assemblage: alkali feldspar + clinopyroxene + biotite + Fe–Ti oxides. Occasional xenocrysts of forsteritic olivine, titanaugite and calcic plagioclase occur in the upper mafic pumice.

3.a. Petrographic zonation

We use the term 'petrographic zonation' to refer to those pumic deposits, and, by inference, the magmas from which they were derived, which exhibit stratification in phenocryst assemblages. Petrographic zonation is normally accompanied by marked chemical zonation, as is the case for Tenerife A, Faial A and Vesuvius A.D. 79, but not for Fogo A. In each of the four cases, less evolved mafic pumice overlies more evolved salic pumice. Representative sample/sample element ratios for these four deposits are given in Figures 5–8. These diagrams are essentially similar to the 'element enrichment' diagrams used by Hildreth (1979), except that we prefer to plot points rather than vertical bars as this permits comparison of more than

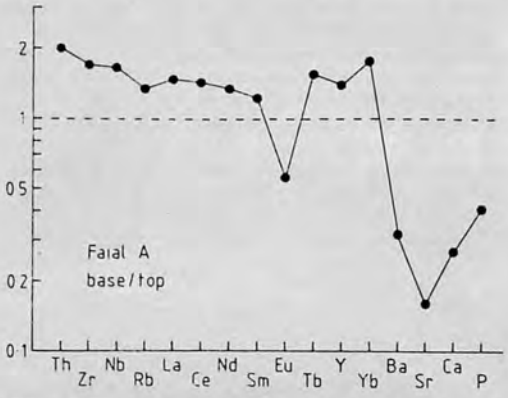

Figure 7. Trace element variation in pumice fall deposit A, Faial. Symbols as Figure 5. Phenocryst assemblage: sanidine + clinopyroxene + biotite + Fe–Ti oxides, with amphibole and plagioclase additionally present in the upper mafic portion.

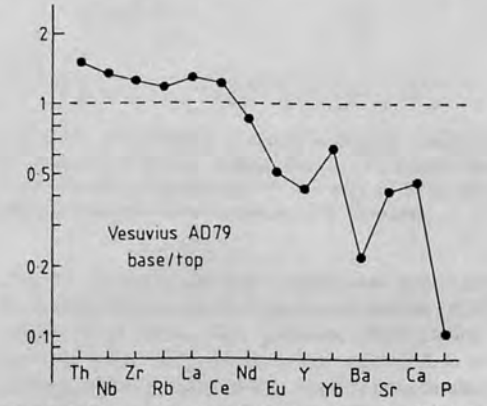

Figure 8. Trace element variation in the pumice fall deposit from the A.D. 79 eruption of Vesuvius, Italy. Symbols as Figure 5. Phenocryst assemblage: sanidine + plagioclase + leucite + clinopyroxene + biotite + amphibole + garnet + scapolite + Fe–Ti oxides (see also Barberi *et al.* 1981).

one pair of samples. Elements which show the greatest variation are plotted in approximate order of increasing atomic number (Y is plotted as a heavy REE). The geochemical differences between the two components in each case mirror the general geochemical trends for each magmatic suite. Ba, Sr, Ca and P normally behave as strongly compatible elements, due to the influences of feldspar, biotite, amphibole/pyroxene, and apatite fractionation (Storey, 1981; Wolff, unpub. Ph.D. thesis, Univ. London, 1983). A distinctive general feature of the Tenerife phonolitic suite, strongly developed in Tenerife A, is the compatibility of the middle rare-earths (MREE); this is due to the presence of sphene in the fractionating assemblage (Wolff, unpub. Ph.D. thesis, Univ. London, 1983). Sphene exhibits a strong preference for the MREE over La, Ce, Yb and Lu (Hellman & Green, 1979; Green & Pearson, 1983; Wörner *et al.* 1983; Wolff, 1984); it is the principal REE-bearing mineral among the phonolite phenocryst assemblage. Amphibole-group minerals also display a preference for the MREE, and although kaersutite is present in the mafic portion of Tenerife A, amphibole is absent from other Tenerife deposits which exhibit similar MREE depletion with fractionation. In any case, some 90–95% of total observed MREE depletion in Tenerife magmas occurs during fractionation of phonolite in the absence or virtual absence of amphibole, but in the presence of sphene; only 5–10% takes place in the fractionation of trachyandesite to phonolite (Wolff, unpub. Ph.D. thesis, Univ. London, 1983). In the Azores examples, negative Eu anomalies are consistent with the presence of feldspar as a phenocryst phase. Elements such as Th, Nb and Zr generally show strong enrichment in the salic pumice. Fogo A contrasts strongly in this respect, in that the mafic zone is only slightly less evolved than the salic component. Vesuvius A.D. 79 shows marked heavy-REE (HREE) depletion in the salic portion, consistent with the presence of melanite garnet in the phenocryst assemblage.

3.b. Occult zonation

Vertical chemical variation in petrographically homogeneous phonolitic or trachytic units is here referred to as occult zonation. Occult zonation is thus an internal feature of the salic capping layer of the zoned magma system. Typically it is manifested as very slight variation in major element concentrations, while some trace elements (especially Ba) may show considerable variation. Three cases are selected here as examples. E and G, with juvenile volumes of the order of 5–10 km^3 of equivalent dense rock, are two large plinian deposits on Tenerife (G is the Granadilla Pumice of Booth, 1973). Both display occult zoning (Figs. 9 and 10, filled circles), chemically similar in type and sign, but lesser in degree, to the petrographic zoning of deposit A (Fig. 5). These changes are continual and progressive from 30% thickness to the top of each deposit (Wolff, unpub. Ph.D. thesis, Univ. London, 1983); zoning is reversed below 30% thickness (see below). E is also petrographically zoned in that banded pumice clasts, bearing phenocrysts typical of intermediate magma, are found in an overlying ignimbrite, considered to represent the closing stages of the same eruption.

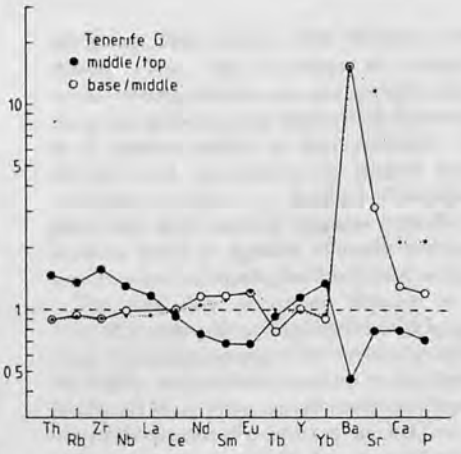

Figure 9. Trace element variation in the Granadilla (G) pumice deposit, Tenerife. Open and filled circles as Figure 6; 'middle' here is approximately 25% thickness above base. The dots represent a hypothetical composition, produced by adding 15% of intermediate contaminant (see text) to the 'middle' composition, divided by the middle composition. This closely models the base/middle pattern for incompatible trace elements, but not for major elements (e.g. Ca, P), indicating that the compositional contrast between the base and middle of G is not due to contamination alone. The phenocryst assemblage throughout G is: alkali feldspar + sodalite + augite + amphibole + biotite + sphene + Fe–Ti oxides.

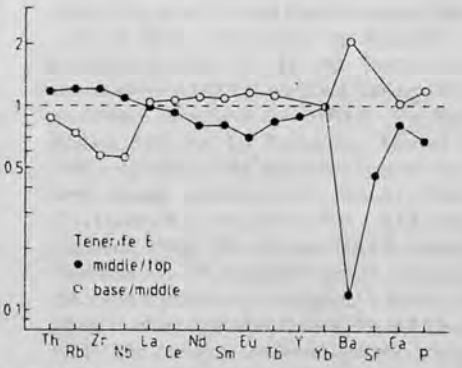

Figure 10. Trace element variation in Tenerife pumice fall E, symbols as Figure 6; 'middle' here is 15% height above base. Phenocryst assemblage in this part of E is: alkali feldspar + augite + biotite + sphene + Fe–Ti oxides.

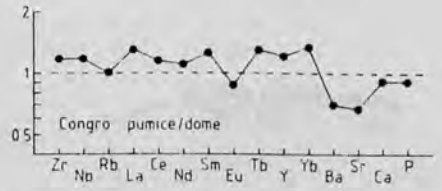

Figure 11. Trace element variation among products of the Congro flank eruption from Agua de Pau, Sao Miguel. Each point is the concentration of an element in the fall deposit divided by its concentration in the trachyte dome extruded at the end of the eruption. Phenocryst assemblage: alkali feldspar + clinopyroxene + biotite + Fe–Ti oxides.

However, banded pumice is restricted to a higher level in the eruption stratigraphy than any analysed sample. Occult zoning is also displayed by the products of the Congro flank eruption from Agua de Pau. Eruption of a very small-volume sub-plinian trachytic pumice deposit (< 0.01 km of equivalent dense rock, Booth, Croasdale & Walker, 1978) was followed by extrusion of a trachyte dome. The two units are closely similar; however, the pumice deposit is slightly enriched in incompatible elements, and depleted in compatible elements, with respect to the dome (Fig. 11).

3.c. Zoning reversals

Reversed zoning is opposite in sign to that so far described. It is not predicted by a simple model for evacuation of magma from a zoned system but has been recorded from a few rhyolitic examples (Eggleston, Osburn & Chapin, 1983). Reversed occult zoning is found in the basal 30% of Tenerife deposits E and G (Figs. 9, 10) and possibly in the lower portion of Fogo A (Fig. 6). The basal part of Tenerife G contains occasional, small (< 2 mm), partly disaggregated fragments of fine-grained intermediate rock with a juvenile phonolitic coating, suggesting contamination of the initially uppermost magma with roof-rock, perhaps during uprise immediately prior to eruption. The whole-rock composition of basal G pumice is not however given by simple addition of the intermediate composition to the most evolved G sample: satisfaction of trace element abundances in basal G requires a more mafic major element composition than is actually found (Fig. 9). Among the phonolites, major element composition varies little for large differences in trace element contents. Thus the less-evolved basal G pumice composition is not due solely to country-rock contamination.

4. Discussion

4.a. Origin of zonation

Both petrographic and occult zonation in individual alkaline eruptive units find close analogues in rhyolitic and rhyolitic–andesitic systems (Smith & Bailey, 1966; McBirney, 1968; Smith, 1979; Hildreth, 1979, 1981; Bacon, 1983). The frequency of compositionally heterogeneous alkaline deposits strongly indicates that the pre-eruptive magma bodies were chemically zoned in a fashion similar to that envisaged for silicic systems, and prompts us to suggest that, in an analogous fashion to rhyolites (Hildreth, 1981), phonolitic and trachytic magmas typically occur as capping layers to systems of mafic intermediate to basaltic alkaline liquid, possibly rooted at deep levels.

The similarlity of zoning features in different evolved systems, of varying degrees of SiO_2-saturation, suggests a common origin for chemical gradients in all the highly differentiated systems so far documented. Michael (1983*a*, *b*) has argued that crystal fractionation is entirely capable of producing the chemical variation observed in the most fully documented example, the rhyolitic Bishop Tuff, California. Despite objections raised by Hildreth (1983) to these arguments, Michael (1983*b*) emphasizes that 'the gradients observed are consistent with crystal–liquid equilibria, *without the need to invoke other processes*' (our italics). Much of the debate on differentiation mechanisms (crystal–liquid *vs.* liquid state) has centred around the behaviour of those trace elements normally considered to be incompatible during fractional crystallization, especially LREE (Hildreth, 1979; Mahood, 1981; Mittlefehldt & Miller, 1983). It is instructive in this regard to compare the behaviour of the REE in phonolitic, trachytic and rhyolitic zoned systems in the light of REE abundances in REE-rich accessory phenocrysts (Fig. 12). In the Tenerife phonolites, strong upward MREE depletion is compatible with the preference of sphene for MREE. For the rhyolitic Bishop Tuff and La Primavera, Mexico (Mahood, 1981), upward LREE depletion is consistent with the very strong preference of allanite (Bishop) and chevkinite (La Primavera) for LREE (Mahood & Hildreth, 1983). The upward HREE depletion in the Vesuvius A.D. 79 magmatic system is consistent with the known preference of garnet, a minor phenocryst phase (melanite) in this deposit, for HREE over other REE. The Azorean trachytic systems, which lack the above phases, display approximately uniform enrichment of all REE. Apatite, which preferentially incorporates the MREE, occurs in all these systems. The slight upward MREE depletion apparent in the Azorean systems is attributed to the influence of apatite, as is the upward decrease in Y/Yb in the Vesuvius system (Fig. 12*c*, *d*). It none the less appears that the influence of apatite on the distribution of REE in zoned systems is subordinate to that of other minor REE-rich phases, where such are present. Comparison of a range of magma types therefore suggests that chemical gradients in felsic and intermediate-felsic magma systems arise through fractionation of observed phenocryst assemblages.

It is desirable to test the feasibility of crystal

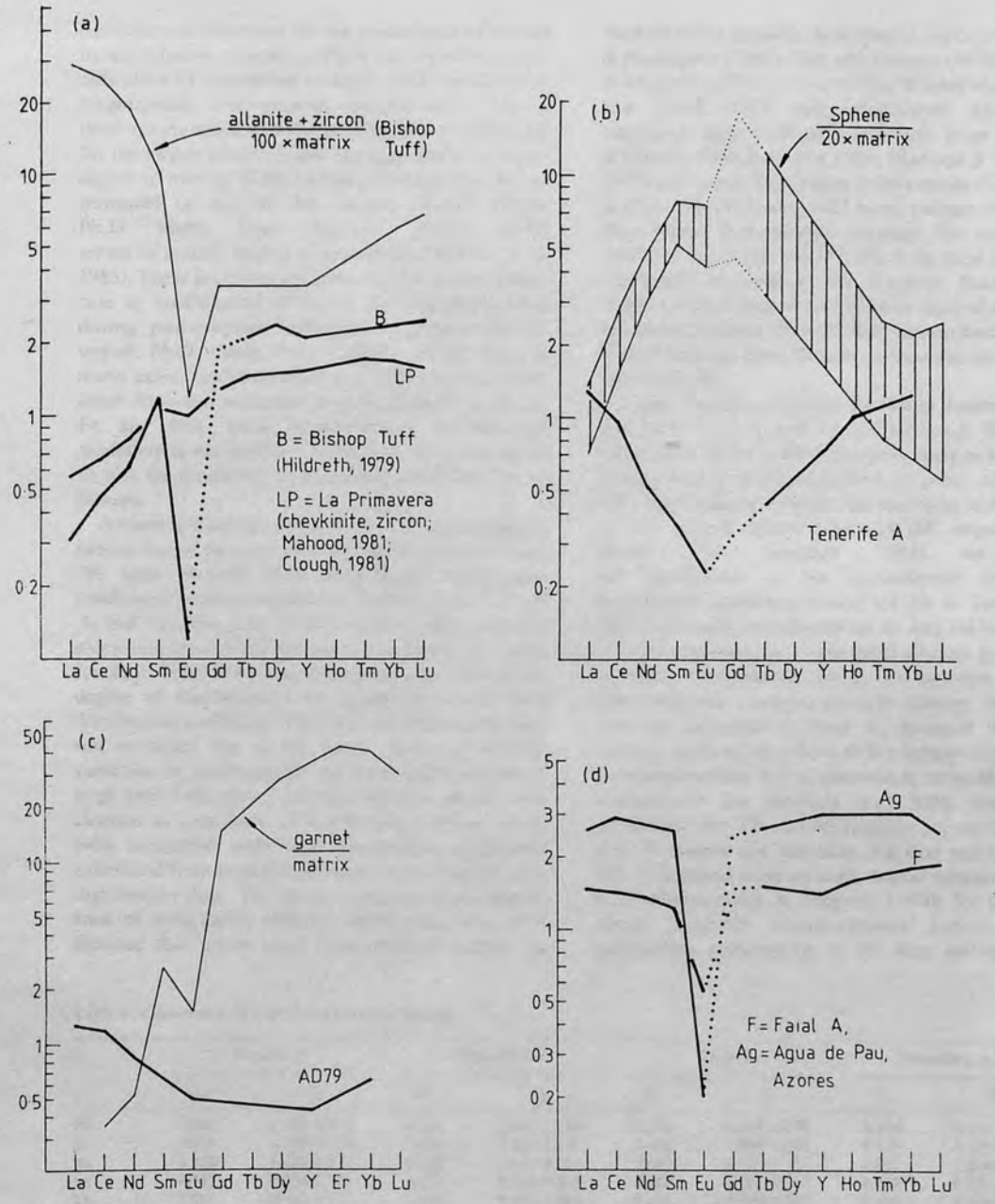

Figure 12. Comparison between REE behaviour in zoned felsic magma systems, of varying degrees of silica-saturation, with the REE preference exhibited by accessory REE-bearing phenocryst phases. (a) REE abundances in early erupted tephra divided by those in late-erupted tephra, for two high-silica rhyolite zoned pyroclastic deposits; B = Bishop Tuff, California (allanite and zircon-bearing, Hildreth, 1979); LP = La Primavera Tala Tuff (Mahood, 1981). The only minerals known to concentrate the REE noted by Mahood (1981) as present at La Primavera are apatite and zircon. However Clough (unpub. Ph.D. thesis, Univ. London, 1981) identified chevkinite in these rocks. Chevkinite exhibits a strong LREE preference and is here considered as essentially identical to allanite as regards its potential effects on REE behaviour in magmas from which it crystallizes. Allanite/matrix and zircon/matrix distributions taken from Mahood & Hildreth (1983). (b) Heavy line: as (a), for Tenerife deposit A. Vertical rule: range of sphene/matrix distributions determined for phonolitic magma by Wörner *et al.* (1983). Distributions for Ce, Nd and Y in sphene/matrix pairs from Tenerife G plot close to the lower end of this range. (c) Heavy line: as (a), for the Vesuvius A.D. 79 deposit. Garnet/matrix data from Schnetzler & Philpotts (1970). (d) Heavy line F: as (a), for Faial A deposit. Heavy line Ag is the concentrations of REE in Fogo deposit D divided by those in Fogo A; the Fogo D magma directly evolved from the Fogo A magma by crystal fractionation over a period of c. 4000 years (Storey, 1981).

fractionation processes for the production of zoning by quantitative modelling. There are, however, many difficulties in attempting to apply such modelling to magmatically heterogeneous volcanic rocks. Among these are imprecise knowledge of partition coefficients for the phases involved, and the uncertainty as to the degree of mixing of the various compositions during transport to and at the surface (Wolff, unpub. Ph.D. thesis, Univ. London, 1983), which serves to modify matrix compositions (Wörner *et al.* 1983). These problems are compounded in the present case by modification of Na, K and Mg abundances during post-eruptive hydration of pumice (Wolff, unpub. Ph.D. thesis, Univ. London, 1983). Also, in many cases, analytical error is a large fraction of the small intra-unit variation in such elements as Si, Al, Fe and Mn. Thus major-element fractionation modelling is not realistic. Instead we have attempted to test the feasibility of fractional crystallization as follows.

Assuming Rayleigh fractionation for the respective production of the most evolved part of each unit from the least evolved, bulk solid/liquid distribution coefficients were calculated for Tenerife A & G, Faial A, and Vesuvius A.D. 79. The most strongly enriched element in the evolved portion (Th in each case, except for Zr in Tenerife G) was selected as a monitor of the degree of fractionation by assuming a zero bulk distribution coefficient. The other units described were not modelled due to the small degree of internal variation in incompatible elements and consequent large errors associated with the selection of one such element as a measure of fractionation. These values were compared with bulk distribution coefficients calculated from modal abundances and trace-element distribution data. The strong compositional dependence of solid/liquid element partitioning behaviour dictated that information from alkaline systems be used wherever possible; accordingly, the data of Berlin & Henderson (1969), Sun and Hanson (1976), Cullers & Medaris (1977), Larsen (1979), Wörner *et al.* (1983) and Wolff (1984, and unpublished data) were employed. Ilmenite/liquid coefficients from rhyolites (Crecraft, Nash & Evans, 1981; Mahood & Hildreth, 1983) and garnet/liquid data from a dacite (Schnetzler & Philpotts, 1970) were used in the absence of data for these phases from alkaline magmas. The two sets of coeffients are compared in Table 3. In most cases, the coefficients required by the Rayleigh fractionation model for each deposit lie within or close to the range of values calculated from the distribution data. Nb and Y were omitted from the comparison due to a lack of literature data.

Large discrepancies exist for Rb in Tenerife A, Zr and Hf in Faial A, and Yb and Hf in A.D. 79. Of the elements in Table 3, Rb is the most likely to be mobile during post-eruptive hydration of glass; as sample AF1 has the highest weight loss on drying and ignition of any sample reported here (Wolff, unpub. Ph.d. thesis, Univ. London, 1983), we attach no significance to the anomalously low bulk distribution coefficient found for Rb in Tenerife A. The high coefficients found for Zr and Hf in Faial A may be explained by a very small amount (*c.* 0.03%) of zircon fractionation. Zircon is a very rare phase in some Azorean trachytic pumices (Storey, 1981) and was not recorded in Faial A; however the small amount required may have either been overlooked or be unrepresented in the phenocryst assemblage. The reasons for the similarly high bulk distribution coefficients for Yb and Hf required for the Vesuvius A.D. 79 magma are less clear. Yb may partition into melanite garnet more strongly than is indicated by the data of Schnetzler & Philpotts (1970) for garnet in dacite. Similarly, crystal-chemical factors suggest substantial partitioning of Hf into andradite-rich

Table 3. Comparison of bulk distribution coefficients

	Tenerife A		Tenerife G		Faial A		Vesuvius A.D. 79	
	D_1	D_2	D_1	D_2	D_1	D_2	D_1	D_2
Rb	0.074	0.223–0.842	0.339	0.316–1.184	0.580	0.314–1.179	0.594	0.312–0.687
Sr	3.819	1.554–33.07	1.453	1.306–7.667	3.644	1.080–7.604	3.179	0.103–3.580
Ba	3.326	1.670–8.004	2.908	2.174–9.123	2.647	2.139–9.161	4.857	2.804–4.183
La	0.742	0.354–0.906	0.678	0.263–0.692	0.437	0.180–0.517	0.369	0.251–0.615
Ce	1.051	0.461–1.397	1.176	0.352–1.085	0.479	0.239–0.507	0.520	0.389–0.798
Nd	1.735	1.190 – 2.456	1.617	0.964–1.802	0.564	0.458–0.670	1.422	0.715–1.654
Sm	2.096	0.841–4.177	1.795	0.608–2.859	0.704	0.376–1.167	—	—
Eu	2.578	1.409–6.304	1.835	1.221–4.025	1.838	1.276–2.471	2.719	0.958–7.326
Tb	1.894	0.860–5.794	1.150	0.560–4.118	0.352	0.407–0.763	—	—
Yb	0.759	0.305–1.119	0.359	0.204–0.798	0.162	0.104–0.227	2.121	0.915–1.417
Zr	0.174	0.066–0.301	0.000	0.043–0.117	0.241	0.005–0.062	0.482	0.110–0.455
Hf	—	—	—	—	0.441	0.031–0.096	0.769	0.260–0.446
Th	0.000	0.039–0.196	0.223	0.035–0.239	0.000	0.015–0.117	0.000	0.014–0.111
Ta	1.139	1.085–2.276	1.101	0.996–1.990	0.481	0.255–0.307	0.611	0.410–0.528

Comparison of bulk distribution coefficients required for the development of zoning by Rayleigh fractionation (D_1), with the range of bulk coefficients calculated from observed modal abundances of phenocrysts and published data on crystal/liquid element distribution (D_2, see text for sources) for Tenerife A, Tenerife G, Faial A, and Vesuvius A.D. 79 pumice fall deposits.

garnet; in the absence of any data, Hf was assumed not to enter A.D. 79 garnet.

In summary, the gradients in trace-element contents in the modelled zoned units are consistent with an origin by crystal fractionation. The modelling is, however, rather poorly constrained, due to the objections noted above.

However, Hildreth's (1979) objections to crystal *settling* as a viable differentiation mechanism cannot easily be refuted. A further objection is that convective velocities in magma bodies exceed settling velocities of crystals by an order of magnitude, thus causing crystals to remain suspended (Sparks, Huppert & Turner, 1984). Possession of a yield strength by the magma may also preclude settling. Many other mechanisms of crystal-liquid separation, such as filter pressing, require highly porphyritic magma; the examples discussed here are all of phenocryst-poor magma. The only currently known differentiation mechanism capable of producing the observed relationships is convective fractionation (McBirney, 1980; Chen & Turner, 1980; Sparks, Huppert & Turner, 1984); specifically, wall-rock crystallization of intermediate magma to yield a low-density boundary layer of evolved magma; this then buoyantly rises to the top of the chamber where it forms a discrete stable capping layer, chemically 'protected' from the underlying magma by a double diffusive interface. Convective fractionation is a near-ubiquitous feature of laboratory experiments, using saturated aqueous solutions, which attempt to simulate processes in cooling magma bodies (Turner & Gustafson, 1981). However, its operation in real magmas has yet to be demonstrated.

Cryptic chemical gradients within the capping layer may arise in a number of ways. Turner & Gustafson (1981) note that in several of their experiments, the capping layer (and the rest of the system) itself split into a fine structure of independently convecting thinner layers separated by double diffusive interfaces. Alternatively, accumulation of evolved liquids, having slightly different densities, at the top of the system would automatically produce a zonation in the capping layer itself, with the least dense (and hence most evolved) liquid increment forming the top of the capping layer.

4.b. Reversed zoning

The occurrence of reversed zoning in three examples suggest that chemical profiles through pyroclastic deposits do not always qualitatively represent an inverted magma chamber stratigraphy. Alternatively it is conceivable (but unlikely) that the magma system itself is in part reversely zoned. In any case the implications for petrologic study of felsic volcanic centres are clear. It has been assumed (e.g. Mahood, 1981) that the relatively small-volume lavas erupted at silicic centres without any precursory explosive activity are representative of the most highly evolved magma produced at the roof of the system. If processes that induce reverse zoning among erupted products commonly operate, this assumption is invalid. The same is true of small-volume pumice eruptions. Only the largest-volume plinian and ignimbrite eruptions found at a particular centre can reasonably be assumed to have sampled the most evolved (among others) liquid produced by the subvolcanic magma system. At the volcanoes studied by us, felsic lavas invariably have much less evolved trace-element abundances that associated pumices of similar major-element compositions (Ridley, 1970*b*; Wolff, unpub. Ph.D. thesis, Univ. London, 1983; Storey, unpub. data). The volumetrically insignificant lavas which emerge at the end of pyroclastic eruptions will, by virtue of normal chemical gradients, also tend to have less-evolved compositions (e.g. Fig. 11; Mahood, 1981).

4.c. The 'Daly gap'

On both Sao Miguel and Tenerife, intermediate volcanic rocks are volumetrically subordinate to their felsic derivatives (Booth, Croasdale & Walker, 1978; Ridley, 1970*a*). Although the extent of the 'Daly gap' at any particular centre is dependent on the geochemical parameters chosen to express it, due to the narrow crystallization interval within which intermeidate magmas are generated in any magma series (Clague, 1978; Wood, 1978), it becomes a very real phenomenon when the pyroclastic volumes are properly computed (Booth, Croasdale & Walker, 1978; Wolff, unpub. data), due to the overwhelming preference of felsic magma for explosive eruption. Magma body zoning provides an attractive explanation for the Daly gap. The capping felsic layer will effectively prevent the denser underlying intermediate magma from reaching the surface (unless the cap is first removed by eruption), resulting in a paucity of erupted intermediate compositions. If the capping layer is very rapidly generated, as is suggested by laboratory experiments (Sparks, Huppert & Turner, 1984; Turner & Gustafson, 1981), then the lack of intermediate volcanics might be expected to be almost total, as is the case on Sao Miguel (Booth, Croasdale & Walker 1978).

4.d. Zonation rates

At the centres discussed here, eruptions from zoned magmatic systems occur on the order of one every few thousand years. The Vesuvius A.D. 79 eruption took place about 3600 years after the previous large eruption from Somma-Vesuvius, which produced a similarly zoned deposit (Barberi *et al* 1981).

On Tenerife, deposits A, E and G are members of

the Granadilla Series, which includes at least four other compositionally zoned and heterogeneous units. The entire Series, comprising at least twenty deposits, probably formed over a period of 10000–20000 years (Booth & Walker, in prep.). Thus the average repose period between eruptions from zoned systems recorded in the Granadilla Series is of the order of 1400–3000 years. The Grandilla Series is overlain by the Fasnia Series, a plinian deposit near the base of which has an age of 28500 years. Some fifteen units overlie this deposit, of which six are zoned (Booth & Walker, in prep.; Wolff, unpub. Ph.D. thesis, Univ. London, 1983). Based on soil thicknesses, Booth & Walker estimate that the youngest of these may be 10000 years old. The average repose period between eruptions from zoned systems in the Fasnia Series is thus of the order of 3000 years.

If it is assumed that all eruptions at one centre are derived from essentially the same magma 'chamber', then it appears that the fractionation processes which produce zoning are operative on the scale of a few thousand years. This rate is consistent with Storey's (1981) documentation of substantial evolution (corresponding to 70% crystallization) of trachytic magma at the Agua de Pau centre over 4000 years. This rapid development of highly differentiated fluid is in agreement with the laboratory experiments, in which evolved capping layers develop at a very early stage by sidewall crystallization and boundary layer uprise (Turner & Gustafson, 1981; Sparks, Huppert & Turner, 1984).

5. Conclusions

Zoned magma systems display a number of unifying features which cut across petrographic association and tectonic setting. Upward zoning from relatively mafic to relatively felsic compositions is common to all, with the exception of reversed zoning which may affect the very top of some systems. Chemical gradients are always consistent with an origin by crystal fractionation, although this does not preclude the operation of other effects in a minor role. The agreement between gross features of zoned systems and predictions from laboratory analogue experiments is encouraging and we endorse the plea of Huppert, Turner & Sparks (1982) that real magma chambers should be studied as complex fluid dynamic systems. We suggest that further progress in this field is likely to be achieved through study of young, fresh pyroclastic deposits, in which evidence for the complex nature of high level magmatic processes is most obvious, abundant and easily interpreted.

Acknowledgements. Wolff wishes to thank the Natural Environment Research Council of Great Britain for a research studentship at Imperial College, and for funding field work on Tenerife. Part of this work was carried out while Storey held an Inner London Education Authority research assistantship at South London College, Knights Hill, London SE27 0TX. Pumice samples from the Azores and Vesuvius were collected by Professor G. P. L. Walker. We are especially grateful to Professor Walker, Dr B. Booth and Dr R. Croasdale for generous access to unpublished data, and to Dr A. C. Mann for providing INAA analyses of the Faial A and Vesuvius A.D. 79 samples. We also thank Drs R. N. Thompson, A. D. Saunders and S. Self for discussion and critical comment. The paper was improved by the comments of Dr R. S. J. Sparks and an anonymous reviewer.

References

ANDERSON, A. T. 1976. Magma mixing: petrological process and volcanological tool. *Journal of Volcanology and Geothermal Research* **1**, 3–33.

BACON, C. R. 1983. Eruptive history of Mount Mazama and Crater Lake Caldera, Cascade Range, U.S.A. *Journal of Volcanology and Geothermal Research* **18**, 57–115.

BARBERI, F., BIZOUARD, H., CLOCHIATTI, R. METRICH, N., SANTACROCE, R. & SBRANA, A. 1981. The Somma-Vesuvius magma chamber: A petrological and volcanological approach. *Bulletin Volcanologique* **44**, 295–315.

BERLIN, R. & HENDERSON, C. M. B. 1969. The distribution of Sr and Ba between alkali feldspar, plagioclase and groundmass phases of porphyritic trachytes and phonolites. *Geochimica et Cosmochimica Acta* **33**, 247–55.

BLAKE, S. 1981. Eruptions from zoned magma chambers. *Journal of the Geological Society of London* **138**, 281–7.

BOOTH, B. 1973. The Granadilla Pumice Deposit of southern Tenerife, Canary Islands. *Proceedings of the Geologists' Association* **84**, 353–70.

BOOTH, B., CROASDALE, R. & WALKER, G. P. L. 1978. A quantitative study of five thousand years of volcanism on Sao Miguel, Azores. *Philosophical Transactions of the Royal Society of London* **A288**, 271–319.

BOOTH, B. & WALKER, G. P. L. in preparation. Products of explosive volcanism on Tenerife, Canary Islands.

BORLEY, G. D. 1974. Aspects of the volcanic history and petrology of the island of Tenerife, Canary Islands. *Proceedings of the Geologists Association* **85**, 259–79.

CHEN, C. F. & TURNER, J. S. 1980. Crystallisation in a double-diffusive system. *Journal of Geophysical Research* **85**, 2573–93.

CLAGUE, D. A. 1978. The oceanic basalt-trachyte association: an explanation of the Daly Gap. *Journal of Geology* **86**, 739–43.

CRECRAFT, H. R., NASH, W. P. & EVANS, S. H., Jr. 1981. Late Cenozoic volcanism at Twin Peaks, Utah: geology and petrology. *Journal of Geophysical Research* **86**, 10303–20.

CULLERS, R. L. & MEDARIS, G. Jr. 1977. Rare earth elements in carbonatites and cogenetic alkaline rocks: examples from Seabrook Lake and Callander Bay, Ontario. *Contributions to Mineralogy and Petrology* **65**, 143–53.

EGGLESTON, E. L., OSBURN, G. R. & CHAPIN, C. E. 1983. Reversely zoned Hells Mesa Tuff and Socorro Cauldron. *EOS, Transactions of the American Geophysical Union* **64**, 884.

FUSTER, J. M., ARANA, V., BRANDLE, J. L., NAVARRO, M., ALONSO, U. & APARICIO, A. 1968. *Geology and Volcanology of the Canary Islands: Tenerife*, 218 pp. Institute 'Lucas Mallada', Madrid.

GREEN, T. H. & PEARSON, N. J. 1983. Effect of pressure on

rare earth element partition coefficients in common magmas. Nature **305**, 414–16.

HELLMAN, P. L. & GREEN, T. H. 1979. The role of sphene as an accessory phase in the high-pressure partial melting of hydrous mafic compositions. *Earth and Planetary Science Letters* **42**, 191–201.

HILDRETH, W. 1979. The Bishop Tuff: evidence for the origin of compositional zonation in silicic magma chambers. In *Ash-flow Tuffs* (eds. C. E. Chapin & W. E. Elston), pp. 43–75. Geological Society of America Special Paper no. 180.

HILDRETH, W. 1981. Gradients in silicic magma chambers: implications for lithospheric magmatism. *Journal of Geophysical Research* **86**, 10153–92.

HILDRETH, W. 1983. Chemical differentiation of the Bishop Tuff and other high-silica magmas through crystallization processes: comment. *Geology* **11**, 622–3.

HUPPERT, H. E. & SPARKS, R. S. J. 1980. The fluid dynamics of a basaltic magma chamber replenished by influx of hot, dense ultrabasic magma. *Contributions to Mineralogy and Petrology* **75**, 279–89.

HUPPERT, H. E., SPARKS, R. S. J. & TURNER, J. S. 1982. Effects of volatiles on mixing in calc-alkaline magma systems. *Nature* **297**, 554–7.

HUPPERT, H. E., TURNER, J. S. & SPARKS, R. S. J. 1982. Replenished magma chambers: effects of compositional zonation and input rates. *Earth and Planetary Science Letters* **57**, 345–57.

LARSEN, L. M. 1979. Distribution of REE and other trace elements between phenocrysts and peralkaline undersaturated magmas, exemplified by rocks from the Gardar igneous province, South Greenland. *Lithos* **12**, 303–15.

LAUGHTON, A. S. & WHITMARSH, R. B. 1975. The Azores–Gibraltar plate boundary. In *Geodynamics of Iceland and the North Atlantic Area* (ed. L. Kristjansson). Dordrecht: D. Reidel.

LESHER, C. E. & WALKER, D. 1983. Soret fractionation of high-silica rhyolite magma. *EOS, Transactions of the American Geophysical Union* **64**, 883.

LIRER, L., PESCATORE, T., BOOTH, B. & WALKER, G. P. L. 1973. Two plinian pumice fall deposits from Somma-Vesuvius, Italy. *Geological Society of America Bulletin* **84**, 759–72.

MCBIRNEY, A. R. 1968. Compositional variations of the climactic eruption of Mount Mazama. In *Andesite Conference Guidebook* (ed. M. H. Dole), pp. 53–7. Oregon State Department of Geology and Mineral Industries Bulletin no. 62.

MCBIRNEY, A. R. 1980. Mixing and unmixing of magmas. *Journal of Volcanology and Geothermal Research* **7**, 357–71.

MAHOOD, G. A. 1981. Chemical evolution of a Pleistocene rhyolitic centre: Sierra La Primavera, Jalisco, Mexico. *Contributions to Mineralogy and Petrology* **77**, 129–49.

MAHOOD, G. A. & HILDRETH, W. 1983. Large partition coefficients for trace elements in high-silica rhyolites. *Geochimica et Cosmochimica Acta* **47**, 11–30.

MARRINER, G. F., NORRY, M. J. & GIBSON, I. L. 1982. The petrology and geochemistry of Agua de Pau volcano, Sao Miguel, Azores. Proceedings of International Symposium on the Activity of Oceanic Volcanoes (IAVCEI), *1980*, 159–73.

MICHAEL, P. J. 1983*a*. Chemical differentiation of the Bishop Tuff and other high-silica magmas through crystallization processes. *Geology* **11**, 31–4.

MICHAEL, P. J. 1983*b*. Chemical differentiation of the Bishop Tuff and other high-silica magmas through crystallization processes: reply. *Geology* **11**, 623–4.

MILLER, C. F. & MITTLEFEHLDT, D. W. 1982. Depletion of light rare-earth elements in felsic magmas. *Geology* **10**, 129–33.

MITTLEFEHLDT, D. W. & MILLER, C. F. 1983. Geochemistry of the Sweetwater Wash Pluton, California: implications for 'anomalous' trace element behaviour during differentiation of felsic magmas. *Geochimica et Cosmochimica Acta* **47**, 109–24.

RIDLEY, W. I. 1970*a*. The abundance of rock types on Tenerife, Canary Islands, and its petrogenetic significance. *Bulletin Volcanologique* **34**, 196–204.

RIDLEY, W. I. 1970*b*. The petrology of the Las Canadas volcanoes, Tenerife, Canary Islands. *Contributions to Mineralogy and Petrology* **26**, 124–60.

SCHNETZLER, C. C. & PHILPOTTS, J. A. 1970. Partition coefficients of rare earth elements between igneous matrix material and rock-forming mineral phenocrysts. II. *Geochimica et Cosmochimica Acta* **34**, 331–40.

SMITH, R. L. 1979. Ash-flow magmatism. In *Ash-flow Tuffs* (eds. C. E. Chapin, W. E. Elston), pp. 5–27. Geological Society of America Special Paper no. 180.

SMITH, R. L. & BAILEY, R. A. 1966. The Bandelier Tuff: a study of ash-flow eruption cycles from zoned magma chambers. *Bulletin Volcanologique* **29**, 83–104.

SPARKS, R. S. J., HUPPERT, H. E. & TURNER, J. S. 1984. The fluid dynamics of evolving magma chambers. *Philosophical Transactions of the Royal Society of London* **A310**, 511–34.

STOREY, M. 1981. Trachytic pyroclastics from Agua de Pau volcano, Sao Miguel, Azores: evolution of a magma body over 4,000 years. *Contributions to Mineralogy and Petrology* **78**, 423–32.

SUN, S. S. & HANSON, G. N. 1976. Rare earth evidence for differentiation of McMurdo volcanics, Ross Island, Antarctica. *Contributions to Mineralogy and Petrology* **54**, 139–55.

TURNER, J. S. & GUSTAFSON, L. B. 1981. Fluid motions and compositional gradients produced by crystallization or melting at vertical boundaries. *Journal of Volcanology and Geothermal Research* **11**, 93–125.

WALKER, G. P. L. & CROASDALE, R. 1971. Two plinian-type eruptions in the Azores. *Journal of the Geological Society of London* **127**, 17–55.

WOLFF, J. A. 1984. Variation in Nb/Ta during differentiation of phonolitic magma, Tenerife, Canary Islands. *Geochimica et Cosmochimica Acta* **48**, 1345–8.

WOOD, D. A. 1978. Major and trace element variations in the Tertiary lavas of Eastern Iceland and their significance with respect to the Iceland geochemical anomaly. *Journal of Petrology* **19**, 393–436.

WÖRNER, G., BEUSSEN, J. M., DUCHATEAU, N., GIJBELS, R. & SCHMINCKE, H. U. 1983. Trace element abundances and mineral melt distribution coefficients in phonolites from the Laacher See Volcano (Germany). *Contributions to Mineralogy and Petrology* **84**, 152–73.

WRIGHT, J. V., SMITH, A. L. & SELF, S. 1980. A working terminology of pyroclastic deposits. *Journal of Volcanology and Geothermal Research* **8**, 315–36.